

Topics in Applied Physics Volume 7

Integrated Optics

Edited by T. Tamir

Second Corrected and Updated Edition



Springer-Verlag Berlin Heidelberg New York 1979

Topics in Applied Physics Volume 7



Topics in Applied Physics Founded by Helmut K. V. Lotsch

Volume 57 **Strong and Ultrastrong Magnetic Fields**

Applications Editor: F. Herlach

Volume 58 **Hot-Electron Transport in Semiconductors**

Editor: L. Reggiani

Volumes 1–56 are listed on the back inside cover

Integrated Optics

Edited by T. Tamir

With Contributions by

E. Garmire J. M. Hammer H. Kogelnik

T. Tamir F. Zernike

Second Corrected and Updated Edition

With 99 Figures

Springer-Verlag Berlin Heidelberg New York 1979

Professor THEODOR TAMIR

**Department of Electrical Engineering, Polytechnic Institute of New York
333 Jay Street, Brooklyn, NY 11201, USA**

3rd Printing of the 2nd Edition 1985

2nd Corrected Printing of the 2nd Edition 1982

**ISBN 3-540-09673-6 2. Auflage Springer-Verlag Berlin Heidelberg New York
ISBN 0-387-09673-6 2nd edition Springer-Verlag New York Heidelberg Berlin**

**ISBN 3-540-07297-7 1. Auflage Springer-Verlag Berlin Heidelberg New York
ISBN 0-387-07297-7 1st edition Springer-Verlag New York Heidelberg Berlin**

This work is subject to copyright. All rights are reserved, whether the whole or part of the material is concerned, specifically those of translation, reprinting, re-use of illustrations, broadcasting, reproduction by photocopying machine or similar means, and storage in data banks. Under § 54 of the German Copyright Law, where copies are made for other than private use, a fee is payable to "Verwertungsgesellschaft Wort", Munich.

**© Springer-Verlag Berlin Heidelberg 1975 and 1979
Printed in Germany**

The use of registered names, trademarks, etc. in this publication does not imply, even in the absence of a specific statement, that such names are exempt from the relevant protective laws and regulations and therefore free for general use.

**Typesetting, printing and bookbinding: Brühlsche Universitätsdruckerei, Giessen
2153/3130-5432**

Preface to the Second Edition

Integrated optics has proven to be a very dynamic and active area, with new significant developments being made at a very fast pace. Because of this rapid advance, the first edition of this book was projected to be relevant for only 2–3 years. It has turned out, however, that the large amount of basic material contained in the book has provided continued interest, which now expresses itself as a demand for a second edition. To accommodate this need, we have decided to issue the present updated paperback edition, which also has a lower price so as to make it more accessible to graduate students.

The paperback edition is essentially identical to the original hard-cover book, except that a new chapter (Chap. 7) has been added. This new chapter reviews briefly the recent advances in the area and provides numerous new references. A few typographical errors in the original edition were corrected.

Due to limitations of both time and space, Chapter 7 can do little more than point the reader to the latest literature. However, we hope that future volumes of Springer optics books will detail the continuing progress of integrated optics.

Brooklyn, New York
July 1979

T. TAMIR

Preface to the First Edition

The new area of integrated optics, which is now about six years old, has been based primarily on the fact that light waves can propagate through and be contained by very thin layers (films) of transparent materials. By combining such layers together and shaping them into appropriate configurations, integrated-optics technology has realized a large variety of components which can perform a wide range of operations on optical waves. Thus, light can be guided, modulated, deflected, filtered, radiated into space or, by using laser action, it can also be generated within a thin-film structure. These components are small and compact and they are expected to promote a variety of goals, of which the most promising is optical signal processing in optical communications. For this, as well as for other related applications, the aim is to develop integrated instrumentation and optical apparatus having miniature dimensions, which are expected to be accompanied by robust, durable and reliable construction, with low power requirements.

Other technological and scientific pursuits of integrated optics include new devices made possible by the development of thin-film structures having special properties, phenomena produced by the concentration of high intensity fields in thin films and effects due to the attendant enhancement of nonlinear and/or active properties of such films. Motivated by so many goals, a host of new fabrication techniques have been developed for both amorphous and crystalline materials. However, integrated optics has been stimulated most strongly by the fact that, after centuries of interest in optical phenomena requiring equipment of relatively large dimensions, the small scale and planar features of thin film components offer intriguing and very promising potentialities for both old and new areas of research and development.

Because it involves a variety of scientific and technological facets, the advancement of integrated optics has needed contributions from investigators having many different backgrounds. Thus, scientists with interest in optics, microwave engineers, specialists in radiation and diffraction, as well as physicists in the areas of semiconductors, crystals, surface phenomena, materials science and other disciplines, have often combined to explore and apply the optical wave phenomena occurring in

thin films. To tie together these various areas, a fairly large number of survey papers have been issued during recent years. However, these surveys usually were either short simplified descriptions of integrated optics and its goals, or they were addressed to a group specializing in a narrow aspect of the broader area. The need has therefore existed for a wider coverage of integrated optics in a manual that would provide a comprehensive exposition of this new area to scientists and engineers in all of the professional groups enumerated above.

The aim of this book is to satisfy this need by serving as a monograph on the state of the present art in integrated optics. We have therefore attempted here to highlight those topics that have received greatest attention and to emphasize those applications and methods that have proven themselves most trustworthy and practical. Because the amount of material already available in this area is quite voluminous and its complete inclusion is beyond the scope of this monograph, we did not aim to achieve the coverage required of a handbook. Nevertheless, an attempt was made to include almost everything reported in the area of integrated optics at least in the form of references. Hence this monograph should serve adequately as a well informed manual that provides a balanced and reasonably detailed coverage of integrated optics and discusses in sufficient depth its most pertinent theoretical and practical aspects.

As the present book represents the joint effort of five contributors, each of whom is responsible for his own chapter, a certain lack of cohesiveness and some repetitions are practically unavoidable. We have attempted to minimize such deficiencies and, whenever appropriate, we have provided cross-references amongst the various chapters. If, nevertheless, the attempt to achieve a well rounded monograph has not been entirely successful, the authors rely on the readers to temper their criticism with the understanding that the time scale for writing, editing and publishing an up-to-date manual on a rapidly growing and very active field is too brief for achieving a more carefully organized book.

The Editor wishes to thank the other contributors for many interesting and productive discussions in connection with the preparation of this book. In particular, the critical comments and the constructive suggestions by Dr. J. M. HAMMER and Dr. H. KOGELNIK on the introductory chapter are greatly appreciated.

Special thanks are due to Miss MARY LEE GRIFFITH for her careful and very competent assistance with the editorial work.

Brooklyn, New York

April 1975

T. TAMIR

Contents

1. Introduction. By T. TAMIR (With 2 Figures)	
1.1. Historical Perspectives	1
1.1.1. The First Six Years	2
1.1.2. The Last Six Years	3
1.1.3. Immediate and Future Prospects	6
1.2. Organization of this Book	8
References	11
2. Theory of Dielectric Waveguides. By H. KOGELNIK (With 25 Figures)	
2.1. Ray Optics of the Slab Waveguide	15
2.1.1. Refraction and Reflection	15
2.1.2. Guided Modes	19
2.1.3. The Goos-Hänchen Shift	25
2.1.4. Effective Guide Thickness	27
2.2. Fundamentals of the Electromagnetic Theory of Dielectric Waveguides	29
2.2.1. Maxwell's Equations	29
2.2.2. Modes of the Waveguide	31
2.2.3. The Wave Equations for Planar Guides	32
2.2.4. Mode Properties Following from Symmetry	34
2.2.5. Orthogonality of the Modes	35
2.2.6. Mode Expansion and Normalization	37
2.2.7. The Variation Theorem for Dielectric Waveguides	40
2.2.8. Power Flow and Stored Energy in a Dielectric Waveguide	42
2.2.9. Variational Properties of the Propagation Constant	44
2.3. Modes of the Planar Slab Guide	45
2.3.1. TE-Modes	46
2.3.2. TM-Modes	50
2.4. Planar Guides with Graded Index Profiles	53
2.4.1. The Parabolic Profile (Harmonic Oscillator)	54
2.4.2. The “ $1/\cosh^2$ ” Profile	55
2.4.3. The Exponential Profile	57

2.4.4. Index Profiles with Strong Asymmetry	59
2.4.5. The WKB Method.	61
2.5. Strip Waveguides	62
2.6. Coupled-Mode Formalism and Periodic Waveguides	66
2.6.1. Excitation of Waveguide Modes	67
2.6.2. Waveguide Deformations	69
2.6.3. Coupled-Wave Solutions	71
2.6.4. Periodic Waveguides	73
2.6.5. TE-TM Mode Conversion	78
References	79
3. Beam and Waveguide Couplers. By T. TAMIR (With 27 Figures)	
3.1. Coupling of Beams to Planar Guides	84
3.1.1. Transverse Couplers	84
3.1.2. The Prism Coupler	86
Coupled-Mode Description	86
Basic Characteristics	89
3.1.3. The Grating Coupler	90
3.1.4. Leaky-Wave Theory of Beam Couplers	93
Inhomogeneous Plane Waves	93
Leaky Waves along Layered Media	96
Leaky Waves along Dielectric Gratings	98
Leaky Waves in Beam Couplers	99
3.1.5. Design Considerations for Prism Couplers	101
Role of Beam Width	102
Effect of Beam Form.	103
Deviations from the Phase-Matching Angle	107
Beam Shaping by Variable Air Gap	107
Calculation of Leaky-Wave Characteristics	107
3.1.6. Design Considerations for Grating Couplers	110
Single-Beam Couplers	110
Effect of Grating Height	113
Effect of Higher-Order Modes	115
Two-Beam Couplers	115
3.1.7. Other Beam Couplers	118
The Thin-Film Tapered Guide	118
The Holographic Coupler.	119
3.2. Waveguide Couplers and Mode Converters	120
3.2.1. Planar-to-Planar Guide Couplers	121
3.2.2. Planar-to-Linear Guide Couplers	123
3.2.3. Linear-to-Linear Waveguide Couplers	124

3.2.4. Waveguide-to-Fiber Couplers	126
3.2.5. Mode Converters	128
3.2.6. Coupling to Radiation Modes	131
3.2.7. Filters and Other Components	133
References	134
4. Modulation and Switching of Light in Dielectric Waveguides	
By J. M. HAMMER (With 11 Figures)	
4.1. Definition of Modulator, Switch, and Scanner	140
4.2. Measures of Relative Merit and Systems Uses	141
4.2.1. Intensity Modulators and Depth of Modulation .	141
4.2.2. Drive Power per Unit Bandwidth at Equivalent In- tensity Modulation of 70%—Specific Energy	143
4.2.3. Insertion Loss	144
4.2.4. Measures of Merit for Switches	145
4.3. Phase, Polarization and Frequency Modulators	146
4.3.1. Phase Modulation	146
4.3.2. Polarization Modulation	146
4.3.3. Frequency Modulators	147
4.4. Physical Effects Used in Light Modulators	147
4.4.1. Electro-Optic Effects	148
Table 4.1.	150
4.4.2. Acousto-Optic Effects	150
Table 4.2.	152
4.4.3. Magneto-Optic Effects	152
4.5. Bulk Modulators	154
4.5.1. Bulk Acousto-Optic Modulators	155
Table 4.3.	160
4.5.2. Bulk Electro-Optic Modulators	161
4.5.3. Bulk Magneto-Optic Modulators	164
4.6. Optical Waveguide Modulators	167
4.6.1. Acousto-Optic Waveguide Modulators	169
4.6.2. Electro-Optic Waveguide Modulator	175
Table 4.4.	183
4.6.3. Magneto-Optic Waveguide Modulator	189
4.7. Comparison of Optical Modulators	192
4.8. Appendix	194
References	198

5. Fabrication and Measurement of Passive Components	
By F. ZERNIKE (With 12 Figures)	
5.1. Methods Used to Produce Waveguiding Layers	202
5.1.1. Substrate Preparation	203
5.1.2. Cleaning of the Substrate	205
5.1.3. Sputtering	206
5.1.4. Plasma Polymerization	211
5.1.5. Spinning and Dipping	213
5.1.6. Ion Migration	214
5.1.7. Proton Bombardment and Ion Implantation	215
5.2. Guide Evaluation	216
5.2.1. Attenuation Measurements	216
5.2.2. Thickness Measurement	220
Interferometry	220
Contact Measurement	221
Measurement during Deposition	222
5.2.3. Index Measurement	222
5.2.4. Index and Thickness Determination from Measurements of the Apparent Refractive Index	223
Data Reduction	229
5.3. Pattern Fabrication	232
5.3.1. Periodic Patterns	232
5.3.2. Non-Periodic Patterns	233
5.3.3. Methods of Material Removal	234
5.3.4. Electron Beam Writing	235
5.3.5. Laser Beam Writing	237
5.3.6. Coupling between Guides	237
5.3.7. Duplication Methods	238
References	239
6. Semiconductor Components for Monolithic Applications	
By E. GARMIRE (With 22 Figures)	
6.1. Waveguides	243
6.1.1. Waveguides Due to Free Carriers	244
Epitaxial Waveguides	246
Diffused Waveguides	247
Ion-Implanted Waveguides	248
6.1.2. Waveguides Due to Material Composition	251
$\text{Ga}_{1-x}\text{Al}_x\text{As}$ Ternary System Waveguides	252
Other Semiconducting Waveguides	256
Insulating Crystal Waveguides	259
6.1.3. Observation of Waveguiding	260

6.2. Three-Dimensional Channel (Strip) Waveguides and Couplers	262
6.2.1. Channel Waveguides	263
Ridged Waveguides	263
Imbedded Guides	265
Strip-Loaded Waveguides	266
6.2.2. Directional Couplers	266
6.3. Lasers	271
6.3.1. GaAs Heterostructure Lasers	271
6.3.2. Lasers Fabricated by Planar Technology	273
6.3.3. Distributed Feedback Lasers	275
6.4. Modulators	279
6.4.1. Electro-Optic Effect in GaAs	279
6.4.2. Electro-Optic Phase Modulators	281
6.4.3. Intensity Modulators.	282
6.5. Detectors	284
6.5.1. Photodiodes	285
6.5.2. Epitaxial Photodetectors	286
6.5.3. Electro-Absorption Detectors	288
6.5.4. Ion-Implanted Photodetectors	289
6.6. Integration	290
6.7. Liquid-Phase Epitaxy	293
6.7.1. Growth Apparatus	293
6.7.2. Growth Procedure	295
6.7.3. Growth Characteristics	298
References	302
7. Recent Advances in Integrated Optics. By T. TAMIR	305
7.1. General Aspects	305
7.2. Passive Components	305
7.3. Active Components	307
7.4. Integration and Other Aspects	308
References	309
Additional References with Titles	321
Further References with Titles (1982 Printing)	328
Subject Index	335

Contributors

GARMIRE, ELSA

Center for Laser Studies, University of Southern California,
Los Angeles, CA 90007, USA

HAMMER, JACOB M.

RCA Laboratories, Princeton, NJ 08540, USA

KOGELNIK, HERWIG

Bell Telephone Laboratories, Holmdel, NJ 07733, USA

TAMIR, THEODOR

Department of Electrical Engineering,
Polytechnic Institute of New York, 333 Jay Street,
Brooklyn, NY 11201, USA

ZERNIKE, FRITS

Perkin-Elmer, Norwalk, CT 06856, USA

1. Introduction

T. TAMIR

With 2 Figures

The area of integrated optics has been concerned with a wide variety of phenomena involving light guided along and controlled by thin dielectric films or strips. The wavelengths of interest lie mostly between 0.1 and 10.0 μm (10^3 – 10^5 Å), this range being determined primarily by available laser frequencies and by material properties. For wavelengths much larger than 10 μm , i. e., in the millimeter region and beyond, metallic waveguiding techniques of the microwave variety have provided a more efficient technology. For wavelengths around 0.1 μm or smaller, the absence of suitable sources and the presence of large absorption and scattering losses impose limitations on the practical use of waveguiding effects.

Following this Introduction, the other chapters specialize in those major aspects of integrated optics that represent the more important concepts and/or the more significant technical achievements in the area. To put all of these into proper perspective, we present here a historical overview of integrated optics, as well as some projections for its applications in the future. These are followed by an outline of the specific topics treated in the subsequent chapters.

1.1. Historical Perspectives

As integrated optics is based on the *guiding* of electromagnetic energy at *optical* frequencies by thin films, its origins have been stimulated and influenced mostly by two separate technical areas, *viz.* microwave engineering and thin-films optics. A special role has also been played by semiconductors, which now appear to be most promising in promoting the goal of monolithic integrated optical circuits. If realized, these circuits would serve as miniature optical counterparts of microwave devices and networks, except that integrated optical circuits would offer the advantages of much larger bandwidth and negligible sensitivity to interference by natural or man-made electromagnetic fields of lower frequencies.

The role played by previous studies of guided waves and by microwave engineering in integrated-optics research is very well documented in KAPANY and BURKE's monograph [1.1], where the origins of optical waveguides are traced to the 1910 work on the dielectric rod by HONDROS and DEBYE [1.2]. We shall therefore skip over a period of about 50 years and concentrate here on the scientific efforts involving planar thin-film dielectric structures rather than metallic and/or circular configurations.

1.1.1. The First Six Years

The period of 1962 to about 1968 saw the inception of several studies of thin-film phenomena, which at the time seemed motivated by different goals. However, many of these efforts ultimately converged into laying the basis for much of what is considered today as belonging to the integrated-optics area. Thus, while planar dielectric waveguides were well understood and used in microwave engineering [1.1] much before 1962, it was only in 1965 that microwave concepts were combined with photolithographic techniques to construct thin-film waveguides as well as other planar components and circuitry for applications in the infrared range by ANDERSON and his group [1.3, 4]. Because of their approach, these investigators employed the term "quasi-microwave optics" to describe that newly developing technology. Although not concerned with such optical waveguide circuitry, the guiding action of planar layers in $p-n$ junctions had been observed and reported earlier in 1963 by YARIV and LEITE [1.5], and BOND et al. [1.6]. Their results were subsequently employed by NELSON and REINARDT [1.7] who showed that the planar guided modes in $p-n$ junctions are instrumental in providing light modulation via the electro-optic effect.

While the above studies were in progress, OSTERBERG and SMITH [1.8] carried out experiments with glass sheets and prisms that, although not yet using laser light, nevertheless provided both optical guidance by planar films and coupling of a light beam into these films. In fact, as shown in Fig. 1.1, their experiment achieved image transmission by coupling through a prism L into a planar guide S_1 , which transferred the light towards a gap; some of this light crossed the gap through a slit U and then was partially captured by another similar glass sheet S_2 , from which optical energy was collected by a second prism R. This produced a beam that, when properly focused, reproduced at I the image of the input aperture a. The guiding along the glass surface was produced by the graded increase of the refractive index, which is particularly enhanced in Pilkington float glass. Viewed as an image trans-

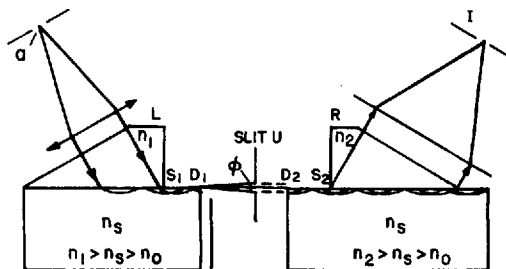


Fig. 1.1. Image-transmission experiment of OSTERBERG and SMITH [1.8]. Note similarity of planar glass waveguides and prism couplers with components used in currents practice

mission device, OSTERBERG and SMITH's set-up can therefore be regarded as a first rudimentary implementation of a passive optical guided-wave apparatus, some elements of which are applicable even today.

The above investigations, as well as the successful prior results on circular dielectric optical guides (or fibers) by SNITZER and OSTERBERG [1.9] and by KAPANY and BURKE [1.10], played a considerable role in arousing interest into planar optical guides. Although the latter were considered as a possible means for long-distance transmission by KARBOWIAK [1.11], their fabrication [1.3, 4, 12, 13] was motivated mostly by applications involving optical surface-wave propagation over short distances only. These applications suggested the use of optical surface waves in data-processing networks, so that terms such as "optical integrated data processors" [1.13] and "optical integrated circuits" [1.14] started being employed around 1968. In 1969, when abbreviating these expressions to "integrated optics". MILLER [1.15] not only coined both an attractive and catchy name, but also heralded the beginning of vigorous efforts to investigate and develop a sound and reliable thin-film technology for optical communications purposes.

1.1.2. The Last Six Years

The year 1968 brought great expectations on the potentialities of integrated optics and served as the start of a period of intense and fruitful activities, which stretch into the present. From the outset, it was projected by some that the ultimate goal of these activities would be to replace integrated-electronics circuits by equivalent, and possibly more effective, integrated-optics circuits. For this purpose, integrated-optics components must be compact and miniature, reliable, with high mechanical and thermal stability, low power consumption and preferably integrable on a common substrate or chip. These requirements stimu-

lated the development of improved thin-film fabrication techniques and promoted numerous studies of new materials, for both passive and active functions.

It can be stated that many of the above goals have by now been achieved and, even though components for integrated-optics circuits are not yet commercially available, their realizability has been demonstrated in the laboratory. For proper perspective, it is interesting to follow the development of thin-film techniques and their application to the construction of passive and active devices by starting with the articles by ANDERSON [1.3], SHUBERT and HARRIS [1.13] and MILLER [1.15], which have been followed by a rapid succession of review papers and/or tutorial articles [1.16-32]; these offer an interesting chronological survey of integrated optics by presenting its state of the art at various stages during the past six years.

Of course, some of the initial efforts following the impetus given in 1968 were intended to improve the properties of planar waveguides and other passive components, such as directional couplers and transitions from one waveguide to another. In integrated optics, these serve the function of transporting light energy in the same sense that wires or conduits carry currents in integrated electronics circuits. It is therefore required that such passive components have low absorption and scattering losses. This requirement was achieved quite early for simple planar guides [1.18], with losses lower than 1 dB/cm being obtainable by thin films of organic material, photoresist, sputtered glass and other suitable media, as listed in [Ref. 1.27, Table I, p. 266].

Because gas lasers were often used as the light source, their beam had to be coupled into the thin-film waveguides. This function, which has no counterpart in integrated electronics, was solved in an efficient manner by HARRIS et al. [1.33], by TIEN and ULRICH [1.34], and by MIDWINTER [1.35] who independently developed greatly improved versions of the prism coupler used by OSTERBERG and SMITH [1.8]. Shortly thereafter, grating couplers, which are less bulky than prism couplers, were introduced by DAKSS et al. [1.36], and by KOGELNIK and SOSNOWSKI [1.37].

In addition to the above components, it was also necessary to develop the active components that would serve as the counterpart of active devices, such as transistors, in integrated electronics. In integrated optics, these components include light sources, modulators and detectors. Because the generation and rapid control of light requires that electric currents interact directly or indirectly with the optical energy, the area of integrated optics dealing with active components falls within the broader technical area of opto-electronics, which includes but is not restricted to miniature planar devices.

Following the demonstration by NELSON and REINHARDT [1.7] of light modulation in thin films, the electro-optic effect was applied by HALL et al. [1.38] to achieve modulation in structures consisting of a high resistivity GaAs epitaxial film on a more heavily doped GaAs substrate; modulation was then obtained by utilizing the electro-optic effect to control the waveguide cut-off or the field polarization. Later, a number of investigators developed other thin-film modulators, which were also utilizing the electro-optic effect but had different configurations and/or employed other electro-optic materials. Some of these used superimposed gratings and took advantage of Bragg diffraction [1.39] to modulate light by spatially deflecting the optical surface wave traveling in the thin film.

The Bragg diffraction principle for deflecting an incoming surface wave was also used by KUHN et al. [1.40] who achieved modulation by replacing the grating with an acoustic wave traveling through the thin film. This electro-acoustic effect was subsequently utilized by other investigators to produce modified versions of modulators and beam deflectors. By taking advantage of Faraday rotation in magnetic materials, TIEN et al. [1.41] constructed a modulator using the magneto-optic effect; however, their approach appears to have fewer followers than the electro-optic and the acousto-optic methods.

Although beams generated by gas and solid-state lasers have been frequently used as light sources, it is evident that much smaller sources must be used to achieve the goal of a truly integrated-optics circuit having miniature dimensions. For this purpose, very promising candidates are the $\text{Al}_x\text{Ga}_{1-x}\text{As}$ heterostructure junction lasers, which have the required thin planar configuration. Based on the studies of KRESSEL and NELSON [1.42], ALFEROV et al. [1.43] and HAYASHI [1.44], these lasers are now available for cw operation at room temperature and they possess long life capabilities [1.45].

Dye lasers also exhibit a desirably small and planar configuration [1.46], but their inherently short life may preclude their use in integrated-optics circuitry for optical communications. Although demonstrated first in dye lasers, the distributed-feedback concept introduced by KOGELNIK and SHANK [1.47] has been successfully applied to the fabrication of AlGaAs lasers [1.48]. These require fine periodic corrugations and, so far, only operation at low temperatures has been obtained [1.49–50], but investigations continue to improve their capabilities for integrated-optics applications. Although also requiring low temperature, another promising miniature source is the mesa laser that, as reported by BLUM et al. [1.51], consists of a $\text{Ga}_{1-x}\text{In}_x\text{As}$ heterostructure in the form of a very thin rhombic resonator grown by selective vapor-phase epitaxy.

Somewhat surprisingly, relatively little effort has been spent on developing miniature planar light detectors. After the infra-red diodes reported by ANDERSON and his associates [1.3, 4], some eight years elapsed until a silicon $p-n$ junction photo-diode was reported by OSTROWSKY et al. [1.52]. Subsequently, studies of photo-detection in GaAs via epitaxial growth, electro-absorption and ion implantation [1.53] have been carried out. These have shown that photo-detectors for integrated optics pose no serious fabrication difficulties; hence their development would probably be more strenuously pursued when more difficult fabrication problems for other components are overcome.

1.1.3. Immediate and Future Prospects

As is evident from the foregoing discussion, a substantially diversified and successful effort has already been carried out in studying and developing components for integrated optics. It is therefore expected that a first optical unit utilizing integrated-optics circuits would be constructed and could perform satisfactorily (at least in pilot form) any day from now. Because most of the effort has been directed towards applications to optics communications, the most likely candidate for such a device might be a single transmit-receive system using optical fibers over a distance of at least a few hundred feet. Conceptual designs of such systems have already been presented and discussed at recent topical meetings [1.20, 32], one of the latest forms [1.54] being shown in Fig. 1.2. As seen therefrom, an optical transmitter is visualized as consisting of a GaAs chip on which the appropriate passive and active components are being grown or deposited. Because GaAs, in conjunction with some of its associated compounds, can provide all the functions necessary in integrated optics, i. e., waveguiding, modulation, detection and lasing,

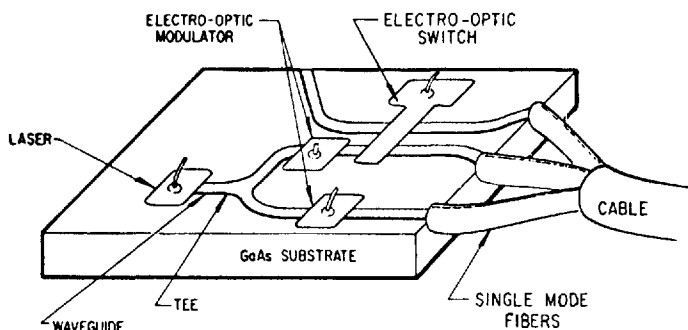


Fig. 1.2. Artist's sketch of a monolithic integrated GaAs transmitter. (After BIUM et al. [1.54])

it could very likely perform a role analogous to that of silicon in integrated electronics. Consequently, GaAs is now regarded by many as the basis for integrated optics on a single wafer or chip—a technology referred to as “monolithic integrated optics”.

As optical fibers with properties superior to either conventional wires at lower frequencies or to waveguides at microwave or millimeter frequencies have by now been developed, it is expected that these fibers would provide the links between the transmitters, relays and receivers that constitute a complex communications system. Such systems are by now definitely considered for the purpose of urban and inter-urban telephone communications, as well as for telemetry, internal communications and operations control inside large planes and ships. This is why the transmitter shown in Fig. 1.2 is connected to a cable containing fibers. Of course, an integrated-optics receiver and/or relay station would then have a very similar appearance to the transmitter chip described in that figure. The simplicity of such a unit and the resemblance of its circuitry to that of an integrated-electronics apparatus is quite evident.

It is also pertinent to observe that, despite the impressive progress already made, the reason for not having yet realized commercial integrated-optics systems is probably due to two extraneous factors. First, the expected use of optical fibers necessitates a simple and reliable splicing method for fibers, as well as an analogous technique for connecting a fiber to a thin-film waveguide. Although both problems motivated numerous investigations since 1970, apparently the results obtained so far have not yet arrived at a fully satisfactory solution. Nevertheless, schemes have been reported [1.55] that look sufficiently promising to expect that this problem will find a suitable solution, at least for multi-mode operation in fibers.

A second reason for the delay in implementing integrated-optics technology is the simple fact that current and near-future projects have as yet no urgent need for its principal advantage—the huge available bandwidth. As of now, even the most crowded intra-urban communication system can easily expand during the next ten years or so by taking full advantage of single side-band microwave systems at millimeter wavelengths. Seeing that optical communications is the most immediate and profitable application of integrated optics, the lack of urgency to develop this area affects its funding, which is generally on the low side. The more modest goal of utilizing integrated-optics circuits and optical fibers to replace larger electronic instruments and bulky cables on ships and planes appears to be adequately funded, but this effort is a relatively small-scale project.

However, future optical instrumentation and systems, in general, and integrated-optics apparatus, in particular, provide the subject for con-

siderable speculations on their potentialities. Without going here into projections that should rightly be in the realm of science fiction, the replacement of larger conventional optical apparatus and, possibly, of some electronic circuitry by integrated-optics instrumentation would undoubtedly open new applications in science and technology. In particular, the huge available bandwidth available at optical frequencies would facilitate office and home access to services that have not been possible so far. Thus, the use of picture phones could be implemented and a large variety of terminals for access to central computers could more easily be introduced.

The very optimistic expectations expressed in the past that integrated optics would replace integrated electronics are nowadays largely muted. It is nevertheless projected that integrated optics will play a significant role in supplying the transition from an entirely electronic technology to a future one that needs optical components for operating at optical frequencies. Thus, even if integrated optics may later serve only as an adjunct to integrated electronics, the use of light as a communications medium indicates that integrated optics is henceforth assured of an important function in modern technology.

1.2. Organization of this Book

In planning the present monograph, we have attempted to combine the historical progress of integrated optics with the development of its technology from the simplest to the most complex components. It is thus natural that Chapter 2 treats the theory of dielectric thin-film waveguides, which were the first and simplest components to be fabricated. These waveguides represent both a basic conceptual aspect of integrated optics and the backbone structure that supports and interconnects an integrated-optics network. Consequently, Chapter 2 discusses the more practical planar guiding configurations and presents the fundamental theoretical considerations that are necessary for the proper understanding of the topics treated in later chapters. Both wide and narrow (strip) guides are discussed and methods for predicting their characteristics are presented.

In addition, Chapter 2 outlines the coupled-mode approach which serves as a powerful tool in understanding a variety of wave phenomena. In particular, the relevance of coupled modes to periodic structures is illustrated. This aspect is particularly important because periodic (grating) configurations play an increasingly important role in integrated optics.

While planar dielectric waveguides support and guide optical waves, the question of efficiently introducing optical energy into these wave-

guides is important for future anticipated uses of integrated-optics circuitry. This question is dealt with in Chapter 3, which discusses in detail the operation and properties of beam couplers, with special emphasis on couplers of the prism and the grating type. It is pertinent here to observe that most of these couplers have been needed because, so far, laboratory work employed conventional (non-integrated) lasers. For future integrated-optics circuitry, in which the laser source is also part of the thin-film structure, such couplers using exterior beams would have less utilization. However, their basic (three-dimensional) operation principles would then most likely be translated into a (two-dimensional) planar configuration, as is already being done in the case of mesa lasers [1.51]. Beam coupling problem and design considerations for efficient couplers will therefore continue to play an important role.

Apart from considering the coupling of beams into waveguides, Chapter 3 also describes other situations involving the coupling or transfer of optical energy from one form into another, such as transitions between waveguides of different cross-sections, mode converters, filters, and radiation losses. However, as most of these topics are closer to very similar ones already considered in the microwave engineering area, their discussion is more concise and the interested reader should refer to the book by MARCUSE [1.56] for theoretical expositions, as well as for additional background and bibliography.

After thus presenting the most significant aspects of passive integrated-optics theory and applications, the active control of optical waves in thin-film structures is dealt with in Chapter 4, where modulators, switches and beam deflectors are discussed. The modulation of light is a relatively new process; even in bulk materials, the physical effects that provide modulation capabilities have been explored, at most, only a few years ahead of similar work involving thin films. Consequently, the subject of light modulation is discussed in Chapter 4 for both bulk and thin-film materials. This subject is viewed therein from two different aspects. On the one hand, modulation of light is considered by separately examining variations in intensity, phase, polarization or frequency. From another point of view, the physical phenomena that provide modulation capabilities are discussed and various techniques involving acousto-optic, electro-optic or magneto-optic processes are presented and compared. A very important practical aspect of modulator operation—the question of drive power requirements and actual overall efficiency—is carefully discussed. In this context, the advantages of thin-film modulators versus their bulk counterparts are emphasized.

As discussed in Subsection 1.1.2, active components also include photodetectors and lasers. However, both lasers and detectors for integrated optics are constructed from semiconducting materials and their

detailed theory of operation is beyond the scope of this monograph. Anticipating that a separate manual in the Topics of Applied Physics series would be dealing with semiconductor lasers, detectors and other devices, we took the attitude that these components could be treated here only briefly and then mostly in the context of their fabrication. This topic has therefore been included in Chapter 6, which is outlined further below.

From the point of view of fabrication, passive structures involving mostly amorphous materials are discussed in Chapter 5. Included therein are descriptions of the methods for depositing films on substrates, *e.g.*, sputtering, plasma polymerization, spinning and dipping, ion migration, proton bombardment and ion implantation, as well as the fabrication of patterns by masking, material removal, electron and laser-beam writing. In addition, Chapter 5 discusses many aspects that are often omitted in journal articles, but these are nevertheless essential for achieving high-quality state-of-the-art results. Thus, the methods for preparing and cleaning the substrate so as to minimize the presence of defects that may seriously degrade performance are carefully presented and specific, successfully tried, procedures are recommended. In addition, the evaluation and measuring of the finished thin-film products are also presented, with questions such as accuracy and tolerances being given special attention. Many of these considerations represent information that is not readily available in the literature.

Finally, Chapter 6 considers the important topic of semiconductor components for monolithic fabrication of integrated-optics circuits. As it concentrates on GaAs and its related compounds, which are presently considered best candidates for totally integrated circuits, this chapter comes closest to, so to say, providing a whiff of things to come in the future of integrated optics. To place its subject into proper perspective, Chapter 6 discusses the fabrication on GaAs substrates of a wide range of semiconductor waveguides and other planar components. In line with the comments made above, lasers and detectors are also briefly described, the emphasis being on their fabrication in the context of GaAs material. Specific questions concerned with GaAs modulators are also mentioned to complete some of the information given in Chapter 4.

To round up all of the above separate topics, Chapter 6 then takes up the projected goal of monolithic integration on a single GaAs chip and presents convincing arguments for predicting that GaAs will play in integrated-optics the same role that silicon so successfully performs in integrated electronics. In conclusion, liquid-phase epitaxy is described, this being a useful process for implementing monolithic integration of all the desired components on GaAs substrates.

References

- 1.1. N. S. KAPANY, J. J. BURKE: *Optical Waveguides* (Academic Press, New York, London, 1972), pp. 1-6.
- 1.2. D. HONDROS, P. DEBYE: Ann. Physik **32**, 465 (1910).
- 1.3. D. B. ANDERSON: "Application of semiconductor technology to coherent optical transducers and spatial filters". In *Optical and Electro-Optical Information Processing*, ed. by J. TIPPETT (M.I.T. Press, Cambridge, Mass., 1965), pp. 221-234.
- 1.4. D. B. ANDERSON, R. R. AUGUST: Proc. IEEE **54**, 657 (1966).
- 1.5. A. YARIV, R. C. C. LEITE: Appl. Phys. Letters **2**, 55 (1963).
- 1.6. W. L. BOND, B. G. COHEN, R. C. C. LEITE, A. YARIV: Appl. Phys. Letters **2**, 57 (1963).
- 1.7. D. F. NELSON, F. K. REINHARDT: Appl. Phys. Letters **5**, 148 (1964).
- 1.8. H. OSTERBERG, L. W. SMITH: J. Opt. Soc. Am. **54**, 1073 (1964).
- 1.9. E. SNITZER, H. OSTERBERG: J. Opt. Soc. Am. **51**, 499 (1961).
- 1.10. N. S. KAPANY, J. J. BURKE: J. Opt. Soc. Am. **51**, 1067 (1961).
- 1.11. A. E. KARBOWIAK: "Optical waveguides". In *Advances in Microwaves* (Academic Press, New York, 1966), pp. 75-113.
- 1.12. E. R. SCHINELLER, R. F. FLAM, D. W. WILMOT: J. Opt. Soc. Am. **58**, 1171 (1968).
- 1.13. R. SHUBERT, J. H. HARRIS: IEEE Trans. MTT **16**, 1048 (1968).
- 1.14. D. B. ANDERSON: "An integrated circuit approach to optical waveguide", Digest Abstract IEEE Microelectronics Symposium, St. Louis, Miss. (1968).
- 1.15. S. E. MILLER: Bell System Tech. J. **48**, 2059 (1969).
- 1.16. J. E. GOELL, R. D. STANDLEY, T. G. LI: Electronics, p. 60 (Aug. 1970).
- 1.17. J. E. GOELL, R. D. STANDLEY: Proc. IEEE **58**, 1504 (1970).
- 1.18. P. K. TIEN: Appl. Opt. **10**, 2395 (1971).
- 1.19. S. E. MILLER: IEEE J. Quant. Electron. QE **8**, 199 (1972).
- 1.20. R. V. POLE, S. E. MILLER, J. H. HARRIS, P. K. TIEN: Appl. Opt. **11**, 1675 (1972).
- 1.21. A. YARIV: Laser Focus **8**, 40 (Dec. 1972).
- 1.22. T. TAMIR: Optik **36**, 209 (1972), **37**, 204 (1973) and **38**, 269 (1973).
- 1.23. E. T. STEPKE: Electro-Optics Systems Design **5**, 18 (1973).
- 1.24. W. S. C. CHANG: IEEE Trans. MTT **21**, 775 (1973).
- 1.25. D. MARCUSE (editor): *Integrated Optics* (IEEE Press, New York, 1973).
- 1.26. H. F. TAYLOR, A. YARIV: Proc. IEEE **62**, 1044 (1974).
- 1.27. W. S. C. CHANG, M. W. MULLER, F. J. ROSENBAUM: *Integrated Optics in Laser Applications*, Vol. 2 (Academic Press, New York, 1974), p. 227.
- 1.28. H. I. SMITH: Proc. IEEE **62**, 1936 (1974).
- 1.29. P. K. CHEO: Appl. Phys. **6**, 1 (1975).
- 1.30. H. KOGELNIK: IEEE Trans. MTT **23**, 2 (1975).
- 1.31. See also selected papers in IEEE Trans. MTT **23**, (Special Issue on Integrated Optics and Optical Waveguides, 1975), pp. 16-92.
- 1.32. R. V. POLE, E. M. CONWELL, H. KOGELNIK, P. K. TIEN, J. R. WHINNERY, A. J. DE MARIA: Appl. Opt. **14**, 569 (1975).
- 1.33. J. H. HARRIS, R. SHUBERT, J. N. POLKY: J. Opt. Soc. Am. **60**, 1007 (1970).
- 1.34. P. K. TIEN, R. ULRICH: J. Opt. Soc. Am. **60**, 1325 (1970).
- 1.35. J. MIDWINTER: IEEE J. Quant. Electron. QE **6**, 583 (1970).
- 1.36. M. L. DAKSS, L. KUHN, P. F. HEIDRICH, B. A. SCOTT: Appl. Phys. Letters **16**, 523 (1970).
- 1.37. H. KOGELNIK, T. P. SOSNOWSKI: Bell System Techn. J. **49**, 1602 (1970).
- 1.38. D. HALL, A. YARIV, E. GARMIRE: Opt. Commun. **1**, 403 (1970) and Appl. Phys. Letters **17**, 127 (1970).
- 1.39. D. P. GIA RUSSO, J. H. HARRIS: Appl. Opt. **10**, 2786 (1971).
- 1.40. L. KUHN, P. F. HEIDRICH, E. G. LEAN: Appl. Phys. Letters **19**, 428 (1971).

- 1.41. P. K. TIEN, R. J. MARTIN, R. WOLFE, R. C. LE CRAW, S. L. BLANK: *Appl. Phys. Letters* **21**, 394 (1972).
- 1.42. H. KRESSEL, N. NELSON: *RCA Rev.* **30**, 106 (1969).
- 1.43. Z. I. ALFEROV, V. M. ANDREEV, V. I. KOROLKOV, E. L. PORTNOI, D. N. TRETYAKOV: *Sov. Phys.-Semicond.* **2**, 1289 (1969).
- 1.44. I. HAYASHI, M. B. PANISH, P. W. FOY: *IEEE J. Quant. Electron.* **QE 5**, 211 (1969).
- 1.45. I. HAYASHI: *Appl. Phys.* **5**, 25 (1974).
- 1.46. F. P. SCHÄFER (editor): *Dye Lasers* (Springer, Berlin, Heidelberg, New York, 1973).
- 1.47. H. KOGELNIK, C. V. SHANK: *J. Appl. Phys.* **43**, 2327 (1972).
- 1.48. H. W. YEN, M. NAKAMURA, E. GARMIRE, S. SOMEKH, A. YARIV, H. L. GARVIN: *Opt. Commun.* **9**, 35 (1973).
- 1.49. C. V. SHANK, R. V. SCHMIDT, B. I. MILLER: *Appl. Phys. Letters* **25**, 200 (1974).
- 1.50. D. R. SCIFRES, R. D. BURNHAM, W. STREIFER: *Appl. Phys. Letters* **25**, 203 (1974).
- 1.51. F. A. BLUM, K. L. LAWLEY, W. C. SCOTT, W. C. HOLTON: *Appl. Phys. Letters* **24**, 430 (1974).
- 1.52. D. B. OSTROWSKY, R. POIRIER, L. M. RIEBER, C. DEVERDUN: *Appl. Phys. Letters* **22**, 463 (1973).
- 1.53. H. STOLL, A. YARIV, R. HUNSPERGER, G. TANGONAN: *Appl. Phys. Letters* **23**, 664 (1973).
- 1.54. F. A. BLUM, K. L. LAWLEY, W. C. HOLTON: *Naval Res. Rev.* **28**, 1 (Feb. 1975).
- 1.55. Refer to the Digest of Technical Papers, Topical Meeting on Optical Fiber Transmission, Williamsburg, Virginia (Optical Society of America, 1975).
- 1.56. D. MARCUSE: *Theory of Dielectric Optical Waveguides* (Academic Press, New York, 1974).

2. Theory of Dielectric Waveguides

H. KOGELNIK

With 25 Figures

Dielectric waveguides are the structures that are used to confine and guide the light in the guided-wave devices and circuits of integrated optics. This chapter is devoted to the theory of these waveguides. Other chapters of this book discuss their fabrication by such techniques as sputtering, diffusion, ion implantation or epitaxial growth. A well-known dielectric waveguide is, of course, the optical fiber which usually has a circular cross-section. In contrast, the guides of interest to integrated optics are usually planar structures such as planar films or strips. Our discussion will focus on these planar guides even though most of the fundamentals are applicable to all dielectric waveguide types.

The simplest dielectric guide is the planar slab guide shown in Fig. 2.1, where a planar film of refractive index n_f is sandwiched between a substrate and a cover material with lower refractive indices n_s and n_c ($n_f > n_s \geq n_c$). Often the cover material is air, in which case $n_c = 1$. As an illustration, we have listed in Table 2.1 the refractive indices of some dielectric waveguide materials used in integrated optics. Typical differences between the indices of the film and the substrate range from 10^{-3} to 10^{-1} , and a typical film thickness is 1 μm . The light is confined by total internal reflection at the film-substrate and film-cover interfaces.

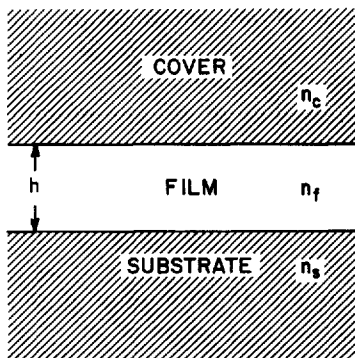


Fig. 2.1. Cross-section of a planar slab waveguide consisting of a thin film of thickness (or height) h and refractive index n_f , sandwiched between substrate and cover materials with indices n_s and n_c .

Table 2.1. Refractive index n of dielectric waveguide materials

Dielectric material	$\lambda [\mu\text{m}]$	n
Fused silica (SiO_2)	0.633	1.46
Typical microscope—slide glass	0.633	1.51
Sputtered Corning 7059 glass	0.633	1.62
$\text{LiTaO}_3 (n_0)$	0.80	2.15
(n_e)	0.80	2.16
$\text{LiNbO}_3 (n_0)$	0.80	2.28
(n_e)	0.80	2.19
GaAs	0.90	3.6

Dielectric waveguides have already been the subject of two textbooks, one by KAPANY and BURKE [2.1] and the other by MARCUSE [2.2], and we can refer the reader to these for a history on the subject as well as for a more complete list of references.

In this text, we have several aims. We hope to give both an introduction to the subject as well as a collection of important results sufficiently detailed to be of use to the experimenter. We also aim to provide a compact theoretical framework of sufficient rigor and generality to be used as the basis for future work and to analyse virtually all waveguide types and devices of interest in integrated optics. In Section 2.1 we discuss the ray-optical picture of light propagation in slab waveguides. This is meant to provide both a first physical understanding as well as an introduction to the concepts and the terminology of dielectric waveguides in general. Some basic results of interest to the experimenter are also developed here. Section 2.2 is a collection of the general fundamentals of the electromagnetic theory of dielectric waveguides and their modes of propagation, including the orthogonality, symmetry, and variational properties of the modes. Section 2.3 gives a detailed listing of the formulas for the modes and fields of the planar slab waveguides, both for the guided TE and TM modes as well as for the radiation modes. Section 2.4 discusses graded index profiles giving the modal solutions for the parabolic, the “ $1/\cosh^2$ ” and the exponential profiles. Brief treatments of graded profiles with an abrupt index step and of the WKB method are also included. Section 2.5 gives a brief discussion of strip waveguides and the application of the effective index method to these structures. The final Section 2.6 is devoted to the development of the general coupled-mode formalism for dielectric waveguides, including its application to the treatment of waveguide deformations and periodic waveguides.

We shall assume throughout this chapter that the guided light is coherent and monochromatic and that the waveguides consist of di-

electric media that are lossless and isotropic. For a discussion of lossy and metal-clad optical waveguides, we refer the reader to the papers by ANDERSON [2.3], REISINGER [2.4], KAMINOW et al. [2.5] and the literature cited therein. Anisotropic dielectric waveguides have been treated by NELSON and MCKENNA [2.6], YAMAMOTO et al. [2.7], RAMASWAMY [2.8, 9] and others.

2.1. Ray Optics of the Slab Waveguide

In this section, we propose to discuss and develop the ray optical model of light propagation in a slab waveguide. Ray optical techniques in connection with slab waveguides have been explored and used by TIEN [2.10], MAURER and FELSEN [2.11], LOTSCH [2.12] and others. We have chosen the slab waveguide, sketched in Fig. 2.1, for two reasons: first, because it is relatively easy to understand and analyze, and second because it is of considerable practical interest in integrated optics. We shall use the ray-optical picture to introduce the basic concepts and terminology of dielectric waveguide theory, including the nature of the modes of propagation, waveguide cutoff, the propagation constants and the effective guide width. In addition, we employ this picture to derive and provide a number of results of interest to the experimenter, such as plots of the propagation constant and of the effective width of slab waveguides. The ray-optical picture is a very simple picture with great intuitive appeal, but it is not as complete a description as that provided by electromagnetic theory, which we discuss later in Sections 2.2 and 2.3. However, the results we present here are in perfect agreement with the latter.

Our picture of light guidance in a slab waveguide is one of light rays tracing a zig-zag path in the film, with total internal reflection of the light occurring at the film-substrate and film-cover interfaces. As reflection and refraction at these dielectric interfaces play an important role in the guiding process, let us briefly review the relevant laws and their consequences.

2.1.1. Refraction and Reflection

Consider an interface separating two lossless, isotropic, homogeneous dielectric media of refractive index n_1 and n_2 as shown in Fig. 2.2, and a coherent light wave incident at an angle θ_1 between the wave normal and the normal to the interface. In general, the wave, having a complex

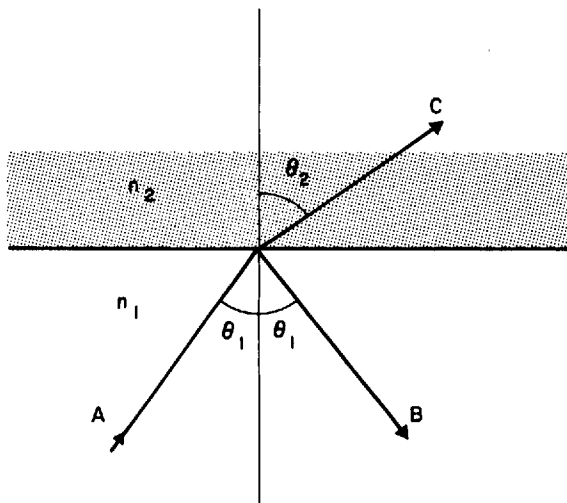


Fig. 2.2. Wave normals of light refracted and reflected at the planar interface between two media of index n_1 and n_2 . Angle of incidence is θ_1

amplitude A at the interface, is partially reflected and refracted as shown. The exit angle θ_2 of the refracted wave C is given by Snell's law

$$n_1 \sin \theta_1 = n_2 \sin \theta_2. \quad (2.1.1)$$

The reflected wave has a complex amplitude B at the interface linearly related to A by a complex reflection coefficient R

$$B = R \cdot A. \quad (2.1.2)$$

The reflection coefficient depends on the angle of incidence and the polarization of the light, and is given by the Fresnel formulas. For TE polarization (i.e. electric fields perpendicular to the plane of incidence spanned by the wave normal and the normal to the interface) we have

$$\begin{aligned} R_{TE} &= (n_1 \cos \theta_1 - n_2 \cos \theta_2) / (n_1 \cos \theta_1 + n_2 \cos \theta_2) \\ &= (n_1 \cos \theta_1 - \sqrt{n_2^2 - n_1^2 \sin^2 \theta_1}) / (n_1 \cos \theta_1 + \sqrt{n_2^2 - n_1^2 \sin^2 \theta_1}). \end{aligned} \quad (2.1.3)$$

The corresponding formula for TM polarisation (with the magnetic fields perpendicular to the plane of incidence) is

$$\begin{aligned} R_{\text{TM}} &= (n_2 \cos \theta_1 - n_1 \cos \theta_2) / (n_2 \cos \theta_1 + n_1 \cos \theta_2) \\ &= (n_2^2 \cos \theta_1 - n_1 \sqrt{n_2^2 - n_1^2 \sin^2 \theta_1}) / (n_2^2 \cos \theta_1 + n_1 \sqrt{n_2^2 - n_1^2 \sin^2 \theta_1}). \end{aligned} \quad (2.1.4)$$

The so-called critical angle θ_c is given by

$$\sin \theta_c = n_2/n_1. \quad (2.1.5)$$

As long as $\theta_1 < \theta_c$ we have only partial reflection and a real valued R . As soon as the critical angle is exceeded ($\theta_1 > \theta_c$), we have $|R|=1$ and total reflection of the light occurs. R is now complex valued and a phase shift is imposed on the reflected light. We write

$$R = \exp(2j\phi), \quad (2.1.6)$$

and extract from the Fresnel formulas the following expressions for the phase shifts ϕ_{TE} and ϕ_{TM} corresponding to the two polarization states

$$\tan \phi_{\text{TE}} = \sqrt{n_1^2 \sin^2 \theta_1 - n_2^2} / (n_1 \cos \theta_1) \quad (2.1.7)$$

$$\tan \phi_{\text{TM}} = \frac{n_1^2}{n_2^2} \sqrt{n_1^2 \sin^2 \theta_1 - n_2^2} / (n_1 \cos \theta_1). \quad (2.1.8)$$

Figure 2.3 shows the dependence of ϕ_{TE} on the angle of incidence θ_1 for a selection of index ratios n_2/n_1 where the values 0.3, 0.5 and 0.7

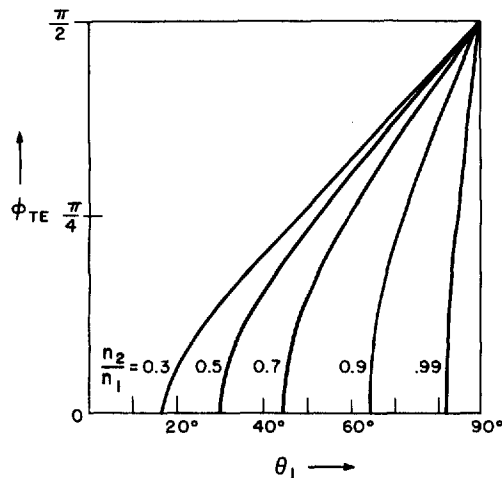


Fig. 2.3. Phase shift ϕ_{TE} of the TE mode as a function of the angle of incidence θ_1

correspond approximately to interfaces between air and GaAs, LiNbO₃, and SiO₂, respectively. We note that the phase shift increases from 0 at the critical angle to $\pi/2$ at grazing incidence ($\theta_1 = 90^\circ$). It increases with infinite slope at $\theta_1 = \theta_c$ and a slope of $(1 - n_2^2/n_1^2)^{-1/2}$ at $\theta_1 = 90^\circ$. The behaviour of ϕ_{TM} is quite similar.

Consider, now, the ("asymmetric") slab waveguide structure shown in Fig. 2.4 with a film of index n_f and substrate and cover materials of index n_s and n_c' . In general, we have $n_f > n_s > n_c'$ and two critical angles of interest, θ_s for total reflection from the film-substrate interface

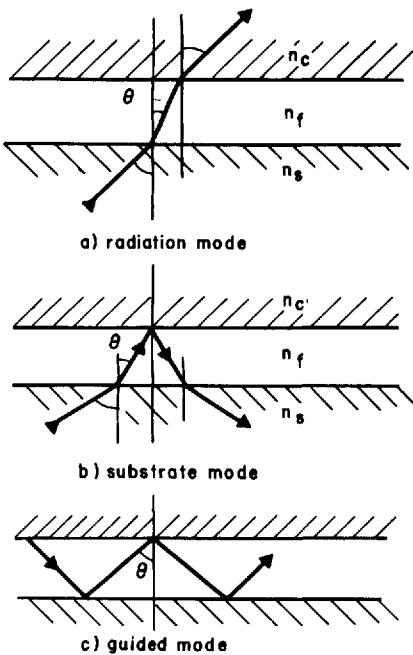


Fig. 2.4a-c. Zig-zag-wave pictures for the radiation modes (a), the substrate radiation modes (b), and the guided modes (c) in a slab waveguide

and $\theta_c < \theta_s$ for total reflection from the film-cover interface. When we examine what happens as the angle of incidence θ is increased, we discover that there are three distinct cases which are sketched in Fig. 2.4. For small angles $\theta < \theta_s, \theta_c$ light incident from the substrate side is refracted according to Snell's law and escapes from the guide through the cover (a). There is essentially no confinement of light, and the electro-

magnetic mode corresponding to this picture is called a "radiation mode" which is discussed in more detail in Section 2.3. When θ is increased somewhat, such that $\theta_s < \theta < \theta_c$, we then find the situation depicted in b). The light incident from the substrate is refracted at the film-substrate interface, totally reflected at the film-cover interface, refracted back into the substrate through which the light escapes from the structure. Again, there is no confinement and we talk of a "substrate radiation mode" (see Sect. 2.3). Finally (c), when θ is large enough, we have $\theta_s, \theta_c < \theta$, i.e., total internal reflection at both interfaces. The light, once it is inside, is trapped and confined in the film and propagates in a zig-zag path. This case corresponds to a guided mode of propagation which we discuss in more detail in the following.

2.1.2. Guided Modes

In Fig. 2.5 we have sketched a side view of the slab waveguide and our choice of the coordinate system. We assume that the light in the guide propagates in the z direction, that confinement occurs transversely in the x direction, and that both the structure and the light are uniform in the y direction perpendicular to xz . Our physical picture of guided light propagation is, then, that of light traveling in zig-zag fashion

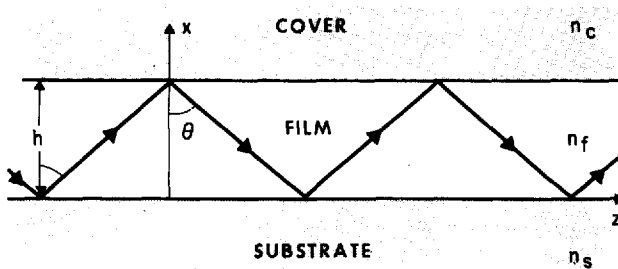


Fig. 2.5. Side-view of a slab waveguide showing wave normals of the zig-zag waves corresponding to a guided mode

through the film. More precisely, it is a picture of two superimposed uniform plane waves with wavenormals which follow the zig-zag path indicated in the figure and which are totally reflected at the film boundaries. These waves are monochromatic and coherent with angular fre-

quency ω , free-space wavelength λ , and they travel with a wavevector $\mathbf{k} n_f$ in the direction of the wave normal where the absolute value of \mathbf{k} is

$$k = 2\pi/\lambda = \omega/c \quad (2.1.9)$$

and c is the velocity of light in vacuum. The fields of these waves vary as

$$\exp[-jk n_f(\pm x \cos \theta + z \sin \theta)]. \quad (2.1.10)$$

For a guided mode of the slab guide, the zig-zag picture predicts a propagation constant β (and the related phase velocity v_p)

$$\beta = \omega/v_p = k n_f \sin \theta, \quad (2.1.11)$$

which is the z -component of the wave vector $\mathbf{k} n_f$. However, not all angles θ are allowed; only a discrete set of angles (and sometimes none) lead to a self-consistent picture that corresponds to what we call the “guided modes”. To examine this in more detail, let us look at a guide cross-section $z=\text{const}$ and add up the phase shifts that occur as we move up from the lower film boundary ($x=0$) with one wave to the other boundary ($x=h$) and then back down again with the reflected wave to where we started from. For self-consistency, the sum of all these phase shifts must be a multiple of 2π . For a film of thickness h we have, specifically, a phase shift of $k n_f h \cos \theta$ for the first transverse passage through the film, a phase shift of $-2\phi_c$ on total reflection from the film-cover interface, another $k n_f h \cos \theta$ on the transverse passage down, and a phase shift of $-2\phi_s$ on total reflection from the film-substrate boundary. Thus, we have the self-consistency condition (also known as the “transverse resonance condition”)

$$2k n_f h \cos \theta - 2\phi_s - 2\phi_c = 2v\pi, \quad (2.1.12)$$

where v is an integer ($0, 1, 2 \dots$) which identifies the mode number. As discussed before, the phase shifts ϕ_s and ϕ_c are functions of the angle θ as described by (2.1.7) and (2.1.8) after the appropriate substitutions for n_1 and n_2 . The above equation is essentially the dispersion equation of the guide yielding the propagation constant β as a function of frequency ω and film thickness h . From (2.1.5) and (2.1.11), we find for guided modes that β is bounded by the plane-wave propagation constants of substrate and film

$$k n_s < \beta < k n_f. \quad (2.1.13)$$

It is often convenient to use an “effective guide index” defined by

$$N = \beta/k = n_f \sin\theta, \quad (2.1.14)$$

which is bounded by

$$n_s < N < n_f. \quad (2.1.15)$$

Figure 2.6 sketches a graphical solution of the dispersion equation (2.1.12) for the fundamental mode ($v=0$) which gives us further information of the propagation characteristics of the guide. We have drawn here, as a function of the angle θ , both the phase shift on film traversal $k n_f h \cos\theta$ (dotted curve) and the sum of the phase shifts $(\phi_s + \phi_c)$ at the film boundaries. We show the latter for two cases, the symmetric guide where $\phi_c = \phi_s$ (solid curve), and the asymmetric guide (dashed curve). The figure shows the angle θ in degrees and radians (0° to 90° , π) and the phase shift ϕ in radians (0 to $\pi/2$). The intersection of the two curves determines the propagation angle θ .

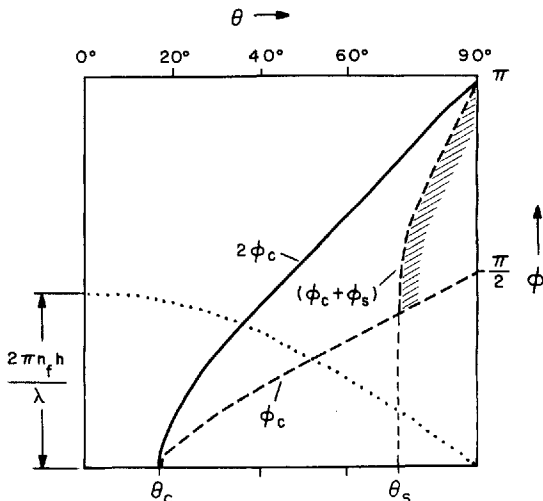


Fig. 2.6. Sketch of graphical solution of the dispersion equation for the fundamental modes of symmetric and asymmetric slab waveguides

curve). Consider the symmetric guide first, where the intersection between the solid and the dotted curve yields the zig-zag angle θ of the fundamental mode. We note that the zig-zags get steeper (θ smaller) as h/λ gets smaller, but there is always a solution even when the film thickness gets very small. This implies that there is no cutoff for the fundamental mode of a symmetric guide. Of course, as the guide gets

thicker, it supports more and more guided modes. Considering the asymmetric guide, we look for an intersection between the dotted and the dashed curve. However, only the portion of the $(\phi_s + \phi_c)$ curve emphasized by shading is above the critical angle θ_s of the film-substrate interface. For sufficiently thin films, we do not get an intersection of the curves above cut-off, which implies that an asymmetric guide cannot always support a guided mode, i.e., there is a cut-off condition even for the fundamental.

Figure 2.7 shows a sketch of an ω - β diagram that restates some of the above discussed dispersion characteristics, which are typical for a dielectric waveguide. The first three guided modes ($v=0, 1, 2$) are shown. At the cut-off frequency, the propagation constants assume the value of the lower bound $n_s k$, and as ω (or the thickness h) increases, β approaches its upper bound $n_f k$ and more and more guided modes exist. In addition to the discrete spectrum of the guided modes, the diagram also shows the continuous spectrum of the radiation modes.

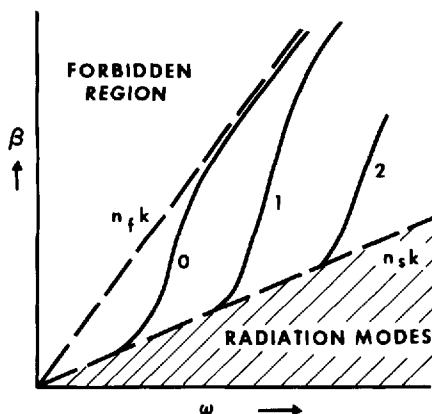


Fig. 2.7. Typical ω - β diagram of a dielectric waveguide

To obtain a more precise ω - β diagram for the asymmetric slab guide, we have to evaluate (2.1.12) numerically. To make the results of such a numerical evaluation more broadly applicable, we introduce normalizations that combine several guide parameters. First, we define a normalized frequency and film thickness V by

$$V = k h \sqrt{n_f^2 - n_s^2}, \quad (2.1.16)$$

and then a normalized guide index b related to the effective index N (and β) by

$$b = (N^2 - n_s^2)/(n_f^2 - n_s^2). \quad (2.1.17)$$

The index b is zero at cut-off and approaches unity far away from it. For small index differences ($n_f - n_s$) we have the simple linear relation

$$N \approx n_s + b(n_f - n_s). \quad (2.1.18)$$

Finally, we introduce a measure for the asymmetry of the waveguide structure defined by

$$a = (n_s^2 - n_c^2)/(n_f^2 - n_s^2). \quad (2.1.19)$$

This measure applies to the TE-modes and ranges in value from zero for perfect symmetry ($n_s = n_c$) to infinity for strong asymmetry ($n_s \neq n_c$ and $n_s \approx n_f$). As an illustration, Table 2.2 lists this asymmetry measure under a_E together with the refractive indices of three waveguide structures of practical interest.

Table 2.2. Asymmetry measures for the TE modes (a_E) and the TM modes (a_M) of slab waveguides

Waveguide	n_s	n_f	n_c	a_E	a_M
GaAlAs, double heterostructure	3.55	3.6	3.55	0	0
Sputtered glass	1.515	1.62	1	3.9	27.1
Ti-diffused LiNbO ₃	2.214	2.234	1	43.9	1093
Outdiffused LiNbO ₃	2.214	2.215	1	881	21,206

For the TE modes, we use (2.1.7) together with the above normalizations to write the dispersion relation (2.1.12) in the form

$$V\sqrt{1-b} = v\pi + \tan^{-1}\sqrt{b/(1-b)} + \tan^{-1}\sqrt{(b+a)/(1-b)}. \quad (2.1.20)$$

A numerical evaluation of (2.1.20) yields the normalized ω - β -diagram shown in Fig. 2.8 which is taken from KOGELNIK and RAMASWAMY [2.13] and where the guide index b is plotted as a function of the normalized frequency V for four different values of the asymmetry measure and for the mode orders $v=0, 1$ and 2 .

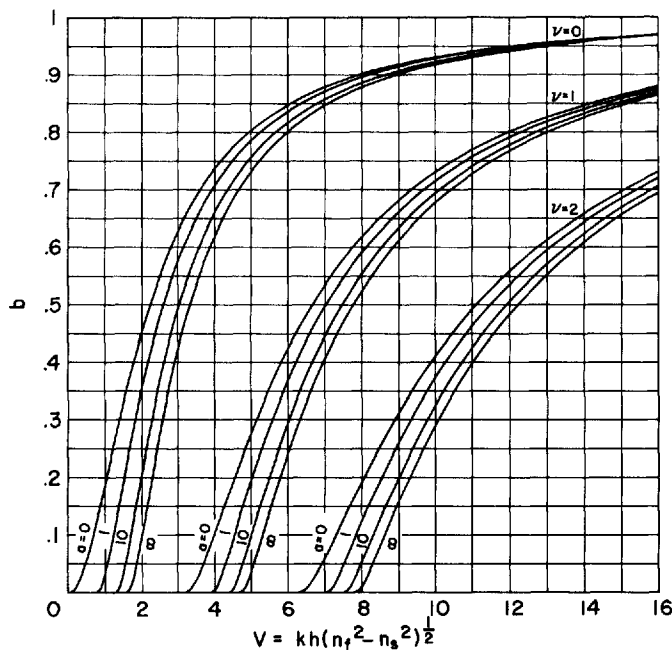


Fig. 2.8. Normalized ω - β diagram of a planar slab waveguide showing the guide index β as a function of the normalized thickness V for various degrees of asymmetry (after [2.13])

Setting $b=v=0$ in the dispersion relation (2.1.20), we determine the cutoff frequency V_0 of the fundamental mode as

$$V_0 = \tan^{-1} \sqrt{a}. \quad (2.1.21)$$

This can also be written in the form

$$(h/\lambda)_0 = \frac{1}{2\pi} (n_f^2 - n_s^2)^{-1/2} \tan^{-1} \sqrt{a}. \quad (2.1.22)$$

The cutoff frequency V_v of the v -th order mode is

$$V_v = V_0 + v\pi, \quad (2.1.23)$$

from which we obtain an approximate formula for the number of guided modes allowed in the waveguide, which is

$$v = \frac{2h}{\lambda} \sqrt{n_f^2 - n_s^2}. \quad (2.1.24)$$

For the TM-mode, we get cut-off conditions of the same form as for the TE-mode and $\omega-\beta$ diagrams that are very similar. In fact, when the index differences ($n_f - n_s$) are small, we can apply the diagram of Fig. 2.8 to the TM modes. However, these statements are only correct if we define the asymmetry measure in a somewhat different manner [2.13], namely, by

$$a = \frac{n_f^4}{n_c^4} \frac{n_s^2 - n_c^2}{n_f^2 - n_s^2}. \quad (2.1.25)$$

Illustrative values for this are given in Table 2.2 under a_M .

2.1.3. The Goos-Hänchen Shift

So far, we have described the light in the waveguide in terms of plane waves and their wave normals and phases. In this subsection and in the next, we consider also the energy of the light and its flow through the guide. To prepare for this, we have to be more precise about what we mean by a light ray. A light ray is defined here as the direction of the Poynting vector or the energy flow of light. Consistent with this is the view of a ray as the axis of a narrow beam of light or wave packet. The relation between wave normal and ray is essentially the spatial analog of the relation between the phase velocity and the group velocity. For the simple case of a plane wave in a homogeneous, isotropic medium the directions of the wave normal and the ray are the same, but in an anisotropic medium the ray generally points in a direction different from that of the wave normal.

The Goos-Hänchen shift that occurs on total reflection from a dielectric interface is another case where the ray behaves differently than the wave normal. Here the reflected ray (B) is shifted laterally relative to the incident ray or wave packet (A), as indicated in Fig. 2.9. This lateral ray shift has turned out to be an important element in the understanding of the flow of energy in dielectric waveguides in terms of the ray picture.

To determine the lateral ray shift, shown as $2z_s$ in Fig. 2.9, consider a simple wave packet consisting of two plane waves incident at two

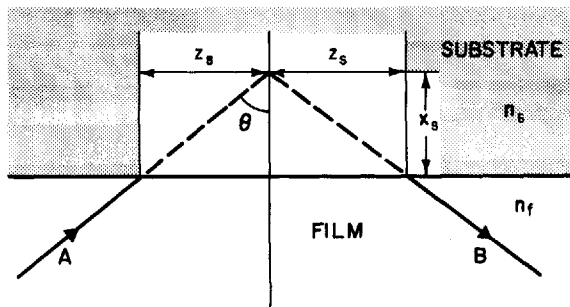


Fig. 2.9. Ray picture of total reflection at the interface between two dielectric media showing a lateral shift of the reflected ray (Goos-Hänchen shift)

slightly different angles. If the z -components of the corresponding wave vectors are $\beta \pm \Delta\beta$, we can write for the complex amplitude $A(z)$ of the incident wave packet at the interface $x=0$

$$\begin{aligned} A &= [\exp(j\Delta\beta z) + \exp(-j\Delta\beta z)] \exp(-j\beta z) \\ &= 2 \cos(\Delta\beta z) \cdot \exp(-j\beta z). \end{aligned} \quad (2.1.26)$$

Before applying the reflection laws (2.1.2) and (2.1.6) to each individual plane wave, we have to remember that the phase shift ϕ occurring on total reflection is a function of θ (and β). For small $\Delta\phi$ and $\Delta\beta$, we can use an expansion of the form

$$\phi(\beta + \Delta\beta) = \phi(\beta) + \frac{d\phi}{d\beta} \Delta\beta. \quad (2.1.27)$$

With this, we obtain for the amplitude $B(z)$ of the reflected wave packet at $x=0$

$$\begin{aligned} B &= \{\exp[j(\Delta\beta z - 2\Delta\phi)] + \exp[-j(\Delta\beta z - 2\Delta\phi)]\} \cdot \exp[-j(\beta z - 2\phi)] \\ &= \cos[\Delta\beta(z - 2z_s)] \cdot \exp[-j(\beta z - 2\phi)], \end{aligned} \quad (2.1.28)$$

where

$$z_s = d\phi/d\beta. \quad (2.1.29)$$

This gives us the lateral shift of the wave packet, i.e., of the ray, in compact and simple form [2.14, 15]. Using (2.1.11), (2.1.7) and (2.1.8), we obtain for the TE-modes

$$k z_s = (N^2 - n_s^2)^{-1/2} \cdot \tan \theta, \quad (2.1.30)$$

and for the TM-modes

$$k z_s = (N^2 - n_s^2)^{-1/2} \tan \theta / \left(\frac{N^2}{n_s^2} + \frac{N^2}{n_f^2} - 1 \right). \quad (2.1.31)$$

As sketched in Fig. 2.9, this lateral ray shift would indicate that the light penetrates to a depth x_s into the substrate before it is reflected, where

$$x_s = z_s / \tan \theta. \quad (2.1.32)$$

If we compare this result with the electromagnetic field solutions to be given in Section 2.3, we find that these predict evanescent fields in the substrate whose decay constants are closely related to this penetration depth x_s of the ray.

2.1.4. Effective Guide Thickness

To obtain a zig-zag ray model of light propagation in the waveguide that is consistent with the flow of energy, we have to incorporate the Goos-Hänchen shifts at the film-substrate and film-cover interfaces, as first suggested by BURKE [2.16]. Figure 2.10 shows a sketch of this ray

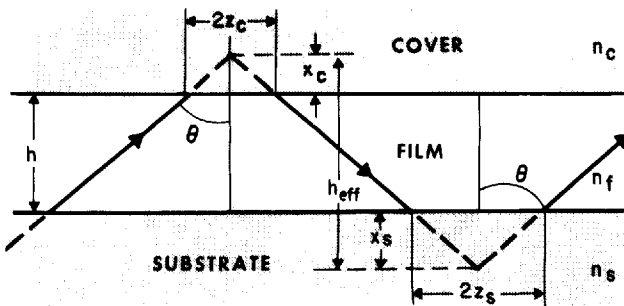


Fig. 2.10. Ray-picture of zig-zag light propagation in a slab waveguide. Goos-Hänchen shifts are incorporated in the model, and the effective guide thickness h_{eff} is indicated

model with lateral shifts $2z_s$ and $2z_c$, and ray penetration depths x_s and x_c . As a consequence of the ray penetration, the guide appears to possess an effective thickness

$$h_{\text{eff}} = h + x_s + x_c \quad (2.1.33)$$

which is larger than h . This is also indicated in the figure. We shall see in later sections that this effective thickness also turns up as a characteristic parameter in the electromagnetic theory of slab guides whenever questions of energy flow or energy exchange arise. The guided light spreads somewhat into the substrate and cover and is essentially confined to a thickness h_{eff} .

To illustrate the degree of light confinement provided by an asymmetric slab waveguide, we evaluate (2.1.33) numerically and plot the normalized effective thickness

$$H = k h_{\text{eff}} \sqrt{n_f^2 - n_s^2} \quad (2.1.34)$$

as a function of the normalized frequency V . For TE modes we have

$$H = V + 1/\sqrt{b} + 1/\sqrt{b+a}, \quad (2.1.35)$$

and the corresponding plots are shown in Fig. 2.11 for four values of the asymmetry measure. Similar plots can be obtained for the TM

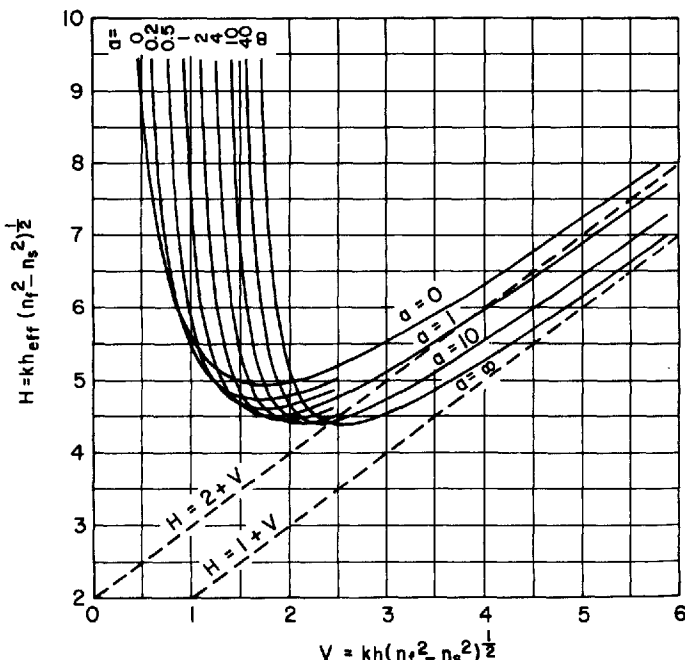


Fig. 2.11. Normalized effective thickness of a slab waveguide as a function of the normalized film thickness V for various degrees of asymmetry (after [2.13])

modes [2.13]. In Fig. 2.11, we note the occurrence of minimum values of $H(V)$, for which we obtain maximum confinement of the light. For highly asymmetric guides ($a=\infty$), for example, we have a minimum of $H_{\min}=4.4$ at $V=2.55$. This implies a minimum effective width of

$$(h_{\text{eff}}/\lambda)_{\min} = 0.7 \cdot (n_f^2 - n_s^2)^{-1/2}. \quad (2.1.36)$$

For a typical thin-film glass waveguide, we have $n_s=1.5$, $n_f=1.6$ and $(h_{\text{eff}}/\lambda)_{\min} \approx 1.3$.

2.2. Fundamentals of the Electromagnetic Theory of Dielectric Waveguides

In this section we propose to collect the, by now well developed, fundamentals of the electromagnetic theory of dielectric waveguides, and to discuss some of the general properties of the waveguide modes. This includes a listing of the relevant forms of Maxwell's equations and of the wave equations, a deduction of modal field properties following from symmetry considerations, a proof for the orthogonality of the modes, and a discussion of mode expansion and normalization, of the variation theorem, of power transport and stored energy, and of variational principles applicable to dielectric waveguides. We will keep this discussion as general as possible to allow for the variety of planar and strip waveguides considered for integrated optics applications.

2.2.1. Maxwell's Equations

Maxwell's equations for source free, time dependent fields are

$$\nabla \times \tilde{\mathbf{E}} = -\partial \tilde{\mathbf{B}} / \partial t \quad (2.2.1)$$

$$\nabla \times \tilde{\mathbf{H}} = \partial \tilde{\mathbf{D}} / \partial t, \quad (2.2.2)$$

where t is time, $\nabla=(\partial/\partial x, \partial/\partial y, \partial/\partial z)$ is the del operator, and $\tilde{\mathbf{E}}(t)$, $\tilde{\mathbf{H}}(t)$, $\tilde{\mathbf{D}}(t)$ and $\tilde{\mathbf{B}}(t)$ are the time dependent vectors of the electric and magnetic field, the electric displacement and the magnetic induction respectively. We assume fields with a periodic time dependence which we write in the form

$$\tilde{\mathbf{E}}(t) = \mathbf{E} \exp(j\omega t) + \mathbf{E}^* \exp(-j\omega t), \quad \text{etc.} \quad (2.2.3)$$

where E is a complex amplitude, ω the angular frequency, and the asterisk indicates a complex conjugate. Assuming a lossless medium with a scalar dielectric constant $\epsilon(\omega)$ and a scalar magnetic permeability μ , we have the constitutive relations

$$\mathbf{D} = \epsilon \mathbf{E}, \quad (2.2.4)$$

$$\mathbf{B} = \mu \mathbf{H}. \quad (2.2.5)$$

With this we get Maxwell's equations for the complex amplitudes of the form

$$\nabla \times \mathbf{E} = -j\omega \mu \mathbf{H}, \quad (2.2.6)$$

$$\nabla \times \mathbf{H} = j\omega \epsilon \mathbf{E}. \quad (2.2.7)$$

These equations are subject to boundary conditions at surfaces where abrupt changes of the material constants occur. Figure 2.12 shows a sketch of such a boundary between two media distinguished by the indices 1 and 2, with the unit vector e_n chosen perpendicular to the

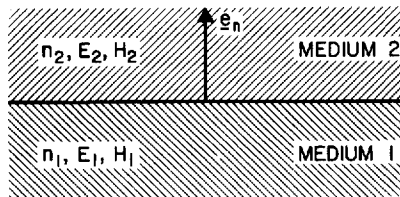


Fig. 2.12. Boundary between two media of indices n_1 and n_2 . The vector e_n is the normal to the surface

surface. In the absence of surface charges and surface currents, we have the conditions

$$\begin{aligned} e_n \cdot (\mathbf{B}_1 - \mathbf{B}_2) &= 0, & e_n \cdot (\mathbf{D}_1 - \mathbf{D}_2) &= 0 \\ e_n \times (\mathbf{E}_1 - \mathbf{E}_2) &= 0, & e_n \times (\mathbf{H}_1 - \mathbf{H}_2) &= 0. \end{aligned} \quad (2.2.8)$$

for the fields E_1, E_2 , etc., at the boundary. In dielectric waveguides we, usually, have a constant permeability $\mu = \mu_0$, which implies equality of the magnetic field vectors $H_1 = H_2$ at the boundary.

In Fig. 2.13 we have sketched a typical waveguide geometry, and indicated the choice of our coordinate system with the guide axis

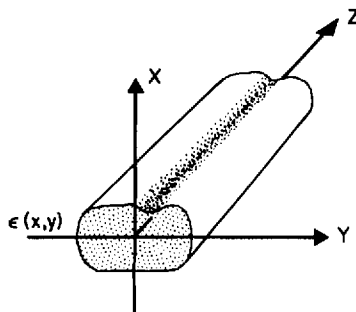


Fig. 2.13. Sketch of a dielectric waveguide and the choice of the coordinate system. The guide axis is chosen to coincide with the z -axis

pointing in the z -direction. Relative to this geometry, we distinguish between the longitudinal field components E_z and H_z , and the transverse field components E_t and H_t ,

$$\mathbf{E} = \mathbf{E}_t + \mathbf{E}_z, \quad \mathbf{H} = \mathbf{H}_t + \mathbf{H}_z. \quad (2.2.9)$$

To separate these components, we write Maxwell's equations in the form

$$\nabla_t \times \mathbf{E}_t = -j\omega\mu\mathbf{H}_z; \quad \nabla_t \times \mathbf{H}_t = j\omega\epsilon\mathbf{E}_z, \quad (2.2.10)$$

$$\nabla_t \times \mathbf{E}_z + \mathbf{e}_z \times \partial \mathbf{E}_t / \partial z = -j\omega\mu\mathbf{H}_t, \quad (2.2.11)$$

$$\nabla_t \times \mathbf{H}_z + \mathbf{e}_z \times \partial \mathbf{H}_t / \partial z = j\omega\epsilon\mathbf{E}_t, \quad (2.2.12)$$

where

$$\nabla_t = (\partial/\partial x, \partial/\partial y, 0) \quad (2.2.13)$$

is the transverse del operator and \mathbf{e}_z is a unit vector pointing in the z -direction. In dealing with waveguide problems, one usually focuses on the transverse components. Once these are known, one can determine the z -components via (2.2.10).

2.2.2. Modes of the Waveguide

As indicated in Fig. 2.13, a dielectric waveguide is characterized by a dielectric constant

$$\epsilon = \epsilon_0 n^2(x, y) \quad (2.2.14)$$

which is independent of the z coordinate. The function $n(x, y)$ is known as the refractive index profile and generally assumes its highest values near the axis. A mode of the waveguide is defined as a field solution of the form

$$\mathbf{E}(x, y, z) = \mathbf{E}_v(x, y) \exp(-j\beta_v z), \quad \mathbf{H}(x, y, z) = \mathbf{H}_v(x, y) \exp(-j\beta_v z), \quad (2.2.15)$$

where v is a mode label (indicating the mode number for example), and β_v is the propagation constant of the mode. For guides providing confinement in two dimensions, such as strip guides or fibers, we need, of course, two labels, but only one is shown here for simplicity. Inserting the modal fields of (2.2.15) into Maxwell's equations (2.2.10–12), we obtain

$$\nabla_t \times \mathbf{E}_{tv} = -j\omega\mu \mathbf{H}_{zv}, \quad \nabla_t \times \mathbf{H}_{tv} = j\omega\varepsilon \mathbf{E}_{zv}, \quad (2.2.16)$$

$$\nabla_t \times \mathbf{E}_{zv} - j\beta_v \mathbf{e}_z \times \mathbf{E}_{tv} = -j\omega\mu \mathbf{H}_{tv}, \quad (2.2.17)$$

$$\nabla_t \times \mathbf{H}_{zv} - j\beta_v \mathbf{e}_z \times \mathbf{H}_{tv} = j\omega\varepsilon \mathbf{E}_{tv}. \quad (2.2.18)$$

The general nature of the solutions to these equations was discussed in detail by MCKENNA [2.17] and in the textbooks of MARCUSE [2.18], KAPANY and BURKE [2.1], and MARCUSE [2.2]. One encounters a situation which is analogous to that encountered in quantum mechanics where one seeks solutions to Schrödinger's equation for various potential distributions and finds two types of solutions, one corresponding to bound states and the other to unbound states. For dielectric waveguides, we find guided modes (bound states) where the energy is confined near the axis, and radiation modes (unbound states) with their energy spread out through the medium surrounding the guide. The guided modes are associated with a discrete spectrum of propagation constants β_v , while the radiation modes belong to a continuum. One also finds evanescent modes with imaginary propagation constants $\beta_v = -j\alpha_v$, and which decay as $\exp(-\alpha_v z)$. Solutions for specific waveguide examples are given in Sections 2.3 and 2.4.

2.2.3. The Wave Equations for Planar Guides

In planar guides, the light is confined in one dimension only, which we choose to be in the x -direction. The refractive index $n(x)$ of a planar guide and the corresponding modal fields are functions of only this coordinate. One can, then, simplify the modal differential equations

(2.2.16–18) by setting $\partial/\partial y=0$. A planar guide supports transverse electric (TE) modes with zero longitudinal electric field ($E_z=0$) and transverse magnetic modes (TM) with zero longitudinal magnetic field ($H_z=0$). In the following, we derive the wave equations governing the two mode types, omitting the mode label v to simplify the notation.

For TE-modes we set $H_y=0$ and get $E_z=0$ from the second of (2.2.16). Eq. (2.2.17) yields $E_x=0$ and

$$\beta E_y = -\omega \mu H_x. \quad (2.2.19)$$

Next we obtain

$$\partial E_y/\partial x = -j\omega \mu H_z \quad (2.2.20)$$

from the first of (2.2.16), and

$$\partial H_z/\partial x + j\beta H_x = -j\omega \epsilon E_y \quad (2.2.21)$$

from (2.2.18). Combining the last three equations, we arrive at a wave equation for E_y

$$\partial^2 E_y/\partial x^2 = (\beta^2 - n^2 k^2) E_y, \quad (2.2.22)$$

where

$$k = \omega/c = \omega/\sqrt{\epsilon_0 \mu_0} \quad (2.2.23)$$

is the propagation constant of free space.

For TM-modes, we start by setting $E_y=0$ and obtain in a similar fashion $H_z=0$, $H_x=0$,

$$\beta H_y = \omega \epsilon E_x, \quad (2.2.24)$$

$$\partial H_y/\partial x = j\omega \epsilon E_z, \quad (2.2.25)$$

$$\partial E_z/\partial x + j\beta E_x = j\omega \mu H_y, \quad (2.2.26)$$

and a wave equation for H_y of the form

$$n^2 \frac{\partial}{\partial x} \left(\frac{1}{n^2} \partial H_y/\partial x \right) = (\beta^2 - n^2 k^2) H_y. \quad (2.2.27)$$

2.2.4. Mode Properties Following from Symmetry

Several phase relationships between the modal field components follow directly from the symmetry of both the waveguide and of Maxwell's equations. We shall use both time-reversal and z -reversal to construct new solutions $\tilde{\mathbf{E}}_2(\mathbf{r}, t)$, $\tilde{\mathbf{H}}_2(\mathbf{r}, t)$ from known solutions $\tilde{\mathbf{E}}_1(\mathbf{r}, t)$, $\tilde{\mathbf{H}}_1(\mathbf{r}, t)$.

As is well known, one can reverse the sign of t in Maxwell's equations to construct a new solution of the form

$$\tilde{\mathbf{E}}_2(\mathbf{r}, t) = \tilde{\mathbf{E}}_1(\mathbf{r}, -t); \quad \tilde{\mathbf{H}}_2(\mathbf{r}, t) = -\tilde{\mathbf{H}}_1(\mathbf{r}, -t). \quad (2.2.28)$$

In terms of the complex amplitudes, this can be written as

$$\mathbf{E}_2(\mathbf{r}) = \mathbf{E}_1^*(\mathbf{r}); \quad \mathbf{H}_2(\mathbf{r}) = -\mathbf{H}_1^*(\mathbf{r}). \quad (2.2.29)$$

Next, we consider z -reversal and assume that

$$\varepsilon(x, y, -z) = \varepsilon(x, y, z), \quad (2.2.30)$$

which is true for all isotropic dielectric waveguides. By reversing the sign of z in Maxwell's equations (2.2.10–12), we can construct new solutions of the form

$$\mathbf{E}_{12}(z) = \mathbf{E}_{11}(-z), \quad \mathbf{E}_{z2}(z) = -\mathbf{E}_{z1}(-z); \quad (2.2.31)$$

$$\mathbf{H}_{12}(z) = -\mathbf{H}_{11}(-z), \quad \mathbf{H}_{z2}(z) = \mathbf{H}_{z1}(-z). \quad (2.2.32)$$

where we have omitted to indicate the (x, y) dependence in order to emphasize the z -reversal operation.

In applying these reversal operations to the modal fields of the form of (2.2.15) we have to distinguish between the propagating modes with real valued β , and the evanescent modes with imaginary β . In the first case, a forward traveling mode will vary as $\exp(-j\beta z)$ and either time reversal or z -reversal yield a backward traveling mode varying as $\exp(j\beta z)$. As the new solution must be unique, the application of (2.2.29), as well as (2.2.31) and (2.2.32) must yield the same result. This requires that

$$\mathbf{E}_{tv} = \mathbf{E}_{tv}^*, \quad \mathbf{H}_{tv} = \mathbf{H}_{tv}^*, \quad (2.2.33)$$

$$\mathbf{E}_{zv}^* = -\mathbf{E}_{zv}, \quad \mathbf{H}_{zv}^* = -\mathbf{H}_{zv}. \quad (2.2.34)$$

We have constructed modal \mathbf{E} and \mathbf{H} fields with real valued transverse components and imaginary z -components. The general implications for

a propagating mode are that the tangential components of its \mathbf{E}' and \mathbf{H} fields are in phase, that their z -components are also in phase, and that the tangential and z -components are 90° out of phase.

The fields of a forward evanescent mode vary as $\exp(-\alpha z)$. Here the time reversal operation produces again a forward wave. Uniqueness requires that these two waves be identical; and because of (2.2.29), this requires that

$$\mathbf{E}_v = \mathbf{E}_v^*, \quad \mathbf{H}_v = -\mathbf{H}_v^*. \quad (2.2.35)$$

We have constructed an evanescent mode with a real valued electric field and an imaginary magnetic field. In general, \mathbf{E}_v and \mathbf{H}_v of an evanescent mode are 90° out of phase.

2.2.5. Orthogonality of the Modes

All modes of a dielectric waveguide are orthogonal to each other [2.18, 19]. This important property holds for both the guided and the radiation modes; it is the basis for much of waveguide theory, including the theories of waveguide excitation, of waveguide discontinuities and waveguide perturbations. We will sketch here a derivation of the orthogonality relations which makes apparent their connection with power conservation and reciprocity.

We start with the complex Maxwell's equation (2.2.6) and (2.2.7) for a lossless, scalar medium and consider two different solutions labeled 1 and 2. We form the dot products of \mathbf{H}_2^* with (2.2.6) and of \mathbf{E}_1 with the complex conjugate of (2.2.7), subtract the results and obtain

$$\nabla \cdot (\mathbf{E}_1 \times \mathbf{H}_2^*) = j\omega(\epsilon \mathbf{E}_1 \cdot \mathbf{E}_2^* - \mu \mathbf{H}_1 \cdot \mathbf{H}_2^*), \quad (2.2.36)$$

where we have used the vector identity

$$\nabla \cdot (\mathbf{a} \times \mathbf{b}) = \mathbf{b} \cdot (\nabla \times \mathbf{a}) - \mathbf{a} \cdot (\nabla \times \mathbf{b}). \quad (2.2.37)$$

Note that (2.2.36) becomes the complex Poynting theorem if we make the labels 1 and 2 equal. Now we exchange the labels 1 and 2 in (2.2.36), take the complex conjugate and add the result to (2.2.36) to obtain

$$\nabla \cdot (\mathbf{E}_1 \times \mathbf{H}_2^* + \mathbf{E}_2^* \times \mathbf{H}_1) = 0. \quad (2.2.38)$$

This theorem is closely related to the Lorentz reciprocity theorem; in fact, we obtain a form of the latter if we replace field 2 in (2.2.38) by its corresponding time reversed field using (2.2.29) with the resulting

$$\nabla \cdot (\mathbf{E}_1 \times \mathbf{H}_2 - \mathbf{E}_2 \times \mathbf{H}_1) = 0. \quad (2.2.39)$$

We proceed by applying the theorem of (2.2.38) to waveguide modes and identify the fields 1 and 2 with two forward modes

$$\mathbf{E}_1 = \mathbf{E}_v(x, y) \exp(-j\beta_v z), \quad \mathbf{E}_2 = \mathbf{E}_\mu(x, y) \exp(-j\beta_\mu z), \quad (2.2.40)$$

which yields

$$\nabla_t \cdot (\mathbf{E}_v \times \mathbf{H}_\mu^* + \mathbf{E}_\mu^* \times \mathbf{H}_v)_t - j(\beta_v - \beta_\mu)(\mathbf{E}_{tv} \times \mathbf{H}_{t\mu}^* + \mathbf{E}_{t\mu}^* \times \mathbf{H}_{tv})_z = 0. \quad (2.2.41)$$

Here we have, again, separated the transverse (t) and the longitudinal (z) components and used the transverse del operator ∇_t . The next step is to integrate (2.2.41) over a cross-section $z = \text{const}$ of the waveguide. Applying the divergence theorem to the first term we get

$$\int_{-\infty}^{+\infty} dx dy \nabla_t \cdot \mathbf{g} = \oint_C ds \mathbf{g} \cdot \mathbf{e}_t \quad (2.2.42)$$

where

$$\mathbf{g} = (\mathbf{E}_v \times \mathbf{H}_\mu^* + \mathbf{E}_\mu^* \times \mathbf{H}_v)_t, \quad (2.2.43)$$

and the line integral extends over an infinitely large curve enclosing the waveguide, with \mathbf{e}_t being a unit vector perpendicular to that curve. It is easy to see that this line integral vanishes if at least one of the two modes is a guided mode with fields decaying exponentially towards infinity. The line integral also vanishes when both modes are radiation modes; the argument to show this is somewhat more complicated and involves the oscillatory nature of the radiation modes [2.18].

The terms remaining after integration are

$$\int_{-\infty}^{+\infty} dx dy (\mathbf{E}_{tv} \times \mathbf{H}_{t\mu}^* + \mathbf{E}_{t\mu}^* \times \mathbf{H}_{tv}) = 0, \quad \beta_v \neq \beta_\mu \quad (2.2.44)$$

where we have dropped the factor $(\beta_\mu - \beta_v)$ as we assume that $\beta_v \neq \beta_\mu$. The z -reversal symmetry allows a further simplification. In order to achieve this, we apply (2.2.44) to a backward traveling mode (labeled $-v$) instead of the corresponding forward mode (labeled v). According to

(2.2.31) and (2.2.32), the fields of the backward traveling mode are given by

$$\mathbf{E}_{t,-v}(x,y) = \mathbf{E}_{t,v}(x,y) \quad (2.2.45)$$

$$\mathbf{H}_{t,-v}(x,y) = -\mathbf{H}_{t,v}(x,y). \quad (2.2.46)$$

With this (2.2.44) becomes

$$\int_{-\infty}^{+\infty} dx dy (\mathbf{E}_{tv} \times \mathbf{H}_{t\mu}^* - \mathbf{E}_{t\mu}^* \times \mathbf{H}_{tv}) = 0, \quad \beta_\mu \neq \beta_v. \quad (2.2.47)$$

Adding the two results yields the simple orthogonality relation

$$\int_{-\infty}^{+\infty} dx dy \mathbf{E}_{tv} \times \mathbf{H}_{t\mu}^* = 0, \quad \beta_\mu \neq \beta_v. \quad (2.2.48)$$

2.2.6. Mode Expansion and Normalization

The orthogonality of the modes allows us to express an arbitrary given field distribution as a superposition of waveguide modes. Doing this, we shall only deal with the transverse field components; the z -components follow from Maxwell's equations, i.e., (2.2.16). To simplify the notation for this subsection, we shall leave out the label t and designate the transverse fields of the forward modes as $\mathbf{E}_{v\mu}(x,y)$ and $\mathbf{H}_{v\mu}(x,y)$.

Assume, first, that only forward propagating modes are present in a given field with the transverse components $\mathbf{E}_t(x,y)$ and $\mathbf{H}_t(x,y)$ in a guide cross-section $z=\text{const}$. This can be represented as a superposition of waveguide modes of the form

$$\mathbf{E}_t(x,y) = \sum_{v\mu} a_{v\mu} \mathbf{E}_{v\mu}(x,y) + \int_0^\infty dv d\mu a(v,\mu) \mathbf{E}(v,\mu; x,y) \quad (2.2.49)$$

$$\mathbf{H}_t(x,y) = \sum_{v\mu} a_{v\mu} \mathbf{H}_{v\mu}(x,y) + \int_0^\infty dv d\mu a(v,\mu) \mathbf{H}(v,\mu; x,y). \quad (2.2.50)$$

The summation here extends over the discrete and finite set of guided modes and the integration extends over the continuous spectrum of radiation modes. The discrete spectra in the above expressions are similar to those encountered in hollow metal waveguides and the continuous spectrum is similar to the angular spectrum of plane waves of a field in free space. It is thus natural to call the continuous labels v and μ "spatial frequencies" and to assign to them the dimension [cm^{-1}].

In order to preserve the same dimensionality for the field distributions of both the guided and of the radiation modes, we have to keep the discrete coefficients $a_{v\mu}$ dimensionless and assign the dimension [cm²] to the coefficients $a(v, \mu)$ of the continuum. It is advantageous to use only positive spatial frequencies; their lower limit, written as 0 in the above equations, actually depends on the particular choice of the labels v and μ .

In (2.2.49) and (2.2.50), we have not explicitly indicated the necessary summation over modes of different polarization (e.g., TE and TM modes) and over degenerate modes with the same spatial frequency (e.g., the even and odd radiation modes to be discussed in Sect. 2.3).

It is convenient to normalize the modal fields by means of the cross power $\bar{P}(v, \bar{v}, \mu, \bar{\mu})$ such that

$$\bar{P} = 2 \int_{-\infty}^{+\infty} dx dy \mathbf{E}_{v\mu} \times \mathbf{H}_{\bar{v}\bar{\mu}}^* = \delta_{v\bar{v}} \delta_{\mu\bar{\mu}} \quad (2.2.51)$$

for discrete modes, where $\delta_{v\bar{v}}$ is the Kronecker delta, and

$$\bar{P} = 2 \int_{-\infty}^{+\infty} dx dy \mathbf{E}(v, \mu) \times \mathbf{H}^*(\bar{v}, \bar{\mu}) = \delta(v - \bar{v}) \delta(\mu - \bar{\mu}) \quad (2.2.52)$$

for continuous modes, where $\delta(v - \bar{v})$ is the delta function. These normalizations express, of course, also the orthogonality demanded by (2.2.48).

When the modes are not normalized, the cross-power \bar{P} of the continuous modes is given by

$$\bar{P}(v, \bar{v}, \mu, \bar{\mu}) = p_{v\mu} \delta(v - \bar{v}) \delta(\mu - \bar{\mu}). \quad (2.2.53)$$

We mention this specifically to make a point about the dimension of the factor $p_{v\mu}$. \bar{P} is measured in Watts; because v and μ are measured in cm⁻¹, the dimension of the delta functions $\delta(v)$ and $\delta(\mu)$ is [cm]. The factor $p_{v\mu}$ is, therefore, measured in Watts/cm². A normalization as in (2.2.52) means that we have set $p_{v\mu}$ equal to 1 Watt/cm². For simplicity, we have not indicated this dimension in (2.2.52), but it should always be remembered when this relation is used below.

The orthonormality relations of (2.2.51) and (2.2.52) allow us to determine the coefficients of the mode expansion in a simple manner. We have

$$a_{v\mu} = 2 \int_{-\infty}^{+\infty} dx dy \mathbf{E}_t \times \mathbf{H}_{v\mu}^* = 2 \int_{-\infty}^{+\infty} dx dy \mathbf{E}_{v\mu}^* \times \mathbf{H}_t, \quad (2.2.54)$$

$$a(v, \mu) = 2 \int_{-\infty}^{+\infty} dx dy \mathbf{E}_t \times \mathbf{H}^*(v, \mu) = 2 \int_{-\infty}^{+\infty} dx dy \mathbf{E}^*(v, \mu) \times \mathbf{H}_t. \quad (2.2.55)$$

The orthonormality relations also permit us to express the power carried by the total field in terms of the expansion coefficients. We obtain

$$P = \int_{-\infty}^{+\infty} dx dy (\mathbf{E}_t \times \mathbf{H}_t^* + \mathbf{E}_t^* \times \mathbf{H}_t)_z = \sum_{v\mu} \sum_{v\mu} a_{v\mu} a_{v\mu}^* + \int_0^{\infty} dv d\mu a(v, \mu) a^*(v, \mu), \quad (2.2.56)$$

where P is measured in Watts. We identify $a_{v\mu} a_{v\mu}^*$ as the power carried by a discrete mode, and $a(v, \mu) a^*(v, \mu)$ as a spectral power density, which implies that a power $a(v, \mu) a^*(v, \mu) \Delta v \Delta \mu$ is carried in the spatial frequency band $\Delta v \Delta \mu$ of the continuous mode spectrum.

In the above discussion, we have noted a formal analogy between the discrete and the continuous modes. In the following, we shall take advantage of this to simplify our notation by writing a_v for $a_{v\mu}$ and $a(v, \mu)$, \mathbf{E}_v for $\mathbf{E}_{v\mu}$ and $E(v, \mu)$, etc., and by writing

$$\sum \text{ for } \sum_{v\mu} + \int \int dv d\mu. \quad (2.2.57)$$

Using this notation, we propose to discuss now the mode expansion of a field which contains forward and backward propagating modes (real β). Subsequently, we will consider evanescent modes. In (2.2.45) and (2.2.46), we have indicated that a backward mode has the same transverse E field distribution as the corresponding forward mode and a transverse H distribution with reversed sign. Because of this, the mode expansion has the form

$$\mathbf{E}_t = \sum (a_v + b_v) \mathbf{E}_v, \quad (2.2.58)$$

$$\mathbf{H}_t = \sum (a_v - b_v) \mathbf{H}_v, \quad (2.2.59)$$

where a_v are the coefficients of the forward waves and b_v are the coefficients of the backward waves. With the help of the orthonormality relations we determine the coefficients as

$$a_v = \int_{-\infty}^{+\infty} dx dy (\mathbf{E}_t \times \mathbf{H}_v^* + \mathbf{E}_v^* \times \mathbf{H}_t), \quad (2.2.60)$$

$$b_v = \int_{-\infty}^{+\infty} dx dy (\mathbf{E}_t \times \mathbf{H}_v^* - \mathbf{E}_v^* \times \mathbf{H}_t). \quad (2.2.61)$$

The power carried by the total field becomes

$$P = \sum (a_v a_v^* - b_v b_v^*), \quad (2.2.62)$$

as expected.

Let us now consider evanescent modes which have imaginary propagation constants. As none of these modes can carry power by itself, we obtain cross power products which are imaginary, and we have to change the orthonormality relation to

$$\bar{P} = 2 \int_{-\infty}^{+\infty} dx dy \mathbf{E}(v, \mu) \times \mathbf{H}^*(\bar{v}, \bar{\mu}) = \pm j \delta(v - \bar{v}) \delta(\mu - \bar{\mu}), \quad (2.2.63)$$

where the occurrence of the + or - sign depends on the particular guide configuration and its mode solutions. Keeping the mode expansion in the form of (2.2.58) and (2.2.59), we obtain for the coefficients of the evanescent modes

$$\pm j a_v = \int_{-\infty}^{+\infty} dx dy (\mathbf{E}_v \times \mathbf{H}_v^* - \mathbf{E}_v^* \times \mathbf{H}_v), \quad (2.2.64)$$

$$\pm j b_v = \int_{-\infty}^{+\infty} dx dy (\mathbf{E}_v \times \mathbf{H}_v^* + \mathbf{E}_v^* \times \mathbf{H}_v). \quad (2.2.65)$$

For the power carried by the field, we get the formula

$$P = \pm j \sum (a_v^* b_v - a_v b_v^*), \quad (2.2.66)$$

which reflects the fact that an evanescent wave cannot carry power by itself, but a combination of forward and backward evanescent waves can lead to tunneling of power through a short region.

2.2.7. The Variation Theorem for Dielectric Waveguides

The variation theorem [2.20] connects the variations $\delta \mathbf{E}$ and $\delta \mathbf{H}$ of the electromagnetic field solutions to the perturbations $\delta(\omega \epsilon)$ and $\delta(\omega \mu)$ of the frequency and of the constants of the medium which are the cause of these variations. The theorem follows directly from the complex Maxwell's equations (2.2.6) and (2.2.7) and can be written in the general form

$$\nabla \cdot (\mathbf{E}^* \times \delta \mathbf{H} + \delta \mathbf{E} \times \mathbf{H}^*) = -j [\delta(\omega \epsilon) \mathbf{E} \cdot \mathbf{E}^* + \delta(\omega \mu) \mathbf{H} \cdot \mathbf{H}^*]. \quad (2.2.67)$$

To apply this theorem to dielectric waveguides [2.21], we consider a waveguide mode with the fields

$$\mathbf{E} = \mathbf{E}_v \exp(-j\beta_v z), \quad \mathbf{H} = \mathbf{H}_v \exp(-j\beta_v z) \quad (2.2.68)$$

and express their variations in the form

$$\delta\mathbf{E} = (\delta\mathbf{E}_v - jz\delta\beta_v \cdot \mathbf{E}_v) \exp(-j\beta_v z), \quad (2.2.69)$$

and similarly for $\delta\mathbf{H}$. If we insert this in the above theorem, we obtain the relation

$$\nabla_t \cdot \mathbf{g} - j\delta\beta_v \cdot \mathbf{S}_z = -j[\delta(\omega\varepsilon)\mathbf{E}_v \cdot \mathbf{E}_v^* + \delta(\omega\mu)\mathbf{H}_v \cdot \mathbf{H}_v^*], \quad (2.2.70)$$

where ∇_t is the transverse del operator,

$$\mathbf{S} = \mathbf{E}_v \times \mathbf{H}_v^* + \mathbf{E}_v^* \times \mathbf{H}_v \quad (2.2.71)$$

is the time averaged Poynting vector, and

$$\mathbf{g} = \mathbf{E}_v^* \times \delta\mathbf{H}_v + \delta\mathbf{E}_v \times \mathbf{H}_v^* - j\delta\beta_v \cdot z\mathbf{S}. \quad (2.2.72)$$

We proceed by integrating (2.2.70) over the cross-section of the guide. As in the derivation of the orthogonality relation in Subsection 2.2.5, we find that the integral over $\nabla_t \cdot \mathbf{g}$ vanishes and obtain

$$\delta\beta_v \cdot \mathbf{P} = \int_{-\infty}^{+\infty} dx dy [\delta(\omega\varepsilon)\mathbf{E}_v \cdot \mathbf{E}_v^* + \delta(\omega\mu)\mathbf{H}_v \cdot \mathbf{H}_v^*], \quad (2.2.73)$$

where

$$\mathbf{P} = \int_{-\infty}^{+\infty} dx dy S_z \quad (2.2.74)$$

is the power carried by the mode. This is the variation theorem for dielectric waveguides. One of the applications of this theorem is the determination of the change $\Delta\beta$ of the propagation constant due to a perturbation $\Delta\varepsilon(x,y)$ of the dielectric constant of the waveguide. Here we have $\delta\omega=0$ and $\delta\mu=0$ and the theorem yields

$$\Delta\beta \cdot \mathbf{P} = \omega \int_{-\infty}^{+\infty} dx dy \Delta\varepsilon \mathbf{E}_v \cdot \mathbf{E}_v^*. \quad (2.2.75)$$

2.2.8. Power Flow and Stored Energy in a Dielectric Waveguide

In this subsection we give a brief discussion of the power flow carried and the energy stored by the fields of a waveguide mode. A more detailed discussion which also explores connections to the zig-zag wave model is given in [2.21].

We have already encountered in earlier sections the time averaged Poynting vector associated with a mode, which is defined by

$$\mathbf{S}(x, y) = \mathbf{E}_v \times \mathbf{H}_v^* + \mathbf{E}_v^* \times \mathbf{H}_v, \quad (2.2.76)$$

and the time averaged power transported by the mode

$$P = \int_{-\infty}^{+\infty} dx dy S_z. \quad (2.2.77)$$

The time average density of the energy stored by the modal fields is given by

$$w(x, y) = \frac{d(\omega \epsilon)}{d\omega} \mathbf{E}_v \cdot \mathbf{E}_v^* + \frac{d(\omega \mu)}{d\omega} \mathbf{H}_v \cdot \mathbf{H}_v^*, \quad (2.2.78)$$

which is written here in a form that allows for dispersive medium constants $\epsilon(\omega)$ and $\mu(\omega)$ [2.22]. The energy W stored per unit guide length is obtained by integrating w over the guide cross section

$$W = \int_{-\infty}^{+\infty} dx dy w(x, y). \quad (2.2.79)$$

The group velocity v_g of the mode is the velocity at which signals carried by the mode propagate. It is determined from the dispersion relation $\omega(\beta)$ of the guide by

$$v_g = d\omega/d\beta. \quad (2.2.80)$$

Applying the variation theorem (2.2.73) to cases where all variations are caused by perturbations in ω alone, we deduce the simple relation

$$P = (d\omega/d\beta) W = v_g W, \quad (2.2.81)$$

which is known to hold for many other waveguide structures.

For the remainder of this subsection, we assume dispersion-free media and distinguish between the electric and magnetic energy (via superscripts ε and μ) and define

$$W_t^\varepsilon = \int_{-\infty}^{+\infty} dx dy \varepsilon \mathbf{E}_t \cdot \mathbf{E}_t^*, \quad W_z^\varepsilon = \int_{-\infty}^{+\infty} dx dy \varepsilon E_z \cdot E_z^*; \quad (2.2.82)$$

$$W_t^\mu = \int_{-\infty}^{+\infty} dx dy \mu \mathbf{H}_t \cdot \mathbf{H}_t^*, \quad W_z^\mu = \int_{-\infty}^{+\infty} dx dy \mu H_z \cdot H_z^*. \quad (2.2.83)$$

Here we have also distinguished between the energy portions stored by the transverse (t) and longitudinal (z) field components, and have left out the mode label v to simplify the notation. Forming dot products of the modal differential equations (2.2.16), (2.2.17) and (2.2.18) with the appropriate field components and combining the results one obtains

$$\nabla_t \cdot \mathbf{E}_z \times \mathbf{H}_t^* - j\beta \mathbf{e}_z \cdot \mathbf{E}_t \times \mathbf{H}_t^* = j\omega \varepsilon \mathbf{E}_z \cdot \mathbf{E}_z^* - j\omega \mu \mathbf{H}_t \cdot \mathbf{H}_t^*, \quad (2.2.84)$$

$$\nabla_t \cdot \mathbf{E}_t \times \mathbf{H}_z^* + j\beta \mathbf{e}_z \cdot \mathbf{E}_t \times \mathbf{H}_t^* = j\omega \varepsilon \mathbf{E}_t \cdot \mathbf{E}_t^* - j\omega \mu \mathbf{H}_z \cdot \mathbf{H}_z^*. \quad (2.2.85)$$

When we integrate this over the guide cross-section, we find, as in Subsection 2.2.5, that the first terms vanish. This leads to the simple relations

$$\beta P = 2\omega(W_t^\mu - W_z^\varepsilon), \quad (2.2.86)$$

$$\beta P = 2\omega(W_t^\varepsilon - W_z^\mu). \quad (2.2.87)$$

Subtracting these two relations we find

$$W^\varepsilon = W_t^\varepsilon + W_z^\varepsilon = W_t^\mu + W_z^\mu = W^\mu, \quad (2.2.88)$$

stating the equality of the stored electric energy W^ε and the stored magnetic energy W^μ . The same relation also follows from the complex Poynting theorem.

By adding (2.2.86) and (2.2.87) we obtain another interesting relation, namely

$$P = \frac{\omega}{\beta} (W_t - W_z) = v_p (W_t - W_z), \quad (2.2.89)$$

where

$$W_t = W_t^\varepsilon + W_t^\mu, \quad W_z = W_z^\varepsilon + W_z^\mu. \quad (2.2.90)$$

This expression relates the phase velocity v_p of the mode to the power flow P and the quantity $(W_t - W_z)$, which can be identified as the electromagnetic momentum flow in the waveguide [2.21]. It should be contrasted to the relation (2.2.81) for the group velocity v_g . Combining these two relations we get

$$v_p/v_g = (W_t + W_z)/(W_t - W_z) \quad (2.2.91)$$

which ties the difference between v_p and v_g to the presence of longitudinal field components.

2.2.9. Variational Properties of the Propagation Constant

To be complete, we should mention briefly the variational properties of the propagation constant β of a guided mode of a dielectric waveguide. As pointed out earlier, there is a close analogy between the dielectric waveguide problem and the potential well problems of quantum mechanics. In quantum mechanics, one has and uses a variational expression for the energy of the ground state which assumes a minimum value when the correct wave functions are inserted (see e.g. [2.23]). For waveguides, we have a similar principle for the propagation constant β , which assumes a maximum value when the correct mode functions are used. BERK [2.24] and KUROKAWA [2.25] give variational expressions for waveguides of quite general type including guides with an inhomogeneous dielectric (refractive index) profile. Variational principles and variational methods can be used for the analysis of guides with relatively complicated index profiles. An example of this is the treatment of optical fibers with graded core profiles by OKOSHI and OKAMOTO [2.26].

We refer the reader to the literature cited above for more detail, and give here as a simple example the variational expression for the propagation constant β of the TE-mode of a planar waveguide with the index profile $n(x)$. This expression follows from the wave equation (2.2.22) and has the form

$$\beta^2 \geq \int_{-\infty}^{+\infty} dx (\psi d^2\psi/dx^2 + n^2 k^2 \psi^2) / \int_{-\infty}^{+\infty} dx \psi^2, \quad (2.2.92)$$

where $\psi(x)$ is a trial function for the field component $E_y(x)$ which must be continuous and must possess first derivatives. The expression yields a lower bound for β^2 which improves as $\psi(x)$ approaches the actual mode distribution $E_y(x)$. For $\psi(x) = E_y(x)$ the right hand side assumes its maximum value which is equal to β^2 .

2.3. Modes of the Planar Slab Guide

In this section we list formulas for the fields of the modes of a planar slab waveguide. We consider the structure and coordinate system shown in Fig. 2.14 where a film of thickness h and uniform refractive index n_f is sandwiched between a substrate of uniform index n_s and a cover of uniform index n_c . This structure has also been called the

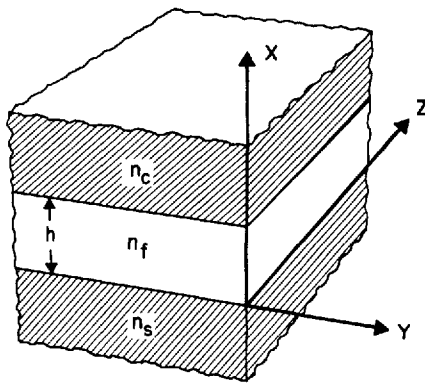


Fig. 2.14. Sketch of an “asymmetric” slab waveguide and the choice of the coordinate system. Note that the z -axis lies in the film-substrate interface

“asymmetric” slab guide. The modal fields can be derived from the wave equations of Subsection 2.2.3, and the corresponding solutions have been discussed by MCKENNA [2.17], TIEN [2.10], MARCUSE [2.2], and others. We follow essentially MARCUSE’s treatment, but cast the results in a simple form which employs the peak values of the fields in substrate, film and cover as well as the phase shifts at the film-substrate and film-cover boundaries that play an important role in the zig-zag wave picture. We have to distinguish between modes of TE and modes of TM polarization. Another distinction is between guided modes and radiation modes, the latter divided into the categories of substrate radiation modes, substrate-cover (also called “air”) radiation modes, and evanescent modes.

In accordance with the wave equation we define various transverse decay (γ_i) and propagation constants (κ_i) by

$$\kappa_c^2 = n_c^2 k^2 - \beta^2 = -\gamma_c^2, \quad (2.3.1)$$

$$\kappa_f^2 = n_f^2 k^2 - \beta^2, \quad (2.3.2)$$

$$\kappa_s^2 = n_s^2 k^2 - \beta^2 = -\gamma_s^2, \quad (2.3.3)$$

where the subscripts s, f, and c refer to substrate, film, and cover respectively.

Table 2.3.

Modes	β	κ_s
guided	$k n_f \rightarrow k n_s$	imaginary
substrate	$k n_s \rightarrow k n_c$	$0 \rightarrow k \sqrt{n_s^2 - n_c^2}$
substrate-cover	$k n_c \rightarrow 0$	$k \sqrt{n_s^2 - n_c^2} \rightarrow k n_s$
evanescent	imaginary	$k n_s \rightarrow \infty$

Table 2.3 shows the ranges of propagation constants β corresponding to the various mode types and categories, and also the associated ranges of the transverse propagation constant κ_s in the substrate. Because of its convenient range, the latter is chosen as the spatial frequency for the continuous mode spectrum.

As we are dealing with a planar problem, all field solutions can be made independent of the y-coordinate.

2.3.1. TE-Modes

From Subsection 2.2.3, we have for the TE-modes

$$H_y = E_x = E_z = 0, \quad (2.3.4)$$

$$H_x = -(\beta/\omega\mu)E_y, \quad (2.3.5)$$

$$H_z = (j/\omega\mu)\partial E_y/\partial x, \quad (2.3.6)$$

with the E_y component obeying the wave equation

$$\partial^2 E_y/\partial x^2 = (\beta^2 - n^2 k^2)E_y. \quad (2.3.7)$$

The boundary conditions of (2.2.8) demand that E_y (and thereby automatically H_x) and $\partial E_y / \partial x$ (and thereby H_z) be continuous across the film boundaries at $x=0$ and $x=h$.

For guided modes we have

$$\begin{aligned} E_y &= E_c \exp[-\gamma_c(x-h)], \quad \text{for } h < x, & \text{(cover),} \\ E_y &= E_f \cos(\kappa_f x - \phi_s), \quad \text{for } 0 < x < h, & \text{(film),} \\ E_y &= E_s \exp(\gamma_s x), \quad \text{for } x < 0, & \text{(substrate).} \end{aligned} \quad (2.3.8)$$

Application of the boundary conditions yields the formulas for the phase shifts

$$\tan \phi_s = \gamma_s / \kappa_f, \quad \tan \phi_c = \gamma_c / \kappa_f, \quad (2.3.9)$$

and the dispersion relation

$$\kappa_f h - \phi_s - \phi_c = v\pi, \quad (2.3.10)$$

where the mode label v is an integer. This is in agreement with the dispersion relation obtained from the zig-zag wave picture (see Sect. 2.1). We also get a relation between the peak fields E_s , E_f and E_c of the form

$$E_f^2(n_f^2 - N^2) = E_s^2(n_s^2 - n_s^2) = E_c^2(n_c^2 - n_c^2), \quad (2.3.11)$$

where $N = \beta/k$ is the effective refractive index.

In the above form, the modes are not normalized for power. We calculate the power P carried by a mode per unit guide width as follows

$$P = -2 \int_{-\infty}^{+\infty} dx E_y H_x = \frac{2\beta}{\omega\mu} \int_{-\infty}^{+\infty} dx E_y^2 = N \sqrt{\frac{\epsilon_0}{\mu_0}} E_f^2 \cdot h_{\text{eff}} = E_f H_f \cdot h_{\text{eff}}, \quad (2.3.12)$$

where

$$h_{\text{eff}} = h + \frac{1}{\gamma_s} + \frac{1}{\gamma_c} \quad (2.3.13)$$

is the effective thickness of the waveguide, as discussed in Subsection 2.1.4.

For the substrate radiation modes, the field distribution is

$$\begin{aligned} E_y &= E_c \exp[-\gamma_c(x-h)] \quad \text{for } h < x, \\ E_y &= E_f \cos[\kappa_f(x-h) + \phi_c] \quad \text{for } 0 < x < h, \\ E_y &= E_s \cos[\kappa_s x + \phi] \quad \text{for } x < 0. \end{aligned} \quad (2.3.14)$$

The boundary conditions require that

$$\tan \phi_c = \gamma_c / \kappa_f, \quad (2.3.15)$$

$$\kappa_s \tan \phi = \kappa_f \tan(\phi_c - \kappa_f h), \quad (2.3.16)$$

and

$$E_f^2(n_f^2 - N^2) = E_c^2(n_f^2 - n_c^2), \quad (2.3.17)$$

$$E_s^2 = E_f^2 \left[1 + \frac{n_f^2 - n_s^2}{n_s^2 - N^2} \sin^2(\phi_c - \kappa_f h) \right]. \quad (2.3.18)$$

Here we have no dispersion relation leading to discrete values for β , and we choose κ_s as the independent continuous variable.

The above field of a substrate mode is exactly the same as that created by a plane wave incident from the substrate side, with $\kappa_s = k n_s \cos \theta_s$ used as a measure for the angle of incidence θ_s . The incident wave is refracted and partially reflected at the film-substrate boundary and totally reflected at the film-cover boundary. The phase shift incurred at that total reflection is $2\phi_c$, and the phase-shift for reflection from the film-cover combination is 2ϕ . Interference between the incident and reflected waves creates the sinusoidal standing wave patterns in film and substrate.

For the cross power $\bar{P}(\kappa_s, \bar{\kappa}_s)$, needed to normalize the substrate modes, we calculate

$$\bar{P} = -2 \int_{-\infty}^{+\infty} dx E_y(\kappa_s) H_x(\bar{\kappa}_s) = \frac{\pi \beta}{\omega \mu} E_s^2 \delta(\kappa_s - \bar{\kappa}_s) = \pi E_s H_s \delta(\kappa_s - \bar{\kappa}_s). \quad (2.3.19)$$

The substrate-cover radiation modes are degenerate; we obtain two independent field solutions for each given κ_s . Great care must be exercised to select two solutions which are orthogonal to each other, as required by the mode expansion formalism. A convenient choice are modal fields which become even or odd functions of x in the limit of a "symmetric" waveguide where $n_s = n_c$. For simplicity, we also call these modes "even" and "odd" in the asymmetric case. Their fields are

for odd modes	for even modes
$E_y = E_c \sin[\kappa_c(x-h) + \phi_c]$;	$E_y = \bar{E}_c \cos[\kappa_c(x-h) + \bar{\phi}_c]$, for $h < x$,
$E_y = E_f \sin(\kappa_f x - \phi)$;	$E_y = \bar{E}_f \cos(\kappa_f x - \phi)$, for $0 < x < h$,
$E_y = E_s \sin(\kappa_s x - \phi_s)$;	$E_y = \bar{E}_s \cos(\kappa_s x - \bar{\phi}_s)$, for $x < 0$,

(2.3.20)

where the same phase shift ϕ is used for both the even and odd modes. Using the boundary conditions one derives the relations for the phase shifts for the odd modes

$$\kappa_s \cot \phi_s = \kappa_f \cot \phi, \quad (2.3.21)$$

$$\kappa_c \cot \phi_c = \kappa_f \cot(\kappa_f h - \phi) \quad (2.3.22)$$

and for the even modes

$$\kappa_s \tan \bar{\phi}_s = \kappa_f \tan \phi, \quad (2.3.23)$$

$$\kappa_c \tan \bar{\phi}_c = \kappa_f \tan(\kappa_f h - \phi). \quad (2.3.24)$$

The connections between the peak fields are

$$E_s^2 = E_f^2 \left(\sin^2 \phi + \frac{\kappa_f^2}{\kappa_s^2} \cos^2 \phi \right), \quad (2.3.25)$$

$$E_c^2 = E_f^2 \left[\sin^2(\kappa_f h - \phi) + \frac{\kappa_f^2}{\kappa_c^2} \cos^2(\kappa_f h - \phi) \right], \quad (2.3.26)$$

$$\bar{E}_s^2 = \bar{E}_f^2 \left(\cos^2 \phi + \frac{\kappa_f^2}{\kappa_s^2} \sin^2 \phi \right), \quad (2.3.27)$$

$$\bar{E}_c^2 = \bar{E}_f^2 \left[\cos^2(\kappa_f h - \phi) + \frac{\kappa_f^2}{\kappa_c^2} \sin^2(\kappa_f h - \phi) \right]. \quad (2.3.28)$$

For the cross power between even or between odd modes we calculate

$$\bar{P} = \frac{\pi \beta}{\omega \mu} [E_s^2 \delta(\kappa_s - \bar{\kappa}_s) + E_c^2 \cdot \delta(\kappa_c - \bar{\kappa}_c)]. \quad (2.3.29)$$

When needed, the second delta function in this expression can be re-written as

$$\delta(\kappa_c - \bar{\kappa}_c) = (\kappa_c / \kappa_s) \delta(\kappa_s - \bar{\kappa}_s), \quad (2.3.30)$$

which follows from the fact that $\kappa_s^2 - \bar{\kappa}_s^2 = \kappa_c^2 - \bar{\kappa}_c^2$.

The cross-power between an even and an odd mode is

$$\bar{P} = \frac{\pi \beta}{\omega \mu} [E_s \bar{E}_s \delta(\kappa_s - \bar{\kappa}_s) + E_c \bar{E}_c \delta(\kappa_c - \bar{\kappa}_c)], \quad (2.3.31)$$

which is not necessarily zero when $\kappa_s = \bar{\kappa}_s$. As we postulate orthogonality between even and odd modes, we have to set

$$\kappa_s E_s \bar{E}_s + \kappa_c E_c \bar{E}_c = 0 \quad (2.3.32)$$

to make the cross-power vanish. After some manipulation, this condition can be rewritten as

$$\cos(\phi_s - \bar{\phi}_s) + \cos(\phi_c - \bar{\phi}_c) = 0, \quad (2.3.33)$$

which becomes a condition for the phase shift ϕ of the form

$$\tan 2\phi = \sin(2\kappa_f h) / \left[\cos 2\kappa_f h + \frac{\kappa_s}{\kappa_c} (1 - \kappa_f^2/\kappa_s^2) / (1 - \kappa_f^2/\kappa_c^2) \right]. \quad (2.3.34)$$

For the symmetric guide we have $\kappa_s = \kappa_c$, and

$$\phi = \kappa_f h / 2. \quad (2.3.35)$$

2.3.2. TM-Modes

Subsection 2.2.3 gives the relations for the TM modes

$$E_y = H_x = H_z = 0, \quad (2.3.36)$$

$$E_x = (\beta/\omega \epsilon) H_y, \quad (2.3.37)$$

$$E_z = -(j/\omega \epsilon) \partial H_y / \partial x, \quad (2.3.38)$$

with the H_y component obeying the wave equation

$$\partial^2 H_y / \partial x^2 = (\beta^2 - n^2 k^2) H_y. \quad (2.3.39)$$

The boundary conditions at $x=0$ and $x=h$ demand the continuity of H_y (and thereby of ϵE_x) and of $n^{-2} \partial H_y / \partial x$ (and thereby of E_z).

The field solutions for the guided modes are

$$\begin{aligned} H_y &= H_c \exp[-\gamma_c(x-h)] && \text{for } h < x, \\ H_y &= H_f \cos(\kappa_f x - \phi_s) && \text{for } 0 < x < h, \\ H_y &= H_s \exp(\gamma_s x) && \text{for } x < 0. \end{aligned} \quad (2.3.40)$$

Using the boundary conditions, we obtain

$$\tan \phi_s = (n_f/n_s)^2 \gamma_s/\kappa_f, \quad \tan \phi_c = (n_f/n_c)^2 \gamma_c/\kappa_f, \quad (2.3.41)$$

and also the now familiar dispersion relation

$$\kappa_f h - \phi_s - \phi_c = v\pi, \quad (2.3.42)$$

where v is an integer. We also get a relation between the peak fields of the form

$$H_f^2(n_f^2 - N^2)/n_f^2 = H_s^2(n_f^2 - n_s^2)q_s/n_s^2 = H_c^2(n_f^2 - n_c^2)q_c/n_c^2, \quad (2.3.43)$$

where the reduction factors q_s and q_c are defined as in Section 2.1. by

$$q_s = (N/n_f)^2 + (N/n_s)^2 - 1, \quad (2.3.44)$$

$$q_c = (N/n_f)^2 + (N/n_c)^2 - 1. \quad (2.3.45)$$

For the power per unit guide width carried by a mode we calculate

$$P = 2 \int_{-\infty}^{+\infty} dx E_x H_y = \frac{2\beta}{\omega \epsilon_0} \int_{-\infty}^{+\infty} dx H_y^2/n^2 = N \sqrt{\frac{\mu_0}{\epsilon_0}} H_f^2 \cdot h_{\text{eff}}/n_f^2 = E_f H_f \cdot h_{\text{eff}} \quad (2.3.46)$$

where the effective thickness for the TM modes is defined as

$$h_{\text{eff}} = h + \frac{1}{\gamma_s q_s} + \frac{1}{\gamma_c q_c}. \quad (2.3.47)$$

The fields of the TM substrate radiation modes are

$$\begin{aligned} H_y &= H_c \exp[-\gamma_c(x-h)] && \text{for } h < x \\ H_y &= H_f \cos[\kappa_f(x-h) + \phi_c] && \text{for } 0 < x < h \\ H_y &= H_s \cos(\kappa_s x + \phi) && \text{for } x < 0. \end{aligned} \quad (2.3.48)$$

The boundary conditions require that

$$\tan \phi_c = (n_f/n_c)^2 \gamma_c/\kappa_f, \quad (2.3.49)$$

$$(\kappa_s/n_s^2) \tan \phi = (\kappa_f/n_f^2) \tan(\phi_c - \kappa_f h), \quad (2.3.50)$$

and

$$H_f^2(n_f^2 - N^2)/n_f^2 = H_c^2(n_f^2 - n_c^2)q_c/n_c^2, \quad (2.3.51)$$

$$H_s^2 = H_f^2 \left[1 + (n_s^2/n_f^2 q_s) \frac{n_f^2 - n_s^2}{n_s^2 - N^2} \sin^2(\phi_c - \kappa_f h) \right]. \quad (2.3.52)$$

Comparing the above expression with the corresponding formulas for the TE modes, we note the appearance of the reduction factors q_s and q_c .

As in the TE-mode case, we use κ_s as the continuous mode label. For the cross-power $\bar{P}(\kappa_s, \bar{\kappa}_s)$ we calculate

$$\bar{P} = 2 \int_{-\infty}^{+\infty} dx E_x(\kappa_s) H_y(\bar{\kappa}_s) = \frac{\pi \beta}{\omega \epsilon_0 n_s^2} H_s^2 \delta(\kappa_s - \bar{\kappa}_s) = \pi E_s H_s \delta(\kappa_s - \bar{\kappa}_s). \quad (2.3.53)$$

As in the TE case, the substrate-cover radiation modes are degenerate and we distinguish between "even" and "odd" modes. Their fields are

for odd modes	for even modes
$H_y = H_c \sin[\kappa_c(x-h) + \phi_c];$	$H_y = \bar{H}_c \cos[\kappa_c(x-h) + \bar{\phi}_c], \text{ for } h < x$
$H_y = H_f \sin(\kappa_f x - \phi);$	$H_y = \bar{H}_f \cos(\kappa_f x - \phi), \text{ for } 0 < x < h$
$H_y = H_s \sin(\kappa_s x - \phi_s);$	$H_y = \bar{H}_s \cos(\kappa_s x - \bar{\phi}_s), \text{ for } x < h,$

(2.3.54)

where ϕ is the same for the even and odd modes. The relations between the phase shifts, as derived from the boundary conditions, are

$$(\kappa_s/n_s^2) \cot \phi_s = (\kappa_f/n_f^2) \cot \phi, \quad (2.3.55)$$

$$(\kappa_c/n_c^2) \cos \phi_c = (\kappa_f/n_f^2) \cot(\kappa_f h - \phi) \quad (2.3.56)$$

for the odd modes, and

$$(\kappa_s/n_s^2) \tan \bar{\phi}_s = (\kappa_f/n_f^2) \tan \phi, \quad (2.3.57)$$

$$(\kappa_c/n_c^2) \tan \bar{\phi}_c = (\kappa_f/n_f^2) \tan(\kappa_f h - \phi) \quad (2.3.58)$$

for the even modes. The peak fields are connected by

$$H_s^2 = H_f^2 [\sin^2 \phi + (n_s^2 \kappa_f / n_f^2 \kappa_s)^2 \cos^2 \phi], \quad (2.3.59)$$

$$H_c^2 = H_f^2 [\sin^2(\kappa_f h - \phi) + (n_c^2 \kappa_f / n_f^2 \kappa_c)^2 \cos^2(\kappa_f h - \phi)], \quad (2.3.60)$$

$$\bar{H}_s^2 = \bar{H}_f^2 [\cos^2 \phi + (n_s^2 \kappa_f / n_f^2 \kappa_s)^2 \sin^2 \phi], \quad (2.3.61)$$

$$\bar{H}_c^2 = \bar{H}_f^2 [\cos^2(\kappa_f h - \phi) + (n_c^2 \kappa_f / n_f^2 \kappa_c)^2 \sin^2(\kappa_f h - \phi)]. \quad (2.3.62)$$

The cross-power between even or between odd modes of different κ_s is

$$\bar{P} = \frac{\pi \beta}{\omega \epsilon_0} \left[\frac{1}{n_s^2} H_s^2 \delta(\kappa_s - \bar{\kappa}_s) + \frac{1}{n_c^2} H_c^2 \delta(\kappa_c - \bar{\kappa}_c) \right]. \quad (2.3.63)$$

As in the TE case, we postulate orthogonality between the even and the odd TM radiation modes and, again, obtain the condition

$$\cos(\phi_s - \bar{\phi}_s) + \cos(\phi_c - \bar{\phi}_c) = 0. \quad (2.3.64)$$

This translates into a condition for ϕ which has the same form as (2.3.34) for the TE mode but with κ_f replaced by κ_f/n_f^2 , κ_s by κ_s/n_s^2 , and κ_c by κ_c/n_c^2 .

2.4. Planar Guides with Graded Index Profiles

Several fabrication processes, in particular diffusion and ion implantation, lead to dielectric waveguide layers with graded index profiles where the refractive index $n(x)$ varies gradually over the cross-section of the guide. We list in this section the known mode solutions for 3 symmetric index profiles of different shapes, namely, the parabolic, the “ $1/\cosh^2$ ”, and the exponential profiles. We also discuss graded profiles with one sharp index discontinuity which correspond to the practical case of diffused guides with a sharp index step at the film-air boundary; and, finally, we briefly mention the application of the WKB method to profiles with a slow index gradation.

The discussion focuses on the TE modes governed by the wave equation (2.2.22) for the E_y component

$$d^2 E_y / dx^2 = (\beta^2 - n^2 k^2) E_y. \quad (2.4.1)$$

The exact solutions available for these modes can be adapted to serve as approximations for the TM modes if the gradient of $n(x)$ is small enough.

The wave equation (2.4.1) has the same form as the Schrödinger equation of quantum mechanics, with $N^2 = \beta^2/k^2$ essentially corresponding to energy level and $n^2(x)$ to the potential energy well; hence, we can draw on the extensive literature of quantum mechanics both for specific solutions and for methods of analysis.

2.4.1. The Parabolic Profile (Harmonic Oscillator)

As sketched in Fig. 2.15, one can use the parabolic profile

$$n^2(x) = n_f^2(1 - x^2/x_0^2) \quad (2.4.2)$$

to approximate the actual index variation of a practical waveguide (shown dashed) near the guide axis ($x=0$) where $n(0)=n_f$. For small x , we can write this as

$$n(x) \approx n_f(1 - \frac{1}{2}x^2/x_0^2). \quad (2.4.3)$$

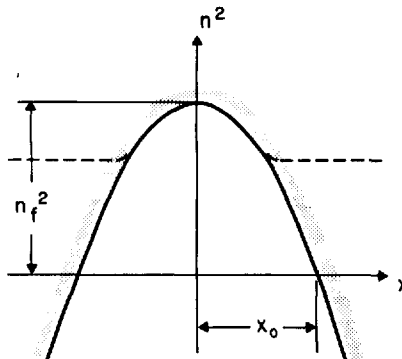


Fig. 2.15. Parabolic index profile (solid curve) and the practical guide profile (dashed curve) which is approximated by it

The index profile of (2.4.2) corresponds to the potential well of the harmonic oscillator (see e.g. [2.23]), and the solutions of the wave equation are

$$E_y = H_v(\sqrt{2}x/w) \exp(-x^2/w^2), \quad (2.4.4)$$

where the H_v are the Hermite polynomials defined by

$$H_v(x) = (-1)^v \exp(x^2) \frac{d^v}{dx^v} \exp(-x^2). \quad (2.4.5)$$

For the lowest orders we have

$$\begin{aligned} H_0(x) &= 1, \\ H_1(x) &= 2x, \\ H_2(x) &= 4x^2 - 2, \\ H_3(x) &= 8x^3 - 12x. \end{aligned} \quad (2.4.6)$$

The Hermite-Gaussian functions of (2.4.4) are also known as the standard description for the modes of laser beams and laser resonators [2.18, 27], where the parameter w is called the “beam radius”. The latter is given by

$$w^2 = (\lambda x_0 / \pi n_f) \quad (2.4.7)$$

and indicates the degree of confinement of the fundamental mode. For the propagation constant β_v and the effective index N_v of a mode of order v , one obtains

$$\beta_v^2 = n_f^2 k^2 - (2v + 1)n_f k/x_0, \quad (2.4.8)$$

$$N_v^2 = n_f^2 - (v + \frac{1}{2})(n_f \lambda / \pi x_0). \quad (2.4.9)$$

The parabolic profile corresponds to a closed well and predicts an infinite set of discrete modes. But as the order v increases, the energy of a mode is spread out further from the guide axis, and eventually the distances x are so large that (2.4.2) can no longer be regarded as a good approximation for the actual guide profile.

2.4.2. The “1/cosh²” Profile

The “1/cosh²” profile is an open well described by

$$n^2(x) = n_s^2 + 2n_s \Delta n / \cosh^2(2x/h). \quad (2.4.10)$$

The corresponding potential is also employed in quantum mechanics [2.23] and is a special case of the PÖSCHL-TELLER potential [2.28]. For

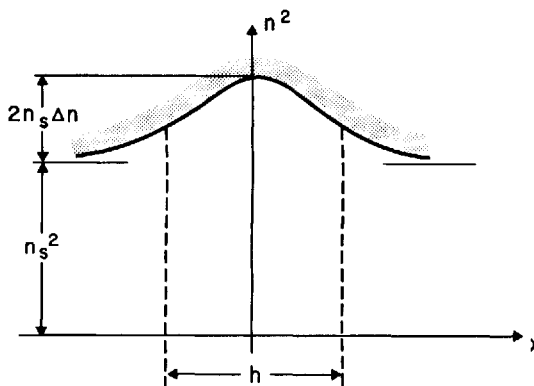


Fig. 2.16. The “ $1/\cosh^2$ ” index profile. The nominal guide thickness h is indicated

small peak index deviations Δn from the substrate index n_s , we have approximately

$$n(x) \approx n_s + \Delta n / \cosh^2(2x/h), \quad (2.4.11)$$

indicating a guiding layer of thickness h , as sketched in Fig. 2.16. As in the case of the uniform slab guide discussed in Section 2.1, it is convenient to use a normalized thickness V , which we define as

$$V = kh\sqrt{2n_s \Delta n}. \quad (2.4.12)$$

The solution of the wave equation (2.4.1) for the “ $1/\cosh^2$ ” profile of (2.4.10) yields a very simple expression for the maximum mode number $s \geq v$ of guided (bound) modes supported by the waveguide, which is

$$s = \frac{1}{2}(\sqrt{1+V^2}-1). \quad (2.4.13)$$

For the propagation constants β_v and the effective indices N_v we obtain

$$\beta_v^2 = n_s^2 k^2 + 4(s-v)^2/h^2, \quad (2.4.14)$$

$$N_v^2 = n_s^2 + (s-v)^2 (\lambda/\pi h)^2. \quad (2.4.15)$$

The modal field distribution is

$$E_y = u_v(2x/h)/\cosh^2(2x/h), \quad (2.4.16)$$

where the u_v are hypergeometric functions [2.23]. For even mode number v we have

$$\begin{aligned} u_v = & 1 - \frac{1}{2}v(2s-v)\sinh^2(2x/h)/(1\cdot 1!) \\ & + \frac{1}{4}v(v-2)(2s-v)(2s-v-2)\sinh^4(2x/h)/(1\cdot 3\cdot 2!) + \dots, \end{aligned} \quad (2.4.17)$$

and for odd v we get

$$\begin{aligned} u_v = & \sinh(2x/h)[1 - \frac{1}{2}(v-1)(2s-v-1)\sinh^2(2x/h)/(3\cdot 1!) \\ & + \frac{1}{4}(v-1)(v-3)(2s-v-1)(2s-v-3)\sinh^4(2x/h)/(3\cdot 5\cdot 2!) + \dots] \end{aligned} \quad (2.4.18)$$

For the lower mode orders these functions simplify to

$$\begin{aligned} u_0 &= 1, \\ u_1 &= \sinh(2x/h), \\ u_2 &= 1 - 2(s-1)\sinh^2(2x/h), \\ u_3 &= \sinh(2x/h)[1 - \frac{2}{3}(s-2)\sinh^2(2x/h)]. \end{aligned} \quad (2.4.19)$$

NELSON and MCKENNA [2.6] give a discussion of an asymmetric graded index profile which is a generalization of the “ $1/\cosh^2$ ” profile for cases where the indices of the substrate and the cover are unequal.

Another profile formally related to the “ $1/\cosh^2$ ” potential has the form

$$n^2(x) = n_f^2[1 - A \tan^2(x/x_0)]. \quad (2.4.20)$$

This is also a special case of the PÖSCHL-TELLER potential for which exact solutions are available, as discussed in detail by GORDON [2.29].

2.4.3. The Exponential Profile

The exponential profile is another case for which exact solutions are available [2.30]. We adapt these here to the symmetric profile sketched in Fig. 2.17 and described by

$$n^2(x) = n_s^2 + 2n_s A n \exp(-2|x|/h), \quad (2.4.21)$$

which, for small $A n$, can be approximated by

$$n(x) \approx n_s + A n \exp(-2|x|/h). \quad (2.4.22)$$

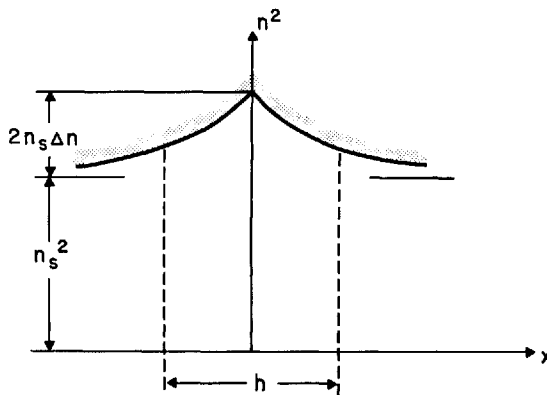


Fig. 2.17. The symmetric exponential profile and the corresponding nominal guide thickness h

Again we introduce a normalized layer thickness V by defining

$$V = kh\sqrt{2n_s \Delta n} . \quad (2.4.23)$$

The solutions for the modal fields of this profile can be expressed in terms of Bessel functions J_p of the first kind and of non-integral order p ,

$$\begin{aligned} E_y &= J_p(V \exp[-x/h]), \quad \text{for } x > 0, \\ &= J_p(V \exp[x/h]), \quad \text{for } x < 0. \end{aligned} \quad (2.4.24)$$

The order p_v is determined by matching the solutions at the boundary $x=0$ for given V . For the even modes, we require that

$$J'_p(V) = 0 , \quad (2.4.25)$$

and for the odd modes we have to demand

$$J_p(V) = 0 . \quad (2.4.26)$$

Each of the two conditions yields approximately V/π discrete solutions for p_v . In terms of p_v , we can write for the propagation constant β_v

$$\beta_v^2 = n_s^2 k^2 + p_v^2/h^2 , \quad (2.4.27)$$

and for the effective index N_v

$$N_v^2 = n_s^2 + p_v^2/(k h)^2. \quad (2.4.28)$$

Fig. 2.18 shows a plot of the quantity

$$(p_v/V)^2 = (N_v^2 - n_s^2)/(2n_s \Delta n) \approx (N_v - n_s)/\Delta n \quad (2.4.29)$$

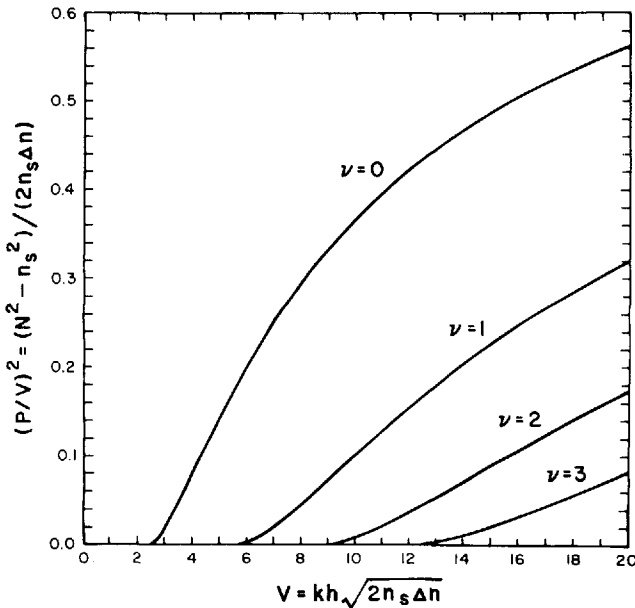


Fig. 2.18. Normalized ω - β diagram for planar guides with an exponential profile. Shown are the dispersion curves for the modes of odd order which correspond to the modes of guides with an asymmetric exponential profile of mode number $\nu = \nu_{\text{asym}}$ as given by (2.4.30). (After [2.31])

for the odd order modes, which is taken from CARRUTHERS et al. [2.31] and represents the results of a numerical solution of (2.4.26).

2.4.4. Index Profiles with Strong Asymmetry

In a class of practical waveguides, a layer of increased index is induced (e.g., by diffusion) in the substrate material. While the induced index change is relatively small, there is often a large step from the substrate index n_s to the cover index n_c which is usually that of air. The result

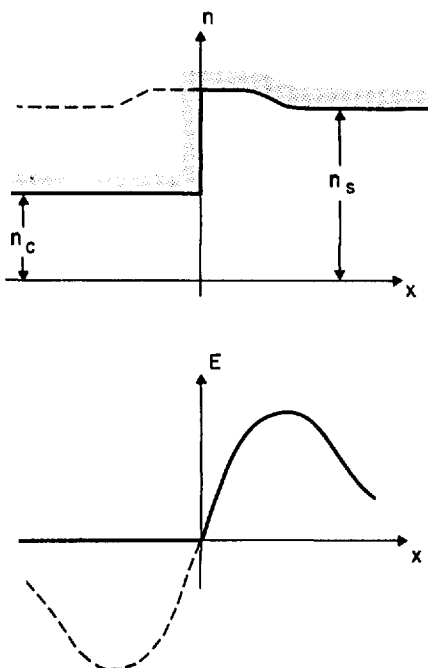


Fig. 2.19. Index profile with strong asymmetry (solid curve) and the associated symmetric profile (dashed curve). The corresponding approximate field distribution $E(x)$ is also shown

is an index profile as that sketched in Fig. 2.19. We call such a profile "strongly asymmetric" because the corresponding asymmetry measure, defined in Section 1, assumes very large values. We shall discuss here a correspondence between strongly asymmetric profiles and symmetric profiles such as those discussed above, which can be used to obtain approximate mode solutions for the asymmetric profiles from solutions known for symmetric ones. This technique has been used by STANDLEY and RAMASWAMY [2.32] for the asymmetric parabolic profile and essentially also by CONWELL [2.30] and CARRUTHERS et al. [2.31] for the asymmetric exponential profile. To obtain a first approximation, one assumes that the field in the cover region ($x < 0$) vanishes, as shown in the Fig. 2.19. The corresponding symmetric profile is indicated by the dashed line. The odd-order mode solutions of symmetric profiles have a zero field at $x = 0$ as sketched in the figure. For $x > 0$ we can therefore use these solutions for the asymmetric profile if we continue them with $E = 0$ for $x \leq 0$. The propagation constants corresponding to these

modes can also be used unaltered for the asymmetric profile as a first approximation. As we only use the symmetric-profile modes of odd order, we renumber the modes using the simple relation

$$2v_{\text{asym}} + 1 = v_{\text{sym}} \quad (2.4.30)$$

between the mode numbers v_{asym} of the asymmetric profile and the mode numbers v_{sym} of the corresponding symmetric profile.

Even though the actual field at the film-air interface is very small, it is not exactly zero. For some applications, such as the design of guided-wave filters with a surface corrugation, one needs to know the field values at the interface. HAUS and SCHMIDT [2.33] have described how one can improve the above approximation and obtain estimates for these field values. They assumed evanescent fields in the cover region with the decay constant γ_c given as usual by

$$\gamma_c^2 = \beta^2 - n_c^2 k^2. \quad (2.4.31)$$

Matching the fields at the boundary $x=0$ they obtain for the y -component of the electric field

$$E_y(0) = \frac{1}{\gamma_c} (dE_y/dx)_{x=0} \quad (2.4.32)$$

which relates the field at the surface $x=0$ to the slope dE/dx . The latter is calculated from the approximate mode solutions discussed above.

Exact solutions for the asymmetric exponential profile were discussed by CONWELL [2.30].

2.4.5. The WKB Method

The WKB method can be used to obtain approximate solutions of the wave equation (2.4.1) for the modes of profiles with slowly varying index $n(x)$. The method is thoroughly treated in the quantum mechanics literature (see e.g., [2.23, 34], and its application to dielectric waveguides has been discussed by GORDON [2.29], FELSEN and MARCUVITZ [2.35], and others. The method involves selection of a trial value for the propagation constant β (or the effective index N) of the waveguide and subsequent determination of the “turning points” x_1 and x_2 as indicated in Fig. 2.20 and described mathematically by

$$n(x_i) = N = \beta/k, \quad i = 1, 2. \quad (2.4.33)$$

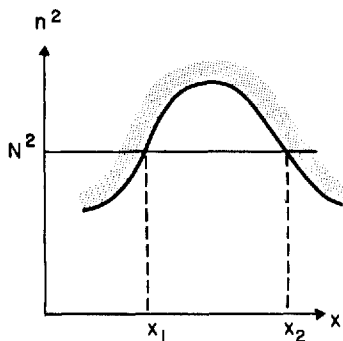


Fig. 2.20. Turning points x_1 and x_2 as determined by intersecting the line $n^2 = N^2$ with the index profile $n^2(x)$

The values of β which obey the condition

$$\int_{x_1}^{x_2} dx \sqrt{n^2 k^2 - \beta^2} = \pi(v + \frac{1}{2}) \quad (2.4.34)$$

with integer v , are the propagation constants β_v predicted by the WKB method. In terms of the effective index, this condition can be written as

$$\int_{x_1}^{x_2} dx \sqrt{n^2 - N^2} = \frac{\lambda}{2} (v + \frac{1}{2}). \quad (2.4.35)$$

For the modal fields, the WKB method predicts oscillatory field distributions in the region where $n(x) > N$ (i.e., $x_1 < x < x_2$) and exponentially decaying fields where $n(x) < N$ (i.e., $x > x_2$ and $x < x_1$).

For the special case of the parabolic profile, the WKB predictions are known to agree exactly with the closed form solutions (2.4.8) available for this profile.

2.5. Strip Waveguides

The planar dielectric guides discussed in the preceding sections provide no confinement of the light within the film plane, i.e., the $y-z$ plane, and confinement takes place in the x -dimension only. Dielectric strip waveguides (also called "3-dimensional" guides) can provide this additional confinement, which we assume to be in the y dimension. In several active integrated optics devices such as lasers or modulators,

this additional confinement can help to bring about desirable savings in drive voltage and drive power for example.

Figure 2.21 shows sketches of the $x-y$ cross sections of four different strip guide types. For simplicity, abrupt transitions of the refractive index are shown, but it should be clear that fabrication techniques such as diffusion may lead to similar cross sections with graded transitions. In all four examples, the light is more or less confined to the material with index $n_f > n_s, n_c, n_l$. The first example (a) shows the cross section of a raised strip guide which can be fabricated by starting with a planar slab guide, masking the strip and removing the surrounding film by sputtering or etching techniques. Masked diffusion or ion implantation leads to embedded strip guides of the kind shown under (b). The ridge guide (c) can be made by techniques similar to the

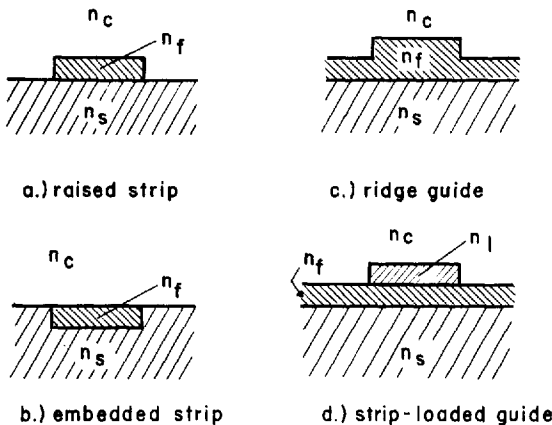


Fig. 2.21a-d. Cross section of four strip waveguide types

ones used for the raised strip guide but with incomplete removal of the surrounding film. The final example shows a strip-loaded guide (d) where a strip of lower index $n_l < n_f$ is deposited onto a planar guide. It has been suggested that both the ridge guide [2.36, 37], and the strip-loaded guide [2.38, 39] can be fabricated with relaxed requirements for resolution and edge roughness. Both strip-guide structures use a "propagating surround", i.e., planar guides on both sides of the strip that allow at least one guided mode.

The analysis of dielectric strip guides is much more complex than that of planar guides, and no exact analytic solutions for the modes of strip guides are available. Numerical calculations have been made for

guides with a core of rectangular cross-section embedded in a uniform surround of lower index. SCHLOSSER and UNGER [2.40] have described a numerical method for the analysis of these rectangular guides which is suited to cases of large aspect ratios (width-to-height ratios) and to cases far away from cutoff. GOELL [2.41] has employed cylindrical space harmonics to analyze rectangular guides with aspect ratios between 1 and 2. MARCATILI [2.42, 43] has obtained approximate analytical solutions applicable to a large class of strip guides for cases sufficiently far away from cut-off.

Another simple tool providing fairly good predictions for the behavior of strip guides is the "effective index method" which we describe in the following. Its application to strip-loaded guides has given good agreement with experimental results [2.39].

To illustrate the method here, we choose the example of a ridge guide. To give, at the same time, a numerical illustration we consider a guide at $\lambda = 0.8 \mu\text{m}$ with indices $n_f = 2.234$, $n_s = 2.214$, $n_c = 1$ which corresponds closely to the Ti-diffused guides in LiNbO_3 . Figure 2.22 shows both the cross-section (x, y) and a top view (z, y) of a ridge guide with a width a . The film thickness h of the ridge region is larger than the film thickness f of the surround as indicated. As a result, the effective index N_h of the ridge region is larger than the effective index N_f of the surround, and the light is essentially confined to the ridge region. The effective index method gives us a more quantitative idea of this guidance in the yz plane. Here, we consider as a first step the two film guides corresponding to the ridge and the surround and determine the corresponding normalized film thicknesses as defined in (2.1.16)

$$\begin{aligned} V_h &= kh\sqrt{n_f^2 - n_s^2}, \\ V_f &= kf\sqrt{n_f^2 - n_s^2}. \end{aligned} \quad (2.5.1)$$

To simplify the argument, both are assumed to be single-mode guides. For our numerical example, we have $h = 1.8 \mu\text{m}$ and $f = 1 \mu\text{m}$, and $V_h = 4.2$ and $V_f = 2.3$. As a second, step we determine the corresponding guide indices b_h and b_f

$$\begin{aligned} b_h &= (N_h^2 - n_s^2)/(n_f^2 - n_s^2), \\ b_f &= (N_f^2 - n_s^2)/(n_f^2 - n_s^2), \end{aligned} \quad (2.5.2)$$

and effective indices N_h and N_f . We can use Fig. 2.8 for this purpose and obtain for the TE-modes of our numerical example $b_h = 0.65$, $b_f = 0.2$, and $N_h = 2.227$, $N_f = 2.218$ where we have taken the data for asymmetry measure $a_E = \infty$ as a good approximation.

Next, consider the symmetric slab guide suggested by the top view of Fig. 2.22 which has a film thickness equal to the width a of the ridge and a film index N_h and substrate index N_f . The effective index method uses the guiding characteristics of this equivalent slab guide to predict

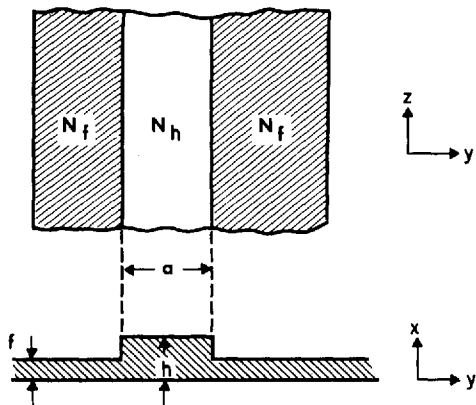


Fig. 2.22. Cross section (x, y) and top view (y, z) of a ridge waveguide. The effective indices N_h and N_f of the ridge and surround regions are indicated

the guiding characteristics of the ridge guide in the y -direction. This is simply done by substituting the effective indices N_h and N_f for the film and substrate indices n_f and n_s in the formulas available for slab guides. In particular, we can define a normalized ridge width V_y in analogy to (2.1.16) by

$$V_y = k a \sqrt{N_h^2 - N_f^2} = k a \sqrt{(n_f^2 - n_s^2)(b_h - b_f)}, \quad (2.5.3)$$

where we have invoked (2.5.2).

This is used in Fig. 2.8 to determine the normalized guide index b and the propagation constant $\beta = kN$ of the ridge guide, where, in analogy with (2.1.17)

$$N^2 = N_f^2 + b(N_h^2 - N_f^2). \quad (2.5.4)$$

For a ridge width of $a = 2 \mu\text{m}$, we get for our numerical example $V_y = 3.14$, $b = 0.64$ and $\beta = 2.224k$. As another example, we can use the

analogue of (2.1.24) to predict the number of guided modes v_y allowed in the y dimension as

$$v_y = \frac{2a}{\lambda} \sqrt{N_h^2 - N_f^2}. \quad (2.5.5)$$

For our example, we have $v_y = 0.4 a/\lambda$.

2.6. Coupled-Mode Formalism and Periodic Waveguides

Many phenomena occurring in physics or engineering can be viewed as coupled-mode processes. Examples for this include the diffraction of x-rays in crystals [2.44], the directional couplers of microwave technology [2.45,46], the energy exchange between electron beams and slow-wave structures in traveling-wave tubes [2.46,47], and the scattering of light by acoustic waves and by hologram gratings [2.49]. The coupled-mode formalism has also proved a very powerful tool in integrated optics, where it has helped in the understanding and analysis of a large variety of important phenomena and devices. These range from the scattering loss due to waveguide irregularities and the behavior of grating couplers and corrugated waveguide filters to distributed feedback lasers, electro-optic or magneto-optic TE-to-TM mode converters and nonlinear optical interactions. SNYDER [2.50] and MARCUSE [2.2] have developed a coupled-mode formalism applicable to a large class of dielectric waveguides including strip-guides and fibers, and they have used it in their analyses of optical fiber deformations. YARIV [2.51] has given a summary of coupled-wave phenomena that occur in integrated optics and presented a perturbation analysis of these for the TE-modes in planar waveguides. In the following subsections, we present the coupled-mode formalism and its derivation in sufficient generality to provide the basis for the treatment of the various coupled-wave phenomena of interest and to permit its application to all practical waveguide structures including strip-guides and fibers. We will first consider the excitation of modes by arbitrary sources in the guide, and then apply that formalism to waveguide deformations such as surface irregularities. This is followed by a listing of the standard coupled-wave solutions both for co-directional and contra-directional interactions, and finally we shall treat periodic waveguides and present results for the specific example of a planar waveguide with periodic surface corrugations.

2.6.1. Excitation of Waveguide Modes

We consider a distribution of sources exciting various waveguide modes and represent these sources by the complex amplitude $\mathbf{P}(x, y, z)$ of the corresponding induced polarization vector. In the presence of these sources, the complex Maxwell's equations have the form

$$\nabla \times \mathbf{E} = -j\omega\mu \mathbf{H}, \quad (2.6.1)$$

$$\nabla \times \mathbf{H} = j\omega\epsilon \mathbf{E} + j\omega \mathbf{P}. \quad (2.6.2)$$

The following steps are now quite analogous to those used in the derivation of the orthogonality relation in Subsection 2.2.5. We consider two different induced polarizations \mathbf{P}_1 and \mathbf{P}_2 and the fields caused by them, and obtain

$$\nabla \cdot (\mathbf{E}_1 \times \mathbf{H}_2^* + \mathbf{E}_2^* \times \mathbf{H}_1) = -j\omega \mathbf{P}_1 \cdot \mathbf{E}_2^* + j\omega \mathbf{P}_2^* \cdot \mathbf{E}_1, \quad (2.6.3)$$

which is essentially the Lorentz reciprocity relation. Now we set $\mathbf{P}_2 = 0$ and identify the field 2 with a mode of the waveguide. As in Subsection 2.2.5, we integrate over the guide cross-section, use the divergence theorem, and find

$$\int \int_{-\infty}^{+\infty} dx dy \frac{\partial}{\partial z} (\mathbf{E}_1 \times \mathbf{H}_2^* + \mathbf{E}_2^* \times \mathbf{H}_1)_z = -j\omega \int \int_{-\infty}^{+\infty} dx dy \mathbf{P}_1 \cdot \mathbf{E}_2^*. \quad (2.6.4)$$

The next step is to expand the transverse components of the field 1 in terms of the modes of the guide according to (2.2.58) and (2.2.59)

$$\mathbf{E}_{1t} = \sum (a_v + b_v) \mathbf{E}_{tv}, \quad \mathbf{H}_{1t} = \sum (a_v - b_v) \mathbf{H}_{tv} \quad (2.6.5)$$

where we use the \sum notation of Subsection 2.2.6. It should be noted that the coefficients $a_v(z)$ and $b_v(z)$ have to be regarded as functions of z in the present context. If we choose for the field 2 a forward running mode

$$\mathbf{E}_2 = \mathbf{E}_\mu \exp(-j\beta_\mu z), \quad \mathbf{H}_2 = \mathbf{H}_\mu \exp(-j\beta_\mu z), \quad (2.6.6)$$

insert these fields and the mode expansion into (2.6.4) and apply the orthogonality relation (2.2.51), we then find that the b_v coefficients drop out and we obtain

$$a'_\mu + j\beta_\mu a_\mu = -j\omega \int \int_{-\infty}^{+\infty} dx dy \mathbf{P} \cdot \mathbf{E}_\mu^*, \quad (2.6.7)$$

where the prime indicates differentiation with respect to z . Similarly we get

$$b'_\mu - j\beta_\mu b_\mu = j\omega \int_{-\infty}^{+\infty} dx dy \mathbf{P} \cdot \mathbf{E}_{-\mu}^* \quad (2.6.8)$$

if we identify the field 2 with a backward running mode

$$\mathbf{E}_2 = \mathbf{E}_{-\mu} \exp(j\beta_\mu z), \quad \mathbf{H}_2 = \mathbf{H}_{-\mu} \exp(j\beta_\mu z). \quad (2.6.9)$$

The above formulas hold only for propagating modes (real β); for the evanescent modes we have to use the orthogonality relation (2.2.63). It is usually convenient to define the amplitudes $A_\mu(z)$ and $B_\mu(z)$ of the forward and backward propagating modes by

$$a_\mu = A_\mu \exp(-j\beta_\mu z), \quad b_\mu = B_\mu \exp(j\beta_\mu z). \quad (2.6.10)$$

The change of these amplitudes due to the presence of sources can then be expressed as

$$A'_\mu = -j\omega \int_{-\infty}^{+\infty} dx dy \mathbf{P} \cdot \mathbf{E}_\mu^* \exp(j\beta_\mu z), \quad (2.6.11)$$

$$B'_\mu = j\omega \int_{-\infty}^{+\infty} dx dy \mathbf{P} \cdot \mathbf{E}_{-\mu}^* \exp(-j\beta_\mu z). \quad (2.6.12)$$

As expected, there is no change in amplitude when no sources are present. It should be emphasized that the above relations are exact; no assumption about the smallness of the perturbation caused by the sources has been made.

The formalism allows for an arbitrary polarization $\mathbf{P}(x, y, z)$ which can be brought about by a variety of physical effects. A standard example is a scalar deformation of the waveguide which is represented by the difference $\Delta\epsilon(x, y, z)$ of the actual dielectric constant from the nominal distribution $\epsilon(x, y)$ and which results in an induced polarization

$$\mathbf{P} = \Delta\epsilon \mathbf{E} \quad (2.6.13)$$

proportional to the field \mathbf{E} in the guide. We shall pursue this case in more detail in the next subsection. To represent loss in the waveguide material, we can use an imaginary-valued $\Delta\epsilon$. Anisotropy in the guide materials can be represented by a tensor perturbation leading to an induced polarization with the components

$$P_i = \Delta \varepsilon_{ij} E_j, \quad (2.6.14)$$

where we have employed the standard tensor notation which assumes summation over repeated indices. The off-diagonal elements of $\Delta \varepsilon_{ij}$ can cause TE-TM mode conversion which has been treated in terms of the coupled-mode formalism by YARIV [2.51], and SOSNOWSKI and BOYD [2.52]. Electro-optic (and other nonlinear optical) effects lead to a $\Delta \varepsilon_{ij}$ of the form

$$\Delta \varepsilon_{ij} = \varepsilon_0 X_{ijk} E_k, \quad (2.6.15)$$

where X_{ijk} is the second-order nonlinear susceptibility and E_k a component of the applied electric field [2.53].

2.6.2. Waveguide Deformations

In this subsection, we discuss in more detail the application of the coupled-mode formalism to scalar waveguide deformations. These are represented by the difference $\Delta \varepsilon(x, y, z)$ in the dielectric constant and an induced polarization of the form given in (2.6.13). We stress again that, so far, the formalism is exact, and we will make no approximations in this subsection. The reader should pay attention to the particular way in which the z -components are handled; this is necessary because only the tangential field components are orthogonal and the mode expansion can be applied only to these components. With (2.6.5) and (2.6.13) we have, therefore,

$$P_i = \Delta \varepsilon E_i = \Delta \varepsilon \sum (a_v + b_v) E_{tv}. \quad (2.6.16)$$

For E_z we obtain from (2.6.2)

$$j\omega(\varepsilon + \Delta \varepsilon) E_z = \nabla_t \times H_t, \quad (2.6.17)$$

which allows us to rewrite expressions for P_z in the following sequence

$$\begin{aligned} P_z &= \Delta \varepsilon E_z = \frac{\Delta \varepsilon}{\varepsilon + \Delta \varepsilon} \frac{1}{j\omega} \nabla_t \times H_t = \frac{\Delta \varepsilon}{\varepsilon + \Delta \varepsilon} \frac{1}{j\omega} \sum (a_v - b_v) \nabla_t \times H_{tv} \\ &= \frac{\Delta \varepsilon \cdot \varepsilon}{\varepsilon + \Delta \varepsilon} \sum (a_v - b_v) E_{zv}, \end{aligned} \quad (2.6.18)$$

where we have used the mode expansion (2.6.5) and the modal Maxwell equation (2.2.16). We are now ready to insert the components of \mathbf{P}

into (2.6.11) and (2.6.12) with the result

$$A'_\mu = -j\omega \int_{-\infty}^{+\infty} dx dy \sum \left[(a_v + b_v) \Delta \varepsilon \mathbf{E}_{tv} \cdot \mathbf{E}_{t\mu}^* + (a_v - b_v) \frac{\Delta \varepsilon \cdot \varepsilon}{\varepsilon + \Delta \varepsilon} \mathbf{E}_{zv} \cdot \mathbf{E}_{z\mu}^* \right] \exp(j\beta_\mu z), \quad (2.6.19)$$

$$B'_\mu = j\omega \int_{-\infty}^{+\infty} dx dy \sum \left[(a_v + b_v) \Delta \varepsilon \mathbf{E}_{t\mu} \cdot \mathbf{E}_{tv}^* - (a_v - b_v) \frac{\Delta \varepsilon \cdot \varepsilon}{\varepsilon + \Delta \varepsilon} \mathbf{E}_{zv} \cdot \mathbf{E}_{z\mu}^* \right] \exp(-j\beta_\mu z), \quad (2.6.20)$$

where we have used the symmetry relations (2.2.31) to express the mode distribution $\mathbf{E}_{-\mu}(x, y)$ in terms of the components of the field $\mathbf{E}_\mu(x, y)$ of the corresponding forward running mode. To simplify these expressions, we introduce tangential and longitudinal coupling coefficients $K_{v\mu}^t(z)$ and $K_{v\mu}^z(z)$ defined by

$$K_{v\mu}^t = \omega \int_{-\infty}^{+\infty} dx dy \Delta \varepsilon \mathbf{E}_{tv} \cdot \mathbf{E}_{t\mu}^*, \quad (2.6.21)$$

$$K_{v\mu}^z = \omega \int_{-\infty}^{+\infty} dx dy \frac{\Delta \varepsilon \cdot \varepsilon}{\varepsilon + \Delta \varepsilon} \mathbf{E}_{zv} \cdot \mathbf{E}_{z\mu}^*, \quad (2.6.22)$$

leading to real and positive quantities for positive $\Delta \varepsilon$. Using these coupling coefficients and the mode amplitudes of (2.6.10) we can rearrange (2.6.19) and (2.6.20) in the final form

$$\begin{aligned} A'_\mu = & -j \sum \left\{ A_v (K_{v\mu}^t + K_{v\mu}^z) \exp[-j(\beta_v - \beta_\mu)z] \right. \\ & \left. + B_v (K_{v\mu}^t - K_{v\mu}^z) \exp[j(\beta_v + \beta_\mu)z] \right\}, \end{aligned} \quad (2.6.23)$$

$$\begin{aligned} B'_\mu = & j \sum \left\{ A_v (K_{v\mu}^t - K_{v\mu}^z) \exp[-j(\beta_v + \beta_\mu)z] \right. \\ & \left. + B_v (K_{v\mu}^t + K_{v\mu}^z) \exp[j(\beta_v - \beta_\mu)z] \right\}. \end{aligned} \quad (2.6.24)$$

These two expressions form the basis for the solution of a number of coupled-mode problems. They show the change in the amplitude of each mode (μ) as a function of the deformation $\Delta \varepsilon$, the modal field distribution, and of the amplitudes of all other modes present in the guide. Depending on the particular problem at hand, one can usually make some simplifying assumptions at this stage. A very common and usually good assumption is that only two guided modes are important and that all other modes can be neglected. This leads to coupled-wave interactions with characteristics that are discussed further in the next subsection. Another

common assumption is that $\Delta\epsilon(x, y, z)$ is only a small perturbation of the dielectric constant $\epsilon(x, y)$ of the waveguide. Often, this is also a good assumption, but there are configurations of interest where it is not justified. An example is the corrugated glass waveguide used for filter devices where a corrugation of the glass-air interface leads to a large $\Delta\epsilon$. This is illustrated further in the discussion of Subsection 2.6.4.

The expressions above point out a general difference between co-directional coupling (e. g., coupling between two forward modes A_μ and A_ν) and contra-directional coupling (e. g., between A_μ and B_ν) which occurs in the presence of E_z components. As K^t and K^z have equal sign, the factor $(K^t + K^z)$ indicates stronger coupling for co-directional interactions as compared to contra-directional interactions where we have the factor $(K^t - K^z)$. This happens because forward and backward modes have E_z components of opposite sign and E_t components of the same sign.

2.6.3. Coupled-Wave Solutions

In a large class of coupled-mode interactions of interest, there are only two guided modes that possess sufficient phase synchronism to allow a significant interchange of energy. One can then neglect all other modes and obtain simple coupled-wave equations that describe the interaction. These equations follow from (2.6.11) and (2.6.12) for the general case addressed by this subsection, and, from (2.6.23) and (2.6.24) for the case of waveguide deformations which we use as an illustration. The solutions to the coupled-wave equations are well known and have been derived in several ways in the literature cited above. We give here only a brief listing of results. We have to distinguish between two different types, co-directional interactions and contra-directional interactions. Co-directional interactions occur between two forward (or two backward) propagating modes, and contra-directional interactions occur between a forward and a backward running mode. To be more precise, it is the relative direction of the group velocities of the modes that is considered here.

We deal with co-directional interactions first and, referring to (2.6.23), call the amplitudes of the two significant waves A ($= A_\mu$) and B ($= A_\nu$). We find that changes in these amplitudes are generally described by differential equations of the form,

$$A' = -j\kappa B \exp(-2j\delta z), \quad (2.6.25)$$

$$B' = -j\kappa A \exp(2j\delta z), \quad (2.6.26)$$

where κ is the coupling constant which, in the simple case considered here, is real and uniform (i.e., independent of z), and δ is a normalized frequency which measures the deviation from synchronism (for which one has $\delta=0$). In the next subsection, these two parameters are derived explicitly for the example of a corrugated waveguide. By means of the simple substitution

$$A=R \exp(-j\delta z), \quad B=S \exp(j\delta z) \quad (2.6.27)$$

we can transform the above into coupled-wave equations of the form

$$R' - j\delta R = -j\kappa S \quad (2.6.28)$$

$$S' + j\delta S = -j\kappa R \quad (2.6.29)$$

For the boundary conditions $R(0)=1$, $S(0)=0$ the solutions of the coupled-wave equations are

$$S(z) = -j\kappa \sin(z \cdot \sqrt{\kappa^2 + \delta^2}) / \sqrt{\kappa^2 + \delta^2}, \quad (2.6.30)$$

$$R(z) = \cos(z \cdot \sqrt{\kappa^2 + \delta^2}) + j\delta \sin(z \cdot \sqrt{\kappa^2 + \delta^2}) / \sqrt{\kappa^2 + \delta^2}. \quad (2.6.31)$$

For the case of synchronism ($\delta=0$), this predicts a sinusoidal interchange of energy between R and S ,

$$S(z) = -j \sin(\kappa z), \quad R(z) = \cos(\kappa z). \quad (2.6.32)$$

A TE-TM mode converter or a directional coupler are examples for this type of interaction.

Next we consider contra-directional interactions with a forward wave of amplitude A ($=A_\mu$) and a backward wave of amplitude B ($=B_\mu$). For these, one finds differential equations of the form (see (2.6.23) and (2.6.24))

$$A' = -j\kappa B \exp(2j\delta z) \quad (2.6.33)$$

$$B' = j\kappa A \exp(-2j\delta z), \quad (2.6.34)$$

and the substitution

$$A=R \exp(j\delta z), \quad B=S \exp(-j\delta z) \quad (2.6.35)$$

transforms these into the coupled-wave equations

$$R' + j\delta R = -j\kappa S \quad (2.6.36)$$

$$S' - j\delta S = j\kappa R. \quad (2.6.37)$$

For this contra-directional interaction, we have to prescribe the boundary condition for the forward wave R at the beginning $z=0$ of the interaction region and for the backward wave S at the end $z=L$. With $R(0)=1$ and $S(L)=0$, we obtain the solutions

$$S(0) = -j\kappa / [\sqrt{\kappa^2 - \delta^2} \coth(L \cdot \sqrt{\kappa^2 - \delta^2}) + j\delta] \quad (2.6.38)$$

$$R(L) = \sqrt{\kappa^2 - \delta^2} / [\sqrt{\kappa^2 - \delta^2} \cosh(L \cdot \sqrt{\kappa^2 - \delta^2}) + j\delta \sinh(L \cdot \sqrt{\kappa^2 - \delta^2})]. \quad (2.6.39)$$

For the example of a corrugated waveguide filter, $S(0)$ represents the amplitude of the light reflected as a function of frequency δ , and $R(L)$ is the amplitude of the transmitted light. For synchronism (which corresponds to the center frequency of the filter or $\delta=0$), the above formulae simplify to

$$S(0) = -j \tanh(\kappa L), \quad R(L) = 1/\cosh(\kappa L). \quad (2.6.40)$$

An illustrative experimental result is given in Fig. 2.23 which is taken from FLANDERS et al. [2.54] and shows the wavelength dependence of the reflectivity $|S(0)|^2$ of a corrugated waveguide filter as measured with a tunable dye laser (solid curve), and predicted by (2.6.38) (dashed curve).

In the distributed feedback structures considered for lasers, we also have a contra-directional coupled-wave interaction, but with some differences compared to the case considered above. First, there is laser gain present in the waveguide, and second there is no incident wave, which is represented by the boundary conditions $R(0)=0$ and $S(L)=0$. For a detailed discussion of this interaction, we refer to KOGELNIK and SHANK [2.55].

2.6.4. Periodic Waveguides

Periodic waveguides are guides with a deformation $\Delta\varepsilon(x, y, z)$ that is periodic in z . These guides are used for a variety of purposes including the construction of filters, grating couplers, and distributed feedback lasers, and for the purpose of phase matching. The physical process that

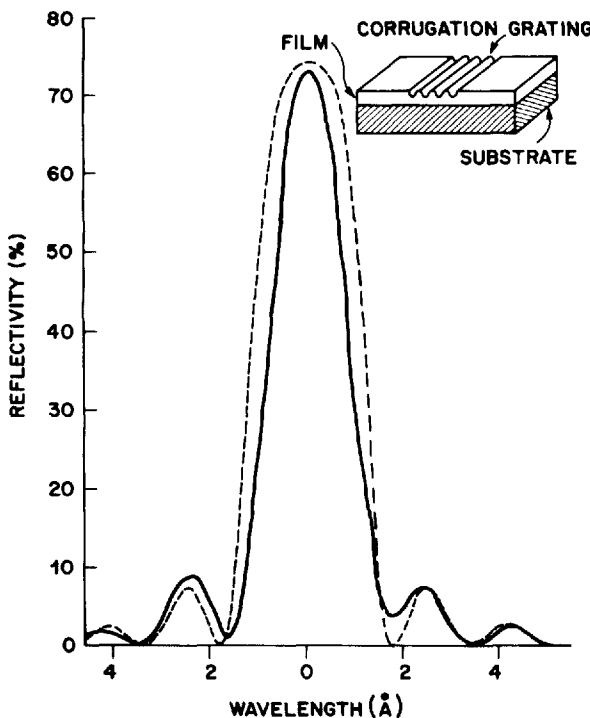


Fig. 2.23. Wavelength response of a corrugated waveguide filter. (After [2.54])

occurs in such a guide is the scattering of light by the periodic structure, which is similar to the light scattering by a diffraction grating. It can be viewed and analyzed as a coupled-mode process. We have already developed above the tools necessary for this analysis and their application is rather straightforward. First, we have to identify two modes which are at least approximately synchronous for a given optical frequency; to these we can apply the coupled-wave solutions given above. What remains to be done is the explicit evaluation of the parameters κ and δ , which we can do with the help of (2.6.21) to (2.6.24).

As an example, we will treat here the case of a corrugated planar slab waveguide, which has been used in experiments with filters and distributed feedback lasers. The modes of the planar slab guide are tabulated in Section 2.3. Figure 2.24 shows a sketch of a corrugated guide with a periodically varying film thickness

$$h(z) = h_0 + \Delta h \cos(Kz), \quad (2.6.41)$$

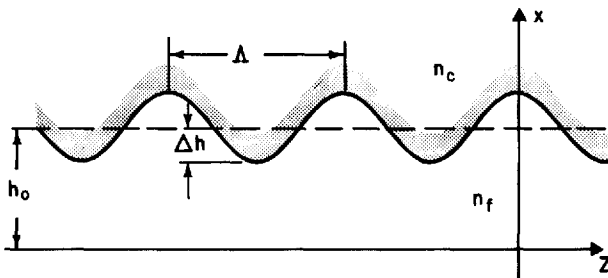


Fig. 2.24. Side view of a corrugated slab waveguide. Here h_0 is the average film thickness, Δh the amplitude of the corrugation, and Λ the period

where K is a grating constant related to the corrugation period Λ by

$$K = 2\pi/\Lambda. \quad (2.6.42)$$

In terms of the refractive indices n_f and n_c of film and cover, the corrugation produces a perturbation $\Delta\varepsilon$ which can be written as

$$\begin{aligned} \Delta\varepsilon &= \varepsilon_0(n_f^2 - n_c^2) && \text{for } h(z) > h_0, \\ \Delta\varepsilon &= -\varepsilon_0(n_f^2 - n_c^2) && \text{for } h(z) < h_0. \end{aligned} \quad (2.6.43)$$

We insert this into (2.6.21) and (2.6.22) to determine the coupling coefficients, restricting the discussion to "backward" scattering from a forward propagating mode (μ) to a backward propagating mode of the same mode number ($-\mu$).

For TE-modes we get $K_{\mu, -\mu}^z = 0$, and

$$\begin{aligned} K_{\mu, -\mu}^t &= \omega \int_{-\infty}^{+\infty} dx \Delta\varepsilon E_y^2 \approx \omega E_c^2 \int_{-\infty}^{+\infty} dx \Delta\varepsilon \\ &= \omega \varepsilon_0 E_c^2 (n_f^2 - n_c^2) \Delta h \cos(Kz) = \kappa(e^{jKz} + e^{-jKz}), \end{aligned} \quad (2.6.44)$$

where we have assumed that Δh is small enough so that we can replace $E_y(x)$ by the constant field value E_c assumed by the mode at the film-cladding interface. The relation of $K_{\mu, -\mu}^t(z)$ to the coupling constant κ of the coupled-wave equations is also indicated. From (2.3.11) and (2.3.12) we can get the normalized value of E_c , and determine κ as

$$\kappa = \frac{\pi}{\lambda} \cdot \frac{\Delta h \cdot n_f^2 - N^2}{h_{\text{eff}}} \cdot \frac{N}{N}, \quad (2.6.45)$$

where N is the effective index and h_{eff} the effective guide thickness as used before. This can be shown to agree with the formula given by MARCUSE [2.2] who also gives results for coupling between modes of unequal mode number. One remarkable thing about this formula is that neither of the subscripts c or s for cladding or substrate appear. This indicates that we get exactly the same coupling constant κ when the corrugation is made on the substrate-film interface instead of the film-cover interface. The reason for this may be found in (2.3.11) which indicates that a smaller value of $(n_f^2 - n_s^2)$ is exactly balanced by a larger value of the field strength E_s at the film-substrate interface.

Figure 2.25, taken from SHANK et al. [2.56], shows the dependence of κ on film thickness h for the example of a GaAlAs waveguide with

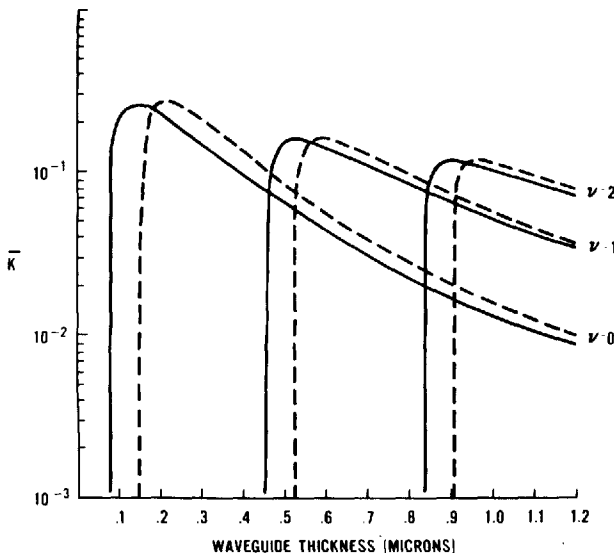


Fig. 2.25. Normalized coupling constant $\bar{\kappa} = \lambda\kappa/(2\pi\Delta h)$ as a function of waveguide thickness for a GaAlAs waveguide with $n_f = 3.59$, $n_s = 3.414$ and $n_c = 1$ (solid curves) and $n_c = 3.294$ (dashed curves) respectively for the three lowest mode orders. (After [2.56])

$n_f = 3.59$, $n_s = 3.414$ and $n_c = 1$ (solid curves) and $n_c = 3.294$ (dashed curves). The normalized quantity $\bar{\kappa} = \lambda\kappa/(2\pi\Delta h)$ is used as the ordinate. We note that the κ of each mode assumes a maximum value fairly close to cut-off.

To determine the normalized frequency δ , we compare the exponentials in (2.6.23) and (2.6.33) and find, neglecting $K_{\mu\mu}$,

$$2\delta = 2\beta_\mu - K. \quad (2.6.46)$$

The scattering is largest at the center frequency where $\delta=0$, which corresponds to a center wavelength λ_0 and a propagation constant $\beta_0=2\pi/\lambda_0$ given by the Bragg condition

$$K=2\beta_0, \quad \lambda_0=2NA. \quad (2.6.47)$$

Referring to these quantities, we can rewrite δ in the form

$$\delta=\beta_\mu-\beta_0=A\beta \approx \frac{d\beta}{d\omega} A\omega = A\omega/v_g, \quad (2.6.48)$$

where $A\omega$ is the radian frequency deviation from the center frequency, and v_g is the group velocity of (2.2.80).

To determine the coupling coefficient for backward scattering of TM modes, we proceed in a similar way by inserting the fields listed in Section 2.3, and particularly (2.3.43) and (2.3.46) into (2.6.21) and (2.6.22). As usual, we find that the algebra is more cumbersome for this case, and a few points deserve special mention. First, we find that both $K_{\mu,-\mu}^t$ and $K_{\mu,-\mu}^z$ are nonzero because of the presence of E_z components. Second, we note that both the E_x components and the values for $A\varepsilon\cdot\varepsilon/(e+A\varepsilon)$ are discontinuous across the film-cover boundary, and we have to take this into account. A consequence of this is the appearance of higher harmonics in the expression for $(K_{\mu,-\mu}^t - K_{\mu,-\mu}^z)$. The higher harmonics, however, do not lead to synchronous waves, and we neglect them by defining κ as the amplitude of the fundamental in the form

$$K_{\mu,-\mu}^t - K_{\mu,-\mu}^z = \kappa [\exp(jKz) + \exp(-jKz)] + \text{harmonics}. \quad (2.6.49)$$

Assuming again that Ah is small enough, we get after some algebra

$$\kappa = \frac{\pi}{\lambda} \cdot \frac{Ah}{h_{\text{eff}}} \cdot \frac{n_f^2 - N^2}{N} \cdot p_c, \quad (2.6.50)$$

which has the same form as the coupling constant of the TE modes, except for the appearance of a reduction factor p_c given by

$$p_c = \frac{1}{2} \left(\frac{n_f^2}{n_c^2} + \frac{n_c^2}{n_f^2} \right) \left(\frac{N^2}{n_f^2} - \frac{N^2}{n_c^2} + 1 \right) / \left(\left(\frac{N^2}{n_f^2} + \frac{N^2}{n_c^2} - 1 \right) \right). \quad (2.6.51)$$

MARCUSE [2.2] has made the additional assumption that $n_f \approx n_c$, and for this case our expression agrees with his. Note that p_c can cause a

considerable reduction. Consider, for instance, the practical example where $n_f \approx n_s \approx N$. Here we find that p_c approaches zero if $n_f/n_c \approx \sqrt{2}$. On the other hand, if all indices are about the same ($n_f \approx n_s \approx n_c \approx N$) we then have $p_c = 1$.

2.6.5. TE-TM Mode Conversion

We have mentioned before that the conversion from TE to TM modes can be regarded as another case of a coupled-wave interaction [2.51, 52]. In this final subsection, we sketch briefly, how this mode conversion is treated with the coupled-mode formalism presented in this section. We consider TE to TM mode conversion due to a tensor perturbation $\Delta\epsilon_{ij}(x)$ of the form

$$\Delta\epsilon_{ij} = \begin{pmatrix} \Delta\epsilon_1 & \eta & 0 \\ \eta & \Delta\epsilon_2 & 0 \\ 0 & 0 & \Delta\epsilon_3 \end{pmatrix} \quad (2.6.52)$$

This can be caused, for example, by application of a *dc* electric field to a planar electro-optic waveguide. Only two modes are assumed present in the guide, a TE mode with the field distribution $E_E(x)$ and a TM mode with the field $E_M(z)$. The corresponding propagation constants are β_E and β_M , and the complex amplitudes are $A_E(z)$ and $A_M(z)$, and we write for the transverse component $E_t(x, z)$ of the total field in the guide

$$E_t = A_E \cdot E_{Et} \exp(-j\beta_E z) + A_M \cdot E_{Mt} \exp(-j\beta_M z). \quad (2.6.53)$$

Only the TM mode contributes to the longitudinal component E_z , which, in analogy to (2.6.18), is written as

$$E_z = \frac{\epsilon}{\epsilon + \Delta\epsilon_3} A_M E_{Mz} \exp(-j\beta_M z) \approx A_M E_{Mz} \exp(-j\beta_M z). \quad (2.6.54)$$

With this, we can use (2.6.14) to calculate the induced polarization and obtain, after insertion into (2.6.11), for the changes of the complex amplitudes

$$A'_E = -j\omega \int_{-\infty}^{+\infty} dx E_{Et}^* \Delta\epsilon_{ij} E_j \exp(j\beta_E z), \quad (2.6.55)$$

$$A'_M = -j\omega \int_{-\infty}^{+\infty} dx E_{Mt}^* \Delta\epsilon_{ij} E_j \exp(j\beta_M z). \quad (2.6.56)$$

If we combine this with (2.6.52), (2.6.53) and (2.6.54), we can write these equations in the form

$$A'_E = -j\Delta\beta_E A_E - j\kappa A_M \exp[-j(\beta_M - \beta_E)], \quad (2.6.57)$$

$$A'_M = -j\Delta\beta_M A_M - j\kappa A_E \exp[j(\beta_M - \beta_E)], \quad (2.6.58)$$

where we have defined the coupling constant as

$$\kappa = \omega \int_{-\infty}^{+\infty} dx \eta E_{Mx} E_{Ey}^* = \omega \int_{-\infty}^{+\infty} dx \eta E_{Mx}^* E_{Ey}, \quad (2.6.59)$$

and the induced changes in the propagation constant as

$$\Delta\beta_E = \omega \int_{-\infty}^{+\infty} dx \Delta\varepsilon_2 E_{Ey} E_{Ey}^*, \quad (2.6.60)$$

$$\Delta\beta_M = \omega \int_{-\infty}^{+\infty} dx (\Delta\varepsilon_1 E_{Mx} E_{Mx}^* + \Delta\varepsilon_3 E_{Mz} E_{Mz}^*). \quad (2.6.61)$$

It is easy to see that (2.6.57) and (2.6.58) can be transformed into the standard form (2.6.28) and (2.6.29) of the coupled-wave equations by using (2.6.27) and a normalized frequency deviation δ of the form

$$2\delta = \beta_M - \beta_E + \Delta\beta_M - \Delta\beta_E \quad (2.6.62)$$

which, again, indicates the degree of deviation from synchronism. The mode conversion problem is now cast in a form that allows us to apply directly the coupled-wave solutions of Subsection 2.6.3. The overlap integrals of (2.6.59), (2.6.60) and (2.6.61) have to be evaluated for each specific case; examples are given in YARIV [2.51], and SOSNOWSKI and BOYD [2.52].

References

- 2.1. N. S. KAPANY, J. J. BURKE: *Optical Waveguides* (Academic Press, New York, 1972).
- 2.2. D. MARCUSE: *Theory of Dielectric Optical Waveguides* (Academic Press, New York, 1974).
- 2.3. W. W. ANDERSON: IEEE J. Quant. Electron. QE-1, 228 (1965).
- 2.4. A. REISINGER: Appl. Opt. 12, 1015 (1973).
- 2.5. I. P. KAMINOW, W. L. MAMMEL, H. P. WEBER: Appl. Opt. 13, 396 (1974).
- 2.6. D. F. NELSON, J. MCKENNA: J. Appl. Phys. 38, 4057 (1967).
- 2.7. S. YAMAMOTO, Y. KOYAMADA, T. MAKIMOTO: J. Appl. Phys. 43, 5090 (1972).

- 2.8. V. RAMASWAMY: *Appl. Opt.* **13**, 1363 (1974).
- 2.9. V. RAMASWAMY: *J. Opt. Soc. Am.* **64**, 1313 (1974).
- 2.10. P. K. TIEN: *Appl. Opt.* **10**, 2395 (1971).
- 2.11. S. J. MAURER, L. B. FELSEN: *Proc. IEEE* **55**, 1718 (1967).
- 2.12. H. K. V. LOTSCH: *Optik* **27**, 239 (1968).
- 2.13. H. KOGELNIK, V. RAMASWAMY: *Appl. Opt.* **13**, 1857 (1974).
- 2.14. K. ARTMANN: *Ann. Physik* **2**, 87 (1948);
H. K. V. LOTSCH: *Optik* **32**, 116, 189, 299, 553 (1970/71).
- 2.15. H. KOGELNIK, T. P. SOSNOWSKI, H. P. WEBER: *IEEE J. Quant. Electron* **QE-9**, 795 (1973).
- 2.16. J. J. BURKE: *Opt. Sci. Newsletter* **5**, 31 (Univ. Arizona, 1971).
- 2.17. J. MCKENNA: *Bell Syst. Tech. J.* **46**, 1491 (1967).
- 2.18. D. MARCUSE: *Light Transmission Optics* (Van Nostrand Reinhold Co., New York, 1972).
- 2.19. R. B. ADLER: *Proc. IRE* **40**, 339 (1952).
- 2.20. W. P. ALLIS, S. J. BUCHSBAUM, A. BERS: *Waves in Anisotropic Plasmas* (John Wiley & Sons, New York, 1962).
- 2.21. H. KOGELNIK, H. P. WEBER: *J. Opt. Soc. Am.* **64**, 174 (1974).
- 2.22. L. D. LANDAU, E. M. LIFSHITZ: *Electrodynamics of Continuous Media* (Pergamon Press, Oxford, 1960).
- 2.23. L. D. LANDAU, E. M. LIFSHITZ: *Quantum Mechanics* (Pergamon Press, Oxford, 1958).
- 2.24. A. D. BERK: *IRE Trans. AP-4*, 104 (1956).
- 2.25. K. KUROKAWA: *IRE Trans. MTT-10*, 314 (1962).
- 2.26. T. OKOSHI, K. OKAMOTO: *IEEE Trans. MTT-22*, 938 (1974).
- 2.27. H. KOGELNIK, T. LI: *Appl. Opt.* **5**, 1550 (1966).
- 2.28. G. PÖSCHL, E. TELLER: *Z. Physik* **83**, 143 (1933).
- 2.29. J. P. GORDON: *Bell Syst. Tech. J.* **45**, 321 (1966).
- 2.30. E. M. CONWELL: *Appl. Phys. Letters* **23**, 328 (1973).
- 2.31. J. R. CARRUTHERS, I. P. KAMINOW, L. W. STULZ: *Appl. Opt.* **13**, 2333 (1974).
- 2.32. R. D. STANLEY, V. RAMASWAMY: *Appl. Phys. Letters* **25**, 711 (1974).
- 2.33. H. A. HAUS, R. V. SCHMIDT: *Appl. Opt.* **15**, 774 (1976).
- 2.34. B. S. JEFFREYS: In "Quantum Theory", Vol. I, ed. by D. R. Bates (Academic Press, New York, 1961).
- 2.35. L. B. FELSEN, N. MARCUVITZ: *Radiation and Scattering of Waves* (Prentice Hall, Englewood Cliffs, N. J., 1973).
- 2.36. S. SOMEKH, E. GARMIRE, A. YARIV, H. L. GARVIN, R. G. HUNSPERGER: *Appl. Opt.* **13**, 327 (1974).
- 2.37. J. E. GOELL: *Appl. Opt.* **12**, 2797 (1973).
- 2.38. H. FURUTA, H. NODA, A. IHAYA: *Appl. Opt.* **13**, 322 (1974).
- 2.39. V. RAMASWAMY: *Bell Syst. Tech. J.* **53**, 697 (1974).
- 2.40. W. SCHLOSSER, H. G. UNGER: In *Advances in Microwaves* (Academic Press, New York, 1966).
- 2.41. J. E. GOELL: *Bell Syst. Tech. J.* **48**, 2133 (1969).
- 2.42. E. A. J. MARCATILI: *Bell Syst. Tech. J.* **48**, 2071 (1969).
- 2.43. E. A. J. MARCATILI: *Bell Syst. Tech. J.* **53**, 645 (1974).
- 2.44. W. H. ZACHARIASEN: *Theory of X-Ray Diffraction in Crystals* (John Wiley & Sons, New York, 1945).
- 2.45. S. E. MILLER: *Bell Syst. Tech. J.* **33**, 661 (1954).
- 2.46. J. R. PIERCE: *J. Appl. Phys.* **25**, 179 (1954).
- 2.47. W. H. LOUISELL: *Coupled Mode and Parametric Electronics* (John Wiley & Sons, New York, 1960).

- 2.48. C. F. QUATE, C. D. W. WILKINSON, D. K. WINSLOW: Proc. IEEE **53**, 1604 (1965).
- 2.49. H. KOGELNIK: Bell Syst. Tech. J. **48**, 2909 (1969).
- 2.50. A. W. SNYDER: J. Opt. Soc. Am. **62**, 1267 (1972).
- 2.51. A. YARIV: IEEE J. Quant. Electron. QE-**9**, 919 (1973).
- 2.52. T. P. SOSNOWSKI, G. D. BOYD: IEEE J. Quant. Electron. QE-**10**, 306 (1974).
- 2.53. I. P. KAMINOW: *An Introduction to Electrooptic Devices* (Academic Press, New York, 1974).
- 2.54. D. C. FLANDERS, H. KOGELNIK, R. V. SCHMIDT, C. V. SHANK: Appl. Phys. Letters **24**, 194 (1974).
- 2.55. H. Kogelnik, C. V. Shank: J. Appl. Phys. **43**, 2327 (1972).
- 2.56. C. V. SHANK, R. V. SCHMIDT, B. I. MILLER: Appl. Phys. Letters **25**, 200 (1974).

3. Beam and Waveguide Couplers

T. TAMIR

With 27 Figures

The basic component of integrated optics is the thin-film dielectric waveguide. As discussed in Chapter 2, this waveguide exhibits properties that make it very similar to metallic guides which have been utilized in carrying energy at microwave frequencies. However, two major differences exist between metallic microwave guides and dielectric optical waveguides. First, typical guide dimensions at optical frequencies are of the order of $1\text{ }\mu\text{m}$ as compared to the typical dimension of 1 cm at microwave frequencies, which is 10^4 larger. Secondly, microwave guides are usually closed and all of the energy flows inside the guide. In contrast, optical dielectric guides are open so that, although most of the energy is within a thin film, the field nevertheless extends also into the exterior space.

The dimensional difference between optical and microwave guides requires different fabrication techniques which are subject to different tolerances and capabilities. These techniques will be treated in Chapters 5 and 6. The present chapter is concerned with the second difference, namely the fact that optical guides are of the open variety. Because of this, many of the techniques for producing the fields in optical guides are quite different from those used in closed metallic guides, even though abundant analogies also exist. One main reason for differences in techniques is the fact that the antennas (or probes) used to excite the fields in microwave guides are usually of relatively small size. In optics, a principal source of energy is a laser beam which can be regarded as being generated by an antenna having a large aperture. Because of the large difference in the antenna size, the excitation problems and their solutions for optical guides are different from those of microwave guides.

The major portion of the present chapter is therefore devoted to the devices that convert the energy of a light beam into a mode (or modes) which are guided by a thin-film dielectric layer. These devices are known as beam couplers and their operation, properties and design problems form the subject of Section 3.1. In particular, we shall discuss therein those aspects of electromagnetic fields that are most intimately related to a proper understanding of beam couplers, such as leaky waves, the properties of dielectric gratings, etc.

The remaining portion of this chapter, i.e., Section 3.2, deals with some of the other passive components that have been developed for integrated-optics applications. These components represent building blocks or links in any planar optical "circuit"; their availability and efficient operation are necessary conditions for making such circuits possible in the future. Included amongst them are couplers or connectors that transfer energy from one waveguide to another waveguide of different size or shape, mode converters, filters and others. For other varieties of planar optical components, reference should be made to Chapter 4, which deals with modulators, and Chapter 6, which considers a variety of components made of crystalline (mostly GaAs) material, including lasers and detectors.

3.1. Coupling of Beams to Planar Guides

The conversion of a laser beam into a surface wave and its reciprocal operation, i.e., the conversion of a surface wave into an outgoing beam, have generated numerous experimental and theoretical investigations. Most of these have been concerned with the coupling of a beam into a *planar* waveguide, i.e., one which has a large width, as opposed to *linear* waveguides of the strip or channel types. As a result, the problem of beam-to-surface-wave coupling is now practically solved for planar guides; for these, grating couplers appear to offer the most satisfactory arrangement for integrated-optics applications.

The various beam couplers for planar guides can be classified into two principal categories: (a) transverse couplers, in which the beam is focused on an exposed cross-section of the guide, and (b) longitudinal couplers, in which the beam is incident obliquely onto the guide. The former category involves the, so-called, "direct" or "head-on" couplers, whereas the latter includes the prism, grating and taper couplers. All of these are discussed separately below, most of the emphasis being placed on the more important prism and grating couplers.

3.1.1. Transverse Couplers

Two typical couplers of the transverse variety are sketched in Fig. 3.1, which shows that the laser beam is incident directly onto the transverse (cross-sectional) plane $z=0$ of the waveguide. The designation of this arrangement as a "direct" or "head-on" coupling is therefore evident. The schemes shown in Fig. 3.1 are scaled-down versions of methods used at

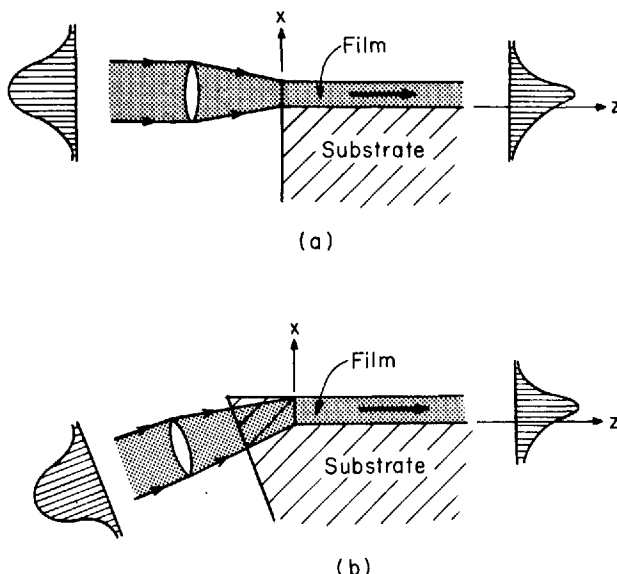


Fig. 3.1a and b. Transverse method for coupling a light beam into a surface wave:
a) Film edge is flush with substrate edge; b) Film edge is embedded in substrate

microwaves for generating a surface wave in a slab by means of a large aperture antenna; however, the antenna at microwaves is usually a horn instead of the lens shown here for optical waves. Consequently, the transverse couplers are also referred to as "end-fire", which is the microwave term for the field incident onto (or radiated from) the planar waveguide.

The conversion of the beam energy into a desired surface wave is achieved in the present case by matching the beam-field incident from the left to the surface-wave field, which is progressing to the right of the $z=0$ boundary. In particular, the fundamental TE_0 mode has the amplitude contour indicated in Fig. 3.1, in agreement with the discussion in Section 2.3. This contour is very similar to the Gaussian shape of a laser beam. The required field matching can therefore be effected by suitable reducing the input beam width so as to conform as closely as possible to the surface-wave field [3.1-3].

If any mismatch occurs between the profile of the incident beam and the shape of the surface-wave field, energy is lost into higher undesirable surface-wave modes and into scattered fields, i.e., radiation modes. In principle, the field-contour matching can be made nearly perfect, for

instance, by appropriately shaping the lens. Thus, the coupling schemes of Fig. 3.1 could be nearly 100% efficient. In practice, however, considerable losses occur if the planar guide boundary (at $z=0$) is not perfectly flat and clean. Also, because the guiding film thickness is of the order of 1 μm , the lens and the laser beam require critical alignment and sensitive micromanipulation. Owing to these restrictive conditions, transverse couplers have been employed in only a few number of cases [3.4-6], as described also in Subsection 6.1.3.

For general integrated-optics applications, the transverse-coupling scheme is therefore not too encouraging and other methods described below appear to be more promising.

3.1.2. The Prism Coupler

The coupling of a beam into a planar structure by means of a prism having a denser refractive index has been considered well before the advent of low-loss optical waveguides. Although the first theoretical studies can be traced to the year 1962 [3.7], the first laboratory experiments have been reported in 1964 by OSTERBERG and SMITH [3.8] who used a prism set-up that is essentially the same as the one in use today for coupling a light beam into an optical surface wave. Later, OTTO [3.9] used a similar set-up to couple photons to plasmons and his technique was subsequently applied by physicists to the study of other surface-wave phenomena, such as phonons, magnons, excitons, etc. [3.10]. However, it was only in 1969 that two research groups, one at the University of Washington and another at the Bell Telephone Laboratories, have independently demonstrated [3.11-12] that prism couplers having high efficiencies can be built for optical surface waves. Afterwards, many investigations have contributed in bringing the theory to a high degree of sophistication and the experimental work has shown that prism couplers can be constructed for highly efficient broad-band operation [3.13-28].

Coupled-Mode Description

The principle of operation of prism couplers is illustrated in Fig. 3.2. Consider first the half-space geometry shown in Fig. 3.2a where the upper medium has a refractive index n_p which is higher than the refractive index n_a of the lower medium, which may be assumed to be air. Under these circumstances, a plane wave incident at an angle θ undergoes total reflection if θ satisfies

$$\theta > \theta_c = \sin^{-1}(n_a/n_p), \quad (3.1)$$

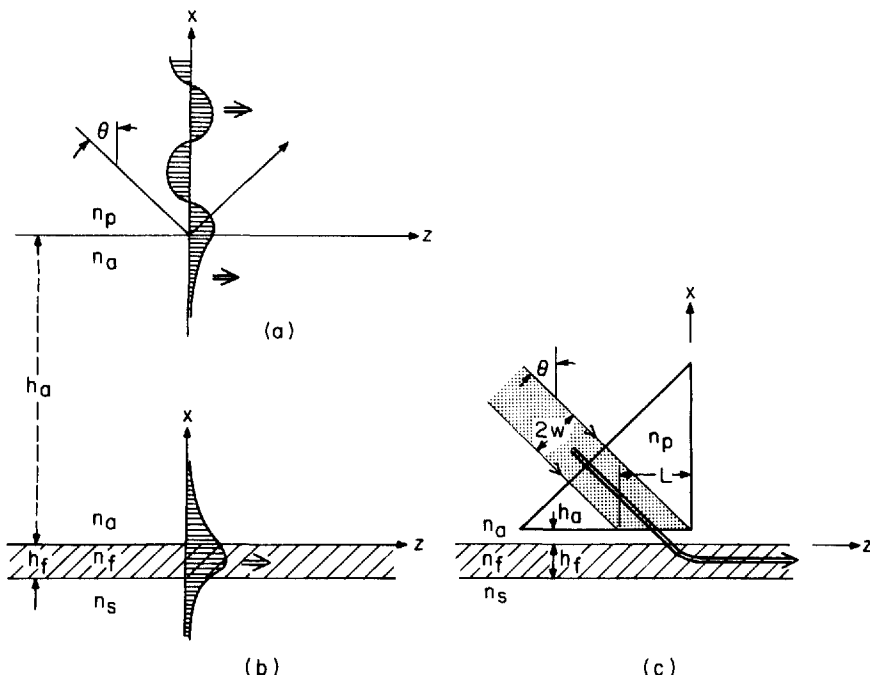


Fig. 3.2a-c. Coupled-mode description of prism couplers: a) Field of a plane wave incident from a denser medium and undergoing total reflection at the interface to a rarer medium, i.e., $\theta > \theta_c = \sin^{-1}(n_s/n_p)$. b) Field of a surface wave propagating along a thin film, with $n_f > n_a, n_s$; c) The two preceding configurations can be brought together by letting h_a become very small, thus obtaining the prism-air-gap-thin-film structure shown here. The incident field now couples to the surface wave via the evanescent field in the air gap

where θ_c is the critical angle of total reflection. Under condition (3.1), the superposition of the incident wave and the totally reflected wave yield a standing wave along the vertical x direction in the denser medium; below the interface $x=0$ between the two media, the field is exponentially decaying with x . The field amplitude is then as indicated in Fig. 3.2a by the shaded contour. The energy flow in both media is horizontal, as suggested by the heavy arrows. Because of this horizontal flow, the entire field can be regarded as a mode that propagates along the z direction. In fact, this field is a radiation mode of the half-space geometry, which is similar to the radiation mode along the planar waveguides discussed in Section 2.3.

Consider next the thin-film waveguide of thickness h_f , in Fig. 3.2b, where it is assumed that a surface wave is propagating, its field amplitude being indicated by the shaded contour. The upper region (cover)

has a refractive index n_c which is taken identical to that in the lower medium in Fig. 3.2a, so that $n_c = n_a$ here. As discussed in Sect. 2.1, the field of the surface wave in both this upper region and in the substrate is decaying exponentially away from the layer. Inside the film, the field varies sinusoidally and the entire surface-wave mode propagates along the horizontal z direction.

The two configurations of Fig. 3.2a and b can be made to approach each other through the medium of refractive index n_a , i.e., we now consider a geometry that combines the two configurations by assuming a height h_a for the common medium, as indicated by the dashed line. In general, we expect that the modes in the combined structure should be different from those of the separate configurations. However, the two separate modes considered before have exponential fields in the common medium. This implies that these modes interact weakly with each other if the height h_a is sufficiently large. The fields in the combined configuration can therefore be obtained by using coupled-mode considerations, which are discussed in Section 2.6. In the present case, the exponential form of the fields in the coupling region implies that energy is transferred via a tunneling effect, which is often referred to as optical tunneling due to frustrated total reflection [3.7, 29, 30].

An important property of weakly coupled modes is that energy can be interchanged between them. Such an interchange is complete if the two modes are phase-matched. In the present case, this condition is satisfied if

$$k_p \sin \theta = \beta_{sw}, \quad (3.2)$$

where k_p is the plane-wave propagation factor in the uppermost medium and β_{sw} is the propagation factor of the surface wave. A complete interchange of energy then occurs if the interaction length (along the longitudinal z direction) is given by

$$\kappa L = \pi/2 \quad (3.3)$$

where κ is the coupling coefficient between the radiation mode of Fig. 3.2a and the surface-wave mode of Fig. 3.2b. Thus, if power is introduced only in the radiation mode, it will be completely transferred to the surface-wave mode after travelling over a distance along z equal to the coupling (interaction) length L given in (3.3).

This coupled-mode approach actually describes the principle of operation of the prism coupler, the realization of which is sketched in Fig. 3.2c. A beam is incident through a prism of index n_p , the angle of incidence θ being chosen so as to satisfy both the total-reflection condition (3.1) and the phase-matching condition (3.2). Hence, within the

incident beam domain shown in Fig. 3.2c, the field is described to a good approximation by the radiation mode of Fig. 3.2a. The medium of index n_a between the prism and the film waveguide is usually air, thus providing an air-gap thickness h_a . The coupling of energy from the radiation mode, which in this case is well identified by the beam field, can occur only over a length L given by

$$L = 2w \sec \theta, \quad (3.4)$$

so that the coupling coefficient κ must have a value given by (3.3) and (3.4) if complete energy transfer is desired. This can be achieved by adjusting the height h_a of the air gap until the desired value of κ is obtained.

Basic Characteristics

The foregoing coupled-mode description of the prism coupler is valid qualitatively but it is only approximate quantitatively. However, the only major quantitative error is that complete transfer of energy from the beam to the surface wave cannot occur even if all media are lossless. This is due to the fact that we have so far neglected the amplitude variation within the beam cross-section. A more accurate analysis shows that a maximum of about 80% of the energy can be coupled in the case of incident beams having uniform or Gaussian profiles [3.17-21], as discussed in Subsection 3.1.5 under *Effect of beam form*.

For many purposes, however, the above description is quite adequate in explaining the major features of the prism coupler. Thus, the coupled-mode approach yields a good estimate for the angle θ in (3.2) and the air-gap thickness h_a in (3.3) and (3.4). In addition, for a beam having a uniform amplitude, it is evident that it must be incident exactly as shown in Fig. 3.2c, i.e., its right-hand boundary must intercept the prism corner. If the beam is shifted to the right of that corner, a portion of the beam domain falls outside the air gap region; this portion of beam energy is reflected or transmitted and thus causes a loss in coupling efficiency. If, on the other hand, the right-hand boundary of the beam falls to the left of the prism corner, energy from the surface wave can be coupled back into the radiation mode of the prism through the air-gap portion which is to the right of the beam boundary. It thus follows that a condition for maximum coupling in the case of a uniform beam is that the right-hand beam boundary just intersects the prism corner. However, exact analysis has shown [3.19-21] that, for maximum excitation of Gaussian beams, the beam must be incident at a distance $z_c = 0.733 w \sec \theta$ to the left of the prism corner, where now w is the beam-spot radius. These quantitative aspects are dealt with further in Subsection 3.1.5 under *Role of beam width*.

An inconvenience of prism couplers is that the prism material must have a high refractive index n_p . This follows because usually the film index n_f is close to that of the substrate n_s , in which case $\beta_{sw} \approx k_f$. Hence, as $\sin \theta$ is smaller than unity, (3.2) implies that $n_p > n_f$, so that the prism must be denser than the film material. In the case of GaAs waveguides (see Section 6.1), their high refractive index requires prisms with very high indices, which are not always easily available; this explains why the transverse (“end-fire”) couplers have been used instead.

Another disadvantage of prism couplers is the critical adjustment of the air gap whose height h_a is usually less than half a vacuum wavelength [3.30]. The fact that dust particles may accumulate in its interior and thus produce losses is a further drawback. These disadvantages can, however, be largely alleviated by using a suitable bonding material to fill the air gap [3.16, 22], a procedure that stabilizes the structure and also increases its realizable efficiency. In this context, also refer to Subsection 3.1.5 for gaps having variable heights, which are capable of achieving theoretical coupling efficiencies close to 100%, with measured values of 88% [3.22].

To conclude the present discussion, we observe that the prism coupler shown in Fig. 3.2c converts a beam into a surface wave and is therefore known as an input coupler or a surface-wave launcher. By reciprocity, a surface wave incident from the right would couple energy into the prism and thus radiate a beam towards the upper left region. This can be described in Fig. 3.2c by simply reversing the directions of the arrows in the diagram. Such a coupler would convert a surface wave into a beam and is therefore known as an output coupler or a beam launcher. Although beam-to-surface-wave and surface-wave-to-beam conversions can be reciprocal operations, practical input and output couplers may involve beams of different forms, in which case these two types of couplers are not exactly reciprocal [3.23]. These aspects are dealt with further in Subsection 3.1.5.

3.1.3. The Grating Coupler

The coupling of a beam into a thin film by means of a dielectric grating has been first reported by DAKSS et al. [3.31] who used a thick photoresist layer exposed to a 4800 Å laser interferometer fringe pattern and subsequently developed to yield a periodicity $d = 0.665 \mu\text{m}$. Their work was immediately followed by that of KOGELNIK and SOSNOWSKY [3.32] who used a thick dichromated gelatin layer, which was exposed holographically so as to produce a fringe pattern inclined at an angle of about 45° with respect to the layer surface; this increased the coupling

efficiency by taking advantage of the Bragg effect caused on the incident light by the slant fringed pattern. These experimental results were followed by many investigations [3.21, 23, 25-56, 59] which achieved a good understanding of grating couplers and other periodic dielectric structures.

As shown in Fig. 3.3, a grating coupler functions similarly to the prism coupler shown in Fig. 3.2c, except that the prism and air-gap configuration is replaced by a grating layer. This grating is often in the form of a photo-resist film which has been exposed to the interference pattern of two

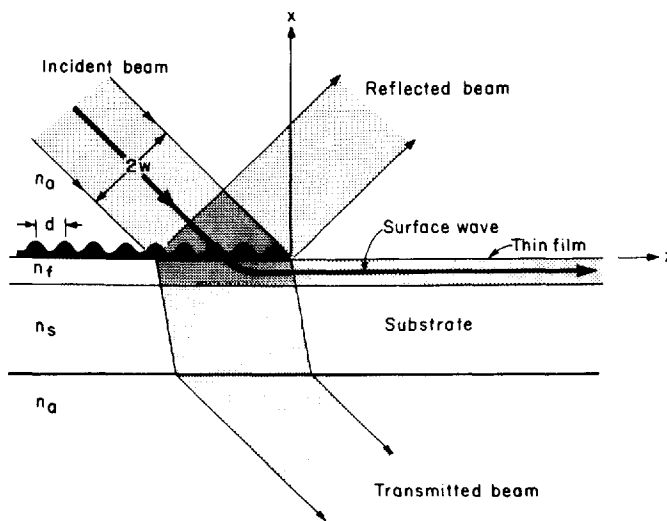


Fig. 3.3. Schematic of a grating coupler. In well designed couplers, the intensities of the reflected and transmitted beams are weak and most of the energy is coupled to the surface wave. If d/λ is large, additional (diffracted) beams may occur which usually cause undesirable losses

oppositely traveling fields obtained by splitting and re-combining a laser beam. Depending on the specific photo-resist and the developing procedure, the grating profile assumes a sinusoidal, triangular or trapezoidal shape; other, less regular and/or asymmetric shapes may also be formed [3.54].

Simple coupling considerations, such as those already described for the prism coupler, can be used to explain also the operation of the grating coupler [3.30-32]. In the latter case, the surface wave supported by the thin film must be accompanied by space harmonics in the grating

region because of the periodic nature of the grating. These harmonics have longitudinal propagation factors given by

$$\beta_v = \beta_0 + (2v\pi/d), \quad v=0, \pm 1, \pm 2, \dots, \quad (3.5)$$

where β_0 is closely equal to the surface-wave propagation factor β_{sw} if the grating acts as only a small perturbation of the thin-film waveguide. Recalling that for surface waves $\beta_{sw} > k_a = 2\pi/\lambda_a$, where λ_a is the wavelength in the upper (usually, air) region, the incident beam cannot be phase-matched to β_0 because its phase along the film is $k_a \sin \theta < k_a$. However, due to the negative values of v in (3.5), values of $|\beta_v|$ smaller than β_0 are possible and they can satisfy a phase-match condition provided

$$k_a \sin \theta = \beta_v \quad (3.6)$$

which can be achieved by taking suitable values of v, d, λ_a and θ .

The foregoing implies that the incident beam can be phase-matched to one of the space harmonics of the surface wave in the grating region. Thus the previous phase-match condition (3.2) is now replaced by (3.6), which is more flexible because it can be satisfied by one or more negative values of v . As all of the space harmonics are coupled together to form the complete surface-wave field in the grating region, energy introduced from the beam into one of these harmonics is also coupled to the fundamental harmonic; as it travels to the right and past the grating region, this fundamental harmonic becomes the familiar surface wave supported by the thin film.

This coupled-wave description of the grating-coupler operation is helpful qualitatively. Thus, as in the prism coupler, an incident beam of uniform intensity couples most efficiently to the surface wave if its boundary just intersects the end of the grating layer, as indicated in Fig. 3.3. Although coupled-wave theory [3.43,55] has been applied to grating couplers, a more sophisticated leaky-wave approach provides a more powerful analytical tool [3.21, 34-41, 45, 47-53, 59], as discussed in the next two subsections.

The main disadvantage of the grating coupler is that a substantial portion of the incident energy is often transmitted through the film and then lost into the substrate because, unlike the prism coupler, the grating does not operate under a total reflection regime. In addition, if the ratio d/λ_a is not sufficiently small, energy can be lost into higher-order diffracted beams produced by the grating. Thus, grating couplers cannot easily attain the high efficiencies of prism couplers. Nevertheless, DALGOUTTE [3.44] achieved a beam-to-surface-wave coupling efficiency of 70.5% by adding a small prism onto a reverse grating coupler. However, this prism destroys the pure planar geometry which is the main

advantage of grating couplers. Although not yet experimentally verified, PENG and TAMIR [2.50, 51] have shown that this efficiency can be nearly 100% if the grating thickness and its profile shape are suitably designed.

Further theoretical and experimental work need to be carried out to fully exploit the capabilities of the grating coupler. However, its essentially planar geometry and relatively easy fabrication by means of the latest etching techniques suggest that the grating coupler is most promising for future integrated optics applications.

3.1.4. Leaky-Wave Theory of Beam Couplers

A good understanding of the operation of beam couplers requires the generalization of the surface-wave concept to that of a leaky wave. As described here, this generalization involves extending the concept of plane waves in free space to inhomogeneous plane-wave fields.

Inhomogeneous Plane Waves

We first recall that a plane wave is a solution of the Helmholtz equation

$$(\nabla^2 + k^2) A = 0, \quad (3.7)$$

where propagation in an unbounded medium is considered. Here A stands for any one component of the electromagnetic field. Assuming a two-dimensional situation ($\partial/\partial y = 0$) and a time dependence of $\exp(j\omega t)$, the solution of (3.7) in rectangular (x, z) coordinates becomes

$$A = A_0 \exp[-j(k_x x + k_z z)], \quad (3.8)$$

where

$$(k_x^2 + k_z^2)^{1/2} = k = \omega/c = 2\pi/\lambda. \quad (3.9)$$

For k_x and k_z real, A in (3.8) is a homogeneous plane wave. Its field is well known and its energy propagates at an angle Φ with respect to the x axis, as determined by k_x and k_z which now are proportional to directional cosines, so that

$$\begin{aligned} k_x &= k \cos \Phi, \\ k_z &= k \sin \Phi. \end{aligned} \quad (3.10)$$

In general, however, k_x and k_z must comply only with (3.9) and they are therefore not restricted to purely real values as implied by (3.10). Thus,

if we let Φ be a complex variable, both k_x and k_z become also complex, in which case they may be written as

$$\begin{aligned} k_x &= b - ja \\ k_z &= \beta - j\alpha \end{aligned} \quad (3.11)$$

The quantities a and α represent amplitude decay¹, as can be determined by inserting (3.11) into (3.8). The field in this case is still a plane wave because its equi-phase and equi-amplitude contours are plane, as illustrated in Fig. 3.4a. However, this wave is known as an inhomogeneous plane wave because of the variation of the field intensity along any equi-phase plane. It can be shown [3.56] that the equi-phase and equi-amplitude contours are orthogonal and that the energy flux (Poynting vector) is oriented parallel to the equi-amplitude lines, as indicated in Fig. 3.4a. The inhomogeneous plane wave thus progresses at a (real) angle $\theta = \tan^{-1}(\beta/b)$ with respect to the x axis.

The reflection and refraction of an inhomogeneous plane wave can be treated as in Subsection 2.1.1 where a homogeneous plane wave was discussed. If we replace the real angles θ_1 and θ_2 in (2.1.3) by the complex angle Φ via (3.10), we obtain that the Fresnel reflection coefficient for perpendicular polarization (TE modes) can be written as

$$R_{\text{TE}} = \frac{k_{x1} - k_{x2}}{k_{x1} + k_{x2}}. \quad (3.12)$$

Similarly, by using (2.1.4) for parallel polarization (TM modes) we get the reflection coefficient

$$R_{\text{TM}} = \frac{k_{x2} - (n_2/n_1)^2 k_{x1}}{k_{x2} + (n_2/n_1)^2 k_{x1}}. \quad (3.13)$$

Here k_{x1} and k_{x2} refer to the values of k_x given by (3.9), but the subscripts 1 and 2 denote the two media with refractive indices n_1 and n_2 , as indicated in Fig. 3.4b. The angles θ_1 and θ_2 here are real, as defined by $\sin^{-1}(\beta/k_1)$ and $\sin^{-1}(\beta/k_2)$, respectively; they should therefore not be confused with the complex angles Φ_1 and Φ_2 defined by (3.10). The value of k_z in the two regions is the same ($k_{z1} = k_{z2} = k_z$) because of the continuity conditions at the $x=0$ boundary.

¹ The decay parameter α is not due to losses in materials, but now α represents a loss due to radiation, as will be clarified soon. As in Chapter 2, all the materials considered here are assumed lossless.

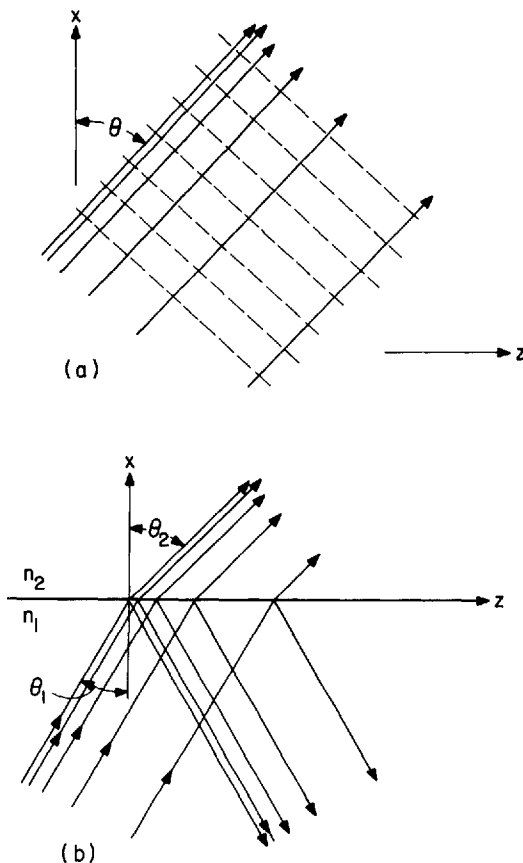


Fig. 3.4a and b. Fields of inhomogeneous plane waves: a) Equi-phase and equi-amplitude contours (shown by dashed and solid lines, respectively) of an inhomogeneous plane wave in free space; b) Reflection and refraction (leakage) of a plane inhomogeneous wave at the interface between two dielectric media. The density of the amplitude (flux) lines suggests the magnitude of the field intensity, which decays in a direction parallel to the equi-phase contours

By virtue of the analogy with homogeneous plane waves, the inhomogeneous plane waves reflect and refract at a dielectric boundary as suggested in Fig. 3.4b, the reflection coefficients being determined by (3.12) or (3.13) for any given value of k_z . However, total reflection does not occur for inhomogeneous plane waves even if the incidence angle θ_1 is larger than the critical angle $\theta_c = \sin^{-1}(n_2/n_1)$. For homogeneous plane waves, total reflection occurs because k_{x1} is real whereas k_{x2} is imaginary so that both R_{TE} and R_{TM} have a magnitude of unity. However,

for inhomogeneous plane waves, both k_{x_1} and k_{x_2} are complex so that, in general, the magnitude of the reflection coefficient cannot be unity.

It therefore follows that inhomogeneous waves refract some energy into the less-dense medium even if incidence occurs beyond the critical angle. However, for $\theta_1 > \theta_c$ and for small inhomogeneity, i.e., $\beta \gg \alpha > 0$ in (3.11), the refracted energy is small (because the magnitude of the reflection is close to unity) and therefore some energy “leaks” out into the upper region 2. Because of this energy leakage, the fields of inhomogeneous plane waves above planar interfaces have been known as leaky waves [3.56,7].

Leaky Waves along Layered Media

When an inhomogeneous plane wave is introduced into a dense dielectric layer, it can bounce between the two boundaries very much like a homogeneous plane wave that produces the surface wave discussed in Section 2.1. In fact, the self-consistency (transverse-resonance) condition (2.1.12) can still be used to identify a mode, which is now of the leaky rather than the surface-wave type. For the present case, the phase shifts Φ_s and Φ_a are complex rather than real, but the picture of the wave inside the layer is still that of a zig-zag wave, as shown in Fig. 2.5. However, because Φ_a and Φ_s (and also k_x and k_z) are complex, the fields in the air and substrate are not purely evanescent but they are of the form described in Fig. 3.4.

In the context of the prism and grating couplers, the guided modes of the leaky-wave type are illustrated in Fig. 3.5. In a prism-air-gap configuration, the refractive indices usually satisfy $n_p > n_f > n_s > n_a$. In this case, the phase shift Φ_s is given by the same expression as that for a film above a substrate with no prism present. However, the phase shift Φ_a at the film-air boundary is a more complicated expression because of the superimposed prism material. As a result, solutions of the transverse-resonance relation (2.1.3) exist only for complex values of k_z , leading to the field depicted in Fig. 3.5a. In this case, the mode consists of an inhomogeneous plane wave which bounces inside the film and leaks into both the air-prism and the substrate regions. However, the leakage into the substrate is near grazing and thus the total energy flux is negligible there [3.57]. In the upper (prism) region, the leakage is at an angle slightly smaller than that of the zig-zag wave in the film. Thus, as the plane wave bouncing inside the film progresses towards the right, most of its energy leaks out into the exterior prism region. This leakage represents energy radiated away in the form of a beam, which progresses through the upper (prism) material. The radiation loss is consistent with a field decay of the form $\exp(-\alpha z)$ along the longitudinal direction.

For dense layers, many leaky-wave modes are possible because the transverse resonance relation admits an infinite number of complex solutions. However, only a few of these solutions exhibit slow leakage, i.e., $\alpha \ll \beta$; these slowly leaking waves can be regarded as being guided over a long distance along the denser layers. It is interesting to observe

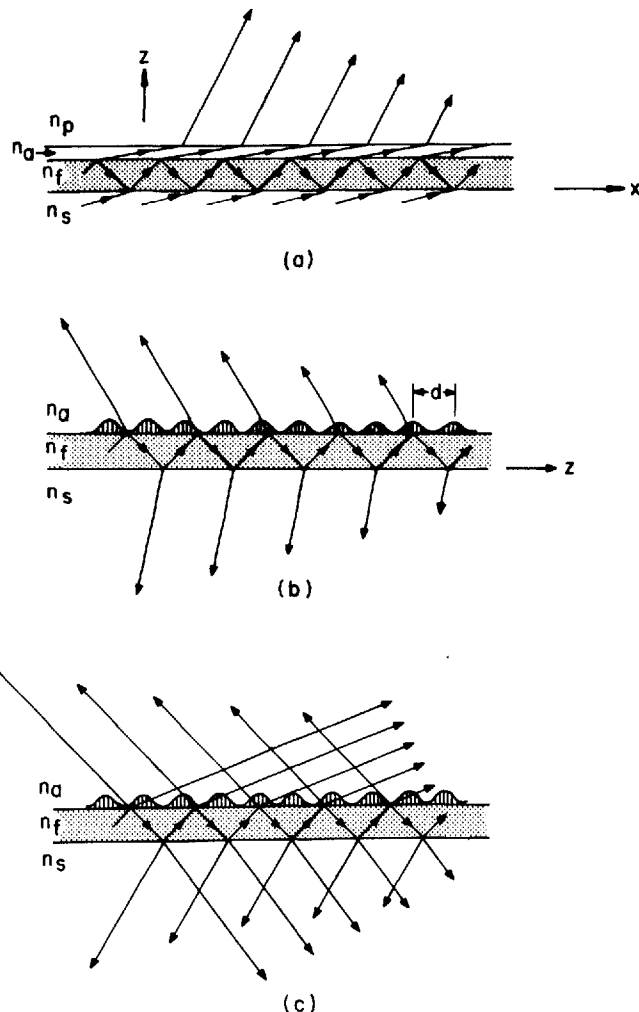


Fig. 3.5 a-c. Modes of the leaky wave type: a) Forward leaky wave guided by prism-air-gap configuration; b) Backward leaky wave guided by a dielectric grating; c) Two-beam leaky wave guided by a dielectric grating. All field amplitudes decay along the longitudinal z direction

that leaky waves also appear along layers having a refractive index n_f lower than n_s of the substrate [3.56, 57, 99]. However, these leaky waves usually decay rapidly with z , i.e., α is comparable to β , so that they are not truly guided by the layer and therefore have found little application so far.

Leaky Waves along Dielectric Gratings

In the case of dielectric gratings, it is not possible to define a reflection coefficient at the film-air boundary because this boundary is not planar due to the presence of the periodic grating. A transverse-resonance condition such as (2.1.3) can nevertheless be used [3.47, 53] provided the scalar quantities therein are replaced by matrices. However, this is beyond the scope of this work and the reader should consult the literature [3.53] for details. Because of periodicity, however, it is clear that a wave bouncing inside the thin film will scatter energy into the upper (cover) region at angles θ_{av} , which are given by

$$k_a \sin \theta_{av} = \beta_v = \beta_0 + (2v\pi/d), \quad v=0, \pm 1, \pm 2 \dots \quad (3.14)$$

where $k_a = k_0 n_a = 2\pi/\lambda_a$ is the propagation factor in the air (cover) medium. Here, β_0 is the propagation factor along z of the wave bouncing inside the layer and d is the grating periodicity. For those values of v such that $|\beta_v/k_a|$ is smaller than unity, θ_{av} is a real angle. Energy is thus scattered from inside the film into the upper region and propagates along directions given by the real angles θ_{av} . Because energy is also scattered back into the layer by the dielectric grating, the grating diffraction orders also produce scattering into the lower (substrate) region at angles θ_{sv} defined by

$$k_s \sin \theta_{sv} = \beta_v \quad (3.15)$$

where β_v are the same as those in (3.14) and $k_s = k_0 n_s$ refers to the plane-wave propagation factor in the substrate medium. Due to the presence of $n_s > n_a$ in (3.15), the number of scattered orders in the substrate is equal to or larger than that in the air region.

It is possible to choose d so that θ_{av} and θ_{sv} are real for only one value $v = -1$. In this case, β_{-1} is usually negative so that the field scattered in the exterior regions is inclined towards the $-z$ direction, as shown in Fig. 3.5b. This describes a leaky wave, which is similar to that in Fig. 3.5a because the fields in both cases are due to leakage out of a wave bouncing inside a film. However, the field in Fig. 3.5a exhibits a leakage whose longitudinal component (along z) progresses along the same direction as the bouncing wave in the layer; this field is therefore known as a forward leaky wave. Layered media, of which the prism configuration

is one example, can support only leaky waves of this *forward* type if conventional dielectrics are used. In contrast, the field in Fig. 3.5b has a leakage whose component along z progresses in a direction opposite to that of the bouncing wave; this is therefore known as a *backward* leaky wave.

It is also seen in Fig. 3.5b that considerable leakage occurs in both the air and substrate regions, in contrast to the situation in Fig. 3.5a where leakage was confined mostly to the upper (prism) region². A more important difference between the two cases is the fact that, by making the quantity $2\pi/d$ sufficiently small, leakage angles θ_{av} and θ_{sv} may occur for several values of v . When this happens, the first few diffraction orders produce leakage of the forward type and the remaining orders account for leakage of the backward type. Each of these orders then causes a beam to radiate into the exterior regions. A two-beam example is illustrated in Fig. 3.5c where one beam is produced by forward leakage (for $v = -1$) and another beam is due to backward leakage ($v = -2$).

Leaky Waves in Beam Couplers

To apply leaky-wave concepts to beam couplers, consider first the basic film-on-substrate configuration of Fig. 3.6a. To the left of the $z=0$ plane, we assume that a surface wave having a propagation factor β_{sw} can be guided. To the right of the $z=0$ plane, we assume that a suitable modification is made so that a leaky wave having a propagation factor $k_z = \beta - j\alpha$ can be supported instead of the surface wave. If now β is very close to β_{sw} and leakage is weak, i.e., $\alpha \ll \beta$, a surface wave varying as $\exp(-j\beta_{sw}z)$ incident from the left will be smoothly transmitted as a leaky wave varying as $\exp(-jk_z z)$ past the $z=0$ plane. Due to the leakage of energy in the region $z > 0$, power is radiated away from the thin film in the form of a beam that progresses at an angle θ in the exterior region. Thus, the plane at $z=0$ can be regarded as a junction between a surface-wave guide and a leaky-wave guide. Because it is assumed that $\beta_{sw} \approx \beta \gg \alpha$, this junction represents only a small discontinuity between the two guides and energy scattering is therefore negligible at $z=0$.

The modification required to transform a surface-wave guide into a leaky one can be either in the form of a prism, as shown in Fig. 3.6b or in the form of a grating, as shown in Fig. 3.6c. The leakage characteristics are determined by this choice of modification, which produces forward leakage in the air region above the prism, as already discussed in conjunction with Fig. 3.5a. For gratings, the leakage produces two

² Leakage in the air region can be eliminated while retaining the leakage in the substrate, thus achieving a situation that is quite analogous to that of the prism coupler. Refer to *Single-beam coupler* of Subsection 3.1.6 for a detailed discussion.

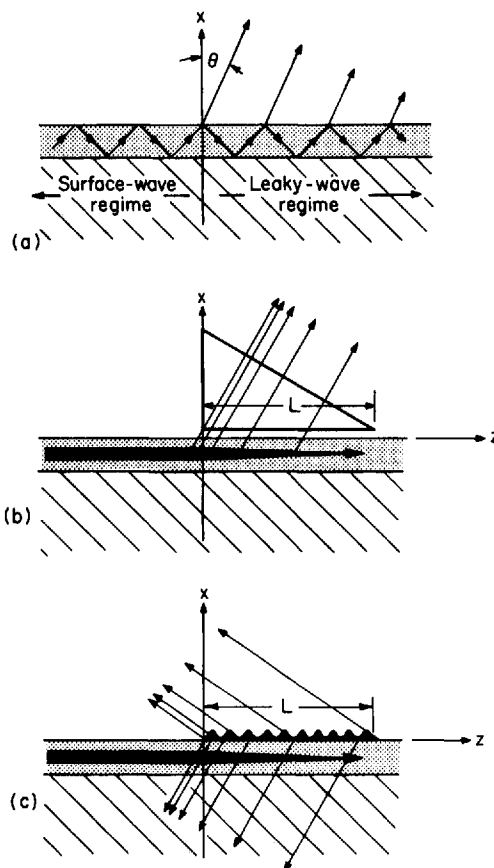


Fig. 3.6a-c. Leaky-wave description of prism and grating couplers: a) Basic film-on-substrate configuration; b) Leakage due to prism; c) Leakage due to grating. In portions b) and c), the density and thickness of flux lines suggests intensity variation. For nearly complete surface-wave-to-leaky-wave-beam conversion it is required that $\alpha L \gg 1$

backward beams, one in each of the two exterior regions, as shown in Figs. 3.6c and 3.5 b, or more than two beams, in which case both forward and backward beams usually occur, as suggested in Fig. 3.5c.

The above describes both prism and grating couplers in a unified manner in terms of a leaky wave that produces outgoing beams. A smooth transition between the surface-wave and the leaky-wave guides requires the condition

$$\beta \approx \beta_{sw} \gg \alpha , \quad (3.16)$$

where β is understood to refer to β_0 (of the fundamental space harmonic) in the case of the grating coupler. It is then evident that, when (3.16) is satisfied, we obtain that (3.10), (3.14) and (3.15) become identical to the phase-match conditions (3.2) and (3.6). The leaky-wave approach can therefore describe the operation of both prism and grating couplers and, as discussed further in Subsection 3.1.5, it greatly facilitates the design of such couplers by emphasizing that the leakage parameter α determines most of the coupling characteristics. Furthermore, this approach shows that if β (or β_0) is not too close to β_{sw} , the proper operation condition requires a phase-match to β (or β_0) rather than to β_{sw} as predicted by the less rigorous mode-coupling description discussed in Subsections 3.1.2 and 3.1.3.

It is also pertinent to observe that the discussion here has dealt with the surface-wave-to-beam operation, as shown in Fig. 3.6, i.e. we described output rather than input couplers. However, as already mentioned at the end of Subsection 3.1.2, reciprocity considerations ensure that the same approach can be applied to input couplers. To achieve this in the context of Fig. 3.6, it is sufficient to reverse the directions of all the arrows, in which case we would have (leaky-wave) beams incident from the right which are converted to surface waves progressing towards the left. Further clarifications of this aspect are discussed in Subsection 3.1.5.

3.1.5. Design Considerations for Prism Couplers

Unless a beam coupler is well designed, the conversion of a beam into a surface wave (or of a surface wave into a beam) will occur with only low efficiency, the bulk of the incoming energy being wasted into undesirable losses. To discuss the features that affect the coupling efficiency most strongly, we shall consider first an output coupler of the prism type.

When the film waveguide is not too thin, more than a single mode can be supported, as discussed in Section 2.1. For any given prism configuration and wavelength, the radiation angle θ of the outgoing beam in an output coupler varies with the mode number. Hence, if the incoming surface-wave energy is in multi-mode form, many beams may appear. When these beams are intercepted by a screen, each one of them appears as a bright line, thus producing a set that is known as “*m*-lines” in the literature because *m* was taken to designate the mode number [3.12]. However, we shall henceforth assume that we are dealing with a single mode in order to simplify the situation. When more than one mode is present, each one of them may be treated independently (provided that no mode coupling occurs due to imperfections). The presence of a single mode can always be ensured by choosing a sufficiently thin film, in agreement with the considerations in Section 2.1 and 2.3.

Role of Beam Width

As discussed previously, a coupler configuration satisfying condition (3.16) has only negligible scattering losses at the junction between the surface-wave and the leaky-wave sections of the thin-film waveguide. For a prism coupler, we have also seen that only a single beam is outgoing through the prism and into the air region. Hence the incident surface-wave energy is transferred into the single leaky-wave beam with nearly 100% efficiency, provided the prism is sufficiently long to leak out all but an insignificant amount of the leaky-wave energy, i.e., the prism length L satisfies $\alpha L \gg 1$. This condition will be assumed to be always satisfied.

However, it is important to recognize that the beam leaked by the prism coupler in Fig. 3.6b has a form that is different from, say, the Gaussian shape of a laser beam. Due to the leaky-wave illumination, this beam has the form sketched in Fig. 3.7, its field being given [3.23, 56] by

$$E = E_0 \exp(-jk_a x_r - \alpha z_r \sec \theta) \operatorname{erfc} \left(\frac{\alpha W}{2} - \frac{x_r}{W} \right), \quad (3.17)$$

where E_0 is a constant, $\operatorname{erfc}(u)$ is the complementary error function of argument u , $k_a = 2\pi/\lambda_a$ is the propagation factor in air, while θ , x_r and z_r are beam coordinates as shown in Fig. 3.7. Here E stands for the field in the air region (outside the prism) and the quantity W is defined by

$$W^2 = -2jx/k_a \cos \theta, \quad (3.18)$$

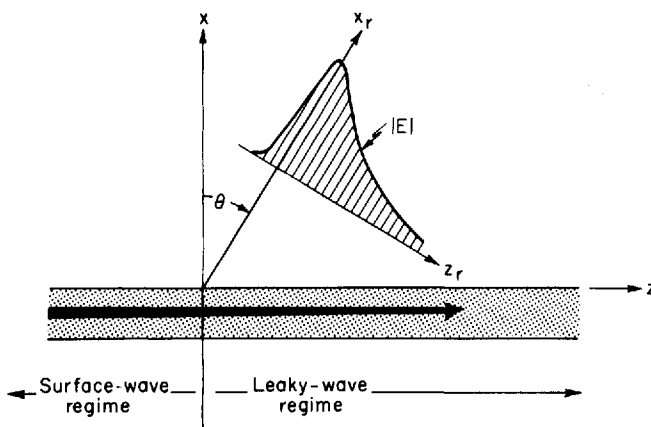


Fig. 3.7. Amplitude profile of a beam produced by the leakage field of a leaky wave

with W being taken in the fourth quadrant of the complex plane. From (3.17) it is clear that the form of the beam is dependent on both the leakage factor α and the beam coordinates θ , x_r , and z_r .

The term involving the erfc function in (3.17) describes the fringing effect that smoothes out the steeper left-hand side of the beam-form $|E|$ in Fig. 3.7. The remaining exponential term describes the leaky-wave variation, which is consistent with that of (3.8) with $k_z = \beta - j\alpha$. If we disregard the fringing effect, which is due to a diffraction process, we may approximate (3.17) and write

$$\left| \frac{E}{2E_0} \right| = \begin{cases} 0, & \text{for } z_r < 0; \\ \exp(-\alpha z_r \sec \theta), & \text{for } z_r > 0. \end{cases} \quad (3.19)$$

Hence the beam profile is nearly exponential, with a beam width w_{eq} given by

$$\alpha w_{eq} = \cos \theta, \quad (3.20)$$

where w_{eq} is defined as the length along z_r where the amplitude of E decreases by $1/e$.

Recalling that, in the present case

$$\sin \theta = \beta/k_0 n_p \approx \beta_{sw}/k_0 n_p, \quad (3.21)$$

where n_p is the prism refractive index, it is clear that θ and w_{eq} are fully determined by the leaky-wave characteristics α and β .

Thus, if a specified beam is to emerge from an output coupler, the values of β and α have to be designed so that (3.20) and (3.21) are satisfied. In particular, α needs to be carefully controlled. In the case of the prism coupler, α is adjusted by changing the height h_a of the air gap, α being larger for smaller h_a . It can be shown [3.18] that α is proportional to $\exp(-2|a_a|h_a)$, where $|a_a|$ is the decay of the surface wave in the air region. Because of this exponential dependence, α varies rapidly with h_a but this is not too critical since the optimum value of h_a is adjusted while assembling the prism coupler, as discussed further below.

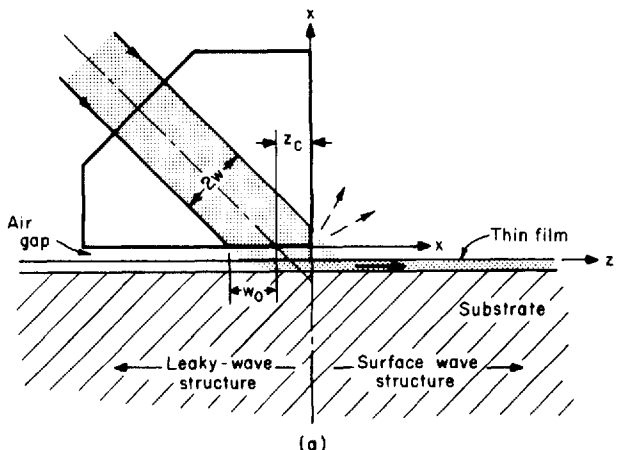
Effect of Beam Form

If the exponential form (3.19) of the beam emerging from an output coupler is no disadvantage and assuming that α is adjusted so as to yield a desirable beam width as given by (3.20), the output coupler can be theoretically 100% effective in converting a surface wave into a beam.

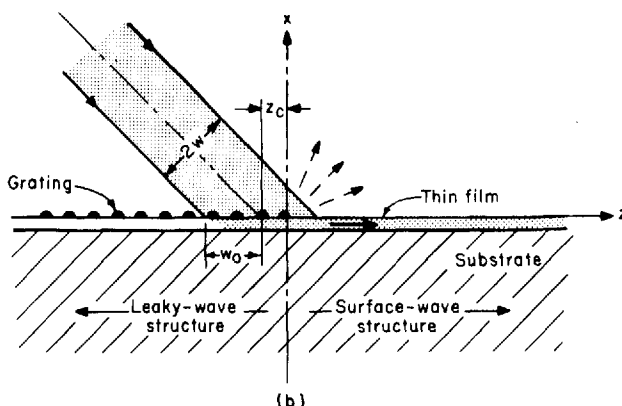
However, this is not the case for an input coupler because, by reciprocity, such a 100% efficiency can be preserved only if the incident beam satisfies the conditions

- it is oriented at exactly the angle θ ;
- it has the same beam width as that given by (3.20);
- it has the same exponential shape as that described by (3.17).

The first condition can be easily satisfied but the other two are more difficult. For a laser beam with a Gaussian shape, the beam form is



(a)



(b)

Fig. 3.8a and b. Alignment of incident beam in prism and grating input couplers for increasing coupling efficiency. Maximum efficiency achievable for Gaussian beams is 80.1%, which is obtained if $z_c/w_0=0.68$ and $z_c/w_0=0.733$

symmetric and the beam width (between points at $1/e$ times the maximum amplitude) is usually taken as $2w$. Then, if we take $2w = w_{eq}$ of (3.20), condition (b) is reasonably satisfied but the beam shape cannot comply with condition (c). It can then be shown [3.21] that, because of the disparity in beam forms, a maximum coupling efficiency of only 80.1% can be achieved. To achieve this efficiency, it is also necessary to orient the incident beam so that its right-hand boundary overshoots the lower side of the prism, as shown in Fig. 3.8a. The exact conditions for this situation are given [3.21] by

$$\alpha w_0 = 1.36, \quad (3.22)$$

$$z_c/w_0 = 0.733, \quad (3.23)$$

where

$$w_0 = w \sec \theta, \quad (3.24)$$

and w is the half beam-width of the Gaussian beam, as defined above, while z_c is the offset length of the beam with respect to the prism, as indicated in Fig. 3.8a.

For beams having uniform illumination, the above conditions are modified [3.18, 30] to

$$\alpha b_0 = 1.25, \quad (3.25)$$

$$z_c/b_0 = 0.5, \quad (3.26)$$

$$b_0 = b \sec \theta, \quad (3.27)$$

where b_0 is the total beam width (measured in the xz plane and perpendicular to the beam axis). The maximum coupling efficiency is 81% for such a beam.

The relatively small differences between the above results for Gaussian and uniform beams suggests that the parameter α and z_c are not too critical when attempting to achieve maximum efficiency. This is supported by Fig. 3.9, where the maximum available coupling efficiency for Gaussian beams is plotted as a function of αw_0 . We can verify from that figure that, if the optimum value $\alpha w_0 = 0.68$ is either doubled or halved, the maximum efficiency of 80% is reduced to only 70%. Thus, if the half beam-width w of a given incident beam is known, the exact value of α can be realized within a factor of 2 without incurring too much coupling loss.

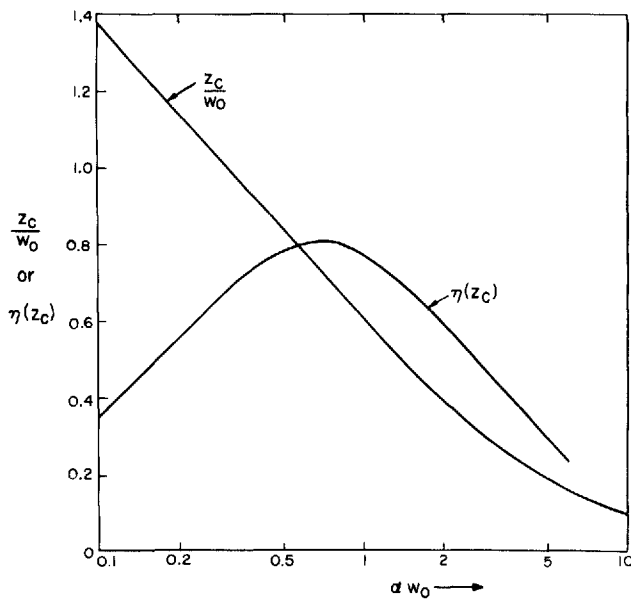


Fig. 3.9. Variation of the maximum available coupling efficiency $\eta(z_c)$ and the off-set distance z_c as functions of αw_0 for Gaussian beams incident on prism couplers

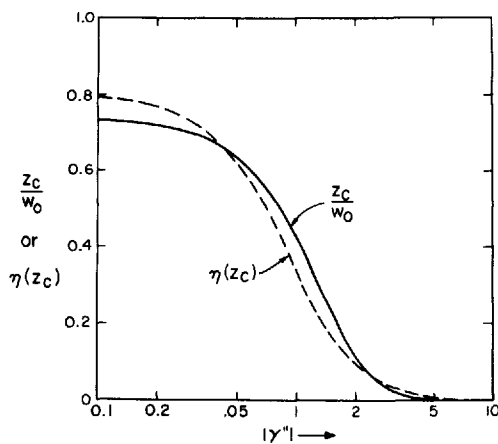


Fig. 3.10. Variation of the maximum available coupling efficiency $\eta(z_c)$ and the off-set distance z_c as functions of angular misalignment $\gamma'' = (\pi\omega/\lambda)\Delta$, for Gaussian beams incident on prism couplers

Deviations from the Phase-Matching Angle

The effect of misaligning the incident beam with respect to the required phase-matching angle has also been estimated [3.21]. The results are given in Fig. 3.10 which shows the maximum available efficiency and the offset distance z_c for Gaussian beams, as a function of γ'' . Here

$$\gamma'' = (\pi w/\lambda) \Delta, \quad (3.28)$$

where Δ is the difference in radians between the exact phase-matching angle θ and the actual incidence angle. As Fig. 3.10 indicates that a loss of 3 dB in coupling efficiency occurs if $|\gamma''| = 1$, Δ must be quite small to avoid losses due to improper angular alignment of the incident beam. In fact, as $\pi w/\lambda$ is the inverse of the far-field divergence of the beam, it follows that Δ must be considerably smaller than this divergence in order to ensure small losses.

Beam Shaping by Variable Air Gap

We recall that the maximum efficiency (about 80%) of input couplers is smaller than the theoretical 100% efficiency of output couplers, because of the exponential beam form emerging from the latter. However, if the outgoing beam had, say, a Gaussian shape, reciprocity considerations would imply that an incident Gaussian beam could be coupled into an input coupler also with nearly 100% efficiency. The beam in an output coupler can be shaped to approximate the Gaussian shape by means of a variable air gap [3.22, 23], as suggested in Fig. 3.11. When so shaped, this air gap results in a value of α that increases from left to right. Hence energy leakage is weaker on the left-hand side and stronger in the right-hand side of the beam. As a result, the strong peak on the left of the exponential beam shown in Fig. 3.7 is shifted towards the right, thus approaching the Gaussian profile shown in Fig. 3.11 a.

A practical implementation of a prism coupler with a tapered gap is shown in Fig. 3.11 b. Advantage is taken of the clamp that holds the slide covered by the thin film and, by careful manipulation and by appropriately varying the pressure of clamping, it is possible to adjust the prism-slide configuration so as to maximize the coupling efficiency. The interested reader should consult references [3.22] and [3.58] for theoretical approaches that deal with structures having variable leaky-wave characteristics.

Calculation of Leaky-Wave Characteristics

Although the discussion here has indicated that, for laboratory purposes, the desired value of α may be obtained by careful adjustment of the air gap h_a , the numerical determination of α may sometimes be

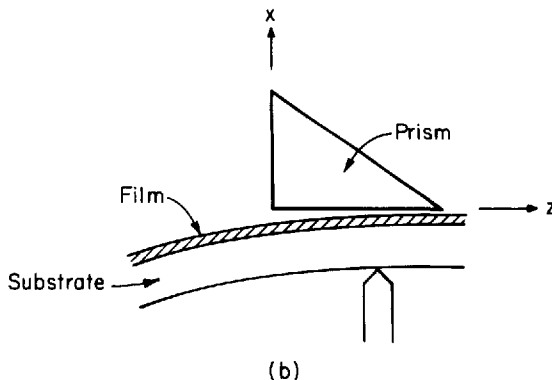
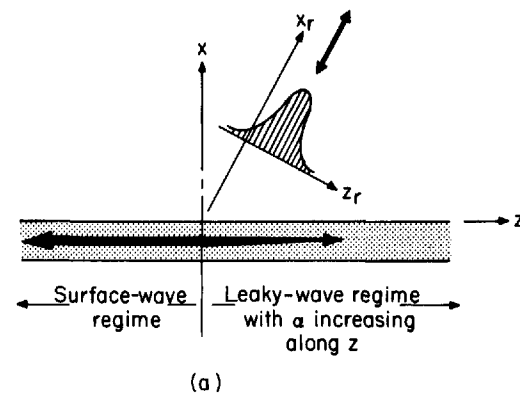


Fig. 3.11a and b. Variable-gap geometry for increasing the coupling efficiency of prism couplers operating with Gaussian beams: a) An output coupler delivering a Gaussian beam with nearly 100% efficiency can also act as an input coupler with nearly 100% efficiency for an incident Gaussian beam; b) Practical realization of a prism coupler having a variable air gap. Pressure is applied to bend the glass slide so that the air-gap height decreases away from the right-hand corner of the prism

also required. This can be achieved either by following the TIEN and ULRICH analysis [3.18] or by applying a transverse-resonance analysis [3.25], as follows.

The four-media prism-coupler configuration is first represented by an equivalent transmission-line network with respect to the transverse x direction, as shown in Fig. 3.12. All of the leaky-wave modes are then given by solving for an eigenvalue equation in the form

$$Z_u + Z_d = 0, \quad (3.29)$$

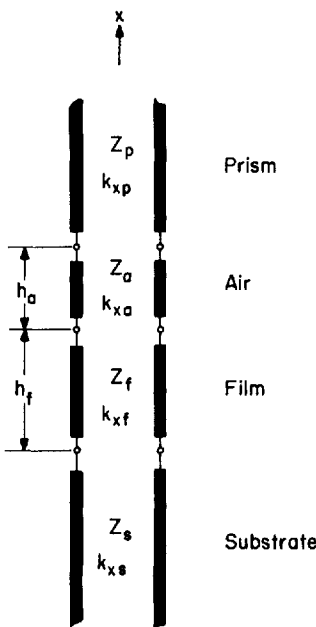


Fig. 3.12. Equivalent transverse network for the prism-coupler configuration

where Z_u and Z_d are the input impedance looking up or down, respectively, at the air-film boundary. These impedances are given by

$$Z_u = \frac{Z_p + jZ_a \tan(k_{xa} h_a)}{Z_a + jZ_p \tan(k_{xa} h_a)} Z_a, \quad (3.30)$$

$$Z_d = \frac{Z_s + jZ_f \tan(k_{xf} h_f)}{Z_f + jZ_s \tan(k_{xf} h_f)} Z_f, \quad (3.31)$$

where k_{xi} and Z_i are propagation factors and characteristics impedances, respectively, in the i -th medium ($i=p,a,f$ or s). These are related by

$$Z_i = \begin{cases} \frac{\omega \mu_0}{k_{xi}} & \text{for TE modes} \\ \frac{k_{xi}}{\omega \epsilon_0 n_i^2} & \text{for TM modes,} \end{cases} \quad (3.32)$$

whereas all k_{xi} satisfy the dispersion relation

$$k_{xi}^2 + k_z^2 = k_0^2 n_i^2 . \quad (3.33)$$

Here $k_0 = 2\pi/\lambda_0$ and λ_0 is the wavelength in vacuum.

Equations (3.30)–(3.33) establish sufficiently many relations to solve (3.29) for the required $k_z = \beta - j\alpha$, which is the desired complex propagation factor along z . Of course, the solutions must usually be obtained by means of a computer and, in general, (3.29) yields an infinite number of k_z , one each for every mode [3.56, 57]. However, we are usually interested only in those leaky-waves modes that appear as perturbations of a surface-wave mode, i.e., $\beta_{sw} \approx \beta \gg \alpha$. Hence the numerical procedure is to first solve for surface waves [in which case $h_a \rightarrow \infty$ in (3.30) so that $Z_u \rightarrow Z_a$] and thus find $k_z = \beta_{sw}$ and then obtain a solution k_z near β_{sw} for finite values of h_a .

As already mentioned previously, the above values of α are well approximated by

$$\alpha h_f = C \exp(-2|a_a h_a|), \quad (3.34)$$

which holds for $|a_a h_a| > 1$. Here C is a complicated function of all Z_i and k_{xi} listed above; its explicit form has been given by TIEN and ULRICH [3.18, 30], while a_a is the imaginary part of k_{xa} .

3.1.6. Design Considerations for Grating Couplers

Single-Beam Couplers

Compared to prism couplers, the design of grating couplers is complicated by the fact that they usually transmit light through the substrate and, in addition, they may support more than a single diffracted order. However, because the substrate refractive index n_s is higher than that of air (or cover) n_a , it is possible to have a beam in the substrate without any transmission through the air region. This can be achieved [3.21, 44, 46] by requiring that the surface wave incident on the grating of an output coupler should be transformed into a leaky wave having no propagating space-harmonics in the air region and only a single propagating one in the substrate. For weak leakage ($\alpha \ll \beta_0 \approx \beta_{sw}$), as is usually the case in practice, these conditions are satisfied only if, by using $\beta_0 = \beta_{sw}$ in (3.14) and (3.15), all of the radiation angles θ_{av} and θ_{sv} are complex, except for $\theta_{s,-1}$.

By simple algebra, it is easy to verify that the above conditions are met if

$$q_i = (k_0 n_i d)^2 - (\beta_{sw} d + 2v\pi)^2 \quad (3.35)$$

is negative for $v=0$ and -1 in air ($i=a$) and $v=0$ and $v=-2$ in the substrate ($i=s$), but is positive for $v=-1$ in the substrate ($i=s$). Obviously, for any guided surface wave, the grating periodicity d can be adjusted to satisfy these requirements. The $v=-1$ space harmonic is then radiating in the substrate, but its leakage angle $\theta_{s,-1}$ is larger than critical for transmission into the air region. Although it is many times thicker than the film guide, the substrate is also exposed to air at its lower boundary. To extract energy from the $v=-1$ harmonic, it is therefore necessary to deform this lower boundary or, as implemented by DALGOUTTE [3.44], to add a prism as shown in Fig. 3.13.

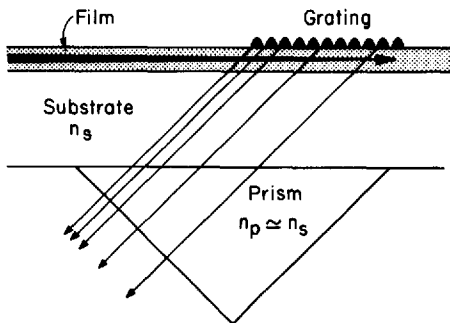


Fig. 3.13. Grating coupler with prism on the substrate for converting an incident surface wave into a single leaky-wave beam. The usual parameters are such that backward leakage occurs in practice

A comparison of Fig. 3.13 with Fig. 3.6 reveals that, from the point of view of surface-wave to leaky-wave conversion, the arrangement of Fig. 3.13 is analogous to that of Fig. 3.6b because only a single output beam results in both cases. The fact that a backward leaky wave occurs in the grating coupler whereas forward leakage appears in the prism coupler is minor and does not affect the analogy. As a result, all of the considerations presented in Subsection 3.1.5 for prism couplers also hold for the single-beam coupler shown in Fig. 3.13. In particular, a maximum coupling efficiency of 80.1% holds when coupling Gaussian beams via an input coupler.

Similarly, the necessity of off-setting the beam for achieving this maximum efficiency also holds for this grating coupler, as shown in Fig. 3.8b. Consequently, we may also use the results of Figs. 3.9 and 3.10. In addition, beam-forming can be realized [3.23, 58] by varying the grating depth or the periodicity (or both) in a manner analogous to varying the air gap in prism couplers. However, this technique has not been applied yet to grating couplers.

If the presence of a prism is acceptable, the design of a prism coupler as shown in Fig. 3.13 therefore follows the rules already discussed in Subsection 3.1.5 except that now the leakage α is obtained by means of a grating instead of an air gap. The periodicity d of the grating is prescribed by the requirements following (3.35). The leakage factor α depends on the grating dimension and form. Some typical dielectric gratings that have been frequently used for couplers are shown in Fig. 3.14. For the holographic grating shown in Fig. 3.14c, the grating layer can be described by a periodically modulated dielectric, as shown;

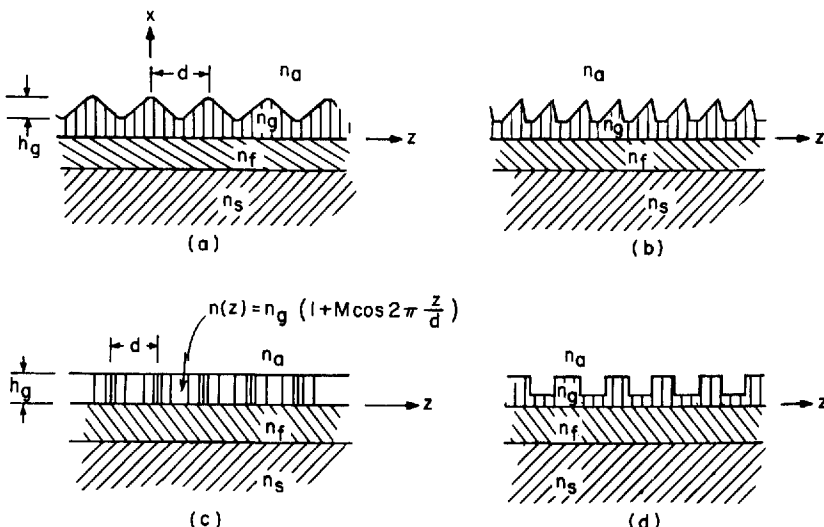


Fig. 3.14a-d. Typical dielectric gratings: a) Symmetric triangular grooves; b) Asymmetric grooves; c) Modulated (holographic) layer; d) Corrugated layer

in this case, α increases with both the layer thickness h_g and the modulation magnitude M . In the case of the other (grooved) gratings, α increases with the groove depth and its value may be affected by the exact shape of the groove profile [3.50, 51].

Effect of Grating Height

Although exact values of α may be calculated by rigorous methods [3.36, 38–40, 47, 48, 50, 53], these methods require expensive and time consuming efforts. Reasonably good approximate results may be obtained by using perturbation techniques [3.34, 35, 52, 53, 59]. In particular, by taking a transverse network similar to that shown in Fig. 3.12, it is possible to obtain [3.52] very accurate values for α and, in addition, to calculate the amplitude of each space harmonic (and therefore the intensity for each radiated beam) in an output coupler. Reciprocity considerations can thereafter be used to evaluate the performance of the same grating as an input coupler. In all cases, the value of α is a complicated function of the grating parameters and therefore the interested reader is referred to the literature for specific results.

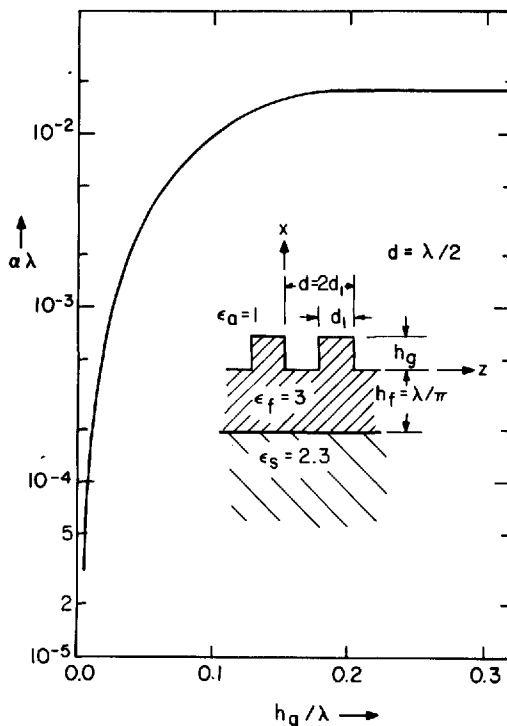


Fig. 3.15. Variation of the leakage $\alpha\lambda$ with normalized grating height h_g/λ for a typical grating. Note that $\alpha\lambda$ increases rapidly at first but then levels off as h_g/λ increases towards larger values

An important result is that, for small values of the grating height h_g , the leakage factor α is proportional to h_g^2 . However, as h_g is further increased, α ultimately reaches a saturation value beyond which it can no longer increase. This happens because the grating grooves appear as a perturbation on a smooth layer that supports a surface wave if no grating is present. Due to the grooves, however, energy from the surface wave is leaked away to form the leaky-wave field. Hence the leakage increases and therefore α initially grows as the grating height h_g increases. However, the grating is located in a region where the incoming surface-wave field is decaying away from the film. Thus, as h_g increases, the grating extends further into a region where the field amplitude ultimately decays to a vanishingly small value. Hence any further increase of h_g acts only as a negligible (second-order) perturbation, so that α levels off as shown in Fig. 3.15.

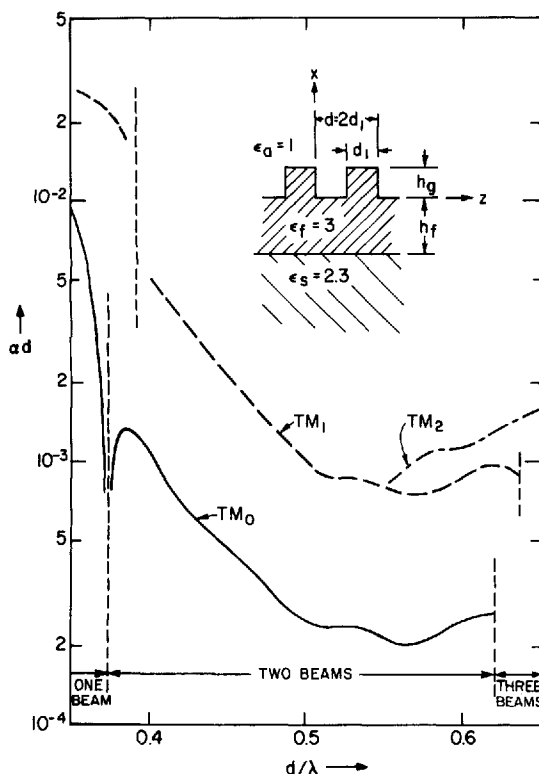


Fig. 3.16. Variation of the leakage αd with d/λ for a typical dielectric grating, showing that (for any given d and λ) the leakage α is larger for the higher modes. The total numbers of leaky-wave beams for any wavelength is also indicated

Because of the saturation effect described in Fig. 3.15, any given combination of film, substrate and grating materials yields values of α that are smaller than the maximum (saturation) value of α_m . The value of h_{gm} at which α starts to level off is given by the transverse distance over which the surface-wave field magnitude decays to $1/e$ times its value at the bottom of the grating grooves [3.47, 48, 53], i.e., $|a_a| h_{gm} = 1$, where $|a_a|$ is the decay factor in the air region. It is therefore not necessary to deposit gratings having grooves deeper than h_{gm} because values of h_g larger than h_{gm} yield no appreciable increase in α .

Effect of Higher-Order Modes

As efficient excitation of a surface wave in an input coupler requires to satisfy conditions (3.22) or (3.25), α_m may be too small in the case of narrow incident beams. This happens especially in the case of infrared light applications [3.60]. To circumvent this difficulty, advantage may be taken of the fact that α increases with the mode number. Thus, for any given thin-film grating configuration that may support more than a single mode, the value of α increases if operation occurs at higher-order modes [3.60]. This can be explained by the fact that a surface wave incident on a grating is characterized by a number of zig-zag bounces (per unit length) that increases with the mode number. As energy may be assumed to be scattered at every reflection on the grating boundary, the total leakage (and therefore the leakage parameter) also increases with the mode number. A typical example is illustrated in Fig. 3.16.

Two-Beam Couplers

Although the single-beam grating coupler of Fig. 3.13 can reach the high efficiencies of prism couplers, the prism required to provide the beam in the substrate is bulky and may therefore be impractical for integrated-optics applications. If the lower substrate boundary is parallel to the thin film, an output coupler will produce at least two beams, of which one is above the grating and the other is below the substrate, both therefore appearing in air regions. To ensure that no more than two such beams occur, it is sufficient to require that q_i in (3.35) be negative for $v=0$ and -2 and positive for $v=-1$ in air ($i=a$).

Of course, the presence of more than a single beam is usually not desired and therefore causes a loss in coupling efficiency. The calculation of this efficiency is then also more complicated because, in either an input or an output coupler, incident energy can be channelled into more than one outgoing direction. As an example, the output coupler of Fig. 3.17a converts an incident surface wave into two out-

going beams. The same coupler, when used as an input coupler as shown in Fig. 3.17b, converts an incident beam into a surface wave, but it also produces reflected and transmitted beams.

Reciprocity considerations can, of course, still be applied but they must be used carefully. If each of the ray paths indicated in Fig. 3.17 is labelled A, B, C, ... to show connections between the various regions, these reciprocity considerations require that any energy transfer η_{IJ} from region I to J be equal to the energy transfer η_{JI} from region J to region I [3.46], provided the field forms are preserved, i.e., if an output beam is of the exponential (leaky-wave) form, then an input beam replacing it must also be exponential. To illustrate this concept, assume that the incoming surface wave in Fig. 3.17a couples 60% of its energy to the beam in the upper region and 40% to the one in the lower region,

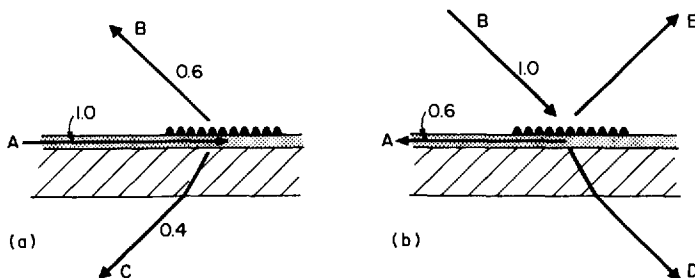


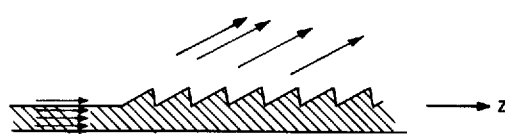
Fig. 3.17a and b. Grating coupler supporting a single diffraction order in the air region: a) An incident surface wave in an output coupler produces two outgoing beams with assumed efficiencies of $\eta_{AB}=0.6$ and $\eta_{AC}=0.4$; b) The same coupler used as an input coupler transforms an incident exponential beam into a surface wave with an efficiency of $\eta_{BA}=0.6$. For a properly aligned incident Gaussian beam, the efficiency is reduced to $\eta_{BA}=0.6 \times 0.8=0.48$

thus establishing $\eta_{AB}=0.6$ and $\eta_{AC}=0.4$. When using this coupler as an input coupler, as in Fig. 3.17b, we have $\eta_{BA}=0.6$ if the incident beam has the proper exponential shape, as discussed in Subsection 3.1.5 under *Effect of beam form*. The remaining energy is then divided between the reflected and transmitted beams, so that $\eta_{BD}+\eta_{BE}=0.4$, but we cannot estimate in what proportion this division takes place unless more information is provided.

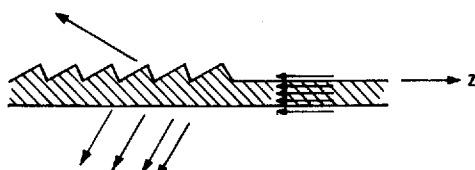
However, if the incident beam is of Gaussian rather than exponential shape, we must contend with a 20% loss due to the beam-form mismatch to the leaky-wave field, as explained in Subsection 3.1.5 under *Effect of beam form*. The above figures are therefore modified so that

$\eta_{BA} = 0.6 \times 0.8 = 0.48$, whereas now $\eta_{BE} + \eta_{BD} = 0.52$. Of course, the present figures assume that the incident beam complies with conditions (3.22) and (3.23) for beam-width size w and offset distance z_c , and that it is aligned at exactly the leaky-wave angle θ . If either of these conditions is not satisfied, η_{BA} is lower and the coupling efficiency decreases.

In general, we may expect that a surface wave incident on an output coupler transfers its energy about equally between the two air regions, so that $\eta_{AB} \approx 0.5$. Hence the expected maximum coupling efficiency of an input coupler is $\eta_{BA} \approx 0.5 \times 0.8 = 0.4$ for an incident Gaussian beam. Of course, if the coupler can support more than a single radiating space harmonic (i.e., more than one diffraction order, thus leading to several beams in each air region), the coupling efficiency can be substantially less than that of prism couplers. However, by properly adjusting the thickness of the thin film and/or that of the grating, η_{AB} and η_{AC} can be made appreciably different from 0.5, thus increasing the energy of one beam at the expense of the other and thereby raising the coupling efficiency. Although not verified experimentally, coupling efficiencies close to 80% have been reported by this method [3.47, 48].



(a) Incidence along + z direction



(b) Incidence along - z direction

Fig. 3.18a and b. Leaky-wave beams produced by a surface wave incident on an asymmetric grating. The number of flux lines (arrows) indicate the power strength in each region

A more sophisticated technique for increasing the coupling to one of the two beams in the air regions is to use dielectric gratings with asymmetric profiles [3.50, 51]. This produces a phenomenon analogous to blazing by diffraction gratings [3.61], which takes the form sketched in Fig. 3.18. Because the grating teeth are asymmetric with respect to the x plane, a surface wave "sees" a different geometry if it is incident from the right or the left. It is therefore intuitively expected that, for example, more energy could be leaked into the lower (substrate) region when incidence occurs from the right whereas most of the energy could go into the upper air region when incidence is from the left, as suggested in Fig. 3.18. In this manner, calculations have shown [3.50] that one of the two beams can be totally suppressed by judiciously shaping the grating profile. However, this blazing effect has not yet been experimentally tested and its implementation for integrated-optics applications may be subject to critical tolerances of the grating profile.

3.1.7. Other Beam Couplers

The Thin-Film Tapered Guide

Although the prism and grating coupler have proved to be reliable and most useful, other beam couplers have also been reported. Of these, an interestingly simple one is the tapered thin-film waveguide coupler devised by TIEN and MARTIN [3.62] and, in somewhat modified form, by SOHLER [3.63].

The principle of the tapered coupler is shown in Fig. 3.19, where it is seen to consist of a thin film that tapers down onto the substrate.

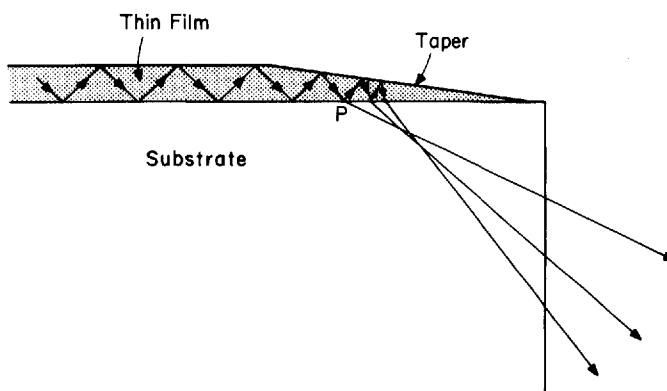


Fig. 3.19. The tapered thin-film waveguide coupler

A surface wave incident on the taper therefore undergoes zig-zag bounces whose angle of incidence on the film-substrate boundaries decreases progressively as the taper narrows down. As a result, at some point P, the angle of incidence becomes smaller than the critical angle of total reflection and therefore energy starts refracting into the substrate. This energy is augmented by that of subsequent rays, so that ultimately most of the incident energy is transformed into an outgoing beam.

Because the beam formed by a tapered coupler is produced by many rays that emerge at slightly different angles, the outgoing beam is characterized by a relatively large divergence, which may be between 1° and 20°. Although the coupling efficiency may be high, with 70% being reported by TIEN and MARTIN [3.62], the high beam divergence detracts considerably from the attractiveness of this coupler. However, the tapered coupler has found applications in those cases where this divergence is not objectionable, for example, in light detectors [3.64], as discussed in Subsection 6.5.1.

The leaky-wave theory that proved to be so useful for dealing with prism and grating couplers does not appear to be readily applicable to tapered couplers. The reason is that the incident surface wave is converted very rapidly into outgoing radiation because the surface-wave mode reaches cut-off conditions within the taper. Energy is then scattered over a wide spectrum of radiation modes, so that a leaky-wave mode cannot be established. Of course, the tapered coupler can be used also as an input coupler; however, its efficiency is usually quite small because it is difficult to align and match the form of the incident beam to the divergent shape indicated in Fig. 3.19. Due to these disadvantages, little theoretical efforts have been spent on investigating tapered couplers.

The Holographic Coupler

Another scheme for beam coupling, as suggested by ASH et al. [3.65], is based on holographic techniques. Its principle is illustrated in Fig. 3.20, wherein a surface wave A incident on a thin-film waveguide is transformed into a leaky-wave beam A' by a grating or other means. This beam A' is used in conjunction with a laser beam R to record a hologram. Subsequent illumination of the hologram with A' will produce a reconstructed beam R . Alternatively, by illuminating the hologram with a conjugate reference beam R^* , it is possible to reconstruct $(A')^*$; when this leaky-wave beam interacts with the leaky-wave structure, it produces a surface wave similar to the initial incident field A .

The great advantage of this holographic scheme is that the grating producing the leaky-wave field need not be at all regular and, in theory,

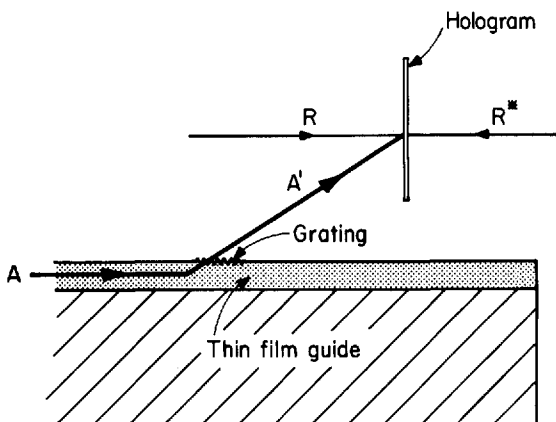


Fig. 3.20. Beam coupling by holographic method (after ASH et al. [3.65]). The grating may be irregular and consist of scratches obtained with an abrasive tool

a random irregularity may in fact be scratched on the film structure to produce the scattered field A' . This is due to the fact that the holographic process adjusts itself automatically so as to duplicate R or A independently of the exact form of the irregularly scattered field A' . Of course, practical considerations (such as the need to capture most of the flux of A' by the holographic plate) do not allow for too much irregularity. However, this method presents very attractive and intriguing potentialities for a number of applications in addition to that of beam coupling. Amongst these applications, ASH et al. [3.65] listed code-translation filtering, multiple beam forming, waveguide connectors with prescribed properties and others.

3.2. Waveguide Couplers and Mode Converters

After the energy from a light beam has been introduced into a planar guide, it is often necessary to transfer it through a variety of other structures for processing or other purposes. A device is therefore necessary to couple this energy from the planar guide to the next structure, and then another device might be required to pass it on to another structure. These devices are known either as couplers, or as transitions, junctions, connectors or converters. However, in view of their main functions, we may classify them either as waveguide couplers, which transfer energy from one type of optical guide to another one, or as mode converters, which transform the energy from one mode to another

mode along the same guide. Although they have not been the subject of so many investigations as beam couplers, these waveguide couplers and mode converters will play an important role in integrated optics and some familiarity with the principal devices is therefore desirable.

3.2.1. Planar-to-Planar Guide Couplers

One of the simpler problems of coupling two different light guides is when both of these guides are planar. Some of the practical schemes for connecting two such guides are shown in Fig. 3.21.

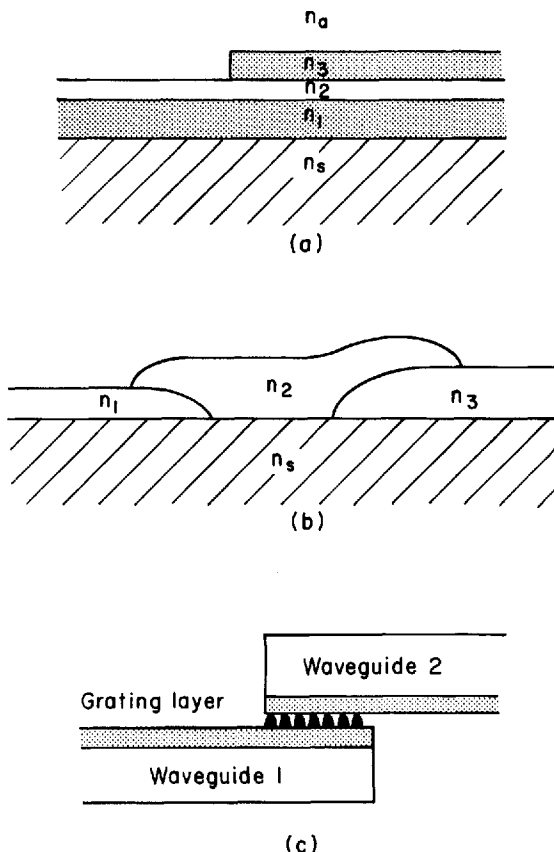


Fig. 3.21a-c. Coupling between two planar guides: a) Two guiding layers sharing a common substrate; b) Two separate thin-film guides coupled by a third layer with tapered connections; c) Two waveguides coupled through a grating layer

When the guiding films are on top of each other, as shown in Fig. 3.21a, it is necessary that their refractive indices n_1 and n_3 be larger than those of the other media involved. The coupling between the two guiding films then occurs because of the evanescent fields that penetrate through the intermediate layer with refractive index n_2 . The energy exchange can be calculated by using the coupled-mode approach outlined in Subsection 2.6.3 and experimental work has confirmed [3.66] that the results obtained by using this approach are excellent. As predicted, in the region where the two guides overlap, energy is interchanged from one to the other guide over every length z satisfying $\kappa z = \pi/2$ in (2.6.32), provided that the two guides have identical propagation factors, i.e., synchronous coupling operation is required. Because of difficulties in maintaining synchronous conditions, the single coupling scheme of Fig. 3.22a has not found much application. These difficulties can be alleviated by using variable coupling, as discussed in Subsection 3.2.3.

A more practical method has been developed by hybrid technology by TIEN et al. [3.67, 8]. As shown in Fig. 3.21b, two film waveguides with refractive indices n_1 and n_3 again share a common substrate but they do not now overlap. Instead, a third layer with refractive index n_2 joins them by means of tapered transitions as indicated. If, for example, a surface wave is incident from the left in the film with index n_1 , energy is radiated into the exterior region when the wave reaches the tapered end of this film, as already discussed in the context of the tapered coupler in Subsection 3.1.7. However, because $n_2 > n_s$, this energy is radiated into the intermediate film with refractive index n_2 rather than into the substrate. The energy then continues as a surface wave into this intermediate film. A similar process occurs if the surface wave is incident from the right into the film with index n_3 , in which case it also continues into the intermediate film via the respective tapered end. By reciprocity, it follows that energy can be coupled out of the intermediate film, depending on the direction of wave travel. Thus, energy can be coupled from left to right (or vice-versa) via the intermediate film. By using a very gentle taper, nearly 100% coupling efficiency could thus be achieved [3.67, 8].

The two previous schemes required a common substrate and they are therefore not suitable for connecting two thin-film waveguides that are placed on separate substrates. In such a case, the two films could be placed on top of each other but separated by a third layer of lower refractive index so that coupling occurs through the intermediary of the evanescent field. However, HSU et al. [3.68, 69] found it more convenient to use a grating layer, as shown in Fig. 3.21c. Of course, if complete energy transfer is required between the two waveguides, the

length of the grating layer and the overlap between the two waveguides must be equal to the coupling length, as determined by the coupled-mode theory outlined in Subsection 2.6.3. A coupling efficiency of 65% has been reported by HSU et al. [3.69].

Other coupling schemes permit a prescribed proportion of the energy to be coupled from one to the other waveguide [3.68], but the work reported so far is too sparse to discuss it in greater detail here.

3.2.2. Planar-to-Linear Guide Couplers

As most of the integrated-optics circuitry is expected to be carried out by means of linear waveguides, i.e., guides of the strip or rib variety, as described in Section 2.5, it will be necessary to transfer into these guides the energy that is carried by planar guides (into which a laser beam had been previously coupled).

The most straightforward approach for this purpose is to gradually taper down the width of the planar guide until it is reduced to the width of the linear guide, as suggested in Fig. 3.22a. This method has been analysed by WYNN and HARRIS [3.70] and effectively implemented by OSTROWSKY et al. [3.71] who used an electron resist for the waveguides and a computer-controlled scanning electron microscope to produce the required horn-shaped structure on the substrate. In general, a surface wave going through the horn transition may lose energy because of scattering and mode conversion. These losses could be reduced by making the horn transition long enough and/or by shaping the horn so as to minimize the loss mechanisms. However, the analysis has shown [3.70] that 90% coupling efficiency could be realized in a linearly tapered horn transition 2 mm long that connects a 50 μm wide planar guide to a 3 μm wide linear guide. Experimental verification of this estimate has so far not been reported.

A different transition, which is analogous to the prism coupler discussed in Subsection 3.1.2, is illustrated in Fig. 3.22b. Here the planar guide is terminated into a slanted end so that the incident surface wave would be totally reflected at the slant edge. This termination plays the role of the prism in beam couplers of the prism variety, except that now the entire process takes place inside the small height h_f of the thin-film waveguides. Thus, the linear guide shown in Fig. 3.22b couples to the planar guide via the evanescent field which appears in the gap between the two guides. The principle of operation of this planar-to-linear coupler is therefore evident but no experimental work has so far been reported on such a device. One difficulty that can be anticipated is that, to achieve good coupling efficiency and single-mode operation,

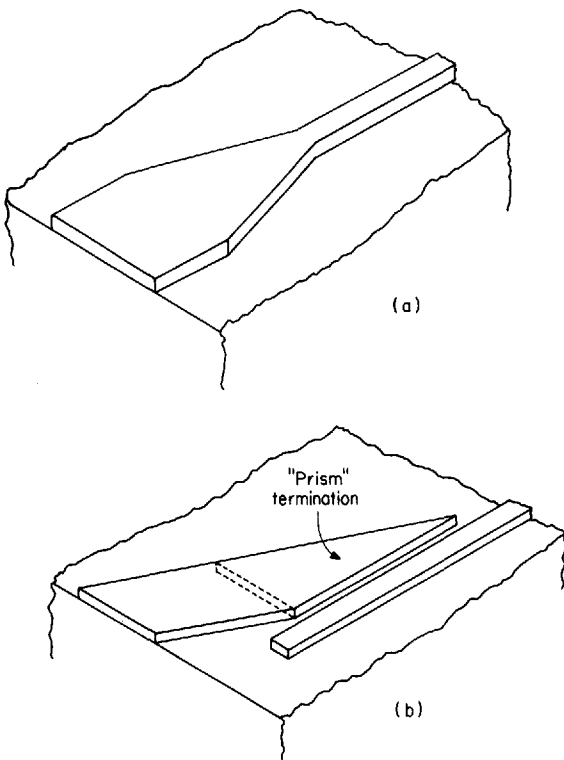


Fig. 3.22a and b. Connecting a planar guide to a linear guide: a) Horn transition; b) Prism and gap transition

it is necessary to have an accurate and well defined gap between the two guides and this may not be easily realizable with presently available fabrication techniques.

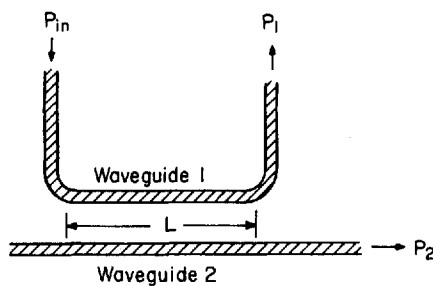
In this context, it is interesting to observe that the principle of operation for the "prism" coupler of Fig. 3.22b is being considered for extracting the output from lasers of the mesa type (see Subsection 6.3.2). However, although a theoretical analysis has already been given [3.72], quantitative experimental results have not yet been reported.

3.2.3. Linear-to-Linear Waveguide Couplers

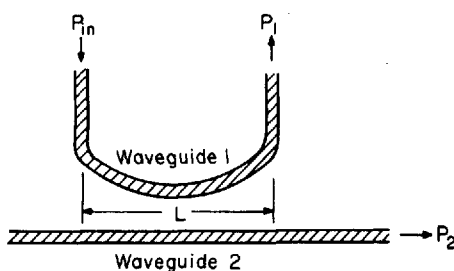
If two identical linear waveguides are parallel and close to each other over a length L , they will couple energy due to the evanescent field between them, as discussed for the case of the synchronous co-directional

coupler in Subsection 2.6.3. In this case, all of the energy can theoretically be transferred from one waveguide to another if the coupling length $L=z$ is chosen to satisfy $\kappa z = (2m+1)(\pi/2)$ in (2.6.32), where $m=0, 1, 2, 3 \dots$

This principle is the basis for the operation of directional couplers, the implementation of which usually takes the form shown in Fig. 3.23. Obviously, two linear waveguides can easily be coupled in this manner and, by suitably choosing the length L , any desired portion of energy from waveguide 1 can be coupled into waveguide 2. Analytic considerations for directional coupling with linear waveguides of the embedded strip type were given by MARCATILI [3.73] and experimental results with strip guides have been reported by FURUTA et al. [3.74]. By using a large number of parallel ion-implanted linear guides, SOMEKH et al. [3.75] have elegantly demonstrated the successive division



(a)



(b)

Fig. 3.23a and b. Directional couplers: a) Synchronous type; b) Tapered coupling. By suitably adjusting the coupling length L , the input power P_{in} may be split into equal or arbitrarily unequal output powers P_1 and P_2 . For complete energy coupling: $P_1=0$ and $P_2=P_{in}$

of energy by coupling amongst several guides. Details of their experimental set-up and a brief discussion of the operation of directional couplers is given in Subsection 6.2.2.

A serious problem in the fabrication of directional couplers for linear waveguides is the fact that tolerances are very critical. Unless these waveguides have a sufficiently uniform cross-section and unless their distance apart is constant through the coupling region, the synchronous condition ($\delta=0$ in Subsection 2.7.3) is not satisfied and complete coupling of energy cannot be achieved from one waveguide to the other. Thus, WILSON and TEH have shown [3.76] that only 50% energy coupling can be obtained if

$$\frac{\delta}{\beta} \approx \frac{0.4}{L}, \quad (3.36)$$

where $\delta=\beta_1-\beta_2$ is the difference between the propagation factors β_1 and $\beta_2=\beta$ in the two waveguides, and L is the coupling length measured in wavelengths. As L is in the range 100λ – $10,000\lambda$, even a small value of δ may seriously degrade the performance of a directional coupler.

To avoid this tolerance difficulty, WILSON and TEH have proposed using a tapered coupling region, as suggested in Fig. 3.23b. Although this is no longer a synchronous coupling operation, nevertheless near-total energy coupling can be theoretically obtained with a substantially smaller tolerance requirement or dimensions. Although WILSON and TEH reported experimental confirmation of this principle only for the case of a planar-to-planar directional coupler, DALGOUTTE et al. [3.77] have recently been successful in applying the tapered-coupling scheme also to linear waveguides.

3.2.4. Waveguide-to-Fiber Couplers

A problem of greatest practical importance is to transfer light energy from a planar or a linear waveguide to an optical fiber, or vice-versa. However, work on these coupling devices has only recently started and no fully satisfactory schemes are as yet available. The difficulty lies primarily in the fact that the fiber core is relatively small and therefore it is difficult to connect it to a waveguide in such a manner that the connection is sufficiently rigid and that the electromagnetic coupling efficiency is high enough.

The principle of leaky-wave radiation discussed in Subsection 3.1.4 has prompted KERSTEN [3.78] to experiment with the coupler shown in Fig. 3.24a. By depositing a high-index fluid drop onto a film wave-

guide, leakage of energy is obtained at an angle θ . It is therefore possible to pick up this energy by inserting a glass fiber into the liquid and orienting it along the angular direction θ . Although a coupling efficiency of 50% was thus achieved, this arrangement is obviously not too satisfactory for a permanent set-up. Also, the coupling efficiency from fiber to waveguide is generally poor because the field in the fiber does not have the proper exponential shape required by the leaky wave, thus resulting in a strong mismatch.

A more rigid coupling scheme has been reported by TIEN et al. [3.79]. As sketched in Fig. 3.24b, this involves a tapered-film coupler, which was already discussed in Subsection 3.1.7. The fiber is introduced into the substrate through a cylindrical hole and is sealed therein with a special cement of appropriate refractive index. The end of the hole is hemispherical and is positioned so as to collect the energy of the beam

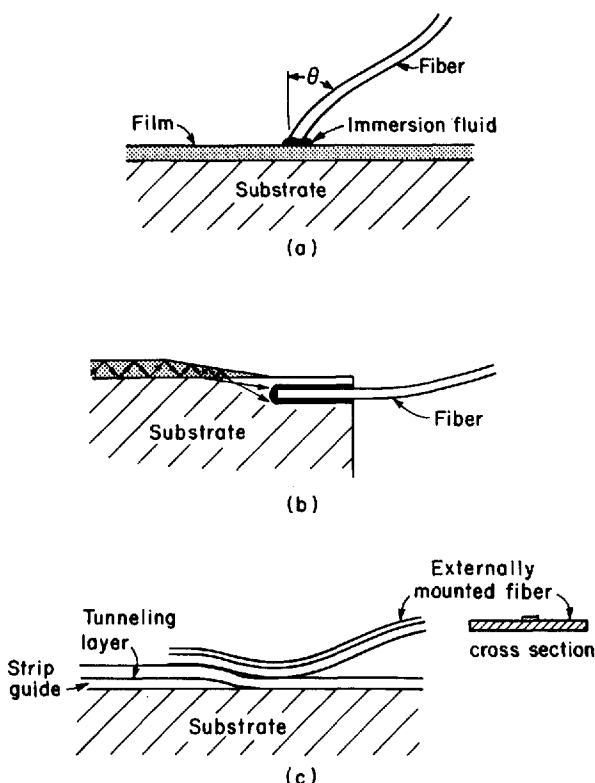


Fig. 3.24a-c. Coupling of a waveguide to a fiber: a) Leaky-wave coupler; b) Tapered-film coupler; c) Coupling using a tapered film and an externally mounted fiber

radiated through the taper when a surface wave is incident. Good matching can thus be established between the field of this beam and the field guided by the fiber. Although a high coupling efficiency can be achieved, this method is applicable primarily to multi-mode fibers but not to single-mode fibers.

Whereas the preceding two schemas coupled a fiber to a planar guide, DALGOUTTE et al. [3.77] have developed couplers between linear guides of the strip variety and fibers. For this purpose, they used a special fiber which is in rectangular rather than circular form and is mounted on an external rectangular fiber of lower refractive index, thus obtaining a stronger fiber structure whose cross-section is shown in Fig. 3.24c. Coupling to a strip guide can then be achieved by clamping this fiber on top of the guide. To obtain a high coupling efficiency and a good match, the end of the strip guide is suitably tapered, as indicated in Fig. 3.24c, and a low-index layer is interposed between the strip guide and the externally mounted fiber. This low-index layer acts as a tunneling region wherein energy is coupled between the strip guide and the fiber via the evanescent field. The tapered end of the guide provides the variable coupling effect discussed above in Subsection 3.2.2. Other coupling schemes similar to that shown in Fig. 3.24c have been proposed by DALGOUTTE et al. [3.77]. In all cases, they used externally mounted fibers and were successful in obtaining a coupling efficiency of 70% not only for guide-to-fiber couplers but also between two externally mounted fibers.

At this point, we would like to observe that connecting or coupling together two separate fibers is one of the most important problems that needs to be overcome in order to ensure the ultimate applicability of fibers to communications and to other industrial purposes. Attempts to solve this so-called "splicing" problem are therefore pursued vigorously at the present time and, whereas some good solutions are already available, especially for connecting multi-mode fibers, this topic lies beyond the scope of this work.

3.2.5. Mode Converters

The conversion of energy from, say, the TE-mode into a TM-mode field can be achieved by introducing anisotropic materials over some distance in the waveguide. The theoretical basis for this operation is outlined in Subsection 2.6.5. In principle, mode conversion arises because a waveguide section loaded by anisotropic materials cannot, in general, support pure TE or TM modes but only combinations of these, i. e., hybrid modes which possess both E_z and H_z longitudinal compo-

nents. Thus, if a surface wave in the TE mode is incident on such an anisotropically loaded section, its field is transformed (for example, via a polarization rotation of the Faraday type in gyromagnetic materials) into a hybrid mode that is continuously changing the ratio of its two TE and TM components as it progresses down the loaded waveguide. If the waveguide dimensions and the length of the anisotropically loaded section are properly adjusted, it is possible to obtain an output field which is of a purely TM type.

In the context of optical waveguides, this type of mode conversion was studied in great detail by WANG and his group [3.80–83]. An experimental verification of their results is described in Fig. 3.25. A thin-film glass waveguide was loaded by a quartz platelet in optical contact, which was achieved by applying pressure to the platelet. Because of the anisotropic nature of quartz, strong TE-TM mode conversion was observed. Although a conversion efficiency of up to 60% was measured, no attempts were made to increase this efficiency to larger values. This kind of mode conversion was also observed in the context of distributed feedback thin-film lasers [3.84, 85], in which case the *substrate* was anisotropic.

By having an acoustic surface wave traverse a thin-film guide (in addition to the optical wave), KUHN et al. [3.86] achieved mode conversion from TE_1 to TE_3 modes and from TM_1 to TM_3 modes. The arrangement for this operation is sketched in Fig. 3.25 b. The mode conversion is produced by the acoustic-optic interaction between the acoustic and optical waves, which requires the condition

$$\beta_1 - \beta_3 = \beta_A, \quad (3.37)$$

where β_1 and β_3 are the propagation factors of either the TE_1 and TE_3 modes, or those of the TM_1 and TM_3 modes, respectively, and β_A is the propagation factor of the acoustic wave. As seen in Fig. 3.25 b the modes were monitored by observing input and output beams coupled to the surface wave in the thin film through grating couplers. Because of their orthogonality properties, no TE-TM conversion occurs in this case and none was observed.

A mode converter to higher-order modes that does not require an acoustic wave has recently been reported by AURACHER [3.87]. As shown in Fig. 3.25 c, this involves two different thin-film waveguides clamped together and forming a wedge. This wedge is filled with an appropriate immersion liquid having a refractive index which is somewhat lower than that of the film guides. If, for example, waveguide I is thinner than waveguide II, more modes will be supported in the latter. To simplify the discussion, let us assume that waveguide I supports one mode

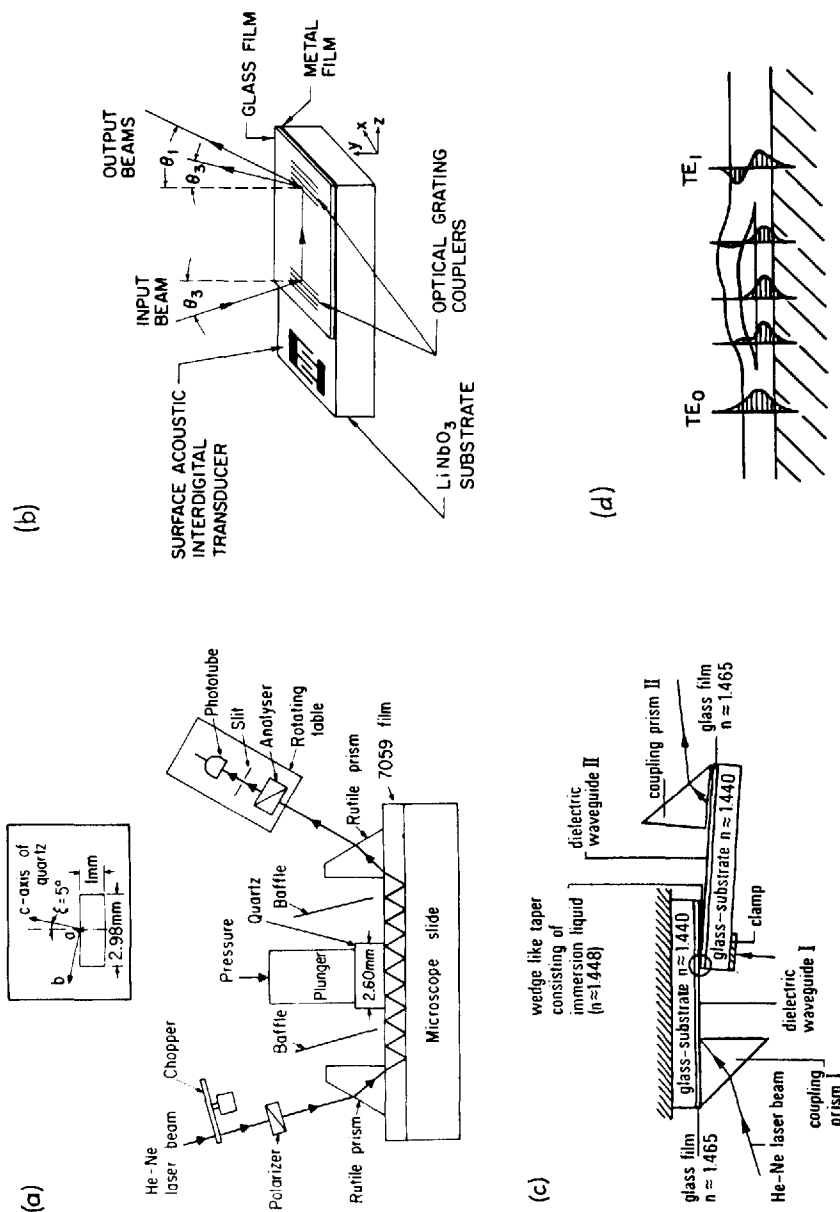


Fig. 3.25a-d. Mode conversion schemes: a) Loading of thin-film waveguide by a quartz platelet having anisotropic properties (after SHAH et al. [3.82]); b) Co-linear acoustic-optic interaction (after KUHN et al. [3.86]); c) Wedge junction (after AURACHER [3.87]); d) Branching waveguide (after YAJIMA [3.100])

whereas waveguide II supports two modes. The single surface-wave mode incident in waveguide I reaches the wedge region by progressing along the usual zig-zag ray path. However, at the film-wedge boundary, the rays do not undergo total reflection and energy is therefore refracted through the wedge region and thus reaches waveguide II. Here, again the rays are totally reflected only at the lower film boundary and energy is refracted back through the wedge region into waveguide I. This process continues down the wedge. The angles of reflection vary along this wedge in a manner analogous to that in the tapered coupler of Fig. 3.19. Because of this variation, some of the rays in waveguide II are at the proper zig-zag angle for the fundamental mode and other rays satisfy the angle for the next higher modes. Thus, both these modes are ultimately excited in waveguide II.

Although this wedge technique has been labelled a mode converter, it is more appropriately regarded as a planar-to-planar coupler between two different waveguides. From this point of view, it is a variation of the coupler of Fig. 3.21c wherein the grating has been replaced by the wedge, which results in higher-order mode excitation. Similar wedge (tapered) schemes have been proposed by DALGOUTTE et al. [3.77] for linear-to-linear guide coupling.

By using a variation of the above tapering schemes, YAJIMA [3.100] has achieved higher-order mode conversion in a so-called "branching" waveguide, as described in Fig. 3.25d. By means of sophisticated deposition techniques, a thin film was split into two sub-layers having a carefully shaped contour. The material separating the two sub-layers, or branches, must have a lower refractive index than that of the film so that the field inside the separating region tends to be evanescent. In this manner, a variable coupling is obtained and the field can then be controlled to achieve the necessary conditions for transforming one mode configuration into another. Thus, in Fig. 3.25d, a $TE_0 - TE_1$ mode conversion is illustrated.

Although it requires careful deposition, the branching scheme developed by YAJIMA [3.100] is very versatile and can be adapted also for mode filtering. This technique could be applied also to linear guides provided, of course, that these linear guides could be deposited with the accuracies required by the special profiles needed for these purposes.

3.2.6. Coupling to Radiation Modes

So far we have discussed the coupling of energy between one guided mode in a waveguide to another mode (or to several modes) in a second waveguide. We have disregarded completely the possible excitation of

radiation modes, except in the case of output beam couplers where the radiated field provided the required outgoing beam. In all other practical cases, the coupling of energy from a guided mode to a radiation mode is undesirable and is usually regarded as a scattering loss.

However, it is important to recognize that losses due to coupling of a guided field into radiation modes can occur whenever irregularities and discontinuities arise. These always appear even in the smoothest transitions but, fortunately, the attendant losses are not too serious. This subject has been treated in considerable depth and the interested reader is referred to the books by MARCUSE [3.88, 89] for detailed and very lucid discussions. Because of the many aspects involved in these problems, each of which may treat a different situation, we shall therefore not pursue this subject here except to mention below some pertinent features concerning bends in waveguides.

The necessity of bending waveguides or designing curved paths for optical strip lines often occurs in integrated optics. Examples of such cases are illustrated in Figs. 3.24c and 3.25d. Because the guided wave cannot easily follow the curved path, radiation or mode conversion losses may occur. These radiation losses are a consequence of the fact that, in the curved region, the field (which extends to infinity) is required to move at a velocity that, for large distances away from the waveguide, is faster than the speed of light. As this is not possible, the field in that far region ceases to be bound to the waveguide and its energy radiates away. As this is, of course, only an intuitively plausible argument, the reader is referred to [Ref. 3.88, p. 398] for a lengthier explanation.

As discussed in considerable detail by MARCATILI [3.90], the radiation losses may be particularly severe in the case of single-mode waveguides that are bent through an insufficiently large radius of curvature. Of particular interest is the case of strip or other linear guides, because these may have to be bent for the purpose of depositing a complete integrated-optics "circuitry" on a substrate. According to

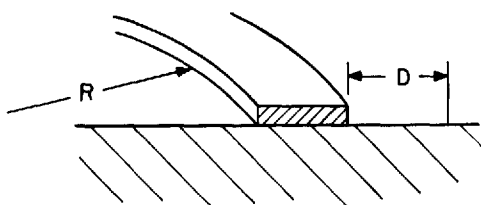


Fig. 3.26. Bent strip waveguide. Here R is the radius of curvature and D is the distance where the field amplitude decreases by a factor of $1/e$.

MARCATILI [3.90], the radiation losses are then negligible provided the radius of curvatures satisfies

$$R < \frac{24\pi^2 D^3}{\lambda^2}, \quad (3.38)$$

where D is now the distance along the substrate where the field amplitude decays by $1/e$, as indicated in Fig. 3.26. Although this criterion is simple, it may not always be easily satisfied. In such cases, other ways of decreasing bending losses are available and these are discussed by MARCATILI [3.90].

3.2.7. Filters and Other Components

Although the present chapter deals with couplers, brief mention will be made here of some other components that have found use in integrated optics. Most of these have little, if any, similarity to coupling functions and they are reported here only because their application is not immediately relevant to the topics treated in the other chapters of this book.

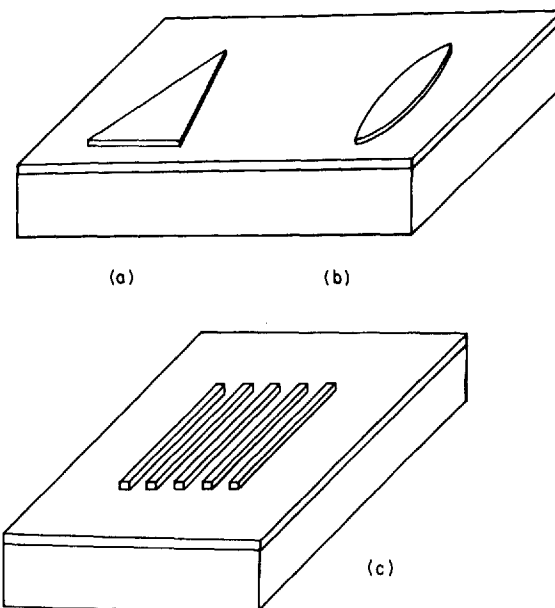


Fig. 3.27a-c. Thin-film planar components: a) Prism; b) Lens, and c) Grating. In all cases, the abrupt (vertical) boundaries may take the form of slanted (tapered) transitions

Amongst the first thin-film components to be examined were shapes other than merely planar waveguides [3.2, 91]. By usually using masking techniques, layers of triangular and lens shapes were deposited, or bars were formed to provide a grating structure, as sketched in Fig. 3.27. These components then function as planar prisms, lens or gratings, respectively, with respect to a surface wave that impinges on them. In fact, by using the equivalent refractive index N as defined in (2.1.14) of Subsection 2.1.2, ULRICH and MARTIN [3.92] have shown that a geometric-optical formulation can be used in two dimensions, which is analogous to the conventional geometrical optics in three dimensions.

Grating structures of the type shown in Fig. 3.27c or Fig. 3.14 have been used as filters [3.93–95, 101–103]. This is accomplished by the stop-band and pass-band properties that are characteristic of any periodic structures. Filtering action was also obtained by SUEMATSU et al. [3.96] who evaporated an aluminum film section on the path of a thin-film waveguide. Because the metallic film absorbs the TE_0 mode considerably less than the TM_0 mode and all of the higher-order modes, this arrangement permitted the filtering out of all but the TE_0 mode. Similar mode-reduction filter properties were also shown by theoretical calculations [3.97, 98], but no further experimental results have been reported.

References

- 3.1. E. R. SCHINELLER, R. P. FLAM, D. W. WILMOT: J. Opt. Soc. Am. **58**, 1171 (1968).
- 3.2. R. SHUBERT, J. H. HARRIS: IEEE Trans. Microwave Theory Tech. MTT-**16**, 1048 (1968).
- 3.3. D. MARCUSE, E. A. J. MARCATILI: Bell System Tech. J. **50**, 43 (1971).
- 3.4. D. HALL, A. YARIV, E. GARMIRE: Opt. Comm. **1**, 403 (1970).
- 3.5. D. HALL, A. YARIV, E. GARMIRE: Appl. Phys. Letters **17**, 127 (1970).
- 3.6. D. B. ANDERSON, J. T. BOYD, J. D. McMULLEN: In *Proc. Symp. Submillimeter Waves* (Polytechnic Press, Brooklyn, N.Y., 1970), p. 191.
- 3.7. L. V. JOGANSEN: Sov. Phys.-Tech. Phys. **7**, 295 (1962); **8**, 985 (1964) and **11**, 1529 (1967).
- 3.8. H. OSTERBERG, L. W. SMITH: J. Opt. Soc. Am. **54**, 1078 (1964).
- 3.9. A. OTTO: Z. Phys. **216**, 398 (1968).
- 3.10. A. S. BARKER, Jr.: Phys. Rev. Letters **28**, 892 (1972). See also the bibliography in reference [3.26].
- 3.11. J. H. HARRIS and R. SHUBERT: "Beam Coupling to Films", Conf. Abstracts, URSI (Int. Sci. Radio Union) Spring Meeting, Washington, D. C. 1969, p. 71.
- 3.12. P. K. TIEN, R. ULRICH, R. J. MARTIN: Appl. Phys. Letters **14**, 291 (1969).
- 3.13. J. E. MIDWINTER, F. ZERNIKE: Appl. Phys. Letters **16**, 198 (1970).
- 3.14. J. H. HARRIS, R. SHUBERT, J. N. POLKY: J. Opt. Soc. Am. **60**, 1007 (1970).
- 3.15. L. N. DERYUGIN, A. N. MARCHUK, V. E. SOTIN: Radioelektronika **13**, 309 and 973 (1970).
- 3.16. V. I. ANIKIN, L. N. DERYUGIN, V. E. SOTIN: Radioelektronika, **14**, 371 (1971).

- 3.17. J. E. MIDWINTER: IEEE J. Quant. Electron. QE-**6**, 583 (1970).
- 3.18. P. K. TIEN, R. ULRICH: J. Opt. Soc. Am. **60**, 1325 (1970).
- 3.19. R. ULRICH: J. Opt. Soc. Am. **60**, 1337 (1970).
- 3.20. J. E. MIDWINTER: IEEE J. Quant. Electron. QE-**7**, 345 (1971).
- 3.21. T. TAMIR, H. L. BERTONI: J. Opt. Soc. Am. **61**, 1397 (1971).
- 3.22. J. H. HARRIS, R. SHUBERT: IEEE Trans. Microwave Theory Tech. MTT-**19**, 269 (1971);
R. ULLRICH: J. Opt. Soc. Am. **61**, 1467 (1971).
- 3.23. T. TAMIR, H. L. BERTONI: "Unified Theory of Optical Beam Couplers", Digest of Technical Papers, Topical Meeting on Integrated Optics (Optical Society of America, 1972), p. MB3-1.
- 3.24. N. S. KAPANY, J. J. BURKE: *Optical Waveguides* (Academic Press, New York, 1972), Chapt. 2, p. 7.
- 3.25. T. TAMIR: Optik **37**, 204 (1973).
- 3.26. R. J. BELL, B. FISHER, I. L. TYLER: Appl. Opt. **12**, 832 (1973).
- 3.27. R. ULRICH: Appl. Phys. Letters **24**, 21 (1974).
- 3.28. R. ULRICH, D. CHEN: Appl. Opt. **13**, 1850 (1974).
- 3.29. L. V. IOGANSEN, L. BERGSTEIN: Appl. Opt. **6**, 2001 (1967).
- 3.30. P. K. TIEN: Appl. Opt. **10**, 2395 (1971).
- 3.31. M. L. DAKSS, L. KUHN, P. F. HEIDRICH, B. A. SCOTT: Appl. Phys. Letters **16**, 523 (1970).
- 3.32. H. KOGELNIK, T. P. SOSNOWSKI: Bell System Tech. J. **49**, 1602 (1970).
- 3.33. L. L. HOPE: Optics Comm. **5**, 179 (1972).
- 3.34. J. H. HARRIS, R. K. WINN, D. G. DALGOUTTE: Appl. Opt. **11**, 2234 (1972).
- 3.35. K. OGAWA, W. S. C. CHANG, B. L. SOPORI, F. J. ROSENBAUM: IEEE J. Quant. Electron. QE-**9**, 29 (1973).
- 3.36. S. T. PENG, T. TAMIR, H. L. BERTONI: Electron. Letters **9**, 150 (1973).
- 3.37. A. J. FOX: Philips Res. Repts. **28**, 306 (1973).
- 3.38. M. NEVIÈRE, P. VINCENT, R. PETIT, M. CADILHAC: Opt. Comm. **8**, 113 (1973).
- 3.39. M. NEVIÈRE, P. VINCENT, R. PETIT, M. CADILHAC: Opt. Comm. **9**, 48 (1973).
- 3.40. M. NEVIÈRE, P. VINCENT, R. PETIT, M. CADILHAC: Opt. Comm. **9**, 240 (1973).
- 3.41. C. ELACHI, C. YEH: Opt. Comm. **7**, 201 (1973).
- 3.42. K. SAKUDA, A. YARIV: Opt. Comm. **8**, 1 (1973).
- 3.43. H. STOLL, A. YARIV: Opt. Comm. **8**, 5 (1973).
- 3.44. D. G. DALGOUTTE: Opt. Comm. **8**, 124 (1973).
- 3.45. K. OGAWA, W. S. C. CHANG: Appl. Opt. **12**, 2167 (1973).
- 3.46. R. ULRICH: J. Opt. Soc. Am. **63**, 1419 (1973).
- 3.47. S. T. PENG, H. L. BERTONI, T. TAMIR: Opt. Comm. **10**, 91 (1974).
- 3.48. S. T. PENG, T. TAMIR, H. L. BERTONI: "Analysis of Thick-Grating Beam Couplers", Digest of Technical Papers, Topical Meeting on Integrated Optics (Optical Society of America, 1974), p. TuB8-4.
- 3.49. J. C. TRACY, L. F. THOMPSON, R. D. HEIDENREICH, J. L. MERZ: Appl. Opt. **13**, 1695 (1974).
- 3.50. S. T. PENG, T. TAMIR: Opt. Comm. **11**, 405 (1974).
- 3.51. S. T. PENG, T. TAMIR: In *Proc. Symp. Optical and Acoustical Micro-Electronics* (Polytechnic Press, N. Y., 1974), p. 377.
- 3.52. K. HANNA, S. T. PENG, T. TAMIR: Appl. Phys. **5**, 325 (1975);
S. T. PENG, T. TAMIR: Appl. Phys. **7**, 35 (1975).
- 3.53. S. T. PENG, T. TAMIR, H. L. BERTONI: IEEE Trans. Microwave Theory Tech. MTT-**23**, 123 (1975).
- 3.54. A. R. NEUREUTHER, F. H. DILL: In *Proc. Symp. Optical and Acoustical Micro-Electronics* (Polytechnic Press, New York 1974), p. 233.

- 3.55. A. YARIV: IEEE J. Quant. Electron. QE-**9**, 919 (1973).
- 3.56. T. TAMIR: Optik **37**, 269 (1973).
- 3.57. R. ULRICH, W. PRETTL: Appl. Phys. **1**, 55 (1973).
- 3.58. A. SAAD, H. L. BERTONI, T. TAMIR: Proc. IEEE **62**, 1552 (1974).
- 3.59. D. G. DALGOUTTE: Appl. Opt. **14**, to be published (1975).
- 3.60. D. FRADIN, P. K. CHEO: J. Opt. Soc. Am. **64**, 1364 (1974).
- 3.61. M. BORN, E. WOLF: *Principles of Optics* (MacMillan Co., New York, 1964), p. 409.
- 3.62. P. K. TIEN, R. J. MARTIN: Appl. Phys. Letters **18**, 398 (1974).
- 3.63. W. SOHLER: J. Appl. Phys. **44**, 2343 (1973).
- 3.64. D. B. OSTROWSKY, R. POIRIER, L. M. REIBER, C. DEVERDUN: Appl. Phys. Letters **22**, 463 (1973).
- 3.65. E. A. ASH, E. SEAFORD, O. SOARES, K. S. PENNINGTON: Appl. Phys. Letters **24**, 207 (1974).
- 3.66. A. IHAYA, H. FURUTA, H. NODA: IEEE J. Quant. Electron. OE-**8**, 546 (1972).
- 3.67. P. K. TIEN, R. J. MARTIN, G. SMOLINSKY: Appl. Opt. **12**, 1909 (1973).
- 3.68. W. S. C. CHANG, M. W. MULLER, F. J. ROSENBAUM: "Integrated Optics" in *Laser Applications*, Vol. 2 (Academic Press, New York, 1974), p. 227. In particular refer to Sect. V. C., p. 300.
- 3.69. H. P. HSU, W. S. C. CHANG, A. BLUM: J. Opt. Soc. Am. **63**, 478 (1973).
- 3.70. R. K. WINN, J. H. HARRIS: "Coupling from Planar to Linear Guides Using Horn Shaped Structures", Digest of Technical Papers, Topical Meeting on Integrated Optics (Optical Society of America, 1974), p. WB8-1.
R. K. WINN, J. H. HARRIS: IEEE Trans. Microwave Theory Tech. MTT-**23**, 92 (1975).
- 3.71. D. B. OSTROWSKY, M. PAPUCHON, A. M. ROY, J. TROTEL: Appl. Opt. **13**, 636 (1974).
- 3.72. R. K. WATTIS: J. Appl. Phys. **44**, 5635 (1973).
- 3.73. E. A. J. MARCATILI: Bell System Tech. J. **48**, 2071 (1969).
- 3.74. H. FURUTA, H. NODA, A. IHAYA: "Optical Directional Coupler Consisting of Optical Stripline", Digest of Technical Papers, Topical Meeting on Integrated Optics (Optical Society of America 1974), p. WB4-1.
- 3.75. S. SOMEKH, E. GARMIRE, A. YARIV, H. L. GARVIN, R. G. HUNSPERGER: Appl. Phys. Letters **22**, 46 (1973).
- 3.76. M. G. F. WILSON, G. A. TEH: Electron. Letters **9**, 453 (1973).
M. G. F. WILSON, G. A. TEH: "Tapered Velocity Coupling Improves Tolerance in Optical Directional Couplers", Digest of Technical Papers, Topical Meeting on Integrated Optics, (Optical Society of America, 1974), p. WB9-1.
- 3.77. D. G. DALGOUTTE, R. B. SMITH, G. ACHUTARAMAYA, J. H. HARRIS, to be published.
- 3.78. R. T. KERSTEN: "Coupling Between Slab-Waveguides and Glass Fibers", Digest of Technical Papers, Topical Meeting on Integrated Optics (Optical Society of America, 1974), pp. WB5-1.
- 3.79. P. K. TIEN, G. SMOLINSKY, R. J. MARTIN: "Theory and Experiment on a New Film-Fiber Coupler", Digest of Technical Papers, Topical Meeting on Integrated Optics (Optical Society of America, 1974), pp. WB6-1.
- 3.80. S. WANG, J. D. CROW, M. SHAH: Appl. Phys. Letters **19**, 187 (1971).
- 3.81. S. WANG, J. D. CROW, M. L. SHAH: IEEE Trans.-Magnetics MAG-**7**, 385 (1971).
- 3.82. M. SHAH, J. D. CROW, S. WANG: Appl. Phys. Letters **20**, 66 (1972).
- 3.83. S. WANG, M. L. SHAH, J. W. CROW: IEEE J. Quant. Electron. QE-**8**, 212 (1972).
- 3.84. J. E. BJORKHOLM, T. P. SOSNOWSKI, C. V. SHANK: Appl. Phys. Letters **22**, 132 (1973).
- 3.85. H. KOGELNIK, C. V. SHANK, J. E. BJORKHOLM: Appl. Phys. Letters **22**, 135 (1973).
- 3.86. L. KUHN, P. F. HEIDRICH, E. G. LEAN: Appl. Phys. Letters **19**, 428 (1971).
- 3.87. F. AURACHER: Opt. Comm. **11**, 187 (1974).

- 3.88. D. MARCUSE: *Light Transmission Optics* (van Nostrand Reinhold Co., New York, 1972), Chapt. 9, p. 340.
- 3.89. D. MARCUSE: *Theory of Dielectric Optical Waveguides* (Academic Press, New York, 1974), Chapt. 4, p. 132.
- 3.90. E. A. J. MARCATILI: Bell System Tech. J. **48**, 2103 (1969).
- 3.91. R. SHUBERT, J. H. HARRIS: J. Opt. Soc. Am. **61**, 154 (1971).
- 3.92. R. ULRICH, R. J. MARTIN: Appl. Opt. **10**, 2077 (1971).
- 3.93. F. W. DABBY, A. KESTENBAUM, V. C. PAEK: Opt. Comm. **6**, 125 (1972).
- 3.94. F. W. DABBY, M. A. SAIFI, A. KESTENBAUM: Appl. Phys. Letters **22**, 190 (1973).
- 3.95. D. C. FLANDERS, R. V. SCHMIDT, C. V. SHANK: "Grating Filters for Thin-Film Optical Waveguides", Digest of Technical Papers, Topical Meeting on Integrated Optics (Optical Society of America, 1974), p. TuB2-1.
- 3.96. Y. SUEMATSU, M. HAKUTA, K. FURUYA, K. CHIBE, R. HASUMI: Appl. Phys. Letters **21**, 291 (1972).
- 3.97. T. TAKANO, J. HAMASAKI: IEEE J. Quant. Electron. QE-**8**, 206 (1972).
- 3.98. T. E. BATCHEMAN, S. C. RASHLIGH: IEEE J. Quant. Electron. QE-**8**, 848 (1972).
- 3.99. D. B. HALL, C. YEH: J. Appl. Phys. **44**, 2271 (1973).
- 3.100. H. YAJIMA: Appl. Phys. Lett. **22**, 648 (1973); H. YAJIMA: In *Proc. Symp. Optical and Acoustical Micro-Electronics* (Polytechnic Press, New York, 1974), p. 339.
- 3.101. K. O. HILL: Appl. Opt. **13**, 1853 (1974).
- 3.102. M. MATSUHARA, K. O. HILL: Appl. Opt. **13**, 2886 (1974).
- 3.103. D. C. FLANDERS, H. KOGELNIK, R. K. SCHMIDT, C. V. SHANK: Appl. Phys. Letters **24**, 194 (1974).

4. Modulation and Switching of Light in Dielectric Waveguides

J. M. HAMMER

With 11 Figures

In this chapter, we will discuss methods of electronically controlling the flow of light in optical waveguides. We will restrict our attention to devices that may be called either modulators or switches. Some of these devices are capable of performing both functions.

In general terms, optical modulators are thought of as devices that place information on a light wave by imposing a time-varying alteration of some measurable property of the wave. The information content is then proportional to the bandwidth of the imposed variation. Switches are thought of as devices which alter the spatial location of a light wave in response to a switching signal. We will try to define these general terms more precisely in the next section.

The point we wish to make here is that optical modulators and switches will find application in a variety of systems only if the economics of using these devices and, indeed, of using light in the first place is favorable when compared to other possible ways of achieving the same purpose. We cannot in this chapter review the economic picture of the systems application of light. We can, however, point out where the real practical and hence economic problems will be with regard to the use of optical modulators and switches.

We may note at once that optical modulators and especially switches have to be important components for the realization of any but the most primitive optical communication or data transmission system. Without electronically controlled optical switches, the switching function in an optical communication or data system must be performed either mechanically or by detecting the light, switching the detected signal electrically and then regenerating a new optical signal. The disadvantage of either of these approaches is obvious. Mechanical switching is inherently slow and frequently unreliable. The second alternative of detection, electronic switching and regeneration is complex and thus likely to be costly in power requirements and components. In addition, this method adds high insertion loss which must be made up by electronic amplification with a consequent reduction in the signal-to-noise ratio.

In the absence of good modulators, information can only be impressed on optical carriers by modulating the light source. This require-

ment places constraints on the possible sources that may be used, and, because of the very nonlinear pumping characteristics of lasers, presents serious problems in obtaining analog types of modulation when coherent light is desired. The use of a modulator, therefore, widens the choice of light sources and allows the chosen light source to be optimized for basic emission characteristics such as, for example, efficiency and coherence.

It is thus of considerable importance to the future of optical communications to have efficient high-speed light modulators and switches. Without these components, system flexibility comparable to that of conventional electronic methods will not be realized. Without sufficient system flexibility, it will be difficult for optical methods to economically compete with conventional alternatives.

Using bulk methods, it has been very difficult to obtain modulators and switches in which the cost of both fabrication and of providing drive power was sufficiently low to seriously compete with conventional communication systems operating above the UHF range.

As will be seen, the chief reason for high drive-power cost resides in the relative weakness of available effects for switching and modulating light. In bulk devices, it proves necessary to provide strong electric, magnetic or acoustic fields which occupy a relatively large volume. Of necessity, therefore, the stored field energy is high and the drive power is proportional to the stored energy. Optical waveguides, which inherently restrict the light flow to regions with at least one dimension on the order of an optical wavelength, are ideally suited to make optimal use of the weak physical effects available. As a result, savings in drive power of greater than an order of magnitude as compared to the bulk devices are expected and have been realized.

4.1. Definition of Modulator, Switch, and Scanner

By modulation we refer to the operation by which information content is placed on a coherent light wave. While it is obvious that a continuous light wave carries no information, it should also be noted that a regularly pulsed light wave such as might be emitted from a mode-locked laser also carries no information. Thus, we will consider a modulator to be a device that alters a detectable property of a light wave in response to an applied electrical signal. For our purposes, the detectable properties of a coherent light wave will be considered to be intensity (amplitude), phase, polarization, and wavelength (frequency).

By switching we refer to the operation by which the spatial location of a coherent light wave is changed in response to an electrical signal.

In a switch, a wave bounded by a circular area A_1 centered at point P_1 on a plane at right angles to the propagation direction is moved in response to an electrical signal to a second area A_2 centered at P_2 on a second plane that need not be parallel to the first plane. This definition of switching then implies either spatial or angular separation between the switched and unswitched beam.

Scanning is an extension of the concept of switching in which the light wave is brought to any of two or more spatial locations in response to an electrical signal. The beam motion may be continuous or discrete. Clearly, then, a number of sequential switches may be used as a scanner. Because of space limitations, we will not further consider scanners in this chapter. We note that a switch will also function as an intensity modulator since the intensity at both P_1 and P_2 will change when the electrical signal is applied.

As will be described at greater length below, some modulators can be directly used as spatial switches while others would require the use of additional devices for conversion to switches.

4.2. Measures of Relative Merit and Systems Uses

The desired performance characteristics of the modulators and switches discussed here are set by the use for which the devices are intended. The ultimate acceptability of a particular device will depend on how well and at what cost it performs its functions. There are four widely used measures for evaluating modulators for systems performance. These measures are extinction ratio or maximum depth of modulation, bandwidth, drive power required per unit bandwidth at a given modulation depth, and insertion loss.

4.2.1. Intensity Modulators and Depth of Modulation

To aid in obtaining broadly useful definitions of measures of merit, we will digress slightly and consider intensity modulators before discussing other types of modulators and measures of merit. We define intensity modulators as devices that vary the intensity of a coherent light wave in response to a time-varying signal. With this type of modulation, a plane wave will take the form $A = G(t) \exp[j(\omega t - \beta z)]$ and the intensity will be given by $I = G^*(t)G(t) = |G|^2$. The quantity $|G^2|$ will be a function of the applied signal and the modulator characteristics.

The extinction ratio or maximum depth of modulation is readily defined for intensity modulators as follows. We suppose that with no

signal applied to the modulator, light leaving the modulator and arriving at a detector is measured to have an intensity I_0 . When maximum signal is applied, the measured intensity is I_m . The extinction ratio or maximum modulation depth, η_m , is then defined as

$$\begin{aligned} \eta_m &= |I_m - I_0|/I_0 \quad \text{for } I_m \leq I_0, \\ \text{and} \quad \eta_m &= |I_m - I_0|/I_m \quad \text{for } I_m \geq I_0, \end{aligned} \quad (4.1)$$

At a signal less than maximum, the modulation depth η is

$$\begin{aligned} \eta &= |I - I_0|/I_0 \quad I_m \leq I_0, \\ \eta &= |I - I_0|/I_m \quad I_m \geq I_0, \end{aligned} \quad (4.2)$$

where I is the detected intensity at the signal level considered.

All the modulators and switches considered in any detail in this chapter rely on physical effects that result in phase rather than absorption changes for light passing through the device. These phase changes can always be related to an equivalent intensity change, so that (4.1) and (4.2) are really sufficient for the definition of modulation depth for all cases of interest. The modulators we will discuss thus formally share a functional equivalence which relates an induced phase shift $\Delta\phi$ to an equivalent intensity modulation. For interference modulators, such as polarization and Bragg phase grating devices, the relation is given by

$$\eta = \sin^2(\Delta\phi/2), \quad (4.3a)$$

as discussed by BORN and WOLF [Ref. 4.1, p. 295] and PINNOW [4.2].

Waveguide devices that use phase change to couple energy from one waveguide to another or to couple energy from one distinct waveguide mode to a second distinct waveguide mode have a relation of the form YARIV [4.3]

$$\eta = 1 - [A + (B\Delta\phi)^2]^{-1}. \quad (4.3b)$$

Simple phase modulators, after detection in heterodyne systems, have an equivalent intensity ratio proportional to the Bessel functions of order equal to the sideband number with argument $\Delta\phi$, as shown by KAMINOW et al. [4.4].

Because of the widespread use of bulk electro-optic polarization and acoustic phase grating modulators, consider for the moment devices

with response given by (4.3a). Assume that the device is arranged so that $\Delta\phi = \pi/2$ with no signal. In this case, an ac signal that, for example, increases $\Delta\phi$ by one radian on the positive half cycle and decreases $\Delta\phi$ by one radian on the negative half cycle will result in a total equivalent change in intensity of 70%. In the more general case of pulse-type signals, a phase change of two radians is also equivalent to 70%. As a result, it has been common to compare modulators on the basis of 70% intensity modulation or 2 radians of phase modulation for pulse-responding devices and one radian of phase for analog modulators. We will follow this practice when comparing the drive power requirements of modulators which we will discuss in the next section.

The extinction ratio is an important measure of merit because the signal to noise ratio at the detector will depend critically on the extinction ratio. Without going into a detailed discussion of light detection, which is outside the scope of this chapter, we point out by way of illustration that if the extinction ratio is on the order of a few percent then most of the detected light will carry no signal. Under these conditions, the noise background in most detectors will be dominated by the noise in the unmodulated received light.

4.2.2. Drive Power per Unit Bandwidth at Equivalent Intensity Modulation of 70%—Specific Energy

Having indicated the relation between induced phase changes and equivalent intensity changes, as applied to the modulators that will be discussed, we may now define an important measure of merit which for brevity will be called the specific energy. The specific energy ($P/\Delta f$)₂ is the drive power required per unit bandwidth to obtain a modulation depth equivalent to an intensity modulation depth of 70%. We use the conventional definition of bandwidth as being the difference between the two closest frequencies at which the equivalent intensity modulation depth falls to fifty percent of the maximum value. Most commonly $P/\Delta f$ is expressed in units of milliwatts per megahertz.

The specific energy is an expression of the power cost of placing information on light. In many systems, specific energy gives a measure of one of the main operating costs and thus serves as an effective measure of merit in comparing modulators for systems application. We will discuss the specific energy required by various modulators later in this chapter.

The bandwidth capabilities of the modulators are important measures of merit. Generally, broad bandwidth is a desirable feature enabling large amounts of information to be placed on the light wave. In

conventional communication systems, bandwidths in the range of 10 percent of the carrier frequency are common. Ten percent of the frequency of a light wave is on the order of 10^{13} Hz which is certainly beyond any likely need in the near and possibly far future. Bandwidths as large as 10^{10} Hz are, however, currently thought of as desirable for modulating proposed millimeter wave carrier systems. Bandwidths on this order are also required to perform certain fast switching operations for data processing. Light as a carrier therefore offers the possibility of enormous bandwidth and, to some extent, modulators will be evaluated on the basis of what fraction of this potential they are capable of providing.

4.2.3. Insertion Loss

We may define the insertion loss for all the modulators and switches we will consider as follows. Let the light intensity entering the modulator be I_{in} , then the insertion loss L is defined as

$$\begin{aligned} L &= 1 - I_m/I_{in} \quad \text{for } I_m \geq I_0, \\ L &= 1 - I_0/I_{in} \quad \text{for } I_m \leq I_0. \end{aligned} \tag{4.4}$$

The insertion loss is sometimes expressed in decibels. Thus,

$$L(\text{dB}) = 10 \log L.$$

In comparing modulators with respect to insertion loss, care must be taken to define the points at which the modulator is considered to start and finish. Thus, for example, if two modulators are to be compared for use in a system in which light from a free standing laser is to be modulated and then transmitted through an external system, it is appropriate to consider the insertion loss as being due to the entire modulator structure including whatever coupling devices are required to introduce and remove the light. On the other hand, if two modulators intended for use in some future system conceived as being entirely on a single waveguide substrate are to be compared, it is probably more meaningful to consider only the loss for light transiting the modulator region of the waveguide. Clearly, a general rule independent of the use for which the modulator is intended cannot be made.

The importance of insertion loss to the economics of using modulators in system is almost self evident but is, alas, occasionally overlooked when new devices are being proposed. In many systems, the single most costly power sink is the laser. Gas lasers, for instance, have power efficiencies which are generally below 10^{-4} . Thus, for example,

a one milliwatt He-Ne laser consumes more than 10 watts of power. If a modulator has a net insertion loss of, say, 10 dB, then 100 watts of power would have to be supplied to obtain one milliwatt of modulated output power. Clearly, if a more efficient laser were used, the overall penalty would be less but even for junction lasers with power efficiencies greater than 10%, few system designers will be content with devices which lose much more power than they transmit. Thus, as is generally the case in comparing devices, the relative importance of insertion loss must be evaluated in context of the particular application when alternative modulation approaches are being compared.

4.2.4. Measures of Merit for Switches

The basic function of an optical switch is to move light from one spatial location to another. Many of the amplitude modulators we will discuss later perform precisely this operation. Included in these are the acousto- and electro-optic grating modulators, various waveguide-to-waveguide couplers and mode-to-mode couplers. In the latter case, additional but usually simple structures have to be provided to spatially separate the modes.

The important requirements for a switch are, with one exception, related to modulator requirements. One of the most important measures of merit is the isolation achieved between the two locations. This is sometimes called the degree of cross-talk. In most of the waveguide devices that can be adapted to serve as switches, the cross-talk is numerically the same as the extinction ratio defined earlier. We will thus, for brevity, identify the extinction ratio with the cross-talk when treating switches.

A second important consideration is the switching time T which we can relate to the bandwidth in the usual way by

$$T = 2\pi/\Delta f. \quad (4.5)$$

In most applications involving switches, the specific energy is less important than the power required, if any, to hold the switch in the "on" condition. We can give no general rule for this power other than to note its importance. Finally, the insertion loss of the switch is as important a measure of merit as it is for modulators.

Thus, with the exception of substituting the holding power for the specific energy, the measures of merit for switches are substantially the same as those for modulators.

4.3. Phase, Polarization and Frequency Modulators

The definition of intensity modulation was discussed in Subsection 4.2.1. This was done there so that a broad definition of the measure of merit for modulators and switches could be stated by using the relation between phase change and equivalent intensity change given in (4.3a) and (4.3b). We will now briefly discuss phase and polarization modulators.

4.3.1. Phase Modulation

Phase modulation is perhaps the simplest form of modulation and, as mentioned earlier, is the fundamental effect used in all the modulators we will discuss. A phase modulator changes the phase of light in response to an applied signal. If the electric field of a plane light wave leaving the modulator with no signal applied is

$$\exp[-j(\omega t - \beta z)],$$

then, when a signal is applied, the field is shifted in phase by an amount $\Delta\phi$ and takes the form $\exp[-j(\omega t - \beta z + \Delta\phi)]$. For a time-varying signal, $\Delta\phi$ is a function of time. This type of modulation may be detected with a heterodyne system [4.4]. The amplitude of the first side-band is then proportional to the Bessel function $J_1(\Delta\phi)$ and the carrier amplitude is proportional to $J_0(\Delta\phi)$.

Simple optical phase modulators have not found any widespread technological use. This is probably due to the complexity of the heterodyne detecting system that is required. It is not clear how a simple phase modulator might be adapted for switching use.

4.3.2. Polarization Modulation

Bulk polarization modulators based on the use of the electro-optic effect are perhaps the most commonly used modulation devices at the present time.

A polarization modulator changes the condition of polarization of light waves in response to an electrical signal. Without loss of generality, we may assume that, with no signal applied, plane linearly polarized light emerges from the modulator. The vector amplitude of the electric field of this wave may be expressed as

$$\mathbf{E} = \hat{x} E_x \exp[j(\omega t - \beta z)] + \hat{y} E_y \exp[j(\omega t - \beta z)]. \quad (4.6)$$

Equation (4.6) is the expression for a plane linearly polarized wave. When $E_x = E_y$, the polarization is at 45° to the x axis.

When a signal is applied, the amplitude becomes

$$E = \hat{x} E_x \exp[j(\omega t - \beta z + \phi_x)] + \hat{y} E_y \exp[j(\omega t - \beta z + \phi_y)] \quad (4.7)$$

where ϕ_x and ϕ_y are functions of the applied signal and thus, in the general case, they are functions of time. If we now define the phase shift $\Delta\phi$ as

$$\Delta\phi = \phi_x - \phi_y \quad (4.8)$$

then (4.7) represents an elliptically polarized wave in which the angle the major axis of the ellipse makes with the x axis depends on $\Delta\phi$. In the special case that $\Delta\phi = \pi$, (4.7) represents a linearly polarized wave whose polarization direction is rotated through 90° from the original direction assumed in (4.6). If a wave such as represented by (4.7) is passed through an analyzer, the transmitted intensity will be given by $\sin^2(\Delta\phi/2)$ [4.1]. The type of polarization modulation represented by (4.6) and (4.7) is characteristic of electro-optic polarization modulators. In the case of magneto-optic polarization modulators, the light remains linear polarized but rotates in direction as a function of the signal. This latter type of rotation (Faraday rotation) will be discussed at greater length in Subsection 4.4.3.

Polarization modulators may be used as switches by passing the beam through suitably oriented birefringent crystals [4.5].

4.3.3. Frequency Modulators

Optical frequency modulators have not found widespread technological use. An optical frequency modulator shifts the frequency (wavelength) of a light wave in response to an applied signal. For the modest shifts in frequency available from optical frequency modulators, detection must be performed with a heterodyne type of system and presents many difficulties. The reported devices are restricted to acousto-optic Bragg modulators. Frequency modulation will be discussed further when acousto-optic modulators are described in Subsection 4.4.1.

4.4. Physical Effects Used in Light Modulators

In the following section we will give a brief survey of the physical effects commonly used in light modulators, which may be classified as electro-optic, acousto-optic, and magneto-optic.

4.4.1. Electro-Optic Effects

Electro-optic effects may be broadly defined to include changes in index of refraction, changes in absorption (electro-absorption) and changes in scattering caused by the application of an electric field to a material through which light is propagating. The latter effect is observed in certain liquid crystals. We will mainly discuss refractive index changes induced by electric fields. If the index change varies linearly with the amplitude of the applied field, the effect is known as the linear electro-optic or Pockels effect.

As explained by NYE [4.6], the Pockels effect is observed only in crystalline solids that lack a center of symmetry. At the present time, the Pockels effect is the most widely used of the physical effects for constructing light modulators.

Index changes proportional to the second and higher even powers of the applied electric field amplitude can be observed in all materials and phases. The second-order effect in liquids is known as the Kerr effect.

The magnitude of the linear electro-optic effect is calculated by using the electro-optic coefficients that relate the changes in refractive index to the amplitude of the applied electric field. The electro-optic coefficients are the elements of a third-rank tensor which interrelates the applied field and light polarization and propagation directions referred to the crystalline axes to the index changes.

NYE [Ref. 4.6, Chap. XIII] gives a detailed description of the meaning and use of the electro-optic tensor. Such a description is beyond the scope of this work but we will give a brief summary.

The refractive index of a general crystalline material is specified by the indicatrix or index ellipsoid. The intersection of a plane passing through the center of the index ellipsoid with the ellipsoidal surface is an ellipse. The length B_i of one of the two principal axes of this ellipse is related to the index of refraction n_i of light propagating in a direction normal to the plane and linearly polarized parallel to that principal axis by $n_i = 1/\sqrt{B_i}$. Light propagating normal to the plane but polarized at an angle parallel to neither principal axes propagates as two waves with velocities (refractive indices) corresponding to the reciprocal square roots of the lengths of the two principal axes and with amplitudes proportional to the cosines of the angles between the polarization direction and the direction of the principal axes.

The linear electro-optic effect can be described by small changes in the size and orientation of the indicatrix caused by an applied field. Since the Pockels effect is very small ($\Delta n \lesssim 10^{-4}$), for most purposes, rotational effects on the indicatrix can be neglected and the significant

changes described through variations in the length of the principal axes of the index ellipsoid.

Crystals that show the linear electro-optic effect are also piezoelectric. Piezoelectricity is an electric field induced stress. This is important because stress variations also produce changes in refractive index through the photo-elastic effect, which we will discuss briefly in the next subsection. Thus, to correctly describe the total index change that takes place when an electric field is applied, it is necessary to prescribe the mechanical constraints placed on the crystal. This is done by specifying the electro-optic coefficients for either the clamped or unclamped conditions. The clamped condition corresponds to a crystal under constant strain and is applicable to situations in which the frequency of the modulating field is well above mechanical crystal resonances. In the unclamped (free) condition, the crystal is under zero stress and the coefficients so specified are used for frequencies well below the mechanical resonances. Thus, generally the clamped coefficients are used for high frequencies and the unclamped coefficients are used for low frequencies.

For linear polarized light propagating perpendicular to a principal plane of the index ellipsoid, the electro-optic refractive index change may be expressed as

$$\Delta n = -n'^3 r' E/2, \quad (4.9)$$

where n' is a linear combination of the principle refractive indices, r' is a linear sum of electro-optic coefficients, and E the appropriate component of the applied electric field. Equation (4.9) is a widely used form and can be applied in all the electro-optic devices we will discuss.

A summary of the use of the electro-optic tensor and tables of electro-optic coefficients were given by KAMINOW in [Ref. 4.7, pp. 447–459]. A sample calculation of the index of refraction for certain propagation directions and polarizations in LiNbO_3 is given in Appendix 4.1.

Because the linear electro-optic effect is basically due to electronic lattice transitions, the response time of the index change approaches the electronic lattice relaxation times, which are in the range 10^{-13} to 10^{-14} sec. Thus, for practical application, the frequency response of the linear electro-optic effect need hardly be considered.

To give some idea of the magnitude of the electro-optic effect, we first note that the phase change in traveling a distance l associated with a given index of refraction change is

$$\Delta\phi = 2\pi l \Delta n / \lambda_0. \quad (4.10a)$$

If a voltage $V_{\lambda/2}$ applied across a gap of width equal to l produces $\Delta\phi = \pi$, the voltage is called the half-wave voltage and is given by

$$V_{\lambda/2} = \lambda_0 / n'^3 r'. \quad (4.10b)$$

Table 4.1. Some typical electro-optic coefficients and refractive index changes for applied fields of 10,000 V/cm

Relative dielectric constant	Material	$\lambda [\mu\text{m}]$	n'	$r' [10^{-12} \text{ m/V}]$	$\frac{\Delta n}{E = 10^4 \text{ V/cm}}$	$V_{\lambda/2} [\text{V}]$
28	LiNbO ₃	0.6328	2.203(n_e)	30 (r_{33})	1.6×10^{-4}	1,970
12.3	GaAs	0.9	3.6(n)	1.2 (r_{14})	2.8×10^{-5}	16,100
8.2	ZnO	0.6328	2.015(n_e)	2.6 (r_{33})	1.1×10^{-5}	29,700

Values of n, r , and ϵ from KAMINOW [4.7]

In Table 4.1 we list typical values of the electro-optic coefficient and refractive index for LiNbO₃, ZnO, and GaAs. These are materials of technological importance which have been used for modulators. Values of Δn calculated from (4.9) when a field of 10⁴ V/cm is applied and values of $V_{\lambda/2}$ calculated from (4.10b) are also listed. We note from Table 4.1 that, even with LiNbO₃ which has one of the strongest electro-optic effects of commercially available materials, a field of 10⁴ V/cm gives an index change of less than two parts in 10⁴ and a half-wave voltage $V_{\lambda/2}$ of almost 2000 V. Nonetheless, all three of these materials have been found useful in the construction of efficient waveguide modulators and LiNbO₃ and a very similar material LiTaO₃ are extensively used in commercially available bulk modulators.

4.4.2. Acousto-Optic Effects

The acousto-optic effect is a change in the index of refraction of a material caused by mechanical strains induced by the passage of an acoustic (strain) wave. The strain and hence the refractive index variation is periodic with a wavelength equal to that of the acoustic wave.

The index changes are caused by the photo-elastic effect, which occurs in all materials and in all material phases: solid, liquid, and gas. The magnitude of the index change caused by a mechanical strain is described by a fourth-rank tensor—the strain-optic tensor. A detailed treatment of the use of this tensor to find the magnitude of the index

changes was given by NYE [4.5]. In general, however, the magnitude of the index change for light propagating in a given direction when a stress is applied in an arbitrary direction is found by using the indicatrix construction briefly described in Subsection 4.4.1. In materials that are electro-optic, strain effects are coupled to electro-optic effects by piezoelectricity. Thus, in crystals showing strong electro-optic effects, it is necessary to include terms in the strain-optic tensor to account for these effects. The electro-optic terms may be responsible for as much as 50% of the total photo-elastic effect, see [Ref. 4.7, pp. 478–488].

In order to actually calculate the refractive index change associated with an acoustic wave, it is necessary to find the strains generated by the wave and then use the strain-optic tensor to find the refractive index changes. The mechanical properties of a general crystal are described by a second-rank tensor which relates stress to strain. The nature of the propagation of an acoustic wave is, in turn, governed by the mechanical properties. Thus, in the most general case, the acoustic wave will propagate as a combination of a shear and compressional wave in a direction other than that in which the wave was launched. Fortunately, in most materials of interest there are sufficient symmetries to reduce the number of tensor components so that, by proper selection of acoustic wave direction and choice of either a compressional or shear wave, simple wave fronts are obtained. Useful treatments of the relation between the index change and the acoustic power were given by PINNOW [4.2], and by SMITH and KORPEL [4.8]. PINNOW [4.2] derived the following relation between the refractive index change and the acoustic power.

$$\Delta n = \sqrt{n^6 p^2 10^7 P_a / 2 \rho v_a^3 A} = \sqrt{M_2 10^7 P_a / 2 A}, \quad (4.11)$$

where

$$M_2 = n^6 p^2 / \rho v_a^3.$$

Here p is the appropriate component of the photo-elastic tensor, v_a is the acoustic velocity, ρ is the density and n is the refractive index. P_a is the total acoustic power in watts and A the cross sectional area in cm^2 occupied by the acoustic wave taken perpendicular to the direction of acoustic propagation. Other units are in the cgs system. M_2 is a commonly used figure-of-merit for acousto-optic materials and is frequently quoted relative to M_2 for fused quartz which has the value $1.51 \times 10^{-18} \text{ sec}^3/\text{gm}$.

In Table 4.2 we list some values of M_2 relative to fused quartz for a few materials that have been used to construct acousto-optic modulators. Using (4.11), Δn is calculated for an acoustic power flux of

100 W/cm^2 and also listed in Table 4.2. The value of 100 W/cm^2 for acoustic power is a rather high but technically achievable level. As can be seen, even for a material such as TeO_2 operating in a shear-wave mode which has an extremely high value of M_2 , Δn is only about six parts in 10^4 .

Table 4.2. Acousto-optic properties of some materials used in acousto-optic modulators. Values adapted from PINNOW [4.2]. M_2 for fused quartz = $1.51 \times 10^{-18} \text{ sec}^3/\text{cm}$. All values are for $\lambda_0 = 0.633 \mu\text{m}$

Material	Wave type	Refractive index	Acoustic attenuation at 500 MHz [dB/cm]	Acoustic velocity $v_a [10^5 \text{ cm/sec}]$	M_2 Relativeto fused quartz	Δn at $P_a/A = 100 \text{ W/cm}^2$
TeO_2	Shear	2.27	4.9	0.617	525	6.2×10^{-4}
PbMoO_4	Longitudinal	2.39	3.3	3.66	23.7	1.3×10^{-4}
LiNbO_3	Longitudinal	2.2	0.05	6.57	4.6	5.8×10^{-5}
Fused quartz	Longitudinal	1.46	3.0	5.96	1.0	2.7×10^{-5}

Table 4.2 includes values of the acoustic attenuation at 500 MHz. High acoustic attenuation will interfere with the operation of devices using acoustic waves by restricting the acceptable path length over which interaction can take place and through heating effects.

4.4.3. Magneto-Optic Effects

While a number of types of magneto-optic effects have been described, the only such effect of real interest for optical modulators is the Faraday effect. TABOR [4.9] gave a brief review of various magneto-optic effects. The Faraday effect in its simplest form is a rotation of the direction of polarization of linearly polarized light caused by an applied magnetic field. In para- and diamagnetic materials, the effect is proportional to the applied field and, in known materials, is too small to be useful for practical devices. In ferromagnetic and ferrimagnetic materials, the rotation is a function of the component magnetization parallel to the light propagation direction. In these cases, the applied magnetic field can be used to change the magnitude or the orientation of the internal magnetization (or both) and thus effects the optical rotation. Very large rotations are observed in certain materials, which we will review in Subsection 4.5.3.

The Faraday rotation may be most simply understood for cubic or isotropic materials as a magnetization dependent difference in the index of refraction for right circularly polarized light as compared to left circularly polarized light propagating in the direction of magnetization. A linearly polarized light wave may be represented as the sum of two circularly polarized waves. In one of the circularly polarized waves, the electric vector rotates clockwise (right circularly polarized) and in the other the electric vector rotates counter clockwise (left circularly polarized). If n^+ is the effective index of refraction for right and n^- the effective index of refraction for left circularly polarized light, the Faraday rotation is equivalent to a rotation of the direction of resultant linear polarization through an angle θ given by

$$\theta = l\pi(n_+ - n_-)/\lambda_0$$

where l is the length of travel.

In ferromagnetic materials, it is common to specify the Faraday rotation per unit length when the sample is magnetized to saturation magnetization. This is called the specific Faraday rotation θ_F and

$$\theta_F = KM_s \cos \gamma, \quad (4.12)$$

where M_s is the saturation magnetization, K is known as the Kundt constant, and γ is the angle between the light propagation direction and the magnetization. Values of θ_F in degrees per centimeter and of $4\pi M_s$ in Gauss are commonly tabulated. See, for example, [Ref. 4.9, p. 1011].

If a magnetic field is applied to a general ferromagnetic material, the direction and magnitude of the magnetization is not simply related to the applied field but depends on both a tensor permeability and the previous history of the sample. One approach for making modulators is to use a dc magnetic field to bring the sample close to magnetic saturation and use the signal field to "tilt" the magnetization [vary the angle γ in (4.12)] and thus modulate the polarization. In this case, the effective component of magnetization in the direction of light propagation may be thought of as being proportional to the applied signal field with a magnetic susceptibility χ_M that depends on the dc magnetization and also on the frequency of signal field, in the form

$$4\pi M = \chi_M H. \quad (4.13)$$

Clearly, χ_M must be specified for the particular material, magnetic history, and orientation chosen. Unfortunately, values of χ_M cannot, in general, be tabulated and must be individually determined because χ_M

is a very sensitive function of the orientations chosen. The ease with which the magnetization can be tilted depends on the anisotropy energy in the tilt direction. Nonetheless, (4.13) will be found useful in our discussion of modulators where it will help to obtain a lower bound on the power required to operate magneto-optic modulators. Using (4.12) with $\gamma=0$, $\cos\gamma=1$ and (4.13), the rotation in degrees for an applied magnetic field H may be formally written as

$$\theta = \chi_M (\theta_F / 4\pi M_S) H l. \quad (4.14)$$

At this point we should note that the simple Faraday rotation found in cubic materials becomes more complex when propagation is at right angles to the magnetization. Here a magnetic birefringence is found (Voigt or Cotton-Mouton effect) resulting in different indices for two orthogonal linear polarized waves. Fortunately, in materials of some interest such as rare-earth garnets, the birefringence is small, e.g., $(n_{||} - n_{\perp}) \sim 10^{-4}$.

Finally, the Faraday rotation in birefringent (uniaxial or biaxial crystals) is no longer a simple rotation of linear polarized light. Here, for propagation in certain directions, rather than a simple rotation, elliptically polarized light with a rotating angle of the major axis of the ellipse is produced by the interaction of the intrinsic Faraday rotation and the material birefringence, see [Ref. 4.9, p. 1016].

The magneto-optic materials are not generally transparent in the visible regions and have thus found more use in the near-infrared and infrared regions. Even in these spectral regions, many materials with large Faraday rotations still strongly absorb light. It is thus common to specify the absorption coefficient α [cm^{-1}] and the Faraday rotation. Most commonly, the tables list as a material figure-of-merit the ratio of twice the specific Faraday rotation to the absorption coefficient $2\theta_F/\alpha$.

4.5. Bulk Modulators

In this section, we will review how the physical effects discussed in Section 4.4 have been applied to construct a variety of optical modulators using bulk materials. A common characteristic of these devices is that the minimum transverse dimensions of the light waves passing through the modulator are determined by the diffraction properties of the light rather than by the properties of the modulator. This is in contrast to the waveguide modulators we will discuss in Section 4.6.

Since the cross-sectional area of the modulator must accommodate that of the light beam, definite lower bounds on required specific energy

are encountered. These bounds are characteristic of the material properties and can be improved only by using a better material. Thus, bulk modulators have inherent limitations which cannot be overcome without controlling the light flow by means other than diffraction limited optics. As will be seen in Section 4.6, properly chosen waveguide devices are capable of overcoming this limitation.

4.5.1. Bulk Acousto-Optic Modulators

Useful acousto-optic modulators are based on the diffraction of light by an acoustic wave. Acousto-optic light diffraction is accomplished by passing the light through a medium in which a traveling acoustic wave has set up an optical phase grating through periodic refractive index changes associated with the acoustic strain field. Two regimes of operation are possible. In the Bragg regime, one finds the highest modulation depth for a given acoustic power, and as a result, most acoustic modulators operate in this regime. Bragg operation requires that the light enters the modulator at a fixed angle to the acoustic wavefronts. Furthermore, the length of the interaction between light and sound must be greater than a certain minimum. As explained below, both these requirements are relaxed in the Raman-Nath regime, as discussed by HAMMER and CHANNIN [4.10].

Figure 4.1 shows the geometry for acousto-optic diffraction in (a) the Raman-Nath regime and (b) the Bragg regime. In both cases, light passing through the sound field parallel to the z -axis (or nearly parallel in the Bragg case) undergoes a phase shift

$$\Delta\phi = \Delta n 2\pi l \sin(2\pi y/\Lambda)/\lambda_0. \quad (4.15)$$

Here Λ is the acoustic wavelength, l the interaction length, and Δn the magnitude of the acoustically induced index change. Δn may be found from (4.11). We neglect the time dependence of the traveling acoustic wave. In both Bragg and Raman-Nath cases, it can be shown that the average effect of the moving index wave is identical to that of a stationary phase grating except that the m -th diffracted order of light is shifted in frequency by $\pm mf_0$, where f_0 is the sound frequency, [4.11].

It is this frequency shift that forms the basis of a frequency modulator. As will be seen below, in the Bragg type of diffraction modulator there is practically only a single diffracted order. This order is shifted in frequency by $+f_0$ when the Bragg angle is arranged to diffract light in the direction of sound propagation and by $-f_0$ for diffraction in the opposite direction. Thus, by varying the acoustic frequency, an

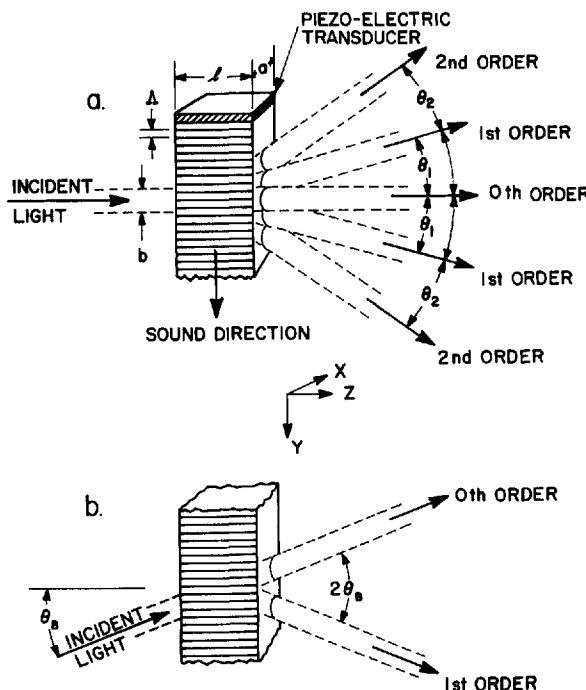


Fig. 4.1a and b. Geometry for acousto-optic diffraction Raman-Nath and Bragg cases

FM modulated light beam is obtained. This effect, which accompanies all acousto-optic diffraction modulators, is generally ignored in most applications of this device. We now separately consider the Bragg and Raman-Nath cases.

The physical basis of the Raman-Nath case is the condition that light diffracted by the sound suffers negligible additional diffraction before leaving the acoustic field. The light is then diffracted into a number of orders at angles given by

$$\sin \theta = m \lambda_0 / \Lambda, \quad m = 0, \pm 1, \pm 2 \dots$$

The intensity of these orders relative to the transmitted intensity in the absence of an acoustic wave, I_0 , is given by [Ref. 4.1, p. 598]

$$I / I_0 = \begin{cases} [J_m(\Delta\phi)]^2 / 2, & |m| > 0 \\ [J_0(\Delta\phi)]^2, & m = 0 \end{cases}$$

where the J 's are the ordinary Bessel functions. The fraction of light removed from the zeroth order is thus

$$\eta_{RN} = (I - I_0)/I = 1 - [J_0(\Delta\phi)]^2. \quad (4.16)$$

The physical basis of the Bragg case is the condition that light diffracted from the incident beam be extensively rediffracted before it leaves the acoustic field. At a particular angle (the Bragg angle θ_B) the phases of the diffracted light cause nearly complete cancellation of all the orders except a single first order. The diffracted light thus ends up mostly in this single first order. A general treatment of the diffraction of light by sound capable of dealing with any diffraction order was given by CHU and TAMIR [4.63].

The Bragg angle is determined by $\sin\theta_B = \lambda/2A$. Note that the angle between incident and diffracted beam is $2\theta_B$. For the Bragg case, the modulation depth for the zeroth order is

$$(I_0 - I)/I_0 = \sin^2(\Delta\phi/2). \quad (4.17)$$

The requirement to operate in the Raman-Nath regime is: $l \ll A^2/\lambda$, and to operate in the Bragg regime is: $l \gg A^2/\lambda$. For this reason, Raman-Nath and Bragg gratings are often called, respectively "thin" and "thick" gratings. Of course, a transition region exists between these extreme cases.

In (4.11) we gave the relation between the acoustic power and the index change. By using (4.11), (4.10a) and (4.17), the modulation depth can be related to the acoustic power. Referring to Fig. 4.2, the appropriate cross-sectional area is la and we obtain

$$\eta = (I_0 - I)/I_0 = \sin^2[(\pi/\lambda_0)\sqrt{10^7 M_2 P_a l/2a}]. \quad (4.18)$$

We now note that the dimensions a and b cannot be freely chosen.

The minimum time required to go from a condition where the acoustic wave interacts with the light beam and "turns off" the undiffracted light to a condition where there is no longer any diffraction is the transit time of the acoustic wave across the beam waist. Referring to Fig. 4.2 it may be seen that this time is just b/v_a and hence the bandwidth $\Delta f = v_a/b$. Thus, b is limited by the bandwidth desired for the modulator. The dimension a is restricted by the diffraction of light which puts a lower bound on the separation of two parallel planes through which a focussed light beam may pass for a given l . We will give an explicit expression for this limitation below. There is, however, a further complication because the Bragg angle depends on the acoustic

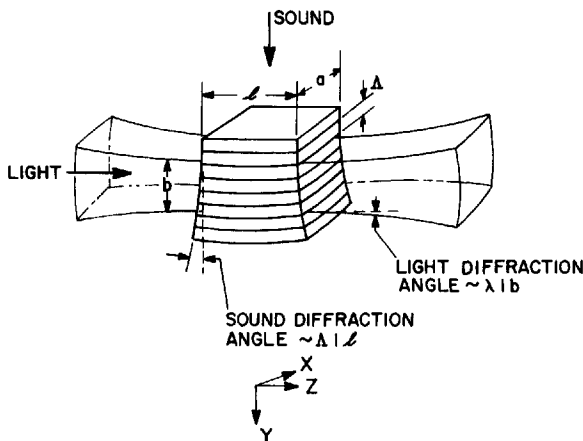


Fig. 4.2. Visualization of the volume of acousto-optic modulators

wavelength and hence on frequency. Thus, for a fixed light-beam entry angle, the depth of modulation is reduced from that of (4.18) if the acoustic frequency is tuned from its center value. The bandwidth is, therefore, limited by both the transit time and the change in Bragg angle. GORDON [4.12] has given a detailed and elegant analysis of this problem, in which he took into account the diffraction properties of both the light and sound waves and found that there is, for a given acoustic power, an intrinsic upper limit on the bandwidth of acousto-optic modulators. This limit is approached when the diffraction angle of the light and that of the sound waves are matched. The matching condition implies that

$$\Lambda/l = \lambda_0/nb. \quad (4.19)$$

Using (4.19), $\Lambda = v_a/f_a$ and the amplitude of $\Delta\phi$ from (4.15) and (4.11), we obtain

$$\Delta f = v_a/b, \quad (4.20a)$$

$$\Delta f \Delta\phi^2 = 10^7 \pi^2 n v_a^2 M_2 P_a / 2 a \lambda_0^3 f_0. \quad (4.20b)$$

We note that, because of the matching condition in (4.19), neither l nor b play a role in setting the required drive power for a given bandwidth.

A modulator figure-of-merit has been defined as

$$M_1 = n v_a^2 M_2 .$$

M_1 is frequently tabulated in addition to M_2 . We may now use (4.20) to obtain an expression for the specific energy of bulk acousto-optic modulators by setting $\Delta\phi$ equal to two radians and solving for $P_a/\Delta f$. Thus

$$(P_a/\Delta f)_2 = 45 f_a \lambda_0^3 a / M_1 \quad (\text{mW/MHz}). \quad (4.21)$$

For convenience, the constants of (4.21) have been adjusted so that $P_a/\Delta f$ is given in units mW/MHz, f_a is in Hz, λ_0 and a in cm and M_1 in cgs units. It should be remembered that (4.21) represents a lower bound on the specific energy. In addition, the value of the thickness a still has a lower bound related to the choice of l actually used in constructing the bulk modulator. It is readily shown for a cylindrical optical beam (where $a=b=2r$) that the minimum radius of a cylinder of length l through which a diffraction limited beam will pass is given by

$$r = \sqrt{\lambda_0 l / \pi n} . \quad (4.22)$$

KAMINOW and TURNER [4.61] point out that, in practical devices, r is multiplied by a safety factor, S , which averages 5. To satisfy both (4.19) and (4.22), the interaction length and optical beam diameter must be

$$\begin{aligned} l &= 4n A^2 / \lambda_0 \\ a = b = 2r &= 2A / \sqrt{\pi} = 2v_a / \sqrt{\pi f_a} . \end{aligned} \quad (4.23)$$

If the diffraction limited value of a from (4.23) is substituted in (4.21), we have

$$\begin{aligned} (P_a/\Delta f)_2 &= 50.8 \lambda_0^3 / M_3 \quad [\text{mW/MHz}] , \\ M_3 &= M_1 / v_a = n v_a M_2 , \end{aligned} \quad (4.24)$$

where λ_0 and M_3 are in cgs units, and M_3 is a third figure-of-merit that has on occasion been used [4.2]. M_1 , M_2 , and M_3 are all quantities that depend entirely on the material properties. Thus, (4.24) places a lower bound on the required specific energy for bulk acousto-optic modulators which depends only on material constants and the wavelength of light. As a result, careful and clever design of a bulk modulator can only assure that the drive power limit of (4.24) is closely approached.

The strong increase of the specific energy with wavelength ($\sim \lambda_0^3$) should be noted when considering the use of bulk acousto-optic modulators for the infrared region.

Table 4.3 gives values of the specific energy calculated from (4.24) by using the materials constants in Table 4.2. If a practical safety factor of five is used, the specific acoustic energies of the last column are obtained. The actual bandwidth attainable will depend on the frequency dependence of the acoustic losses. Of the materials listed, only LiNbO_3 has sufficiently low loss to have a reasonable prospect of being operated in the microwave region.

Table 4.3. Calculated values of specific acoustic energy for bulk modulators made with some useful acousto-optic materials. $\lambda_0 = 0.633 \mu\text{m}$. See Table 4.2 for additional material constants. The required electrical power depends on the efficiency of the transducer and is not considered in this table

Material	$(P_a/\Delta f)_2 [\text{mW/MHz}]$			
	M_1 $[10^{-6} \frac{\text{cm}^2 \cdot \text{sec}}{\text{gm}}]$	M_3 $[10^{-11} \frac{\text{cm} \cdot \text{sec}^2}{\text{gm}}]$	Theoretical limit	Practical safety factor = 5
TeO_2 (shear)	6.85	11.1	0.12	0.6
PbMoO_4 (Long)	11.4	3.13	0.41	2.05
LiNbO_3 (Long)	6.60	1.00	1.29	6.45
SiO_2 Fused Quartz (Long)	0.79	0.13	9.8	49.0

In considering the drive power requirements for acousto-optic modulators, it should be remembered that losses in the electrical-to-acoustic-wave transducers must be taken into account. At relatively low frequencies, losses below 3 dB can be expected. The losses go up rapidly (10 dB or greater) as the microwave range is approached. An additional and hidden power cost is added in the electrical frequency modulator.

Commercial acoustic modulators have been limited to bandwidths below 50 MHz. Generally, extinction ratios close to 100% and insertion losses below 1 dB are available in the bulk acousto-optic modulators.

4.5.2. Bulk Electro-Optic Modulators

All practical bulk electro-optic modulators make use of Pockel's effect materials and basically operate as polarization modulators. In most applications, analysers are added to convert to intensity modulation. A schematic of a typical arrangement is shown in Fig. 4.3. The electric field is produced by the application of a voltage V between the upper and lower electrodes. Typically, the electro-optic crystal chosen for this

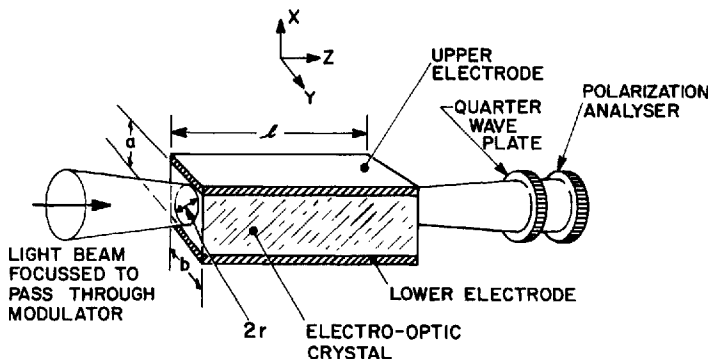


Fig. 4.3. Typical bulk electro-optic modulator

type of transverse field arrangement has a strong electro-optic effect for light polarized parallel to the field direction, the x direction of Fig. 4.3, and zero electro-optic effect for polarization parallel to y . For instance, if LiNbO_3 is used, the "c" crystalline axis would be set parallel to x and the a or b axis parallel to y . For x polarized light, the appropriate r' would be r_{33} and for y polarized light: $r'=0$. The entering light is then arranged to be polarized at 45° to x . With no voltage applied, the output light will be elliptically polarized because of the natural birefringence of the crystal. It is impractical to fabricate the l dimension with sufficient precision to ensure a linearly polarized output. Instead, a quarter-wave plate is frequently placed between the output and the analyzer. The quarter-wave plate is rotated so that the analyzer passes the desired fraction of the light for the chosen operating conditions. The conditions are then as described in Subsection 4.2.1. The quarter-wave plate is also useful to adjust for gross changes caused by temperature variations. Application of a signal voltage rotates the axis of elliptically polarized light to obtain modulation, as described in Subsection 4.3.2.

For crystals of the LiNbO_3 type used in the geometry of Fig. 4.3, $\Delta\phi$ of (4.8) is given directly by (4.9) and (4.10a) with $r' = r_{33}$ and $n' = n_e$. Using these equations in (4.3), the modulation depth is

$$\eta = \sin^2(\pi n_e^3 r_{33} l V / 2a \lambda_0). \quad (4.25)$$

We will now discuss the power required to operate bulk electro-optic modulators. These devices, when constructed with insulating crystals, may be considered to represent pure reactances to an external circuit. As such they absorb no power, reflecting it back into the driving circuits. Practically, however, this power is totally wasted in the supply network and must be supplied by the generator. In fact, for any broadband application, the device reactance would be shunted by a resistance equal to the reactance and then a transformer would be used to match the impedance of the combination to the generator. The reactive power is, in fact, equal to the energy stored in the applied field multiplied by the angular frequency. We will use this identification to calculate the specific energy for electro-optic modulators in a very general way, which need not directly consider how the fields are applied. A similar calculation will be given in the next subsection where we discuss magneto-optic modulators.

The electric field energy stored in an elemental volume of material of dielectric constant ϵ is

$$dU = \mathbf{E} \cdot \mathbf{D} dx dy dz / 2.$$

We may formally integrate this relation over a total volume V_M and obtain

$$P/\Delta f = U = (\pi/2)(\epsilon_0 \epsilon E^2) V_M, \quad (4.26)$$

where ϵE^2 is understood as being a properly averaged quantity related to an applied voltage and ϵ_0 is the permittivity of space. For the simple geometry of Fig. 4.3, neglecting fringing, E is in fact just V/a and the volume is lab . When light is traveling through the material, the phase change, $\Delta\phi$, associated with the field amplitude E is given by (4.9) and (4.10a) and is equal to $\pi ln'^3 r' E / \lambda_0$. Solving for E , we obtain

$$E = \lambda_0 \Delta\phi / \pi ln'^3 r'. \quad (4.27)$$

Substituting (4.27) into (4.26) and assuming a rectangular volume

$$P/\Delta f = \epsilon_0 \epsilon \lambda_0^2 ab \Delta\phi^2 / \pi n'^6 r'^2 l. \quad (4.28a)$$

The specific energy is obtained when $\Delta\phi$ is equal to two radians

$$(P/\Delta f)_2 = 4 \times 10^9 \varepsilon_0 \varepsilon \lambda_0^2 a b / \pi n'^6 r'^2 l \quad [\text{mW/MHz}]. \quad (4.28 \text{b})$$

For convenience, we have adjusted the numerical factor by multiplying with 10^9 to convert W/Hz to mW/MHz. All other units are MKS. As we have already explained in Subsection 4.5.1, a , b , and l cannot be independently chosen in bulk modulators. For a cylindrical beam in which $a=b=2r$, (4.22) may be used in (4.28b) and the specific energy becomes

$$(P/\Delta f)_2 = 16 \times 10^9 S^2 \varepsilon_0 \varepsilon \lambda_0^3 / \pi^2 n'^7 r'^2 \quad [\text{mW/MHz}] \quad (4.29 \text{a})$$

and the modulation depth of (4.25) becomes

$$\eta = \sin^2 [\pi^{3/2} n'^{7/2} r_{33} \sqrt{l V / 4 S \lambda_0^{3/2}}]. \quad (4.29 \text{b})$$

In this case, we have specifically included the safety factor S . Thus, as in the case of the bulk acousto-optic modulator, the lower bound on the specific energy for electro-optic bulk modulators is independent of the dimensions chosen and depends only on the wavelength of light and on the material constants. Here, too, a cubic dependence on λ_0 makes the outlook for the use of bulk electro-optic modulators at infrared wavelengths dim.

We anticipate our discussion of waveguide devices and we assume that the dimension a can be set by means other than diffraction, but that b is limited by diffraction from a one-dimensional aperture rather than a circular aperture, as in (4.22), so that

$$b = \sqrt{2l\lambda_0/n'}. \quad (4.30)$$

Substituting (4.30) in (4.28b), the specific energy for the “one-dimensional” case is

$$(P/\Delta f)_2 = (4\sqrt{2} \times 10^9 / \pi) (\varepsilon_0 \varepsilon \lambda_0^2 / n'^6 r'^2) (a \sqrt{\lambda_0 / n' l}) \quad [\text{mW/MHz}] \quad (4.31)$$

Using the material constants listed in Table 4.1, the specific energy for a bulk LiNbO₃ modulator operating at $\lambda_0=0.63 \mu\text{m}$ is $0.45 S^2 \text{ mW/MHz}$, which for a safety factor of 5 puts a practical lower bound of 11.0 mW/MHz on the specific energy. Commercial bulk electro-optic modulators more often have values closer to 20 mW/MHz . Bulk modulators of a material such as ZnO are entirely impractical. With a safety factor of 5 a ZnO modulator would require 816 mW/MHz .

The practical bandwidths of bulk modulators are essentially limited by the high specific energy and by the relatively high drive voltages required to get a useful extinction ratio. Equation (4.29 b) indicates that, by increasing l , the drive voltage can be reduced indefinitely. Actually, it is not possible to grow crystals of indefinite size so that practically l is limited to a few centimeters. Drive voltages on the order of one hundred volts or more are required.

A LiNbO₃ modulator with a bandwidth of 50 MHz requires a power supply yielding between 0.2 and 0.5 watts of *rf* drive at about 100 or more volts, which is reasonably practical. The power supply for a modulator to reach 500 MHz needing 2 to 5 watts at over 100 volts becomes very difficult. Commercial bulk electro-optic modulators generally offer bandwidths around 25 MHz. It is not possible, as of this writing, to purchase a 50 MHz bulk electro-optic modulator. The commercial bulk electro-optic modulators have very low insertion losses and have extinction ratios that approach 100% provided great care is used in bringing them into proper alignment with the laser beam.

4.5.3. Bulk Magneto-Optic Modulators

Bulk magneto-optic modulators, as contrasted to bulk acousto-optic and electro-optic modulators, have not reached the state of usefulness required for commercial production. We will nonetheless give a brief account of how they operate and develop formal expressions for the required specific energy so that some assessment of the potential usefulness of magneto-optic modulators can be made.

Descriptions of bulk magneto-optic modulators have been given by a number of authors over the last 15 years or so. These include PERSHAN and BLOEMBERGEN [4.13], BLOEMBERGEN et al. [4.14], HANLON and DILLON [4.15], and LE CRAW [4.16]. A variety of methods have been proposed and a few have also been demonstrated. We will not discuss methods that restrict the operation to regions near magnetic resonance because of the limited bandwidth and high signal losses of these approaches. Basically, what we will discuss are devices that dc bias the magnetization of a ferromagnetic magneto-optic material and then use an ac field to "tilt" the magnetization as was described in Subsection 4.4.3. The arrangement used by LE CRAW [4.16] is an example, a schematic of which is shown in Fig. 4.4. The modulator is a cylinder of magneto-optic material. LE CRAW used gallium doped YAG. Light propagates in the z direction parallel to the cylindrical axis. A helical coil is wrapped around the cylinder to provide the signal magnetic field parallel to z and a dc bias magnetic field is applied in the x direction.

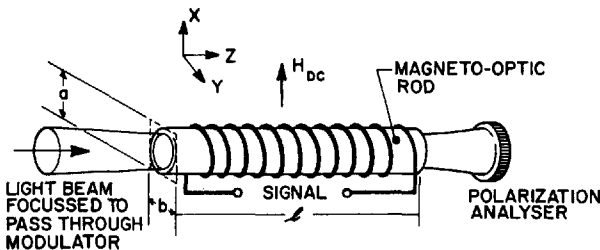


Fig. 4.4. Schematic of bulk magneto-optic modulator

With no current flowing in the signal coil, linearly polarized light both enters and emerges from the modulator. When a signal current flows through the coil, a component of magnetization is induced parallel to the z axis and the angle of the electric vector of the emerging linearly polarized light is rotated from the zero signal position. Using (4.15), we can write the modulation depth of light emerging from the analyzer as

$$\eta = \sin^2 [\chi_M (\theta_F / 4\pi M_S) H l], \quad (4.32)$$

where H is the (average) magnetic field produced by the current flow. We emphasize again that χ_M is a function of H_{dc} and depends strongly on the anisotropy energies of the material for the direction chosen. Clearly, these should be selected so that a signal field "tilts" M in the "easy" direction.

We may calculate the specific energy using arguments similar to those given in Subsection 4.5.2. Thus, in analogy with (4.26) but using cgs units to correspond with most tabulations of magneto-optic properties, the case of magnetic fields yields

$$P/\Delta f = (1/8)(\chi_M - 1) H^2 V_M. \quad (4.33)$$

Solving (4.14) for H in terms of the Faraday rotation θ and substituting in (4.33), we have

$$P/\Delta f = (10^2/8)[(\chi_M - 1)/\chi_M^2](4\pi M_S/\theta_F)^2 (a b/l) \theta^2 \quad [\text{mW/MHz}]. \quad (4.34a)$$

We have assumed a rectangular rod of cross-sectional area ab ; for a circular rod of radius r , ab would be replaced by πr^2 . A Faraday rotation of one radian corresponds to a phase shift $\Delta\phi$ of two radians; thus the specific energy is obtained from (4.34a) by setting $\theta = 57^\circ$ (one radian)

$$(P/\Delta f)_2 = 4.1 \times 10^4 [(\chi_M - 1)/\chi_M^2] (4\pi M_S/\theta_F)^2 (a b/l) \quad [\text{mW/MHz}]. \quad (4.34b)$$

For convenience, we have adjusted the constants so that $P/\Delta f$ is given in mW/MHz. The other units are cgs with M_S in gauss and θ_F in degrees/cm.

In this case, as in the bulk electro-optic modulator, ab and l or r and l are related through the diffraction properties of light. For cylindrical geometry, using (4.22) and a cross-sectional area of πr^2 , (4.34b) becomes

$$(P/\Delta f)_2 = 4.1 \times 10^4 S^2 [(\chi_M - 1)/\chi_M^2] (4\pi M_S/\theta_F)^2 (\lambda_0/n) \quad [\text{mW/MHz}]. \quad (4.35)$$

We note that (4.35), which is a lower limit on the required specific energy, is independent of the dimensions chosen and depends only on material properties and the wavelength. Again, anticipating our discussion of waveguide devices and allowing a to be independent of l but taking b to be diffraction limited, we have using (4.30) in (4.34b)

$$(P/\Delta f)_2 = 4.1 \times 10^4 S [(\chi_M - 1)/\chi_M^2] (4\pi M_S/\theta_F)^2 (\sqrt{2\lambda_0/n} l) a \quad [\text{mW/MHz}]. \quad (4.36)$$

It is very difficult at this time to find values of χ_M for materials that have been used, but very high values, perhaps in the range 10^2 – 10^3 , might be expected. The measured specific energy in LE CRAW's experiment is 0.9 mW/MHz. From his data: $4\pi M_S = 270$ Gauss, $\theta_F = 112^\circ/\text{cm}$ at $\lambda_0 = 1.52 \mu\text{m}$ and we calculate from (4.35) that $(P/\Delta f)_2$ is approximately $18.2 S^2/\chi_M$ mW/MHz. For $S \sim 5.0$, we infer $\chi_M \sim 500$. This indicates that carefully made bulk devices of this material would require powers on the order of 0.3 mW/MHz.

We have not emphasized the general problem of absorption in magneto-optic materials which must always be considered. It appears from (4.35) that the specific energy increases only as the first power of λ_0 , as contrasted to the λ_0^3 dependence for bulk acousto and electro-optic devices. This seems to indicate that magneto-optics is the way to go for infrared modulators. Further reinforcement for this view is provided by the general increase in transparency of magneto-optic materials at longer wavelength. A word of caution, however, is in order in that θ_F is wavelength dependent. The dependence of θ_F on λ_0 is, however, quite variable from material to material. Some show an increase, some a decrease, and others, depending on the range, showing both. Nonetheless, magneto-optic modulators do not in fact pay as strong an inherent wavelength penalty as do the other bulk modulators and must be considered very promising for use in the infrared region where they offer the prospect of both very low specific energy and low insertion loss.

4.6. Optical Waveguide Modulators

In the preceding sections, we have tried to clarify the physical basis and some of the limitations on the operation of bulk modulators of coherent light. A fundamental restriction, common to all the bulk modulators we discussed, was the requirement that the cross-sectional area of the modulator be sufficiently large to allow the light beam to pass through. This requirement sets minimum drive power requirements which are independent of the dimensions because, to obtain a required phase shift, the interaction must continue for a minimum length that puts a lower bound on the cross-section area through the diffraction relation. The total applied energy, however, is proportional to the total volume and hence, for fixed interaction length, it is proportional to the cross-sectional area.

Thus, in bulk modulators, the cross-sectional area restriction comes about because of the diffraction properties of coherent light flowing in essentially unbounded media. Optical waveguides provide a way of overcoming this problem and restricting the cross-sectional area of light flow to regions with transverse dimensions on the order of the wavelength of light for essentially unbounded distance in the direction of light flow. However, diffraction limited optics, at best, can only restrict the cross-section of a coherent light wave to regions with transverse dimensions in the range 10 to 100 wavelengths for the required interaction length. It thus becomes apparent that savings in power of from one to two orders of magnitude should become possible if light modulators make use of optical waveguide structures. Power savings of this order have indeed been realized and a number of examples will be cited later on.

In this section, we will attempt to review how light guiding structures may be used to make modulators. We will again restrict our attention to the three effects we have discussed earlier for the bulk modulators, namely, acousto-optic, linear electro-optic and magneto-optic effects.

The use of waveguides presents additional problems in materials not found in the bulk modulators. At the same time, with light-guiding configurations it becomes possible to perform operations on light that are not practical or in some cases even conceptually realizable when dealing with light flow in unbounded regions. Phenomena such as coupling from waveguide to waveguide or coupling among waveguide modes have no real counterpart in diffraction limited optics. Yet, these operations provide the possibility of making perhaps the most efficient modulators yet conceived.

It is perhaps best to start the technical description of waveguide switches and modulators by contrasting the waveguide and bulk approaches in a general way. In bulk modulators, laser light is focussed

so as to pass through a volume containing active material. An applied field changes the index of refraction of the material so that light undergoes a phase change. The generalized field could be an electric, magnetic or an acoustic field. Characteristically, the volume of interaction consists of a single active material in a bulk modulator. This material must fulfill only the modulator requirements.

In waveguide modulators, laser light is coupled by any of the means discussed in Chapter 3 into a thin film supported on a substrate or restrained between a substrate and a cover. The refractive index of the film must be higher than that of the substrate and higher than that of any covering layer in order that the film act as a waveguide. In addition, the optical fields of the guided wave penetrate some distance into the substrate and the cover depending on the indices and the film thickness. Thus, in its most simple form, the waveguide modulator requires two materials. At least one of these must fulfill the requirements of the modulator while both must have the correct relative static refractive indices. In this case, as in the bulk modulator, an applied field causes phase changes in the guided light. But, here the changes can occur through an effect in the material of the waveguide film, an effect in the material of the substrate, or both.

As a result, the waveguide devices are restricted to materials which not only have a desired active property, as for example, a good acousto-optic figure of merit, but which are also capable of being formed into a waveguide in combination with another material that has a different refractive index. The active material can be used for the waveguide or the substrate, or indeed the top layer. Thus, the choice of materials for waveguide modulators is much more highly restricted than the choice available for bulk modulators, but when suitable materials are found they can be combined in a variety of ways. As a result, the problem of finding suitable material combinations has taken the attention of many workers in the field. The problem of fabricating the waveguides to ensure good waveguide characteristics then becomes intimately coupled to the materials problem. Details of many of these efforts are given in Chapters 5 and 6.

If we assume that some reasonable film substrate combination for a desired effect is available, we may then contrast the methods required to apply the field with those of the bulk devices.

In the case of a bulk device, almost the entire volume of material is subject to the action of the applied field. In the case of the waveguide device, however, it is essential that only the small guiding regions containing optical energy be subject to the applied field. Otherwise, the advantage of small volume is lost. Practically, this means that applied fields must be excluded from most of the substrate which generally has

relatively large thickness because of mechanical requirements. Thus, waveguide modulators require configurations for applied fields that restrict the field to the vicinity of the guiding film.

This requirement is met in a variety of ways. In acousto-optic devices, surface acoustic waves are generated which travel parallel and as far as possible congruent with the guiding film. In electro-optic and magneto-optic devices using insulating materials, the fringing field of electrodes deposited on or near the film surface are used. In devices employing semi-conductors, the properties of junctions are used to restrict the main applied field to the vicinity of the guiding region.

We may summarize the contrasts between the bulk and waveguide devices as follows. The bulk device requires only a single material while the waveguide device requires a combination of materials with specified optical properties. Both devices require means to apply fields that are restricted to the active material regions which contain light. In the bulk device, almost the entire volume of material is active, contains light, and can be immersed in the field. In the waveguide device, only a small fraction of the total material contains the light and can be immersed in the field if the full advantage of the waveguide device configuration is to be realized.

As a result of these restrictions on the waveguide devices, a number of ingenious methods of applying the fields have been proposed and many have been demonstrated. We will now try to make these concepts clearer by describing specific examples of waveguide modulators. It is not physically possible to describe all the device approaches already reported in the literature in this single chapter. We will, however, try to discuss examples of typical methods emphasizing, where possible, those that have been experimentally demonstrated. We will try to gain some idea of the measures of merit of the waveguide modulators and make a tentative assessment of their usefulness. It should be borne in mind that the study of waveguide modulators is a young field and the devices we will now discuss are still largely in the research stage. Nonetheless, some notable results have already been obtained so that there is good promise that a number of useful waveguide modulators will emerge.

4.6.1. Acousto-Optic Waveguide Modulators

The first reported experiment demonstrating the diffraction of an optical guided wave by an acoustic wave was that of KUHN et al. [4.17]. Their general approach has been elaborated by many subsequent investigators, including OHMACHI [4.18, 19], SCHMIDT et al. [4.20], and WILLIE and HAMILTON [4.21]. An early theoretical treatment of colinear acousto-optic interactions was given by CHANG [4.22]. A fairly extensive

theoretical treatment of the general problem of acoustic wave interactions with guided light has been given by GIALLORENZI [4.23], and GIALLORENZI and MILTON [4.24]. Some other experimental approaches will be discussed below.

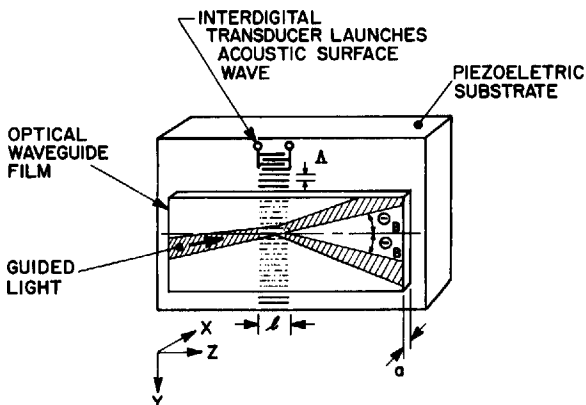


Fig. 4.5. Schematic of acousto-optic waveguide modulator

The type arrangement used by KUHN et al. [4.17] is shown in Fig. 4.5. A glass film of index n_t greater than the index n_s of α quartz is deposited on a α quartz crystal substrate. Interdigital electrodes deposited on regions of the quartz not covered with film launch an acoustic surface wave in the quartz substrate which travels in the y direction and passes through the area of the substrate upon which the waveguide film is deposited. Light is launched into the waveguide at an angle θ_B to the acoustic wavefronts and is diffracted by the periodic refractive index changes induced in both the substrate and the waveguide by the acoustic wave. Here we have an example of a case where the active property of the substrate, the piezoelectric effect, is used to create the desired effect.

OHMACHI [4.18], and WILLIE and HAMILTON [4.21] used similar arrangements in which the acoustic wave is launched in the substrate material. SCHMIDT et al. [4.20] were able to launch the acoustic wave in the optical waveguiding layer directly. Before citing results of these experiments, we will try to give a brief analysis of this type of device.

The physical basis of the acousto-optic interaction has been described in Section 4.5. The condition on the interaction length l to determine if the operation is in the Bragg or Raman-Nath regime are valid here. The intensity of the diffracted light is given in terms of the strain induced

phase shift $\Delta\phi$ by the same relations, (4.15) and (4.16) for the Raman-Nath case and (4.17) for the Bragg case, as in the bulk modulators. The difference in analysis is in computing the phase shift $\Delta\phi$.

When computating the phase shift, account must be taken of the fact that the acoustic wave is interacting with a guided optical wave. In the bulk modulators, both the optical and acoustic fields can be taken, to good approximation, as being uniform over the region in which they interact. In the waveguide, the acoustic surface wave and the guided light wave, however, do not have uniform intensity distribution in the x direction. Therefore, to calculate the actual phase change induced by the non-uniform strain on the non-uniform light energy distribution, it is necessary to evaluate a fairly complex overlap integral. An outline of this problem was given by KUHN et al. [4.17]. GIALLORENZY [4.23], and GIALLORENZY and MILTON [4.24] gave additional treatment of this type of problem. Their results can be used for certain cases if great precision is needed.

For our purposes, however, we may use (4.15) to find $\Delta\phi$, (4.18) to find η and (4.21) to estimate the specific energy for comparison purposes by recognizing that the value of M_1 must be that appropriate to surface waves and that a is related to the guide thickness. In fact, we may take a to be the guide thickness divided by an overlap factor ξ . The quantity ξ may be found by evaluating the overlap integral between the transverse distribution of energy in the guided optical mode and the transverse distribution of energy in the acoustic surface wave. Thus, ξ is a number which is equal to one when the acoustic strain field congruently overlaps the optical field, and is less than one for all cases that the two fields do not completely overlap. Also, ξ may well be dominated by the nature of the acoustic surface wave rather than by the distribution in the optical guided wave. In general, the distribution of acoustic energy in the x direction will have an exponential distribution similar to the evanescent fields of guided optical waves described in Section 2.4. Thus, at the lower acoustic frequencies (longer acoustic wavelength) the energy of the acoustic wave may extend over long distances in the x direction reducing the overlap to small values. Without going into elaborate detail, however, we would expect that ξ will, in fact, be on the order of the ratio of the guide thickness h_f to the surface acoustic wavelength. Using (4.21), we may write the expression for the specific energy of waveguide acousto-optic modulators operating in the Bragg regime

$$(P_a/\Delta f)_2 = 45 \lambda_0^3 f_a h_f / \xi M_1 [\text{mW/MHz}]. \quad (4.38)$$

Some interesting results should be noted. In the optimum case, the use of surface acoustic waves places a lower bound on the required power which

depends on the overlap factor and the waveguide thickness. This comes about because the effective thickness a is the penetration of the surface acoustic wave into the material. Thus, if the optical guided wave is restricted to a thickness h_f much less than A , ξ will be small and no saving in power will be realized. It should also be remembered that the bound set by (4.38) will be reached only when the acoustic transducers are arranged so that the angular spread due to diffraction of the acoustic surface wave parallel to the waveguide plane in the z direction is matched to the diffraction spread in the y direction of the guided optical mode.

For these reasons, the optical-waveguide surface-acoustic-wave modulator may not show the strong decrease in the required specific power when compared to the bulk device that might have been expected from simpler considerations. Alas, the dimension a of (4.21) cannot always be made as small as the thickness of an optical waveguide.

At this point, it will be interesting to survey the results of some of the experiments cited earlier. In the experiment of KUHN et al. [4.17] the center operating frequency was 191 MHz. The authors did not report the bandwidth but it may be inferred from their data. From (4.30) and (4.20a) we have

$$\Delta f = v_a / \sqrt{2l\lambda_0/n} . \quad (4.40)$$

The acoustic beam width l is equal to the transducer width 0.035" or 0.0889 cm. With the 16 μm transducer spacing for 191 MHz reported, the surface acoustic wave velocity may be inferred to be 3×10^5 cm/sec giving a bandwidth of ~ 100 MHz. An acoustic power of 0.18 W is measured (the input electrical power is 2.5 W) for a deflection efficiency of 66%. Adjusting to 70% deflection would require an increase of power by a factor of 1.09 to 200 mW giving a specific acoustic energy of 2.0 mW/MHz. The actual specific electrical energy is 28 mW/MHz. Using (4.38) and assuming $h_f \approx 10^{-4}$ cm, the predicted specific acoustic energy is 0.27 mW/MHz. Here the larger measured specific energy comes about mainly because of poor overlap between the guided optical mode which is largely confined to the optical film and the surface acoustic mode which is largely confined to the substrate. This is nonetheless an encouraging result when compared to the specific acoustic energy of approximately 10 mW/MHz required for an ideal bulk acousto-optic modulator made of the same material (see Table 4.3).

We may compare this result with the more recent work of WILLIE and HAMILTON [4.21] on a very similar system operating at $f_a = 290$ MHz and consisting of an α quartz substrate with a sputtered Ta_2O_5 waveguide. We again infer Δf using (4.40) with $l = 0.055$ cm, $\Delta f = 127$ MHz. The reported acoustic power for 93% diffraction of the TM_1 waveguide mode

at 6328 Å is 175 mW corresponding to 138 mW for 70% modulation. This gives a specific energy of 1.1 mW/MHz. If we again, perhaps unreasonably, assume M_1 to be that of bulk quartz, (4.38) predicts a specific energy of 0.4 mW/MHz. The value for M_1 of Ta_2O_5 has not been reported, but the appropriate value of M_1 to use would average between the two materials. Significantly, the authors found much higher required powers for the TE_0 waveguide mode which would be expected to be more highly confined to the tantalum pentoxide waveguide film than the TM_1 mode.

OHMACHI [4.18] used $LiNbO_3$ as a substrate on which he launched the surface acoustic wave in an As_2S_3 waveguide film. The As_2S_3 has a high figure of merit M_2 in bulk applications but is not transparent in the visible. With an l of 2 mm and a surface acoustic wave velocity of 3.64×10^5 cm/sec, the theoretical value of Δf is 83 MHz and his best power measurement (27 mW for 93% diffraction) gives a specific energy of only 0.29 mW/MHz at $\lambda_0 = 1.15 \mu m$. OHMACHI estimated the overlap factor as $\xi = 0.05$ for his system. He reports the effective figure of merit for the combined system at $f_a = 200$ MHz to be $M_2 = 214 \times 10^{-18}$ sec $^3/gm$, or $M_1 = 70.9 \times 10^{-6}$ cm 2 sec/gm. This is approximately 90 times greater than that of fused quartz. Using OHMACHI's estimate of M_1 , (4.38) would predict 0.02 mW/MHz for $\xi = 1$ indicating that the overlap factor is perhaps slightly larger (~ 0.07) than OHMACHI's estimate.

It should be noted that, in all three experiments discussed, the transducer width l was not chosen to optimize the bandwidth as presumed in (4.38). Thus, the specific energies we calculate here are idealized values intended to give an idea of what might be expected if the geometry were optimized. Hence, despite the very encouraging results, all three experiments cited thus far suffered, to some extent, from the use of an acoustic surface wave that does not overlap the guided optical wave and a non-optimum choice of transducer width l . The latter problem can be readily corrected but the former problem requires a different waveguide system.

In the experiments of SCHMIDT et al. [4.20], a high-index layer was produced by out-diffusion [4.64] and provided both the optical waveguide and surface acoustic wave medium, so that much better overlap between the two waves may, in principle, be obtained. Unfortunately, in this particular experiment, the opposite problem arose. The waveguide itself must be very thick because of the small index change between the out-diffused layer and the remainder of the $LiNbO_3$ which acts as a substrate. Thus, the optical wave is not confined as tightly as the surface acoustic wave. This problem may be overcome using recently reported waveguides made by diffusing metallic niobium into $LiTaO_3$,

as discussed by HAMMER and PHILLIPS [4.25]. These materials will be described at somewhat greater length in the next section.

In the reported experiment of SCHMIDT et al., the device was operated in the Raman-Nath regime. Here we cannot directly use (4.38) and it is not necessary to satisfy all the diffraction matching requirements implied by this equation. The authors cited a specific energy for 100% diffraction into all orders (i.e., the zeroth order completely "turned off") of 25 mW/MHz.

There is a general problem in addition to those already mentioned in using the surface acoustic wave approach in practical applications. The requirements on the number of transducer finger pairs to get efficient electrical power to acoustic power coupling is in conflict with the requirement for broad-band acoustic response to the electrical signal. We must point out that none of the papers we have cited, which use a surface acoustic wave to diffract an optical guided wave, have reported a measurement of the frequency response of the modulated light. At the present time, these devices must be considered to be very promising but they require further development.

There are alternate ways of applying acousto-optics to modulate guided waves. The acoustic wave may be used to couple energy between guided modes of the optical waveguide or between a guided mode and a radiation mode. In the latter case, coupling of light into or out of the waveguide is implied. Coupling among various guided modes of the waveguide and between guided and radiation modes by the use of gratings has been described in detail in Chapter 3. Basically, the periodic phase changes induced by an acoustic wave are considered to play a role analogous to the phase gratings described earlier. A detailed theory of acousto-optic interactions using the coupled-mode approach was given by CHU and TAMIR [4.63].

KUHN et al. [4.26] have demonstrated coupling between the TE_1 and TE_3 modes of a glass waveguide deposited on a metal layer which in turn is deposited on a $LiNbO_3$ substrate upon which the surface waves are launched colinearly with the guided optical waves. They achieved 55% conversion efficiency at $f_a = 320$ MHz but did not report the required power. As they pointed out, the conversion is very narrow-band and might find use as an optical filter. SHAH [4.27] and BRANDT et al. [4.28] reported $TE-TM$ mode conversion using acoustic shear waves launched perpendicular to the waveguide plane. In SHAH's work, a series of electrodes are bonded to a $LiNbO_3$ transducer, which in turn is bonded to SiO_2 cover in intimate contact with a 7059 Corning glass waveguide. The electrodes are spaced with a periodicity d chosen to satisfy the phase match condition $\beta_{TE} - \beta_{TM} = 2\pi/d$.

Thus, acoustic waves launched by the transducer traverse the waveguide setting up a periodic disturbance that acts as a coupling perturbation. The frequency response here is related to the transit time of the acoustic waves across the waveguide thickness and thus can in principle be high. The interaction is, however, weak and the coupling takes place at twice the frequency of the applied signal. SHAH reports that a required power of 4.5 watts is required to obtain only 8% TE to TM conversion over a bandwidth of 17.5 MHz. This amounts to 250 mW/MHz for the 8% conversion. It is not clear what the correct law is for projecting the power requirements to higher conversion efficiencies.

In a related experiment, SHAH [4.29] used interdigital electrodes in a similar geometry to launch shear waves at right angles to the waveguide plane. The geometric arrangement provides a periodic perturbation which results in a thin grating type of diffraction in the waveguide plane rather than TE-TM mode coupling. Although a bandwidth of 300 MHz is reported, the specific power is 20 mW/MHz for 10% total diffraction out of the zeroth order. This projects to approximately 1 W/MHz if 70% modulation could be reached. The approach of launching the acoustic wave perpendicular to the waveguide plane strongly reduces the efficiency of the interaction, as compared to the surface wave methods. This is so because perpendicular launching requires that acoustic energy be supplied over an area which is in no way reduced by the waveguide characteristics when compared to the bulk modulators. Thus, although the frequency response capabilities are not strongly limited by the transit time of the acoustic wave across the waveguide thickness, the power requirements appear excessive. Further study of this approach may perhaps result in ways of overcoming its limitations.

A general comparison of the acousto-optic waveguide modulators with other waveguide modulators will be made after the electro-optic and magneto-optic modulators are discussed in the next two sections. All the acoustic diffraction modulators can be used to obtain frequency modulated light and all can be used as amplitude modulators and/or switches.

4.6.2. Electro-Optic Waveguide Modulator

It is perhaps reasonable to start our discussion of electro-optic waveguide modulators with a very brief review of the current literature. There have been well over thirty publications concerned with various experimental and theoretical aspects of this type of device in the last few years. While no claim for completeness is made, we will mention some of these now. Reported experimental approaches include polarization rotators and

phase modulators using either semiconductor junctions or insulating electro-optical materials. Examples were given by REINHART et al. [4.30], REINHART and MILLER [4.31], CHEO [4.32], WILSON and REINHART [4.44], KAMINOW et al. [4.4], MARTIN [4.34], and FUKUNISHI et al. [4.35]. Amplitude modulators using electro-optic scattering effects in liquid crystal waveguides were described by CHANNIN [4.36], and SHERIDAN et al. [4.37]. Electro-optically induced diffraction grating modulators were reported by HAMMER [4.38], GIARUSO and HARRIS [4.39], POLKI and HARRIS [4.40], HAMMER et al. [4.41], and PHILLIPS and HAMMER [4.25]. Modulators based on waveguide cut off effects were described by HALL et al. [4.42] and CHANNIN [4.43]. CHEO [4.44] observed an electro-optic induced lensing modulator.

Many of these papers deal with guides in which the light is restricted in only one direction. MARTIN [4.34] gave an example of an electro-optic modulator in which the light is restricted in two dimensions by a so-called channel or strip guide. In his example the guides were highly multimode devices that tend, as we will see, to negate some of the advantage hoped for in reducing transverse dimensions. In addition, some of the semi-conducting polarization modulators mentioned earlier have a degree of restriction in the second dimension smaller than what would be allowed in unbounded media. We will mention below many theoretical descriptions of electro-optic mode converters, i.e. TE_i to TE_j or TE_i to TM_j . There have been no experimental reports of electro-optic TE_i to TE_j or TM_i to TM_j converters. Another theoretically efficient and attractive device, namely, an electro-optically switched or controlled coupler between adjacent strip or channel guides has as yet not been reported experimentally. Passively coupled strip guides have been reported by SOMEKH et al. [4.45] who pointed out that their approach lends itself readily for use in an electro-optically controlled coupling modulator.

We should mention here, although we will not further discuss this class of device, that free-carrier effects have also been used to construct modulator like devices. REINHART [4.46] observed efficient electro-absorption in aluminium-gallium-arsenide double heterostructures at $\lambda \sim 0.9 \mu\text{m}$ with specific energies on order of 0.1 mW/MHz . McFEE et al. [4.47] observed optically pumped free-carrier deflection for $10.6 \mu\text{m}$ (CO_2 laser) radiation.

At this point we will give a brief listing of some of the theoretical papers. WANG et al. [4.48, 49 and 50] treated mode converters in systems with passive waveguides on anisotropic (electro-optic) or gyrotropic (magneto-optic) substrates. CHANG and LOH [4.51] gave theoretical calculations for Ge and GaAs phase modulators at $10.6 \mu\text{m}$. SOSNOWSKI and BOYD [4.52] analyzed electro-optic TE - TM mode conversion.

YAMAMATO et al. [4.53] treated TE-TM mode conversion in anisotropic and gyrotropic waveguides. MARCATILLI [4.54] and TAYLOR [4.55] dealt with electro-optic coupling modulation between parallel guides. YARIV [4.3] gave a general coupled-mode theory applicable to a variety of devices including parallel guide couplers and a variety of mode to mode couplers using gratings.

It is apparent even from this brief listing that a number of ways of using the electro-optic effects to construct waveguide modulators have been proposed and a good fraction of these have been experimentally demonstrated. We believe that the electro-optic waveguide modulators which make use of the Pockels effect have shown the greatest promise and, because of obvious space limitations, we will restrict our attention in the remainder of this subsection to devices using the linear electro-optic effect.

The devices we will discuss may be listed as follows: simple phase modulators, polarization modulators, phase grating modulators, coupling modulators between adjacent planar or strip guides ("directional" coupler modulation). Before giving a more detailed description of these modulators we would like to point out that the specific energy requirement for all of these devices is subject to the same type of limitations discussed earlier. Briefly, for a given interaction length, the specific energy depends on the cross-sectional area occupied by the driving field. Optimum use is made of the driving field if the optical field and the applied driving field are congruent. If the optical field occupies a smaller volume than the applied field, some of the latter is wasted. If the applied field occupies a smaller volume than the optical field, the interaction strength is diminished.

As we suggested in discussing the acoustic modulators, it is convenient to represent the effect of overlap by a factor ξ which is equal to one for congruent overlap and is less than one for all other cases. With this factor, the specific energy for all the electro-optic waveguide modulators discussed here can be represented using (4.28 b) as

$$(P/\Delta f)_2 = 4 \times 10^9 / \pi (\epsilon_0 \epsilon \lambda_0^2 / n'^6 r') (a/\xi_a) (b/\xi_b) (1/l) \quad [\text{mW/MHz}] \quad (4.41)$$

where we now identify a as the effective thickness of the guided mode measured in the x direction, ξ_a the overlap factor in the x direction, b the effective width of the guided mode measured in the y direction, and ξ_b the overlap factor in the y direction. Equation (4.41) applies to the general case of a strip or channel guide.

If a one-dimensional guide is used, b is set by diffraction considerations. We may then use (4.31), which was derived for this case, by adjusting

a with its overlap factor. Here there will be no confusion in letting $\xi_a = \xi$ and

$$(P/\Delta f)_2 = (4\sqrt{2} \times 10^9/\pi)(\epsilon_0 \epsilon \lambda_0^2/n'^6 r'^2)(\sqrt{\lambda_0/n' l})(a/\xi). \quad (4.42)$$

To get an idea of how the specific energy of waveguide modulators compares to that of bulk modulators, we make the approximation that, in a one-dimensional guiding system, a is on the order of a wavelength in the medium and, in a strip guide, b is also on this order. Then, for modulators made of the same material, the ratios of the specific energies in the waveguide cases to those in the bulk cases may be found by dividing (4.41) or (4.42) by (4.29). We thus have, assuming $S, \xi = 1$,

$$\begin{aligned} (P/\Delta f) \text{ waveguide}/(P/\Delta f) \text{ bulk} &\sim \sqrt{\lambda/l} && \text{(planar guide)} \\ (P/\Delta f) \text{ waveguide}/(P/\Delta f) \text{ bulk} &\sim \lambda/l && \text{(Strip guide)} \end{aligned} \quad (4.43)$$

For $\lambda = 1 \mu\text{m}$ and $l = 0.1 \text{ cm}$, (4.43) indicates a reduction of the specific energy by more than an order of magnitude in one-dimensional waveguide and three orders of magnitude in strip-waveguide modulators when compared to bulk devices.

The advantage of using the waveguide configuration is thus clear. Because the wave can be restrained by the waveguide to travel in a limited cross-sectional area over an essentially unlimited interaction length, large savings in specific energy can be expected.

A further practical advantage will become apparent when we discuss some actual devices below. The voltage required for a given modulation depth is also strongly reduced in the waveguide case as compared to the bulk case. This comes about because, when using the waveguide format, we can apply low voltages across gaps on the order of size of wavelengths to obtain high fields. In the bulk case, the voltage must be applied across gaps which are at least ten times larger. The practical advantage of low voltage operation is that it simplifies power supply requirements allowing transistor and IC units to be used.

We will now discuss an example of a simple phase modulator that has been reported by KAMINOW et al. [4.4]. In this experiment, two coplanar electrodes separated by a gap g are deposited on the surface of a waveguide formed by out diffusion in LiNbO_3 . The guided light propagates parallel to and under the gap in the electrodes so that the fringing field of a voltage applies to the electrodes overlaps the region in which light is propagating. Orientations are chosen so that the electric vector of a TE mode is parallel to the c axis of the LiNbO_3 . Thus, the appropriate indexes of refraction and electro-optic coefficients for this particular

device are $n' = n_e$ and $r' = r_{33}$. Since the beam is not restrained in the direction parallel to the surface, (4.42) may be applied to estimate the specific energy. The authors observed that, despite the highly multimode character of the out-diffused guide, the effective a is on the order of the gap dimension of 50 μm rather than the waveguide thickness of 500 μm . Under these conditions, with $l=0.62$ cm and assuming ξ is unity, (4.42) predicts a specific energy of 0.59 mW/MHz. The authors report that 0.19 mW/MHz is required for one radian of phase shift which translates to a specific energy of 0.76 mW/MHz ($\Delta\phi=2$ rad); this implies $\xi=0.78$ and is comparable with the authors' estimate. These values are not much less than what would be obtained with an ideal bulk modulator of LiNbO_3 . This is mainly because the highly multimode nature of the waveguide used makes the dimensions comparable to limiting dimensions for bulk modulators.

We should at this point note that electrodes deposited on the surface of a waveguide device waste electric field in the space above the waveguide so that electro-optic waveguide devices using surface electrodes start out with a disadvantage in this respect.

Despite the inherent disadvantage of the multimode guide, the results are still very promising. The large safety factor required for a real bulk modulator is avoided so that the actual specific energy is still a factor of five lower than the bulk case.

To date, reported demonstrations of waveguide polarization modulators have been restricted to devices based on the use of guiding planes formed in the junction region of semi-conduction diodes. One of the earliest of these devices was reported by NELSON and REINHART [4.60]. In their experiment, which is typical of many subsequent observations, the guiding region formed by a high-index epi-layer near the junction plane is reinforced by the depletion layer formed when a gallium phosphide diode is back biased. The waveguide thickness of these devices thus often varies with applied voltage. Orientations are chosen so that the strong field developed across the depletion layer by even modest voltages produces a different index change for TE as compared to TM modes. If both modes are initially excited by a linear polarized wave, the emergent beam will in general be elliptically polarized with the angle that the axis of the ellipse makes with a reference axis being dependent on the applied voltage. Thus, this device is analogous in operation to conventional bulk polarization modulators. We note that, in these devices, the electro-optic effect does not couple TE to TM modes in the waveguide. Neglecting losses due to random scattering or absorption, the intensity of all the modes both TE and TM originally launched into the waveguide are unaffected by the electro-optic effect. Only the relative phase velocities of the modes are changed. As a result, phase match between TE and TM

modes is not required as it would be in mode converter devices where energy is actually exchanged among the modes concerned.

It is characteristic of junction modulators that the electric field is restricted to the depletion layer. It would be hoped that the waveguiding layer might be designed to be almost congruent with the depletion layer to give high overlap factors. Thus, we would theoretically expect the junction devices to make very efficient use of the modulation power. This may be contrasted to devices, such as the simple phase modulator just described and the grating modulators that will be described below, where the applied fields is introduced by electrodes located on one surface of the waveguide. In these devices, as mentioned earlier, the effective field is that due to the fringing field between the coplanar electrodes. Here some of the field is wasted in the region above the electrodes which contain no guided light giving lower values of ξ .

It is clear, however, that very careful design must be incorporated into the junction type modulators if indeed the depletion region is to be congruent with the guiding region. In gallium aluminum arsenide (dH) modulators, it is found that the relative location and size of the guiding layers becomes a function of the applied voltage. The effect is sufficiently strong so that in many dH modulator samples the phase shift is not linear with applied voltage as would be expected for a fixed guiding layer. A detailed study of this problem was given by WILSON and REINHART [4.31].

Nonetheless, the results of REINHART and MILLER [4.33] using GaAs— $\text{Al}_x\text{Ga}_{1-x}\text{As}$ double heterostructures to modulate light at the 1.153 μm line of HeNe are encouraging. They project their results measured with devices having a length l of 404 μm to devices with $l=0.1$ mm (1000 μm) and predict specific energies of 0.42 mW/MHz (2 rad phase) and requiring only 7 volts for one radian of polarization rotation which is, as discussed earlier, equivalent to 70% in intensity.

The appropriate electro-optic coefficient for their orientation [100] is r_{41} . Using GaAs values from Table 4.1 with their reported dimensions of $a=0.14 \mu\text{m}$ and $b=50 \mu\text{m}$, (4.41) predicts a specific energy of 0.41 mW/MHz for $\xi_a=\xi_b=1$. In fact, ξ_b is unity in this geometry and we may thus infer a total overlap of factor $\xi_a=0.98$, which is an excellent result. Insertion loss measurements on the modulated light are not reported but extinction ratios greater than 20 dB are observed. Finally, we note that the expectation of an order of magnitude improvement, as compared to bulk devices, is well realized.

The idea of using periodic electrodes to create an electro-optic phase diffraction grating was described by LEDGER and ASH [4.56] for use with bulk materials. This method is particularly suitable for waveguide devices. HAMMER [4.38] described the use of periodic elec-

trodes to form a grating on thin LiNbO_3 slabs and proposed its application to actual waveguide geometries and GIA RUSSO and HARRIS [4.39], and POLKY and HARRIS [4.40] demonstrated waveguide grating modulation using a Kerr liquid waveguide. HAMMER et al. [4.41] demonstrated efficient grating modulation on epitaxial ZnO on sapphire waveguides. HAMMER and PHILLIPS [4.25] described a very efficient grating modulator using $\text{LiNb}_x\text{Ta}_{1-x}\text{O}_3$ on LiTaO_3 waveguides. We will discuss the latter experiment in some detail. The waveguide is formed by diffusing metallic niobium into LiTaO_3 substrates to form a guiding layer of $\text{LiNb}_x\text{Ta}_{1-x}\text{O}_3$ which has a higher refractive index than pure LiTaO_3 in all orientations.

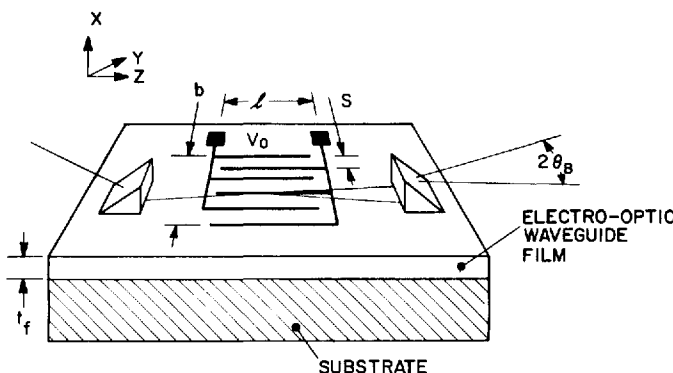


Fig. 4.6. Schematic of electro-optic grating modulator

A schematic diagram of the arrangement is shown in Fig. 4.6. Laser light is coupled into the guide by a prism coupler at the left and coupled out of the guide with a second prism coupler at the right. A chrome-gold interdigital circuit of length $l = 3 \text{ mm}$ and of spacing $s = 7.6 \mu\text{m}$ is formed by photolithography on the waveguide surface. The assembly can be rotated around the X axis so that the angle the guided light makes with the fingers may be varied. When this angle is adjusted to the Bragg angle θ_B and voltage is applied between the interleaved fingers, light is diffracted at an angle $2\theta_B$ from the direction of the main beam.

The voltage applied between the interleaved fingers generates a periodic electric field whose intensity falls off with distance from the plane of the fingers. The in-plane component of this field acts through the appropriate electro-optic coefficient r' on the particular waveguide mode propagating to form an index of refraction or phase grating with

fundamental period $2s$. At any distance beneath the waveguide surface, the amplitudes of the various Fourier field components may be calculated. It is readily shown that the fundamental spatial frequency dominates. Analogously to Bragg diffraction from acoustic waves, a thick or Bragg grating will be produced when the condition $2\pi\lambda_0 L \gg (2s)^2$ is satisfied. Such gratings have the property of diffracting light into a solitary first order when light enters the grating at the internal Bragg angle (angle measured in the waveguide) θ'_B given by

$$\sin \theta'_B \sim \theta'_B = \lambda_0/2(2s)n' = \pi/2s\beta. \quad (4.44)$$

The Bragg angle measured when light is coupled out of the waveguide is $\theta_B \sim \lambda_0/2(2s)$. As the angle is varied from θ_B , the diffracted intensity is reduced. The angular range for a 50% reduction, or the half width, can be shown to be $\Delta\theta_B \approx 4s/L$ for small θ_B such that $\theta_B \approx \sin \theta_B$.

The fraction of the light diffracted depends on the amplitude of the electro-optically induced phase shift $\Delta\phi$. $\Delta\phi$ is given by (4.9) and (4.10a) with E taken as the amplitude of the fundamental in-plane Fourier field component. The field E depends linearly on the applied voltage V .

In terms of $\Delta\phi$, the fractional diffraction is given by $I/I_0 = \sin^2 \Delta\phi/2$ and is thus formally identical to the amplitude modulation obtained when a polarization modulated beam is passed through an analyser. This has the general form $I/I_0 = \sin^2 BV_0$, where I_0 is the intensity of the beam passing out of the circuit when $V_0 = 0$, and I is the intensity of the diffracted beam when V_0 is applied. Because it is so frequently necessary to find the correct electro-optic coefficients to be used when an electro-optic waveguide modulator is being designed, sample calculations for LiNbO_3 - LiTaO_3 waveguides are given in Appendix 4.8.

In Table 4.4 the results obtained in Appendix 4.8 for waveguides consisting of pure LiNbO_3 are summarized. The values used are shown in the table. The optimum angles would change by a relatively small amount if LiTaO_3 numbers were used in place of the LiNbO_3 values for optimization. For $\text{LiNb}_x\text{Ta}_{1-x}\text{O}_3$ we would expect the coefficients to fall between those of the niobate and those of the tantalate and depend on the compositional variable x . Similarly, the values of n_0 and n_e would be bracketed by the values of the unmixed crystals.

The significance of being able to operate at arbitrary angles in either the $a-c$ (Y -cut) plane or $b-c$ (X -cut) plane is clear from the table. Consider, for example, Y -cut samples. If ψ was chosen equal to zero (propagation parallel to the optic axis), a large index difference $\Delta n'$ and, hence, a strong waveguide but zero electro-optic effect would be obtained. At 90° there would be a weaker guide but an appreciable electro-optic effect, namely, $r' = r_{33} = 30 \times 10^{-12} \text{ m/V}$. Operating at 51° , however, a

Table 4.4. Effective indices of refraction and electro-optic coefficients for LiNbO_3 and LiTaO_3 (see Figs. 4.7 and 4.11): $\Delta n' = n'(\text{LiNbO}_3) - n'(\text{LiTaO}_3)$

At 6328 Å

	n_0	n_t	$[10^{-12} \text{ m/V}]$			
			r_{13}	r_{33}	r_{22}	r_{51}
LiNbO_3	2.295	2.203	+ 10	+ 30	+ 6	+ 28
LiTaO_3	2.177	2.181	+ 7	+ 30	~ 1	+ 20

ψ_{opt} calculated using LiNbO_3 values for the electro-optic coefficients

E parallel to W.G plane and perpendicular to propagation direction

	ψ	0°	90°	ψ_{opt}	
				$+ 56.1^\circ$	$- 46.6^\circ$
<i>X-Plates</i>					
TE	r'	r_{22}	r_{33}	- 33.2	+ 36.2
	n'	n_0	n_t	2.230	2.245
	$n'(\text{LiTaO}_3)$	n_0	n_t	2.180	2.179
	$\Delta n'$	0.118	0.021	0.050	0.066
TM	r'	- r_{22}	- r_{13}	- 11.6	- 3.1
	n'	n_0	n_0	n_0	n_0
	$n'(\text{LiTaO}_3)$	n_0	n_0	n_0	n_0
	$\Delta n'$	0.118	0.118	0.118	0.118

Y-Plates

	ψ	0°	90°	$\pm 51.4^\circ$
TE	r'	0	r_{33}	± 34.4
	n'	n_0	n_t	2.237
	$n'(\text{LiTaO}_3)$	n_0	n_t	2.179
	$\Delta n'$	0.118	0.021	0.058
TM	r'	0	r_{13}	+ 7.8
	n'	n_0	n_0	n_0
	$\Delta n'$	0.118	0.118	0.118

E Perpendicular to
W.G. Plane

TE	r'	- r_{22}	0	+ 2.3
----	------	------------	---	-------

relatively strong index difference $\Delta n' \approx 0.06$ is associated with the maximum electrooptic effect $r' \approx 34 \times 10^{-12} \text{ m/V}$.

The results obtained by HAMMER and PHILLIPS [4.25] are shown in Fig. 4.7, where I/I_0 in percent is plotted against voltage for the TE_0

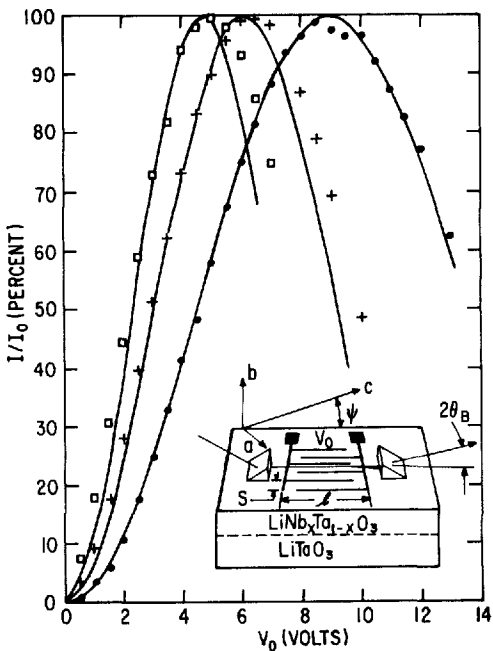


Fig. 4.7. Measured modulation depth for electro-optic grating modulator in $\text{LiNb}_x\text{Ta}_{1-x}\text{O}_3$ on LiTaO_3 waveguides. 4976 Å (squares), 5598 Å (crosses), and 6328 Å (circles). Solid lines are plots of $\sin^2 BV$ normalized at 70%

mode at three wavelengths: 4976 Å (squares), 5598 Å (crosses), and 6328 Å (circles). At 6328 Å, 100% modulation is obtained at approximately 9 V. The specific energy calculated from the capacitive power $(\pi/2)CV^2/4f$ using the measured capacitance of 20 picofarads is: 0.37 mW/MHz ($V=3.5$ V) at 4970 Å, 0.63 mW/MHz ($V=4.5$ V) at 5592 Å and 1.4 mW/MHz ($V=6.6$ V) at 6328 Å.

Using the values given in [4.25] of $a=1.5$ μm, $b=0.04$ cm and the constants listed in Tables 4.1 and 4.4 at $\lambda_0=0.6328$ μm, (4.41) predicts a specific energy of 0.18 mW/MHz for $\xi=1$. The total overlap factor is thus 0.13. We note that the dimension b is at least twice as large as needed, so design improvement could reduce the specific power by a factor of 2. These are also very encouraging results and, as with the polarization modulator previously described, at least an order of magnitude improvement over bulk devices of the same material can be achieved. The authors report waveguide losses below 1 dB/cm at 6328 Å so that low insertion losses would be anticipated.

The waveguide grating modulators are, therefore, very interesting devices which can make good use of advantages offered by optical waveguides. This approach provides amplitude modulation directly without requiring further processing either in or outside the waveguide plane. In addition, the spatial separation of the diffracted beam from the original beam allows the grating modulator to be used directly in switching applications and also makes it conceptually possible to cascade a few such devices on a single waveguide and accomplish more complex switching functions than could be obtained with only one grating.

The final electro-optic waveguide device discussed here is one which has not yet been reported experimentally, but which has been proposed as early as 1969 by MARCATILI [4.54]. With recent improvements in electro-optic waveguides, it seems likely that strip guides in insulating or semi-conducting materials or multilayers in junction type devices can be fabricated with good precision (see, e.g., [4.25, 45, 57]).

With these improved techniques, it now appears likely that it will be possible to form adjacent strip or channel waveguides and vary the coupling between them using the electro-optic effect.

MARCATILI [4.54] described a closely related device and gave an extensive analysis which allows the coupling between adjacent strip guides to be calculated for a number of cases. SOMEKH et al. [4.45] analysed passive strip guide couplers in AlGaAs and pointed out the possibility of electrically controlling the coupling between the adjacent stripes. TAYLOR [4.55] gave an analysis of the type of electro-optic strip guide coupler we will briefly describe below. The reason for the wide interest in this approach is that by using channel guides, both the dimensions a and b of (4.41) can be reduced to sizes on the order of a wavelength and the advantage discussed earlier of further reduction in specific energy obtained.

We consider the device shown schematically in Fig. 4.8. Two single-mode strip guides of electro-optic materials are deposited on a common substrate. The two guides run parallel to each other and are separated by a gap g for a length l . Outside this length, the guides separate. Electrodes are provided as shown so that, if voltage is applied to the outer electrodes with respect to the inner, the fringing electric field in guide 1 has opposite sign to that in guide 2. If guide 1 and 2 are identical so that the phase match condition $\beta_1 = \beta_2$ is met, light flowing in guide 1 will couple into guide 2 and vice versa provided the gap g is sufficiently small so that the evanescent fields of the two guides overlap. If l were very long and all the light was initially in guide 1, after a given distance all the light would be coupled into guide 2 and then, after flowing a similar distance the light would couple back into 1 and so forth. The distance for

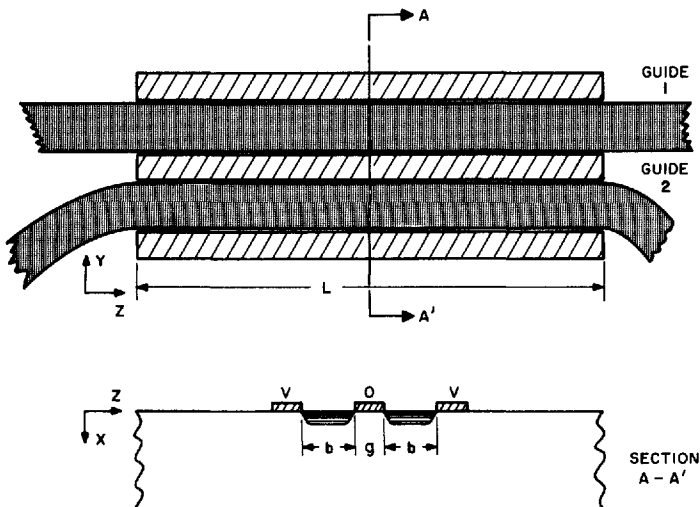


Fig. 4.8. Schematic of electro-optic "stripe" guide coupling modulator

coupling all the light from 1 to 2 under phase match conditions is called the critical coupling length and is given by

$$L = \pi/2\kappa \quad (4.45)$$

as discussed in Subsection 2.8.3, where κ is known as the coupling constant and will be calculated below.

If the two guides are not phase matched

$$\beta_1 \neq \beta_2$$

or

$$\Delta = |\beta_1 - \beta_2| \neq 0 \quad (4.46)$$

all the light will not be coupled and the period of maximum coupling will be shortened. It has been shown that, if the initial intensity of light in guide 1 is I_1 and the initial intensity of light guide 2 is $I_2 = 0$, the coupling ratio is [4.3, 45]

$$(I_1/I_2) = [\kappa^2/(\kappa^2 + \Delta^2)] \sin^2 [\kappa^2 + \Delta^2)^{1/2} z] \quad (4.47)$$

and, if $\Delta^2 \gg \kappa^2$, no light is coupled.

We consider the effect of applying a voltage to the electrodes of Fig. 4.8. With no voltage applied $\beta_1 = \beta_2$ and, if l is chosen using (4.45), all the light is coupled from guide 1 to guide 2. If a voltage is applied and if the directions are chosen so that fields in the y direction produce changes in index of refraction, the effective index of guide 1 will change in the opposite direction from that of guide 2 and phase match will be destroyed, thus changing the amount of light coupled between the two guides [4.55].

We will now give a brief summary of a simplified analysis of this type of device. We assume that the guide thickness a was chosen so that in a one-dimensional guide of this thickness, the TE_0 mode would propagate but the TE_1 mode would just be cut off. This assumption allows the dimension a to be eliminated from the wave propagation expressions.

Under these conditions the coupling constant κ using MARCATIL's analysis is given by

$$\kappa = \frac{(2k_2^2/\beta)(\delta/b)}{1 + (k_2\delta)^2} \exp(-g/\delta) \quad (4.48)$$

where

$$\beta = (2\pi n_s/\lambda_0) \sqrt{2(\Delta n - \delta n)/n_s + 1} \quad (4.49)$$

$$\Delta n = n_f - n_s$$

$$\delta n = \beta/k - n_s$$

$$k = 2\pi/\lambda_0$$

$$k_2 = \pi/(b + \lambda_0/\pi) \sqrt{2n_s \Delta n}$$

$$\delta = (1/\pi) [(2\sqrt{2n_s \Delta n}/\lambda_0)^2 - (b + \lambda_0/\pi) \sqrt{2n_s \Delta n}]^{-1}.$$

The electro-optic modulation relies on changing Δ . Small electro-optic changes in the guide refractive indices will not change κ to first order. It is readily shown that

$$\Delta = \pi r' n'^3 (2E_y)/2\lambda, \quad (4.50)$$

where E_y is multiplied by 2 because of the "push-pull" electrode arrangement, and r' is the effective electro-optic coefficient for the orientation chosen.

For simplicity in this brief review, we assume that the sample is a y -cut plate of LiNbO_3 related waveguide. If the propagation direction is taken parallel to a crystalline axis and the light polarized parallel

to the c axis as is the case for the TE_{11} wave, then n_s is the extraordinary index n_e and r' is identical to r_{33} . Thus from (4.50) we get

$$\Delta = \pi r_{33} n_e^3 E_y / \lambda_0.$$

Setting

$$E_y = V \xi / b, \quad (4.51)$$

we obtain

$$\Delta = \pi r_{33} n_e^3 \xi V / \lambda_0 b. \quad (4.52)$$

The switching characteristics of the modulator, if the dimensions Δn and β are known, may now be calculated. As an example, choose

$$\begin{aligned} b &= 5 \mu\text{m} \\ \delta n &= 1.75 \times 10^{-3} \\ \beta &= 21.9 \mu\text{m}^{-1} \\ k_2 &= 0.465 \mu\text{m}^{-1} \\ \delta &= 0.959 \mu\text{m}^{-1}. \end{aligned}$$

These values would give a single mode (TE_{11}) stripe guide in $\text{LiNb}_x\text{Ta}_{1-x}\text{O}_3$ with $x \sim 0.1$, [4.25]. Substituting these values in (4.48), the coupling coefficient is

$$\kappa = 31.6 \exp(-g/0.959) [\text{cm}^{-1}], \quad (4.53)$$

where the gap g between the guides is measured in micrometers.

Using (4.47) and (4.53) and taking $r_{33} = 30 \times 10^{-12} \text{ V/m}$, we calculate I_1/I_2 for three values of g , $g = 1, 2, \text{ and } 3 \mu\text{m}$. These are plotted in Fig. 4.9. The solid curves are the maximum values of I_1/I_2

$$(I_1/I_2)_{\max} = \kappa^2 / (\kappa^2 + \Delta^2).$$

The dotted portion, shown only for $g = 2 \mu\text{m}$, is the complete expression. For $g = 1, 2, 3 \mu\text{m}$, the critical coupling lengths L are 1.14, 0.4, and 0.14 cm, respectively. As can be seen, 100% shut off takes place at $V = 2$ volts with $g = 2 \mu\text{m}$.

The brief treatment given here is very approximate but is intended to give a feeling of the type of design parameters and performance that might be expected. For $g = 2 \mu\text{m}$, $l = 0.4 \text{ cm}$. The specific-energy is approximately $18 \times 10^{-6} \text{ W/MHz}$.

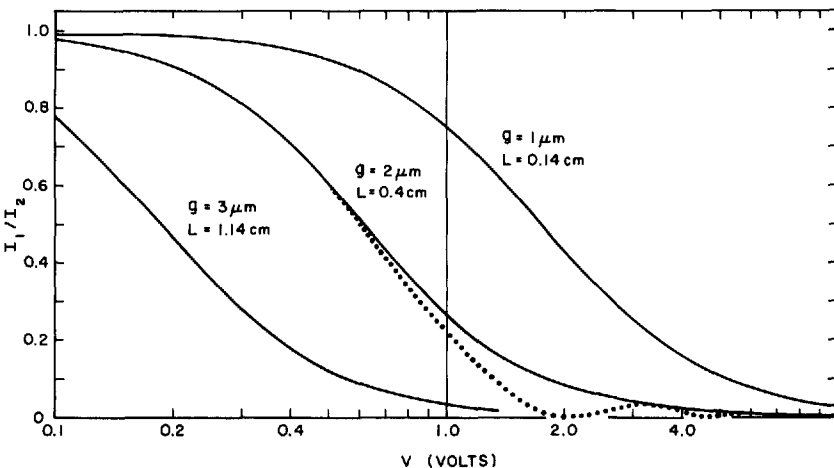


Fig. 4.9. Plot of fraction of light coupled from guide 1 to guide 2 in electro-optic stripe guide modulator as function of applied voltage

Thus, the electro-optic strip guide coupling modulator should be capable of truly outstanding performance. High transfer is possible at low voltage and power. The voltage requirements are a factor of five less and power requirements are at least an order of magnitude lower than the power required by the one dimensional waveguide modulator.

4.6.3. Magneto-Optic Waveguide Modulator

Although there have been many theoretical treatments of magneto-optic waveguide mode converters and other modulators, to the best of the author's knowledge the only reported experiments are those of TIEN et al. [4.58], and TSENG et al. [4.65]. Before discussing the experiments, we will give a brief listing of some of the theoretical treatments. WANG and his colleagues have published a number of papers that treat the general problem of mode conversion in gyrotropic and anisotropic media, [4.48-50,59]. YARIV [4.3] gave a generalized coupled-mode theory which may be applied to magneto-optic waveguides. YAMAMATO et al. [4.53] treated anisotropic and gyrotropic waveguides by a normal mode analysis, which may be applied to magneto-optic modulators. Clearly, any analysis that treats the effect of anisotropy on the propagation of light in optical waveguides may be applied to the case where the anisotropy is introduced or modified by the application of electric or magnetic fields. Thus, the treatments given earlier in this book may be so applied and will not be discussed further at this point.

In the experiment of TIEN et al. [4.58], a waveguide film of $\text{Y}_3\text{Ga}_{1.1}\text{Sc}_{0.4}\text{Fe}_{3.5}\text{O}_{12}$ was epitaxially grown on a $\{1,1,1\}$ $\text{Gd}_3\text{Ga}_5\text{O}_{12}$ substrate. In an earlier work, TIEN et al. [4.62] gave some details of the growth and waveguide properties of these and related garnet films. The growth conditions are arranged so that the magnetization can be rotated freely in the plane of the film. For rotation of M in the plane, an anisotropy field H_1 of less than 1 Oe is estimated. The $4\pi M_s$ of the film is given as 600 G. Thus, the effective magnetix susceptibility χ_M is on the order of [$M_s/H_1 \sim 50$].

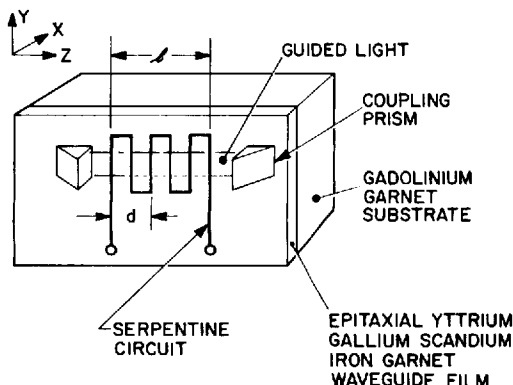


Fig. 4.10. Schematic of magneto-optic waveguide modulator

A schematic of the experimental arrangement is shown in Fig. 4.10. For $1.15 \mu\text{m}$ light propagating in the z direction, components of magnetic field in the z direction cause a Faraday rotation which in a bulk sample would rotate the direction of polarization for light (linearly polarized in the xy plane) through some angle θ around z . In the waveguide, this effect provides a coupling between TE and TM modes. The energy exchange is described by (4.47) of the previous subsection. $I_1 \rightarrow I_{\text{TE}}$ is the intensity of the TE mode and $I_2 \rightarrow I_{\text{TM}}$ that of the TM mode. Thus, in order to get appreciable energy transfer, it is necessary to match the phase velocities of the two modes, i.e., $A = \beta_{\text{TE}} - \beta_{\text{TM}}$ must be very small or zero. This condition is, however, not met in the experimental film itself. Rather, phase match is achieved by perturbing the waveguide with a periodic structure [4.3]. For this purpose, a periodic variation in magnetic field is supplied by having the signal current flow in the serpentine structure shown in Fig. 4.10. The period d is chosen so that

$$2\pi/d = A. \quad (4.54)$$

In operation, a dc bias field parallel to the waveguide plane and at 45° to z is applied. Current flow in the circuit rotates the net magnetic field and hence the magnitude of the z component of the magnetic field varies around the value set by the *dc* bias field. This ensures that the largest value of χ_M is used. Conversion from TE_0 to TM_0 is observed by coupling the light out of the waveguide using rutile prism film couplers. Because of the high birefringence of the rutile, TE_i modes are coupled out at a different angle from TM_i modes. The angular separation is around 20° between the TE_0 and TM_0 modes.

All the energy will be coupled from one mode to the other when (4.54) is satisfied (exact phase match) and the waves interact for a distance equal to the critical coupling length L given by (4.45). TIEN et al. [4.58] calculated the coupling coefficient κ to equal $\gamma\theta_F$ where θ_F is the Faraday rotation and γ measures the depth of modulation of the actual rotation. At exact phase match: $\Delta=0$ and the conversion ratio is given by (4.47) which becomes $I_{TE}/I_{TM}=\sin^2\gamma\theta_F$. For $\gamma=0.8$ and $z=0.6$ cm, the conversion is calculated as 62% while a 52% conversion is measured using a dc signal current of 0.5 A. Since the light is guided in only one dimension, we may use (4.36) to estimate a lower bound on the specific energy for this experiment. TIEN et al. gave the waveguide thickness, $h_f=a=3.5$ μm , $\theta_F=208^\circ/cm$, and $l=0.6$ cm. Using $4\pi M_s=600$ g and our estimate of $\chi_M \sim 50$, the predicted specific energy is only $24/\xi \mu W/MHz$. This is indeed a low value. Although the authors do not specifically give a measured value of the specific energy, we may roughly estimate it to be below 1 mW/MHz from their comment that a 100 mW supply provided an 80 MHz bandwidth and would have apparently provided much more if they had better detectors available.

We might also note that this experiment uses surface electrodes and suffers the same type of loss of driving field as do the electro-optic devices using surface electrodes. In addition, the circuit height h used is apparently greater than required by the diffraction limit. We might therefore expect that the overlap factor is small and the specific energy for an optimized modulator of this type may indeed be on the order of tens of $\mu W/MHz$. We thus see that, with material parameters similar to those reported by TIEN et al. [4.58] infrared waveguide modulators requiring only tens of $\mu W/MHz$ might be achieved.

The insertion loss is not reported but low waveguide losses in the infrared have been observed using similar materials. There has been no reported measurement of the range of wavelengths over which a device such as just been described might be operated.

The experiments of TSENG et al. [4.65] are closely related to those just discussed. The periodic magnetic field is, however, provided by

permanent magnets so that only low frequency modulation can be obtained by varying the bias (dc) field.

4.7. Comparison of Optical Modulators

The two most striking differences between the bulk and the waveguide modulators are found in comparing the drive power and the size. Waveguide modulators require anywhere from one to three orders of magnitude less specific energy (mW/MHz) than bulk modulators and are correspondingly smaller in actual dimensions. We think it important to comment very briefly on how these devices might be used to advantage before discussing the relative performance of the various types of waveguide modulators.

Although the waveguide modulator could be packaged to act as a bench modulator, it is more likely to be used in conjunction with fiber optic transmission lines. In this use, the requirements that the modulator places on the guided beam will have to be carefully assessed in choosing among alternatives. "One-dimensional" modulators such as the acousto-optic or the electro-optic diffraction grating types require beams which are diffraction limited parallel to the waveguide plane. The range of included angle in this direction must be relatively small, so that the guided light must originate in a relatively large transverse aperture. In modulators such as the proposed strip guide coupling modulators, the light is restrained in two dimensions but, unless the guides are strong the light beam entry angles must also be restricted. A choice cannot therefore be made without specifying the fiber optic to planar waveguide coupler. Direct couplers between these two types of guiding systems are still under study, as discussed in Chapter 3. These comments are intended to serve as a caution to make the reader aware of potential problem areas that may in the future weigh as heavily in choosing a particular device as the power and performance characteristics to which this chapter was largely devoted.

Before leaving this topic, we should also point out a problem area which may be better solved by use of bulk rather than waveguide modulators. This is the problem of handling high optical powers. Because of the high concentration of light in optical waveguides, average laser powers of about half a watt start producing nonlinear effects which may disrupt operation. Thus, bulk modulators will probably continue to be used to handle very high power laser beams. In addition, at least at the present time, it is more difficult to obtain diffraction limited output beams and very low insertion losses (below about 2 dB) with the wave-

guide than with bulk modulators. The latter difficulties may, however, be solved as the waveguide coupling problems receive further study.

It thus appears at this time that waveguide modulators and switches will find their largest use in the emerging field of optical communications, especially systems based on fiber optic transmission lines. On the other hand, bulk modulators are likely to find continuing use to handle high laser powers for diffraction limited systems, such as used for holographic data processing and space communications.

We can at this point make no general dictum that would be useful for deciding which of the waveguide modulators or, indeed, which of the physical effects will dominate the future. We have seen working examples of waveguide modulators based on acousto-optics, electro-optics, and magneto-optics. Many of these examples have produced units that show the reduction in specific energy hoped for in going to the waveguide format. We can say at this time that modulators requiring specific energies on the order of 0.1 mW/MHz using all three physical effects we have discussed have been demonstrated and that specific energies below 10 μ W/MHz can be expected in the not too distant future.

We can also say that, at the present time, modulators based on the use of linear electro-optic effect materials are in a more advanced state of development than those based on acousto-optic or magneto-optic effects. And in turn, the acousto-optic devices are certainly more numerous than the two (experimental) examples of magneto-optic waveguide modulators that we know about.

At the risk of being proved wrong next month or perhaps next year we might guess that electro-optic modulators and switches will dominate the modulation and switching field in the visible and near infrared regions of the spectrum ($\lambda_0 = 0.5$ to $1.06 \mu\text{m}$). The electro-optic modulators hold an advantage over the acousto-optic in the relative simplicity of their drive power requirements. Thus, to drive an electro-optic modulator at a bandwidth of $\Delta f = f_2 - f_1$, the highest frequency needed is f_2 , but the center acoustic frequency has to be added in the case of an acousto-optic modulator. As higher bandwidths are required, this fact presents a severe problem to the acousto-optics. Waveguide acousto-optic devices will continue to find use for specialized signal processing tasks for which they are uniquely suited and the explanation of which is beyond the scope of this chapter.

At wavelengths much above one micrometer, both the acousto-optic and electro-optic modulators pay a high specific energy price. For both types $P/\Delta f \propto \lambda_0^3$. This gives an advantage to the magneto-optic modulators which are transparent in the infrared and which do not have to pay a severe penalty in specific energy when going to long wavelengths. The appearance of a suitable magneto-optic waveguide material which is

transparent at short wavelengths would perhaps make the magneto-optic modulator competitive in the visible.

In the nearer future, the one-dimensional waveguide modulators, such as the very successful electro-optic grating types, will probably find their way into systems where they will be used mainly for switching. This assumes that the fiber-waveguide coupling problem is tractable. The one-dimensional devices do not rely on close control of the guide propagation characteristics and thus do not present severe fabrication difficulties.

At a later time, the strip guide coupling modulators or mode-to-mode coupling modulators will probably become more significant. These more elegant devices offer lower drive power and voltage-current requirements. They do, however, present much more critical problems in manufacture because they require close control of waveguide material properties and geometry to insure good phase match and to make the actual interaction length equal the critical coupling length, so that good extinction ratios are obtained.

Basically, all the answers are not as yet in. We are, as mentioned at the beginning of this section, dealing with very new devices which are either in the research or initial development stage.

We might conclude this chapter by commenting that, at the present time, there are two areas in which we believe research can be most fruitful in resolving the future of optical waveguide modulators and switches. We still need new materials and methods for forming active optical waveguides. Just one example—a good material system for a magneto-optic modulator at 10.6 μm is required. More importantly, we need a good simple and cheap way of coupling optical fibers to high index of refraction planar or strip optical waveguides.

4.8. Appendix

The general equation of the index ellipsoid is written as [Ref. 4.7, pp. 447–449]

$$B_{11}X_1^2 + B_{22}X_2^2 + B_{33}X_3^2 + 2B_{22}X_2X_3 + 2B_{12}X_1X_2 + 2B_{13}X_1X_3 = 1 \quad (4.55)$$

In reduced notation 1,1 = 1; 2,2 = 2; 3,3 = 3; 2,3 = 4; 1,3 = 5; and 1,2 = 6. In this notation, (4.55) becomes

$$B_1X_1^2 + B_2B_2^2 + B_3X_3^2 + 2B_4X_2X_3 + 2B_5X_1X_3 + 2B_6X_1X_2 = 1 \quad (4.56)$$

where

$$B_1 = a_{10} + r_{11}E_1 + r_{12}E_2 + r_{13}E_3 \quad (4.57)$$

The notation 1, 2, 3, corresponds to the a , b , c or the X , Y , Z crystal axes. Both LiNbO_3 and LiTaO_3 have 3m symmetry and the electro-optic tensor reduces to

$$\begin{Bmatrix} 0 & -r_{22} & r_{13} \\ 0 & -r_{22} & r_{13} \\ 0 & 0 & r_{33} \\ 0 & r_{51} & 0 \\ r_{51} & 0 & 0 \\ -r_{22} & 0 & 0 \end{Bmatrix}. \quad (4.58)$$

The a 's reduce to

$$a_3 = 1/n_e^2 \quad (4.59)$$

and

$$a_1 = a_2 = a_0 = 1/n_0^2 \quad (4.60)$$

where n_0 is the ordinary and n_e the extraordinary index of refraction.

The equation for the index ellipsoid now becomes

$$(a_0 - r_{22}E_2 + r_{13}E_3)X_1^2 + (a_0 + r_{22}E_2 + r_{13}E_3)X_2^2 + (a_3 + r_{33}E_3)X_3^2 + 2r_{51}E_2X_2X_3 + 2r_{51}E_1X_1X_3 + 2r_{22}E_1X_1X_2 = 1. \quad (4.61)$$

We wish to consider crystals with light propagating in the $X-Z$ or $Y-Z$ planes. In our notation, these are 1-3 or 2-3 planes. Consider first light propagating at an arbitrary angle in the $Y-Z$ (2-3) plane. In the coordinates shown in Fig. 4.11 assume that light propagates along the Y_3 axis.

In order to find the index of refraction and the electro-optic coefficient for propagation in the Y_3 direction, the equation of the ellipse formed by the intersection of a plane at right angles to Y_3 with the index ellipsoid must be found. The major and minor axes of this ellipse will have values a_{major} and a_{minor} , and the index of refraction for components of polarization parallel to a_{major} will be

$$n_m = 1/\sqrt{a_{\text{major}}}$$

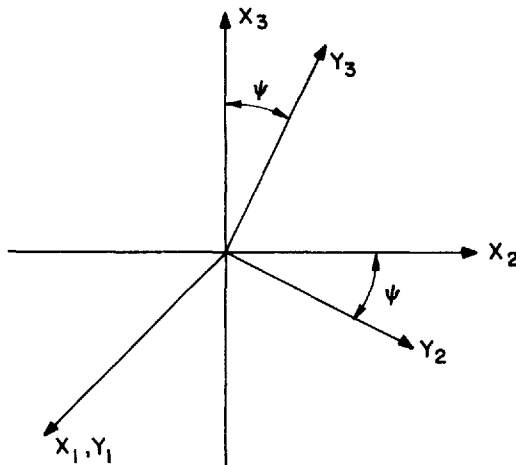


Fig. 4.11. Coordinates for use in calculating effective indices of refraction and electro-optic coefficients from index ellipsoid

and for those parallel to a_{minor}

$$n_{\text{min}} = 1/\sqrt{a_{\text{minor}}}.$$

The equation for the ellipse is most conveniently found by transforming coordinates. Thus, from Fig. 4.11,

$$\begin{aligned} X_1 &= Y_1 \\ X_2 &= Y_2 \cos \psi + Y_3 \sin \psi \\ X_3 &= -Y_2 \sin \psi + Y_3 \cos \psi. \end{aligned}$$

The general equation for the index ellipsoid can now be written in transformed coordinates. To get an appropriate index ellipse we set $Y_3=0$ in the transformed equation. The resultant equation of the index ellipse is

$$(a_0 - r_{22}E_2 + r_{13}E_3)Y_1^2 + (a_0 + r_{22}E_2 + r_{13}E_3)\cos^2 \psi Y_2^2 + (a_3 + r_{33}E_3)\sin^2 \psi Y_2^2 - 2r_{51}E_2 Y_2^2 \sin \psi \cos \psi = 1. \quad (4.62)$$

Electro-optic cross terms $Y_i Y_j$, which represent small field-induced second-order rotations of the axis, are ignored.

It is convenient to transform the electric field components to the new coordinate system. Denoting the transformed fields by primes, we have

$$\begin{aligned} E_2 &= E'_2 \cos \psi + E'_3 \sin \psi, \\ E_3 &= E'_3 \cos \psi - E'_2 \sin \psi. \end{aligned} \quad (4.63)$$

At this point, we recognize that TE waves are polarized along Y_2 . Therefore, the coefficient of the Y_2^2 term will give the desired refractive index for TE waves. Furthermore, for the interdigital grating and other devices with fields applied parallel to the waveguide plane and at right angles to the propagation direction, the only field component of interest is E'_2 . Thus, taking $E'_2 = 0$ in (4.63) and using (4.62), we find the coefficient of Y_2^2 to be

$$a_0 \cos^2 \psi + a_3 \sin^2 \psi + (r_{22} \cos^3 \psi - r_{13} \sin \psi \cos^2 \psi - r_{33} \sin^3 \psi - 2r_{51} \sin \psi \cos^2 \psi) E_2 = 1/\sqrt{n}. \quad (4.64)$$

Expanding and using (4.60), we obtain

$$n = n' - n'^3 r' E_2 / 2, \quad (4.65)$$

where

$$n' = n_E n_0 / \sqrt{n_E^2 \cos^2 \psi + n_0^2 \sin^2 \psi}, \quad (4.66)$$

and

$$\begin{aligned} r' &= r_{22} \cos^3 \psi - r_{13} \sin \psi \cos^2 \psi - r_{33} \sin^3 \psi \\ &\quad - 2r_{51} \sin \psi \cos^2 \psi. \end{aligned} \quad (4.67)$$

Since the electro-optic term is a linear combination of the r 's and varies with ψ , we may seek an optimum value of ψ to maximize the electro-optic effect. Differentiating the electro-optic term of (4.64) with respect to ψ and setting the differential equal to zero, we obtain the equation

$$\tan^2 \psi - (A/C) \tan \psi - B/C = 0 \quad (4.68)$$

where $A = 3r_{22}$, $B = r_{13} + 2r_{51}$, and $C = 2(r_{13} + 2r_{51}) - 3r_{33}$.

The optimum values of ψ are

$$\psi_{\text{opt}} = \arctan \left[\frac{3r_{22} \pm \sqrt{9r_{22}^2 + 8(r_{13} + 2r_{51})^2 - 12r_{33}(r_{13} + 2r_{51})}}{4(r_{13} + 2r_{51}) - 6r_{33}} \right]. \quad (4.69)$$

A similar analysis may be made for propagation in the $X-Z$ (1-3) plane (Y -plates). The results of this analysis give

$$n' = n_e n_0 / \sqrt{n_e^2 \cos^2 \psi + n_0^2 \sin^2 \psi} \quad (4.70)$$

$$r' = r_{33} \sin^3 \psi + (r_{13} + 2r_{51}) \cos^2 \psi \sin \psi, \quad (4.71)$$

$$\psi_{\text{opt}} = \pm \arctan \sqrt{r_{13} + 2r_{51} / [2(r_{13} - 2r_{51}) - 3r_{33}]} \quad (4.72)$$

For this case, fields perpendicular to the plane also cause an electro-optic effects with

$$r'_1 = -r_{22} \cos^2 \psi.$$

For TM waves, it is readily shown that

$$\begin{aligned} X\text{-plates} & \left\{ \begin{array}{l} n' = n_0 \\ r' = -(r_{22} \cos \psi + r_{13} \sin \psi) \end{array} \right. \\ Y\text{-plates} & \left\{ \begin{array}{l} n' = n_0 \\ r' = r_{13} \sin \psi. \end{array} \right. \end{aligned}$$

References

- 4.1. M. BORN, E. WOLF: *Principles of Optics*, 2nd ed. (Macmillan Co., New York, 1964).
- 4.2. D. A. PINNOW: IEEE J. Quant. Electr. QE-6, 223 (1970).
- 4.3. A. YARIV: IEEE J. Quant. Electr. QE-9, 919 (1973).
- 4.4. I. P. KAMINOW, J. R. CARRUTHERS, E. H. TURNER, L. W. STULZ: Appl. Phys. Letters 22, 540 (1973).
- 4.5. V. J. FOWLER, J. SCHLAFFER: Proc. IEEE 54, 1437 (1966).
- 4.6. J. F. NYE: *Physical Properties of Crystals* (Oxford at the Clarendon Press, London, 1957).
- 4.7. R. J. PRESSLEY (Ed.): *Handbook of Lasers* (Chemical Rubber Company, Cleveland, 1971).
- 4.8. T. M. SMITH, A. KORPEL: IEEE J. Quant. Electr. QE-1, 283 (1965).
- 4.9. W. J. TABOR: In *Laser Handbook*, ed. by F. T. Arrechi and E. O. Schulz-DuBois (North Holland Publishing Co., Amsterdam, 1972), pp. 1011-1027.
- 4.10. J. M. HAMMER, D. J. CHANNIN: Appl. Opt. 10, 2203 (1972).
- 4.11. R. ADLER: IEEE Spectrum 4, 42 (1967).
- 4.12. E. I. GORDON: Proc. IEEE 54, 1391 (1966).
- 4.13. P. S. PERSHAN, N. BLOEMBERGEN: In *Advances in Quantum Electronics* (Columbia University Press, 1961), pp. 187-199.
- 4.14. N. BLOEMBERGEN, P. S. PERSHAN, L. R. WILCOX: Phys. Rev. 120, 2015 (1960).
- 4.15. J. T. HANLON, J. F. DILLON, Jr.: J. Appl. Phys. 36, 1269 (1965).

- 4.16. R. C. LE CRAW: Intermagnetics Conference, Stuttgart, Germany (1966), unpublished. Text available from R. C. LE CRAW, Bell Telephone Laboratories, Murray Hill, N. J., USA.
- 4.17. L. KUHN, M. L. DAKSS, P. F. HEIDRICH, B. A. SCOTT: *Appl. Phys. Letters* **17**, 265 (1970).
- 4.18. Y. OHMACHI: *J. Appl. Phys.* **44**, 3928 (1973).
- 4.19. Y. OHMACHI: *Electron. Letters* **9**, 539 (1973).
- 4.20. R. V. SCHMIDT, I. P. KAMINOV, J. R. CARRUTHERS: *Appl. Phys. Letters* **23**, 417 (1973).
- 4.21. D. A. WILLIE, M. C. HAMILTON: *Appl. Phys. Letters* **24**, 159 (1974).
- 4.22. W. S. C. CHANG: *IEEE J. Quant. Electr.* **QE-7**, 167 (1971).
- 4.23. T. G. GIALLORENZI: *J. Appl. Phys.* **44**, 242 (1973).
- 4.24. T. G. GIALLORENZI, A. F. MILTON: *J. Appl. Phys.* **45**, 1762 (1974).
- 4.25. J. M. HAMMER, W. PHILLIPS: *Appl. Phys. Letters* **24**, 545 (1974).
- 4.26. L. KUHN, P. F. HEIDRICH, E. G. LEAN: *Appl. Phys. Letters* **19**, 428 (1971).
- 4.27. M. L. SHAH: *Appl. Phys. Letters* **23**, 75 (1973).
- 4.28. G. B. BRANDT, M. GOTTLIEB, J. S. CONROY: *Appl. Phys. Letters* **23**, 53 (1973).
- 4.29. M. L. SHAH: *Appl. Phys. Letters* **23**, 556 (1973).
- 4.30. F. K. REINHART, D. F. NELSON, J. MEKINNA: *Phys. Rev.* **177**, 120 (1969).
- 4.31. F. K. REINHART, B. I. MILLER: *Appl. Phys. Letters* **20**, 36 (1972).
- 4.32. P. K. CHEO: *Appl. Phys. Lett.* **23**, 439 (1973).
- 4.33. L. O. WILSON, F. K. REINHART: *J. Appl. Phys.* **45**, 2219 (1974).
- 4.34. W. E. MARTIN: *J. Appl. Phys.* **44**, 3703 (1973).
- 4.35. S. FUKUNISHI, M. UCHIDA, S. MIYAZAWA, J. NODA: *Appl. Phys. Letters* **24**, 424 (1974).
- 4.36. D. J. CHANNIN: *Appl. Phys. Letters* **22**, 365 (1973).
- 4.37. J. P. SHERIDAN, J. M. SCHNUR, T. G. GIALLORENZI: *Appl. Phys. Letters* **22**, 560 (1973).
- 4.38. J. M. HAMMER: *Appl. Phys. Letters* **18**, 147 (1971).
- 4.39. D. P. GIARUSO, J. H. HARRIS: *Appl. Opt.* **10**, 2786 (1971).
- 4.40. J. N. POLKY, J. H. HARRIS: *Appl. Phys. Letters* **21**, 307 (1972).
- 4.41. J. M. HAMMER, D. J. CHANNIN, M. T. DUFFY: *Appl. Phys. Letters* **23**, 176 (1973).
- 4.42. D. HALL, A. YARIV, E. GARMIRE: *Appl. Phys. Letters* **17**, 127 (1970).
- 4.43. D. J. CHANNIN: *Appl. Phys. Letters* **19**, 128 (1971).
- 4.44. P. K. CHEO: *Appl. Phys. Letters* **22**, 241 (1973).
- 4.45. S. SOMEKH, E. GARMIRE, A. YARIV, H. L. GARVIN, R. G. HUNSPERGER: *Appl. Phys. Letters* **22**, 46 (1973).
- 4.46. F. K. REINHART: *Appl. Phys. Letters* **22**, 372 (1973).
- 4.47. J. H. MCFEE, R. E. NAHORY, M. A. POLLACK, R. A. LOGAN: *Appl. Phys. Letters* **23**, 571 (1973).
- 4.48. S. WANG, M. SHAH, J. D. CROW: *IEEE J. Quant. Electron.* **QE-8**, 212 (1972).
- 4.49. S. WANG, J. D. CROW, M. SHAH: *Appl. Phys. Letters* **19**, 189 (1971).
- 4.50. S. WANG, M. SHAH, J. D. CROW: *J. Appl. Phys.* **43**, 1861 (1972).
- 4.51. W. S. C. CHANG, K. W. LOH: *IEEE J. Quant. Electron.* **QE-8**, 463 (1972).
- 4.52. T. P. SOSNOWSKI, G. D. BOYD: *IEEE J. Quant. Electron.* **QE-10**, 306 (1974).
- 4.53. S. YAMAMOTO, Y. KOYAMADA, T. MAKIMOTO: *J. Appl. Phys.* **43**, 5090 (1972).
- 4.54. E. A. J. MARCATILI: *Bell Syst. Tech. J.* **48**, 2103 (1969).
- 4.55. H. F. TAYLOR: *J. Appl. Phys.* **44**, 3257 (1973).
- 4.56. J. F. ST. LEDGER, E. A. ASH: *Electron. Letters* **4**, 99 (1968).
- 4.57. W. E. MARTIN, D. HALL: *Appl. Phys. Letters* **21**, 325 (1972).
- 4.58. P. K. TIEN, R. J. MARTIN, R. WOLFE, R. C. LE CRAW, S. L. BLANK: *Appl. Phys. Letters* **21**, 397 (1972).
- 4.59. S. WANG, M. SHAH, J. D. CROW: *IEEE Trans. on Magnetics MAG-7*, 385 (1971).

- 4.60. D. F. NELSON, F. K. REINHART: *Appl. Phys. Letters* **5**, 148 (1964).
- 4.61. I. P. KAMINOW, E. H. TURNER: *Proc. IEEE* **54**, 1374 (1966).
- 4.62. P. K. TIEN, R. J. MARTIN, S. L. BLANK, S. H. WEMPLE, L. J. VARNERIN: *Appl. Phys. Letters* **21**, 207 (1972).
- 4.63. R. S. CHU, T. TAMIR: *IEEE Trans. Microwave Theory Tech.* **MTT-18**, 486 (1970).
- 4.64. I. P. KAMINOW, J. R. CARRUTHERS: *Appl. Phys. Letters* **22**, 326 (1973).
- 4.65. S. C. TSENG, A. R. REISINGER, E. A. GIESS, C. G. POWELL: *Appl. Phys. Letters* **24**, 265 (1974).

5. Fabrication and Measurement of Passive Components

F. ZERNIKE

With 12 Figures

Since thin films have been used in optics for a considerable length of time, one would expect that the necessary techniques for the production and the evaluation of planar guides were all available when the idea of optical waveguides was first conceived. However, by and large, this was not so. The reason is that, in almost all applications of thin films in classical optics, the films are used at perpendicular or close to perpendicular incidence; the light passes through the film in its shortest dimension, and so, even though in some cases the beam may pass through the film many times, the total optical path in the film is very small. In addition, for most classical applications, such as anti-reflection coatings and multi-layer dielectric mirrors, one does not need to know the mechanical thickness or the refractive index of each layer to a great degree of accuracy. All that is necessary is an accurate knowledge of the optical thickness—a dimension that can be monitored quite easily during deposition—and a nominal value of the refractive index. Indeed, when one peruses the literature on optical thin films, it is remarkable that the index of a film is hardly ever given to an accuracy better than two decimal places.

The thin films needed for optical waveguides, however, have quite different requirements. First of all, the light is transmitted in the plane of the film, so that the optical path can easily be on the order of centimeters long.

Secondly, in waveguide applications the optical thickness of the film is of no importance, but instead one needs to know separately its refractive index and its mechanical thickness, or (in less demanding applications) at least its apparent refractive index $N = \beta/k$. Also, the light is not transmitted totally inside the film but rather it travels in a composite medium made up of the film, the substrate and the cladding. Thus, the materials used for all three layers have to be of good optical quality and free of scattering defects. In addition, the boundaries between the different layers should be smooth to avoid losses caused by scattering at the interfaces. Exactly how smooth the surfaces have to be depends on the particular design of the guiding layer and on the order of the mode. In general, the higher the difference in refractive

index between the guide and the surrounding media and the higher the mode number, the higher will be the losses caused by scattering at the boundaries. Thus, a film of a high index material may appear to be more lossy when deposited on a low index substrate than when deposited on a higher index substrate.

It should perhaps be emphasized that the word used here to describe the surface is "smooth" in distinction to "flat". The surfaces needed for the deposition of optical waveguides need not be flat; i.e., no great deal of care is necessary to obtain the extreme flatness that optical polishers are so proud of. Rather one needs a surface that is free of defects such as scratches, pits and digs. Optical flatness is of only minor importance. As a result, new methods of film deposition and evaluation have been and are still being developed specifically for use in optical waveguides. Some of the more prominent methods known at this time are described in this chapter.

By employing thin films as planar waveguides, one can obtain useful information about new materials, new deposition techniques, etc. To make an optical circuit, one has to be able to make patterns in these films. If these patterns are simple and relatively large, such as lenses, prisms, etc., they can be made by the use of mechanical masks. However, if high resolution patterns, such as gratings and strip guides, are required, the masks to be employed become more complicated. Some methods currently used to make these latter types of masks are described in the second part of this chapter.

5.1. Methods Used to Produce Waveguiding Layers

The methods used to produce waveguiding layers can be divided into two classes: those in which the layer is made by the deposition of a material on a substrate, and those in which the higher-index layer is produced in the substrate itself by some chemical or physical reaction. In the first type, the index change between the guide and the substrate is discontinuous, whereas in the second type a gradual index change occurs.

Methods belonging to the first class are sputtering, plasma polymerization and the production of a film from a liquid by spinning or by dipping. Vacuum evaporation—the method most commonly used for the production of thin films for classical optics applications—is seldom used in integrated optics since it produces films with relatively high losses. In the second class one finds proton bombardment, ion implantation, and ion migration.

Before discussing these methods in detail, the methods used for preparation of the substrates must first be considered.

5.1.1. Substrate Preparation

As mentioned in the introduction to this chapter, the substrate on which the film is to be deposited does not need to be optically flat, but it has to be free of defects such as scratches and pits. However, since a portion of the energy is transmitted as an evanescent wave in the substrate, this substrate has to be defect-free below its surface as well. If the surface was polished by the techniques prevailing in most optical shops, this condition is quite likely not satisfied. In the normal polishing of glass, one tries to obtain a smooth surface, and often also a particular figure (spherical or flat, for example). To arrive at this, the rough cut glass blank is fine ground and subsequently polished. Each step is continued with increasingly finer polishing powder, until all scratches from the previous step have disappeared. If done properly, this does indeed provide a good surface polish. However, damage from previous grinding steps may still be present directly under the surface. There is much evidence to suggest that the topmost surface of the glass actually melts during the polishing operation and that the edges of the cracks are rolled over until they are closed, leaving the crack very much present immediately under the surface [5.1]. Again, for most normal classical optics applications, this type of polish is perfectly adequate; the subsurface cracks cannot be detected optically, therefore they will be harmless in normal applications. However, if a waveguiding film is deposited on such a surface, the evanescent wave associated with the light in the guide does travel precisely in the damaged area and, as a result, the guide is very lossy.

One way around this problem is to first grow a layer with an index lower than that of the guide, before growing the actual guide. If this layer is thick enough, the evanescent wave of the guide is very weak at the boundary between the original substrate and this first film; thus the losses from the damage layer are negligible. The method presumes, however, that the damage layer does not propagate into the low-index layer, and this is apparently not always the case. It has been found that, in some cases, presumably due to stresses in the top layer which propagate into the deposited film, the layer grown on the polished surface shows surface irregularities.

A better method, of course, is to polish the substrate in such a manner that no damage layer is present. This can be done by prolonging each

successive polishing step longer than is ordinarily done in classical-optics applications. A common rule of thumb seems to be that each step must be three times longer.

In general, purely mechanical polishing, such as described here, does tend to leave scratches, even if each step is prolonged in the manner described above. This is due to the fact that the actual removal is done by mechanical scraping, i.e. by the action of the grinding power, which is never infinitely small. To obtain a scratch-free surface, then, one has to go to a non-mechanical polishing method. Purely chemical polishing does provide a damage-free surface, but not a smooth one. A combination of chemical and mechanical polishing, known as chemo-mechanical, or chem-mech. polishing, is widely used in the semiconductor industry. In this method, the material to be removed is first attacked by the chemical and the much softer reaction product is then rubbed off by the action of very fine abrasive material. In the optical industry, this method has not been used extensively, at least not intentionally. There is much discussion as to whether the customary iron oxide (rouge) polishing methods are chemo-mechanical or not. Newer materials, such as Syton, are chemo-mechanical and are beginning to be used. Since the damage-free polishing of glass surfaces is also of great importance in very high power lasers, it is to be expected that these materials will be developed more fully in the near future.

In many instances, and certainly when one is trying out new films or new film configurations, the need is for a substrate cheap enough so that a number of experiments can be done at not too great a cost in substrates. Nevertheless, one does still require a substrate with a polish good enough to make a reasonably low-loss waveguide. For many purposes, the flame polish on commercially available microscope slides is adequate, and, as a matter of fact, is far superior to the average optical polish. This type of slide can be obtained from a number of suppliers, in $25 \times 76 \text{ mm}^2$ size. However, it usually comes with ground edges, and the originally good polish on the surfaces is often damaged during this grinding process. It is therefore advantageous to order the glass individually wrapped, with cut, i.e., non-ground, edges.

PITT [5.2] reported that the unpolished substrates tend to produce protuberant growths of $1\text{--}5 \mu\text{m}$ diameter and many film thicknesses in height. He ascribed these to minor defects in the substrates and noted that Syton polishing of the substrates eliminates them.

A very good, but more expensive substrate, is available from Corning Glass Works in their 7059 type glass, in squares of $75 \times 75 \text{ mm}^2$. The surfaces are polished to a finish better than that of the average microscope slide and are flat to about one wavelength per centimeter.

5.1.2. Cleaning of the Substrate

Before the film is deposited, the substrate has to be cleaned thoroughly. This should, of course, be done without destroying its surface quality. It should therefore be realized that some cleaning solutions can etch the surface of glass to a small but significant extent. STILLWELL and DOVE [5.3], for example, found that soda lime glass is severely etched by hot alconox solutions. The author similarly noted that slides of 7059 glass showed a deterioration of their surfaces when cleaned in alconox. BRANDT et al. [5.4], however, reported very good results on quartz and pyrex substrates by using only small amounts of alconox in warm (40°C) distilled water (20 mg in 250 ml typically). However, their results are not supported by measured losses in actual waveguides.

GOELL [5.5] reported using a cleaning method developed for use in silicon semiconductor technology [5.6]. The slides are first cleaned ultrasonically several times in alternate baths of trichlorethylene and acetone, and are then scrubbed with a mildly abrasive detergent. Subsequently they are boiled, first in a mixture of 7–2–1 parts by volume of water, 30% unstabilized H_2O_2 and 27% NH_4OH , and then in a mixture of 7–2–1 of water, 30% unstabilized H_2O_2 and 37% HCl. Finally they are cleaned with filtered distilled water and spun dry.

A simple, but effective, procedure is used in the author's laboratory. The slides are scrubbed with a mixture of filtered deionized water, ORION¹ industrial cleaner and a small amount of ammonium hydroxide. The scrubbing is done with a cotton swab; the commercially available Q-tips are very well suited to this purpose. The slides are rinsed subsequently, first in running hot water, and then in deionized water. The hot water rinse was found to be indispensable to remove the soap. The slides are then blown dry with nitrogen.

A simple and quick inspection method is now needed, since almost any well washed slide appears immaculately clean under normal room light. One such method is the water break method [5.8, 14]. The cleaned slide is dipped in deionized water and the drying pattern is observed. If the slide is free of organic residue, the water wets the slide evenly and disappears slowly, almost completely by evaporation, showing interference colors as the layer becomes thinner. In a different and slightly more sensitive method, the slide is sprayed with deionized water using a fine spray gun (a painters' air brush is well suited) and the wetting of the slide is observed. Both methods, however, show an organic residue only. In general, an inorganic residue is much more detrimental to the operation of the waveguide.

¹ Manufactured by Puritan Chemical Company.

An inexpensive and surprisingly good method to examine the slides for the presence of inorganic residue is to install a small, more or less collimated, light source (e.g. a microscope illuminator) in a blackened box which is open on one side, so that the light from the illuminator is directed towards the opening of the box. The slide is held in the light beam, and observed against the black background in such a way that no direct or reflected light is seen (see Fig. 5.1). Small specks of dirt

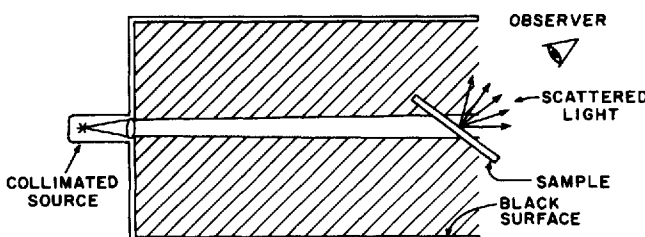


Fig. 5.1. Schematic representation of a simple instrument for the examination of surfaces

and surface imperfections now become clearly visible because they scatter the light. In this manner, both the surface quality and the cleanliness of the sample can be investigated. After some practice, one learns to discriminate between removable residue and non-removable pits and digs in the surface.

5.1.3. Sputtering

Good low-loss optical films have been deposited by sputtering. Extensive and detailed descriptions of the different methods of sputtering have been given elsewhere [5.8]. However, to explain some of the properties of sputtered films and some of the problems of the sputtering process, its more pertinent points are given here.

Sputtering is the process in which material is removed from a surface as the result of a bombardment by atoms or ions with energies in excess of about 30 eV. Since it is easier to accelerate charged particles, ions are normally used. The particles that are moved from the target surface can be collected on a conveniently located substrate to form a thin film. Thus the process can be used to remove material (onto the substrate).

The bombarding particle penetrates the surface of the target material and transfers its momentum to the lattice of the target, thereby knocking

one or more target atoms out of their equilibrium positions. If these "knocked on" atoms are close to the surface, they themselves may emerge, but more probably they will hit a surface atom from below, and cause it to fly off. The energy needed to move a lattice atom from its equilibrium position is on the order of 20 eV, but the energy necessary to remove an atom from the surface is only about 3–5 eV. Hence the film formed on the substrate is built up by a slow accumulation of atoms with appreciable energy. This is quite likely the reason for the low-loss properties and the durability of sputtered films.

In the applications considered here, the target is often an insulator, and rf sputtering is used. The rate at which a material is sputtered is proportional to the product of the sputtering yield, i.e. the number of sputtered atoms per incident ion, and the number of ions striking the target. While this last number is proportional to the current in the discharge, the sputtering yield increases with the voltage. As a result, one expects an increase in the sputtering rate with the power fed into the discharge.

The sputtering yield is obviously not the same for all target materials and all gases. Light gases, such as helium and hydrogen, have a very low sputtering yield. Moreover, because they can carry a disproportionately large share of the discharge current, small amounts of these gases in a plasma can alter the sputtering rate significantly. Hence the purity of the plasma is important.

In addition, the sputtering yield for a given type of atom in a compound target depends on the probability that the incident ion will cause that type of atom to be dislodged from the surface. Thus, in a compound target, the sputtering yields for the different types of atoms depend also on the composition of the target material. As a result, it is possible that some atoms in the target are sputtered more easily than others, thus causing a layer of changed composition on the surface of the target. This compositional change continues until an equilibrium is reached between the ratio of the different atoms in the target and their sputtering rates.

Even if the target does not change composition, a film deposited by sputtering from a compound cathode does not, in general, have the same composition as the target material. This is due to the fact that the different atoms from the cathode do not all find a suitable bonding site within a given time period, and are therefore re-emitted. Hence some types of atoms stick to the surface better than others. Moreover, this sticking coefficient is temperature dependent and, since the substrate holder is grounded, electrons from the discharge are attracted to it, causing heating. Consequently the temperature of the glass, or other insulating surface on which the material is to be deposited, may well

be much higher than the temperature of the substrate holder; moreover, this temperature may be dependent on the substrate material. As a result, the same target material can form films with different properties on different substrates. The author has found, for example, that sputtering from a Corning 7059 glass target produced films on a KDP substrate with a much lower index than films produced from the same target on glass substrates. There is, of course, no reason why the target in an rf discharge has to be an insulator. Metal compounds, such as oxides and nitrides, can be deposited by sputtering from a metal target in the appropriate reactive gas. This is known as reactive sputtering.

In general, sputtering does provide durable, low-loss films. Its drawback, however, is the extremely low rate at which the films grow, average rates being on the order of 30 \AA/min . However, if the discharge conditions are kept stable, the growth rate is linear with time and, once the rate is known, films of well defined thickness can be made by sputtering for a predetermined period of time [5.9].

For optical waveguides, the requirement is for films with uniform thickness and uniform refractive index. As a first measure to obtain uniform thickness, the target is made sufficiently larger than the sub-

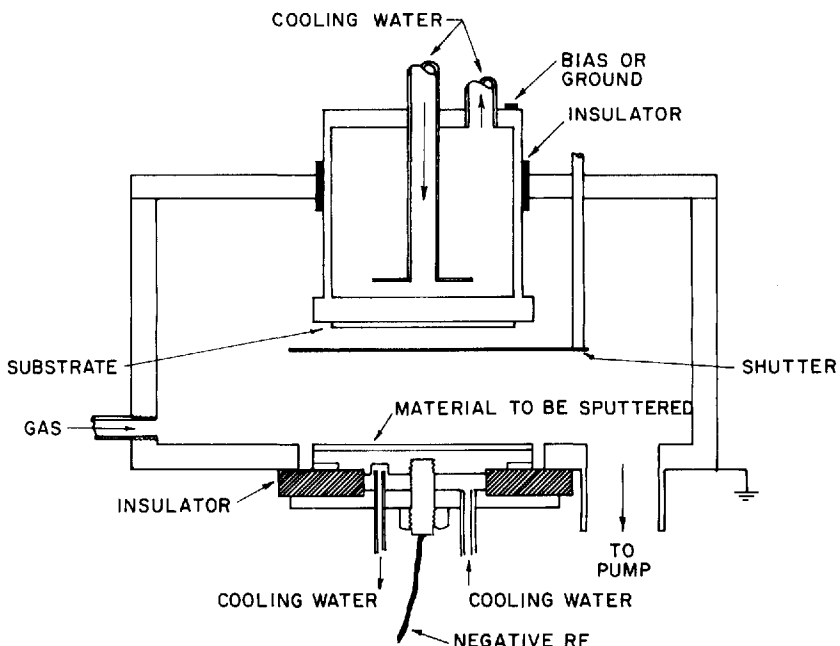


Fig. 5.2. Typical rf sputtering tank

strate. Secondly, to avoid complicated monitoring and cooling procedures, one would of course like to have a target that produces films of the same composition and at the same rate, even if the sputtering parameters are varied relatively widely.

An rf sputtering tank consists basically of a vacuum enclosure in which a discharge can be maintained between a cathode (the target) and the rest of the tank which is grounded (see Fig. 5.2). A substrate holder is mounted parallel to the cathode. Both the target and the substrate holder are water cooled. To prevent sputtering from the cathode support, a grounded shield is placed within one darkspace distance from the cathode, or, as shown here, the spacing between the tank and the cathode support is held to less than one darkspace distance.

Because of the charge distribution in an rf plasma, some sputtering takes place on all the exposed surfaces, but, since most of these surfaces are coated with material from the target (from previous runs), this does not cause any appreciable contamination. At the beginning of a run, however, the surfaces contain contaminants adsorbed from the air. These contaminants are removed during the initial phases of the subsequent run. To prevent any deposition of target material on the substrates, a shutter is used to cover the substrates during this pre-sputtering operation.

With a sputtering apparatus similar to that shown in Fig. 5.2, it was found in the author's laboratory that, with a 20 cm diameter cathode and a target to substrate spacing of 4.5 to 6 cm, films of better than 1% thickness uniformity could be deposited over a diameter of more than 8 cm at pressures ranging from 2.5 to 20×10^{-3} Torr. To insure repeatability between runs, it was found important to bond the target material to the water cooled backing plate. Epoxy was used as the cement.

The substrate holder is insulated from the rest of the tank since, in some applications, it is desirable to bias it. Both the input power and the voltage on the cathode are monitored. For constant voltage and input power, the sputtering rate was found to be linear with time.

A different method of sputtering is to use the type of apparatus used for ion beam etching (see Subsection 5.3.3). Here a collimated beam of ions is produced by an ion gun and is directed against the target, which can now be placed in a high vacuum. A separate filament, located in the high vacuum, close to the ion beam, emits electrons which are trapped in the ion beam and are used to avoid the build up of a charge on the target. This method has several advantages: the beam can strike the target at an angle, which results in a higher sputtering yield, and no electrons strike the substrate, so that the temperature of the substrate can be controlled much more easily. Moreover, since the

conductivity of the target is of no importance, a dc ion beam can be used. A disadvantage of the method is that the diameter of the ion beam is relatively small, so that it is difficult to obtain deposited films of uniform thickness.

One of the earliest materials that was used successfully to produce low-loss films by sputtering is Corning 7059 glass. This is a pyrex type of glass which is produced in large sheets of about 1.5 mm thickness from which circular sputtering cathodes can be cut, although this is rather difficult because the glass is extremely brittle. This material offers vivid proof that the sputtered film does not necessarily have the same composition as the target material, in that films sputtered on 7059 substrates from a 7059 target form waveguiding layers, i.e. they have a higher index than the starting material. The bulk composition of 7059 glass is 50.2% SiO₂, 25.1% BaO, 13.0% B₂O₃, 10.7% Al₂O₃ and 0.4% As₂O₃ by weight [5.10]. NISHIMURA et al. [5.11] have shown that the sputtered films have a different barium content than the bulk. ESCA analysis in the author's laboratory found no evidence of boron in films sputtered from a 7059 target in pure oxygen. In addition, it was observed that the refractive index of the sputtered film varied as a function of the power at which the deposition was done [5.12]. This was also found by PITTS who sputtered 7059 in argon, in argon oxygen mixtures, and in oxygen [5.2]. He noticed that the oxygen content greatly influenced the loss and the refractive index of the sputtered films. Films sputtered in pure argon had an index of 1.7 and losses greater than 100 dB/cm. However, 20% oxygen produced low-loss films, with an index only about 1% higher than that of the bulk. As a function of the sputtering power, the index at 6328 Å could be made to vary from 1.53 to 1.59.

A material that appears to be less sensitive to the sputtering power is a mixture of BaO and SiO₂. Such mixtures can be prepared in pure form by the reaction $x \text{BaCO}_3 + y \text{SiO}_2 \rightarrow x \text{BaO} \cdot y \text{SiO}_2 + x \text{CO}_2$ and can be hot pressed into ceramic discs for use as cathodes. GOELL [5.13] has experimented with varying values of x and y . He found that, as the weight percentage of BaO is changed from about 24% to about 46%, the index of the film changes from 1.51 to 1.61. Again, the film index is higher than that of bulk glass of the same composition as the target, but prepared by rapid quenching from the melt.

Films of higher indices have been made by sputtering of tantalum and niobium. HENSLER et al. [5.14] used metal cathodes to sputter tantalum films which were then oxidized. They reported an index of 2.2767 at 4880 Å, 2.2423 at 5154 Å and 2.2136 at 6328 Å for the TE waves with a slightly different value for TM waves. Very detailed work on this same method was done by FUJIMORI et al. [5.15].

In the author's laboratory, it was found that Ta_2O_5 films reactively sputtered from Ta cathodes showed lower losses than those made by oxidation of a metal film. However, the losses were very dependent on the exact conditions during sputtering.

McGRAW and ZERNIKE [16] have described films of Nb_2O_5 made by reactive sputtering of niobium in an argon-oxygen mixture. They report an index of 2.370 at 4880 Å and 2.276 at 6328 Å.

5.1.4. Plasma Polymerization

If an electrical discharge is passed through a gas containing an organic compound with low molecular weight, polymerization can occur, and, under the proper conditions, a smooth, clear, pinhole free film can be made to form on the walls and on the electrodes of the apparatus. The thickness of such films can range from about 200 Å to several micrometers.

A typical apparatus for such plasma polymerization is shown in Fig. 5.3. The lower electrode is connected to a 13.56 MHz generator through an impedance matching network. This electrode is cooled by water from a constant temperature bath and it is supported 10 cm above the base plate by insulating legs. The substrates are placed on this electrode. The upper electrode is held at ground potential. In a typical run, the chamber is first evacuated by an oil diffusion pump to a pressure of 2×10^{-6} Torr or less. The gate valve is then closed and subsequently the system is pumped by a mechanical pump through a throttle valve. At this point, argon is admitted through an inlet in the top plate. The monomers are introduced into the argon stream from heated reservoirs through variable leak valves.

By this method, SMOLINSKY et al. [5.17] have grown good optical waveguiding films by polymerization of each of the following: cyclohexane, acetone, hexene-1, isopropyl silane, vinyltrimethyl silane (VTMS) and hexamethyldisiloxane (HMDS). Methylmethacrylate was also tried but this produced a film that turned brown after several days exposure to daylight.

The growth rate of the films is linear with time and is essentially constant even if the monomer concentration is varied by a factor of 5. At 200 W input, VTMS films grow at about 2000 Å/min. At increased growth rates, nodules of polymer embedded in the film begin to show up.

The conventional polymerization process consists of the addition of a radical or an ionic species to a double bond, producing a new reactive species which can then link itself to another unsaturated molecule in a sequential process. The processes taking place in the discharge are

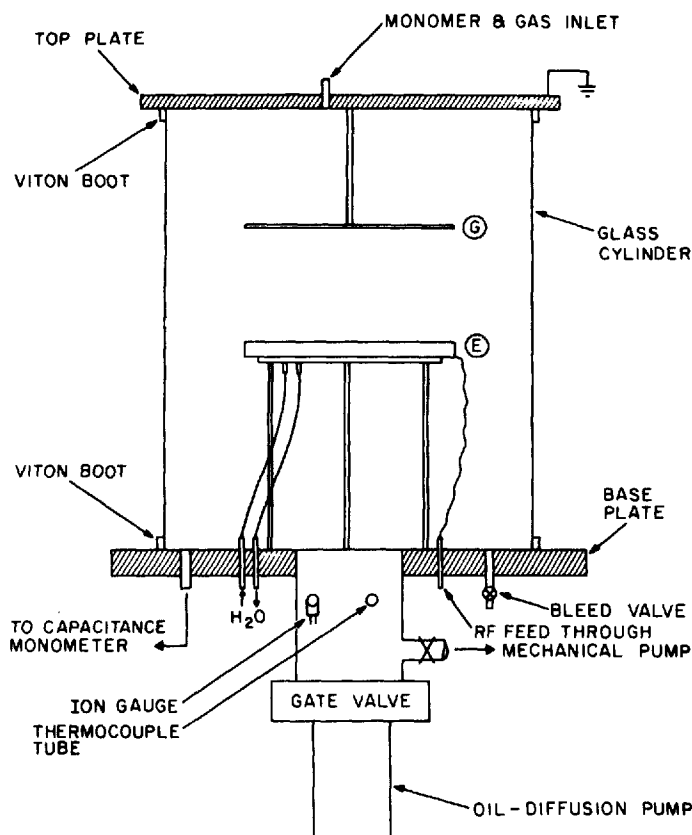


Fig. 5.3. Typical set-up for plasma polymerization. From [5.18])

more complex, as is quite clearly shown by the fact that films can be made by plasma polymerization of HMDS, $(\text{CH}_3)_3\text{SiOSi}(\text{CH}_3)_3$, a molecule that contains no unsaturated group. The molecules undergo fragmentation and ionization in the discharge, producing a compound that possesses two- and three-dimensional bonding rather than a linear structure. As a result of this highly cross-linked structure, the polymer films have good thermal stability and are inert to mild acids, alkalis and most organic solvents.

VASILE and SMOLINSKY [5.18] have described the rf plasma polymerization of HMDS and VTMS, $\text{CH}_2=\text{CHSi}(\text{CH}_3)_3$, in great detail, and have examined the effects of the different parameters involved in the film formation. They have also performed elemental analysis, infrared spectroscopy and electron spin resonance experiments on these

films, and have reported that the polymer films have a carbon-silicone ratio which is less than that of the monomers. As an example, VTMS has a carbon to silicon ratio of 5, whereas in the polymer made from it the carbon-silicon ratio can range from 2.7 to 4 depending on the discharge parameters. In addition, the polymers possess potentially reactive radical sites and, as a result, the exact composition of the films can be influenced by exposure to air, nitric oxide and chlorine directly after the polymerization.

As expected, the optical properties of the films also change as a result of such treatment. For example, heating a film at 140°C in oxygen produced a decrease in its refractive index, the amount of the decrease being dependent on the duration of the heat treatment [5.17]. At 6328 Å, for example, the index decreased from 1.5310 to 1.4797 in 180 min. This decrease was accompanied by a decrease in film thickness. This change in properties appears to be permanent; identical results were obtained after 6 months.

Hence these films promise the interesting possibility of very precise tuning, of a resonator or of coupled waveguides, etc., by a heat treatment after the films are deposited. Another way of varying the index is to grow a film using a mixture of two monomers, such as HMDS and VTMS. In this way, the index of the film can be varied during growth by changing the ratio of the monomer mixture.

In addition, these organo-silicon films have extremely low losses. In some of the best films, losses as low as 0.04 dB/cm for the TE₀ mode at 6328 Å have been reported. However, no data as to the thickness of this film, the allowed number of modes, etc. were provided [5.17]. Characteristic of the low losses is the fact that often no *m* lines are seen in the output from these films. (See also under attenuation measurements, Subsect. 5.2.1). This indicates that these films are completely amorphous.

In sputtering and in plasma polymerization [5.19], thickness variations in the films can be made by the use of mechanical masks. If the mask is a few millimeters high and has a straight edge, the thickness variation shows a short taper. The length of this taper can be increased by undercutting the edge of the mask and decreased by making the mask thinner. Aluminum masks were found to be most useful. Masks made of ordinary soda lime glass may leave a deposit on the film under the mask. This deposit is readily washed off in water.

5.1.5. Spinning and Dipping

Many varnishes, epoxies, etc. can be deposited onto glass substrates to form waveguides. Three methods of deposition are used: 1) the slide is

covered with the material and is spun around an axis normal to its surface to remove the excess; 2) the slide is dipped in the material and withdrawn slowly; 3) the slide is covered with the material and then turned upright so that excess material runs off. ULRICH and WEBER [5.20] have reported films of polyurethane, epoxy, lead silica glass and photoresist made by the last method. Losses of 0.3 dB/cm were measured in the epoxy films.

The greatest advantage of these techniques is that a film can be made extremely quickly. However, the film thickness cannot be controlled very accurately. Another advantage is the fact that the films can be doped, for example, with a dye [5.21]. Many films deposited in this manner undergo a change in refractive index upon illumination by ultraviolet light. Thus they can be used for the production of strip guides (see Subsect. 5.3.2).

A very interesting application of this deposition method was described by SOSNOWSKI and WEBER who made birefringent films [5.22]. They used poly(methylmethacrylate), (PMMA), deposited from a solution of chloroform and toluene, and polystyrene deposited from a xylene solution. Both were air dried. The polystyrene indices were measured to be 1.5862 for the TE mode and 1.5886 for the TM mode. The birefringence is due to stress in the film set up during the evaporation of the solvent.

5.1.6. Ion Migration

By applying an electric field to a heated glass plate, ions in the glass plate can be made to migrate to the negative electrode. In a soda-lime glass plate, for example, a SiO_2 surface layer free of Na can be produced in this fashion. If a molten salt is present at the cathode, ions from this salt can migrate into the glass. IZAWA and NAKAGOME [5.23] have used this method to produce both planar guides and strip guides. They start with a borosilicate glass. The glass is partially submerged in molten salts which contain the platinum anode. In a recess on top of the glass, the cathode (also made of platinum) is immersed in molten potassium nitrate. The entire set-up is heated to 530°C.

In the first diffusion step, the molten salts at the anode are thallium nitrate, sodium nitrate and potassium nitrate. Some of the Na^+ and K^+ ions in the glass are exchanged with Tl^+ ions, forming a high-index layer. In the second step, only sodium nitrate and potassium nitrate are used at the anode. Now the Na^+ and the K^+ ions diffuse into the surface, causing the Tl^+ ions to migrate even further into the substrate.

In this manner, a high-index layer is formed a short distance under the surface.

By masking the surface of the borosilicate glass with a glass film, which blocks Ti^+ diffusion, and then etching narrow lines in the mask, the method can be used to make strip guides.

5.1.7. Proton Bombardment and Ion Implantation

It is well known that when a solid is bombarded by heavy ions, these ions can be implanted in the solid. Due to the mechanism by which the ions lose their energy in the solid, the concentration of implanted ions has a Gaussian profile. The depth under the surface of the maximum of this profile (the range), depends on the target material, the type of ions, and their energy [5.24]. Representative calculated penetration depths for the noble gases are given in Table 5.1 which was reported in [5.25].

Table 5.1. Calculated penetration depths for the noble gases. (From [5.25])

Energy [keV]	Depth [\AA]			
	Ion			
	Ne^+	Ar^+	Kr^+	Xe^+
50	1200	580	345	300
100	2950	1180	632	495
150	3860	2040	890	685
200	4800	2750	1170	880
300	6780	4280	1750	1240

In fused silica, the implanted ions and the lattice displacements caused by the implantation process produce an increase in the refractive index. The amount of this change depends on the number of particles per unit volume. Thus, optical waveguides can be produced by proton bombardment and by ion implantation. The maximum index change in these waveguides depends on the number of particles per unit volume (up to a saturation value). The depth of the waveguide under the surface depends on the energy of the bombarding particles.

Early work on the creation of waveguides in fused silica by proton bombardment was done by SCHINELLER et al. [5.26], who reported a

change in index (at the maximum of the Gaussian profile) of $\Delta n_{\max} = 10^{-17} D$, where D is the density of protons per cm^3 . More recent work on ion bombardment of fused silica was done by STANDLEY et al. [5.27], who used a variety of ions ranging from helium to bismuth with energies in the range of 32–200 keV. They investigated the index variation and the losses of the resulting waveguides for the different ions and determined the effects of surface preparation, surface temperature during bombardment, ion species and dose, and post-bombardment annealing. Their best results were obtained with lithium ions, for which the index change was $\Delta n = 2.1 \times 10^{-21} D$. As a typical result, they obtained an index of 1.493 and a loss of 1.8 dB/cm by implanting 10^{15} Li^{+7} particles per cm^2 with the substrate at 220 °C. Annealing for 1 hour at 300 °C reduced the index to 1.468 and the loss to below 0.2 dB/cm. (These index values are at 6328 Å, the index of non-irradiated fused silica is 1.457).

For fabrication methods using crystalline substrates, the reader is referred to Sections 6.2 and 6.7.

5.2. Guide Evaluation

After the waveguide is fabricated, by deposition or otherwise, its properties need to be measured. Most important are the attenuation, the apparent index $N = \beta/k$, which was defined in (2.1.14) of Section 2.1, and the index and the thickness of the guide.

5.2.1. Attenuation Measurements

While the refractive index and the thickness are two quantities that need to be known if specific designs are required, perhaps the most basic measure of the quality of a guide is its attenuation. A very first evaluation of this property can be made by observing the guide in the same black box that was used to examine the cleanliness of the substrate, as discussed in Subsection 5.1.2. Guides with a large loss due to scatter appear uniformly hazy in this test. Even so, such guides often still do allow transmission of a guided mode, but one observes the attenuation as soon as light is coupled in; the characteristic streak of light scattered from the guide disappears in a centimeter or so. Also, if the loss is indeed caused by scatter, this streak is very bright. In such cases the attenuation is in the order of 20 dB/cm. A more accurate number is often not of interest since the guide most likely is not useful.

In low-loss guides, a more meaningful preliminary test is to couple the guided light out and to observe the output on a screen. Usually this output consists of a bright short line parallel to the plane of the guide², with a much weaker series of spots continuing in a slightly curved line on its top and bottom. This series of spots, known as the *m*-line, is caused by scatter in the plane of the guide. It is present in all but the very lowest loss guides. When making this observation, the surfaces of the input prism should be clean and well polished because scatter from these surfaces can also send light into the *m*-lines.

The problem becomes much more interesting and difficult when a more accurate quantitative measurement of the attenuation is required. Several early workers measured the scattered light intensity as a function of the length of the guide [5.28]. This can be done, for example, by moving a fiber-optic probe along the length of the guide and recording the signal emitted from the other end of the fiber. From this data, one can then deduce the attenuation in the guide.

In a much cruder version of the same type of measurement, the guide is photographed a number of times using progressively shorter exposures. The length of the guide, as recorded in the different photographs, is then measured, and from this the attenuation is found [5.28].

If the scatter in the guide is relatively uniform, a fairly good measurement can be obtained by either of these methods. However, if the scatter is much stronger in some places than in others, these methods become unreliable. The same is true for low attenuation (less than about 1 dB/cm).

Obviously, the best method to measure attenuation is to measure the transmitted power as a function of the length of the guide. This measurement can be made accurately only if the input coupling to the guide is kept constant, as should also be the case in the previous methods. This means that the change in length of the guide has to be accomplished without disturbing the input coupling, i.e. in practice, without taking the guide out of the experimental set up. For films with *N* values less than about 2.0, this measurement can be made by using a sliding output prism [5.12, 29]. This prism is contacted onto the guide using a small amount of index matching oil (with an index equal to that of the prism or slightly lower) and is translated mechanically towards the input prism. The output signal is processed by a logarithmic amplifier and recorded as a function of the position of the output prism. A typical record of such a measurement is shown in Fig. 5.4. Note that the recorded signal is linear as a function of guide length

² If the output does not appear as a narrow line, the output prism is too tightly coupled. Releasing the pressure on the clamp a little immediately narrows the line.

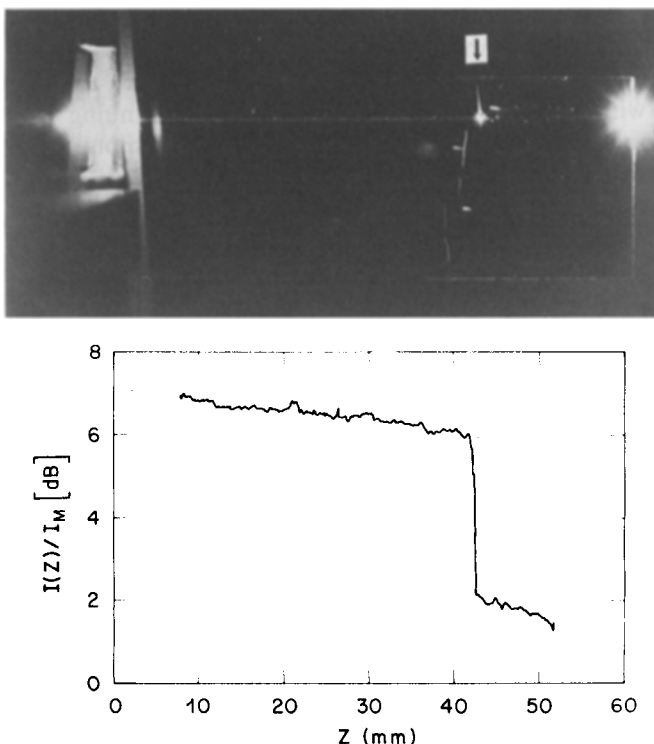


Fig. 5.4. Typical record of an attenuation measurement, plus a photograph of the measured slide. At both locations of the shallow scratch, the losses are locally very high, but they return to the previous value after that. (From [5.30])

and that the slope is constant on both sides of the sudden change due to the scratch in the film.

In this measurement, it is crucial that all the light in the guide be coupled out by the sliding prism, and detected. WEBER et al. [5.30] use a small, delicately held prism, with an index only slightly higher than that of the film, to insure that the meniscus of the matching oil does not couple light out past the detector. In the author's laboratory, a large prism is used (base length 2 cm) and it is held against the film by the surface tension of only a small amount of index matching liquid.

Since matching liquids are used in this method, it follows that the measurement cannot be made in this fashion for guides with N values higher than about 2.0. For such guides, a fairly reliable estimate for the attenuation can still be arrived at by using a clamped-on output

prism to measure the transmitted signal as a function of guide length at a number of discrete points. The difficulty here is, of course, that the clamping of the prism has to be tight enough to insure 100% output coupling, but has to be accomplished without disturbing the input coupling. This can be done by mounting the sample itself rigidly and using, for both input and output, light clamping frames that are supported by the sample to which they are clamped. Each frame holds a prism and its opposing anvil. In this manner any slight twisting or other motion of the sample during the reclamping of the output prism does not alter the clamping of the input prism or the input coupling. Figure 5.5 shows such a clamping frame.

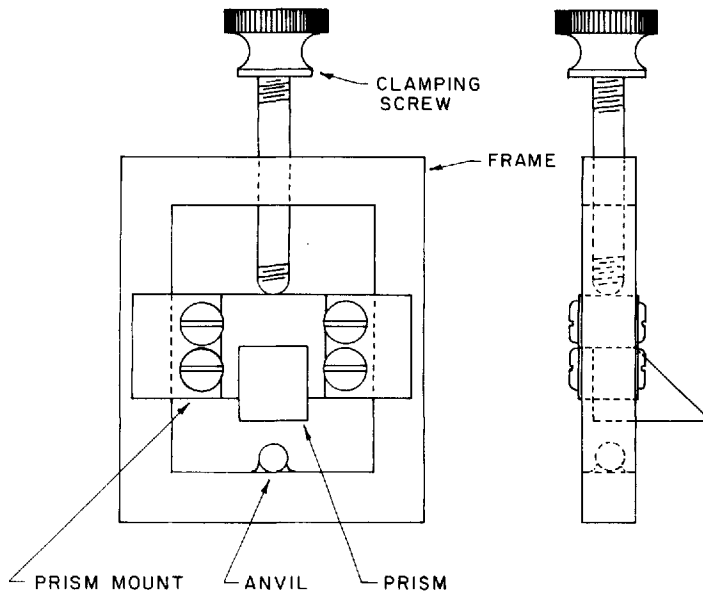


Fig. 5.5 Clamping frame, front and side view. The prism mount slides loosely in the frame

Attenuation measurements on multimode guides can provide some interesting insight into the cause of the loss. Often the higher-order modes show a larger attenuation. This is due to scattering at the film boundaries; since the electric field at these boundaries is larger for higher-order modes any scattering caused by imperfections of the interface will be stronger. On the other hand, if the scattering is in the film itself, or if the film has a small amount of absorption, one may

find that the higher-order mode has a lower loss than the next lower mode, due to the fact that a larger fraction of its energy is transmitted in the substrate.

As was pointed out by MARCUSE [5.31], the influence of boundary imperfections is larger for a greater difference in index between the material on either side of the boundaries. Thus, a film of a high-index material deposited on a high-index substrate will show a much lower loss for a given mode than it would if it were deposited on a low-index substrate.

From these considerations, it is clear that it is relatively meaningless to give a number for the attenuation of a specific material, unless the exact conditions under which the loss was measured are specified.

5.2.2. Thickness Measurement

To measure the physical thickness (as opposed to the optical thickness) of a film, one needs a step discontinuity, i.e., a transition region from the uncoated to the coated substrate. The thickness is measured across this step. Since in many cases the substrates are not optically flat, the film has to come up to its full thickness within a very short distance from the step.

Interferometry

A relatively coarse measurement of film thickness can be obtained by two-beam interferometry. The stepped area is used as one mirror in a modified Michelson interferometer and the step height is determined by measuring the fringe displacement. Because of the need for relatively abrupt steps, this measurement is almost always performed in an interferometric microscope. In this instrument, matched objectives are used in both the measuring and the reference legs of a Twyman-Green interferometer, thus allowing the observation of a small area of the sample. The visibility of the fringes is determined by the difference in the reflectivities of the sample and the reference mirror. Thus, by having an uncoated reference mirror, one can obtain good fringe contrast even from an uncoated sample.

However, care has to be taken that the observed fringes are indeed caused by interference with the beam that is reflected from the top surfaces of the film and the uncoated substrate. Often one also sees fringes caused by interference with the beam reflected from the substrate through the film. Comparison of the two types of fringes shows that the shift across the step in the latter set of fringes is in the opposite direction from that in the first set, and is also smaller by a factor $(n - 1)$, where n

is the refractive index of the film. Usually these fringes are much weaker, but in some cases, for example if the film to be measured has a lower index than the substrate and an optical thickness close to one quarter wave, they are dominant and can cause errors.

For films thicker than a few fringes and for very abrupt steps, it becomes difficult to follow the fringe pattern. It is then often necessary to use white light fringes. Because the intensity varies sinusoidally across the fringes in this type of interferometer, it is difficult to determine the exact center of a fringe. Therefore, unless densitometric measurements are performed, this type of measurement is only good to an accuracy of about 600 Å.

To make more definite measurements, one needs a method in which the fringes are much sharper. Such a better fringe definition can be obtained by the use of multiple beam interferometry. Here the interference is obtained between the sample and a flat reference surface held almost parallel to it. Often the reference surface is the flat first surface of the microscope objective. If used properly, this is perhaps the most accurate method for making thickness measurements; accuracies of better than 10 Å are possible. However, the method has some drawbacks. Chief among these is the fact that the sample has to have a relatively high reflectivity, making a metal coating necessary, which is time consuming. In addition, if the layer is later to be used as a waveguide in the location where the measurement was made, care has to be taken that the metal used is one that can be removed without ruining the surface of the layer (see Subsect. 5.3.3). Another drawback is that the reference flat has to be close to the sample in order to get good fringe finesse. In most applications, this means that the reference surface is pressed against the sample. Unless a floating contact head is used, distortion of the sample can result, making it difficult to define the start and finish of the step across which the thickness is being measured. Lastly, for abrupt steps and films thicker than one fringe, it may become difficult to follow the fringe across the step, in which case one has to resort to two-beam interferometry and white-light fringes for a rough thickness determination to determine the integral part of the number of fringes across the step.

Contact Measurement

A different method of thickness measurement is the stylus method. Here the hemispherical end of a diamond stylus is dragged across the step and the movement of the stylus is detected and amplified electronically and recorded. In principle, this measurement can give very accurate readings, while also giving an indication of the horizontal profile

of the step. However, especially for soft films, penetration of the stylus into the film gives rise to inaccuracies. SILVER and CHOW [5.32], in a careful comparison of various thickness measuring methods, found a constant deviation of about 200 Å for films of 3000 Å thickness using the Talisurf instrument manufactured by Taylor, Taylor and Hobson.

Measurement during Deposition

It is, of course, very desirable to be able to measure the thickness of the film during deposition. In that way, the film can be grown until a pre-determined value is reached, at which point the process is terminated. Such a measurement can be made by measuring the frequency change of a resonant quartz crystal as a function of the mass of the film deposited on it [5.33]. However, the accuracy of the method depends greatly on the temperature of the quartz sensor and this limits its applicability. In sputtering, for example, the electron bombardment of the substrate heats up the quartz, thus making the measurement unreliable, while deflection of the electrons by a magnetic field disturbs the plasma and produces a non-uniform thickness on the substrate.

5.2.3. Index Measurement

An often mentioned method of index measurement is ellipsometry. From the literature, one can gather the impression that ellipsometry allows the precise determination of the index and an integral fraction of the thickness of a film. In practice, however, this measurement is possible only if one knows the index of the substrate very accurately. This is especially true if the film index is close to the index of the substrate, a condition which is often met in integrated optics.

Another often mentioned method is due to ABELES [5.34]. Here the refractive index of a film is determined by finding Brewster's angle for the film. The reflectivity (as a function of incident angle for light linearly polarized in the plane of incidence) is measured both for the film-coated substrate, and for the uncoated substrate. Brewster's angle for the film is, of course, that angle where the two thus obtained curves cross. The refractive index of the film is then equal to the tangent of this angle.

This method is relatively simple to implement for films whose indices are quite different from the index of the substrate. However, if the film index is only a little higher (or lower) than that of the substrate, the two curves are very close together and may actually cross more than once, due to instabilities in the apparatus, thereby rendering the method useless. Also, since the index of the film is almost always larger than

1.5, its Brewster's angle is larger than 57° and consequently (since $A\bar{n} = A\alpha/\cos^2 i$) the angle of incidence i has to be measured to an accuracy of better than a minute of arc to provide a third decimal accuracy in the refractive index n . Nevertheless, since this method is relatively simple to implement, it is often used for quick, low-accuracy index determinations.

5.2.4. Index and Thickness Determination from Measurements of the Apparent Refractive Index

If the index and the thickness of the film are large enough to allow guidance of an optical wave, the most direct method to measure either the index or the thickness of the film is by measuring the effective index N . The simplest way to determine N is by measuring the coupling angle, using a prism coupler. In many applications, such as the coupling between guides, the value of N itself is of importance, but, in addition, the actual refractive index and/or the thickness of the guide can be derived from N through the modal equation. In a single-mode guide, one of these quantities has to be known for the other to be computed, i.e., the thickness can be computed from N and the index; conversely, the index can be computed from N and the thickness. However, if two modes are allowed in the guide, both the index and the thickness can be computed from the two values of N . If more than two modes are allowed, the method becomes self checking and greater accuracy can be obtained by a least-square fitting method. Hence an accurate measurement of N is very useful.

To find the coupling angle, the angle of incidence on the prism for which a given mode is excited is measured. By referring to Subsection 3.2.2, one can infer that the value of N for this mode is given by

$$N = n_p \sin [A + \sin^{-1}(\sin i / n_p)]. \quad (5.1)$$

To determine N , one therefore needs to know, in addition to the angle of incidence i , the angle A between the base and the incident face of the prism and the refractive index n_p of the prism (see Fig. 5.6). The angle i is considered positive when the incident beam lies between the normal to the prism and its base. In other words, in Fig. 5.6 the angle i is shown as positive. It is easily seen that the errors in these three quantities all add about equally to the error in N , the exact contributions depending on the case at hand. Thus, to obtain the smallest error in N , it is advantageous to know A and n_p to an accuracy much better than the obtainable accuracy in i . The accuracy to which N is

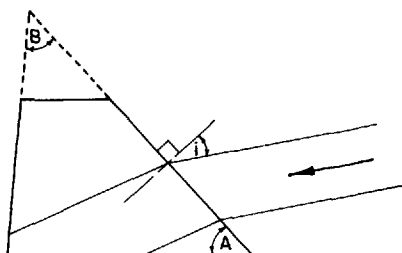


Fig. 5.6. Illustrating the angles in a prism as used in the text

then known is approximately equal to the accuracy Δi in the angle of incidence. In other words, if N has to be known to 1 part in 10^4 , the angle of incidence must be measured to about the same accuracy, i.e., to about 20 seconds of arc. The possible values of N for the different modes lie between n_f and n_s , where n_f is the film index and n_s is the index of the substrate. Thus, to be able to measure all the modes, one needs a prism with A and n_p chosen so that all the values of N can be obtained for useful values of i . In practice, the useful values of i and the dimensions of the prism are determined by the fact that, to couple into the guide, the beam has to be incident on the edge of the coupling area, which for clamped prisms is usually under the flat top of the prism. Clearly more than one prism is needed to measure different guides with widely varying indices.

To measure the angle i one needs a reference, and the most convenient choice for this is the normal to the prism. Although in many publications this is neglected, this normal is often more difficult to establish accurately than the coupling angle itself. The reason for this is the following. In most applications, one tends to focus the beam on the area where the prism is closest to the guide, in order to obtain sufficiently strong coupling. That is to say, the coupling angle is found by using a focused beam. However, to find the normal, one determines the angular position of the prism for which the beam reflected from the surface of the prism comes back on itself, i.e., the reflected beam is opposite in direction but collinear with the incident beam. This is most easily done by auto-collimation. However, a difficulty arises here, since it is not possible to auto-collimate a focused beam. This is illustrated in Fig. 5.7, which shows that a beam focused on a flat mirror is recollimated by the focusing lens and as a result is parallel to the incident beam on its return path. Even if the mirror is not exactly in the focal spot, as is the case for the entrance face of the coupling prism, the return beam is still almost parallel to the incident beam, so that the auto-

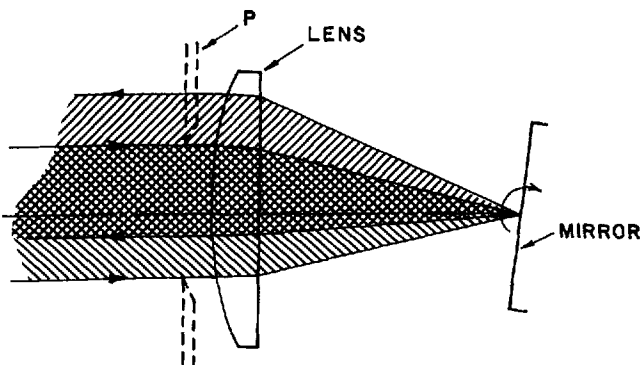


Fig. 5.7. Recollimation of a beam focused on a mirror

collimator cannot distinguish that the mirror is not perpendicular to the beam. To find if the mirror is perpendicular to the beam in this arrangement, one has to resort to a spatial, rather than an angular, discrimination; i. e., one can place an aperture stop in the beam at P . The signal from a photocell in the return beam is then largest when the mirror is perpendicular. However, it is easily seen that this method is not very sensitive. Assuming, for example, that the beam diameter at P is 5 mm and that the focusing lens has a focal length of 20 cm, a rotation of the mirror over an angle of 1 minute of arc changes the signal by less than 1%. Moreover, to obtain true readings, the aperture at P has to be perfectly centered on the axis of the lens, a condition which is not easily verified. However, if the lens is omitted and a collimated beam is incident on the mirror, its perpendicularity can be ascertained to an angle comparable to the diffraction limit of the collimated beam. This means, for example, that for a 5 mm diameter beam the signal from the photocell will vary by more than 50% for a rotation of 20 sec of arc.

It is clear from the above that the normal to the prism surface can be found to the desired accuracy by using a collimated beam of about 5 mm diameter. However, if a lens is subsequently inserted to launch the beam into the waveguide for a determination of the coupling angle, the accuracy of the measurement deteriorates again. Hence it is preferable to work with a collimated beam throughout. A convenient setup is schematically shown in Fig. 5.8. To avoid excessive astigmatism, the beam splitter should be a cube beam splitter, or a thin membrane. The correct position of the pinhole in front of detector d_1 , to assure auto-collimation, can be found by using the above explained fact that a focused beam cannot be auto-collimated, i.e., one puts an extra lens

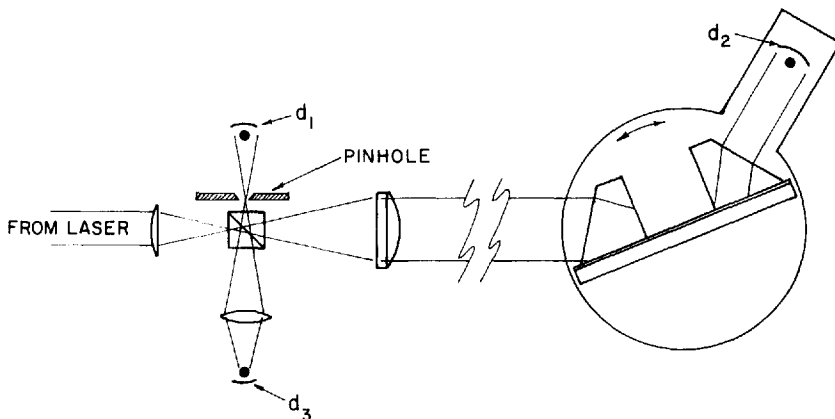


Fig. 5.8. Autocollimator and angle measuring equipment

in the collimated beam and a plane mirror at its focal point. The mirror is rotated so that the reflected beam more or less overlaps the incident beam and the pinhole is then adjusted to give a maximum signal from the detector d_1 . The signal from detector d_3 is directly proportional to the source brightness and can be used to normalize the signal from detector d_2 used to observe the output from the waveguide.

An additional advantage of the collimated beam is that the prism does not have to be very strongly coupled to the guide, which makes for a smaller error due to the inaccurate knowledge of the gap thickness, as explained below. A disadvantage, especially when the prism is clamped onto the guide, is that often only a region smaller than the beam diameter is sufficiently close to the guide to provide adequate coupling, resulting in a smaller signal into the guide.

The second quantity in (5.1) that has to be known is the angle A of the measuring prism. It is advisable to measure this angle to a greater accuracy than necessary. This can, of course, be done once and for all when the prism is first made. To allow this greater accuracy, the prism has to have faces at least as large as the diameter of the beam used in the measurement, i.e. larger than 5 mm. As pointed out by ULRICH and TORGE [5.35], it is preferable not to have any angles in the prism that are 30° , 45° , 60° or 90° since this may give rise to undesirable reflections or transmissions from the prism.

It is advantageous to measure the angle B also. By silvering the backface of the prism, one can then determine the refractive index of the prism quickly, by auto-collimating, first on the incidence face and

then on the backface. If the angle between these two readings is D , the refractive index of the prism is given by $n_p = \sin D / \sin B$. Obviously, this latter measurement can be made only for prisms for which $n_p \sin B < 1$.

To excite the different modes it is best to place the guide on a rotating table, and provide an input and an output prism. Means to make the entrance face of the input prism (and the guide itself) normal to the incident beam are necessary. In addition, a lateral movement of the mount is helpful to position the entrance prism so that the incident beam strikes the edge of the coupling area. In many cases, no output prism is necessary since a streak of scattered light is seen as soon as the light is coupled into the guide. However, an output prism is often helpful for accurate measurements, and for low-loss guides. Since the angle of the output with respect to the guide does not vary as the angle of incidence is varied, a detector can be mounted on an arm that rotates with the table.

To find the different modes, it is best to work with a tightly clamped prism and a focused beam first. After the approximate angular positions for the different modes are found in this way, the focusing lens is taken out, the prism is clamped less tightly, and the input angles are measured accurately.

By properly averaging a number of readings, both of the normal to the prism and of the angles for which maximum coupling is observed, one can determine the coupling angle for the different modes to the above mentioned accuracy of 20 sec or better. A necessary condition for such accuracy is, of course, that the rotating table has to be good to an accuracy of better than 20 sec of arc. If this is not the case, one can still obtain an accuracy better than that of the table by measuring the coupling angle a number of times with the sample in different angular positions with respect to the table.

Depending on the type of waveguide at hand, the angles at which the different modes occur follow a definite sequence. If a discontinuous step exists in the refractive index between guide and substrate, as in a deposited film, the dependence of N_i on the thickness of the guide for the different modes is as shown in Fig. 5.9. The lower-order modes are closer together than the higher-order ones. Thus, in a multimode guide, one can often find out if a mode-like coupling at a given angle is indeed a mode by plotting the measured modes and seeing if the angle in question fits in the sequence.

If the index changes continuously between guide and substrate, a different sequence of the modes occurs, whose exact structure depends on the particular shape of the curve of index versus guide thickness [5.36].

In addition to the different values of N_i , the data reduction requires a knowledge of the refractive index of the substrate. This quantity can

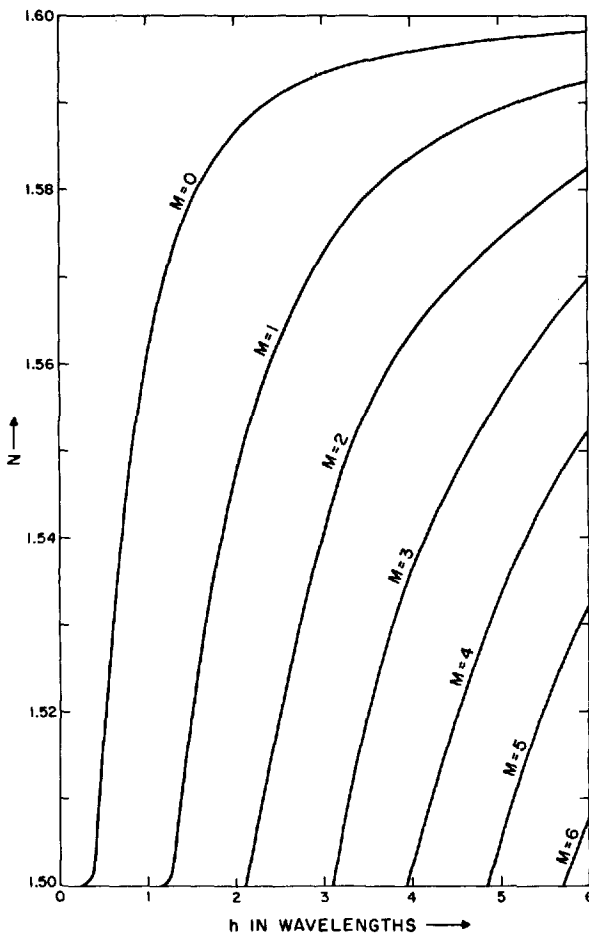


Fig. 5.9. Typical curves showing N as a function of h for a number of modes. The numbers relate to a guide with $n_s = 1.5$, $n_f = 1.6$ and $n_c = 1.0$

be measured at the same time that the measurements for N are made. If the prism-guide combination is rotated beyond the angle at which the highest-order mode occurs, the light couples into the substrate, and, as the angle is increased further, one can often see the beam reflecting many times against the two faces of the substrate. At the angle where this coupling just occurs, i.e., where the light is seen to come out of the end of the substrate, the value of N determined from (5.1) is the refractive index of the substrate.

Data Reduction

Once the angles of incidence for the different modes have been measured, N_i can be calculated for each of the modes using (5.1). These values of N_i can then be used to compute the index and/or the thickness of the film.

There are three different cases:

- 1) The guide supports only one mode and either n_f or h is known from a separate measurement. The unknown quantity (h or n_f) can then be computed.
- 2) The guide supports two modes. In this case n_f and h can both be computed from the two N_i values.
- 3) The guide supports more than two modes. Now both n_f and h can be computed with increased accuracy by the use of a least-square fitting routine.

In any of these cases, one uses the modal equation

$$2\pi Bh - M\pi = \phi'_c + \phi_s \quad (5.2)$$

and

$$n_f^2 = B^2 + N^2. \quad (5.3)$$

In (5.2), the thickness h of the film, is given in wavelengths.

Also

$$\begin{aligned} \phi'_c &= \phi_c + \sin(2\phi_c) \cos(2\phi_p) \exp(-4\pi P_c s) \\ \phi_c &= \tan^{-1}(P_c/B) \\ \phi_s &= \tan^{-1}(P_s/B) \\ \phi_p &= \tan^{-1}[P_p/(n_p^2 - N^2)^{1/2}] \end{aligned} \quad (5.4)$$

where

$$P_c^2 = (N^2 - n_c^2) \quad \text{and} \quad P_s^2 = N^2 - n_s^2. \quad (5.5)$$

The value ϕ'_c given by (5.4) is used because the value of N is measured under the prism and is thus the "loaded" N of the guide.³

Because of the transcendental nature of (5.2) a computer is indispensable to the data reduction. The calculation can be made in a

³ Equation (5.4) is an approximation derived from

$$\tan \phi'_1 = \frac{\tan \phi_p + \tan \phi_c + (\tan^2 \phi_p \tan \phi_c - \tan \phi_p) \tanh^2(-2\pi P_c s)}{(\tan^2 \phi_p + 1) \tanh(-2\pi P_c s)}$$

by using the fact that, for large x ; $\tanh(-x) = 1 - 2 \exp(-2x)$.

straightforward manner only in the case where the index n_f of the guide is known, and one wants to find h from n_f and N_0 . In all the other cases, one solves the modal equation by substituting a value of n_f (larger than the largest of the values N_i) in the equation

$$2\pi Bh - M\pi - \phi'_c - \phi_s = R \quad (5.6)$$

and by changing n_f in an iterative approximation in such a way that $R \rightarrow 0$. The iteration should be continued until the precision to which n_f is computed is compatible with the accuracy to which the values N_i were measured. In the first two cases, this means that the computation can be stopped when the step by which n_f is changed in successive iterations is an order of magnitude smaller than the measurement accuracy. In the third case, the limiting precision is that compatible with the rms error. In general, then, if the values of N_i are measured with an accuracy of 10^{-5} , there is no need to continue the iteration after the steps have become as small as 10^{-7} . The computer used for the data reduction should, of course, be capable of the required precision.

The one parameter that has not been discussed, and that is, in fact, difficult to measure accurately, is the thickness of the gap. Clearly, if one assumes a wrong value for s , one does make the computation with a value of N that is not quite correct. In most cases, however, a fairly large error in s is allowable before the error in N caused by it becomes comparable in magnitude to the measurement error, and in many cases only a small error results if the prism is neglected completely. However, it is prudent to compute the exact influence of s whenever high accuracy is needed. In those measurements where s needs to be known accurately, a low-index layer of controlled thickness can be deposited on the guide. The prism is contacted onto this layer with a cement, or a matching fluid with the same index as the prism [5.37].

It is of interest to note that the error in h is almost always larger than the error in n_f . This is due to the fact that n_f is calculated from (5.3) while h is calculated from (5.2). Since B is normally small compared to N , a small error in B results in a much larger error in h than in n_f .

If in a single-mode film neither h nor n_f are known, it may still be possible to find both quantities by changing n_c , for example by using an index-matching fluid. Thus either a different value of N is found for this "new" guide, and the two values of N can be used in much the same way as they would be in a two-mode guide or the "new" guide will actually sustain two modes from which h and n_f can be found. This is done by finding that value of n_f for which both values of N give the same value of h .

If a guide allows more than two modes, the film index and the thickness are overdetermined. One can now define an error sum

$$\sigma = \sum_i (N_i - \bar{N}_i)^2 \quad (5.7)$$

where N_i are the observed values and \bar{N}_i are the computed values. The best values of n_f and h are those for which σ is a minimum. Since the modal equation cannot be expressed in closed form, this minimum cannot be found analytically, and again a numerical solution has to be used. Several numerical techniques can be used to do this. ULRICH and TORGE, for example, have described a gradient method [5.35]. In the author's laboratory a similar method is used. First, approximate values of n_f and h are computed by the method of case 2) using the N values for the lowest and the highest order mode. These two values are used because they give the highest accuracy, as can be understood from Fig. 5.9. Using these values of n_f and h , the computer determines σ for the nine combinations of n_f , h and $(n_f \pm \Delta n_f)$ and $(h \pm \Delta h)$, where Δn_f and Δh are both small values. It finds the values of n_f and h for which σ is smallest and once again extends around these values using smaller quantities Δn_f and Δh . This iteration is continued until the change in n_f and h between two iterations has become small compared to the accuracy to be expected. At this point n_f , h , and σ are printed out.

Table 5.2. Indices and thicknesses of a Baria-Silica film as determined using different laser wavelengths

Wavelength [nm]	Measured index	Number of modes	Measured thickness	
			in wavelengths	in micrometers
632.8	1.60081	4	3.668	2.322
514.5	1.60808	5	4.505	2.318
488.0	1.61042	5	4.744	2.315
476.5	1.61178	5	4.852	2.312

Table 5.2 gives the result of an index and thickness measurement on a film with many modes. The measurement was made for different wavelengths and thus provided a check on the thickness measurement. As can be seen, the values of h , as measured at the different wavelengths, are consistent to within $\pm 0.2\%$.

5.3. Pattern Fabrication

The patterns needed in integrated optics can be divided into two distinct classes: those that are periodic, such as grating couplers [5.38] and filters [5.39], and those that have no periodicity at all.

5.3.1. Periodic Patterns

Because of their periodicity, the first type can be made conveniently by using optical interference patterns [5.40]. If two beams intersect at an angle 2θ , the fringe spacing is

$$d = \lambda_0 / (2n \sin \theta), \quad (5.8)$$

where λ_0 is the vacuum wavelength, and n is the refractive index of the material in which the two waves interfere. (The angle θ is also considered to be measured inside this material.) This interference pattern can be used to expose photoresist. The resulting resist pattern itself may then be used as an optical element, or it may be used as a mask in a subsequent etching process.

If the photoresist is deposited on a glass substrate, reflection against the back of the glass may produce disturbing interference patterns. These can be eliminated by exposing the photoresist through the substrate, by contacting a glass wedge onto the back of the substrate during the exposure, using index fluid, or by pre-exposing the entire slide to a level well below that needed for complete exposure [5.40]. The effect of the last procedure is to increase the gamma of the emulsion and, as a result, lower contrast patterns (including those due to dust on the optics) are suppressed.

If the two beams intersect at an angle 2θ in air, the refractive index in (5.8) is 1, and the smallest value obtainable for d is larger than $\lambda_0/2$. However, if the derived periodic element is to be used to interact with light in a waveguide, without coupling it out, the fringe spacing has to be smaller than the wavelength of the light in the guide [5.41]. As was demonstrated by DALGOUTTE [5.42], d can be made smaller by contacting a prism onto the photoresist surface using an index matching liquid. In this manner, SHANK and SCHMIDT [5.43] have obtained structures with a spacing of 1108 Å. An interesting variation of this method was used by TSANG and WANG [5.44], who submerge their sample, coated with positive photoresist, in a prism like container filled with photoresist developer. Because of this submersion, the photoresist is developed, i.e., the exposed material is removed while it is being exposed. This results in deeper corrugations in the photoresist.

5.3.2. Non-Periodic Patterns

A large amount of high resolution mask technology is used in the electronics industry for the manufacture of integrated circuits. Though much of this can be carried over to optical waveguide technology, there are some distinct differences. The two major differences are the need for very smooth edges and the aspect ratio of optical waveguides. Because of these points, the photolithography methods commonly used for integrated circuits cannot be used here. Consider, for example, an optical modulator with a guide 6 mm long and 2 μm wide. If the mask for this guide were made by photographic reduction of a line 2 mm wide, this line would have to be 6 m long! The problem cannot be circumvented by a step and repeat method; even for a 1% difference in index between guide and surround, the edges of the guide have to be smooth to better than 500 Å in order to keep the attenuation below 1 db/cm [5.31]. This imposes tolerances on the step and repeat camera that are impossible to meet.

The unique requirement for very smooth long lines can be met by the use of a focused laser beam or a focused electron beam to write the patterns. For a proper appreciation of the problems involved in the making of masks, the final use of the generated pattern needs to be understood first. In general, four different ways of pattern generation and use can be distinguished:

- 1) The pattern is generated in a positive resist, deposited on top of a planar guide.⁴ After development, a metal coating is applied to the entire surface and subsequently the resist and the metal covering it are washed off. The remaining metal pattern is then used as a barrier in an etching procedure in which all but the wanted portions of the slab guide are removed.
- 2) The pattern is generated in either a positive or a negative resist and the resist itself is used as a barrier during a subsequent etching procedure.
- 3) The pattern is generated in a positive resist and the resist is used as a mask in ion implantation.
- 4) The pattern is generated in a material whose index increases as a result of exposure to the generating radiation, thus producing the guide directly. In a variation of this procedure, the pattern is written in a negative resist which, after development, forms the waveguide.

⁴ Resists are called positive when the exposed area is removed upon development. In other words, if the resist is considered black, the exposing radiation writes a white line, making a positive image.

5.3.3. Methods of Material Removal

As was mentioned in Subsection 5.1.3, sputtering can be used as a method to remove material. This could be done by merely positioning the properly masked sample directly on the cathode of the same sputtering apparatus that was used to deposit the planar guide. However, if the mask is a resist (and thus an organic material) the sputter etching operation has to be performed in an argon plasma to avoid burning up the mask. Even then, the small amount of oxygen freed from the rest of the cathode by the sputtering action is often enough to oxidize the mask. To prevent any oxidation, the cathode should be metallic and a getter type of metal, such as titanium, is preferred. A small amount of the titanium sputtered off the cathode is redeposited on it, leaving a thin titanium deposit on the sample also. This deposit can be removed by sputter etching for a very short time on a glass cathode.

A better controlled method of sputter etching is known as ion-beam machining, and uses the apparatus described in Subsection 5.1.3. Since the ion beam is generated in a separate ion gun, the sample itself can be located in a very high vacuum and kept at lower temperatures.

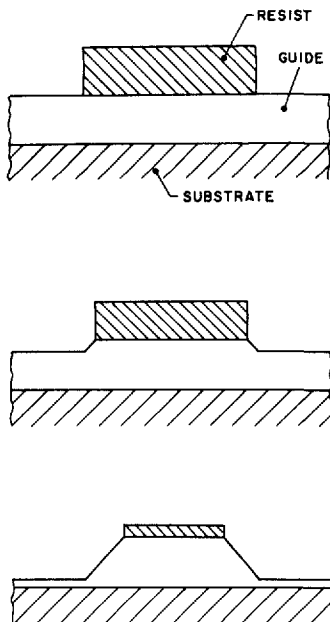


Fig. 5.10. Three successive stages in the etching of a resist-covered glass waveguide

Moreover, the beam is collimated and well defined; this allows a larger freedom in the exact use of the mask; for example, blazed gratings can be fabricated, by having the ion beam incident at an angle on a pattern of parallel lines [5.46].

An important point in both methods of etching is that the ion bombardment removes the mask also. Photoresist masks, for example, are removed at about the same rate as glass. As a result, even if the mask has perpendicular sides to begin with, the finished guide after etching has a trapezoidal cross-section with sides at about 45° (see Fig. 5.10). This also means that the sides of the trough written in the photoresist have to be smooth over their entire height. A line which is smooth on the bottom but not towards the top does not produce a smooth side after etching.

Some metals sputter slower than glass. However, not all of these can be used; it was found, for example, that aluminum cannot be deposited and removed from a slab guide without ruining the surface of the guide. Moreover, its edges do not remain smooth during the sputtering. Manganese can be used, its edges remain smooth during sputter etching, it sputters at about 1/5 the rate of glass [5.47], and it can be removed without damage to the guide.

5.3.4. Electron Beam Writing

The high resolution and the dimensional precision achievable with electron-beam exposure of resists, as developed for the writing of integrated circuit masks [5.48], make this method highly suitable for waveguide mask making also. Both positive [5.49] and negative [5.50] resists exist. Exposures necessary are on the order of 10^{-4} Coulomb cm^{-2} at 10 to 14 kV for the positive resist, and 4×10^{-4} Cb cm^{-2} at 20 kV for the negative resist.

Since electron beams can, at best, be scanned over only a few millimeters before lens aberrations become too large, the sample has to be moved if large patterns need to be written. OSTROVSKY et al. [5.51], for example, focus their beam to a 300 Å diameter spot, and use a digital method. To write a line, a number of adjacent rectangles are written, whose length is equal to the width of the line. The carriage is moved from rectangle to rectangle, but the individual rectangles are written by steering the electron beam. Errors in the carriage motion are detected interferometrically and are corrected by adjusting the beam position.

Though OSTROVSKY et al. used a digital method of control, this is partly due to the fact that their apparatus was designed to make masks

for integrated circuits. Analog or hybrid digital-analog methods would appear to have advantages in view of the desired edge smoothness. GOELL [5.47] has written small patterns by scanning the beam in analog fashion over a stationary sample. BALLANTYNE and TANG [5.52] used a hybrid method to write grating patterns; each grating line is drawn in analog fashion, but the steps from line to line are made digitally.

In a positive resist, the ultimate resolution achievable with electron beam exposure is limited by undercutting of the resist. This is caused by scattering of the electrons in the resist layer, and by back-scattering from the surface under the resist. As a result, the written line is wider at the bottom of the resist layer than at the top. Moreover, the amount of undercutting varies. Thus, if two lines are written very close together, the line of resist separating them may come off. Postbaking, i.e., baking after development, can cure the undercutting [5.49], but this does, of course, not help after the resist has separated from the substrate. However, if a metal lift-off technique is used, as described under Item 1) in Subsection 5.3.2, the undercutting is an advantage, since it prevents the formation of a connection between the metal on the resist and the metal in the groove, as shown in Fig. 5.11. As a result, the edge smoothness of the metal line (remaining after the resist is washed off) is determined by the edges of the line written in the resist, and not by shearing of the metal.

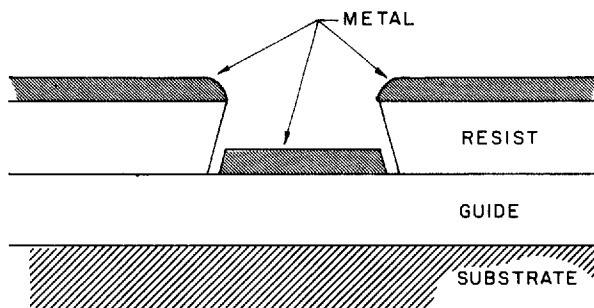


Fig. 5.11. Electron-beam written line in positive resist overcoated with metal

In negative electron resists, the scattering of the electrons again causes a widening of the line at the substrate-resist interface [5.50]. However, since the line determines where the resist remains after development, the result when two lines are written close together is much less catastrophic than with positive resists; i.e., the lines overlap slightly, but the space between them is not totally lost.

5.3.5. Laser Beam Writing

If a focused laser beam is used to write the pattern, only the sample is usually translated. Thus, the smoothness of the edges of a written line depends on the quality of the translating stage, the uniformity of the resist sensitivity and the processes taking place during development. Very smooth lines can be written in positive photoresist (Shipley AZ 1350) [5.53]. However, a metal lift-off process (as used with electron beam writing) does not work here, since the groove width in the resist is wider at the top than at the bottom. As a result, after evaporation, the metal on the resist is connected to the metal in the groove; when the resist is washed off, the breaking of this connection causes rough edges on the remaining metal line.

Consequently, the resist itself has to be used as the etch mask. However, since this is a positive resist, the outline of the guides to be written has to be exposed, rather than the guide itself. In other words, at least two lines have to be written for every guide. Also, the smallest distance between two guides written in this manner is equal to the width of the written line, and, unless the sample is optically flat, the narrowest such line is about $2 \mu\text{m}$ wide.

It was originally reported [5.53] that the necessary edge smoothness cannot be obtained in negative photoresists. However, some of the newer resists, such as Kodak 747, appear to have the desired properties, but special care is needed during development.

Direct writing of guides in Kodak KPR photoresist films was reported by WEBER et al. [5.54]. Recently, the same group [5.55] has reported a technique called photolocking. In this technique, a moderately volatile dopant is dissolved in a lower-index polymer and this mixture is deposited as a thin film on a glass substrate. By exposing the film to a focused argon laser beam at 3640 \AA , the dopant is locally locked in the film. After the exposure, the unreacted dopant is removed by heating. A guide written in this fashion, and which allowed one mode in the vertical and two modes in the horizontal direction, was measured to have a loss of $0.20 \pm 0.05 \text{ dB/cm}$. Virtually the same loss was found in planar guides of the same material, showing that no additional loss was caused by the edges of the channel guide.

5.3.6. Coupling between Guides

Coupled waveguides form the basis of a number of essential components, such as switches, directional couplers, filters, etc. To obtain adequate coupling over a reasonable length, the distance between the

guides should be small. However, as was pointed out above, difficulties arise when one tries to write two guides close together. To circumvent this problem, rib guides can be used. These can be either ribs of thicker material on a film of the same material which is below cut-off [5.56], or ribs of a low-index material on a film which is below cut-off when covered by air, but above cut-off when covered by the low-index material [5.57]. Coupling between two such rib guides is obtained in a structure as shown in Fig. 5.12. Because of the connecting layer, which

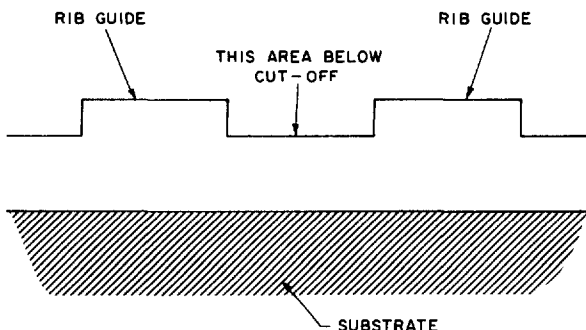


Fig. 5.12. Coupling between two rib guides. The connecting layer is below cut-off

is below cut-off, the coupling here is relatively strong even though the distance between the guides is large. Clearly, one way in which such a coupler can be made is by removal of the planar guide [5.58]. A similar structure is caused by electron scatter when two parallel guides are written in negative electron resist [5.50].

5.3.7. Duplication Methods

A number of methods to be used for duplication of integrated optical circuits have been reported. ULRICH et al. [5.59] described a method in which grooves are embossed in a thermoplastic substrate. These grooves had been filled with a liquid which was then solidified. PUECH [5.60] has described a method to make the die necessary to do the embossing.

Optical contact printing of waveguide patterns has been reported [5.53] using a duplication method first developed by SMITH et al. [5.61].

An electron projection method similar to one first described by O'KEEFE [5.62] has been used by OSTROVSKY [5.63]. This method uses

a master mask written in a TiO_2 coating on a fused silica substrate. The entire mask is coated with a thin film of palladium and is situated in a vacuum. The mask is illuminated through the fused silica substrate by an ultraviolet source. Where no TiO_2 is present the ultraviolet light strikes the palladium and electrons are emitted. A magnetic field is used to re-image these electrons onto the wafer to be exposed.

SPEARS and SMITH [5.64] have reported a lithography method using X-rays which, because of its high resolution capabilities, looks promising for optical waveguides.

References

- 5.1. L. HOLLAND: *The Properties of Glass Surfaces*, (John Wiley, New York 1964), Chapt. 1.
- 5.2. C. W. PITI: Electron. Letters **17**, 401 (1973).
- 5.3. G. R. STILLWELL, D. B. DOVE; J. Appl. Phys. **34**, 1941 (1963).
- 5.4. G. B. BRANDT, E. P. SUPERTZI, T. HENNINGSSEN: Appl. Opt. **12**, 2898 (1973).
- 5.5. J. E. GOELL: Appl. Opt. **12**, 737 (1973).
- 5.6. W. KERN, D. A. PUOTINEN: RCA. Rev. **31**, 187 (1970).
- 5.7. D. O. FEDER, D. E. KOONTZ: Symposium on cleaning of electronic device components and materials, ASTM Spec. Tech. Publ. 246 (1959), p. 40.
- 5.8. See, for example: L. I. MAISSEL, M. H. FRANCOMBE: *An Introduction to Thin Films* (Gordon and Breach, New York, 1973).
- 5.9. W. J. COLEMAN: Appl. Opt. **13**, 946 (1974).
- 5.10. P. D. DAVIDSE, L. I. MAISELL: J. Vac. Sci. Techn. **4**, 33 (1967).
- 5.11. T. NISHIMURA, Y. MURAYAMA, K. DOTA, H. MATSUMARU: Digest of the third symposium on the deposition of thin films by sputtering (Bendix Corp., Rochester, 1969), p. 96.
- 5.12. F. ZERNIKE, E. L. SLOAN, J. C. WEBSTER, R. B. McGRAW, W. L. KNECHT: "Digest of Technical Papers". Topical Meeting on Integrated Optics, Guided Waves, Materials and Devices, Las Vegas, Nev., Febr. 1972, paper TuA9.
- 5.13. J. E. GOELL: Appl. Opt. **12**, 737 (1973).
- 5.14. D. H. HENSLER, J. D. CUTHERBERT, R. J. MARTIN, P. K. TIEN: Appl. Opt. **10**, 1037 (1971).
- 5.15. M. FUJIMORI, M. SASAKI, M. HONDA: "Digest of Technical Papers". Topical Meeting on Integrated Optics, Guided Waves, Materials and Devices, Las Vegas, Nev., Feb. 1972, paper TuA2.
- 5.16. R. B. McGRAW, F. ZERNIKE: Paper presented at 76th Annual Meeting of the American Ceramic Society, Chicago Ill., April 28—May 2, 1974.
- 5.17. P. K. TIEN, G. SMOLINSKY, R. J. MARTIN: Appl. Optics **11**, 637 (1972).
- 5.18. M. J. VASILE, G. SMOLINSKY: J. Electrochem. Soc. **119**, 451 (1972).
- 5.19. P. K. TIEN, R. J. MARTIN, G. SMOLINSKY: Appl. Opt. **12**, 1909 (1973).
- 5.20. R. ULRICH, H. P. WEBER: Appl. Opt. **11**, 428 (1972).
- 5.21. R. ULRICH, H. P. WEBER: Appl. Phys. Letters **20**, 38 (1972).
- 5.22. T. P. SOSNOWSKI, H. P. WEBER: Appl. Phys. Letters **21**, 310 (1972).
- 5.23. T. IZAWA, H. NAKAGOME: Appl. Phys. Letters **21**, 584 (1972).
- 5.24. J. LINDHARD, M. SCHARF: Phys. Rev. **124**, 128 (1961).
- 5.25. J. B. SCHROEDER, H. D. DIESELMAN: J. Appl. Phys. **40**, 2559 (1969).

- 5.26. E. R. SCHINELLER, R. P. FLAM, D. W. WILMOT: *J. Opt. Soc. Am.* **58**, 1171 (1968).
- 5.27. R. D. STANLEY, W. M. GIBSON, J. W. RODGERS: *Appl. Opt.* **11**, 1313 (1972).
- 5.28. J. E. GOELL, R. D. STANLEY: *Proc. IEEE* **58**, 1504 (1970).
- 5.29. F. ZERNIKE, J. W. DOUGLAS, D. R. OLSON: *J. Opt. Soc. Am.* **61**, 678 (1971).
- 5.30. H. P. WEBER, F. A. DUNN, W. N. LEIBOLT: *Appl. Optics* **12**, 755 (1973).
- 5.31. D. MARCUSE: *Bell Syst. Tech. J.* **48**, 2902 (1969).
- 5.32. M. D. SILVER, E. K. CHOW: *J. Vac. Sci. Techn.* **2**, 203 (1965).
- 5.33. K. I. CHOPRA: "Thin Film Phenomena" (McGraw-Hill Book Company, New York, 1969), p. 91.
- 5.34. F. A. ABELES, in: "Advanced Optical Techniques" edited by A.C.S. van Heel (John Wiley, New York, 1967), p. 143.
- 5.35. R. ULRICH, R. TORGE: *Appl. Opt.* **12**, 2901 (1973).
- 5.36. See, for example P. K. TIEN, S. RIVA-SANSEVERINO, R. J. MARTIN, A. A. BALLMAN, J. BROWN: *Appl. Phys. Letters* **24**, 503 (1974).
- 5.37. F. ZERNIKE, J. E. MIDWINTER: *IEEE J. Quant. Electr.* **QE-6**, 577 (1970).
- 5.38. M. L. DAKSS, L. KUHN, P. F. HEIDRICH, B. A. SCOTT: *Appl. Phys. Letters* **16**, 523 (1970).
- 5.39. D. C. FLANDERS, H. KOGELNIK, R. V. SCHMIDT, C. V. SHANK: *Appl. Phys. Letters* **24**, 194 (1974).
- 5.40. M. J. BEESLEY, J. G. CASTLEDINE: *Appl. Opt.* **9**, 2720 (1970).
- 5.41. F. W. DABBY, A. KESTENBAUM, U. C. PEAK: *Opt. Comm.* **6**, 125 (1972).
- 5.42. D. G. DALGOUPTE: *Opt. Comm.* **8**, 124 (1973).
- 5.43. C. V. SHANK, R. V. SCHMIDT: *Appl. Phys. Letters* **23**, 154 (1973).
- 5.44. W. TSANG, S. WANG: *Appl. Phys. Letters* **24**, 196 (1974).
- 5.45. J. E. GOELL, R. D. STANLEY, W. M. GIBSON, J. W. RODGERS: *Appl. Phys. Letters* **21**, 72 (1972).
- 5.46. H. L. GARVIN, E. D. WOLF: "Digest of Technical Papers". Topical Meeting on Integrated Optics, New Orleans, La., January 1974, paper ThA6; also, H. L. GARVIN, E. GARMIRE, S. SOMEKH, H. STOLL, and A. YARIV: *Appl. Optics* **12**, 455 (1973).
- 5.47. J. E. GOELL: *Appl. Opt.* **12**, 729 (1973).
- 5.48. A. N. BROERS, M. HATZAKIS: *Scientific American* **227**, 34 (1972).
- 5.49. J. HALLER, M. HATZAKIS, R. SRINIVASAN: *IBM J. Res. Dev.* **12**, 251 (1973).
- 5.50. J. C. DUBOIS, M. GAZARD, D. B. OSTROVSKY: *Optics Comm.* **7**, 237 (1973).
- 5.51. D. B. OSROVSKY, M. PAPUCHON, A. M. ROY, J. TROTEL: *Appl. Opt.* **13**, 636 (1974).
- 5.52. J. M. BALJANTYNE, C. L. TANG: "Digest of Technical Papers". Topical Meeting on Integrated Optics, New Orleans, La., January 1974, paper ThA8.
- 5.53. F. ZERNIKE, J. C. WEBSTER, R. B. McGRAW: "Digest of Technical Papers". Topical Meeting on Integrated Optics, New Orleans, La., January 1974, paper ThA2.
- 5.54. H. P. WEBER, R. ULRICH, E. A. CHANDROSS, W. J. TOMLINSON: "Digest of Technical Papers". Topical Meeting on Integrated Optics, Guided Waves, Materials and Devices, Las Vegas, Nev., February 1972, paper TuA8.
- 5.55. E. A. CHANDROSS, C. A. PRYDE, W. J. TOMLINSON, H. P. WEBER: *Appl. Phys. Letters* **24**, 72 (1974).
- 5.56. P. KAISER, E. A. J. MARCATILI, J. E. MILLER: *Bell Syst. Tech. J.* **52**, 265 (1973).
- 5.57. H. FUTURA, H. NODA, A. IHAYA: *Appl. Optics* **13**, 322 (1974).
- 5.58. J. E. GOELL: *Appl. Opt.* **12**, 2797 (1973).
- 5.59. R. ULRICH, H. P. WEBER, E. A. CHANDROSS, W. J. TOMLINSON, E. A. FRANKE: *Appl. Phys. Letters* **20**, 213 (1972).
- 5.60. C. PUECH: *Opt. Comm.* **7**, 135 (1973).
- 5.61. H. I. SMITH, F. J. BACHNER, N. EFRENOW: *J. Electrochem. Soc.* **118**, 821 (1971).

- 5.62. T. W. O'KEEFE: IEEE Trans. **ED 17**, 465 (1970).
- 5.63. D. B. OSTROVSKY: "Digest of Technical Papers". Topical Meeting on Integrated Optics, New Orleans, La., January 1974, paper ThAl.
- 5.64. D. L. SPEARS, H. I. SMITH: Solid State Techn. **15**, 21 (1972).

6. Semiconductor Components for Monolithic Applications

E. GARMIRE*

With 22 Figures

In monolithic integrated optics, all optical functions must be obtained in a single material. These optical functions can be broadly categorized as light generation, guiding, coupling, modulation and detection. Active functions such as light generation, modulation and detection generally require crystals rather than amorphous light guides. The only material to date in which all functions have been obtained is GaAs. The existence of continuous lasers in GaAs operating at room temperature is a prime incentive for considering this material. This chapter will be devoted to the fabrication of optical circuit elements in crystals, with special importance placed on GaAs and related III-V semiconductor compounds. The spectral region in the red or near infra-red will be emphasized, because this is a region of low loss for optical fibers and therefore of interest for optical communication systems. We shall describe ways to produce optical waveguides in crystals, particularly of the semiconductor variety, both planar and channel guides being considered. We shall discuss ways to fabricate active elements in GaAs which generate, modulate and detect the light. Finally, the growth processes of liquid-phase epitaxy will be discussed in some detail, as crystal growth is a necessary step for the realization of integrated optics using GaAs.

6.1. Waveguides

The first requirement for a crystal to be suitable for integrated optics is that it can be fabricated as a dielectric waveguide, in the form of a layer of good optical quality with refractive index higher than the substrate. The refractive index can be controlled largely by changing the material composition, as in the guides of Chapter 5. To a smaller extent, in semiconductors it can also be controlled by the electrical properties. Both of these effects have been utilized to make waveguides in crystals.

* Article was written when the author was with the Standard Telecommunication Laboratories, Harlow, Essex, England, on leave from California Institute of Technology, Pasadena, California.

We consider first guiding due to the electrical properties in semiconductors.

6.1.1. Waveguides Due to Free Carriers

Waveguides can be made from a resistive or pure layer of GaAs on *n*-type substrates of the same material. This is because the presence of free carriers in a semiconductor lowers the refractive index from that of the pure material. A layer with no free carriers will have a higher refractive index than a substrate with a high carrier concentration. If the depression of the refractive index due to the free carriers is sufficiently large in the substrate, the pure layer will guide light. We shall show that this effect is sufficiently strong in *n*-type GaAs to enable excellent guides to be made. We shall discuss the magnitude of this effect and describe techniques for the fabrication of layers with no free carriers in GaAs and properties of the resulting waveguides.

The depression of the refractive index is primarily due to the negative contribution of the free-carrier plasma to the dielectric constant. Its magnitude is calculated in the same fashion as for a plasma, using the free-carrier effective mass m^* in place of the free-electron mass. In a semiconductor with N free carriers per unit volume, the change in refractive index due to free carriers is [6.1]

$$\Delta n_s = -\frac{N \lambda_0^2 e^2}{\epsilon_0 n_s 8\pi^2 m^* c^2}. \quad (6.1)$$

Here n_s is the refractive index of the semiconductor at a free space wavelength λ_0 , e is the free carrier charge, ϵ_0 is the permittivity of vacuum, and c is the velocity of light. As a numerical example in *n*-type GaAs, $\Delta n_s = 0.01$ when $N = 5 \times 10^{18}$ carriers/cm³ for $\lambda_0 = 1 \mu\text{m}$. This refractive index change between pure and *n*-type material is large enough to permit guiding of light if a pure layer sufficiently thick can be fabricated on an *n*-type GaAs substrate. In order to see how thick the guiding layer must be, we must relate this refractive index change to the waveguiding conditions obtained in Subsection 2.1.2.

The modes in a waveguiding layer of GaAs with one surface exposed to air are, to a very good approximation, the anti-symmetric modes of a symmetric guide of twice the layer thickness [6.2]. This is because the refractive index of GaAs is so high that the light field is essentially zero at the GaAs-air interface. The guided modes therefore have a waveguide cutoff condition which is the same as for the anti-symmetric (odd) modes of a symmetric guide, which was derived in Section 2.3.

In order to confine light in a guide of thickness h , the refractive index discontinuity Δn between the guide and substrate must be [6.2]

$$\Delta n \geq \frac{(2M-1)^2}{2n_s} \left(\frac{\lambda_0}{4h} \right)^2, \quad (6.2)$$

where M is the number of asymmetric modes propagating.

Combining (6.1) and (6.2), we can obtain a waveguide cutoff condition for semiconductor waveguides formed by a resistive layer on a lower resistivity substrate [6.1]. The required difference in carrier concentration between the substrate and guiding layer is expressed as a function of the guide thickness by

$$N_s - N_f > \frac{(2M-1)^2 \pi^2 \epsilon_0 m^* c^2}{4e^2 h^2}. \quad (6.3)$$

If the carrier concentration in the film N_f is much less than that in the substrate N_s , (6.3) reduces to a condition on the substrate carrier concentration only. As an example, n -type GaAs with $N_s = 5 \times 10^{18}$ carriers/cm³ will guide light in a 1 μm or thicker layer. It is not possible to guide light in layers much thinner than this because GaAs substrates with substantially higher carrier concentrations are not available. It is the exceptionally small effective mass of electrons in GaAs ($0.08 m_e$) that makes the plasma contribution so large. In other semiconductors, as well as in p -type GaAs, this effect is much smaller and guiding is then possible only in much thicker layers. Control of free carriers is a convenient way to make waveguides in GaAs and has proved very useful for studies of integrated optics.

It is interesting to note that the free carrier cutoff condition, (6.3), is independent of wavelength; this is due to the λ_0^2 dependence of the plasma contribution to the refractive index which cancels the λ_0^2 dependence of the waveguide cutoff condition. This means that if a resistive layer is thick enough to guide light at one wavelength, it will guide at all wavelengths, in the approximation of this model. However, the free carriers in the substrate may introduce some optical absorption, which limits the range over which these guides can be used.

If the guided light is well-confined to the resistive layer, free-carrier losses are negligible. As confinement becomes poor near waveguide cutoff, however, losses due to substrate free carriers may become substantial. Typically $10^{18}/\text{cm}^3$ n -type GaAs has a loss [6.3] at 1 μm of about 40 db/cm so that, if more than 10% of the guided light travels in the substrate, losses larger than 4 db/cm are introduced. The free-

carrier loss is proportional to N , so that the same guided light distribution will suffer less loss in substrates with smaller carrier concentrations. However, smaller substrate carrier concentrations produce poorer confinement and more loss unless thicker guides are used. The waveguide parameters which yield minimum loss will depend on the particular design requirements.

Light of wavelength $10.6 \mu\text{m}$ is subject to much more loss than light at $1 \mu\text{m}$ because the free-carrier loss is proportional to λ_0^2 . This means that low-loss guides at $10.6 \mu\text{m}$ require particularly good light confinement and must be at least $10 \mu\text{m}$ thick, even though (6.3) indicates that much thinner layers have sufficient refractive index change to guide light.

Waveguides formed by resistive layers on n -type substrates in GaAs have the primary advantage of relative ease of fabrication, as we shall show in the next sections. Their disadvantage is the inability to vary the refractive index and the carrier concentration independently, the inability to make guides thinner than $1 \mu\text{m}$, and possible free-carrier losses. We shall discuss three types of waveguides which have been made using the electrical properties of GaAs to control the refractive index. These are shown schematically in Fig. 6.1.

Epitaxial Waveguides

A commercially available source of GaAs optical waveguides is epitaxial layers of high resistivity GaAs grown on low-resistivity GaAs substrates, as sketched in Fig. 6.1a. This is the same material that is used for Gunn oscillators and for field effect transistors, and the vapor or liquid phase epitaxial techniques for its fabrication are well developed [6.4]. Waveguiding has been observed and cutoff measured at $1.15 \mu\text{m}$ in these epitaxial guides [6.2], and Δn was shown to be consistent with that expected from (6.1). This demonstrates that the plasma effect of the free carriers is their chief contribution to the refractive index at $1 \mu\text{m}$. The additional contributions to the refractive index expected when light is close to the bandgap have been shown to be negligible at $1 \mu\text{m}$. Epitaxial layers several micrometers thick exhibit good quality single mode guiding with low losses ($< 4 \text{db/cm}$) in the near infrared. At $10.6 \mu\text{m}$, high resistivity epitaxial layers $20 \mu\text{m}$ or thicker have been shown to form useful guides [6.5].

Commercial GaAs epitaxial layers are of good enough quality that losses due to material and interface perturbations are negligible. When the free-carrier losses are minimized, these layers make excellent guides that have been used for modulators, lasers and detectors, devices which will be described in later sections of this chapter. Besides their com-

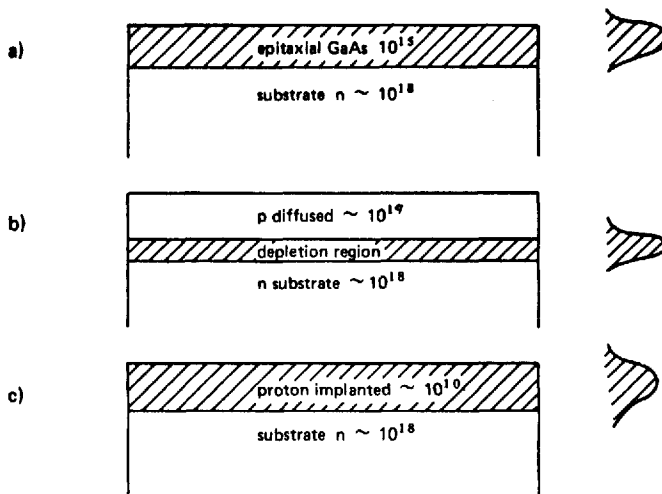


Fig. 6.1 a-c. Three methods of guiding light by free carriers in GaAs. The shaded regions have higher refractive index and form the waveguides. Typical free-carrier concentrations per cubic centimeter are shown, and approximate guided light profiles are sketched. Examples are a) high resistivity epitaxy on *n*-type substrate, b) depletion region of a reverse-biased *p*–*n* junction and c) proton implantation of *n*-type substrate

mmercial availability and low losses, a final advantage of these over other types of free-carrier guides is the ease of applying an electric field across a pure epitaxial layer for active elements.

Diffused Waveguides

Diffusion of acceptor impurities into *n*-type GaAs can produce a layer of *p*-type material at the surface as well as an imbedded depletion region in which the free carriers are compensated, as shown in Fig. 6.1b. The region depleted of free carriers has a higher refractive index than the surrounding *n* and *p* regions, and can contribute to confinement of light near the depletion layer.

The depletion region width is generally too thin (on the order of $0.1 \mu\text{m}$) to be expected to confine light strongly. However, the *p*-region can have a higher refractive index than the *n*-region and it can thus contribute to guiding. This is because the effective mass of holes is ten times larger than the effective mass of electrons in GaAs, so that the same number of holes depress the refractive index only one tenth as much as the electrons. Light guiding in diffused *pn* junctions was

identified very early in GaAs lasers [6.6]. However, there are neither published studies of the refractive index profiles of GaAs *pn* junctions, nor careful studies of guided light distributions, so that comparisons between theory and experiment are not possible.

Careful studies of guiding of 0.6 μm light in GaP diffused *pn* junctions have been published [6.7] and indicate some discrepancy with models based purely on free-carrier considerations. Additional contributions to the refractive index are expected to come from the dopant [6.8] as well as from the electro-optic effect, and these may be required for a full understanding of guiding in *pn* junctions.

Diffusion of *pn* junctions for use as GaAs lasers is a well established technique and the same method may be used to fabricate waveguides. Into *n*-type bulk GaAs, Zn is diffused at typically 750°C for 5 min. inside a diffusion furnace. The source is Zn_3As_2 which is placed along with the polished substrate in an evacuated, sealed quartz ampoule.

One common use of *pn* junction guiding at the present time is in single heterostructure lasers [6.9]. This structure results from the liquid phase epitaxy of a single Zn-doped GaAlAs layer on bulk GaAs. The diffusion of the Zn dopant during growth places the *pn* junction depletion region about 3 μm below the GaAlAs layer. The lower refractive index of the *n*-region confines light to the active region.

Many of the properties of guiding in GaAs *pn* junction layers have not yet been studied. It remains to be seen whether these can be useful passive waveguides, but their use in pulsed lasers is well documented. An accurate description of their characteristics awaits further experiments. For active elements, these guides have some real use. They have been shown for lasers, and can be used as modulators or detectors. While these guides are expected to have fairly high optical losses due to free carriers, because the depletion layer is so thin, they have the advantage of being easily made by diffusion techniques, which are available in most laboratories. This should be a fruitful area for more research.

Ion-Implanted Waveguides

High-resistivity layers and resulting waveguides can be fabricated in GaAs by using ion implantation, shown in Fig. 6.1c. Bombardment of material by energetic protons or by other light ions produces a layer with changed properties due to damage. In semiconductors, ion implantation generally compensates both *n*- and *p*-type material, forming a layer of high resistance. The energetic ions are thought to cause displacements of the lattice, which trap carriers, thereby lowering the free-carrier concentration. This results in a layer of higher refractive index than the bulk, with a thickness given by the penetration range of the

ions into the material. Protons travel into GaAs about one micrometer for each hundred keV of energy.

Three hundred keV protons are readily available from commercial ion implantation machines. In order to provide uniform implantation, the ion beam should be swept rapidly back and forth across the polished, bulk GaAs target during implantation. Doses are typically 5×10^{14} protons/cm² and slices of bulk GaAs as large as several centimeters on a side can be implanted. To minimize channeling effects, the GaAs target should be slightly misaligned from the axis of the beam.

The proton damage which compensates free carriers also introduces optical losses. In practice, it is possible to eliminate sufficient optical loss while maintaining sufficient compensation. Implantation damage can be removed by annealing, i.e., heating in flowing gas (typically H₂ or N). The anneal temperature and time are variables that allow partial removal of damage sufficient to reduce optical loss while not destroying the guiding property. It has been found in GaAs that excellent waveguides can be fabricated with optical losses less than 10 db/cm using 300 keV protons [6.10]. Without proper annealing the optical loss is unacceptably high, but it decreases dramatically by over two orders of magnitude in decibels with increasing anneal temperature. The lowest losses reported occur for 30 min anneals at 500 °C of *n*-type substrates with 2×10^{18} carriers/cm³ implanted with a dose of 3×10^{14} protons/cm².

As the substrate carrier concentration is reduced, a smaller implantation dose is required and consequently a smaller optical loss results for the same anneal conditions. The smaller substrate concentration reduces the refractive index discontinuity, however, which results in a longer tail of the light distribution in the substrate. This can be seen in Fig. 6.2, where intensity scans of the guided light distribution are shown for different substrate conductivity. The tail of the guided light distribution travelling in the substrate is subject to free-carrier losses. As the fraction of light travelling outside the guide increases, this free carrier loss becomes increasingly important. This means that the optical loss cannot be reduced indefinitely by reducing the implantation dose or by increasing the anneal. The optimum dose, anneal and substrate carrier concentration are a compromise between damage loss and free-carrier loss, and appear to give loss at 1.15 μm of about 4 db/cm, but more experiments may determine even lower losses.

From (6.3) it can be determined that 300 keV protons, with a range of 3 μm, should require a substrate carrier concentration of at least $6 \times 10^{17}/\text{cm}^3$ for guiding to be achieved. This does, in fact, correspond to the observed waveguide cutoff, which indicates that the plasma contribution to the refractive-index change predominates over damage-induced effects.

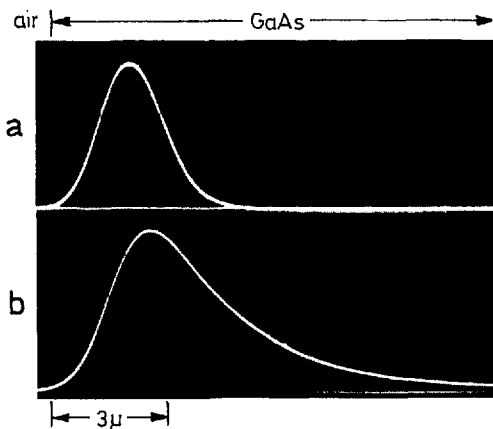


Fig. 6.2a and b. Proton-implanted GaAs mode intensity profiles [6.10], as monitored on the oscilloscope of the image-scanning system shown in Fig. 6.5. Substrate electron free-carrier concentrations are a) $6 \times 10^{18}/\text{cm}^3$, and b) $2 \times 10^{18}/\text{cm}^3$

When the number of free carriers in the implanted layer is very much less than those in the substrate, the exact profile of the damage is not important. However, as annealing increases and optical loss decreases, the nature of the implantation damage becomes important. The protons tend to travel rapidly through GaAs without causing much damage until near the end of their range. This means that annealing eliminates the weak compensation near the surface before removing the excess damage near the end of the range. This has implications not only on the guiding properties, tending to result in submerged guides, but has strong effects on the electrical properties of the guides. Unannealed implanted layers make poor Schottky barriers with large amounts of leakage current. As annealing progresses, the quality of the Schottky barriers increases, but the carrier concentration near the surface becomes so high that the field no longer extends into the submerged guiding region. As a result, active components have not yet been fabricated in ion-implanted GaAs guides. The solution to this difficulty is to successively implant GaAs with several proton energies, which have different penetration depths, so that the damage profile is essentially uniform. If this is done, active functions (such as modulation) should succeed in GaAs proton-implanted guides.

Ion-implanted GaAs guides have the same disadvantages as other guides formed by elimination of free carriers, i.e., the inability to separate guiding and electrical properties, as well as residual free-carrier

loss. In addition, they have substantial implantation loss. However, implantation has several decided advantages: implanted guides are very easy to make if an ion-implantation machine is available, large areas can be implanted at the same time with very uniform properties, and, conversely, localized areas can be implanted through masks. Also, excellent channel guides can be easily made. It is probable that ion implantation will be useful for producing waveguides in specific parts of an integrated optical circuit, just as implantation has been useful for specific parts of integrated electronic circuits.

Ion implantation produces waveguides in fused quartz [6.11]. In this case, the increased refractive index is due to atomic displacement rather than to electrical compensation. Refractive index changes are somewhat higher than in GaAs and optical losses are very much lower, but no work has been done on crystalline material [6.12].

6.1.2. Waveguides Due to Material Composition

A larger refractive index change is available by varying material composition. It is well known, for example, that the refractive index of glasses depends on their material composition. In general, any two materials with different chemical compositions will have different refractive indices. If transparent material of higher refractive index can be fabricated as a good quality film over a different material of lower refractive index as substrate, an optical waveguide can be the result. The first planar optical guides which utilized different material composition were liquid-quartz sandwiches [6.11] and epoxy-glass sandwiches [6.13].

The ability to have a good optical quality thin layer upon a substrate of different material composition is the first requirement for guiding. With amorphous materials, thin layers are made easily and extensive variation is possible as to composition and refractive index. As discussed in Chapter 5, many amorphous materials have been made into optical waveguides by varying material composition using methods such as sputtering [6.14], vapor deposition [6.15], solution deposition [6.16], oxidation [6.17], ion bombardment [6.11], and ion exchange [6.18]. The materials used include photoresist, polymers, gelatins, amorphous layers of crystals, liquids, glasses. The advantage of amorphous material is that there is no necessity of matching lattice constants between the guiding layer and substrate. The only requirement is that the amorphous film have good optical properties.

Although it is relatively easy to make good quality amorphous films (note how many varieties there are), it is difficult to perform active

functions in them. Optically pumped thin-film dye lasers have been made by using liquid guides [6.19], but electrical excitation is not possible. Nd doped glass thin-film waveguides have also shown light amplification, but again with optical pumping [6.20]. The only amorphous modulators which have been made are in a liquid film [6.21] or have used slower acousto-optic interactions [6.22].

$\text{Ga}_{1-x}\text{Al}_x\text{As}$ Ternary System Waveguides

In general, versatility in the ability to make active circuit elements requires crystalline films rather than amorphous films. Large electro-optic, magneto-optic or acousto-optic coefficients, good electrical properties, laser action, all are needed to make active circuit elements, and these properties generally come from crystalline films. Good crystal growth requires close lattice match. This is a severe requirement and only special systems are successful. Fortunately GaAs has a close lattice match to AlAs. In the ternary system $\text{Ga}_{1-x}\text{Al}_x\text{As}$, the AlAs concentration can be changed at will, thus changing the refractive index without substantially altering the lattice constant. Hence good quality epitaxial layers of $\text{Ga}_{1-x}\text{Al}_x\text{As}$ can be grown to make optical waveguides. This system was the basis of the first crystalline waveguides, which were used in heterostructure lasers [6.23]. $\text{Ga}_{1-x}\text{Al}_x\text{As}$ has a refractive index at $1.15 \mu\text{m}$ which is less than that of GaAs by an amount [6.24]

$$\Delta n = -0.4x. \quad (6.4)$$

Keeping this in mind, it is possible to design waveguides of the desired properties on GaAs substrates by varying the parameter x .

A dielectric waveguide requires a layer of increased refractive index, and the inclusion of AlAs decreases the refractive index. Hence a waveguide can be obtained by means of a layer of GaAs grown on top of a layer of $\text{Ga}_{1-x}\text{Al}_x\text{As}$, which acts as an isolation layer, for separating the guide from the GaAs substrate. This configuration is shown in Fig. 6.3a. Since the dielectric discontinuity for the GaAs guide is determined by the AlAs concentration in the isolation layer, the wave-guiding condition (6.2) can be expressed as a function of x using (6.4). For the propagation of only one mode in a layer of GaAs of thickness h bounded by air on one side and $\text{Ga}_{1-x}\text{Al}_x\text{As}$ on the other,

$$0.022\left(\frac{\lambda_0}{h}\right)^2 < x < 0.07\left(\frac{\lambda_0}{h}\right)^2. \quad (6.5)$$

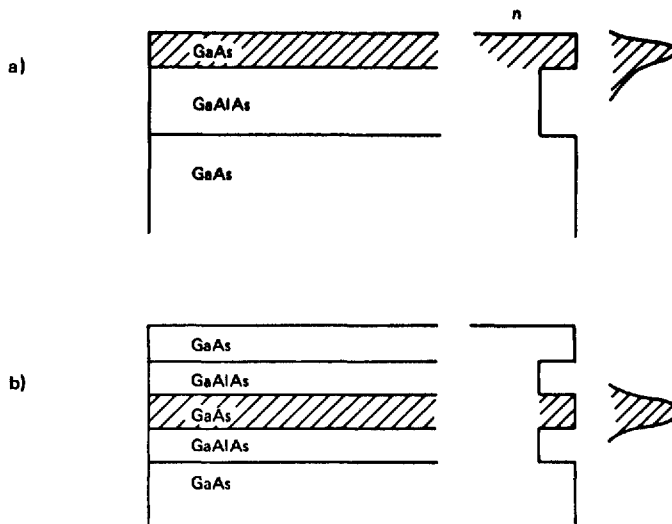


Fig. 6.3a and b. GaAs-Ga_{1-x}Al_xAs waveguiding structures, refractive index profiles n , and sketches of guided light intensity. The shaded GaAs layer forms the light guide in a) air-covered structure, and b) double heterostructure

For 1 μm light propagating in a 3 μm layer, $0.0025 < x < 0.007$; this is a very small amount of aluminum, which is hard to control during growth. Larger amounts of aluminum result in guides which are usually multimode. On the other hand, a 1 μm guide requires $0.02 < x < 0.07$, a range which can be grown. Guides of width 3 μm will typically be multimode unless the Al concentration is very small, while guides of width smaller than 1 μm can be made single mode. This should be compared with the waveguides due to free carriers which have a smaller refractive index change and are generally single mode.

Any guided light that penetrates the isolation layer into the substrate radiates away as a loss. It is important to show that this loss can be made negligibly small for reasonable thicknesses of the isolation layer. The coupling of light from the guide into the substrate through the isolation layer may be calculated by the overlap of the guided mode intensity in the substrate with the radiation field there [6.25]. This results in an exponential loss coefficient α for guided light of wavelength λ_0 which is given by

$$\alpha \sim \frac{\lambda_0^3 H P^2 \sin^2(H h_t) \exp(-2Ph_i)}{\pi^3 n_s \Delta n^2 h_t}, \quad (6.6)$$

where h_f is the guiding film width, h_i is the thickness of the isolation layer, and H and P are the transverse propagation constants (wave-numbers) inside and below the guiding layer, respectively [6.26]. The propagation constants are determined by solving for the light distribution in the guide, as shown in Chapter 2. As a numerical example, a single-mode guide 1 μm thick with $x=0.05$ requires an isolation layer thicker than 4.3 μm in order to reduce this leakage loss to less than 4 db/cm. When thicker guides or larger dielectric discontinuities are used, thinner isolation layers suffice.

Since free carriers are not required for optical waveguiding in this structure, the optical loss due to free carriers can be eliminated by using pure material with few free carriers. The remaining source of loss is the edge roughness of the epitaxial layers. This is known to be a problem since liquid phase epitaxy of GaAlAs does not usually produce perfect layers. Material and interface perturbations introduce sources of loss. The effect of epitaxial layer imperfections on optical loss has not been studied in depth, but indications are that this is the factor that limits losses in these guides to values greater than 7 db/cm at the present time [6.54]. Advances in the art of liquid phase epitaxy should reduce the losses of these guides considerably.

The two-layer structure we have described here (shown in Fig. 6.3a) is simple, versatile, and very useful for semiconducting optical waveguides. The guiding properties do not rely on free carriers, and suitable electrical doping can be chosen for active elements without destroying the guiding. This structure shows much potential for use in integrated-optics systems.

The double heterostructure shown in Fig. 6.3b provides a useful buried guide. In this case, the GaAs guiding layer is covered above as well as below with GaAlAs, resulting in a symmetric guide, as opposed to the unsymmetric air-covered GaAs guides discussed above. As shown in Chapter 2, the symmetric guide has no waveguide cutoff condition for the lowest mode. The higher-order antisymmetric modes, however, obey (6.5) where h now represents half the symmetric guide thickness. To avoid higher-order modes when $x \sim 0.3$, the symmetric guide thickness must be less than 1/2 wavelength. On the other hand, if the guide becomes too thin, much of the light travels outside the guide. In practice, the guide thickness should be $> 0.2\lambda$.

The guiding properties of these layers have been studied by looking at the mode profiles of laser light generated by double heterostructures, as well as by transmitting light through them [6.27]. These studies indicate that the dielectric waveguide can be qualitatively described as nearly symmetric, with abrupt dielectric steps. The constant dielectric profile is perturbed by gradients that are most likely due to slight Al

concentration gradients arising from the solution growth. As with the two-layer structure described above, waveguide losses at the present time are due to imperfections in liquid phase epitaxy. The double heterostructure of GaAs-GaAlAs is common, versatile, and has been put to use not only for lasers, but also for waveguides and modulators. These structures show much promise for integrated optics.

We have shown that, in order to obtain single-mode guiding, layers of GaAs must be very thin, or else the AlAs concentration in the isolation layer must be very small. Very thin guides ($\sim 0.3 \mu\text{m}$) have the advantage of requiring small modulation powers and of concentrating light energy for lasers. These will be useful for monolithic integrated-optics circuits. Coupling into such thin guides from external circuits is difficult, however, and there are occasions when thicker guides are desirable. It is difficult to grow an isolation layer with refractive index sufficiently close to that of GaAs to make single-mode guides thicker than $1 \mu\text{m}$. It is possible, however, to produce aluminum gradients in a single $\text{Ga}_{1-x}\text{Al}_x\text{As}$ layer, in a fashion which results in a single-mode optical waveguide several micrometers thick.

It is a property of the liquid phase epitaxial growth of $\text{Ga}_{1-x}\text{Al}_x\text{As}$ that, as the growth proceeds, the value of x decreases. This will be discussed in more detail in Section 6.7. The decrease in x occurs because aluminum has a high segregation coefficient, and grows out rapidly from the melt into the crystal. When a small melt volume is used, or when growth is rapid, the concentration of aluminum is easily depleted. Thus, the top portion of the crystal layer, which is grown last, has a smaller AlAs concentration and a higher refractive index than the region right below it. This satisfies the condition for confinement of light that a layer of higher refractive index be supported by a region of lower refractive index. In Fig. 6.4 is sketched the light intensity I guided near

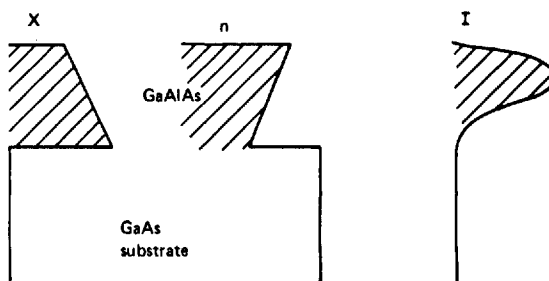


Fig. 6.4. AlAs gradient x , refractive index n , and guided light profile I for single-layer graded $\text{Ga}_{1-x}\text{Al}_x\text{As}$ guides

the surface by the increased refractive index produced by a gradient in x . Large AlAs gradients have been grown by a special wiping technique in liquid phase epitaxy, and single-mode low-loss waveguides 3 μm wide have been obtained [6.26]. This technique is very helpful for the fabrication of single-mode guides several wavelengths thick.

A single uniform layer of $\text{Ga}_{1-x}\text{Al}_x\text{As}$ grown on a GaAs substrate can form a leaky guide, which is comprised of a layer of smaller refractive index on a larger refractive index substrate. In this case, the strong grazing incidence reflection of guided light at the higher refractive index boundary partially confines the light. The weak component which refracts into the substrate upon each reflection results in lossy propagation. The exponential loss coefficient α is calculated by the overlap of guided modes with substrate modes and is given by [6.26]

$$\alpha = \frac{\lambda_0^2}{8\sqrt{n_s^3 \Delta n} h^3}. \quad (6.7)$$

When $h = 10 \mu\text{m}$, and $x = 0.4$, $\alpha \sim 1 \text{ cm}^{-1}$ (a loss of 4 db/cm) which is sufficiently small to make the guide useful. Leaky guiding has been observed in $\text{Ga}_{0.4}\text{Al}_{0.6}\text{As}$ layers with thicknesses varying from 4 to 15 μm , and good agreement with (6.7) was obtained [6.26]. This means that thick single layers of GaAlAs on GaAs can form useful guides. However, the losses increase dramatically as the guides become thinner. The possible guiding of thick refractive index layers must be taken into account when interpreting layered-structure waveguide results. For most applications, thinner guiding layers utilizing aluminum gradients are more useful.

Other Semiconducting Waveguides

The III-V semiconductors are the most promising crystal family for monolithic integrated optics because of their large electro-optic effect, good electrical properties for modulators and contacts, detectors and lasers. We have already examined waveguiding in GaAlAs ternary structures which have a good lattice match to GaAs. If we look more generally at the III-V compounds we can find other systems which may have promise.

Table 6.1 lists III-V compounds of interest, their approximate refractive indices, lattice constants, and band-gaps. From this information, we can see that InAs and GaSb have larger refractive indices than GaAs, so that single layers of $\text{Ga}_{1-x}\text{In}_x\text{As}$ or $\text{GaAs}_{1-x}\text{Sb}_x$ grown on GaAs substrates might be expected to guide light. However, the transmission is farther from the visible than is obtainable with GaAs. Further-

Table 6.1. Refractive index n at 1 μm wavelength, lattice constant, and bandgap wavelength λ for III-V compounds [6.27]

III-V compound	$n(\lambda \sim 1 \mu\text{m})$	lattice constant [\AA]	$\lambda(\text{band-gap}) [\mu\text{m}]$
GaAs	3.3	5.64	0.87
AlAs	2.9	5.66	0.58
GaP	3.0	5.45	0.45
InP	3.1	5.87	0.92
InAs	3.5 ^a	6.06	3.4
GaSb	3.8 ^a	6.09	1.77

^a These approximate refractive indices refer to wavelengths in the transparent region of the crystal, not close to the band-gap.

more, it must be noted that the lattice constants of these compounds are far from that of GaAs, so that crystal quality of grown layers is expected to be poor. However, it has been demonstrated that by grading the InAs concentration in a $\text{Ga}_{1-x}\text{In}_x\text{As}$ layer, by increasing x as the layer is grown, the strain may be reduced sufficiently for waveguiding layers to result [6.28].

The other III-V compounds have smaller refractive indices than GaAs and can be used as isolation layers, in a fashion similar to $\text{Ga}_{1-x}\text{Al}_x\text{As}$. From Table 6.1, we see that the lattice of AlAs is closest to GaAs, making it indeed the most favorable material for ternary waveguiding structures.

By using quaternary layers, it should be possible to tailor lattice match and refractive index somewhat independently so as to obtain useful strain-free, good quality films for optical waveguides [6.29]. The slight discrepancy between AlAs and GaAs lattice constants introduces strain into the thin layers of double heterostructure layers, but the strain can be reduced by the addition of a small fraction of GaP. GaP can also be used in $\text{Ga}_{1-x}\text{In}_x\text{As}$ layers to bring the lattice constant into a better match with GaAs as well as to bring the band-gap closer to the visible. At the present time, research in III-V compounds for optical waveguides has been centered around GaAlAs as the simplest system and one in which considerable technology has already been developed for heterostructure lasers. This material is most commonly grown by liquid phase epitaxy [6.30], although recently molecular beam epitaxy has been introduced [6.31].

In addition to III-V semiconductors, II-VI compounds have been used to make waveguiding components. Poor electrical properties make

this material less attractive than III-V compounds, but each of the optical functions required for integrated optics can be fabricated in II-VI semiconductors. The existence of a sizeable electro-optic effect, laser action, and photoconductivity in II-VI compounds makes them possible candidates for integrated-optics crystals. So far, only the injection laser has not been made in II-VI crystals.

Of II-VI compounds, ZnO and ZnS were first sputtered on glass to make amorphous guides composed of small crystallites [6.14]. Partially oriented crystallites have some average nonlinear and electro-optic properties that should make them useful for some applications [6.33]. However, with epitaxial methods, good quality single crystal ZnO has been grown on sapphire [6.34]. Using the method of close-spaced chemical vapor transport, the heated Al_2O_3 substrate is suspended close to a heated ZnO powder source in a flow of hydrogen gas. The growth rate depends on the temperatures chosen, typically 750–850 °C for the substrate and 50° hotter for the source. Growth rates of between 0.25 and 1.3 $\mu\text{m}/\text{min}$ were reported with the *c* axis of hexagonal ZnO grown on (01 $\bar{1}$ 2)-oriented Al_2O_3 lying in the plane of the film. The samples were subsequently polished with chromium oxide before use as waveguides. Depending on the application, the films can be made *n*-type semiconducting or resistive. The large refractive index difference between ZnO and Al_2O_3 (about 0.3) allowed six 6328 Å modes to propagate in a film 1 μm thick. The inability to vary the refractive index discontinuity is a disadvantage of this system. However, ZnO is electro-optic, can be doped to be an excellent photiconductor, is transparent from 0.4 to 2 μm and also has a large nonlinear polarizability. These properties, as well as the ability to make large films with low losses (<1 dB/cm), make this a promising film for active integrated optics.

The semiconducting II-VI compounds have been made into waveguides by diffusion of a higher refractive index II-VI species into bulk substrates. Low-loss guides have been made by diffusing Se into CdS [6.35], Cd into ZnSe, Cd into ZnS and Se into ZnS [6.36]. These guides are transparent to red light and can be studied with 6328 Å laser light. The guides that were reported were multimode and rather lossy, but further control of the diffusion process should eliminate these problems. The II-VI semiconductors show no fundamental barriers to the development of waveguiding optical components, although their poorly controlled electrical properties put them at a decided disadvantage to III-V semiconductors.

Germanium and silicon are not of great interest for monolithic integrated optics because of their lack of electro-optic effect and laser action, as well as because their transmission is farther into the infrared.

Optical waveguiding has been observed in both, however, and they may prove useful for integrated-optics detectors. Guiding has been observed in a high resistance Si layer grown on a low resistivity Si substrate [6.37] at 3.39 μm , and in an amorphous Ge film sputtered on IRTRAN [6.38] at 10 μm .

Insulating Crystal Waveguides

Research is proceeding rapidly to find crystal systems other than semiconductors in which integrated-optics circuits can be built. These will, of necessity, lack injection laser and detector capability and the possibility of monolithic integrated optics. However, they may involve large electro-optic or magneto-optic effects, which are applicable to the design of modulators.

LiNbO_3 is one of the best modulator materials, and forms excellent mixed crystals with LiTaO_3 , which has a smaller refractive index. A simple diffusion technique has recently been developed [6.79] to fabricate guides of $\text{LiNb}_{x}\text{Ta}_{1-x}\text{O}_3$ on LiTaO_3 substrates. Metallic Nb, evaporated onto polished LiTaO_3 , diffuses into the substrate at 1100°C a distance which is typically about 1 μm , producing a layer with a 1% increase in refractive index. These excellent single-mode guides have optical losses as low as 1 dB/cm and can be used for efficient modulation. This technique is simple and shows much promise for useful integrated-optics components.

An epitaxial-growth-by-melting technique has been used to fabricate guides of LiNbO_3 on LiTaO_3 [6.39]. This method relies on the fact that the melting temperature of LiTaO_3 is higher by about 300°C than that of LiNbO_3 . The epitaxial layer was grown from a powder at a temperature of 1250°C, melted and then cooled at a rate of about 20°C/h. Waveguiding layers have also been made from LiNbO_3 and LiTaO_3 by thermal out-diffusion of Li, leaving a non-stoichiometric form with a slightly higher refractive index [6.40]. The crystal is held in vacuum at 1100°C for over 20 h. The resultant Li-depleted guiding layers are about 500 μm thick and highly multimode, but they have very low losses and have been made into a modulator.

Another electro-optic crystal system, which has been grown epitaxially, from water solution, is ADP-KDP mixed crystal, $(\text{NH}_4)_x\text{K}_{1-x}\text{H}_2\text{PO}_4$ on KDP, although in an orientation not suitable for modulation [6.41].

More recently, the sillenites have been developed as piezoelectric crystals which show promise for integrated optics crystals [6.42]. Bismuth germanate ($\text{Bi}_{12}\text{GeO}_{20}$) forms the substrate on which bismuth gallate (12 Bi_2O_3 : 1 Ga_2O_3) and bismuth titanate (6 Be_2O_3 : 1 TiO_2) are

grown. As in epitaxial growth of LiNbO_3 , the melting point of the epitaxial layers is lower than that of the substrate. In this case, however, epitaxial growth occurred in the liquid phase via dipping directly into melts of the desired film composition. Films less than two micrometers thick were grown which supported only two or three waveguide modes. The films are transparent in the visible and near-infrared and are of good optical quality.

The large magneto-optic effect in iron-garnets has led to their epitaxial growth for waveguide modulators. The garnets have a general formula $R_3B_5O_{12}$, where R can be Y, La, Bi, trivalent rare earth ions, or some mixture of these ions, and B can be either Fe, Ga, Al or some mixture of these trivalent cations. The lattice constant can be varied continuously by mixing rare-earth ions, so that perfect lattice match between film and substrate can be obtained. As an example, $\text{Eu}_3\text{Ga}_5\text{O}_{12}$ was grown on $\text{Gd}_3\text{Sc}_2\text{Al}_3\text{O}_{12}$ in a film $2.4 \mu\text{m}$ thick, forming a wave-guiding layer transparent in the visible [6.43]. The dipping method of liquid phase epitaxy was used. For magneto-optic modulation, $\text{Y}_3\text{Fe}_{4.3}\text{Sc}_{0.7}\text{O}_{12}$ films were grown on $\text{Gd}_3\text{Ga}_5\text{O}_{12}$ (111) substrates. Although these guides make excellent modulators, they are transparent only at wavelengths longer than $1 \mu\text{m}$. For optical communications applications in which the wavelength used is expected to be near the GaAs laser emission at 8800\AA , these films may have limited use.

In electro-optic materials, waveguides can be formed in a bulk crystal by the increased refractive index due to an applied electric field, as was proposed [6.44] in GaAs and observed [6.45] in LiNbO_3 . However, the refractive index change induced by the electric field is small, and only relatively thick layers will guide light. This effect will be discussed further in Section 6.3.

6.1.3. Observation of Waveguiding

This completes our discussion of the ways to make optical waveguides in crystals. Let us now consider the observation of light guiding. In GaAs the most convenient method to couple the light into the guide is directly into a cleaved end by focusing with a microscope objective. The experimental setup is diagrammed in Fig. 6.5. Light from a $1.15 \mu\text{m}$ He-Ne laser is coupled into and out of cleaved parallel faces with microscope objectives. The exit face near-field image is projected onto an image converter or scanned past a detector in order to display an intensity profile in real time on an oscilloscope. Waveguide losses are determined by measuring the power out versus power in as a function of waveguide length. This also determines the coupling efficiency, which

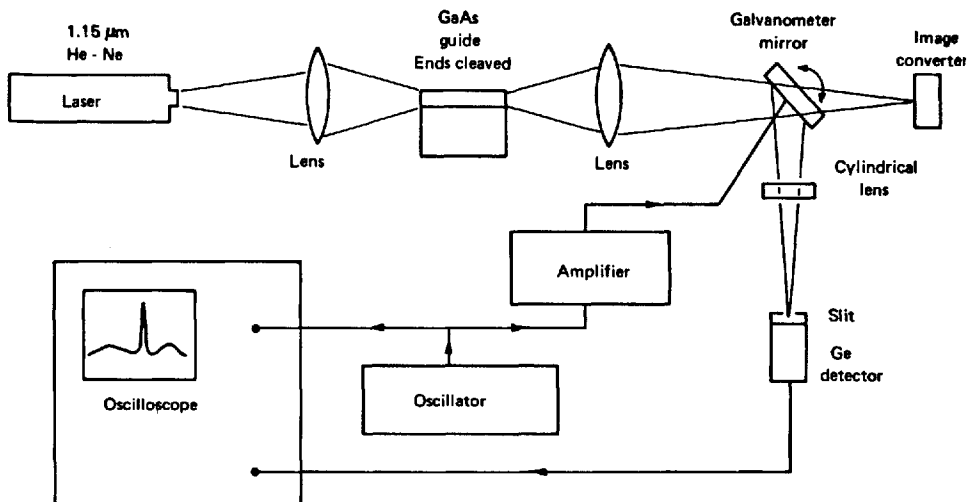


Fig. 6.5. Experimental apparatus for the observation of optical waveguiding [6.10]. Galvanometer mirror image-scanning apparatus may be removed to view the waveguide exit face on an image converter

depends on the *f* number of the input light and on the waveguide thickness. Direct endfire coupling requires crystals which cleave well, or can be easily polished at a corner, and it excites continuum modes as well as guided modes, which can complicate the interpretation of results. On the other hand, this coupling can be used for submerged guides and channel guides, and its alignment is as quick as that of prism couplers (see Subsect. 3.2.2).

The techniques for studying guiding in passive structures discussed in Chapter 5 are not suitable for GaAs waveguides. Prism couplers cannot be used since they must be of a higher refractive index than the guide, and there are no materials, which are transparent at $1 \mu\text{m}$, that have a higher index of refraction than GaAs. Loss measurement by visual observation of the scattered light is not possible since the guides are transparent only in the infrared.

Two other methods of coupling light into a waveguide are the grating and the tapered film. Grating couplers have been made for $10.6 \mu\text{m}$ light in GaAs [6.5] but not in the near infrared. Tapered film coupling should be effective if appropriate tapers can be fabricated, but these techniques have not yet been developed in GaAs. Cleaving and end-fire coupling remain the simplest and easiest techniques for studying the waveguiding properties of GaAs and related crystals.

With the development of planar guides and techniques for studying them, it is time to turn our attention to three-dimensional channel waveguides needed for circuitry applications.

6.2. Three-Dimensional Channel (Strip) Waveguides and Couplers

After having discussed methods for the fabrication of planar waveguides, we need to develop techniques for making three-dimensional channel (or strip) guides. In such guides the light is confined in two dimensions, which facilitates the fabrication of separate optical circuits, and the coupling of energy from one circuit to another. Waveguide channels can be made either ridged (lying on top of the substrate), or imbedded in the substrate, or by strip-loading planar guides. The three types, shown in Fig. 6.6, will be discussed in this section, along with

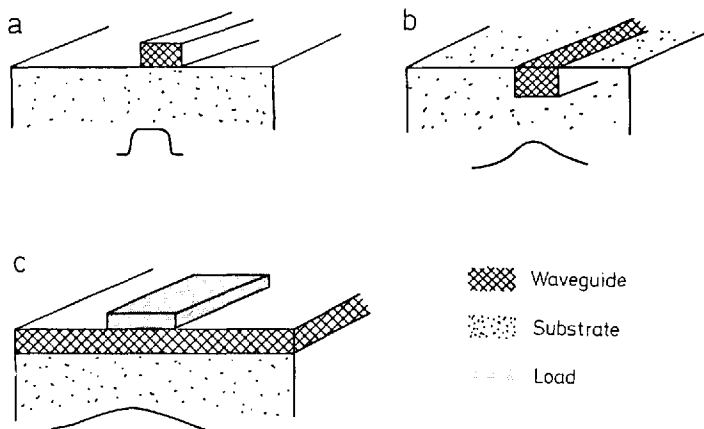


Fig. 6.6a-c. Diagrams of channel guide configurations with accompanying light distributions, including a) Ridged channel (strip) guide, b) imbedded channel guide and c) strip-loaded planar guide

their characteristics and fabrication techniques. GaAs will be emphasized for the reasons discussed in Section 6.1. Finally, coupling between adjacent channel guides will be considered.

6.2.1. Channel Waveguides

The transverse mode profile of guided light depends on the type of channel, as shown schematically in Fig. 6.6. The ridged guide (Fig. 6.6a) has air on either side of the waveguide channel, which results in highly multimode guided light propagation because of the large dielectric discontinuity in the transverse direction. The guided light profile typically fills the channel and has no field penetration into the air. By contrast, the strip-loaded guide (Fig. 6.6c) typically supports only one mode and the tail of the light distribution outside the guide can be large or small, depending on the amount of the loading. The imbedded guide has properties between those of the ridged and strip-loaded guides and the number of propagating modes depends on the dielectric discontinuity between the channel guide and the imbedding medium. The optimum channel structure for a given application will depend on the light intensity profile required by the circuit design. Single-mode strip-loaded or imbedded guides with long tails to the light distribution will be used when coupling between channels is required, while multi-mode ridged or imbedded guides can ensure no cross-talk between channels.

Ridged Waveguides

Ridged guides are usually made by etching away unneeded material from planar guides by means of chemical, rf sputtering or ion-beam etch techniques. Ion-beam etch (micro-machining) is the most controllable method of removing superfluous sections of a planar epilayer, and was described in Chapter 5. Ridged channel guides have been fabricated in epitaxial films of high resistivity GaAs grown on low resistivity substrates by ion-beam micro-machining through a photoresist mask [6.46]. The surface of the photoresist is replicated in the epitaxial layer by the milling action of the ion-beam [6.47]. An example of smooth channels, which were fabricated by exposing the photoresist with a holographically prepared mask and ion polishing the sample after ion machining, is shown in Fig. 6.7. The edge deviations appear to be less than a few hundred Angstroms. By controlling the shape of the developed photoresist, and by orienting the ion beam at appropriate angles, the channel cross-sectional shape can be tailored.

Chemical etching is less controllable than ion machining or rf sputter etching, but is commonly used to make mesa stripe-geometry heterostructure lasers. By altering the crystal orientation and reaction rate, different mesa channel profiles can be obtained [6.48]. Figure 6.8 shows mesas etched by $3\text{H}_2\text{SO}_4:1\text{H}_2\text{O}_2:1\text{H}_2\text{O}$ through a photolithographically prepared aluminum mask. With the use of good masks and

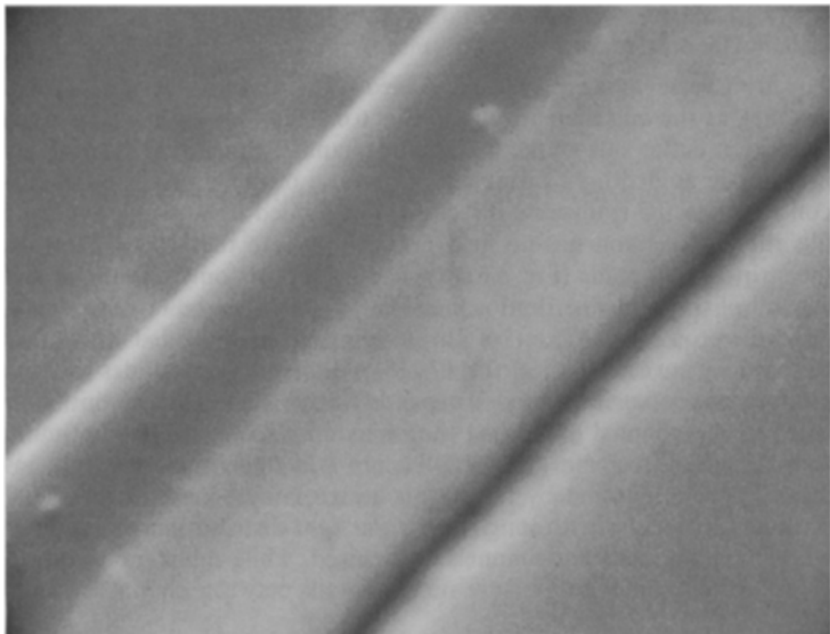


Fig. 6.7. SEM photograph of an ion-beam machined ridged channel in GaAs 1.4 μm high and 2.0 μm wide [6.47]

carefully controlled processing, useful ridged channel guides can be made by chemical etching.

The growth of ridged channels directly on substrate material by epitaxy through a mask is difficult, but useful for some purposes. The orientational dependence of the growth rate of GaAs limits the flexibility of this technique. However, with the control possible from vapor phase

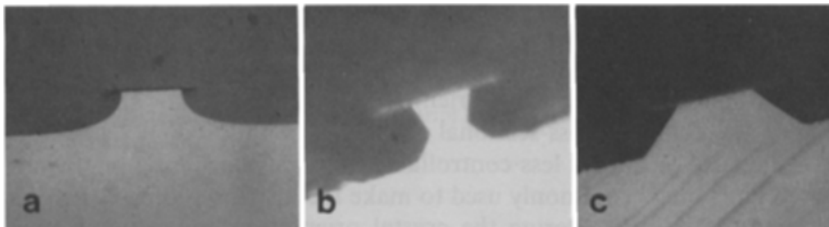


Fig. 6.8a-c. Typical chemically etched mesa profiles obtained on (100) GaAs [6.48] using diffusion-limited etch (a), and ratelimited etch for stripes oriented perpendicular to {011}; b) and {011} c)

epitaxy, excellent mesas have been grown through an oxide mask for use as ridged lasers [6.49].

Imbedded Guides

Imbedded channels can be made by filling in around a ridged channel with material similar to the substrate material. This has been done in GaAs by regrowth of $\text{Ga}_{1-x}\text{Al}_x\text{As}$ using molecular beam epitaxy [6.50]. A ridged guide 10 μm wide and 0.5 μm thick was chemically etched from a planar guide consisting of a GaAs layer separated from the GaAs substrate by a $\text{Ga}_{1-x}\text{Al}_x\text{As}$ isolation layer. The ridged guide was re-inserted into the molecular beam epitaxy machine to imbed it in $\text{Ga}_{1-x}\text{Al}_x\text{As}$, producing guides with losses as low as 4 dB/cm. Growing the imbedding layer by the simpler techniques of liquid phase epitaxy rather than by molecular beam epitaxy requires careful control of the growth process before good results can be achieved. Nevertheless, this is a promising method for the future and one impetus for improving liquid phase epitaxy techniques.

Molecular beam epitaxy has been used in a shadow masking technique to produce a lateral variation in aluminum concentration resulting in imbedded channel guides [6.51]. If the molecular beams of Al and GaAs are incident on the substrate from different angles, a wire mask can shadow only the Al beam, leaving a channel of GaAs imbedded in the $\text{Ga}_{1-x}\text{Al}_x\text{As}$ layer grown elsewhere. This simple, elegant technique is available only if a molecular beam epitaxy system is available.

Channel guides have been imbedded in GaAs by proton implantation through a gold mask [6.52]. As discussed in Subsection 6.1.1 under *Ion-Implanted Waveguides*, bombardment compensates the free carriers and thus increases the refractive index to form a light guide. The same implantation and anneal conditions used for planar guides are required for the channel guides; also, the guide depth remains the same, i. e., 3 μm for 300 keV protons. A negative gold mask 2 μm thick keeps the protons from penetrating the GaAs outside the guide areas. The high resolution gold mask can be fabricated directly on the GaAs by ion-beam machining through a photographically prepared negative photoresist mask. The stochastic process of ion bombardment with 10^{14} protons/ cm^2 and the subsequent annealing help to smooth out any defects in the gold mask. The resulting channels have the same loss as planar guides (~ 7 dB/cm) and good uniformity of propagation velocities. These guides have been used to make excellent directional couplers.

A final technique for fabrication of imbedded guides is diffusion through a mask, which may introduce compensating ions or a higher index material. The latter has been demonstrated in II-VI compounds

[6.35, 36] by diffusing Cd into ZnSe through a SiO mask. Guides 10 μm wide by 3 μm deep have been fabricated with losses less than 3 dB/cm. No results on the diffusion of channel guides in GaAs have been reported to date, but diffusion is certainly another fabrication method which should be included in useful methods for channel guide fabrication in GaAs.

Strip-Loaded Waveguides

Strip-loaded guides (Fig. 6.6c) may have the loading strip made out of the same material as the guide (rib waveguides) or out of a different material (optical strip-line). A strip of different material placed over the guide loads the planar layer to confine light to the strip. Ridges of sputtered glass have been used to load planar higher-index glass guides [6.53]. Because of the high index of refraction of GaAs, the loading strip must have a high refractive index and should consist of GaAs or GaAlAs. Loading strips may be sputtered, grown, or etched from a planar layer. The latter has been done in GaAs using a high resistivity guide and a low resistivity substrate and loading strip [6.80]. A single-mode guide resulted from a strip 2 μm thick and 10 μm wide placed upon a 5 μm thick planar guide. The light travels inside the guide rather than in the loading strip, thereby diminishing fabrication smoothness tolerances.

Rib guides, in which the loading strip is the same material as the guide, can be made by the same techniques as ridged guides, if a bridge of planar guiding layer is left beside the channels. This has been done by ion beam etching in GaAs [6.46]. Because of the high refractive index of GaAs, the rib does not need to be very high in order to load the guide sufficiently to confine light to a strip. This has been demonstrated using anodization as a technique to remove thin layers of GaAs from the unprotected surface outside the strip [6.54]. The growth of the oxide layer during anodization consumes GaAs at a controlled rate which is dependent on the applied voltage (7.4 \AA/V). If a waveguide pattern is first generated in an oxidized surface, anodization of the exposed portions outside the strip etches down the surface and results in ribs 0.1 μm having a width of 10 μm or smaller and a thickness of about 1 μm . Unlike ridged guides, these rib guides have the advantage of single transverse mode propagation, and individual modes can be excited and propagated separately.

6.2.2. Directional Couplers

Once the techniques of fabricating channel guides are developed, optical circuits can be fabricated. Light can be sent around bends, from one

element to another in an optical circuit, or coupled from one circuit to another. The latter can be accomplished by coupling between two adjacent parallel guides, i. e., a directional coupler.

As discussed in Chapter 3, there is an interchange of light energy between the guides if two parallel guides have a small power leak between them. This leakage occurs when the waveguide mode profiles in adjacent channels overlap.

Cumulative energy exchange requires the light to propagate with nearly the same velocity in each channel. When the propagation vectors in two channels differ by a small amount Δk , and all the light is initially fed into one channel, the power flow down two channels obeys the following equations [6.46].

$$P_0(z) = \cos^2 sz + \left(\frac{\Delta k}{2}\right)^2 \frac{\sin^2 sz}{s^2}, \quad (6.8a)$$

$$P_1(z) = \frac{K^2}{s^2} \sin^2 sz, \quad (6.8b)$$

where

$$s^2 = K^2 + \left(\frac{\Delta k}{2}\right)^2. \quad (6.8c)$$

The coupling constant K controls the transfer of energy; its value depends on the overlap of the mode profiles, i. e., on the channel spacing, guide width and dielectric discontinuity. For well-confined modes

$$K = \frac{2k_x^2 q_x \exp(-q_x c)}{k_z b (q_x^2 + k_x^2)} \quad (6.9)$$

where b is the channel width, c is the separation between channels, k_x and k_z are the propagation constants along the x and z axes, respectively, and q_x is the exponential falloff in the x direction outside the guide. When the two parallel channels have the same phase velocity, $\Delta k=0$ and all the power switches from channel 0 to 1 in a distance given by $K L=(m+1/2)\pi$, $m=0, 1, 2, \dots$. This makes an optical directional coupler between circuits, whose length depends on the coupling coefficient, as is also discussed in Subsection 2.6.3.

Excellent two-channel optical directional couplers have been made in GaAs using adjacent proton-implanted channel guides [6.46]. The guides had cross-sections of $3 \mu\text{m} \times 3 \mu\text{m}$, an index discontinuity of about $\Delta n \sim 0.005$ and a separation of $3 \mu\text{m}$ between guides. The coupling is demonstrated in Fig. 6.9. In a) the power distribution halfway along a directional coupler is observed by scanning the output plane of a sample of length $L/2$. The coupling of half the light from the initial into

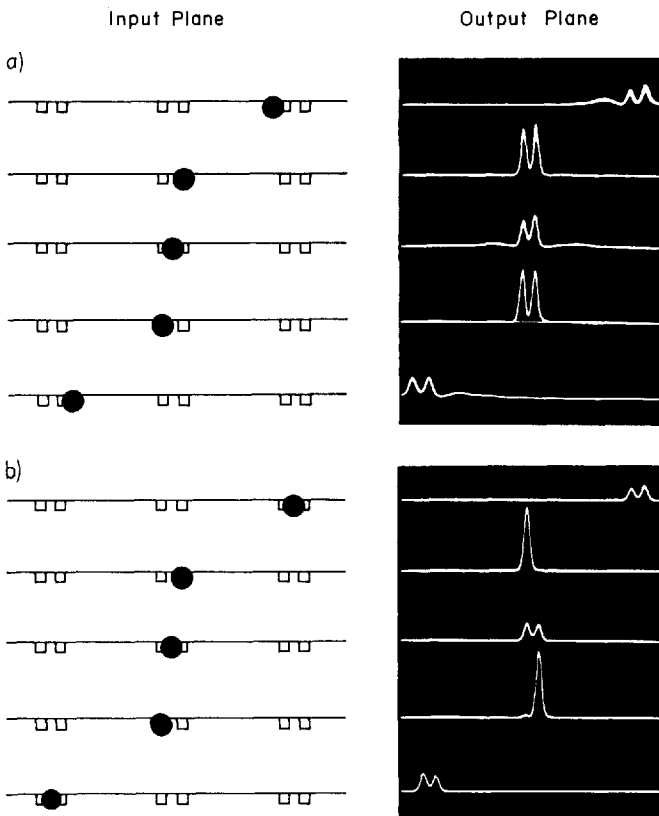


Fig. 6.9a and b. Three pairs of directional couplers on the same substrate. In the diagram of the input plane the black dot indicates the point at which the input light was focused [6.46]. The light intensity distribution at the corresponding output plane is demonstrated by a series of scans taken by the apparatus diagrammed in Fig. 6.5 for a) a sample 1 mm long, which is half the length of the directional coupler, demonstrating the division of light between the two channels and b) a sample 2.1 mm long, the full length of the directional coupler, demonstrating complete exchange of light power between the two channels

the adjacent channel can be seen in the second and fourth oscilloscope traces. In b) a full-length directional coupler causes complete coupling from the initial channel into the adjacent one, as also observed in the second and fourth oscilloscope traces. The observed 2 mm coupling length is consistent with (6.9), when known dielectric discontinuity and channel dimensions are included. The existence of complete coupling means that the two channels are synchronous and have the same phase velocity.

When more than two channels are adjacent, the light does not oscillate between only two of them, but spreads throughout the available channels. When an infinite number of channels are adjacent, the light field amplitude spreads out with a Bessel function distribution. When all the light enters the zeroth (central) channel, the field in the n th channel is given by [6.47]:

$$E_n(z) = (-i)^n J_n(2Kz) \exp(-\frac{1}{2} \alpha z). \quad (6.10)$$

Typical light distributions are shown in Fig. 6.10. The energy spreads out from the central channel into adjacent ones with the expected Bessel function distribution. The multichannel directional coupler is a useful device for determining quickly the coupling constant between adjacent channels, information which is necessary in order to determine the length needed for a two-channel directional coupler. Because of the

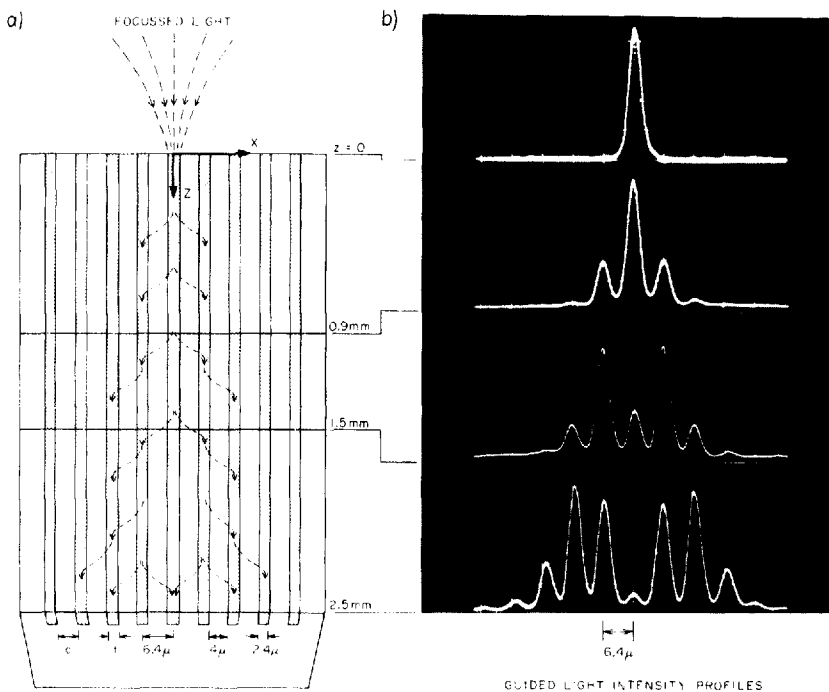


Fig. 6.10a and b. Multi-channel optical waveguide directional coupler [6.52] described by a) sketch showing the flow of light energy into adjacent channels and b) photographs of guided light intensity profiles for various lengths. The profiles have been displayed relative to the sketch at the proper value of z . The intensity scale is arbitrary

spread of light energy, the coupling constant can be determined in a single length, rather than in the two lengths required by two-channel devices. For example, each of the profiles in Fig. 6.10 correspond to $K = 0.52 \text{ mm}^{-1}$. From the coupling constant, important guide properties can be inferred. For example, the dielectric discontinuity can be determined if the guide dimensions are known.

When the propagation velocities are not identical, $\Delta k \neq 0$. In that case, the phase velocity synchronism of the fields is absent, and the effectiveness of the coupling is reduced. Some fraction of the total energy in a two-channel directional coupler oscillates between the two channels with the faster period s , given in (6.8c). While all the power is never transferred to the opposite channel, all the lights returns to the initial channel when $sL = \pi$. This suggests that an optical switch can be made if Δk can be changed. The value of Δk needed to entirely spoil synchronous coupling ($KL = \pi/2$) is given by $sL = \pi$ or $\Delta k L = \sqrt{3}\pi$. A light modulator based on the modulation of Δk in a directional coupler will be discussed in Section 6.4.

Imbedded channel directional couplers such as the proton-implanted couplers already discussed have large coupling coefficients because of the large overlap of modes. This is due to the small dielectric discontinuity between the channels and the intervening region. The same property is true of directional couplers made with strip-loaded channels. Ridged channels, however, have air between them and the dielectric discontinuity is so large that no significant coupling is possible. It is possible, however, to couple ridged channels by leaving a thin bridge of waveguiding material between the two channels, as sketched in Fig. 6.11. This leaves a path for light to leak through and increases the coupling constant. The resulting structure can be thought of as adjacent rib guides. Such a ridged directional coupler has been made by ion beam machining GaAs through a mask and the effectiveness of the bridge in coupling light between adjacent channels has been demonstrated [6.47].

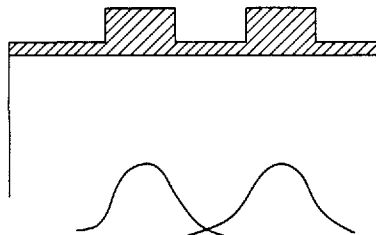


Fig. 6.11. Diagram of ridged directional coupler with coupling bridge between channels, along with a sketch of overlapping guided light intensity profiles

This completes our discussion of passive optical waveguides in crystalline materials. We turn our attention now to active circuit elements for monolithic integrated optics.

6.3. Lasers

An important step in the development of integrated optics is the fabrication of light sources which are miniature, convenient, cheap, rugged and compatible with planar optical circuits. For single-mode and single-frequency low-dispersion requirements, lasers are needed. GaAs-GaAlAs heterostructure lasers are the only sources that fulfill all these criteria. The room-temperature continuous lasers using this material make GaAs and its related III-V compounds of special interest for integrated optics. We shall describe briefly GaAs heterostructure lasers and techniques for integrating them into planar optical circuits; in particular, the use of feedback other than by cleaved facets will be discussed.

6.3.1. GaAs Heterostructure Lasers

One example of a room-temperature continuous laser is shown in Fig. 6.12. Laser action takes place in the GaAs layer at the *pn* junction. Under forward electrical bias, current is converted to light by the recombination of injected electrons with holes in the active region. The light is confined to the *p*-GaAs active region by the layers of $\text{Ga}_{0.7}\text{Al}_{0.3}\text{As}$ on either side, since their lower refractive index provides the dielectric discontinuity for an optical waveguide. The layers of GaAlAs reduce the laser threshold by confining both the injected carriers and the laser light to the active region. This heterostructure is required for room temperature continuous operation. The layer of *p*⁺-GaAs is grown for ohmic contact purposes, since GaAlAs makes poor ohmic contacts. It is the ability to grow good layers of GaAlAs by liquid phase epitaxy on GaAs and to alter the Al concentration at will that makes these materials so exceptionally favorable for room-temperature cw laser operation.

Stimulated laser light occurs in the injection region along the stripe contact. The light reflection necessary for laser action occurs from the cleaved end facets, utilizing the 30% reflection per face from the high dielectric discontinuity. The light fills the stripe 17 μm wide and 0.4 μm deep and is emitted out at the end face of the crystal with typical powers of 10–30 mW. The threshold current above which laser action takes place

is typically 6000 A/cm^2 , or a total current of 250 mA. The exact design of a room-temperature, double heterostructure laser is fairly critical, requiring low threshold and excellent heat sinking to reduce the thermal impedance. The laser is bonded with Sn, active side down to a copper or diamond heat sink.

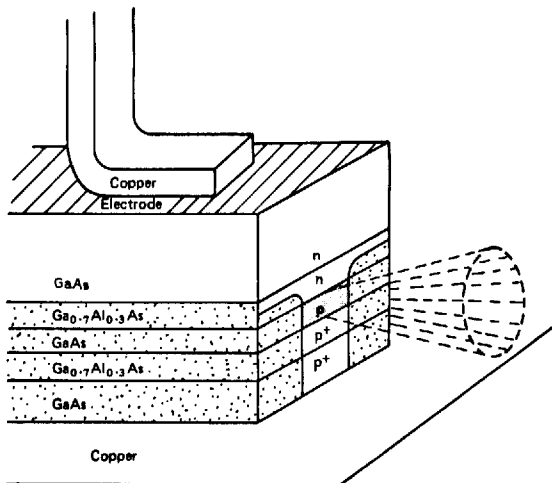


Fig. 6.12. Stripe geometry double heterostructure laser. Dotted areas have been proton bombarded to be resistive so that current flows only in the stripe region from whose active region (shaded area) light is emitted. Typical stripes are 17 μm wide, with an active region 0.4 μm thick. GaAs dice typically are 400 μm long and 100 μm thick and are mounted with the substrate up so that good thermal contact with the copper heat sink is available for the active layer

The double heterostructure lasers described here [6.55], which run continuously at room temperature, are small, convenient and processed in batches. As such, they are suitable as light sources that can be bonded directly to a fiber for optical communication systems. For integrated optics, however, these devices are not compatible with planar technology. Although the layers are grown on wafers by liquid phase epitaxy and ohmic contacts are applied by evaporation, a wafer is subsequently cleaved into bars 0.4 mm long and then sawn into dice 0.2 mm wide. The cleaving, which provides the flat parallel mirror surfaces for laser feedback, is not a planar process, and the miniature laser dice are not compatible with monolithic integrated-optics circuits.

6.3.2. Lasers Fabricated by Planar Technology

For monolithic integrated optics purposes, lasers must be compatible with planar technology. This means that laser feedback must be provided in a fashion other than by cleaving, which produces dice rather than planar structures. A mesa laser supported by a planar substrate, which is the same structure as the ridged channel guide, would suffice if the mesa walls can be made flat enough to provide good laser mirrors. Such a GaAs mesa laser has been grown by vapor phase epitaxy on planar substrates through oxide masks [6.49]. By selection of the (110) face for growth, and by using appropriate diamond shaped masks, GaAs mesas were grown with excellent vertical (111) faces. The mesas, about 16 μm high and 300 μm tip-to-tip in the longest dimension, are shown in Fig. 6.13. Crystal growth planes determine the diamond shape of the mesas grown through holes in the SiO_2 mask and shown in Fig. 6.13a. In Fig. 6.13b an electron micrograph of the grown mesa shows the high quality of the facet which enables it to be used as a laser mirror. Optically pumped laser action was observed in these mesa lasers operating at liquid nitrogen temperature. The excitation source was a doubled Nd:YAG laser operating at 0.532 μm . The longitudinal mode structure of the cavity formed by the parallel mesa faces 175 μm apart was observed. Zinc-diffused *pn* junctions have also been made in these mesas and the results are electrical injection lasers which have excellent mode spectra. These lasers are the first semiconductor lasers of any type to use as-grown crystalline facets for optical feedback. Coupling to the optical circuit is expected to be by evanescent wave coupling [6.56] into planar guides in the substrate. These lasers will be useful in an integrated-optics system based on GaAs-InGaAs, if the problems of poor lattice match in these materials can be overcome and heterostructures can be grown. Unfortunately, GaAlAs is not grown successfully by vapor phase epitaxy, and crystal growth of laser mirrors would require development of liquid phase epitaxial methods of facet growth through masks.

In addition to crystal growth, etch techniques such as those discussed in Section 6.2 for channel guides may be developed with sufficient control to produce laser mirrors. In particular, etch by ion-beam sputtering is a technique that allows control over edge angle and definition. Facets can be fabricated which should be good enough for laser action, as demonstrated by the smooth ridged channel in Fig. 6.7. Coupling from such a layer into optical circuits could involve an air gap to a neighboring ion-beam etched channel guide, or evanescent coupling into another layer. Chemical etches can cause different shaped mesas, as seen in

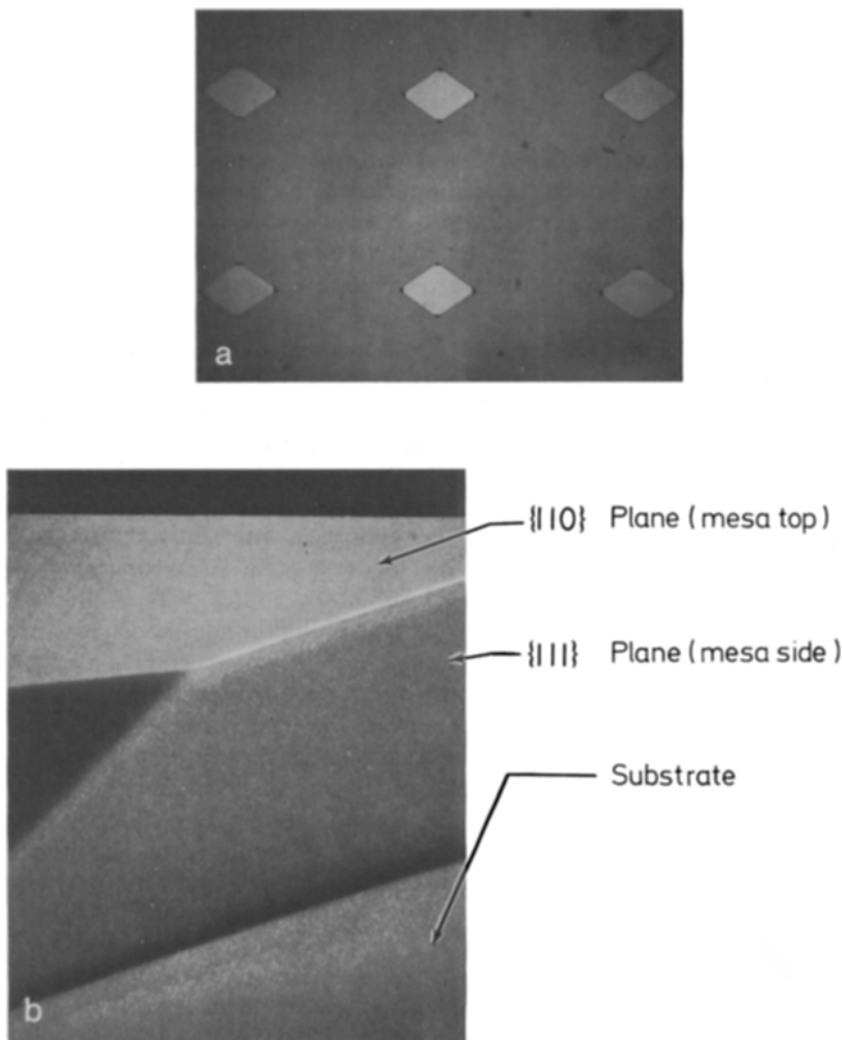


Fig. 6.13a and b. GaAs mesas grown by vapor-phase epitaxy for use as surface laser [6.49], including a) photograph from above of six diamond-shaped mesas which have been grown through a mask, 300 μm in the longest dimension and b) electron micrograph of grown facet of mesa to be used as laser mirror; height of mesa is 16 μm

Fig. 6.8, depending on etch characteristics. It is possible to consider plane mirrors fabricated by chemical etch, but this would require extremely accurate control.

6.3.3. Distributed Feedback Lasers

For use with GaAlAs and for versatility in integrated optics laser sources, it is necessary to develop planar-technology feedback other than mesa mirror facets for use with double heterostructure lasers. Such a mechanism is distributed feedback due to periodic perturbations in the laser or wave guide properties. The use of distributed feedback due to corrugation of the waveguide appears to show the most promise for versatile planar technology lasers.

Due to the stop-band effect produced by periodic structures, a corrugated guide reflects guided light if the corrugated grating has a period which is a multiple order of half the wavelength of light in the guide. Because the refractive index of GaAs is so large, (~ 3.6), the required corrugation spacing for reflection of laser light (77 K) at 8240 Å from a grating of fundamental order is 1150 Å. Such a fine grating spacing requires special fabrication techniques. The finest corrugations have been made by ion-beam etching through a grating mask of photoresist. The grating is developed in the photoresist after it has been holographically exposed by interfering two plane waves of laser light at the appropriate angle. If the two waves make equal angles θ with the normal to the photoresist surface, light of wavelength λ will interfere to produce a grating of spacing [6.57]

$$d = \lambda / (2 \sin \theta). \quad (6.11)$$

The smallest grating spacing that can be achieved holographically is half the wavelength of the exposing laser light (when the two beams are incident 180° apart). Using the 4880 Å line of the argon laser, the smallest grating that can be exposed on photoresist is 2440 Å. If a 3450 Å spacing is chosen, the grating may be used in third order to provide feedback for a GaAs laser at 8300 Å. The surface of the guiding layer of GaAs is spin-coated with photoresist (Shipley 1350). After careful exposure and development (in order to retain the grey scale), a grating remains in the photoresist. Because of the high refractive index of GaAs, the guided light is so well confined that it does not sense the presence of this grating and it is necessary to etch the grating into the surface of the GaAs.

Both ion-beam and chemical etch have been used to fabricate gratings in GaAs. To date, the ion beam has produced the finest corrugations in GaAs, 1000 Å deep, fabricated uniformly over areas of 1 cm² [5.58]. The ion beam replicates the shape of the photoresist into the GaAs guide, for any orientation of the crystal. To obtain a given groove shape, it is usual to obtain it first in photoresist. Variation

of exposure and development time allow a variation of groove shape. It is possible to blaze the grating, however, by using an ion beam incident from an angle. A typical grating on GaAs is shown in Fig. 6.14. Any residual surface damage due to the ion beam should be annealed away before optical pumping.

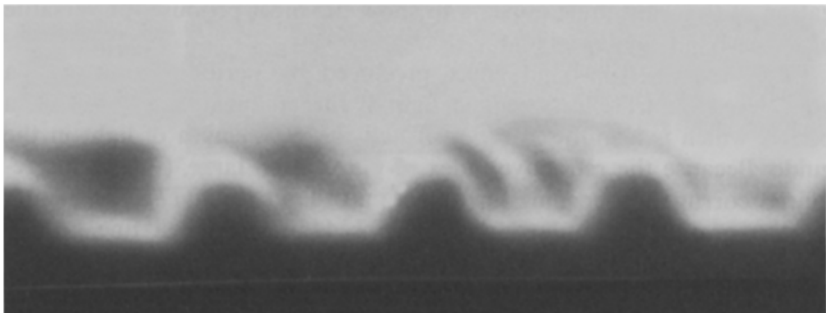


Fig. 6.14. Cross-section of grating pattern ($0.41 \mu\text{m}$ periodicity) in GaAs [6.46]. Scanning electron microscope magnification is $55,000 \times$. This periodicity is close to that required for third order distributed feedback gratings

The chemical etch produces different groove shapes depending on crystal orientation. This can be inferred from Fig. 6.8, in which the chemically etched mesa shape depends on type of etch and crystal orientation. The selective etch technique has been shown to produce excellent gratings with good groove depth at 2400\AA periodicity and with every expectation of reaching the fundamental spacing of 1100\AA with high quality [6.81]. The groove depth can be made deeper with selective chemical etch than with ion beam etch, but it has the drawback that the grooves must line up with the (011) direction on the (100) face.

The effectiveness of the ion-beam etched corrugation has been checked [6.59] by optically pumping a corrugated GaAs waveguide at liquid nitrogen temperature with a nitrogen-pumped dye laser at 6300\AA . The grating was used in third order to provide feedback with a period near 3450\AA . Optical waveguides consisting of both high resistivity epilayers on low resistivity substrates, and of GaAs-GaAlAs layers were used. The optical pumping threshold was 10^4W/cm^2 , comparing favorably to thresholds of optically pumped GaAs lasers with cleaved mirrors. The GaAs laser wavelength is determined by the corrugation period and was tuned over a range of 45\AA by varying the

corrugation spacing. This proves not only the effectiveness of the corrugation, but also demonstrates the ability to select the lasing wavelength of distributed feedback lasers.

Further reduction in threshold power and better mode properties can be expected from fundamental gratings rather than from gratings used in the third order. Gratings of the fundamental 1150 Å spacing have been exposed by introducing a high index medium in optical contact with the photoresist in order to reduce the effective light wavelength. By exposing the photoresist through a rectangular quartz prism using index matching immersion oil, as shown in Fig. 6.15, λ in (6.11) becomes λ_0/n_i , where n_i is the refractive index of the matching oil and λ_0 is the wavelength of light in vacuum [6.58]. This means that the grating spacing can be reduced to $\lambda_0/2n$. If the He-Cd UV laser is used at 3250 Å, then the 1100 Å spacing can be achieved [6.58, 60], and fundamental period corrugation feedback is possible.

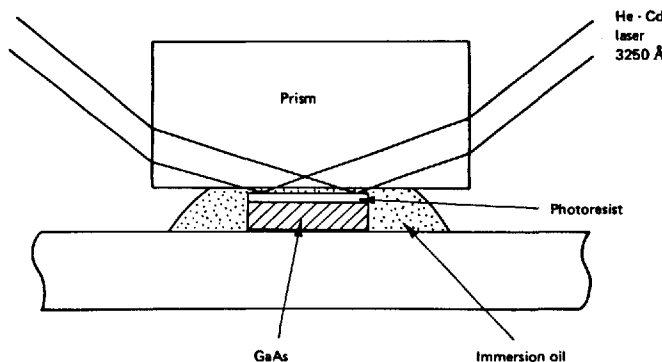


Fig. 6.15. Experimental arrangement for exposing 0.11 μm gratings in photoresist [6.58]. The two laser plane waves traverse quartz and index matching oil in order to interfere in a standing wave with a smaller spacing than in air

Gratings of fundamental period have been prepared in GaAs with a spacing of 1150 Å by ion-beam etch, and laser operation was achieved by the same optical pumping technique described above in connection with third-order gratings [6.58]. The threshold was roughly the same as with the third-order gratings, and not lower, as theoretically expected, presumably because the grating quality was somewhat degraded. However, much better mode structure was observed. With a short pumping length (150 μm), single mode operation was obtained with a linewidth less than 1 Å. With a longer pumping length and higher

pumping power, multi-longitudinal-mode oscillation was observed. Seven modes had a spacing of 1 Å, which agreed well with the mode spacing expected for the pumped cavity length of 700 μm.

The usefulness of distributed-feedback lasers lies not in the optically pumped lasers which have been fabricated so far, but in their use with double heterostructure lasers. Since the light is guided in a submerged layer of these structures, and the corrugation interacts with the guided light, it is necessary to develop techniques for growing the top layers of the double heterostructure on the corrugated lower layers. Such a device is shown in Fig. 6.16, utilizing the five-layer localized gain region laser, in which the carriers are confined in a region smaller than the light. These lasers have been fabricated without corrugations, using feedback from cleaved faces, and have been shown to have the lowest threshold of any laser [6.61]. This structure has the additional advantage for distributed feedback lasers that the corrugation and any resultant surface defects will not affect the electrical activity of the laser, since the electrically active layer is separated from the corrugated optical guiding layer.

Development of such distributed feedback heterostructure lasers requires crystal growth on corrugated layers. Research in this area

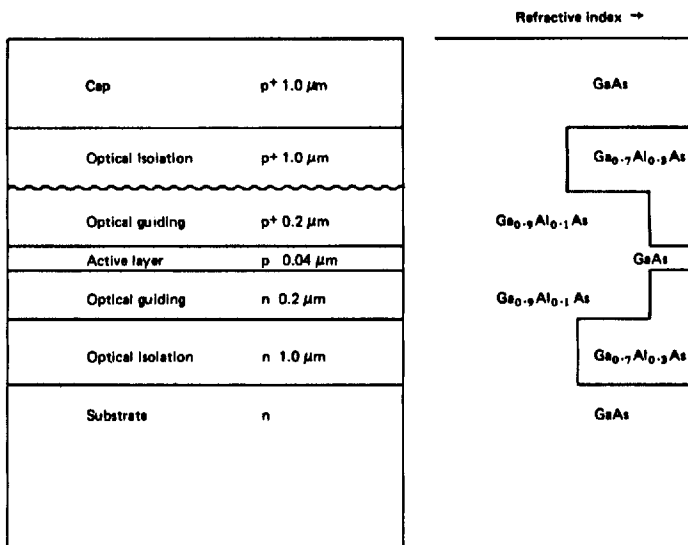


Fig. 6.16. Localized gain region heterostructure laser with distributed feedback, and corresponding refractive index profile. The corrugation is placed on top of the optical guiding layer, and separated from the electrically active layer

is developing so that room temperature distributed feedback double heterostructure injection lasers are expected to be available soon for use in monolithic integrated optics circuits. Successful growth of GaAlAs on a 3500 Å corrugated GaAs surface was demonstrated [6.62] by subsequently selectively etching away the regrown GaAlAs layer and demonstrating that the corrugation was still present with undegraded quality. Optically pumped laser action using feedback from a submerged corrugation has been demonstrated [6.82]. A fundamental corrugation of 1100 Å was applied to a GaAs waveguide, which was isolated from the substrate by a $\text{Ga}_{0.7}\text{Al}_{0.3}\text{As}$ layer. A layer of $\text{Ga}_{0.5}\text{Al}_{0.5}\text{As}$ was grown upon the corrugated GaAs waveguide, the large AlAs content allowing this layer to transmit the optical pumping light at 6400 Å. Such an experiment demonstrates that crystal growth upon corrugations is good enough to permit laser action.

The first injection distributed-feedback laser was demonstrated in a single heterostructure GaAs diode laser [6.83]. The *pn* junction was diffused into the GaAs substrate, which was corrugated by ion milling at the third harmonic (3500 Å). The threshold current densities required were comparable to those of cleaved single heterostructure lasers, and pulsed operation at liquid nitrogen temperature was observed. The faces were saw-cut, 10° apart so that mirror-feedback was eliminated. Proof of distributed feedback was the tuning of the laser wavelength over 130 Å by changing the grating period, and the absence of shift in wavelength with increasing excitation current. Multimode operation 5 Å wide was typical.

With the development of double heterostructure distributed-feedback lasers operating continuously at room temperature with many hours operation time, the necessary light source for monolithic integrated optics in GaAs will be achieved.

6.4. Modulators

Chapter 4 on modulation and beam deflection deals with several types of light modulators. In this section, we shall review the modulation methods for light in GaAs which show promise for modulators in monolithic optical circuits.

6.4.1. Electro-Optic Effect in GaAs

Its large electro-optic effect makes GaAs an excellent material for modulators. It has a zinc-blende structure with (110) cleavage planes.

The electro-optic coefficient is $r_{41} = 1.4 \times 10^{-12} \text{ m/V}$ [6.63]. When the guide plane is (001) and light enters along (110), TE waves (polarized in the plane of the guide) see a change in refractive index given by

$$n = \pm(1/2)n_f^3 r_{41} E, \quad (6.12)$$

while the coefficient for TM waves (polarized perpendicular to the guide) is zero. These changes are discussed extensively in Chapter 4. While the value of r_{41} is not as large in GaAs as in some other materials, the large value of n_f^3 renders this a very effective electro-optic material.

The electrode configuration required for application of the electric field are very different for semiconductors, compared to insulators. The contact is applied directly on top of the GaAs guide, rather than on either side of the guide, as with insulators. Because GaAs is a semiconductor, the large electric fields needed for electro-optic modulation can be applied by back-biased metal-semiconductor junctions (Schottky barriers) or by *pn* junctions. The field is supported in the depletion region of the semiconductor, which is swept free of carriers to a depth D . If one side of the junction has a higher carrier concentration, its depletion region can be ignored compared to that of the lower conductivity. In this case, the depletion depth is given by $D = \varepsilon E/eN$, where N is the free carrier concentration (in the higher resistance region) and E is the peak value of the electric field [6.64]. If the depletion region has a uniform charge distribution, the field falls off linearly with depth. The maximum depth to which a field can be applied is determined from the field at which the material breaks down. In GaAs, the breakdown field is roughly independent of doping level and has a value $E_B = 5 \times 10^5 \text{ V/cm}$. This means that the maximum depletion width is inversely proportional to the carrier concentration. Numerically, the maximum depth D_m in micrometers is related to the carrier concentration N in one cubic centimeter by $D_m = 1.5 \times 10^{16}/N$. Modulation efficiency will be optimized when the depletion region extends across the guide. A look at the numbers indicates that this could be a strong limit on purity requirements for thicker waveguiding layers [6.1].

Electro-optic modulation has been studied extensively in GaAs and related compounds. As discussed in Subsection 4.4.1, the phase change for TE modes in a guide of orientation (100), thickness h and length L is given by (4.9) and (4.10), which yield

$$\Delta\phi = \pi L n_f^3 r_{41} V/(h\lambda_0). \quad (6.13)$$

This assumes that the depletion region fills the guide and that the field is constant across the guide. This condition will be satisfied if

there are few free carriers that are swept out by the applied field in the waveguiding region. In this case the field falls off abruptly in the substrate. Because the maximum field that can be applied is that at breakdown, the guide must be a minimum length L_m before a phase change of π can be achieved. This length, given by $L_m = 2\lambda_0/(n_g^3 r_{41} E_B)$, is independent of guide thickness as long as the depletion region fills the guide. This behavior should be contrasted to that of insulating materials discussed in Chapter 4. In GaAs, the minimum half-wave retardation length is an encouragingly short 0.8 mm. The voltage needed to achieve a given modulation will be smaller if h is smaller so that efficient modulators will use guides that are as thin as possible.

6.4.2. Electro-Optic Phase Modulators

Electro-optic modulation has been studied in GaAs waveguides by endfire coupling light into the waveguides, applying a field, and by analyzing the light emerging from the exit cleave of the modulator. As discussed in Subsection 4.7.2, if the light is incident with its polarization 45° to the (100) crystal axes, and a crossed polarizer is placed in the output beam, the resulting transmission depends on the squared sine of the applied voltage, as long as the depletion region fills the guide. This behavior was observed at 1.15 μm in Schottky barriers placed upon high resistivity GaAs epilayers grown by vapor phase on low resistivity substrates [6.2]. The waveguides were 10 μm thick, and the modulator was 2.4 mm long. The ratio of output to input voltage was given by

$$\frac{I}{I_0} = \sin^2 \left[\frac{\pi}{2} \left(\frac{V - 12}{84} \right) \right], \quad (6.14)$$

where 84 represents the half-wave voltage and the off-set of 12 volts is due to the zero-bias phase shift. The zero-bias phase shift is due to the combined effects of strain birefringence and the built-in electric field at zero bias in a Schottky barrier. These effects are always present, but are often unpredictable, and the applied voltage for maximum transmission is not usually expected to be zero. These thick waveguides require large voltages to achieve high fields and large modulation effects; thinner waveguides would be more efficient.

Electro-optic modulation has been performed [6.65] at 1.15 μm in double heterostructures of GaAs-GaAlAs of width only 0.15–0.2 μm . The phase difference was linear with applied bias voltage (in this case across the pn junction), with a large zero-field phase shift. The depletion

depth in these layers was 0.6 μm , filling the guide. Because of the very thin guides, a potential of 8 V was sufficient to cause a 60° change in phase in a sample only 0.4 mm long. The power needed to phase-modulate the light by 1 rad was of the order of 0.1 mW per 1-MHz bandwidth. The high-frequency modulation is limited by the series resistance and by the capacitance of the device, and 4 GHz was the highest cutoff frequency so far determined. These double heterostructures make excellent, efficient phase modulators and have much potential for use in integrated optics.

At 10.6 μm , phase modulation has been measured in GaAs using 20 μm wide high resistance epitaxial films with Schottky barrier electrodes [6.66]. An excellent linear dependence of phase shift with reverse bias voltage was observed with no zero-field built-in phase shift. Because of the thick film, much larger voltages and longer lengths were needed to achieve the same phase change. A 17 μm thick film, 1 cm long, required 80 V for a 32° phase shift. Clearly, the waveguides should be as thin as possible if high efficiency is required.

Phase modulation has been studied extensively at 6328 Å in GaP reverse-bias *pn* junction diodes [6.67]. In this case, the exact nature of the guide is not fully understood, although light was guided in a 2 μm region and excellent modulators were made. A GaP diode of 1.5 mm length used as a phase modulator needed only 1.5 mW of power per MHz bandwidth for a modulation index of 1 rad at a wavelength of 0.633 μm resulting in an intensity modulation depth of over 80%.

6.4.3. Intensity Modulators

For many integrated-optics applications, intensity modulation is often required. In monolithic integrated-optics circuits, intensity modulation can be obtained from electro-optic polarization modulation by using GaAs in an orientation in which an applied field converts TE into TM modes, as discussed in Subsection 4.1.2. A metallic electrode can be designed which absorbs the TM but not the TE light. The design of such an intensity modulator has been suggested for GaAs [6.68] but the device has not yet been fabricated. The crystal orientation required is the (110) guide plane with light entering along ($\bar{1}10$). Since this is the same orientation as for the mesa lasers grown through masks by vapor phase epitaxy, such a modulator may prove the most convenient for this GaAs integrated-optics systems.

As discussed in Chapter 4, an intensity modulation can also be achieved using the electro-optic effect by controlling waveguide cutoff with an electric field. TE modes in (100) guides covered by metal electrodes or air have cutoff conditions which are affected by the applied

field. With GaAs, the maximum change in refractive index obtainable at the breakdown field is $\Delta n = 1.6 \times 10^{-3}$. This is sufficient to confine light in a guide of width 3 μm . Waveguide definition by the application of an applied field to bulk material can therefore be used only to create relatively thick guides. Because the refractive index change is positive or negative, depending on crystal orientation, it is possible to create or destroy guiding with an applied field. The destruction of guiding by applied field is possible only for waveguides whose dielectric discontinuity is comparable to that induced by the applied field. In practice, this limits this modulation method to guides 2 μm or wider. This method is also not suitable for the symmetric *pn* junction waveguides which have no cutoff condition.

Waveguide cutoff modulation has been demonstrated in high resistivity layers of GaAs 12 μm thick grown on lower resistivity substrates [6.44]. By selecting the substrate carrier concentration carefully, the refractive index discontinuity was chosen so that the guide was just below waveguide cutoff. In this case, the substrate carrier concentration was $2 \times 10^{16} \text{ cm}^{-3}$. The resulting modulation showed a factor of three increase of light intensity in the waveguide with 70 V applied. In this device, care must be taken in determining the crystal orientation, as the refractive index change may be positive or negative, depending on whether the crystal is 'up' or 'down'. Waveguide cutoff modulation provides intensity modulation in the (100) orientation, but requires more power than some other modulators. No effort has been made to optimize the design of waveguide cutoff modulators in GaAs, however, and further research in this area is necessary to determine how useful they will be.

Intensity modulators made with directional couplers show much promise for modulation in GaAs. In the semiconductor device, the electrodes are applied directly on top the guide. A field applied to only one will destroy synchronism and switch light from one channel to the other. In Subsection 6.2.3 we demonstrated that maximum modulation is obtained when $\Delta k L = \sqrt{3}\pi$, where L is the coupler length. As this is $\sqrt{3}$ larger than the change required for phase modulation, the coupler length must be at least $\sqrt{3} L_m$, or 1.4 mm. The ion-implanted channel coupler had a coupling length longer than this, so should be suitable for directional coupler modulation [6.46], if ion-implanted guides can be developed which support Schottky barrier fields. The directional coupler modulator remains a wide-open field for investigation in GaAs. This will probably be one of the most versatile and useful intensity modulators, when couplers with suitable electrical properties are developed.

When the light frequency is near the bandgap of GaAs, optical attenuation is dependent on applied electric field (electro-absorption)

and this physical effect can be used to make an intensity modulator. The applied field shifts the band-edge, increasing the absorption of light. GaAlAs double heterostructures were fabricated with band-edges close to the light to be modulated. The change in absorption was two orders of magnitude for only 8 V applied [6.69]. The performance of the double heterostructure electro-absorption modulators was, for a small wavelength region, similar to that of the electro-optic phase modulator: 90% modulation of intensity at $\lambda_0 = 0.9 \mu\text{m}$ for a diode only 0.5 mm long and 50 μm wide with a bias change of only 4 V. Together with a typical capacitance of 25 pF, the characteristic power for 90% intensity modulation is about 0.2 mW/MHz. By adding prescribed amounts of Al into the guide, its bandgap can be designed to be as close as desired to the light to be modulated and electro-absorption should prove to be a useful intensity modulation mechanism. The TM and TE modes are subject to different amounts of absorption, so that polarization modulation results also from electro-absorption and this acts as a mode filter.

For completeness, we mention the possibility of modulating the laser light source directly. Switching the laser drive current from zero limits the modulation rate because of the delay while the electron density builds up to the level needed for gain and laser action. This delay typically limits modulation to the 100 MHz range. By prebiasing the laser just below threshold, the modulation speed can be increased. Direct modulation of double-heterostructure lasers at 1 Gbit/sec rates has been reported using 130 mA current bias and 20 mA modulation amplitude [6.70]. The light amplitude modulation was essentially 100%. Because the laser has a tendency to oscillate, modulation is hard to control, especially in single mode lasers. Thus, separate modulation is preferable in most instances.

6.5. Detectors

Detectors for monolithic integrated-optical circuits make use of the photoconductive properties of semiconductor junctions. The requirement for a photodetector is that incident light be absorbed in such a way as to liberate free carriers. The application of a field will sweep out the charges, producing photocurrent in the external circuit. Semiconductors are photosensitive to light whose energy is larger than their bandgap energy, if they are pure, or to light whose energy is larger than the levels of impurity atoms, defect centers, or traps. The bandgap can be shifted by diffusing with dopants or impurities, by ion bombardment, or by application of an applied field (Franz-Keldesh effect).

Detectors can be made for integrated optics if, by any of the above processes, a localized area on a semiconductor chip can be made photosensitive.

6.5.1. Photodiodes

A reverse-biased junction confines the electric field to the photosensitive region. This will be either a *pn* junction, or a metal-semiconductor junction (Schottky barrier). In the former, the photosensitive region is near the junction, which is usually diffused or grown several microns into the substrate. These junctions will make excellent detectors for the double heterostructure guides shown in Fig. 6.3b, which are buried symmetric structures with cladding above the waveguide. The Schottky barrier will be the best configuration for guides at the surface, shown in Fig. 6.3a.

The *pn* junction photo-diodes are available commercially and are made of silicon or germanium. When light of frequency higher than the bandgap shines on the *pn* junction, carriers are released. The sensitivity cutoff is $1.2 \mu\text{m}$ for silicon and $1.7 \mu\text{m}$ for germanium, i.e., light of wavelengths shorter than these will be detected. Silicon is an excellent photodetector for use with optical fibers in an optical communication system. This is because the region of low optical loss for fibers, which is in the range 0.8 to $1 \mu\text{m}$ wavelength, coincides with the high sensitivity of the silicon photodetector.

A *pn* junction provides the field necessary to sweep out the free carriers liberated by the absorbed light, and to provide the detection signal. If no external bias voltage is applied, the built-in field of the depletion region of the *pn* junction separates the photo-generated carriers, and the detector works in the photo-voltaic mode. More sensitivity is provided by applying a reverse bias field to the *pn* junction, so that it behaves as a photo-conductive detector. In this way, a substantial fraction of the incident light generates detectable current. When used with the usual 50Ω load, the speed of the semiconductor diode is usually limited by the capacitance of the device. With proper design to minimize diode area, the response time can be of the order of nanoseconds or faster. Higher gain and speed are provided by avalanche photodiodes. These detectors utilize a high bias voltage, near breakdown, so that the avalanche process causes gain in the photocurrent.

Silicon *pn* junction diodes have been used to make an integrated-optics detector [6.71] in the hybrid arrangement shown schematically in Fig. 6.17. A silicon wafer was used as the substrate on top of which a glass optical waveguide was sputtered. The guide was isolated from the substrate by a layer of SiO_2 , formed by oxidation of the silicon.

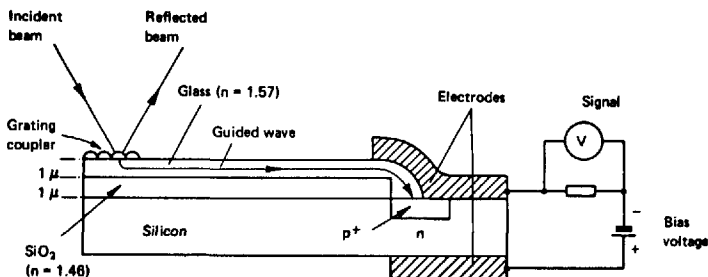


Fig. 6.17. Schematic of a hybrid integrated optics detector in silicon [6.71]

The guided light wave is coupled into the silicon substrate at the point where the SiO_2 layer stops, using principles similar to the tapered coupler. The geometry can be seen in the figure. The silicon was made into a detector in the region of the guide taper by forming a localized boron-diffused pn junction in the silicon, about 1 μm below the surface. Electrodes applied to the localized junction region collect the current generated by the absorption of the guided beam of 6328 Å light. This detector can be optimized by using a diode area as small as the guided light beam. If the structure were about 50 μm in diameter, the capacitance would be small enough for the RC time constant across a 50 Ω load to be less than the diffusion rate limit of about 10 GHz.

A monolithic integrated-optics detector involves the introduction of localized areas of lower bandgap material into the higher bandgap waveguide. These have been fabricated by epitaxy, by electro-absorption, and by ion implantation. Diffused monolithic integrated-optics detectors remain to be demonstrated. Each of these monolithic detectors will be discussed here.

6.5.2. Epitaxial Photodetectors

The localized epitaxial growth of lower bandgap material for integrated-optics detectors has been studied [6.72] in $\text{In}_x\text{Ga}_{1-x}\text{As}$ grown on GaAs. The resulting structure is shown in Fig. 6.18 b. Because of severe lattice mismatch, vapor phase epitaxial growth was performed in a way that allowed the $\text{In}_x\text{Ga}_{1-x}\text{As}$ composition to be graded from GaAs to the desired composition as the localized region was grown. This reduced the crystalline imperfections which are generally introduced by the strain of lattice mismatch.

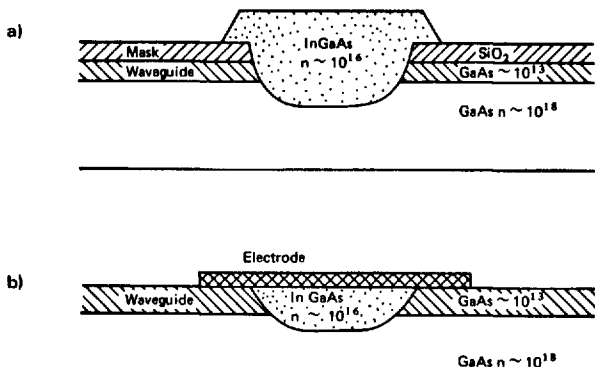


Fig. 6.18a and b. Steps in the processing of an epitaxially grown $\text{In}_x\text{Ga}_{1-x}\text{As}$ integrated-optics detector: a) After etching hole through SiO_2 mask and regrowth with InGaAs , b) Completed detector, after removing mask, polishing InGaAs flush and evaporating Pt electrode

The integrated-optics photodetector was fabricated as follows: a high resistivity layer of GaAs 5 μm thick was grown by vapor-phase epitaxy on a low resistivity substrate to act as the optical waveguide. Pyrolytically deposited silicon dioxide was used as a mask, with holes 125 μm in diameter opened by photolithography. Chemical etch removed the GaAs in the detector hole area, where InGaAs was to be grown. The silicon dioxide served as a mask against growth, so that epitaxial growth of InGaAs was obtained only in the regions where holes were etched in the waveguide. The resulting growth is shown schematically in Fig. 6.18a. Final polishing made the grown areas flush with the surface of the waveguide, after the mask was removed. Platinum Schottky barrier electrodes were evaporated, 0.125 mm in diameter, forming the completed detector, sketched in Fig. 6.18b.

These integrated Schottky barrier photodetectors had excellent photo-response characteristics. They were operated in the avalanche mode with gains of 250 and had a quantum efficiency up to 50%. Their base bandwidth was 2 GHz, limited by their capacitance, which could be reduced by using a smaller area electrode. The integrated-optics detectors were studied using 1.06 μm light, which was coupled into a cleaved end of the waveguide. The detector was optimized to this wavelength sensitivity by the inclusion of about 20% InAs.

Development of similar integrated-optics structures in GaAlAs by liquid phase epitaxy is essential for the optimum versatility in detector design. An example of such a system, sketched in Fig. 6.19,

could incorporate a detector of GaAs grown into a hole in a $\text{Ga}_{1-x}\text{Al}_x\text{As}$ waveguide which was isolated from the GaAs substrate by a $\text{Ga}_{1-y}\text{Al}_y\text{As}$ layer, where $y > x$. The fabrication of such a system awaits the perfection of techniques for liquid phase epitaxy through a mask. The InGaAs devices are fabricated by vapor phase epitaxy, which has proved difficult for GaAlAs. When the epitaxial techniques are developed, these detectors should be most useful for integrated-optics applications. The electrical, material properties and geometry can be chosen as necessary to decrease the capacitance as much as possible and therefore to increase the speed of the detector.

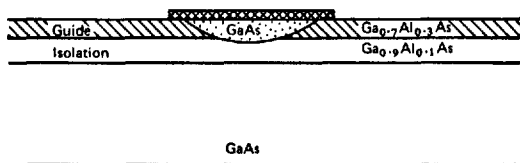


Fig. 6.19. Design for GaAlAs integrated-optics detector involving etch and regrowth of GaAs in a localized region of a $\text{Ga}_{1-x}\text{Al}_x\text{As}$ guide grown on a $\text{Ga}_{1-y}\text{Al}_y\text{As}$ isolation layer ($y > x$)

6.5.3. Electro-Absorption Detectors

The bandgap of a semiconductor can be shifted slightly to longer wavelengths by the application of an electric field. This is the electro-absorption effect which was discussed in Section 6.4. A field applied to a semiconductor increases the optical absorption for light near the bandgap; the absorption generates hole-electron pairs, which are swept out by the applied field, thus producing photo-current. If the bandgap of the electro-absorbing material is tailored to the wavelength of light, electro-absorption makes a useful detector. In the double heterostructures, it is possible to achieve fields up to 300,000 V/cm, very near the breakdown field, with only 10 V applied bias, because the active region is thin, ranging from 0.4 to 1 μm . In this case, electro-absorption generates photo-current for light as far as 0.3 eV below the bandgap energy.

An electro-absorption integrated optics detector has been demonstrated in reverse-biased *pn* junction double heterostructures [6.47]. Light of wavelength 1.06 μm was guided in the heterostructure, and photocurrents were measured with up to 16 V reverse bias voltage applied. The bandgap of the double heterostructure was only 0.86 μm , yet up to 1 mA of photo-current was detected. The photo-current

was found to closely follow the electro-absorption at large reversebias values. As with electrical absorption, the photo-currents were polarization dependent, larger for TM than for TE modes, by typically a factor of 5. No significant photo-current multiplication was observed at bias values up to 16 V, but the quantum efficiency was close to 100%. The time constant in the devices built so far was determined by the capacitance of the diode, which can be minimized by careful design so that the speed is in the GHz range.

The advantage of electro-absorption as a detector is that it is not necessary to fabricate a localized region of different bandgap. With proper design, the waveguide is transparent except in the electrode region where the field is applied and detection takes place. Electro-absorption is a useful technique for integrated-optics detectors, provided that the band-gap of the guiding material is properly chosen and the light to be detected is fairly narrow-band.

6.5.4. Ion-Implanted Photodetectors

Ion implantation is another way of decreasing the band-gap, in order to increase absorption and photo-current. In Section 6.1, the properties of proton-implanted GaAs were discussed. The damage of the energetic ions leaves defect centers which trap electrons. It has been shown that a good fraction of the optical losses of implanted layers are due to electrically active traps [6.73]. These can be liberated by the incident light. If a field is applied in the form of a back-biased Schottky barrier, the photo-induced carriers are swept through the depletion region, causing photo-current.

A proton-implanted integrated optics photo-detector has been fabricated [6.74] in GaAs. The waveguide was an epitaxial layer 3.5 μm thick of high resistivity GaAs on a low resistivity substrate. Protons of 300 keV energy were bombarded in a localized portion of the guide with a flux $2 \times 10^{15}/\text{cm}^2$. The result was a damage profile that peaked about 2.5 μm below the surface, near the peak of the guided optical distribution. A 30 minute anneal at 500°C reduced the optical loss in the detector region to 90 db/cm. The Schottky barriers, made of evaporated aluminum, were 0.275 mm square and withstood as much as 40 V.

Ion implantation increased the cutoff wavelength of the photo-sensitivity curve from 0.85 to 0.9 μm and also introduced a photo-sensitive tail which, at 0.92 μm , had a tenth the peak response, and which fell to 1/50 the peak response at 1.15 μm . Typical quantum efficiencies, measured at 1.06 μm , were 16% and they can be expected to be improved with further optimization of implantation damage and light profiles.

Typical photo-currents were 20 μA for a reverse bias of 20 V. The response time was not measured, but it was found to be shorter than 200 nsec.

The advantage of ion-implanted detectors over others fabricated so far in GaAs is the ease with which localized areas may be implanted. A gold mask protects the regions that are not to be implanted. Through a very simple process, an epitaxial lossless GaAs-GaAlAs surface optical waveguide may be implanted in a localized area and converted to a detector.

In addition to epitaxy, electro-absorption and ion implantation, the bandgap can be lowered by the diffusion of impurities. In order to be useful as a detector, the impurity absorption must be a process that creates free carriers. Free carrier absorption or conduction-band absorption to a higher band will not create photocurrent, so that it cannot be useful for detection. However, if the impurities introduce new deep levels which can be ionized by light, the semiconductor can be used as a detector. Impurity diffusion in a selected region of the semiconductor would make an integrated-optics detector; however, this has not yet been reported.

This completes our discussion of integrated-optics detectors. Detectors seem to present very few fundamental difficulties in the design and fabrication of optical circuits. The use of semiconductor junction detectors is an advanced art and the challenge for integrated optics is careful design to minimize the response time for any given application.

6.6. Integration

The above completes our discussion of components for monolithic integrated optics. We shall now consider techniques for integration of these components onto a substrate. At the present time, monolithic integration techniques are only beginning to be developed in active waveguiding materials. Presumably, some of the techniques used in passive materials will carry over to active materials, while some new methods will also be brought forward. In the case of GaAs, research on techniques for integration of optical components remains definitely in the area of materials science. While no complete integration experiments have yet been performed, we shall construct simple examples for ways to incorporate the individual components for integrated optics into a single monolithic element. These are untried and perhaps not the most elegant solutions; they are presented here as tutorial examples.

In order to have a laser and non-absorbing waveguide on the same chip, it will be necessary to have either successive guiding layers with

different aluminum concentrations and to couple light from one layer into another, or to have different regions of a guiding layer with different aluminum concentrations. These two basic designs are shown in Fig. 6.20. The designs we show here all utilize the double-heterostructure distributed feedback laser, although the single-heterostructure laser can be used for pulsed operation and possibly other feedback mechanisms may prove more valuable.

The design of Fig. 6.20a utilizes the coupling of light from one layer into the layer below by using a tapered coupler [6.75]. This design involves growing all needed layers of the structure and then selectively

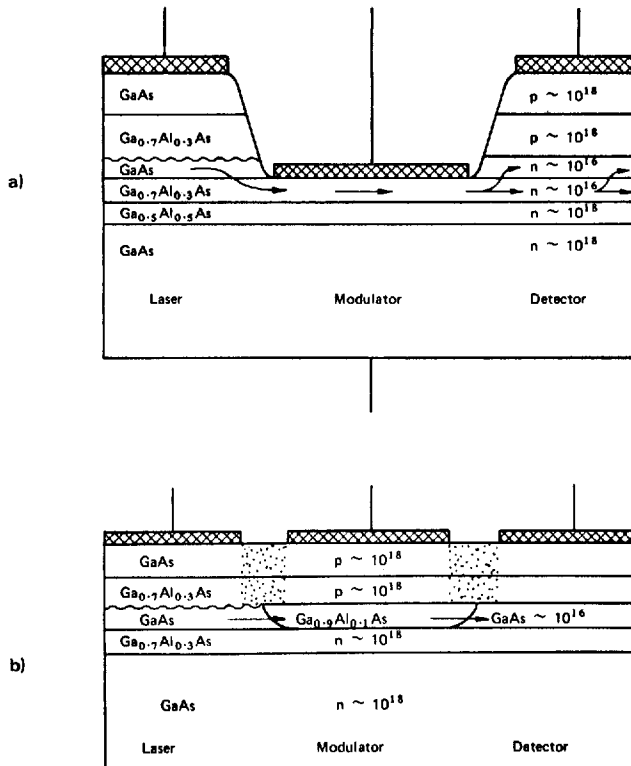


Fig. 6.20a and b. Monolithic integrated-optical circuits consisting of distributed feedback laser, modulator and detector. The arrows indicate the light path. The cross-hatched areas are the electrodes: a) Etched modulation region uses tapered coupling into a different layer and requires no crystal regrowth over the modulator. b) Light path remains in the same plane because crystal regrowth alters the AlAs content as required. Dotted regions are proton implanted for electrical isolation

etching away the top layers. Light at the GaAs wavelength is generated in a GaAs heterostructure laser portion of the chip, which is operated under forward bias. The diagram indicates distributed feedback, but facet formation by chemical or ion-beam etch is also possible. The GaAs laser light requires a guiding layer of GaAlAs in which to perform the integrated-optics functions such as modulation. The GaAs chip is etched in selected regions, through a mask, leaving a taper, so that the laser light couples into the layer below, which is transparent because it contains aluminum. This layer will guide light if its refractive index is higher than an isolation layer below it, and if the GaAs layer above it is removed.

In the guiding $\text{Ga}_{0.7}\text{Al}_{0.3}\text{As}$ region, all the logic functions will be performed: e.g., modulation, multiplexing, coupling light between circuits, filtering, analyzing, mode selection, etc. In the diagrams, we have shown only modulation in the guiding region. All the techniques discussed in previous sections for fabrication of circuit elements and modulators can be applied to this waveguiding layer. In the detection region, the modulated light leaks back into the lossy GaAs *pn* junction region where a reverse-bias field converts the hole-electron pairs generated by the absorbed light into photocurrent. One disadvantage of the design described here is that the top layer in the modulation region contains aluminum. It has been found that it is very difficult to make good electrical contacts to GaAlAs. If the contacting problem can be solved, or if a very thin layer of GaAs can be left remaining on the surface to provide good contacts, but not enough to introduce optical attenuation, then this design should be useful. The advantage of this system is that the crystal growth requirements are less severe than in the design of Fig. 6.20b.

Figure 6.20b shows a design that solves the contacting problems, but involves regrowth on GaAlAs, a problem which has not been solved satisfactorily by liquid phase epitaxy to date. The isolation layer and GaAs layer are grown first. The sample is removed from the furnace, a SiO_2 mask is pyrolytically deposited, and the GaAs selectively etched away in the region which is to be the guiding region. The sample is returned to the furnace with the SiO_2 mask in place, to protect against growth in the GaAs areas. A guiding layer with a small aluminum concentration is regrown in the etched areas on the isolation layer of higher aluminum concentration. The sample is removed from the furnace, the SiO_2 mask removed, and the top surface polished in order to remove any overgrowth of GaAlAs. This method is similar to the detector fabrication outlined in Fig. 6.18. The grating is fabricated in the laser region as described in Section 6.3. Finally the whole sample is replaced in the furnace and the top two optical isolation and contacting

layers are grown over the entire sample. After masked contact deposition, ion implantation provides electrical isolation of the various regions: laser, modulator, and detector.

It can be seen that the fabrication of monolithic integrated-optical circuits involves the solution of some very challenging materials science problems. Regrowth by liquid phase epitaxy, both over GaAs and GaAlAs in selected areas, selective etching, and regrowth through masks, all must be perfected for truly integrated optical circuits to come into fruition. The challenges for research clearly lie in the field of crystal growth.

6.7. Liquid-Phase Epitaxy

In the preceding section it was made clear that advances must be made in the epitaxial growth of $\text{Ga}_{1-x}\text{Al}_x\text{As}$ if integration is to become a reality. For this reason, we discuss liquid-phase epitaxy, which is used for the fabrication of lasers and is therefore the growth technique that is the most developed.

6.7.1. Growth Apparatus

Liquid phase epitaxy of GaAlAs uses a gallium melt, which dissolves the GaAs seed crystals and aluminum, as well as the necessary electrical dopants. A polished substrate of GaAs is placed under the melt and the temperature is lowered as growth occurs. In most arrangements the melts are pushed over the substrate using a graphite boat and slider arrangement. The furnace is usually horizontal, and involves a linear slider motion. The details of this system will be described here, but we shall also mention some of the advantages of using a vertical furnace having a rotary slider motion.

The growth apparatus is shown in Fig. 6.21. A three-zone horizontal diffusion furnace produces a uniform temperature (or required small temperature gradient) in the range of 750°–900°C over the boat length of about 10–30 cm. A precision temperature controller maintains a stable temperature in the range ± 0.01 –0.1°C. A temperature programmer, which can be a motor-driven potentiometer, causes the temperature to be lowered at a rate between 0.5–0.1°C/min. A thermocouple made of platinum/platinum-rhodium provides the accurate temperature sensing. Its quartz shield is designed to act as a push stop for the graphite boat.

The boat is machined from high purity graphite, with many different designs having been used. There is a well for each melt and a space at the

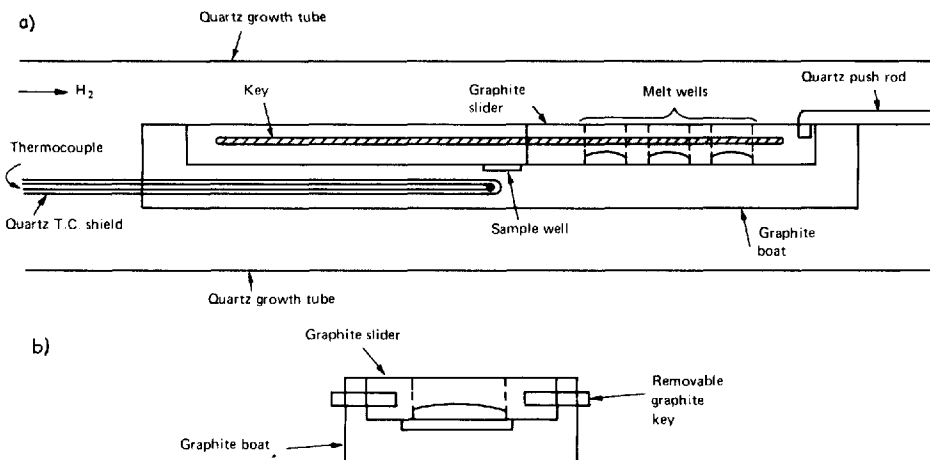


Fig. 6.21a and b. Graphite boat and slider for liquid phase epitaxy of $\text{Ga}_{1-x}\text{Al}_x\text{As}$ in a horizontal quartz growth tube: a) Side view of apparatus, b) End view of graphite slider and boat

beginning and end of the boat for the sample to sit under the graphite. Either the melts slide over the substrate, placed in a recess in the base, or the substrate is placed in a recessed part of a slider and pushed under stationary melts. The substrate recess is slightly larger than the melt hole so that the sample is held down during growth by the edge of the graphite melt wells. Convenient means of putting the substrate in and removing it without disturbing the melts is necessary if they are to be reused. It is useful also to design the boat so that the sample may begin a run uncovered, so that it is exposed to the flushing gas flow. The graphite boat also needs provision for the attachment of a quartz push rod, which will move the melts over the sample. Better handling is obtained if a pull as well as a push motion are incorporated. The boat should sit without moving up against the quartz thermocouple shield inside the quartz growth tube.

Tolerances on movement of the boat and slider during growth are extremely critical because the melt must be wiped off the sample before it enters the next melt. This wiping is usually done with the edge of the well in the graphite boat, and must be done with precision. Some melt carry-over improves the wetting and equilibrium growth conditions, while too much carry-over spoils the aluminum concentration and leads to unreproducibility. A clearance in the range of 12–125 μm is normally left between the wiping graphite well edge and the substrate. Such small tolerances require careful design and machining of the

graphite boat and slider so that the sliding motion is smooth and without jitter. High purity, high density graphite can be machined to sufficient tolerance and can be mechanically polished with alumina to a shiny surface to promote smooth sliding. In the boat design of Fig. 6.21, sliding takes place along a removable key, which provides sufficient constraint for the slider along with the ability to lift apart the boat pieces.

The graphite boat is placed in a quartz growth tube, with a good seal between the push rod and the end plate. Flowing hydrogen provides a reducing atmosphere. It is most important that all oxygen and water vapor be eliminated; the presence of aluminum makes this more critical than for the growth of pure GaAs. This is because aluminum oxide does not vaporize at the growth temperature, and it is important to keep it from forming. Epitaxy takes place at temperatures higher than 700°C to ensure that gallium oxide vaporizes and does not present a problem. The presence of water vapor will etch hot GaAs. A palladium diffuser purifies the hydrogen to a level <1 ppm of water or oxygen, with a flow rate typically 5 ml/h. An additional requirement, if luminescent structures are to be grown, is the elimination of copper because of its deep traps when it is an impurity. This means that all the piping should be stainless steel or glass. A silicone oil bubbler provides a positive gas pressure head inside the growth tube at all times, to keep oxygen or water vapor from seeping in at any moveable joints.

6.7.2. Growth Procedure

The thickness of the layer that will be grown depends on the depth of the melt above the substrate and on the temperature drop (assuming equilibrium growth conditions), as will be discussed in detail later. Melt thicknesses typically 0.5–3 mm are used. The thinner melts require a graphite plug in order to press the melt flat, as gallium has a high cohesion and tends to form a ball. Equilibrium growth is difficult to achieve. If the melt is to be exactly saturated at the growth temperature, melt components must be weighed extremely accurately and the temperature controlled very precisely. In fact, most systems include an excess GaAs. The aluminum is dissolved first and any remaining GaAs (typically 20%) not needed for equilibrium floats on the surface. This tends to introduce a slight supersaturation, because the GaAs concentration will be highest at the top of the melt. Furthermore, moving the slider may introduce a temperature change, if there are any thermal gradients in the system. This means that the melt may not be in equilibrium. In practice, the thickness of the layer grown is plotted as a function of the growth time, for various growth times, and extrapolated to zero time. The zero-

time growth indicates the degree of supersaturation or undersaturation and a temperature gradient can be purposely introduced to counteract these effects. In this way, layers only 400 Å thick can be grown. In GaAlAs melts, the supersaturation depends on the thermal history of the melt, in ways which are not totally understood but which are reproducible. As long as care is taken to reproduce the thermal history of a melt, the temperature gradient required to eliminate dump growth or etchback can be introduced empirically and thin layers can be grown.

The rate of temperature decrease must be sufficiently slow if the entire melt volume is to participate in the growth. Typical growth rates are often 0.5°C/min, but more controlled growth occurs at rates of 0.1°C/min or slower. The need for slow growth and reproducible thermal history in GaAlAs is due to the high segregation coefficient of aluminum. Its density in the solid is much higher than in the liquid. This means that local depletion of aluminum in the liquid will occur if growth occurs faster than the diffusion rate for aluminum. As long as the growth system is used in a reproducible fashion, slight deviations from equilibrium need not be detrimental. The time required for a given thickness of grown layer is generally determined empirically and is the order of ten minutes for one micrometer at a cooling rate of 0.2°C/min.

Good growth requires clean, flat, strainfree and low dislocation density GaAs substrates. Bulk GaAs is grown in ingots and slices are cut in the desired orientation; (100) and (111) are usual, the former of special interest because of its perpendicular cleavage planes. Slices are cut by wire saw, typically 0.4 mm thick; they generally have an area greater than 4 cm². Mechanical lapping removes saw marks, then mechano-chemical polishing on a pad with an etch such as bromine-methanol, NaOCl or 3H₂SO₄:1H₂O₂:1H₂O thins the sample to the prescribed thickness. The substrate is then cleaved to a size which carefully fills the substrate recess in the boat. Each substrate is measured to determine the amount of final etch required to obtain the exact thickness required. Proper substrate thickness is necessary for successful wiping after growth, a process that requires accurate tolerances. Control of etch rate is obtained by careful control of etch temperature and by use of an argon bubbler agitation. A final rinse in doubly distilled water and blowing dry with nitrogen complete the processing.

All ingredients for the melts must be as pure as possible and thoroughly cleaned before use. Pure gallium can be bought in pellets that may be weighed and used without further processing. The gallium may also be melted under dilute HCl (to prevent formation of oxides), measured, frozen, and subsequently cleaned of residual acid. The GaAs seed crystals should be numerous and small, to promote rapid melting or regrowth for equilibrium stabilization. They can be cleaned by a thorough

degreasing, free etch, rinse and blow dry. Only a small amount of aluminum is needed, obtained from a measured length of pure wire, or scraped from a pure ingot. Some aluminum oxide will be present, and since it will not dissolve in the melt, it is advantageous to keep this to a minimum and to use a reproducible method of aluminum preparation. Furthermore, the aluminum must be placed under rather than on top of the gallium, else the oxide skin may keep the aluminum from dissolving into the gallium. Typical amounts needed for growth are 1 gm gallium, 0.05 gm GaAs, 0.005 gm aluminum. The exact amounts needed for different results will be discussed later.

After the melt ingredients are loaded into the proper wells, the substrate is placed in its recess in the boat, uncovered by graphite, and the boat is loaded into the quartz growth tube. After flushing first with nitrogen and then with hydrogen, the furnace is heated to 500°C for an hour before proceeding with heating to the growth temperature. After flushing and bakeout, the graphite boat is pushed over the sample while the furnace is heated to the growth temperature. This is necessary to protect it from dissociation by outdiffusion of arsenic. It is the advanced rate of this process that limits the high temperature operation to 900°C.

The melts are moved in succession over the substrate by means of the push rod. Often the first melt is an etch melt composed of gallium undersaturated with GaAs, so that 10–20 µm of the substrate is removed, providing a clean, flat, strain-free surface for growth. The layers are then grown one after another with a minimum time in between, so that growth continues in as smooth a fashion as possible. For thicker layers, several minutes are required, although the thinnest layers require only seconds under the growth melt. The necessary growth time is a strong function of aluminum concentration, which will be shown later.

The final wipeoff is critical in determining the top smoothness. If any melt is left on the surface, GaAs continues to grow out from the melt as the temperature is dropped to room temperature. This extra layer is often very thick, reaching as much as 20 µm. Successful wiping can be performed if the exact tolerance and cleanliness are maintained, but the yield is often low. For example, too close a tolerance causes scratches and too large a tolerance does not wipe clean. In some laboratories, a flexible graphite "brush" or "felt" is used as a wiper. More commonly, a quench melt is used. The sample is passed under a gallium melt which contains no GaAs and is then wiped. Any residual gallium melt covering the sample causes some etchback, since it is undersaturated, but this is regrown as the temperature drops to room temperature. In this way, thin top layers of GaAs can be grown.

Even the best liquid-phase epitaxy does not leave the surface polish-smooth. There are often ripples the order of one millimeter apart. These are sufficiently smooth not to affect waveguiding losses, but are not smooth enough for some applications, such as uniform photoresist layers needed for grating fabrication. In this case, polishing has been used to produce flat surfaces. Carefully controlled mechanical or chemical polishing can reduce a 20 μm GaAs layer to a 3–5 μm guide with a flat smooth surface.

6.7.3. Growth Characteristics

After growth, any remaining gallium is removed by warm dilute HCl. To measure the growth of relatively thick layers, a section is cleaved off, stained and observed in a microscope. Typical stains will selectively color or etch the GaAlAs, such as dilute NaOCl in water (1:400) or 4HNO₃:1H₂O. For thinner layers, angle lapping or cylinder lapping is required before staining to achieve sufficient resolution.

The aluminum concentration can be obtained by photo-luminescence, cathodo-luminescence or an electron microprobe on an angle-lapped portion, or on the top layer. If each successive melt is smaller than the last, a portion of each growth is exposed and can be analyzed. In photo-luminescence and cathodo-luminescence, measurement is made of the wavelength of light that is emitted by samples excited by blue or ultraviolet light, or by a low energy electron beam. The AlAs concentration can be determined by comparison with the known measurements of luminescence. The electron microprobe measures the energy of X-rays, which are emitted during the impact of the electron beam of an electron microscope, and compares the relative intensities of the elemental components. In each case, the spatial resolution is determined by the diffusion of excited electrons, which is of the order of one micrometer.

The expected equilibrium growth behavior is shown in Fig. 6.22. The curves [6.76] are plotted from the known thermodynamic properties of the three-component melt. From the contour of constant AlAs in the solid (straight lines) and a specific growth temperature (contour of constant temperature for first formation of solid), the required melt composition can be determined. This determines the amount of aluminum and GaAs to add in preparation of the melt.

As the temperature is dropped equilibrium growth proceeds along the cooling curves (dotted lines). The thickness of the layer grown for a given temperature drop can be determined from the effective melt thickness and the decrease in the percentage of arsenic in the liquid. Because the

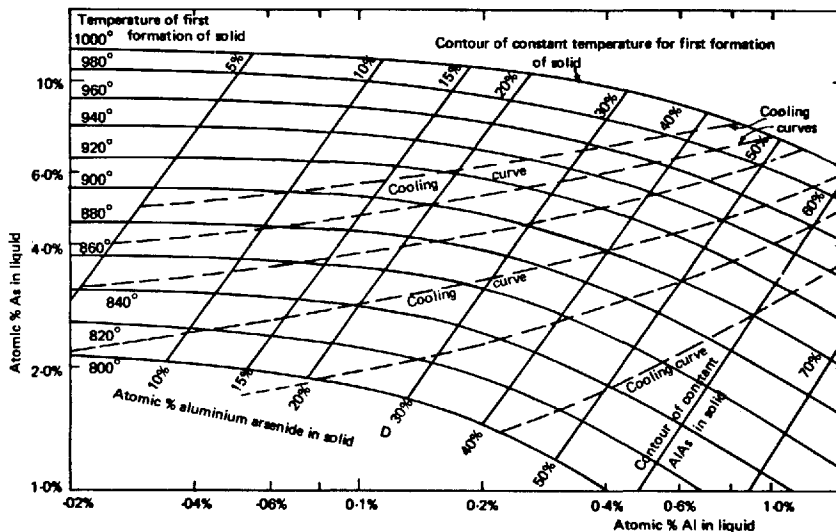


Fig. 6.22. Equilibrium growth curves for $\text{Ga}_{1-x}\text{Al}_x\text{As}$ liquid phase epitaxy showing constituents of the solid and the melt at various temperatures, and cooling curves

decrease of arsenic in the liquid represents the amount of arsenic grown into the solid, the layer thickness is determined if the density of the solid is known. In fact, the thickness grown is

$$h = 2 \Delta y \eta T \quad (6.15)$$

where Δy is the decrease in the fraction of arsenic in the melt, T is the effective melt thickness, and η is the ratio of the melt density to the solid density, and is approximately unity. As an example, for 30% aluminum, at 860°C, cooling 20°C causes a decrease in arsenic concentration of 0.5% (determined from the cooling curve), so that a 1 mm melt thickness grows a layer 10 μm thick. The effective melt thickness to be used in this expression may be considerably smaller than the physical melt thickness. As it depends on the cooling rate, diffusion and convection rates of the melt constituents, it usually is determined empirically.

It can be seen from the slope of the cooling curves that the percentage of aluminum arsenide in the solid does not remain a constant, but decreases as growth proceeds. The reason for this fall-off is the large segregation coefficient of aluminum. That is, the much higher fraction of AlAs in the solid than of aluminum in the liquid. This means

that the aluminum depletes more rapidly from the melt than the arsenic, and subsequent equilibrium growth must have a smaller AlAs concentration. The decrease in AlAs concentration is determined by the temperature drop during growth. However, for a given temperature drop, thicker layers are grown if thicker melts are used. This means that the gradient will be smaller for thicker melts (the temperature drop required for a given layer thickness is smaller). While thicker melts are used to reduce the AlAs concentration gradient, it can be made purposely large by using thin melts. In the first section we discussed GaAlAs waveguides fabricated with thin melts making optical use of this concentration gradient.

These cooling curves have been experimentally verified and found to describe growth proceeding at rates 0.2 °C/min, or slower [6.76]. The concentration gradient in the epitaxial layer is a property of liquid phase epitaxy which must be taken into account when designing a structure to be grown. If growth proceeds faster than 0.2 °C/min, the AlAs concentration gradient is larger because the effective melt thickness decreases.

The addition of electrical dopants into the melts will yield electrically active devices. In the absence of doping, with stringent cleanliness, concentrations $\sim 10^{13}/\text{cm}^3$ in GaAs layers have been achieved. More typically, $\sim 10^{16}/\text{cm}^3$ epitaxial layers are grown. Typical dopants added to the melts are tin for *n*-type doping and zinc for *p*-type doping, with silicon or germanium for the active region. The small amount of dopants added rarely make a change in the epitaxial growth properties other than electrical doping. In the case of tin, however, because the solubility of GaAs in tin is 4.5 times higher than in gallium and 5% of the melt is tin, it is necessary to add excess GaAs to saturate the melt. Typical proportions and constituents [6.77] used for liquid phase epitaxy of double heterostructures at 850 °C are shown in Table 6.2.

The furnace we described in this section was horizontal, and the slider motion was linear. More accurate control of temperature profiles is obtained with use of a vertical furnace with a rotary motion for the graphite slider. In this way, the sample remains at the same temperature as it moves from melt to melt, because of cylindrical symmetry. Any radial temperature gradient has only a small effect, and a required vertical temperature gradient can be impressed without introducing a temperature gradient in the direction of the substrate movement. The only disadvantage of the vertical system is the limit to the size of the substrates and melt wells that can be fit into a fixed diameter tube.

This completes our discussion of liquid phase epitaxy of $\text{Ga}_{1-x}\text{Al}_x\text{As}$. We have presented a rather descriptive outline with few references because, although a great deal of work has been done in many labora-

Table 6.2. Typical melt constituents for double-heterostructure laser

Melt	Material	Atomic percent
1. Etch	Ga	97.5
	As	2.5
2. <i>n</i> -type	Ga	92.1
	As	2.9
	Al	0.5
	Sn	4.5
3. Active	Ga	93.8
	As	4.1
	Si	2.1
4. <i>p</i> -type	Ga	91.4
	As	2.8
	Al	0.8
	Zn	5.0
5. Cap	Ga	91.0
	As	4.0
	Zn	5.0

tories, many of the techniques remain those of an art. Different laboratories use procedures that differ in minor details in ways whose importance have not yet been proven. No one procedure has been found conclusively to be the best. Good thermal control and good cleanliness are the two essential requirements. Proper wipeoff and uniform slider motion remain steps that must be performed with care.

Development of the ability to grow on structures rather than planar surfaces is a present challenge, as is the ever-increasing control and perfection of planar layers, particularly for development of double heterostructure lasers with long lives. A recent issue (1974) of the Journal of Crystal Growth was devoted exclusively to the techniques of liquid phase epitaxy of $\text{Ga}_{1-x}\text{Al}_x\text{As}$ and would serve as the best starting point for references on the subject. A few earlier references are listed in [6.78].

Acknowledgements. The author gratefully acknowledges the hospitality of Standard Telecommunication Laboratories during the period of writing this chapter, as well as their imparting information about liquid phase epitaxy of heterostructure lasers. In particular, special thanks are due G. H. B. Thompson, for stimulating discussions and for making this opportunity available. The author also gratefully acknowledges California Institute of Technology, where, in the stimulating research environment of the laboratory of Professor Yariv, the author developed much of her understanding of integrated optics in GaAs.

References

- 6.1. See, for example, E. GARMIRE: NEREM 72, Solid State Circuits Conference Proceedings (NEREM, Boston, 1972), p. 115—118.
- 6.2. D. HALL, A. YARIV, E. GARMIRE: Opt. Commun. **1**, 403 (1970).
- 6.3. E. P. RASHEVSHAYA, V. I. FISTUL': Sov. Phys.-Solid State **9**, 2849 (1968).
- 6.4. B. E. BARRY: *GaAs and Related Compounds* (Institute of Physics, London, 1971), Paper 19.
- 6.5. P. K. CHEO: Appl. Opt. **12**, 500 (1973).
- 6.6. A. YARIV, R. C. C. LEITE: Appl. Phys. Letters **2**, 55 (1963).
- 6.7. F. K. REINHART, D. F. NELSON, J. MCKENNA: Phys. Rev. **177**, 1208 (1969).
- 6.8. J. ZOROOFCHI, J. K. BUTLER: J. Appl. Phys. **44**, 3697 (1973).
- 6.9. M. PANISH, I. HAYASHI, SUMSKI: IEEE J. Quant. Electr. QE-**5**, 210 (1969).
- 6.10. E. GARMIRE, H. STOLL, A. YARIV: Appl. Phys. Letters **21**, 87 (1972).
- 6.11. R. SCHINELLER: Microwaves **7**, 77 (1968).
- 6.12. R. STANLEY, W. GIBSON, J. RODGERS: Appl. Opt. **11**, 1313 (1972).
- 6.13. R. SHUBERT, J. HARRIS: IEEE Trans. Microwave Theory Techniques MTT-**16**, 1648 (1968).
- 6.14. P. K. TIEN, R. ULRICH, R. J. MARTIN: Appl. Phys. Letters **14**, 291 (1969).
- 6.15. M. J. RAND, R. D. STANLEY: Appl. Opt. **11**, 2482 (1972).
- 6.16. D. B. OSTROWSKY, A. JACQUES: Appl. Phys. Letters **18**, 556 (1971).
- 6.17. D. H. HENSLER, J. D. CUTHBERT, R. J. MARTIN, P. K. TIEN: Appl. Opt. **10**, 1037 (1971).
- 6.18. T. IZAWA, H. NAKAGOME: Appl. Phys. Letters **21**, 584 (1972).
- 6.19. H. KOGENNIK, C. SHANK: Appl. Phys. Letters **18**, 152 (1971).
- 6.20. H. YAJIMA, S. KAWASE, Y. SEKIMOTO: Appl. Phys. Letters **21**, 407 (1972).
- 6.21. D. P. GIA RUSSO, J. HARRIS: Appl. Opt. **10**, 2786 (1971).
- 6.22. L. KUHN, M. DAKSS, P. HEIDRICH, B. SCOTT: Appl. Phys. Letters **17**, 265 (1970).
- 6.23. ZH. I. ALFEROV, V. M. ANDREEV, E. L. PORTNOI, M. K. TRUKN: Sov. Phys. Semiconductors **3**, 1107 (1970).
- 6.24. NEUBERGER: *III-V Semiconducting Compounds* (Plenum Press, New York 1971).
- 6.25. D. MARCUSE: IEEE J. Quant. Electr. QE-**8**, 661 (1972).
- 6.26. E. GARMIRE: Appl. Phys. Letters **23**, 403 (1973).
- 6.27. F. K. REINHART, I. HAYASHI, M. B. PANISH: J. Appl. Phys. **42**, 4466 (1971).
- 6.28. C. M. WOLFE, G. E. STILLMAN, I. MELNGALLIS: "Digest of Technical Papers". Topical Meeting on Integrated Optics, 1974 (Opt. Soc. Am., Washington, D.C., 1974), p. MA8.
- 6.29. R. D. BURNHAM, N. HOLONYAK, D. R. SCIFRES: Appl. Phys. Letters **17**, 455 (1970).
- 6.30. B. I. MILLER, E. PINKAS, I. HAYASHI, R. J. CAPIK: J. Appl. Phys. **43**, 2817 (1972).
- 6.31. A. Y. CHO, M. B. PANISH, I. HAYASHI: *GaAs and Related Compounds* (Institute of Physics, London, 1971), p. 18.
- 6.32. W. VON MÜNCH: J. Crystal Growth **9**, 144 (1971).
- 6.33. N. UESUGI, H. ITO, H. INOBA: "Digest of Technical Papers". Topical Meeting on Integrated Optics, 1974 (Opt. Soc. Am., Washington, D.C., 1974), p. MB10.
- 6.34. J. M. HAMMER, D. J. CHANNIN, M. T. DUFFY, J. P. WITTKE: Appl. Phys. Letters **21**, 358 (1972).
- 6.35. H. F. TAYLOR, W. E. MARTIN, D. B. HALL, V. N. SMILEY: Appl. Phys. Letters **21**, 95 (1972).
- 6.36. W. E. MARTIN, D. B. HALL: Appl. Phys. Letters **21**, 325 (1972).
- 6.37. VINCENT: Top. Meeting on Integ. Opt., 1972 (Opt. Soc. Am., Washington, D.C., 1972).
- 6.38. W. S. C. CHANG, K. W. LOH: Appl. Opt. **10**, 2361 (1971).

- 6.39. S. MIYAZAWA: *Appl. Phys. Letters* **23**, 198 (1973).
- 6.40. I. P. KAMINOW, J. R. CARRUTHERS: *Appl. Phys. Letters* **22**, 326 (1973).
- 6.41. V. RAMASWAMY: *Appl. Phys. Letters* **21**, 183 (1972).
- 6.42. A. A. BALLMAN, H. BROWN, P. K. TIEN, R. J. MARTIN: *J. Crystal Growth* (1974).
- 6.43. P. K. TIEN, R. J. MARTIN, S. C. BLANK, S. H. WEMPLE, L. J. VARNERIN: *Appl. Phys. Letters* **21**, 207 (1972).
- 6.44. D. HALL, A. YARIV, E. GARMIRE: *Appl. Phys. Letters* **17**, 127 (1970).
- 6.45. D. J. CHANNIN: *Appl. Phys. Letters* **19**, 128 (1971).
- 6.46. S. SOMEKH, E. GARMIRE, A. YARIV, H. GARVIN, R. HUNSPERGER: *Appl. Opt.* **13**, 327 (1974).
- 6.47. S. SOMEKH, E. GARMIRE, A. YARIV, H. GARVIN, R. HUNSPERGER: *Appl. Opt.* **12**, 455 (1973).
- 6.48. A. R. GOODWIN, D. H. LOVELACE, P. R. SELWAY: *Opto-Electronics* **4**, 311 (1972).
- 6.49. F. A. BLUM, K. L. LAWLEY, W. C. SCOTT, W. C. HOLTON: *Appl. Phys. Letters* **24**, 430 (1974).
- 6.50. J. C. TRACY, W. WIEGMAN, R. A. LOGAN, F. K. REINHART: *Appl. Phys. Letters* **22**, 511 (1973).
- 6.51. A. Y. CHO, F. K. REINHART: *Appl. Phys. Letters* **21**, 355 (1972).
- 6.52. S. SOMEKH, E. GARMIRE, A. YARIV, H. GARVIN, R. HUNSPERGER: *Appl. Phys. Letters* **22**, 46 (1973).
- 6.53. H. FUTURA, H. NODA, A. IHAYA: "Digest of Technical Papers." Topical Meeting on Integ. Opt. 1974 (Opt. Soc. Am., Washington, D.C., 1974), p. WB4.
- 6.54. F. K. REINHART, R. A. LOGAN, T. P. LEE: *Appl. Phys. Letters* **24**, 270 (1974).
- 6.55. See, for example, L.A. D'ASARO: *Physics and Technology of Semiconductor Light Emitters and Detectors*, edited by A. PROVA (North-Holland Publishing Co., Amsterdam, 1973).
- 6.56. R. K. WATTS: *J. Appl. Phys.* **44**, 5635 (1973).
- 6.57. H. GARVIN, E. GARMIRE, S. SOMEKH, H. STOLL, A. YARIV: *Appl. Opt.* **12**, 455 (1973).
- 6.58. H. W. YEN, M. NAKAMURA, E. GARMIRE, S. SOMEKH, A. YARIV, H. L. GARVIN: *Optics Commun.* **9**, 35 (1973).
- 6.59. M. NAKAMURA, H. YEN, A. YARIV, E. GARMIRE, S. SOMEKH, H. L. GARVIN: *Appl. Phys. Letters* **23**, 224 (1973);
see also M. NAKAMURA, A. YARIV, H. W. YEN, S. SOMEKH, H. L. GARVIN: *Appl. Phys. Letters* **22**, 515 (1973).
- 6.60. C. V. SHANK, R. V. SCHMIDT: *Appl. Phys. Letters* **23**, 154 (1973).
- 6.61. G. H. B. THOMPSON, P. A. KIRKBY: *Electronics Letters* **9**, 295 (1973).
- 6.62. M. NAKAMURA, K. AIKI, J. UMEDA, A. YARIV, H. W. YEN, T. MORIKAWA: *Appl. Phys. Letters* **24**, 466 (1974).
- 6.63. See, for example, A. YARIV: *Quantum Electronics* (John Wiley & Sons, New York, 1967), p. 310.
- 6.64. S. M. SZE: *Physics of Semiconductor Devices* (John Wiley & Sons, New York, 1969).
- 6.65. F. K. REINHART, B. I. MILLER: *Appl. Phys. Letters* **20**, 36 (1972).
- 6.66. P. K. CHEO: *Appl. Phys. Letters* **23**, 439 (1973).
- 6.67. F. K. REINHART: *J. Appl. Phys.* **39**, 3426 (1968);
F. K. REINHART, D. F. NELSON, J. MCKENNA: *Phys. Rev.* **177**, 1208 (1969).
- 6.68. E. GARMIRE, H. STOLL: *IEEE J. Quant. Electr. QE-8*, 763 (1972).
- 6.69. F. K. REINHART: *Appl. Phys. Letters* **22**, 372 (1973).
- 6.70. M. CHOWN, A. R. GOODWIN, D. F. LOVELACE, G. H. B. THOMPSON, P. R. SELWAY: *Electron. Letters* **9**, 34 (1973).
- 6.71. D. B. OSTROWSKY, R. POIRIER, L. M. REIBER, C. DEVERDUN: *Appl. Phys. Letters* **22**, 463 (1973).

- 6.72. G. E. STILLMAN, C. M. WOLFE, A. G. FOYT, W. T. LINDLEY: *Appl. Phys. Letters* **24**, 8 (1974);
C. M. WOLFE, G. E. STILLMAN, I. MELNGAILIS: "Digest of Technical Papers." Topical Meeting on Integrated Optics, 1974 (Opt. Soc. of Am., Washington, D.C., 1974), p. MA8;
G. E. STILLMAN, C. M. WOLFE, I. MELNGAILIS: "Digest of Technical Papers", Topical Meeting on Integrated Optics, 1974 (Opt. Soc. of Am., Washington, D.C., 1974) p. MA9.
- 6.73. H. M. STOLL, A. YARIV, R. HUNSPERGER, E. GARMIRE: "Digest of Technical Papers". Topical Meeting on Integrated Optics, 1974 (Opt. Soc. of Am., Washington, D.C., 1974) p. THA9.
- 6.74. H. STOLL, A. YARIV, R. HUNSPERGER, G. TANGONAN: *Appl. Phys. Letters* **23**, 664 (1973).
- 6.75. P. K. TIEN, R. J. MARTIN, G. SMOLINSKY: *Appl. Optics*, **12**, 1909 (1973).
- 6.76. G. H. B. THOMPSON, P. A. KIRKBY: *J. Crystal Growth* **27**, 70 (1974).
- 6.77. Typical growth compositions for double heterostructure lasers grown at Standard Telecommunication Laboratories, Harlow, England, P.R. SELWAY (private communication).
- 6.78. E. PINKAS, B. I. MILLER, I. HAYASHI, P. W. FOY: *J. Appl. Phys.* **43**, 2827 (1972);
J. M. BLUM, K. K. SHIH: *J. Appl. Phys.* **43**, 1394 (1972);
H. F. LOCKWOOD, M. ETTERBERG: *J. Crystal Growth* **15**, 81 (1972).
- 6.79. J. M. HAMMER, W. PHILLIPS: *Appl. Phys. Letters* **24**, 545 (1974).
- 6.80. F. A. BLUM, D. W. SHAW, W. C. HOLTON: *Appl. Phys. Letters* **24**, July 15 (1974).
- 6.81. L. COMERFORD, P. ZORY: *Appl. Phys. Letters* **25**, 208 (1974).
- 6.82. C. V. SHANK, R. V. SCHMIDT, B. I. MILLER: *Appl. Phys. Letters* **25**, 203 (1974).
- 6.83. D. R. SCIFRES, R. D. BURNHAM, W. STREIFER: *Appl. Phys. Letters* **25**, 203 (1974).

7. Recent Advances in Integrated Optics

T. TAMIR

The purpose of this chapter is to briefly review the advances that have occurred since 1975 in most of the areas covered by the preceding chapters. Consistent with the material covered by this book, the emphasis here is on planar structures, with fiber-optics components and technology being referred to only if they bear directly on some of the topics reviewed below.

7.1 General Aspects

Considerable progress has been made in the sophistication, fabrication and in the theoretical analysis of planar passive and active components during the last four years. However, most of the components developed during this period rely on the same basic principles and general phenomenological aspects that are presented in the preceding chapters. To obtain a good flavor of the progress made, the reader is advised to scan the proceedings of pertinent conferences [7.1–5] and to refer to special journal issues [7.6–7] that have appeared since 1975.

Due to the strong continued interest shown by scientists from many disciplines, the demand for descriptive papers on integrated optics has motivated a number of tutorial reviews covering general [7.8–11] or specialized [7.12–14] aspects of this area. Several books that bear on specific topics of the integrated-optics area have also been published [7.15–18].

7.2 Passive Components

Interest in producing optical waveguides with lower losses has motivated studies into guiding configurations that show desirable absorption and dispersion characteristics. While two-dimensional multi-layer waveguides have been investigated [7.19–26] in order to better understand their guiding properties, special attention has been paid to anisotropic media [7.27–30] because of their potential for modulation and mode

conversion, and to metal-clad waveguides [7.31–34] which may serve as polarizers. However graded-index waveguides [7.35–46] and three-dimensional waveguides having strip or other specialized cross-sections [7.47–58] have been studied more extensively because of their greater suitability for use on small integrated-optics “chips”. The fabrication of the various optical waveguides has also been reported [7.59–67] in considerable detail.

The problems associated with joining two separate waveguides have been explored. In particular, the step discontinuity that appears when two waveguides of different height or width are connected has been estimated [7.68–71]. While the adverse effects of such a discontinuity can be reduced by tapers, studies of such tapers have revealed [7.72–76] that considerable mode conversion may occur unless proper design is enforced. Different discontinuities, such as waveguide bends [7.77–81], branches [7.82–85] and other related transitional configurations [7.86–92] have also been studied.

To avoid an abrupt transition from one waveguide to another, the method of transferring energy by co-directional coupling has been further explored [7.93–101], and the advantages of using tapered rather than constant coupling have been demonstrated [7.95, 96, 99]. Various fabrication methods for producing suitable transitions between wave-guiding regions have also been developed [7.101–107].

Beam-to-waveguide couplers have continued to attract considerable attention [7.108–130] because of their basic function in coupling a laser beam into a planar structure. As prism couplers had already been well developed by 1975, only a few studies have been concerned with them [7.109–111]. In contrast, grating couplers have been considered much more extensively [7.112–130] because of greater difficulties in the design and fabrication of this beam-coupler device. However, recent work has shown [7.118, 122–126] that, by choosing gratings with suitably blazed asymmetric profiles, it is possible to achieve a very efficient beam coupler whose operation compares well with that of a prism coupler. As recent fabrication techniques of such gratings have greatly improved [7.130–137], the construction of such blazed gratings now appears realistic [7.130, 135, 137].

Another function of dielectric gratings is to serve as frequency filters [7.138–140], but filtering action was achieved also by means of selective co-directional coupling [7.141–143]. It should also be noted that recent work on gratings having variable periodicity [7.13, 140] opens up intriguing possibilities for both frequency and spatial discrimination of signals by means of dielectric gratings.

Perhaps the most difficult coupling problem is that of transferring optical energy from a planar waveguide to a fiber. As this poses a very serious challenge to the implementation of integrated-optics systems, a

number of investigations were addressed to overcome that problem [7.144–157]. At this stage, no serious obstacles appear to exist in connecting multi-mode planar waveguides to multi-mode fibers. However, if one of these two guiding structures is single-mode, a satisfactory solution is still being sought for a connection that is sufficiently efficient, strong and reliable for practical use outside the laboratory.

A component that has recently attracted greater attention than in the past is the integrated-optics lens, which takes the form of an appropriate change in the thin-film waveguide and/or the substrate. While several lens shapes were explored [7.158–166], it was shown that geodesic lenses [7.158–161] are very effective in discriminating between guided beams that are only slightly divergent from each other. As the spherical aberration introduced by such lenses can be made negligible, they are excellent candidates for data processing using multi-beam techniques [7.160].

7.3 Active Components

Because it was found quite early that they can operate at room temperature [1.42–45, 7.160–162] and their small size makes them easily suitable for integration on small chips, semiconductor lasers have generated a very large amount of research papers since 1975, probably more than any other components in the integrated-optics area. Consequently only a small sampling of these papers can be given here [7.12, 13, 167–212].

Amongst the many varieties of heterostructure lasers, the distributed feedback (DFB) and the distributed Bragg reflection (DBR) structures have shown great promise for simple operation, spectrally pure laser output and possibly small sensitivity to wavelength variation with temperature [7.188, 195–208]. In the DFB laser, a periodic waveguide (usually, a corrugated film) forms an integral part of the active lasing region and serves to stabilize the laser operation because the wavelength and period dimensions must comply with a Bragg condition [7.13, 174, 188, 195–200]. The DBR laser also contains a periodic portion, but this is now outside the active region; thus, the DBR laser consists of a lasing region with the end mirrors being replaced by periodic waveguides which provide total reflection at wavelengths satisfying a Bragg condition [7.13, 200–208].

One difficulty with heterostructure laser outputs is that the outgoing beam has rather large vertical divergence due to the small height of the active film. This has been circumvented in twin-line lasers [7.209–213] that consist of two coupled waveguides, of which one is a thin active

waveguide whereas the other serves as a passive output waveguide which is relatively thick. Thus, the energy generated by the thin active guide is coupled to the passive thick guide, which can produce an output beam with considerably smaller divergence.

Detectors have usually been studied in conjunction with semiconductor laser investigations and results have been reported on in a few papers [7.177, 213, 261].

Intensive work has also continued in the development of faster broadband modulators, switches and beam deflectors. In this context, considerable progress has been made with devices using Bragg-type acousto-optic interactions [7.214–218], which also include schemes for achieving convolution of two separate acoustic signals [7.219]. However, because of their lower power requirements and faster possible speed, more attention has been paid to devices using the electro-optic effect [7.220–252].

Most electro-optic switches consist of two or more sections of coupled waveguides [7.223–230], which are often subject to cross-talk because of the sensitivity to the coupling length and to other waveguide parameters. However, by dividing each of the waveguides into separate sections to which different switching voltages are applied, it was found possible [7.224, 255] to achieve very reliable configurations having a crossover ratio of better than 26 dB. This so-called $\Delta\beta$ -reversal technique has stimulated the development of an impressive array of switching devices [7.227, 229, 236, 237], which include an efficient switch and amplitude modulator [7.252] having data rates in excess of $100 \text{ mbit}\cdot\text{s}^{-1}$ with drive voltages as low as 3 V. Other electro-optic switches rely on different mechanisms to implement the switching action, such as bifurcation [7.232, 238], mirror action [7.233] or total internal reflection [7.234, 235], and others [7.239, 241].

Although the stress on switches has been motivated by orientation towards digital processing, amplitude modulators have also been developed [7.243–257]. While most of these are also based on electro-optic interactions [7.243–252], other mechanisms have been considered, including electrostriction [7.253], liquid-crystal waveguides [7.254], electro-absorption [7.256] and opto-optic interactions [7.257]. Devices for analog-to-digital conversion of signals have also been explored [7.258, 259].

7.4 Integration and Other Aspects

The aim of producing a fully integrated optical system on a small wafer (or “chip”) is still being pursued as a goal for the integrated-optics area. However, efforts at integrating many varieties of operational components

on a single chip are still at the laboratory stage. Nevertheless, very promising results have already been obtained, particularly with subsystems involving GaAs materials [7.14, 260–265]. The obstacles to larger-scale integration occur because heterostructure lasers are based primarily on GaAs compounds whereas switches, modulators and passive components are more effectively fabricated in other materials that are less lossy and/or provide stronger electro-optic effects, such as LiNbO₃.

It is therefore very likely that the solution for large-scale integrated systems will be provided by hybrid integration, which involves two or more materials that may be bonded together [7.14]. Alternatively, integrated optics may be restricted to monofunctional chips, which involve many elements of a single variety (such as switches), rather than more complex multifunctional chips which include many or all varieties of components [7.10]. Of course, the answer still lies with the materials technology that will be developed in the near future.

Apart from the immediate needs dictated by optical communications, integrated-optics research has meanwhile directly generated a broad spectrum of other components characterized by guided light [7.266–270] and even x-rays [7.271]. In addition, integrated optics has played a creative role in related studies, such as wave interaction in passive and active periodic media [7.272–275], which were probably stimulated by Bragg-type interactions in distributed-feedback lasers.

In this context, perhaps one of the most interesting and intriguing areas is the transmission and reconstruction of images passing through long fibers. While its beginnings may be traced to image transmission through simple optical waveguides [7.276–278], this area of research now combines holographic techniques with the nonlinear mixing of several wave components in an attempt to achieve real-time three-dimensional reconstruction of images that have passed through long and dispersive optical channels [7.279–284].

References

- 7.1. Tech. Digest, 1976 Topical Meeting on Integrated Optics, Salt Lake City, Utah, USA (Opt. Soc. Am., 1976).
- 7.2. 1976 IEEE International Semiconductor Laser Conference, Special Issue of IEEE J. QE-13, 553 (1977).
- 7.3. Proc. AGARD/NATO Symp. Optical Fibers, Integrated Optics and Their Military Applications, London, England (1977).
- 7.4. Tech. Digest, 1977 Intern. Conf. Integrated Optics and Optical Fiber Communication, Tokyo, Japan (1977).
- 7.5. Tech. Digest, 1978 Topical Meeting on Integrated and Guided Wave Optics, Salt Lake City, Utah, USA (Opt. Soc. Am., 1978).
- 7.6. Special Issue on Integrated Optics. IEEE J. QE-13, 121 (1977).

- 7.7. Special Issue on Devices for Optical-Fiber Communications, IEEE J. QE-**14**, 789 (1978).
- 7.8. E. M. CONWELL: Integrated optics. Phys. Today **29**, 48 (May 1976).
- 7.9. P. K. TIEN: Integrated optics and new wave phenomena in optical waveguides. Rev. Mod. Phys. **49**, 361 (1977).
- 7.10. H. KOGELNIK: Review of integrated optics. Fiber and Int. Optics **1**, 227 (1977).
H. KOGELNIK: Coupled-Wave Devices. Proc. NATO Adv. Study Inst. Fiber and Integrated Optics, Corsica, France (June/July 1978)
- 7.11. A. YARIV: Guided-wave optics. Sci. American **240**, 64 (Jan. 1979).
- 7.12. J. J. DEGNAN: The waveguide laser: A review. Appl. Phys. **11**, 1 (1976).
- 7.13. A. YARIV, M. NAKAMURA: Periodic structures for integrated optics. IEEE J. QE-**13**, 233 (1977).
- 7.14. D. B. ANDERSON: Integrated optical spectrum analyzer: an imminent "chip". IEEE Spectrum **15**, 22 (1978).
- 7.15. J. A. ARNAUD: *Beam and Fiber Optics* (Academic Press, New York 1976).
- 7.16. M. S. SODHA, A. K. GHATAK: *Inhomogeneous Optical Waveguides* (Plenum Publishing, New Delhi 1977).
- 7.17. H. C. CASEY, Jr., M. B. PANISH: *Heterostructure Lasers* (Academic Press, New York 1978).
- 7.18. H. G. UNGER: *Planar Optical Waveguides and Fibers* (Oxford University Press, Oxford 1978).
- 7.19. H. A. HAUS, H. KOGELNIK: Electromagnetic momentum and momentum flow in dielectric waveguides. J. Opt. Soc. Am. **66**, 320 (1976).
- 7.20. P. YEH, A. YARIV, C. S. HONG: Electromagnetic propagation in periodic stratified media. J. Opt. Soc. Am. **67**, 423 (1977).
- 7.21. J. D. LOVE, C. WINKLER: Attenuation and tunneling coefficients for leaky rays in multi-layered optical waveguides. J. Opt. Soc. Am. **67**, 1627 (1977).
- 7.22. P. K. CHEO, R. WAGNER: Infrared electro-optic waveguides. IEEE J. QE-**13**, 159 (1977).
- 7.23. S. MIYANAGA, M. IMAI, T. ASAKURA: Radiation pattern of light scattering from the core region of dielectric-slab-optical waveguides. IEEE J. QE-**14**, 30 (1978).
- 7.24. S. KAWAKAMI, M. IKEDA: Transmission characteristics of a two-mode optical waveguide. IEEE J. QE-**14**, 608 (1978).
- 7.25. C. VASALLO: Radiating normal modes of lossy planar waveguides. J. Opt. Soc. Am. **69**, 311 (1979).
- 7.26. D. O. NORTH: Dielectric-waveguide modal properties. IEEE J. QE-**15**, 17 (1979).
- 7.27. D. MARCUSE: Coupled-mode theory for anisotropic optical waveguides. Bell Syst. Tech. J. **54**, 985 (1975).
- 7.28. V. K. AGRAWAL, Y. MIYAZAKI, Y. AKAO: Analysis of hybrid modes in an optical waveguide bounded at one side by a gyromagnetic medium. Opt. Commun. **16**, 104 (1976).
- 7.29. K. KITAYAMA, N. KUMAGAI: Theory and applications of coupled optical waveguides involving anisotropic or gyrotropic materials. IEEE Trans. MTT-**25**, 567 (1977).
- 7.30. D. MARCUSE: Modes of a symmetric slab optical waveguide in birefringent media. IEEE J. QE-**14**, 736 (1978); QE-**15**, 92 (1979).
- 7.31. Y. YAMAMOTO, T. KAMIYA, H. YANAI: Characteristics of optical guided modes in multi-layer metal-clad planar optical guide with low-index dielectric buffer layer. IEEE J. QE-**11**, 729 (1975).
- 7.32. M. OHTAKA, M. MATSUHARA, N. KUMAGAI: Analysis of the guided modes in slab-coupled waveguides using a variational method. IEEE J. QE-**12**, 378 (1976).
- 7.33. K. NOSU, J. HAMASAKI: The influence of the longitudinal plasma wave on the propagation characteristics of a metal-clad-dielectric-slab waveguide. IEEE J. QE-**12**, 745 (1976).

- 7.34. K. H. ROLLKE, W. SOHLER: Metal-clad waveguide as cutoff polarizer for integrated optics. *IEEE J. QE-13*, 141 (1977).
- 7.35. G. B. HOCKER, W. K. BURNS: Modes in diffused optical waveguides of arbitrary index profile. *IEEE J. QE-11*, 270 (1975).
- 7.36. A. M. SCHEGGI, P. F. CHECCACCI, R. FALCIAI: Dispersion characteristics in quasi-step and graded-index slab waveguides by ray-tracing techniques. *J. Opt. Soc. Am.* **65**, 1022 (1975).
- 7.37. H. F. TAYLOR: Dispersion characteristics of diffused channel waveguides. *IEEE J. QE-12*, 748 (1976).
- 7.38. J. F. LOTSPEICH: A perturbation analysis of modes in diffused optical waveguides. *Opt. Commun.* **18**, 567 (1976).
- 7.39. I. SAVATINOVA, E. NADJAKOV, L. MASHEV: Determination of refractive index profiles in diffused optical waveguides. *Appl. Phys.* **12**, 293 (1977).
- 7.40. A. K. GHATAK, E. KHULAR, K. THYAGARAJAN: Modes in optical waveguides formed by silver-sodium ion exchange. *IEEE J. QE-14*, 389 (1978).
- 7.41. J. HEIBEL, E. VOGES: Index profiles of planar optical waveguides determined from the angular dependence of reflectivity. *IEEE J. QE-14*, 501 (1978).
- 7.42. L. MASHEV: Mode dispersion characteristics of graded-index optical waveguides. *Appl. Phys.* **17**, 189 (1978).
- 7.43. I. P. KAMINOW, L. W. STULTZ: Loss in Ti-diffused LiNbO_3 waveguides. *Appl. Phys. Lett.* **33**, 62 (1978).
- 7.44. L. MASHEV, L. TSONEV, S. MIRONOV, M. GARSIA: Wave propagation in uniaxial graded-index optical waveguides. *Appl. Phys.* **19**, 43 (1979).
- 7.45. A. HARDY: Beam propagation through parabolic-index waveguides with distorted optical axis. *Appl. Phys.* **18**, 223 (1979).
- 7.46. J. D. LOVE, A. K. GHATAK: Exact solutions for TM modes in graded-index slab waveguides. *IEEE J. QE-15*, 14 (1979).
- 7.47. T. R. RANGANATH, W. T. TSANG, S. WANG: Tapered edge ridge waveguides for integrated optics. *Appl. Opt.* **14**, 1847 (1975).
- 7.48. E. GARMIRE, T. McMAHON, M. BASS: Propagation of infrared light in flexible hollow waveguides. *Appl. Opt.* **15**, 145 (1976).
- 7.49. N. UCHIDA: Optical waveguide loaded with high refractive-index strip film. *Appl. Opt.* **15**, 179 (1976).
- 7.50. G. B. HOCKER: Strip-loaded diffused optical waveguides. *IEEE J. QE-12*, 232 (1976).
- 7.51. K. D. LAAKMANN, W. H. STEIER: Characteristic modes of hollow rectangular dielectric waveguides. *Appl. Opt.* **15**, 1334 (1976).
- 7.52. H. KRAMMER: Propagation of modes in curved hollow metallic waveguides for the infrared. *Appl. Opt.* **16**, 2163 (1977).
- 7.53. R. A. STEINBERG, T. G. GIALLORENZI: Modal fields of anisotropic channel waveguides. *J. Opt. Soc. Am.* **67**, 523 (1977).
- 7.54. M. GESHIRO, M. OHTAKA, M. MATSUHARA, N. KUMAGAI: Modal analysis of strip-loaded diffused optical waveguides by a variational method. *IEEE J. QE-14*, 259 (1978).
- 7.55. P. M. PELOSI, P. VANDENBULCKE, C. D. W. WILKINSON, R. M. DE LA RUE: Propagation characteristics of trapezoidal cross-section ridge optical waveguides. *Appl. Opt.* **17**, 1187 (1978).
- 7.56. J. C. CAMPBELL: Tapered waveguides for guided wave optics. *Appl. Opt.* **18**, 900 (1979).
- 7.57. K. OGUSU, S. KAWAKAMI, S. NISHIDA: Optical strip waveguide: an analysis. *Appl. Opt.* **18**, 908 (1979).
- 7.58. T. FINDAKLY, E. GARMIRE, H. T. MOON: Comparison of losses in imperfect surface-diffused and buried optical waveguides. *Optics Lett.* **4**, 149 (1979).

- 7.59. W. T. TSANG, C. C. TSENG, S. WANG: Optical waveguides fabricated by preferential etching. *Appl. Opt.* **14**, 1200 (1975).
- 7.60. M. S. CHANG, W. S. C. CHANG, B. L. SOPORI, H. R. VANN, M. W. MULLER, M. G. CRAFORD, D. FINN, W. O. GROVES, A. H. HERZOG: GaAs optical waveguide structures at 10.6 μm wavelength. *Appl. Opt.* **14**, 1572 (1975).
- 7.61. W. STUTIUS, W. STREIFER: Silicon nitride films on silicon for optical waveguides. *Appl. Opt.* **16**, 3218 (1977).
- 7.62. G. STEWART, C. A. MILLAR, P. J. R. LABOURN, C. D. W. WILKINSON, R. M. DE LA RUE: Planar optical waveguides formed by silver-ion migration in glass. *IEEE J. QE-13*, 192 (1977).
- 7.63. S. VALETTE, G. LABRUNIE, J. C. DEUTSCH, J. LIZET: Planar optical waveguides achieved by ion implantation in zinc telluride. *Appl. Opt.* **16**, 1289 (1977).
- 7.64. B. L. SOPORI, W. S. C. CHANG: Low-loss Na-glass waveguides. *IEEE J. QE-14*, 323 (1978).
- 7.65. G. STEWART, P. J. R. LABOURN: Fabrication of ion-exchanged optical waveguide from dilute silver nitrate melts. *IEEE J. QE-14*, 935 (1978).
- 7.66. W. T. TSANG, A. Y. CHO: Molecular beam epitaxial writing of patterned GaAs epilayer structures. *Appl. Phys. Lett.* **32**, 491 (1978).
- 7.67. L. W. STULTZ: Titanium in-diffused LiNbO₃ optical waveguide fabrication. *Appl. Opt.* **18**, 2041 (1979).
- 7.68. B. RULF: Discontinuity radiation in surface waveguides. *J. Opt. Soc. Am.* **65**, 1248 (1975).
- 7.69. T. E. ROZZI: Rigorous analysis of the step discontinuity in planar dielectric waveguide. *IEEE Trans. MTT-26*, 738 (1978).
- 7.70. T. E. ROZZI, G. H. IN'T VELD: Field and network analysis of interacting step discontinuities in planar dielectric waveguides. *IEEE Trans. MTT-27*, 303 (1979).
- 7.71. K. MORISHITA, S. I. INAGAKI, N. KUMAGAI: Analysis of discontinuities in dielectric waveguides by means of the least squares boundary residual method. *IEEE Trans. MTT-27*, 310 (1979).
- 7.72. A. R. NELSON: Coupling optical waveguides by tapers. *Appl. Opt.* **14**, 3012 (1975).
- 7.73. A. F. MILTON, W. K. BURNS: Mode coupling in optical waveguide horns. *IEEE J. QE-13*, 828 (1977).
- 7.74. W. K. BURNS, A. F. MILTON, A. B. LEE: Optical waveguide parabolic coupling horns. *Appl. Phys. Lett.* **30**, 28 (1977).
- 7.75. T. K. LIM, B. K. GARSIDE, J. P. MARTON: An analysis of optical waveguide tapers. *Appl. Phys.* **18**, 53 (1979).
- 7.76. G. A. TEH, V. C. Y. SO, G. I. STEGEMAN: Tapered block coupling and mode conversion in integrated optics. *IEEE Trans. MTT-27*, 265 (1979).
- 7.77. M. MIYAGI, S. KAWAKAMI, S. NISHIDA: Bending losses of a doubly clad slab waveguide. *Opt. Commun.* **14**, 123 (1975).
- 7.78. E. F. KUESTER, D. C. CHANG: Surface-wave radiation loss from curved dielectric slabs and fibers. *IEEE J. QE-11*, 903 (1975).
- 7.79. M. MIYAGI, S. NISHIDA: Bending losses of dielectric rectangular waveguides for integrated optics. *J. Opt. Soc. Am.* **68**, 316 (1978).
- 7.80. H. F. TAYLOR: Losses at corner bends in dielectric waveguides. *Appl. Opt.* **16**, 711 (1977).
- 7.81. D. MARCUSE: Radiation losses of parabolic-index slabs and fibers with bent axes. *Appl. Opt.* **17**, 755 (1978).
- 7.82. H. YAJIMA: Coupled mode analysis of dielectric planar branching waveguides. *IEEE J. QE-14*, 749 (1978).
- 7.83. H. NAITO, K. MUTO, T. NAKAYAMA: Mirror-type optical branch and switch. *Appl. Opt.* **17**, 101 (1978).

- 7.84. D. R. SCIFRES, R. D. BURNHAM, W. STREIFER: Branching waveguide coupler in a GaAs/GaAlAs injection laser. *Appl. Phys. Lett.* **32**, 658 (1978).
- 7.85. J. L. MERZ, R. A. LOGAN: Dual-beam laser: A GaAs double-cavity laser with branching output waveguides. *Appl. Phys. Lett.* **32**, 661 (1978).
- 7.86. J. T. BOYD, D. B. ANDERSON: Radiation pattern of an end-fire optical waveguide coupler. *Opt. Commun.* **13**, 353 (1975).
- 7.87. R. HERRMANN, J. HERTEL: Mode launching on a multi-mode slab-waveguide by a plane wave. *Appl. Phys.* **9**, 307 (1976).
- 7.88. T. KUROKAWA, S. OIKAWA: Optical waveguide intersections without light leak. *Appl. Opt.* **16**, 1033 (1977).
- 7.89. R. G. HUNTSPELTER, A. YARIV, A. LEE: Parallel end-butt coupling for optical integrated circuits. *Appl. Opt.* **16**, 1026 (1977).
- 7.90. C. VASSALLO: On a rigorous calculation of the efficiency for coupling light power into optical waveguides. *IEEE J. QE-13*, 165 (1977).
- 7.91. Y. K. LEE, S. WANG: Electro-optic guided-to-unguided mode converter. *IEEE J. QE-12*, 273 (1976).
- 7.92. H. YAJIMA: Dielectric bypass waveguide mode order converter. *IEEE J. QE-15*, 482 (1979).
- 7.93. D. MARCUSE: Electro-optic coupling between TE and TM modes in anisotropic slabs. *IEEE J. QE-11*, 759 (1975).
- 7.94. A. F. MILTON, W. K. BURNS: Tapered velocity couplers for integrated optics. *Appl. Opt.* **14**, 1207 (1975).
- 7.95. D. VINCENT, J. W. Y. LIT: Effects of a thin overlying film on optical waveguides and couplers. *J. Opt. Soc. Am.* **66**, 226 (1976).
- 7.96. R. B. SMITH: Analytic solutions for linearly tapered directional couplers. *J. Opt. Soc. Am.* **66**, 893 (1976).
- 7.97. R. T. KERSTEN: A directional coupler with large waveguide separation. *Opt. Commun.* **17**, 124 (1976).
- 7.98. J. C. CAMPBELL, D. W. BELLAVANCE: Monolithic laser/waveguide coupling by evanescent fields. *IEEE J. QE-13*, 253 (1977).
- 7.99. T. FINDAKLY, C. L. CHEN: Optical directional couplers with variable spacing. *Appl. Opt.* **17**, 769 (1978).
- 7.100. M. KOBAYASHI, H. TERUI: Optical demultiplexer using coupling between non-identical waveguides. *Appl. Opt.* **17**, 3253 (1978).
- 7.101. V. RAMASWAMY, R. D. STANLEY: Radiation patterns from parallel, optical waveguide directional couplers - parameter measurements. *Bell Syst. Tech. J.* **57**, 2685 (1978).
- 7.102. R. T. KERSTEN, H. BOROFFKA: Ion implantation into fused quartz for integrated optical circuits. *Opt. Commun.* **17**, 119 (1976).
- 7.103. S. SOMEKH, H. C. CASEY: Dry processing of high resolution and high aspect ratio structures in $\text{GaAs}-\text{Al}_x\text{Ga}_{1-x}\text{As}$ for integrated optics. *Appl. Opt.* **16**, 126 (1977).
- 7.104. K. KURATA, Y. ONO, M. MORIOKA, K. ITO, M. MORI: Near-infrared high-power LED's with $\text{Ga}_{1-x}\text{Al}_x\text{As}$ epitaxially grown junctions. *IEEE J. QE-13*, 525 (1977).
- 7.105. I. LADANY, M. ETTERBERG, H. F. LOCKWOOD, H. KRESSEL: Al_2O_3 half-wave films for long-life cw lasers. *Appl. Phys. Lett.* **30**, 87 (1977).
- 7.106. J. T. BOYD, C. M. CHUANG, C. L. CHEN: Fabrication of optical waveguide taper couplers. *Appl. Opt.* **18**, 506 (1979).
- 7.107. J. L. MERZ, R. A. LOGAN, A. M. SERGENT: GaAs integrated optical circuits by wet chemical etching. *IEEE J. QE-15*, 72 (1979).
- 7.108. R. K. WINN, J. H. HARRIS: Beam coupling to linear waveguides using lens-like waveguide. *Appl. Opt.* **14**, 1213 (1975).
- 7.109. H. HEIBLUM: The prism coupler and the dielectric bend: similarities and anomalous behavior. *IEEE J. QE-12*, 463 (1976).

- 7.110. I. J. KURLAND, H. L. BERTONI: Birefringent prism couplers for thin-film optical waveguides. *Appl. Opt.* **17**, 1030 (1978).
- 7.111. H. KOGELNIK: Coupler equations for tapered beam-to-film couplers and their solutions. *Arch. Elektr. Übertr.* **32**, 191 (1978).
- 7.112. W. STREIFER, D. R. SCIFRES, R. D. BURNHAM: Coupling coefficients for distributed feedback single- and double-heterostructure diode lasers. *IEEE J. QE-11*, 867 (1975).
- 7.113. D. G. DALGOUTTE, C. D. W. WILKINSON: Thin grating couplers for integrated optics. *Appl. Opt.* **14**, 2983 (1975).
- 7.114. J. T. BOYD, K. S. KUO: Composite prism-grating coupler for coupling light into high refractive index thin-film waveguides. *Appl. Opt.* **15**, 1681 (1976).
- 7.115. D. MARCUSE: Exact theory of TE-wave scattering from blazed dielectric gratings. *Bell Syst. Tech. J.* **55**, 1295 (1976).
- 7.116. C. C. GHIZONI, B. U. CHEN, C. L. TANG: Theory and experiment on grating couplers for thin-film waveguides. *IEEE J. QE-12*, 69 (1976).
- 7.117. W. STREIFER, D. R. SCIFRES, R. D. BURNHAM: TM-mode coupling coefficients in guided-wave distributed feedback lasers. *IEEE J. QE-12*, 74 (1976).
- 7.118. W. STREIFER, D. R. SCIFRES, R. D. BURNHAM: Analysis of grating-coupled radiation in GaAs:GaAlAs lasers and waveguides. *IEEE J. QE-12*, 422 and 494 (1976).
- 7.119. W. W. RIGROD, D. MARCUSE: Radiation loss coefficients of asymmetric dielectric waveguides with shallow sinusoidal corrugations. *IEEE J. QE-12*, 673 (1976).
- 7.120. P. H. H. HSIEH, C. G. FONSTAD: Coupling coefficient calculations for lead-tin telluride distributed feedback lasers. *IEEE J. QE-13*, 17 (1977).
- 7.121. W. STREIFER, D. R. SCIFRES, R. D. BURNHAM, R. I. MACDONALD: On grating-coupled radiation from waveguides. *IEEE J. QE-13*, 67 (1977).
- 7.122. T. TAMIR, S. T. PENG: Network methods for integrated-optics devices. *Proc. Intern. Conf. Applic. Holography and Data Processing* (Pergamon Press, Oxford 1977) p. 437.
- 7.123. W. Y. WANG, T. J. DILaura: Bragg effect waveguide coupler analysis. *Appl. Opt.* **16**, 3230 (1977).
- 7.124. D. MARCUSE: Thick dielectric grating on asymmetric slab waveguide. *Bell Syst. Tech. J.* **56**, 329 (1977).
- 7.125. T. TAMIR, S. T. PENG: Analysis and design of grating couplers. *Appl. Phys.* **14**, 235 (1977).
- 7.126. K. C. CHANG, T. TAMIR: Bragg-reflection approach for blazed dielectric gratings. *Opt. Commun.* **26**, 327 (1978).
- 7.127. Y. YAMAMOTO, T. KAMIYA, H. YANAI: Improved coupled mode analysis of corrugated waveguide and lasers. *IEEE J. QE-14*, 245 and 620 (1978).
- 7.128. W. STREIFER, A. HARDY: Analysis of two-dimensional waveguides with misaligned or curved gratings. *IEEE J. QE-14*, 935 (1978).
- 7.129. W. H. LEE, W. STREIFER: Radiation loss calculation for corrugated dielectric waveguides. *J. Opt. Soc. Am.* **68**, 1701 (1978).
- 7.130. T. AOYAGI, Y. AOYAGI, S. NAMBA: High efficiency blazed grating couplers. *Appl. Phys. Lett.* **29**, 303 (1976).
- 7.131. S. AUSTIN, F. T. STONE: Fabrication of thin periodic structures in photoresist. *Appl. Opt.* **15**, 1071 (1976).
- 7.132. S. AUSTIN, F. T. STONE: Thin periodic structures in photoresist: Fabrication and experimental evaluation. *Appl. Opt.* **15**, 2126 (1976).
- 7.133. J. S. WEI, C. C. TANG: Coupling to film waveguide with reusable plastic gratings. *Appl. Opt.* **15**, 289 (1976).
- 7.134. P. K. TIEN: Method of forming novel curved-line gratings. *Optics Lett.* **1**, 64 (1977).
- 7.135. R. L. AAGARD: Design and fabrication of a blazed replica grating coupler for optical waveguides. *Optics Lett.* **1**, 67 (1977).

- 7.136. H. NISHIHARA, Y. HANNA, T. SUHARA, J. KOYAMA: Direct writing of optical gratings using a scanning electron microscope. *Appl. Opt.* **17**, 2342 (1978).
- 7.137. M. K. SHAMS, D. BOTEZ, S. WANG: Preferential chemical etching of blazed gratings in (110)-oriented GaAs. *Optics Lett.* **4**, 96 (1979).
- 7.138. M. MATSUHARA, K. O. HILL, A. WATANABE: Optical waveguide filters: Synthesis. *J. Opt. Soc. Am.* **65**, 804 (1975).
- 7.139. C. S. HONG, J. B. SHELLAN, A. C. LIVANOS, A. YARIV, A. KATZIR: Broadband grating filters for thin-film optical waveguides. *Appl. Phys. Lett.* **31**, 276 (1977).
- 7.140. A. KATZIR, A. C. LIVANOS, J. B. SHELLAN, A. YARIV: Chirped gratings in integrated optics. *IEEE J. QE-13*, 296 (1977).
- 7.141. M. KOBAYASHI, H. TERUI, K. EGASHIRA: Optical-mode filters using coupling between two non-identical waveguides. *Appl. Opt.* **17**, 486 (1978).
- 7.142. R. C. ALFERNES, P. S. CROSS: Filter characteristics of co-directionally coupled waveguides with weighted coupling. *IEEE J. QE-14*, 843 (1978).
- 7.143. R. C. ALFERNES, R. V. SCHMIDT: Tunable optical waveguide directional coupler filter. *Appl. Phys. Lett.* **33**, 161 (1978).
- 7.144. J. GUTTMANN, O. KRUMPHOLZ, E. PFEIFFER: Optical fiber stripline coupler. *Appl. Opt.* **14**, 1225 (1975).
- 7.145. D. VINCENT, J. W. Y. LIT: Film-fiber coupling in integrated optics. *Appl. Opt.* **14**, 1256 (1975).
- 7.146. D. G. DALGOUTTE, R. B. SMITH, G. ACHUTARAMAYYA, J. H. HARRIS: Externally mounted fibers for integrated optics interconnections. *Appl. Opt.* **14**, 1860 (1975).
- 7.147. B. S. KAWASAKI, D. C. JOHNSON: Bulb-ended fiber coupling to LED sources. *Opt. Quantum Electron.* **7**, 281 (1975).
- 7.148. T. OZEKI, B. S. KAWASAKI: Efficient power coupling using taper-ended multi-mode optical fibers. *Electron. Lett.* **12**, 607 (1976).
- 7.149. C. C. TIMMERMAN: Highly efficient light coupling from GaAlAs lasers into optical fibers. *Appl. Opt.* **15**, 2432 (1976).
- 7.150. F. L. THIEL, R. M. HAWK: Optical waveguide cable connection. *Appl. Opt.* **15**, 2785 (1976).
- 7.151. E. WEIDEL: Light coupling problems for GaAs laser-multi-mode fiber coupling. *Opt. Quantum Electron.* **8**, 301 (1976).
- 7.152. J. M. HAMMER, R. A. BARTOLINI, A. MILLER, C. C. NEIL: Optical grating coupling between low-index fibers and high-index film waveguides. *Appl. Phys. Lett.* **28**, 192 (1976).
- 7.153. H. P. HSU, A. F. MILTON: Single-mode coupling between fibers and indiffused waveguides. *IEEE J. QE-13*, 224 (1977).
- 7.154. C. H. BULMER, M. G. F. WILSON: Single-mode grating coupling between thin-film and fiber optical waveguides. *IEEE J. QE-14*, 741 (1978).
- 7.155. G. A. TEH, G. I. STEGEMAN: Coupling from a thin-film to an optical fiber. *Appl. Opt.* **17**, 2483 (1978).
- 7.156. J. C. CAMPBELL: Coupling of fibers to Ti-diffused LiNbO₃ waveguides by butt-joining. *Appl. Opt.* **18**, 2037 (1979).
- 7.157. Y. UEMATSU, T. OZEKI, Y. UNNO: Efficient power coupling between an MH LED and a taper-ended multi-mode fiber. *IEEE J. QE-15*, 86 (1979).
- 7.158. C. M. VERBER, D. W. VAHEY, V. E. WOOD: Focal properties of geodesic waveguide lenses. *Appl. Phys. Lett.* **28**, 514 (1976).
- 7.159. B. U. CHEM, E. MAROM, A. LEE: Geodesic lenses in single-mode LiNbO₃ waveguides. *Appl. Phys. Lett.* **31**, 263 (1977).
- 7.160. D. W. VAHEY, V. E. WOOD: Focal characteristics of spheroidal geodesic lenses for integrated optical processing. *IEEE J. QE-13*, 129 (1977).
- 7.161. W. H. SOUTHWELL: Geodesic optical waveguide lens analysis. *J. Opt. Soc. Am.* **67**, 1293 (1977).

- 7.162. W. H. SOUTHWELL: Inhomogeneous optical waveguide lens analysis. *J. Opt. Soc. Am.* **67**, 1004 (1977).
- 7.163. D. B. ANDERSON, R. L. DAVIS, J. T. BOYD, R. R. AUGUST: Comparison of optical waveguide lens technologies. *IEEE J. QE-13*, 275 (1977).
- 7.164. G. I. HATAKOSHI, S. I. TANAKA: Grating lenses for integrated optics. *Optics Lett.* **2**, 142 (1978).
- 7.165. G. E. BETTS, J. C. BRADLEY, G. E. MARX, D. C. SCHUBERT, H. A. TRENCHARD: Axially symmetric geodesic lenses. *Appl. Opt.* **17**, 2346 (1978).
- 7.166. G. E. BETTS, G. E. MARX: Spherical aberration correction and fabrication tolerances in geodesic lenses. *Appl. Opt.* **17**, 3969 (1978).
- 7.167. I. HAYASHI, M. B. PANISH, P. W. FOY, S. SUMSKI: Junction lasers which operate continuously at room temperature. *Appl. Phys. Lett.* **17**, 109 (1970).
- 7.168. J. J. HSIEH, J. A. ROSSI, J. P. DONNELLY: Room temperature cw operation of GaInAsP/InP double heterostructure diode lasers. *Appl. Phys. Lett.* **28**, 709 (1976).
- 7.169. C. J. NUESE, G. H. OLSEN, M. ETTERBERG, J. J. GANNON, T. J. ZAMEROWSKI: cw room temperature in In_xGa_{1-x} /In $_xGa_{1-x}$ P lasers. *Appl. Phys. Lett.* **29**, 807 (1976).
- 7.170. K. A. SHORE, M. J. ADAMS: The effects of carrier degeneracy on transport properties of the double heterostructure injection laser. *Appl. Phys.* **9**, 161 (1976).
- 7.171. W. STREIFER, R. D. BURNHAM, D. R. SCIFRES: Substrate radiation losses in GaAs heterostructure lasers. *IEEE J. QE-12*, 177 (1976).
- 7.172. V. P. GRIBKOVSKII, V. N. KONONENKO, G. I. RYABTSEV, V. A. SAMOILYUKOVICH: Trapped radiation in injection lasers. *IEEE J. QE-12*, 322 (1976).
- 7.173. D. O. NORTH: Theory of modal character, field structure, and losses for semiconductor lasers. *IEEE J. QE-12*, 616 (1976).
- 7.174. K. AIKI, M. NAKAMURA, J. UMEDA: Frequency multiplexing light source with monolithically integrated distributed-feedback diode lasers. *Appl. Phys. Lett.* **29**, 506 (1976).
- 7.175. K. KAJIYAMA, S. HATA, S. SAKATA: Effects of spontaneous emission on dynamic characteristics of semiconductor lasers. *Appl. Phys.* **12**, 209 (1977).
- 7.176. F. K. REINHART, A. Y. CHO: Al $_y$ Ga $_{1-y}$ As/Al $_x$ Ga $_{1-x}$ As laser structures for integrated optics grown by molecular-beam epitaxy. *Appl. Phys. Lett.* **31**, 457 (1977).
- 7.177. J. L. MERZ, R. A. LOGAN: Integrated GaAs-Al $_x$ Ga $_{1-x}$ As injection lasers and detectors with etched reflectors. *Appl. Phys. Lett.* **30**, 530 (1977).
- 7.178. W. W. ANDERSON: Gain-frequency-current relation for Pb $_{1-x}$ Sn $_x$ Te double heterostructure lasers. *IEEE QE-13*, 532 (1977).
- 7.179. H. PREIER, M. BLEICHER, W. RIEDEL, H. PFEIFFER, H. MAIER: Peltier cooled PbSe double-heterostructure lasers for IR-gas spectroscopy. *Appl. Phys.* **12**, 277 (1977).
- 7.180. E. SAKAKI, L. L. CHANG, R. LUDEKE, C. A. CHANG, G. A. SAI-HALASZ, L. ESAKI: In $_{1-x}$ Ga $_x$ As-GaSb $_{1-y}$ As $_y$ heterojunctions by molecular beam epitaxy. *Appl. Phys. Lett.* **31**, 211 (1977).
- 7.181. F. C. JAIN, J. W. MARCINEC: A single-heterostructure MOS injection laser. *IEEE J. QE-14*, 398 (1978).
- 7.182. J. K. BUTLER, J. B. DELANEY: A rigorous boundary value solution for the lateral modes of stripe geometry injection lasers. *IEEE J. QE-14*, 507 (1978).
- 7.183. D. KATO: High-reflectivity cavity mirrors for high-performance (GaAl)As diode lasers. *IEEE J. QE-14*, 563 (1978).
- 7.184. R. D. DUPUIS, P. D. DAPKUS: Single longitudinal-mode cw room-temperature Ga $_{1-x}$ Al $_x$ As-GaAs channel-waveguide lasers grown by metal-organic chemical vapor deposition. *Appl. Phys. Lett.* **33**, 724 (1978).
- 7.185. H. NAGAI, Y. NOGUCHI: InP-Ga $_x$ In $_{1-x}$ As $_y$ P $_{1-y}$ double-heterostructure for 1.5 μ m wavelength. *Appl. Phys. Lett.* **32**, 234 (1978).

- 7.186. B. I. MILLER, J. H. MCFEE, R. J. MARTIN, P. K. TIEN: Toom-temperature operation of lattice-matched InP/GaInAs/InP double-heterostructure lasers grown by MBE. *Appl. Phys. Lett.* **33**, 44 (1978).
- 7.187. W. T. TSANG, R. A. LOGAN, M. ILEGEMS: High-power fundamental-transverse-mode strip buried heterostructure lasers with linear light-current characteristics. *Appl. Phys. Lett.* **32**, 311 (1978).
- 7.188. T. KURODA, S. YAMASHITA, M. NAKAMURA, J. UMEDA: Channeled-substrate-planar structure distributed-feedback semi-conductor lasers. *Appl. Phys. Lett.* **33**, 173 (1978).
- 7.189. A. THOMPSON: The reliability of a practical $\text{Ga}_{1-x}\text{Al}_x\text{As}$ laser device. *IEEE J. QE-15*, 11 (1979).
- 7.190. R. L. HARTMAN, M. E. SCHUMAKER, R. W. DIXON: Continuously operated double heterostructure lasers with 70 °C lifetimes as long as two years. *Appl. Phys. Lett.* **31**, 756 (1977).
- 7.191. H. KRESSL, M. ETTERBERG, I. LANDANY: Accelerated step-temperature aging of $\text{Al}_x\text{Ga}_{1-x}\text{As}$ heterojunction laser diodes. *Appl. Phys. Lett.* **32**, 305 (1978).
- 7.192. W. T. TSANG, R. A. LOGAN: GaAs- $\text{Al}_x\text{Ga}_{1-x}\text{As}$ strip buried heterostructure lasers. *IEEE J. QE-15*, 451 (1979).
- 7.193. R. D. DUPUIS, P. D. DAPKUS: Preparation and properties of $\text{Ga}_{1-x}\text{Al}_x\text{As-GaAs}$ heterostructure lasers grown by metalorganic chemical vapor deposition. *IEEE J. QE-15*, 128 (1979).
- 7.194. D. R. SCIFRES, W. STREIFER, R. D. BURNHAM: GaAs/GaAlAs diode lasers with angled pumping stripes. *IEEE J. QE-14*, 223 (1978).
- 7.195. H. M. STOLL, D. H. SEIB: Multiply resonant distributed-feedback lasers. *IEEE J. QE-12*, 53 (1976).
- 7.196. C. C. GHIZONI, J. M. BALLANTYNE, C. L. TANG: Theory of optical-waveguide distributed feedback lasers: A Green's function approach. *IEEE J. QE-13*, 843 (1977).
- 7.197. H. A. HAUS, C. V. SHANK: Antisymmetric taper of distributed feedback lasers. *IEEE J. QE-12*, 532 (1976).
- 7.198. K. AIKI, M. NAKAMURA, J. UMEDA: Lasing characteristics of distributed-feedback GaAs-GaAlAs diode lasers with separate optical and carrier confinement. *IEEE J. QE-12*, 597 (1976).
- 7.199. M. A. DIFORTE, M. PAPUCHON, C. PUECH, P. ALLEMAND, D. B. OSTROWSKY: Tunable optically pumped GaAs-GaAlAs distributed-feedback lasers. *IEEE J. QE-14*, 560 (1978).
- 7.200. W. STREIFER, D. R. SCIFRES, R. D. BURNHAM: Coupled wave analysis of DFB and DBR lasers. *IEEE J. QE-13*, 134 (1977).
- 7.201. H. W. YEN, W. NG, I. SAMID, A. YARIV: GaAs distributed Bragg reflector lasers. *Opt. Commun.* **17**, 213 (1976).
- 7.202. M. OKUDA, K. MURATA, K. OONAKA: Optimum design of a distributed Bragg reflector laser with optical loss in the corrugated waveguide. *Opt. Commun.* **16**, 30 (1976).
- 7.203. C. C. TSENG, D. BOTEZ, S. WANG: Optically pumped epitaxial GaAs waveguide lasers with distributed Bragg reflectors. *IEEE J. QE-12*, 549 (1976).
- 7.204. W. NG, A. YARIV: Highly collimated broadside emission from room-temperature GaAs distributed Bragg reflector lasers. *Appl. Phys. Lett.* **31**, 613 (1977).
- 7.205. K. AIKI, N. NAKAMURA, J. UMEDA: A frequency-multiplexing light source with monolithically integrated distributed-feedback diode lasers. *IEEE J. QE-13*, 220 (1977).
- 7.206. S. WANG: Design considerations for the DBR injection laser and the waveguiding structure for integrated optics. *IEEE J. QE-13*, 176 (1977).

- 7.207. T. KAWAMURA, M. YAMANISHI, M. AMEDA, N. MIKOSHIBA: Optically pumped GaAs lasers with two-dimensional Bragg reflectors. *IEEE J. QE-13*, 806 (1977).
- 7.208. M. K. SHAMS, S. WANG: GaAs-GaAlAs LOC-DBR laser with high differential quantum efficiency. *Appl. Phys. Lett.* **33**, 170 (1978).
- 7.209. Y. SUEMATSU, M. YAMADA, K. HAYASHI: Integrated twin-guide AlGaAs laser with multi-heterostructure. *IEEE J. QE-11*, 457 (1975).
- 7.210. H. KAWANISHI, Y. SUEMATSU, K. KISHINO: GaAs-Al_xGa_{1-x}As integrated twin-guide lasers with distributed Bragg reflectors. *IEEE J. QE-13*, 64 (1977).
- 7.211. K. OTSUKA: A proposal on coupled waveguide lasers. *IEEE J. QE-13*, 895 (1977).
- 7.212. M. YAMADA, Y. SUEMATSU: Analysis of an integrated twin-guide laser with coupled-wave theory. *IEEE J. QE-13*, 201 (1977).
- 7.213. K. H. NICHOLS, W. S. C. WANG, C. M. WOLFF, G. E. STILLMAN: GaAs waveguide detectors for 1.06 μm. *Appl. Phys. Lett.* **31**, 631 (1977).
- 7.214. C. S. TSAI, M. A. ALHAIDER, LE T. NGUYEN, B. KIM: Wideband guided-wave acoustooptic using multiple surface acoustic waves. *Proc. IEEE* **64**, 318 (1976).
- 7.215. K. W. LOH, W. S. C. CHANG, W. R. SMITH, T. GRUDKOWSKI: Bragg-coupling efficiency for guided acoustooptic interaction in GaAs. *Appl. Opt.* **15**, 156 (1976).
- 7.216. L. T. NGUYEN, C. S. TSAI: Efficient wideband guided-wave acoustooptic Bragg diffraction. *Appl. Opt.* **16**, 1297 (1977).
- 7.217. Y. NOMURA, M. NUNOSHITA, T. NAKAYAMA: Efficiency of thin-film acoustooptic light deflectors. *Appl. Opt.* **16**, 2729 (1977).
- 7.218. S. K. YAO, C. S. TSAI: Acoustooptic Bragg-diffraction with application to ultrahigh data rate laser communication systems. *Appl. Opt.* **16**, 3032, 3044 (1977).
- 7.219. W. S. C. CHANG, C. S. TSAI, R. A. BECKER, J. W. YAO: Convolution using guided acoustooptical interaction in thin-film waveguides. *IEEE J. QE-13*, 208 (1977).
- 7.220. J. C. CAMPBELL, F. A. BLUM, D. W. SHAW, K. L. LAWLEY: GaAs electrooptic directional-coupler switch. *Appl. Phys. Lett.* **27**, 202 (1975).
- 7.221. W. E. MARTIN: A new waveguide switch/modulator for integrated optics. *Appl. Phys. Lett.* **26**, 562 (1975).
- 7.222. I. P. KAMINOW, L. W. STULZ: A planar electrooptic prism switch. *IEEE J. QE-11*, 633 (1975).
- 7.223. M. PAPUCHON, Y. COMEMBALE, X. MATHIEU, D. B. OSTROWSKY, L. REIBER, A. M. ROY, B. SEJOURNE, M. WERNER: Electrically switched optical directional coupler: COBRA. *Appl. Phys. Lett.* **27**, 289 (1975).
- 7.224. R. V. SCHMIDT, H. KOGELNIK: Electrooptically switched coupler with stepped $\Delta\beta$ reversal using Ti diffused LiNbO₃ waveguides. *Appl. Phys. Lett.* **28**, 503 (1976).
- 7.225. H. KOGELNIK, R. V. SCHMIDT: Switched directional couplers with alternating $\Delta\beta$. *IEEE J. QE-12*, 396 (1976).
- 7.226. R. V. SCHMIDT, L. L. BUHL: Experimental 4×4 optical switching network. *Electron. Lett.* **12**, 575 (1976).
- 7.227. R. A. STEINBERG, T. G. GIALLORENZI: Performance limitations imposed on optical waveguide switches and modulators by polarization. *Appl. Opt.* **15**, 2440 (1976).
- 7.228. V. RAMASWAMY, R. D. STANDLEY: A phased, optical, coupler-pair switch. *Bell Syst. Tech. J.* **55**, 767 (1976).
- 7.229. R. A. STEINBERG, T. G. GIALLORENZI: Design of integrated optical switches for use in fiber data transmission systems. *IEEE J. QE-13*, 122 (1977).
- 7.230. R. A. STEINBERG, T. G. GIALLORENZI, R. G. PRIEST: Polarization-insensitive integrated-optical switches. *Appl. Opt.* **16**, 2166 (1977).
- 7.231. D. H. BELLEVANCE, K. L. LASLEY: GaAlAs Schottky directional-coupler switch. *Appl. Phys. Lett.* **31**, 836 (1977).
- 7.232. M. PAPUCHON, A. M. ROY, D. B. OSTROWSKY: Electrically active optical bifurcation: BOA. *Appl. Phys. Lett.* **31**, 266 (1977).

- 7.233. H. NAITON, S. NODA, K. MUTO, T. NAKAYAMA: Mirror-type optical switch array. *Appl. Opt.* **17**, 3975 (1978).
- 7.234. S. K. SHEEM: Total internal reflection integrated-optics switch. *Appl. Opt.* **17**, 3679 (1978).
- 7.235. C. S. TSAI, B. KIM, F. R. EL-AKKARI: Optical channel waveguide switch and coupler using total internal reflection. *IEEE J. QE-14*, 513 (1978).
- 7.236. E. GARMIRE, S. D. ALLEN, J. MARBURGER, C. VERBER: Multi-mode integrated optical bistable switch. *Optics Lett.* **3**, 69 (1978).
- 7.237. P. S. CROSS, R. V. SCHMIDT, R. L. THORNTON, P. W. SMITH: Optically controlled two channel integrated-optical switch. *IEEE J. QE-14*, 577 (1978).
- 7.238. H. SASAKI, I. ANDERSON: Theoretical and experimental studies on active Y-junctions in optical waveguides. *IEEE J. QE-14*, 883 (1978).
- 7.239. K. YAMANOUCHI, M. YASUMOTO, K. SHIBAYAMA: Optical switching device using leaky surface waves. *IEEE J. QE-14*, 863 (1978).
- 7.240. H. OGAWARA, H. YAMAMOTO: Optical waveguide switch (3×3) for an optical switching system. *Appl. Opt.* **17**, 1182 (1978).
- 7.241. V. RAMASWAMI, M. D. DIVINO, R. D. STANLEY: Balanced bridge modulator switch using Ti-diffused LiNbO_3 strip waveguides. *Appl. Phys. Lett.* **32**, 644 (1978).
- 7.242. H. OGAWARA: Optical waveguide 3×3 switch. *Appl. Opt.* **18**, 510 (1979).
- 7.243. J. F. LOTSPEICH: Modulation-sensitivity enhancement in electro-optic slab waveguides. *J. Opt. Soc. Am.* **65**, 797 (1975).
- 7.244. Y. OHMACHI, J. NODA: Electro-optic light modulator with branched ridge waveguide. *Appl. Phys. Lett.* **27**, 544 (1975).
- 7.245. W. K. BURNS, A. B. LEE, A. F. MILTON: Active branching waveguide modulator. *Appl. Phys. Lett.* **29**, 790 (1976).
- 7.246. T. R. RANGANATH, S. WANG: Ti-diffused LiNbO_3 branched-waveguide modulators: Performance and design. *IEEE J. QE-13*, 290 (1977).
- 7.247. Y. K. LEE, S. WANG: Electro-optic Bragg-deflection modulators. *Appl. Opt.* **15**, 1565 (1976).
- 7.248. J. C. AN, Y. CHO, Y. MATSUO: Electro-optic-distributed Bragg-reflection modulators for integrated optics. *IEEE J. QE-13*, 206 (1977).
- 7.249. M. IZUTSU, Y. YAMANE, T. SUETA: Broad-band traveling-wave modulator using a LiNbO_3 waveguide. *IEEE J. QE-13*, 287 (1977).
- 7.250. G. ARNOLD, P. RUSSER: Modulation behavior of semiconductor lasers. *Appl. Phys.* **14**, 255 (1977).
- 7.251. G. L. TANGONAN, D. L. PERSECHINI, J. F. LOTSPEICH, M. K. BARNOSKI: Electro-optic diffraction modulation in Ti-diffused LiTaO_3 . *Appl. Opt.* **17**, 3259 (1978).
- 7.252. R. V. SCHMIDT, P. S. CROSS: Efficient optical waveguide switch/amplitude modulator. *Optics Lett.* **2**, 45 (1978).
- 7.253. M. S. CHANG: Bragg electrostriction in optical waveguides. *Appl. Opt.* **16**, 1960 (1977).
- 7.254. J. R. WHINNERY, C. HU, Y. S. KWON: Liquid-crystal waveguides for integrated optics. *IEEE J. QE-13*, 262 (1977).
- 7.255. A. R. REISINGER, D. W. BELLEVANCE, K. L. LAWLEY: Intensity modulation in GaAlAs metal-gap channel waveguides. *Appl. Phys. Lett.* **32**, 663 (1978).
- 7.256. J. C. CAMPBELL, J. C. DEWINTER, M. A. POLLACK, R. E. NAHORY: Buried heterojunction electroabsorption modulator. *Appl. Phys. Lett.* **32**, 471 (1978).
- 7.257. R. W. GRAY, L. W. CASPERSON: Opto-optic modulation based on gain saturation. *IEEE J. QE-14*, 893 (1978).
- 7.258. H. F. TAYLOR, M. J. TAYLOR, P. W. BAUER: Electro-optic analog-to-digital conversion using channel waveguide modulators. *Appl. Phys. Lett.* **32**, 559 (1978).
- 7.259. H. F. TAYLOR: An optical analog-to-digital converter - design and analysis. *IEEE J. QE-15*, 210 (1979).

- 7.260. C. P. LEE, S. MARGALIT, A. YARIV: Double-heterostructure GaAs injection lasers on semi-insulating substrates using carrier crowding. *Appl. Phys. Lett.* **31**, 281 (1977).
- 7.261. M. K. SHAMS, H. NAMIZAKI, S. WANG: *p-n* junction detector directly integrated with GaAlAs LOC-DBR laser. *Appl. Phys. Lett.* **32**, 179 (1978).
- 7.262. M. K. SHAMS, H. NAMIZAKI, S. WANG: Monolithic integration of GaAs-GaAlAs light modulators and distributed-Bragg-reflector lasers. *Appl. Phys. Lett.* **32**, 314 (1978).
- 7.263. D. B. ANDERSON, J. T. BOYD, M. C. HAMILTON, R. R. AUGUST: An integrated-optics approach to the Fourier transform. *IEEE J. QE-13*, 268 (1977).
- 7.264. J. T. BOYD, D. B. ANDERSON: Effect of waveguide optical scattering on the integrated optical spectrum analyzer dynamic range. *IEEE J. QE-14*, 437 (1978).
- 7.265. J. T. BOYD, C. L. CHEN: Integrated optical waveguide and charge-coupled device image array. *IEEE J. QE-13*, 282 (1977).
- 7.266. S. YAMAMOTO, Y. OKAMURA, T. MAKIMOTO: Analysis and design of semi-leaky-type thin-film optical waveguide isolator. *IEEE J. QE-12*, 764 (1976).
- 7.267. V. HINKOV, W. SOHLER: Reduced depth polarizer for integrated optics. *Appl. Phys.* **14**, 229 (1977).
- 7.268. M. J. SUN, M. W. MULLER, W. S. C. CHANG: Thin-film waveguide gyrators: a theoretical analysis. *Appl. Opt.* **16**, 2986 (1977).
- 7.269. D. VINCENT, J. W. Y. LIT: Thin-film beam splitter for integrated optics. *J. Opt. Soc. Am.* **67**, 533 (1977).
- 7.270. R. P. KENAN: Theory of crossed-beam diffraction gratings. *IEEE J. QE-14*, 924 (1978).
- 7.271. R. H. PANTELL, P. S. CHUNG: Transmission of x-rays through curved waveguides. *IEEE J. QE-14*, 694 (1978).
- 7.272. S. R. SESADRI: Higher-order wave interactions in a periodic medium. *Appl. Phys.* **10**, 165 (1976).
- 7.273. D. L. JAGGARD: Stability of higher-order Bragg interactions in active periodic media. *Appl. Phys.* **13**, 185 (1977).
- 7.274. S. R. SESADRI: Symmetric first-order Bragg interactions in an active dielectric waveguide. *Appl. Phys.* **15**, 377 (1978).
- 7.275. S. R. SESADRI: Waves in an active medium guided by a reactive surface with reactance of gain modulation. *Appl. Phys.* **14**, 35 (1977).
- 7.276. R. ULRICH: Image formation by phase coincidence in optical waveguides. *Opt. Commun.* **13**, 259 (1975).
- 7.277. A. YARIV: On transmission and recovery of three-dimensional image information in optical waveguides. *J. Opt. Soc. Am.* **66**, 301 (1976).
- 7.278. R. ULRICH, T. KAMIYA: Resolution of self-images in planar optical waveguides. *J. Opt. Soc. Am.* **68**, 583 (1978).
- 7.279. D. M. BLOOM, G. C. BJORKLUND: Conjugate wave-front generation and image reconstruction by four-wave mixing. *Appl. Phys. Lett.* **31**, 592 (1977).
- 7.280. S. M. JENSEN, R. W. HELIWARTH: Observation of the time-reversed replica of a monochromatic optical wave. *Appl. Phys. Lett.* **32**, 166 (1978).
- 7.281. A. YARIV, J. AU YEUNG, D. FEKETE, D. M. PEPPER: Image phase compensation and real-time holography by four-wave mixing in optical fibers. *Appl. Phys. Lett.* **32**, 635 (1978).
- 7.282. A. YARIV: Phase conjugate optics and real-time holography. *IEEE J. QE-14*, 650 (1978).
- 7.283. R. NORMANDIN, G. I. STEGEMAN: Nondegenerate four-wave mixing in integrated optics. *Optics Lett.* **4**, 58 (1979).
- 7.284. R. W. HELIWARTH: Theory of phase-conjugation by four-wave mixing in a waveguide. *IEEE J. QE-15*, 101 (1979).

Additional References with Titles

- D. B. ANDERSON, R. R. AUGUST, J. E. COKER: Distributed feedback double-heterostructure GaAs injection laser with fundamental grating. *Appl. Optics* **13**, 2742 (1974).
- J. A. ARNAUD, A. A. M. SALEK: Guidance of surface waves by multilayer coatings. *Appl. Optics* **13**, 2343 (1974).
- G. D. AUMILLER, E. A. CHANDROSS, W. J. TOMLINSON, H. P. WEBER: Submicrometer resolution replication of relief patterns for integrated optics. *J. Appl. Phys.* **45**, 4557 (1974).
- F. AURACHER, H. H. WITTE: New directional coupler for integrated optics. *J. Appl. Phys.* **45**, 4997 (1974).
- F. AURACHER: A photoresist coupler for optical waveguides. *Optics Comm.*, **11**, 191 (1974).
- A. AZEMA, J. BOTINEAU, F. GIRES, A. SAISY: Low-frequency TM modes guided in a dielectric slab deposited on a conducting substrate. *Appl. Phys.* **19**, 145–147 (1979).
- D. F. BARBE (ed.): *Charge-Coupled Devices*, Topics in Applied Physics, Vol. 38 (Springer, Berlin, Heidelberg, New York 1980).
- M. K. BARNOWSKI, R. G. HUNSPERGER, R. G. WILSON, G. TANGENAN: Proton-implanted GaP optical waveguide. *J. Appl. Phys.* **44**, 1925 (1973).
- F. BERGLER, R. ULRICH: Preparation and characterisation of Ge/GaAs waveguides for 10.6 μm. *Wave Electronics* **1**, 153 (1975).
- F. A. BLUM, D. W. SHAW, W. C. HOLTON: Optical striplines for integrated optical circuits in epitaxial GaAs. *Appl. Phys. Letters* **25**, 116 (1974).
- F. A. BLUM, K. L. LAWLEY, F. H. DOERBECK, W. C. HOLTON: Monolithic GaAs injection mesa lasers with grown optical facets. *Appl. Phys. Letters* **25**, 620 (1974).
- D. P. BORTFELD: Mode-dependent retardation in (Ga, Al)P waveguide modulators. *IEEE J. Quant. Electron.* **QE 11**, 108 (1975).
- D. P. BORTFELD: Analysis of heterojunction optical waveguides with a modulated region smaller than the guide width. *IEEE J. Quant. Electron.* **QE 10**, 551 (1974).
- J. T. BOYD: Totally internally reflecting thin-film optical cavities. *Appl. Optics* **11**, 2635 (1972).
- J. T. BOYD, D. B. ANDERSON: Radiation pattern of an end-fire optical waveguide coupler. *Optics Comm.* **13**, 353 (1975).
- G. B. BRANDT: Two wavelength measurements of optical waveguide parameters. *Appl. Opt.* **14**, 946 (1975).
- G. B. BRANDT: Birefringent coupler for integrated optics. *Appl. Optics* **13**, 1359 (1974).
- L. J. BRILLSON, E. M. CONWELL: Optical guided waves in CdS_xSe_{1-x} diffused layers. *J. Appl. Phys.* **26**, 5289 (1975).

- R. D. BURNHAM, D. R. SCIFRES, W. STREIFER: Low-divergence beams from grating-coupled composite guide heterostructure GaAlAs diode lasers. *Appl. Phys. Letters* **26**, 644 (1975).
- W. K. BURNS, A. F. MILTON: Mode conversion in planar-dielectric separating guides. *IEEE J. Quant. Electron.* **QE 11**, 32 (1975).
- J. I. BUROV, N. THAN, N. V. ANASTASOVA: Reflection, transmission and conversion of acoustic surface waves incident normally onto a quartz wedge with plane Y, X-cut. *Appl. Phys.* **20** (1979, to be published).
- J. I. BUROV, N. THAN, N. V. ANASTASOVA: Optical methods for measuring the amplitude response of surface acoustic wave devices. *Appl. Phys.* **20** (1979, to be published).
- J. C. CAMPBELL, F. A. BLUM, D. W. SHAW: GaAs electro-optic channel-waveguide modulator. *Appl. Phys. Letters* **26**, 640 (1975).
- J. R. CARRUTHERS, I. P. KAMINOW, L. W. STULTZ: Diffusion kinetics and optical wave-guiding properties of outdiffused layers in lithium niobate and lithium tantalate. *Appl. Optics* **13**, 2333 (1974).
- W. M. CATON: Propagation constants in diffused planar optical waveguides. *Appl. Optics* **13**, 2750 (1974).
- W. M. CATON: Electro-optic light modulation in a planar zinc-blende-type crystal waveguide. *J. Appl. Phys.* **46**, 260 (1975).
- W. S. C. CHANG: Integrated optics at 10.6 μm wavelength. *IEEE Trans. Microwave Theory and Tech. MTT* **23**, 31 (1975).
- D. J. CHANNIN, J. M. HAMMER, M. T. DUFFY: Scattering in ZnO sapphire optical waveguides. *Appl. Optics* **14**, 923 (1975).
- P. K. CHEO, M. GILDEN: Microwave modulation of CO₂ lasers in GaAs optical waveguides. *Appl. Phys. Letters* **25**, 272 (1974).
- P. K. CHEO: Thin-film waveguide devices. *Appl. Phys.* **6**, 1 (1975).
- A. Y. CHO, W. C. BALLAMY: GaAs planar technology by molecular beam epitaxy (MBE). *J. Appl. Phys.* **46**, 783 (1975).
- J. J. CLAIR, J. M. C. JONATHAN, J. L. STEHLE: A new device for realization of gratings and modulation grids. *Optics Comm.* **13**, 183 (1975).
- T. W. COLE: An improved acousto-optical light modulator. *Optics Commun.* **13**, 192 (1975).
- E. M. CONWELL: Modes in anisotropic waveguides formed by diffusion. *IEEE J. Quant. Electron.* **QE 10**, 608 (1974).
- J. D. CROW, N. F. BORELLI, T. P. SEWARD, J. CHODAK: Lightguiding in photochromic glasses. *Appl. Opt.* **14**, 580 (1975).
- R. H. DEITCH, E. J. WEST, T. G. GIALLORENZI, J. F. WELLER: Sputtered thin films for integrated optics. *Appl. Optics* **13**, 712 (1974).
- P. DI VITA, R. VANUCCI: Geometrical theory of coupling errors in dielectric optical waveguides. *Optics Commun.* **14**, 139 (1975).
- R. DORNAHUS, G. NIMTZ: "The Properties and Applications of the Hg_{1-x}C_xTe Alloy System", in Springer Tracts in Modern Physics, Vol. 78 (Springer, Berlin, Heidelberg, New York 1976) pp. 1-119.
- W. DUNCAN, C. R. STANLEY: A CdS-Si photodetector for integrated optics. *Optics Comm.* **10**, 371 (1974).
- V. EVTUHOV, A. YARIV: GaAs and GaAlAs devices for integrated optics. *IEEE Trans. Microwave Theory Tech. MTT* **23**, 44 (1975).
- C. ELACHI, C. YEH: Mode conversion in periodically disturbed thin-film waveguides. *J. Appl. Phys.* **45**, 3494 (1974).
- C. ELACHI, C. YEH: Distribution networks and electrically controllable couplers for integrated optics. *Appl. Optics* **13**, 1372 (1974).
- L. B. FEELSEN, S. Y. SHIN: Rays, beams and modes pertaining to the excitation of dielectric waveguides. *IEEE Trans. Microwave Theory Tech. MTT* **23**, 150 (1975).

- D. FINN, W. A. GRAVES, L. G. HELLWIG, M. G. CRAFORD, W. S. C. CHANG, M. S. CHANG, B. C. SOPORI: Low-loss large-area GaAs/GaAsP heterostructure as optical waveguide at 10.6 m. *Optics Comm.* **11**, 201 (1974).
- S. R. FRITSCHE, W. ROTHMUND: Sputtering during ion implantation into gallium arsenide. *Appl. Physics* **7**, 39 (1975).
- H. FURUTA, H. NODA, A. IHAYA: Novel optical waveguide for integrated optics. *Appl. Optics* **13**, 322 (1974).
- K. FURUYA, Y. SUEMATSU: Mode dependent radiation losses of dielectric waveguides with external higher-index layers. *Trans. IECE* **57C**, 411 (1974). In Japanese.
- T. A. GALANTOWICZ: Lineshape measurement for coupling to waveguide modes in the prism-film coupler. *Appl. Optics* **13**, 2525 (1974).
- A. GEDEON: Effective thickness of optical waveguides in tunable directional couplers. *J. Opt. Soc. Am.* **64**, 615 (1974).
- A. GEDEON: Formation and characteristics of graded-index optical waveguides buried in glass. *Appl. Physics* **6**, 223 (1975).
- M. GESHIRO, M. OOTAKA, M. MATSUHARA, N. KUMAGAI: Analysis of wave modes in slab waveguide with truncated parabolic index. *IEEE J. Quant. Electron.* **QE 10**, 647 (1974).
- A. K. GHATAK, K. THYAGARAJAN: Ray and energy propagation in graded-index media. *J. Opt. Soc., Am.* **65**, 169 (1975).
- K. H. HÄGELE, R. ULRICH: Pyroelectric loss measurement in LiNbO₃:Ti guides. *Optics Lett.* **4**, 60 (1979).
- U. HALLER, W. HEROLD, H. OHNSORGE: Problems arising in the development of optical communication systems. *Appl. Phys.* **17**, 115–122 (1978).
- J. HAMASAKI, K. WOSU: A partially-clad-dielectric-slab waveguide for integrated optics. *IEEE J. Quant. Electron.* **QE 10**, 822 (1974).
- A. HARDY: Beam propagation through parabolic-index waveguides with distorted optical axis. *Appl. Phys.* **18**, 223–226 (1979).
- I. HAYASHI: Recent progress in semiconductor lasers—cw GaAs lasers are now ready for new applications. *Appl. Phys.* **5**, 25 (1974).
- M. HEIBLUM, J. H. HARRIS: Analysis of curved optical waveguides by conformal transformation. *IEEE J. Quant. Electron.* **QE 11**, 424 (1975).
- R. D. HENRY: Thin-film optical magnetic mode converters. *Appl. Phys. Letters* **26**, 408 (1975).
- K. O. HILL: Aperiodic distributed parameter waveguides for integrated optics. *Appl. Opt.* **13**, 1853 (1974).
- J. J. HUPERT: Evanescent fields in physics and their interpretations in terms of flow graphs. *Appl. Phys.* **6**, 131 (1975).
- M. IZUTSU, T. SUETA: Coupled mode analysis of light modulation in dielectric waveguides. *Appl. Physics* **5**, 307 (1975).
- A. JACQUES, D. B. OSTROWSKY: The grating coupler: comparison of theoretical and experimental results. *Optics Commun.* **13**, 74 (1975).
- D. L. JAGGARD, A. R. MICKELSON: The reflection of electromagnetic waves from almost periodic structures. *Appl. Phys.* **19**, 405–412 (1979).
- I. P. KAMINOW, V. RAMASWAMY, R. V. SCHMIDT, E. H. TURNER: Lithium niobate ridge waveguide modulator. *Appl. Phys. Letters* **24**, 622 (1974).
- I. P. KAMINOW, W. L. MAMMEL, H. P. WEBER: Metal clad optical waveguides: analytical and experimental study. *Appl. Optics* **13**, 396 (1974).
- I. P. KAMINOW: Optical waveguide modulators. *IEEE Trans. Microwave Theory Tech. MTT* **23**, 57 (1975).
- D. KATA: Nondestructive technique for the precise evaluation of optical waveguides. *Appl. Phys. Letters* **25**, 406 (1974).

- M. KAWABE, H. KOTANI, K. MASUDA, S. NAMBA: Heterostructure $\text{CdS}_{1-x}\text{Se}_x$ -CdS surface lasers for integrated optics. *Appl. Phys. Letters* **26**, 46 (1975).
- S. KAWAKAMI: Relation between dispersion and power-flow distribution in a dielectric waveguide. *J. Opt. Soc. Am.* **65**, 41 (1975).
- R. T. KERSTEN, W. RAUSCHER: Allow-loss thin film optical waveguide for integrated optics made by vacuum evaporation. *Optics Comm.* **13**, 189 (1975).
- R. T. KERSTEN: A new method for measuring refractive index and thickness of liquid and deposited solid thin films. *Optics Comm.* **13**, 327 (1975).
- R.J. KEYES (ed.): *Optical and Infrared Detectors*, Topics in Applied Physics, Vol. 19 (Springer, Berlin, Heidelberg, New York 1977).
- R.H. KINGSTON: *Detection of Optical and Infrared Radiation*, Springer Series in Optical Sciences, Vol. 10 (Springer, Berlin, Heidelberg, New York 1978).
- V.A. KISELEV: Diffraction coupling of radiation into a thin-film waveguide. *Sov. J. Quant. Electron.* **4**, 872 (1975).
- J. KISHIBIKI, H. SASAKI, N. CHUBACHI, N. MIKOSHIBA, K. SHIBAYAMA: Thickness dependence of acousto-optic diffraction efficiency in ZnO-film optical waveguides. *Appl. Phys. Letters* **26**, 362 (1975).
- H.P. KLEINKNECHT, A.E. WIDMER: (GaAl)P optical-waveguide modulators fabricated by liquid-phase epitaxy. *J. Appl. Phys.*, **45**, 3453 (1974).
- H. KOGELNIK, V. RAMASWAMY: Scaling rules for thin film optical waveguides. *Appl. Opt.* **13**, 1857 (1974).
- E.A. KOLOSOVSKY, D.V. PETROV, A.V. TZAREV: Frequency dependence of acoustooptics interaction efficiency in anisotropic graded-index waveguides. *Appl. Phys.* **20** (1979) to be published.
- C.J. KRAMER, M.N. ARAGHI, P. DAS: Real-time convolution using acousto-optic diffraction from surface waves. *Appl. Phys. Letters* **25**, 180 (1974).
- H. KRESSEL (ed.): *Semiconductor Devices for Optical Communication*, Topics in Applied Physics, Vol. 39 (Springer, Berlin, Heidelberg, New York 1980).
- E.F. KUESTER, D.C. CHANG: Propagation, attenuation and dispersion characteristic of inhomogeneous dielectric waveguides. *IEEE MTT* **23**, 98 (1975).
- A. KUMAR, K. THYAGARAJAN, H.K. GHATAK: Modes in inhomogeneous slab waveguides. *IEEE J. Quant. Electron.* **QE 10**, 902 (1974).
- T.K. LIM, B.K. GARSIDE, J.P. MARTON: An analysis of optical waveguide tapers. *Appl. Phys.* **18**, 53–62 (1979).
- H.K.V. LOTSCH: Comments on "Propagating modes of a metal-clad-dielectric-slab waveguide for integrated optics". *IEEE J. QE-9*, 780 (1973).
- J.F. LOTSPEICH: Single-crystal electro-optic thin-film waveguide modulators for infrared laser systems. *Appl. Optics* **13**, 2529 (1974).
- H.F. MAHLEIN, R. OVERBACHER, W. RAUSCHER: An integrated optical TE-TM mode splitter. *Appl. Physics* **7**, 15 (1975).
- W.E. MARTIN: Refractive index profile measurement of diffused optical waveguides. *Appl. Opt.* **13**, 2112 (1974).
- L. MASHEV: Mode dispersion characteristics of graded-index optical waveguides. *Appl. Phys.* **17**, 189–192 (1978).
- L. MASHEV, L. TSONEV, S. MIRONOV, M. GARSIA: Wave propagation in uniaxial graded-index optical waveguides. *Appl. Phys.* **19**, 43–46 (1979).
- A. MATSUDA, H. MIZUNO, T. TAKAYAMA, M. SAITO, M. KIKUCHI: 'Stopping effect' on guided light in As-S by a laser beam. *Appl. Phys. Letters* **24**, 314 (1974).
- M. MATSUHARA, K.O. HILL: Optical waveguide band-rejection filters: design. *Appl. Optics* **13**, 2886 (1974).
- M. MATSUHARA, A. WATANABE: Coupling of curved transmission lines and application to optical directional couplers. *J. Opt. Soc. Am.* **65**, 163 (1975).
- H. MIKELSKIS: Zusammenhang zwischen srunkenform und efficiency holographischer beugungsgitter. *Optik* **39**, 516 (1974).

- R. MITTRA, T. ITOH: A method for measuring the refractive index profile of thin-film waveguides. *IEEE Trans. Microw. Theory Tech. MTT* **23**, 176 (1975).
- M. MIYAGI, S. KAWABAMI, S. NISHIDA: Bending losses of a doubly-clad slab waveguide. *Opt. Comm.* **14**, 123 (1975).
- S. MIYAZAWA, S. FUSHIMI, S. KONDO: Optical waveguide of LiNbO_3 thin film grown by liquid phase epitaxy. *Appl. Phys. Letters* **26**, 8 (1975).
- M. NAKAMURA, K. AIKI, J. UMEDA, A. YARIV, H. W. YEN, T. MORIKAWA: Liquid phase epitaxy of GaAlAs on GaAs substrates with fine surface corrugations. *Appl. Phys. Letters* **24**, 466 (1974).
- M. NAKAMURA, K. AIKI, JUN-ICHI UMEDA: GaAs-Ga_{1-x}Al_xAs double heterostructure distributed-feedback diode lasers. *Appl. Phys. Letters* **25**, 487 (1974).
- A. NISHIWAKI, T. MIZUNO, S. HATTORI: Driving power for light modulators with inter-digital electrodes. *Optics Commun.* **13**, 78 (1975).
- J. NODA, N. UCHIDA, M. MINAKATA, T. SAKU, S. SAITO, Y. OHMACHI: Electro-optic intensity modulation in LiTaO_3 ridge waveguide. *Appl. Phys. Letters* **26**, 298 (1975).
- A. A. OLINER (ed.): *Acoustic Surface Waves*, Topics in Applied Physics, Vol. 24 (Springer, Berlin, Heidelberg, New York 1978).
- D. B. OSTROWSKY, A. M. ROY, J. SEVIN: Integrated optical waveguide examination using anti-Stokes fluorescence. *Appl. Phys. Letters* **24**, 553 (1974).
- M. B. PANISH: Heterostructure injection lasers. *IEEE Trans. Microwave Theory Tech. MTT* **23**, 20 (1975).
- H. PREIER: Recent advances in lead-chalcogenide diode lasers. *Appl. Phys.* **20**, Nov. (1979).
- H.-J. QUEISSER (ed.): *X-Ray Optics, Applications to Solids*, Topics in Applied Physics, Vol. 22 (Springer, Berlin, Heidelberg, New York 1977).
- V. RAMASWAMY: Propagation in asymmetrical anisotropic film waveguides. *Appl. Optics* **13**, 1363 (1974).
- V. RAMASWAMY, R. D. STANLEY: Growth strains and losses in Nb-diffused LiTaO_3 optical film waveguides. *Appl. Phys. Letters* **26**, 10 (1975).
- E. V. K. RAO, D. MOUTONNET: Buried optical waveguides in fused silica by high energy oxygen ion implantation. *J. Appl. Phys.* **46**, 422 (1975).
- F. K. REINHART, R. A. LOGAN: Monolithically integrated AlGaAs double heterostructure optical components. *Appl. Phys. Letters* **25**, 622 (1974).
- F. K. REINHART, R. A. LOGAN: GaAs-AlGaAs double heterostructure lasers with taper-coupled passive waveguides. *Appl. Phys. Letters* **26**, 516 (1975).
- W. W. RIGROD, J. H. MCFEE, M. A. POLLACK, R. A. LOGAN: Index-profile determination of heterostructure GaAs planar waveguides from mode-angle measurements at 10.6 μm wavelength. *J. Opt. Soc. Am.* **65**, 46 (1975).
- R. P. SALATHÉE: Diode lasers coupled to external resonators. *Appl. Phys.* **20**, 1–18 (1979).
- B. SALEH: *Photoelectron Statistics*, Springer Series in Optical Sciences, Vol. 6 (Springer, Berlin, Heidelberg, New York 1978).
- M. SARUWATARI, T. IZAWA: Nd-glass laser with three-dimensional optical waveguide. *Appl. Phys. Letters* **24**, 603 (1974).
- H. SASAKI, J. KUSHIBIKI, N. CHUBACHI: Efficient acousto-optic TE-TM mode conversion in ZnO films. *Appl. Phys. Letters* **25**, 476 (1974).
- I. SAVATINOVA, E. NADJAKOV: Modes in diffused optical waveguides. *Appl. Phys.* **8**, 245–250 (1975).
- I. SAVATINOVA, P. SIMOVA, L. TSONEV: Losses in diffused optical waveguides. *Appl. Phys.* **20** (1979, to be published).
- D. SCHICKETANZ, G. ZEIDLER: GaAs-double-heterostructure lasers as optical amplifiers. *IEEE J. Quant. Electron. QE* **11**, 65 (1975).
- D. R. SCIFRES, R. D. BURNHAM, W. STREIFER: Highly collimated laser beams from electrically pumped SH GaAs/GaAlAs distributed-feedback lasers. *Appl. Phys. Letters* **26**, 48 (1975).

- R. V. SCHMIDT, I. P. KAMINOW: Metal-diffused optical waveguides in LiNbO₃. *Appl. Phys. Letters* **25**, 458 (1974).
- R. V. SCHMIDT, D. C. FLANDERS, C. V. SHANK, R. D. STANDLEY: Narrow-band grating filters for thin-film optical waveguides. *Appl. Phys. Letters* **25**, 651 (1974).
- R. V. SCHMIDT, I. P. KAMINOW: Acousto-optic Bragg deflection in LiNbO₃ Ti-diffused waveguides. *J. Quant. Elec.* **QE 11**, 32 (1975).
- S. R. SESHADRI: Asymmetric first-order Bragg interactions in an active dielectric waveguide. *Appl. Phys.* **17**, 141-149 (1978).
- A. SIMON, R. ULRICH: A fiber-optical interferometer. *Appl. Phys. Lett.* **31**, 77 (1977).
- E. SPILLER, J. S. HARPER: High resolution lenses for optical waveguides. *Appl. Optics* **13**, 2105 (1974).
- R. D. STANDLEY, V. RAMASWAMY: Nb diffused LiTaO₃ optical waveguides: planar and embedded strip guides. *Appl. Phys. Letters* **25**, 711 (1974).
- G. E. STILLMAN, C. M. WOLFE, I. MELNGAILIS: Monolithic integrated In_xGa_{1-x}As Schottky-barrier waveguide photodetector. *Appl. Phys. Letters* **25**, 36 (1974).
- H. M. STOLL, D. H. SEIB: Distributed feedback GaAs homojunction injection laser. *Appl. Optics* **13**, 1981 (1974).
- Y. SUEMATSU, M. YAMADA: Oscillation modes and mode control in semi-conductor lasers with stripe geometry. *Trans. IECE* **57C**, 434 (1974). In Japanese.
- Y. SUEMATSU, M. YAMADA, K. HAYASHI: A multi-hetero-AlGaAs laser with integrated twin guide. *Proc. IEEE* **63**, 208 (1975).
- Y. SUEMATSU, K. FURUYA: Refractive index distribution and group delay characteristics in multimode dielectric optical waveguides. *Trans. IECE* **57C**, 289 (1974). In Japanese.
- Y. SUEMATSU, K. FURUYA: Quasi-guided modes and related radiation losses in optical dielectric waveguides with external higher index surroundings. *IEEE Trans. Microw. Theory Tech.* **MTT 23**, 170 (1975).
- O. I. SZENTESI, E. A. NOGA: Parylene C films for optical waveguides. *Appl. Optics* **13**, 2457 (1974).
- K. TADA, K. HIROSE: A new light modulator using perturbation of synchronism between two coupled guides. *Appl. Phys. Letters* **25**, 561 (1974).
- P. K. TIEN, D. P. SCHINKE, S. L. BLANK: Magneto-optics and motion of the magnetization in a film waveguide optical switch. *J. Appl. Phys.* **45**, 3059 (1974).
- P. K. TIEN, S. RIVA-SANSEVERINO, R. J. MARTIN, G. SMOLINSKY: Two-layered construction of integrated optical circuits and formation of thin-film prisms, lenses and reflectors. *Appl. Phys. Letters* **24**, 547 (1974).
- P. K. TIEN, S. RIVA-SANSEVERINO, R. J. MARTIN, A. A. BALLMAN, H. BROWN: Optical waveguide modes in single-crystalline LiNbO₃-LiTaO₃ solid-solution films. *Appl. Phys. Letters* **24**, 503 (1974).
- P. K. TIEN, G. SMOLINSKY, R. J. MARTIN: Radiation fields of a tapered film and a novel film-to-fiber coupler. *IEEE Trans. Microw. Theory Tech.* **MTT 23**, 79 (1975).
- W. J. TOMLINSON, H. P. WEBER, C. A. PRYDE, E. A. CHANDROSS: Optical directional couplers and grating couplers using a new high-resolution photolocking material. *Appl. Phys. Letters* **26**, 303 (1975).
- J. C. TRACY, L. F. THOMPSON, R. D. HEIDENREICH, J. L. MERZ: Gratings for integrated optics by electron lithography. *Appl. Optics* **13**, 1695 (1974).
- C. S. TSAI, LE T. NGUYEN, S. K. YAO, M. A. ALHAIDER: High-performance acousto-optic guided-light-beam device using two tilting surface acoustic waves. *Appl. Phys. Letters* **26**, 140 (1975).
- W-T. TSANG, S. WANG: Grating masks suitable for ion-beam machining and chemical etching. *Appl. Phys. Letters* **25**, 415 (1974).
- W-T. TSANG, C-C. TSENG, S. WANG: Optical waveguides fabricated by preferential etching. *Appl. Optics* **14**, 1200 (1975).

- C. C. TSENG, W. T. TSANG, S. WANG: A thin film prism as a beam separator for multi-mode guided waves in integrated optics. *Opt. Comm.* **13**, 342 (1975).
- C. C. TSENG, S. WANG: Integrated grating-type Schottky-barrier photodetector with optical channel waveguide. *Appl. Phys. Letters* **26**, 632 (1975).
- S. UEHARA, K. TAKAMOTO, S. MATSUO, Y. YAMAUCHI: Optical intensity modulator with three-dimensional waveguide. *Appl. Phys. Letters* **26**, 296 (1975).
- R. ULRICH: Image forming by phase coincidence in optical waveguides. *Optics Commun.* **13**, 259 (1975).
- R. ULRICH: Light-propagation and imaging in planar optical waveguides. *Nouv. Rev. Opt.* **6**, 253 (1975).
- R. ULRICH, G. ANKELE: Self-imaging in homogeneous planar optical waveguides. *Appl. Phys. Lett.* **27**, 337 (1975).
- R. ULRICH: Representation of codirectional coupled waves. *Optics Lett.* **1**, 109 (1977).
- R. ULRICH: "Integrated Optics", in Proc. 3rd Europ. Conf. Optical Communication (VDE-Verlag, Berlin 1977) pp. 160.
- R. ULRICH, T. KAMIYA: Resolution of self-images in planar optical waveguides. *J. Opt. Soc. Am.* **68**, 583 (1978).
- P. VINCENT, M. NEVIERE: Corrugated dielectric waveguides: A numerical study of the second-order stop-bands. *Appl. Phys.* **20** (1979, to be published).
- A. WAGENDRISTEL: Determination of diffusion profiles in thin film couplers by x-ray diffraction. *Appl. Physics* **7**, 175 (1975).
- R. K. WATTS, M. DE WIT, W. C. HOLTON: Non-oxide chalcogenide glass film for integrated optics. *Appl. Optics* **13**, 2329 (1974).
- J. C. WEBSTER, F. ZERNIKE: Push-pull thin-film optical modulator. *Appl. Phys. Letters* **26**, 465 (1975).
- W. D. WESTWOOD, J. W. Y. LIT: Sectional thin film grating. *J. Opt. Soc. Am.* **64**, 1631 (1974).
- I. O. WILSON, F. K. REINHART: Phase modulation nonlinearity of double-heterostructure p-n junction diode light modulators. *J. Appl. Phys.* **45**, 2219 (1974).
- M. G. F. WILSON, G. A. TEH: Tapered optical directional coupler. *IEEE Trans. Microw. Theory Tech. MTT* **23**, 85 (1975).
- V. E. WOOD, N. F. HARTMAN, C. M. VERBER, R. P. KEVAN: Holographic formation of gratings in optical waveguiding layers. *J. Appl. Phys.* **46**, 1214 (1975).
- L. YANG, J. M. BALLANTYNE: Epitaxial growth over optical gratings on GaAs. *Appl. Phys. Letters* **25**, 67 (1974).
- F. ZERNIKE: Luneburg lens for optical waveguide use. *Opt. Comm.* **12**, 379 (1974).

Further References with Titles (1982 printing)

The following references provide a representative list of publications that have appeared mostly from 1979 to early 1982, as well as a few older articles that have been inadvertently left out in previous editions of this book. Because of the great wealth of papers publishing during the last few years, this list is obviously not complete and the reader is referred to the references included in those papers for greater coverage.

The editor is indebted to Dr. H. KOGELNIK, Bell Telephone Laboratories; Dr. F. J. LEONBERGER, M.I.T. Lincoln Laboratory; and to Prof. C. S. TSAI, University of California at Irvine, for providing a large portion of this bibliography.

- ACKLEY, D. E., ENGLEMANN, R. W. H.: High-power leaky-mode multiple-stripe laser. *Appl. Phys. Lett.* **39**, 27 (1981).
- ALFERNESS, R. C.: Optical directional couplers with weighted coupling. *Appl. Phys. Lett.* **35**, 260 (1979).
- ALFERNESS, R. C.: Polarization-independent optical directional coupler switch using weighted coupling. *Appl. Phys. Lett.* **35**, 748 (1979).
- ALFERNESS, R. C.: Efficient waveguide electrooptic TE↔TM mode converter/wavelength filter. *Appl. Phys. Lett.* **36**, 513 (1980).
- ALFERNESS, R. C.: Guided-wave devices for optical communication. *IEEE J. QE-17*, 946 (1981).
- ALFERNESS, R. C., BUHL, L. L.: Electrooptic waveguide TE↔TM mode converter with low drive voltage. *Opt. Lett.* **5**, 473 (1980).
- ALFERNESS, R. C., BUHL, L. L.: Waveguide electrooptic polarization transformer. *Appl. Phys. Lett.* **38**, 655 (1981).
- ALFERNESS, R. C., ECONOMOU, N. P., BUHL, L. L.: Picosecond optical sampling technique for measuring the speed of fast electrooptic switch/modulators. *Appl. Phys. Lett.* **37**, 597 (1980).
- ALFERNESS, R. C., ECONOMOU, N. P., BUHL, L. L.: Fast compact optical directional coupler switch/modulator. *Appl. Phys. Lett.* **38**, 214 (1981).
- ALFERNESS, R. C., SCHMIDT, R. V., TURNER, E. H.: Characteristics of Ti-diffused LiNbO₃ optical directional couplers. *Appl. Opt.* **18**, 4012 (1979).
- AMMITTAY, A., EINZIGER, P. D., TAMIR, T.: Experimental observation of anomalous electromagnetic absorption in thin-layered media. *Optics Commun.* **37**, 383 (1981).
- ARVIDSSON, G., THYLEN, L.: Electrooptic integrated-optics spectrum analyzer: and experimental investigation. *Appl. Opt.* **21**, 797 (1982).

- AURACHER, F., KELL, R.: Method for measuring the rf modulation characteristics of Mach-Zehnder-type modulators. *Appl. Phys. Lett.* **36**, 626 (1980).
- BARNOSKI, M. K., CHEN, B. U., JOSEPH, T. R., LEE, J. Y. M., RAMER, O. G.: Integrated optic spectrum analyzer. *IEEE Trans. CAS*-**26**, 1113 (1979).
- BAVA, G. P., ORTA, R.: Optical frequency mixing in planar waveguides: influence of crystal orientation. *Appl. Phys. A* **26**, 185 (1981).
- BLAUVELT, H., BAR-CHAIM, N., FEKETE, D., MARGALIT, S., YARIV, A.: AlGaAs lasers with micro-cleaved mirrors suitable for monolithic integration. *Appl. Phys. Lett.* **40**, 289 (1982).
- BLOOM, D. M., MOLLENAUER, L. F., LIN, C., TAYLOR, D. W., DEL GAUDIO, A. M.: Direct demonstration of distortionless picosecond-pulse propagation in kilometer-length optical fibers. *Opt. Lett.* **4**, 297 (1979).
- BOTEZ, D., CONNOLLY, J. C.: Single-mode positive-index cw constricted double-heterojunction large-optical-cavity AlGaAs lasers with low threshold-current temperature sensitivity. *Appl. Phys. Lett.* **38**, 658 (1981).
- BOTEZ, D., HERSKOWITZ, C. J.: Components for optical communication systems: a review. *Proc. IEEE* **68**, 689 (1980).
- BULMER, C. L., SHEEM, S. K., MOELLER, R. P., BURNS, W. K.: High efficiency flip-chip coupling between single-mode fibers and LiNbO₃ channel waveguides. *Appl. Phys. Lett.* **37**, 351 (1980).
- BURNS, W. K., HOCKER, G. B.: End fire coupling between optical fibers and diffused channel waveguides. *Appl. Opt.* **16**, 2048 (1977).
- BURNS, W. K., KLEIN, P. H., WEST, E. J.: Ti-diffusion in Ti:LiNbO₃ planar and channel optical waveguides. *J. Appl. Phys.* **50**, 6175 (1979).
- CAMPBELL, J. C., DE WINTER, J. C., POLLACK, M. A., NAHORY, R. E.: Buried heterostructure electroabsorption modulator. *Appl. Phys. Lett.* **32**, 471 (1978).
- CANCELLIERI, G.: Mode coupling in grated-index optical fibres due to microbending. *Appl. Phys. A* **26**, 51 (1981).
- CARENCO, A., MENIGAUS, L., DELPECH, P.: Multiwave length GaAs rib waveguide directional coupler with stepped $\Delta\beta$ Schotky electrodes. *J. Appl. Phys.* **50**, 5139 (1979).
- CARNEY, J. K., FONSTAD, C. G.: Double-heterojunction laser diodes with multiply segmented contacts. *Appl. Phys. Lett.* **38**, 303 (1981).
- CARTER, A. C., FORBES, N., GOODFELLOW, R. C.: Monolithic integration of optoelectronic, electronic and passive components in GaAlAs/GaAs multilayers. *Electron. Lett.* **14**, 72 (1982).
- CHANG, K. C., SHAH, V., TAMIR, T.: Scattering and guiding of waves by dielectric gratings with arbitrary profiles. *J. Opt. Soc. Am.* **70**, 804 (1980).
- CHANG, K. C., TAMIR, T.: Simplified approach to surface-wave scattering by blazed dielectric gratings. *Appl. Opt.* **19**, 282 (1980).
- CHEN, B., PASTOR, A. C.: Elimination of LiO₂ out-diffusion waveguide in LiNbO₃. *Appl. Phys. Lett.* **30**, 570 (1977).
- CHEN, P. C., YU, K. L., MARGALIT, S., YARIV, A.: Embedded epitaxial growth of low-threshold GaInAsP/InP injection lasers. *Appl. Phys. Lett.* **38**, 301 (1981).
- CHEN, YI-XIN, CHANG, WM. S. C., LAU, S. S., WIELUNSKI, L., HOLMAN, R. L.: Characteristics of LiNbO₃ waveguides exchanged in TINO₃ solution. *Appl. Phys. Lett.* **40**, 10 (1982).
- COHEN, L. G., LIN, C., FRENCH, W. G.: Tailoring zero chromatic dispersion into the 1.5–1.5 μm low loss spectral region of single-mode fibers. *Electron. Lett.* **15**, 334 (1979).
- COLDREN, L. A., IGA, K., MILLER, B. I., RENTSCHLER, J. A.: GaInAsP/InP stripe-geometry laser with a reactive-ion-etched facet. *Appl. Phys.* **37**, 681 (1980).
- COLDREN, L. A., MILLER, B. I., RENTSCHLER, J. A.: Monolithic two-section GaInAsP/InP active-optical-resonator devices formed by reactive ion etching. *Appl. Phys.* **38**, 315 (1981).

- COLOMBINI, E.: Design of thin-film Luneberg lenses for maximum focal length control. *Appl. Opt.* **20**, 3589 (1981).
- CONWELL, E. M., BURNHAM, R. D.: Materials for integrated optics: GaAs. *Am. Rev. Mater. Sci.* **8**, 135 (1978).
- CROSS, P. S., KOGELNIK, H.: Sidelobe suppression in corrugated-waveguide filters. *Opt. Lett.* **1**, 43 (1977).
- CROSS, P. S., SCHMIDT, R. V.: A 1 Gbit/s integrated optical modulator. *IEEE J. QE-15*, 1415 (1979).
- DIXON, R. W.: Current directions in GaAs laser device developments. *Bell. Syst. Tech. J.* **59**, 669 (1980).
- DUTTA, S., JACKSON, H. E., BOYD, J. T.: Reduction of scattering from a glass thin-film optical waveguide by CO₂ laser annealing. *Appl. Phys. Lett.* **37**, 512 (1980).
- DUTTA, S., JACKSON, H. E., BOYD, J. T., HICKERNELL, F. S., DAVIS, R. L.: Scattering loss reduction in ZnO optical waveguides by laser annealing. *Appl. Phys. Lett.* **39**, 206 (1981).
- FEKETE, D., BURNHAM, R. D., SCIFRES, D. R., STREIFER, W., YINGLING, R. D.: Self-aligned GaAs/GaAlAs semiconductor laser with lateral spatial variation in thickness grown by metalorganic-chemical vapor deposition. *Appl. Phys. Lett.* **38**, 607 (1981).
- FEKETE, D., STREIFER, W., SCIFRES, D. R., BURNHAM, R. D.: High-speed laser modulation with integrated optical injection. *Appl. Phys. Lett.* **37**, 975 (1980).
- FINDAKLY, T., GARMIRE, E.: Reduction and control of optical waveguide losses in glass. *Appl. Phys. Lett.* **37**, 855 (1980).
- FUKUMA, M., NODA, J.: Optical properties of Ti-diffused LiNbO₃ strip waveguides and their coupling-to-a-fiber characteristics. *Appl. Opt.* **19**, 491 (1980).
- FUKUMA, M., NODA, J., IWASAKI, H.: Optical properties in titanium-diffused LiNbO₃ strip waveguides. *J. Appl. Phys.* **49**, 3693 (1978).
- GARMIRE, E., EVANS, G., NIESEN, J.: Longitudinal mode control in GaAs lasers using a three-mirror active-passive cavity. *Appl. Phys. Lett.* **39**, 789 (1981).
- GAYLORD, T. K., MOHARAM, M. G.: Planar dielectric grating diffraction theories. *Appl. Phys. B* **28**, 1 (1982).
- GIBBS, H. M., McCALL, S. L., VENKATESAN, T. N. C.: Optical bi-stability. *Optics News* **5**, 6 (1979).
- GLASS, A. M., KAMINOW, I. P., BALLMAN, A., OLSON, D. H.: Absorption loss and photo-refractive index change in T_k ; LiNbO₃ crystals and waveguides. *Appl. Opt.* **19**, 276 (1980).
- GOLDBERG, L.: Interferometric method for measuring the diffused channel waveguide-index profile. *Appl. Opt.* **20**, 3580 (1981).
- GRUSS, A., TAM, K. T., TAMIR, T.: Blazed dielectric gratings with high beam-coupling efficiencies. *Appl. Phys. Lett.* **36**, 523 (1980).
- HAAVISTO, J., PAJER, G. A.: Resonance effects in low-loss ring waveguides. *Opt. Lett.* **5**, 510 (1980).
- HAMMER, J. M., BOTEZ, D., NEIL, C. C., CONNOLLY, J. C.: High-efficiency high-power butt coupling of single-mode diode lasers to indiffused LiNbO₃ optical waveguides. *Appl. Phys. Lett.* **39**, 943 (1981).
- HARDER, C., LAU, K. Y., YARIV, A.: Bistability and pulsations in cw semiconductor lasers with a controlled amount of saturable absorption. *Appl. Phys. Lett.* **39**, 382 (1981).
- HAUS, H. A., FONSTAD, C. G., JR.: Three-waveguide couplers for improved sampling and filtering. *IEEE J. QE-17*, 2321 (1981).
- HAUS, H. A., HO, P. T.: Effect of noise on active mode-locking of a diode laser. *IEEE J. QE-15*, 1258 (1979).
- HAUS, H., KIRSCH, S., MATHYSSEK, K., LEONBERGER, F. L.: Picosecond optical sampling. *IEEE J. QE-16*, 870 (1980).

- VON HELMOLT, C. H.: Integrated optic strip waveguides driven by surface acoustic waves. *J. Opt. Commun.* **4**, 142 (1981).
- HO, P. T.: Comments on host dispersion in ultrashort pulse generation with GaAs lasers. *Solid-State and Electron Dev.* **3**, 246 (1979).
- HONG, C. S., SHELLAN, J. B., LIVANOS, A. C., YARIV, A., KATZIR, A.: Broad-band grating filters for thin-film optical waveguides. *Appl. Phys. Lett.* **31**, 276 (1977).
- HORIKOSHI, Y., FURUKAWA, Y.: Temperature sensitive threshold current of InGaAsP-InP double heterostructure lasers. *Jpn. J. Appl. Phys.* **18**, 809 (1979).
- IEEE Trans. CAS-**26**, No. 12 (1979). Special issue on integrated and guided wave optical circuits and systems.
- IPPEN, E. P., EILENBERGER, D. J., DIXON, R. W.: Picosecond pulse generation by passive modelocking of diode lasers. *Appl. Phys. Lett.* **37**, 367 (1980).
- IZUTSU, M., SHIKAMA, S., SUETA, T.: Integrated optical SSB modulator/frequency shifter. *IEEE J. QE-17*, 2225 (1981).
- KATZ, J., MARGALIT, S., WILT, D., CHEN, P. C., YARIV, A.: Single-growth embedded epitaxy AlGaAs injection lasers with extremely low threshold currents. *Appl. Phys. Lett.* **37**, 987 (1981).
- KEILMANN, F., BAI, Y. H.: Periodic surface structures: frozen into CO₂ laser-melted quartz. *Appl. Phys. A* **28** (August 1982).
- KIM, B., TSAI, C. S.: Thin-film tunable optical filtering using anisotropic and noncollinear acoustooptic interaction in LiNbO₃ waveguides. *IEEE J. QE-15*, 642 (1979).
- KIMURA, T.: Single-mode systems and components for longer wavelengths. IEEE Trans. CAS-**26**, 987 (1979).
- KOGELNIK, H.: Filter response of nonuniform almost-periodic structures. *Bell Syst. Tech. J.* **55**, 109 (1976).
- KOGELNIK, H.: Limits in integrated optics. *Proc. IEEE* **69**, 232 (1981).
- KRESSEL, H. (ed.): *Semiconductor Devices for Optical Communication*, 2nd ed., Topics Appl. Phys., Vol. 39 (Springer, Berlin, Heidelberg, New York 1982).
- KUBOTA, K. et al.: Traveling wave optical modulator using directional coupler LiNbO₃ waveguide. *IEEE J. QE-16*, 754 (1980).
- LEE, C. C., LIAO, K. Y., TSAI, C. S.: Wideband guided-wave acoustooptic Bragg deflector using a tilted-finger chirp transducer. *IEEE J. QE-15*, 1166 (1979).
- LEONBERGER, F. J.: High-speed operation of LiNbO₃ electrooptic interferometric waveguide modulators. *Opt. Lett.* **5**, 312 (1980).
- LEONBERGER, F. J.: Applications of guided-wave interferometers. *Laser Focus* **18**, 125 (1982).
- LEONBERGER, F. J., BOZLER, C. O.: GaAs directional coupler switch with stepped $\Delta\beta$ reversal. *Appl. Phys. Lett.* **27**, 202 (1977).
- LEONBERGER, F. J., BOZLER, C. O., MCCLELLAND, R. W., MELINGAILIS, I.: Oxide-confined GaAs optical waveguides formed by lateral epitaxial growth. *Appl. Phys. Lett.* **38**, 313 (1981).
- LEONBERGER, F. J., DONNELLY, J. P., BOZLER, C. O.: GaAs $p^+n^-n^+$ directional-coupler switch. *Appl. Phys. Lett.* **29**, 652 (1976).
- LEONBERGER, F. J., WOODWARD, C. E., BECKER, R. A.: 4-bit 828 Megasample/s electro-optic guided-wave analog-to-digital converter. *Appl. Phys. Lett.* **40**, 575 (1982).
- LIN, C., KOGELNIK, H., COHEN, L. G.: Optical pulse equalization and low dispersion transmission in single-mode fibers in the 1.3–1.7 μm spectral region. *Opt. Lett.* **5**, 476 (1980).
- MARCATILI, E. A. J.: Optical subpicosecond gate. *Appl. Opt.* **19**, 1468 (1980).
- MARCUSE, D.: Optimal electrode design for integrated optics modulators. *IEEE J. QE-18*, 393 (1982).

- MCKENNA, J., REINHART, F. K.: Double-heterostructure GaAs-Al_xGa_{1-x}¹¹⁰ p-n-junction-diode modulator. *J. Appl. Phys.* **47**, 2069 (1976).
- MIKAMI, O.: LiNbO₃ coupled-waveguided TE/TM mode splitter. *Appl. Phys. Lett.* **36**, 491 (1980).
- MIKAMI, O., NODA, J., FUKUMA, M.: Directional coupler type light modulator using LiNbO₃ waveguides. *Trans. IECE Jpn. E-61*, 144 (1978).
- MIKAMI, O., ZEMBUTSU, S.: Modified balanced-bridge switch with two straight waveguides. *Appl. Phys. Lett.* **35**, 145 (1978).
- MINAKATA, M., SAITO, S., SHIBATA, M., MIYAZAWA, S.: Precise determination of refractive-index changes in Ti-diffused LiNbO₃ waveguides. *J. Appl. Phys.* **49**, 4677 (1978).
- MINAKATA, M.: Efficient LiNbO₃ balanced bridge modulator/switch with ion-etched slot. *Appl. Phys. Lett.* **35**, 40 (1979).
- NAHORY, R. E., POLLACK, M. A., DE WINTER, J.C.: Temperature dependence of InGaAsP double-heterostructure laser characteristics. *Electron. Lett.* **11**, 695 (1979).
- NAKAMURA, M.: Single-mode operation of semiconductor injection lasers. *IEEE Trans. CAS-26*, 1055 (1979).
- NEYER, A., SOHLER, W.: High-speed cutoff modulator using a Ti-diffused LiNbO₃ channel waveguide. *Appl. Phys. Lett.* **35**, 256 (1979).
- NEYER, A., VOGES, E.: High-frequency electrooptic oscillator using an integrated interferometer. *Appl. Phys. Lett.* **40**, 6 (1982).
- NG, W., HONG, C. S., MANASEVIT, H., DAPKUS, P. D.: Low threshold 1.3 μm. GaInAsP/InP buried heterostructure lasers by liquid phase epitaxy and metalorganic chemical vapor deposition. *Appl. Phys. Lett.* **39**, 188 (1981).
- OHMACHI, Y., NODA, J.: LiNbO₃ TE↔TM mode converter using collinear acoustooptic interaction. *IEEE J. QE-13*, 43 (1977).
- OLIVIER, M., PEUZIN, J. P., DANIEL, J. S., CHALLETON, D.: Absorption spectra of garnet films between 1.0 and 1.8 μm by guided wave optical spectroscopy. *Appl. Phys. Lett.* **38**, 79 (1981).
- OLSEN, G. H., NUÈSE, C. J., ETTERBERG, M.: Low-threshold 1.25 μm vapor-grown InGaAsP cw lasers. *Appl. Phys. Lett.* **34**, 262 (1979).
- PUN, E. Y. B., YI-YAN, A.: Fabrication of periodic waveguides by ion exchange. *Appl. Phys. Lett.* **38**, 673 (1981).
- RAMER, O. G.: Single-mode fiber-to-channel waveguide coupling. *J. Opt. Commun.* **4**, 122 (1981).
- RAMER, O. G.: Integrated optic electrooptic modulator electrode analysis. *IEEE J. QE-18*, 386 (1982).
- RAMER, O. G., NELSON, C., MOHR, C.: Experimental integrated optic circuit losses and fiber pigtailing of chips. *IEEE J. QE-17*, 970 (1981).
- RANGANATH, T. R., WANG, S.: Suppression of Li₂O out-diffusion from Ti-diffused LiNbO₃ optical waveguides. *Appl. Phys. Lett.* **30**, 376 (1977).
- REINHART, F. K.: Electroabsorption in Al_yGa_{1-y}As-Al_xGa_{1-x}As double heterostructures. *Appl. Phys. Lett.* **22**, 372 (1973).
- SALATHÉ, R. P.: Diode lasers coupled to external resonators. *Appl. Phys.* **20**, 1 (1979).
- SCHLAAK, H. F.: Optical PCM clock regenerator with integrated optical directional coupler. *J. Opt. Commun.* **3**, 31 (1981).
- SCHMIDT, R. V., ALFERNES, R. C.: Directional coupler switches modulators, and filters using alternating $\Delta\beta$ techniques. *IEEE Trans. CAS-26*, 1099 (1979).
- SCHMIDT, R. V., CROSS, P. S., GLASS, A. M.: Optically induced crosstalk in LiNbO₃ waveguide switches. *J. Appl. Phys.* **51**, 9 (1980).
- SESHADRI, S. R.: Asymmetric first-order Bragg interactions in an active dielectric waveguide. *Appl. Phys.* **17**, 141 (1978).

- SESHADRI, S. R.: Symmetric first-order Bragg interactions in an active dielectric waveguide. *Appl. Phys.* **15**, 377 (1978).
- SESHADRI, S. R.: TE-TE mode coupling at oblique incidence in a periodic dielectric waveguide. *Appl. Phys.* **25**, 211 (1981).
- SESHADRI, S. R.: Three-mode coupling in a passive dielectric waveguide with index modulation. *Appl. Phys.* **23**, 311 (1980).
- SHAKIR, S. A., TURNER, A. F.: Method of poles for multilayer thin film waveguides. *Appl. Phys. A* **28** (August 1982).
- SHARMA, A. B., HALME, S. J., BUTUSOV, M. M.: *Optical Fiber Systems and Their Components*, Springer Ser. Opt. Sci., Vol. 24 (Springer, Berlin, Heidelberg, New York 1981).
- SHELTON, J. C., REINHART, F. K., LOGAN, R. A.: GaAs-Al_xGa_{1-x}As rib waveguide switches with MOS electrooptic control. *Appl. Opt.* **17**, 2548 (1978).
- SHIMA, K., HANAMITSU, K., FUJIWARA, F., TAKUSAGAWA, M.: Buried convex waveguide structure (GaAl)As injection lasers. *Appl. Phys.* **38**, 605 (1981).
- SMITH, P. W.: Hybrid bistable optical devices. *Opt. Eng.* **19**, 456 (1980).
- SPIE Vol. 176, Guided Wave Optical Systems and Devices (1979).
- SUHARA, T., HANADA, Y., NISHIHARA, H., KOYAMA, J.: Monolithic integrated microgratings and photo-diodes for wavelength demultiplexing. *Appl. Phys. Lett.* **40**, 120 (1982).
- TAMIR, T.: Microwave modeling of periodic waveguides. *IEEE Trans. MTT-29*, 979 (1981).
- TAMIR, T.: Guided-wave methods for optical configurations. *Appl. Phys.* **25**, 201 (1981).
- TANGONAN, G. L., BARNOSKI, M. K., LOTSPEICH, J. F., LEE, A.: High optical power capabilities of Ti-diffused LiTaO₃ waveguide modulators. *Appl. Phys. Lett.* **30**, 238 (1977).
- TAYLOR, H. F.: An optical digital-to-analog converter. *Proc. IEEE* **63**, 1524 (1975).
- THIOULOUSE, P., CARENCO, A., GUGLIELMI, R.: High-speed modulation of an electrooptic directional coupler. *IEEE J. QE-17*, 535 (1981).
- THYLEN, L., STENSLAND, L.: Lensless integrated optics spectrum analyzer. *IEEE J. QE-18*, 381 (1982).
- TSAI, C. S.: Guided wave acoustooptic Bragg modulators for wide-band integrated optic communications and signal processing. *IEEE Trans. CAS-26*, 1072 (1979).
- TSAI, C. S., WANG, J. K., LIAO, K. Y.: Acoustooptic time-integrating correlators using integrated optics technology. *SPIE* **180**, 160 (1979).
- TSANG, D. Z., WALPOLE, J. N., GROVES, S. H., HSIEH, J. J., DONNELLY, J. P.: Intracavity loss modulation of GaInAsP diode lasers. *Appl. Phys. Lett.* **38**, 120 (1981).
- TSANG, W. T.: Low current threshold and high lasing uniformity GaAs-Al_xGa_{1-x}As double heterostructure lasers grown by molecular beam epitaxy. *Appl. Phys. Lett.* **34**, 473 (1979).
- TSANG, W. T.: A graded-index waveguide separate-confinement laser with very low threshold and a narrow Gaussian beam. *Appl. Phys. Lett.* **39**, 134 (1981).
- WRIGHT, P. D., NELSON, R. F., WILSON, R. B.: Monolithic integration of InGaAsP heterostructure lasers and electrooptic devices. *IEEE J. QE-18*, 249 (1982).
- YAMADA, S., MINAKATA, M., NODA, J.: Analog-to-digital conversion experiments using a LiNbO₃ balanced bridge modulator. *Appl. Phys. Lett.* **39**, 124 (1981).

Subject Index

- Absorption 166
- Acoustic wave 5, 169, 170
- Acousto-optic devices 169
 - effect 150, 167
 - figure of merit 151
 - interaction 170, 308
 - materials 160
 - properties 152
- Air gap 89, 90, 107
- Alconox 205
- Aluminum 235
- Amorphous materials 251
- Analog-to-digital conversion 308
- Angle
 - , complex 94
 - , critical 17, 87
 - Annealing 249, 276
 - , post-bombardment 216
- Anodization 266
- Aspect ratio 233
- Asymmetry measure 23
- Attenuation 216, 217, 219
 - , acoustic 152
- Auto-collimation 224, 225
- Bandwidth 143, 157, 160, 164, 173, 191
- Beam coupler (see also grating coupler, prism coupler, etc.) 2, 9, 83
 - deflectors 9, 308
 - form 103
 - shaping 107
- Bi-refringence 214
- Blazing effect 118
- Boat 293, 295
- Boundary conditions 30
- Bragg angle 157, 181
 - condition 77, 307
 - diffraction 5, 182
 - effect 91
 - regime 155, 157, 170, 171
- “Branching” waveguide 131
- Carrier concentration 245
- Cleaved mirrors 276
- Chips 306, 309
- Collimated beam 225
- Coupled mode theory 8, 66, 174, 177, 189
- Coupled-wave equations 71, 72, 73
- Coupler 306
 - Couplers, directional 125, 262, 267, 270, 283
 - , grating 4, 84, 90, 261, 306
 - , holographic 119
 - , input 90, 107, 115
 - , ion-implanted channel 283
 - , longitudinal 84
 - , output 90, 107, 115
 - , prism 2, 4, 86, 223, 261, 306
 - , strip guide 185
 - , tapered 118, 261, 291
 - , transverse 84, 90
 - , waveguide 9, 84, 120
- Coupling 262, 273
 - angle 223, 224
 - , co-directional 71, 306
 - coefficients 70, 188, 191
 - constant 75, 186, 187, 267
 - , contra-directional 71, 72
 - , direct 261
 - efficiency 101, 105, 107, 115, 117, 128
 - modulators 185, 189, 194
 - , synchronous 122, 270
 - , tapered 126, 127
- Coupling length, critical 186, 191
- Cross power 38
- Cross-talk 145
- Crystal growth 278
- Crystalline films 252
- Crystals 243
- Cut-off conditions 25, 119, 244, 245
 - frequency 24
- Damage loss 249
- Data-processing 3
- Data system 139

- Depletion region 280
 Detectors 4, 6, 9, 84, 119, 284, 285, 287, 308
 Dielectric rod 2
 Diffracted beams 92
 — — light 157
 Diffraction 167, 169
 — limited 166, 167
 Diffraction limited beam 159
 Diffusion 274, 265, 284, 290
 Dipping 10, 202, 213
 Dispersion relation 47
 Dopants 300
 Drive power requirements 167
 Drive voltages 164
 Duplication methods 238
 4β -reversal technique 308
- Effective mass** 245, 247
Electro-absorption 283, 288
Electro-acoustic effect 5
Electrodes 283
Electro-optic coefficients 148, 150, 178, 180, 195, 308
 — — effect 2, 5, 148, 149, 151, 167, 169, 279
 — — modulation 187
 — — polarization modulators 147
 — — refractive index change 149
 — — scattering 176
 — — waveguide 179
- Ellipsometry** 222
Energy flow 87
 — — flux 94
 — — leakage 127
 — — specific 143, 159, 162, 163, 166, 172, 173, 174, 175, 177, 179, 180, 184, 185, 188, 191, 193
 — — specific acoustic 160
 — — stored 42, 43
Epitaxial growth 286
 — — layer 246, 263
Epitaxy 264
 —, liquid phase 10, 255, 265, 287, 292, 293
 —, molecular beam 265
 —, vapor-phase 5, 273, 287
Epoxy 213, 214
Equilibrium growth 295
Etch mask 237
Etching 232, 235
 —, chemical 263, 274, 275, 287
 —, ion beam 209, 263, 266, 275, 277
 —, sputter 234, 235
Extinction ratio 142, 143, 164, 180
- Faraday rotation** 5, 152, 153, 154, 165, 190
Fibers 6, 7, 192, 193, 307
Films, organo-silicon 213
Filters 84, 133, 306
Focused beam 224, 227
Franz-Keldesh effect 284
Free carrier 244, 246, 247, 250
 — — effects 176
 — — losses 245
Fresnel coefficient 94
 — — formulas 16
Fringes 220
Furnace 293, 297
Fused silica 215, 216
- GaAs** 5, 6, 10, 243, 244, 245, 247, 248, 279, 280, 309
Garnet 190
Goos-Haenchen shift 25
Grating 83, 98, 190, 202, 275, 276, 309
 — — diffraction orders 98
 — — height 113
Grating profile 91, 93
 — —, asymmetric 118
Grating thickness 93
Growth apparatus 293
 — — rates 296
Group velocity 42
Guides (see *waveguides*)
- Half-wave voltage** 150
Hermite-Gaussian functions 55
Hologram 119
Hypergeometric functions 57
- Image transmission** 2, 309
Imbedded channels 265
Imbedding 262
Index (see *refractive index*)
Information content 140
Infra-red 2, 6, 115, 243
Insertion loss 144, 180, 184, 191
Insulators 280
Integration 10, 290, 308
 —, hybrid 309
Interaction, volume of 168, 169
Interdigital grating 197
Interferometric microscope 220
Interferometry, multiple-beam 221
 —, two-beam 220, 221
Ion beam 234
 — — sputtering 273

- Ion bombardment 216, 235, 284
- — implantation 10, 202, 215, 248, 251, 289
- — migration 10, 202, 214
- Iron-garnets 260
- Isolation layer 252
- Junction 99
- Kerr effect 148
- — liquid waveguide 181
- Kundt constant 153
- Laser 9, 84, 307
 - beam 83, 84
 - , distributed-feedback 275, 277, 279, 307
 - , double heterostructure 275, 278, 309
 - , dye 5
 - , GaAs 248
 - , heterostructure 5, 248, 252, 271, 284, 307
 - , mesa 5, 9, 124, 263, 273
 - , twin-line 307
- Lead silica glass 214
- Leakage, slow 97
- Leaky guide 256
- Leaky wave 83, 93
 - —, backward 99, 111
 - —, forward 99
- Lens 307
 - , geodesic 307
- Light modulator (see modulators)
- Liquid crystals 148
- Lithography 233
 - , x-ray 239
- Lorentz reciprocity theorem 36
- Loss, attenuation 283
- Losses 265
 - , absorption 246, 248, 266
 - , free carrier 249
 - , radiation 96, 132, 253
- “m-lines” 101, 217
- Magneto-optic effect 5, 152, 167, 169
 - — waveguide 189
- Mask 213, 235
- Masking, shadow 265
- Material composition 251
- Maxwell's equations 29
- Measure of merit 141, 143
- Melt 293, 296
- Mesa laser (see laser, mesa)
- Metal coating 221, 233
- Metal semiconductor junctions 280
- Michelson interferometer 220
- Microwaves 1
- Modal equation 230, 231
- Mode conversion 78, 305, 306
- Mode converters 9, 84, 120, 128, 176, 189
 - —, electro-optic 176
- Mode coupling 88
 - — expansion 37
 - — filter 284
 - — number 20
 - — orthogonality 35
- Modes 244
 - , anti-symmetric 244
 - , coupled 120
 - , evanescent 32
 - , guided 25, 32
 - , number of
 - , radiation 19, 32, 45, 85, 87, 131, 253
 - , symmetric 244
 - , TE 46
 - , TM 50
- Modulation 2, 5, 9, 140
 - , amplitude 145, 185
 - , cut-off 283
 - , electro-optic 280
 - , frequency 147, 156
 - , intensity 161, 282
 - , phase 146, 176, 282
 - , polarization
- Modulation depth 141, 142, 157, 162, 163, 165
 - —, maximum 142
- Modulator 4, 9, 139, 233, 279, 305, 308
 - , acousto-optic 176
 - , acousto-optic bulk 155
 - , acousto-optic waveguide 169
 - , amplitude 176, 308
 - , bulk 154, 160, 164, 167, 169, 179, 192
 - , definition of 140
 - , electro-optic 176
 - , electro-optic bulk 161–164
 - , electro-optic waveguide 175, 177
 - figure-of-merit 159
 - , infrared 166
 - , intensity 141, 283, 284
 - , junction 180
 - , lensing 176
 - , magneto-optic 189
 - , magneto-optic polarization 147
 - , phase 176, 177, 178, 282
 - , polarization 176, 179
 - , waveguide 167, 168, 169, 192, 193, 194
 - , waveguide grating 185

- Monolithic devices 244, 290
 - — integration (see integration)
- Monomers 211
- Niobium 210
- Optical communications 3, 6, 7, 139, 193
 - — pumping 276, 279
- Orthonormality relation 40
- Overlap factor 171, 173, 177, 184, 191
 - — integral 171
- Palladium 239
- Pattern 232
 - fabrication 232
 - generation 233
- Penetration depths 27, 215
- Periodic electrodes 180
 - — structures (see gratings)
- Perturbation techniques 113
- Phase matching 88, 92, 101, 107, 175, 179, 186, 187, 190
 - — shift 147
- Photoconduction 284
- Photodetector (see detectors)
- Photodiodes 285
- Photo-elastic effect 149, 150
- Photolithography (see lithography)
- Photolocking 237
- Photoresist 4, 90, 214, 232, 263, 275, 277
 - films 237
 - mask 235
 - , negative 235, 237
 - , positive 232, 233, 235, 237
 - , undercutting 236
- Photo-voltaic mode 283
- Piezoelectric effect 170
- Piezoelectricity 149
- Plasma 86, 244, 246, 249
- p-n junctions 2, 248, 280, 282, 285, 288, 292
- Pockels effect 148, 177
- Polarization rotators 175
- Polarizer 306
- Polishing 296, 298
 - , chemical 204
 - , chem-mechanical 204
 - , glass 203
 - , mechanical 204
- Polymer 211
 - films 213
- Polymerization 211, 213
 - , plasma 10, 202, 211, 212, 213
- Polystyrene 214
- Polyurethane 214
- Postbaking 236
- Power 40, 47
 - , drive 143, 160
 - flow 42
 - , reactive 162
- Poynting theorem 35
- Pre-sputtering 209
- Prism 226
- Propagation constant 46
- Proton bombardment 10, 202, 215
- Quaternary layers 257
- Raman-Nath regime 155, 157, 170, 174
- Reciprocity 90, 101, 107, 116, 122
- Reconstruction of images 309
- Reflection coefficient 16
 - —, total 17, 86, 88, 95
- Refractive index 201, 244, 246, 249, 252
 - —, apparent 201, 216
 - —, effective 21, 223
 - —, graded 2, 53
- Refractive index changes 150
 - — — matching fluid 217, 218, 230, 232
 - — — measurement 222, 231
 - — — profile 32
- Response time 149
- Safety factor 159, 160, 163, 179
- Sample cleanliness 206
- Scanner, definition of 140
- Scanning 141
- Scatter 217
- Schottky barriers 250, 280, 281, 282, 283, 285, 287, 289
- Segregation coefficient 255, 299
- Semi-conduction diodes 179, 285
- Semi-conductor 1, 10, 244, 245, 256, 280
 - junctions 176
- Silicon 7, 258, 285
- Sillenites 259
- Snell's law 16
- Space harmonics 91, 111, 113, 117
- Spinning 10, 202, 213
- Splicing 7
- Sputtered glass 4
- Sputtering 10, 202, 206, 207, 208, 209, 213, 222, 234, 235
 - rate 207
 - , reactive 208, 211

- Sputtering, rf 207, 209, 263
 - yield 207, 209
- Standing wave 87
- Sticking coefficient 207
- Strip loading 262
- Stylus method 221
- Substrate preparation 203
 - —, thermoplastic 238
- Surface acoustic waves 169, 171, 173, 174
- Surface electrodes 179, 191
 - — quality 206
 - — wave 84, 86, 88, 91
- Switches 9, 139, 145, 193, 308
 - , definition of 140
 - switching 140, 185
 - time 145
- Systems uses 141

- Talisurf 222
- Tantalum 210
- Target 206
- Thickness, effective 27
 - measurement 220, 222, 231
 - , optical 201
 - uniformity 209
- Titanium 234
- Tolerances 126
- Transition 306
- Transverse resonance 20, 96, 97, 98, 108
- Tunneling 88

- Vacuum evaporation 202
- Variation theorem 40
- Variational expression 44
- Varnishes 213

- Water break method 205
- Water, deionized 205
- Waveguide 8, 243, 244, 246, 305
 - , anti-symmetric 254
 - , asymmetric 18
 - bends 132, 306
 - , channel 176, 262, 267
 - , circular 3
 - , closed 83
 - , coupled 237
 - coupling 167
 - , crystalline 252, 259
 - cut-off 176, 249, 282
 - deformations 69
 - , dielectric 83
 - filter 73
 - , graded-index 306
 - , ion-implanted 265
 - , linear 123
 - , liquid crystal 176
 - losses 260
 - , metallic 83
 - , open 83
 - , periodic 73
 - , planar 2, 123, 214, 251, 306
 - , rectangular 64
 - , rib 238, 266
 - , ridge 63, 65, 262, 263, 265
 - , slab 19
 - , strip 8, 62, 125, 176, 185, 202, 214, 215, 262, 266, 306
 - , symmetric 254
- Waves, plane inhomogeneous 93
- Width, minimum effective 29
- Wipeoff 297
- WKB method 61

- Zig-zag path 19, 96